# The Loma Prieta, California, Earthquake of October 17, 1989—Marina District

THOMAS D. O'ROURKE, *Editor*

STRONG GROUND MOTION AND GROUND FAILURE
THOMAS L. HOLZER, *Coordinator*

**U.S. GEOLOGICAL SURVEY PROFESSIONAL PAPER 1551-F**


UNITED STATES GOVERNMENT PRINTING OFFICE, WASHINGTON : 1992

**DEPARTMENT OF THE INTERIOR**

**MANUEL LUJAN, JR.,** *Secretary*

**U.S. GEOLOGICAL SURVEY**

**Dallas L. Peck,** *Director*



Manuscript approved for publication, June 11, 1992

Text and illustrations edited by George A. Havach

---

For sale by the Book and Open-File Report Sales, U.S. Geological Survey,
Federal Center, Box 25286

Collapsed four-story wood-frame building at southwest corner of Divisadero and Jefferson Streets. Local subsidence caused by soil liquefaction is visible at street corner. Heaved and fractured pavement is oriented perpendicular to direction of strongest seismic shaking. Underground water, gas, and wastewater pipelines were considerably damaged at this site. View southward; photograph courtesy of T.D. O'Rourke.

CONTENTS

THE LOMA PRIETA, CALIFORNIA, EARTHQUAKE OF OCTOBER 17, 1989:
STRONG GROUND MOTION AND GROUND FAILURE

MARINA DISTRICT

# INTRODUCTION

By Thomas D. O'Rourke,
Cornell University

## CONTENTS



## INTRODUCTION

During the earthquake, a total land area of about 4,300 km$^2$ was shaken with seismic intensities that can cause significant damage to structures (Plafker and Galloway, 1989; McNutt and Toppazada, 1990). The area of the Marina District of San Francisco is only 4.0 km$^2$—less than 0.1 percent of the area most strongly affected by the earthquake—but its significance with respect to engineering, seismology, and planning far outstrips its proportion of shaken terrain and makes it a centerpiece for lessons learned from the earthquake.

The Marina District provides perhaps the most comprehensive case history of seismic effects at a specific site developed for any earthquake. The reports assembled in this chapter, which provide an account of these seismic effects, constitute a unique collection of studies on site, as well as infrastructure and societal, response that cover virtually all aspects of the earthquake, ranging from incoming ground waves to the outgoing airwaves used for emergency communication.

An aerial view and map of the Marina District are presented in figure 1. The Marina District encompasses the area bounded by San Francisco Bay on the north, the Presidio on the west, and Lombard Street and Van Ness Avenue on the south and east, respectively. Nearly all of the earthquake damage in the Marina District, however, occurred within a considerably smaller area of about 0.75 km$^2$, bounded by San Francisco Bay and Baker, Chestnut, and Buchanan Streets.

At least five major aspects of earthquake response in the Marina District are covered by the reports in this chapter: (1) dynamic site response, (2) soil liquefaction, (3) lifeline performance, (4) building performance, and (5) emergency services.

## DYNAMIC SITE RESPONSE

One of the most important response characteristics of the Marina District was the amplification of earthquake motion, with notably stronger shaking in the Marina District than in surrounding areas on bedrock and firmer soils. In this chapter, several studies are focused on evaluating subsurface conditions and assessing the factors contributing to site amplification.

Bonilla reviews the historical development of the Marina District and delineates in considerable detail the locations of natural-sand deposits, fill associated with tipping from shore and seawall construction, and hydraulic fill placed in preparation for the 1915 Panama-Pacific International Exposition. Bonilla, Bardet and others, Taylor and others, and O'Rourke and others provide a comprehensive view of subsurface conditions, based on an examination of hundreds of soil borings and soundings. The three-dimensional picture that emerges from these studies shows that the Marina District is underlain by a bedrock basin, approximately 100 m deep, filled with alluvial and marine sedimentary deposits on which loose sandy fills have been placed to develop new land next to the bay. The remarkable degree of resolution with which the subsurface conditions have been characterized is unusual for any site and, in this instance, provides an excellent framework within which to evaluate site response.

Boatwright and others evaluate the amplification of ground motion with the records of seismographs deployed after the earthquake to measure aftershocks. These records show a relatively high amplification for the central part of the Marina District, with ground motion in the bedrock magnified by a factor of 6 to 10 in the frequency range 0.7–1.5 Hz, corresponding to the predominant response

frequencies of many Marina District buildings. On the basis of the aftershock data, Boatwright and others estimate that ground motions from the main shock may have been equivalent to those at the Outer Harbor Wharf in Oakland, where a peak ground acceleration of 0.29 *g* was recorded.

Liu and others report that ground-motion amplification during aftershocks in the Marina District depended on both ground-motion direction and earthquake location. Their data show significant three-dimensional characteristics. Upon first arrival, ground motion was aligned with the direction of the incoming wave, after which a widely varying path of horizontal motion can be traced, indicating multiple reflections and wave scattering. Liu and others also show that the highest spectral-ratio peaks are associated with ground-motion components parallel to the major axis of the underlying bedrock basin, thereby demonstrating a relation between bedrock topography and the amplification of surface relative to bedrock waves.

Bardet and others compare the results of one- and two-dimensional analytical models of site response in the Marina District, showing clearly the importance of two-dimensional simulations in accounting for the amplification of seismic shaking. Their two-dimensional analyses show peak acceleration at the ground surface as high as 0.23 *g*, approximately twice as large as that calculated from their one-dimensional model. The two-dimensional effects resulted mainly from the geometry of the bedrock basin and stiff soil layers, an outcome consistent with the ground-motion data presented by Liu and others.

Stewart and Hussein evaluate the nonlinear dynamic-response properties of soft clay and silt, typical of the deposits underlying the Marina District. Their laboratory data and proposed model of soil behavior provide a sound experimental basis for the analytical modeling of nonlinear site response.

## SOIL LIQUEFACTION

Liquefaction is the temporary loss of soil strength caused by high water pressures generated in the soil as a

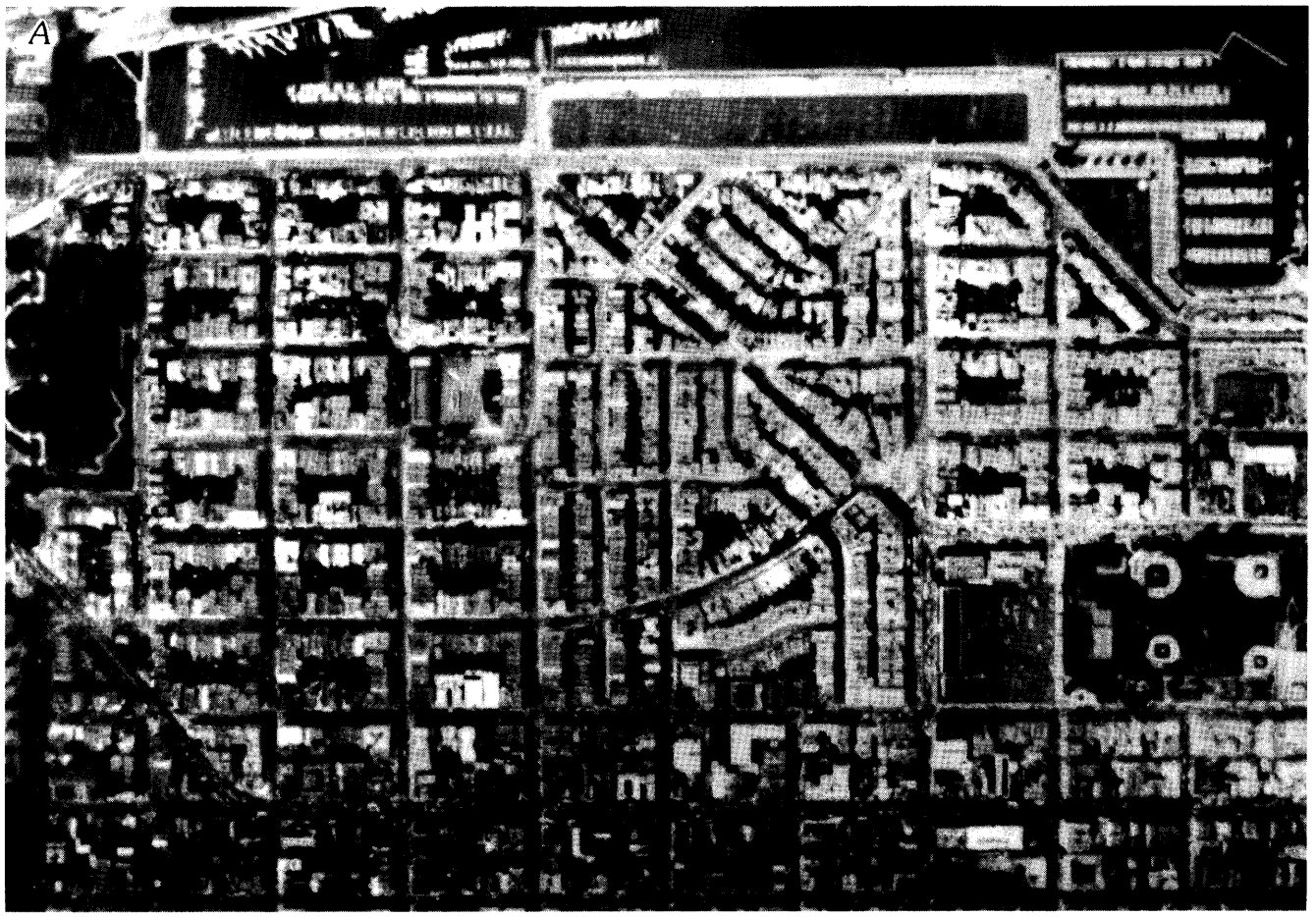


Figure 1.—Marina District of San Francisco. *A*, Marina District 2 days after the earthquake, showing areas of conspicuous damage and earthquake effects. Photograph taken from a height of 2,000 m; courtesy of Pacific Aerial Surveys, Oakland, Calif. *B*, Sketch maps showing locations of the Marina District within San Francisco and of areas of figure 1*A*.

result of earthquake shaking. Under conditions of severe shaking, the strength loss may be so large that the ground behaves as a liquid, with consequent foundation failures, damage to utilities, settlement, and lateral deformation.

The reason for the liquefaction hazard is shown clearly by the geologic and historical development of the Marina District, as described by Bonilla. Much of the liquefaction hazard is related to how soils were placed to develop the areas adjacent to San Francisco Bay. From 1851 to 1912, both marsh and bay were filled in a piecemeal fashion by loosely dumping natural sand, much of which was excavated from dunes and beaches in the vicinity of the old shoreline. In 1912, hydraulic fill was placed principally in an artificial lagoon enclosed by a seawall, which still provides support and horizontal stability for parts of the Marina District. This hydraulic fill consists of sand and silt, dredged and pumped into the lagoon. The Marina District, therefore, is built on three types of sandy soils, including natural sand, loose sand placed by tipping from the shoreline and seawall, and hydraulic fill.

The properties and liquefaction behavior of these different soils are an important aspect of our investigations and are directly relevant to other places where these types of soils exist. Bardet and others show that liquefaction, in the form of sand boils, was most conspicuous throughout areas underlain by hydraulic fill. O'Rourke and others explore the postliquefaction consolidation of the different deposits. (Postliquefaction consolidation is the volume loss and settlement that result as soils densify during the dissipation of high water pressures triggered by an earthquake.) These researchers show that the most widely used methods of site exploration, utilizing the standard penetration test, are not sufficiently refined for predicting the postliquefaction consolidation of hydraulic fill. Instead, other methods of site exploration, such as the cone penetration test, are required to evaluate properly the stratification of hydraulic fill and thus to identify more accurately the sandy layers that actually liquefy.

Taylor and others describe the behavior of the Marina District's seawalls and waterfront during the earthquake. Lateral displacements and settlements as high as 600 mm were observed near the St. Francis Yacht Club. Deformation analysis of the main seawall in the Marina District shows approximately 150 mm of lateral movement, which is consistent with the observed performance of the seawall. This type of validation and refinement of analytical

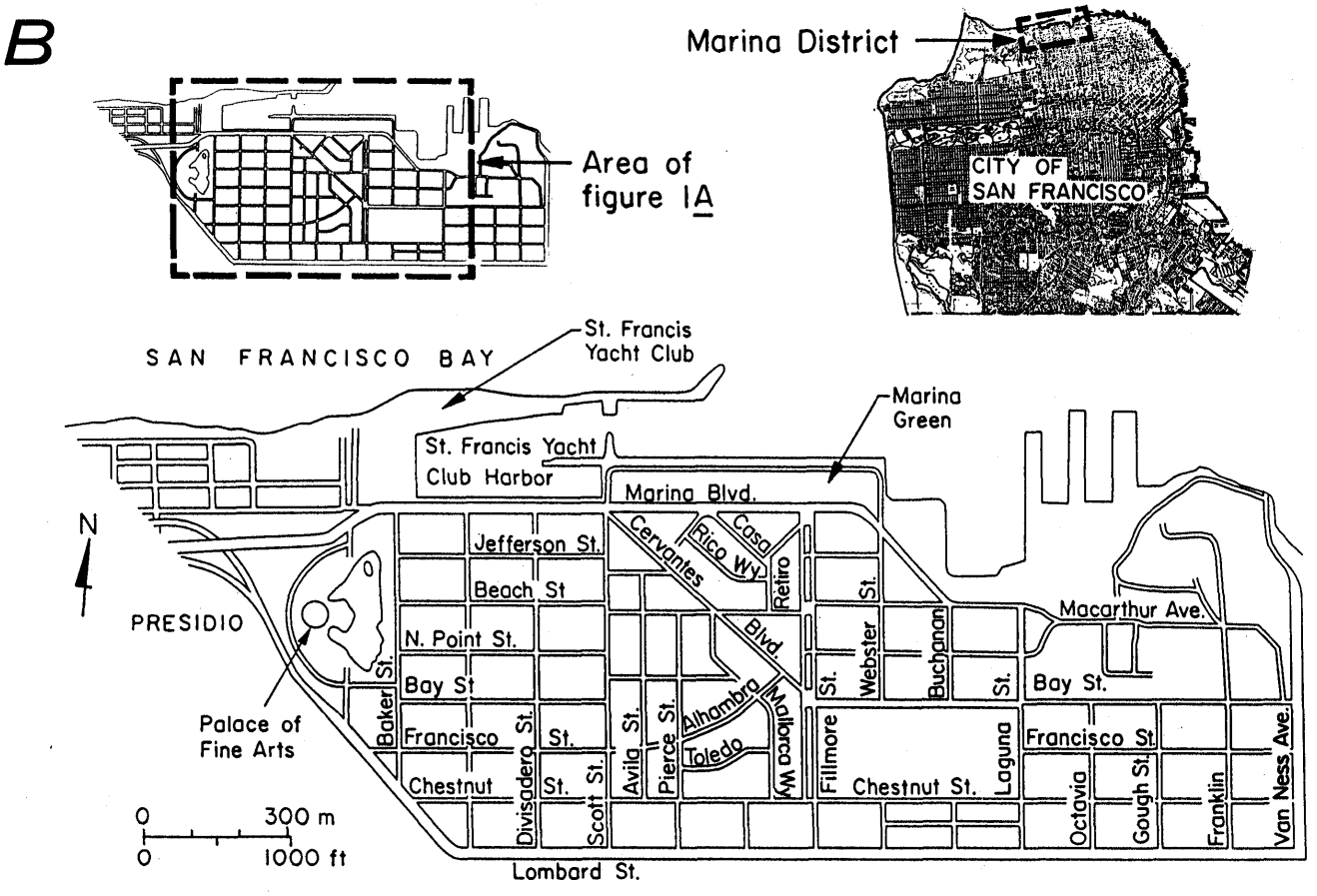


Figure 1.—Continued.

models on the basis of observations is an important step in forecasting the seawall and shoreline response in the Marina District during a larger earthquake.

## LIFELINE PERFORMANCE

Lifelines are systems for the distribution of critical resources, such as water supplies, transportation arteries, gas and liquid-fuel complexes, telecommunication and electric-power systems, and wastewater-conveyance networks. These facilities are important for life support and the restoration of community and economic activity after an earthquake.

In the Marina District, there were 123 repairs to pipelines of the Municipal Water Supply System (MWSS) of San Francisco, more than three times the number of repairs throughout the rest of the city. The loss of water from this system severely hampered firefighting efforts in the district. Approximately 13.6 km of gas-distribution piping was replaced, and more than 20 percent of the wastewater-collector lines were repaired or replaced.

O'Rourke and others report on the damage to lifelines in the Marina District and show that damage to the MWSS and wastewater-conveyance system was caused primarily by soil deformation associated with postliquefaction consolidation. The remarkable correlation between pipeline damage and surface settlement, both with respect to magnitude and spatial distribution, is perhaps the clearest demonstration in any earthquake of pipeline-network vulnerability to liquefaction-induced ground deformation.

## BUILDING PERFORMANCE

Earthquake effects in the Marina District provide a graphic illustration of the damage that can occur to certain types of buildings, particularly those constructed before the adoption of appropriate seismic codes and for which retrofitting has not been implemented. The most severe damage occurred in four-story, wood-frame corner buildings, which are the subject of the report by Harris and Egan, focusing on ground conditions and structural damage. Their study shows that the highest concentration of most heavily damaged buildings correlates with the areas of fill placed by tipping from the former shorelines and seawall, with somewhat less damage in areas of hydraulic fill. Building damage is shown to be related closely to the fundamental frequency of the structure. The most heavily damaged buildings had fundamental frequencies of approximately 0.8 to 1.2 Hz, which corresponds to the frequency range of greatest site amplification reported by Boatwright and others. Dynamic analyses indicate displacements of about 300 mm for heavily damaged buildings, which is consistent with the permanent deformation actually observed in many of these structures.

A particularly interesting aspect of Harris and Egan's work is the difference in the response of wood-frame corner buildings from that of buildings which had unreinforced-masonry or concrete first stories but were otherwise similar in construction. The buildings with masonry and concrete first stories, which had fundamental frequencies of about 3 Hz, were damaged on average about 10 times less severely than their wood-frame counterparts. Such observations emphasize the importance of fundamental frequency and the substantial improvements in structural response associated with stiffening structures at soft-soil sites.

## EMERGENCY SERVICES

Scawthorn and others describe the emergency-response services of the police and fire departments, ambulance crews, and Marina District residents. Their study brings into focus some of the most important lessons learned in the Marina District.

San Francisco is served by two in-ground water-supply systems, the MWSS and the Auxiliary Water Supply System (AWSS); the AWSS is operated exclusively for firefighting purposes. Water was available from neither of these systems after the earthquake. As previously mentioned, the MWSS was severely disrupted by the effects of liquefaction in the Marina District. The AWSS had likewise been damaged by liquefaction nearly 5 km away, and water was completely lost from a reservoir supplying city areas adjacent to the bay.

Of critical importance in controlling and suppressing the fire in the Marina District were the fireboat, which was dispatched to the St. Francis Yacht Club Harbor, and the Portable Water Supply System (PWSS). The PWSS consists of special hose tenders, with 1,600 m of 125-mm-diameter hose and associated equipment, which can draw water from the bay and underground cisterns. This system was responsible for stopping the fire in the Marina District, thereby saving the community from considerably more severe fire damage. The acquisition of the PWSS, as well as the planning and training for its use under emergency conditions, proved to be of inestimable value in reducing earthquake-related losses.

Scawthorn and others draw attention to the congested radio traffic between firefighters and the central communications center. This traffic, which far exceeded the capacity of the allotted channels, underscores a need for additional channels and improved oversight by means of aerial reconnaissance. These investigators also point out the important role played by Marina District residents in assisting emergency-service personnel.

## CONCLUDING REMARKS

The Marina District has been a focal point of media coverage, postearthquake investigations, and rehabilitation efforts. In the first few months after the earthquake, special studies were undertaken by geotechnical staff at the University of California, Berkeley (Mitchell and others, 1990), the U.S. Geological Survey (1990), and the National Center for Earthquake Engineering Research (O'Rourke and others, 1990). These initial studies were used to acquire data and evaluate site conditions for use by city and district residents in the rehabilitation and seismic remediation of the area. Additional studies sponsored by the National Science Foundation, the U.S. Geological Survey, and the National Center for Earthquake Engineering Research helped to establish a detailed and vigorous program for the assessment of earthquake effects in the Marina District. Many of the reports in this chapter are the result of research sponsored by these national organizations. Studies commissioned by the city of San Francisco (Harding Lawson Associates and others, 1991) have focused on liquefaction hazards, with a first-time, systematic review of the sites vulnerable to liquefaction-induced ground deformation and their potential effect on lifeline systems. These studies have involved an engineering evaluation of liquefaction and lifeline hazards in the Marina District, with recommendations for retrofitting, site stabilization, and infrastructure planning.

The investigations and studies stimulated by the Marina District have important ramifications not only for local residents but also for the larger community of people living in places vulnerable to earthquakes. Lessons learned regarding the pattern of ground deformation relative to subsurface conditions and its effect on lifelines and buildings will help in the mapping of hazard zones as part of a statewide effort engendered by the Seismic Hazards Mapping Act passed by the California Legislature (1990). Lessons learned about dynamic site response, liquefaction, lifeline performance, and emergency services are relevant to all seismically vulnerable areas and help to achieve the goals of earthquake-damage mitigation embodied in the National Earthquake Hazards Reduction Program.

The Marina District is a microcosm of the type of site response and damage patterns that can be sustained not only in the San Francisco Bay area but also at locations of reclaimed land and soft sedimentary deposits throughout the world. The findings reported in this chapter, therefore, contribute to improved engineering and planning practices for sites most vulnerable to earthquakes and most in need of assistance to reduce existing hazards.

*Acknowledgment.*—I thank Laurie Mayes of Cornell University for helping in the organization and coordination of this publication.

## REFERENCES CITED

California State Legislature, 1990, Public Resources Code, chap. 1168, sec. 2690 ff.

Harding Lawson Associates, Dames & Moore, Kennedy/Jenks/Chilton, and EQE Engineering, 1991, Liquefaction study, Marina District and Sullivan Marsh area, San Francisco, California; final report prepared for San Francisco Department of Public Works: San Francisco, 144 p.

McNutt, S.R., and Toppazada, T.R., 1990, Seismological aspects of the 17 October 1989 earthquake, *in* The earthquake, sec. 1 *of* McNutt, S.R., and Sydnor, R.H., eds., The Loma Prieta (Santa Cruz Mountains), California, earthquake of 17 October 1989: California Division of Mines and Geology Special Publication 104, p. 11–27.

Mitchell, J.K., Tahir, M., Kayen, R.E., and Seed, R.B., 1990, Soil conditions and earthquake hazard mitigation in the Marina District of San Francisco: report to the mayor of San Francisco.

O'Rourke, T.D., Stewart, H.E., Blackburn, F.T., and Dickerman, T.S., 1990, Geotechnical and lifeline aspects of the October 17, 1989 Loma Prieta earthquake in San Francisco: Buffalo, N.Y., National Center for Earthquake Engineering Research Technical Report NCEER–90–0001, 49 p.

Plafker, George, and Galloway, J.P., eds., 1989, Lessons learned from the Loma Prieta, California earthquake of October 17, 1989: U.S. Geological Survey Circular 1045, 48 p.

U.S. Geological Survey, 1990, Effects of the Loma Prieta earthquake on the Marina District, San Francisco, California: Open-File Report 90–253.

THE LOMA PRIETA, CALIFORNIA, EARTHQUAKE OF OCTOBER 17, 1989:
STRONG GROUND MOTION AND GROUND FAILURE

MARINA DISTRICT

# GEOLOGIC AND HISTORICAL FACTORS AFFECTING EARTHQUAKE DAMAGE

By M.G. Bonilla,
U.S. Geological Survey

## CONTENTS

[Table 1 follows references]



ABSTRACT

A northwest-trending valley in the bedrock surface is buried by firm Pleistocene bay clay, dense to very dense Pleistocene sand, soft Holocene bay deposits, loose to dense Holocene beach and dune sands, and artificial fill that have an aggregate maximum thickness of about 90 m. Depth to the ground-water table is generally less than 2.7 m (9 ft) except in one area of thick dune sand; the ground-water table is quite shallow in some places where no surface effects of liquefaction related to the earthquake were reported.

Artificial filling of a cove at the site of the Marina District proceeded gradually from the late 1860's to 1912, when major hydraulic filling was done for the Panama-Pacific International Exposition. The remains of thousands of piles driven for the exposition probably still exist and may have affected long-term ground settlement and earthquake-related ground displacements.

Previous studies suggest that ground motion was amplified on both natural and artificially filled ground because of the configuration of the bedrock surface and the position and thickness of various clay and sand deposits underlying the fill, but that most of the settlement, liquefaction, and damage to pipelines, building foundations, streets, sidewalks, and curbs occurred in areas of artificial fill consisting mainly of loose sand.

## INTRODUCTION

During the earthquake, substantial damage occurred in the Marina District of San Francisco, even though it was 100 km (60 mi) from the epicenter. Factors that influenced the damage included liquefaction, differential settlement, amplification of ground motion, and the types and conditions of the buildings. To understand the reasons for the damage and to anticipate the effects of future earthquakes, various studies have been conducted and described, among them a preliminary report on the geology and the artificial fills that underlie the Marina District (Bonilla, 1990), and a report that discussed the relations of the geology, historical development, and earthquake effects (Bonilla, 1991). The present study is a summary and expansion of the cited reports, including information about the historical development of the Marina District and the composition and distribution of bedrock, unconsolidated Pleistocene and Holocene deposits, and artificial fills. Its purpose is to provide background information for current and future scientific and geotechnical investigations of the Marina District, and its emphasis is on those aspects of the geology and historical development that are pertinent to understanding past and future earthquake effects.

Both customary and metric units are used in this report, because many of the anticipated geotechnical users prefer customary units; furthermore, the original data for some illustrations are in customary units and cannot be conveniently or accurately shown in metric units. Dual units are given in the text and, where practical, in the illustrations also.

Although much information is available about the Marina District, much still remains unknown. Where necessary, I have made interpretations even if the information is scanty. The bases for my interpretations are described in the text or shown on the maps and cross sections, to allow the reader to judge the reliability of the interpretations.

The location of the Marina District and of streets and localities referred to in the text are shown in figure 1. For brevity, the Marina District is referred to as "the Marina" in the following text.

# GEOLOGY

## SOURCES OF INFORMATION

The geologic map of the Marina District (fig. 2) is derived from old maps, photographs, boreholes, and previously published geologic maps. The positions of shorelines and marsh areas are from U.S. Coast Survey maps dated 1851 through 1869. Areas of dune sand, beach sand, and beach sand covered by dune sand were interpreted on the basis of (1) the sand patterns shown on the maps, (2) areas of higher ground shown by hachures or contours on the maps, and (3) other historical information including photographs taken in 1856 through 1887. The area of undivided Quaternary sedimentary deposits shown near Chestnut and Scott Streets is inferred from hachures and sand patterns shown on the 1851 map. The areas of undivided Quaternary and Franciscan bedrock are slightly modified from the maps by Schlocker (1974, pl. 1) and Schlocker and others (1958). The areas of artificial fill were delineated primarily from topographic and planimetric maps, including those by the U.S. Coast Survey dated 1851 through 1895, Lawson (1908, map 17), and Leurey (1914, fig. 3). The information on these maps was supplemented by a photograph taken in 1912, historical accounts, and boreholes.

The boreholes used in this study are identified by an alphanumeric code related to a grid that is referenced to the Marina street pattern (fig. 3); for example, the borehole in the northwest corner of figure 3 is referred to as 3A1. The last number in the code was assigned serially according to the date of drilling, if known. The sources, dates, and other pertinent information about the boreholes are listed in table 1. Many of the borehole logs are considered proprietary information by landowners, and readers interested in copies of these logs should contact the listed sources for the owners' names.

The locations of many of the boreholes drilled for the Panama Pacific International Exposition are uncertain, and so their locations as shown in figure 3 may differ from locations used by other workers. Whitworth (1932, pl. 24) showed the boreholes on a small-scale (approx 1:90,000) map, and described their locations in relation to both streets and exposition buildings, but some of his descrip-

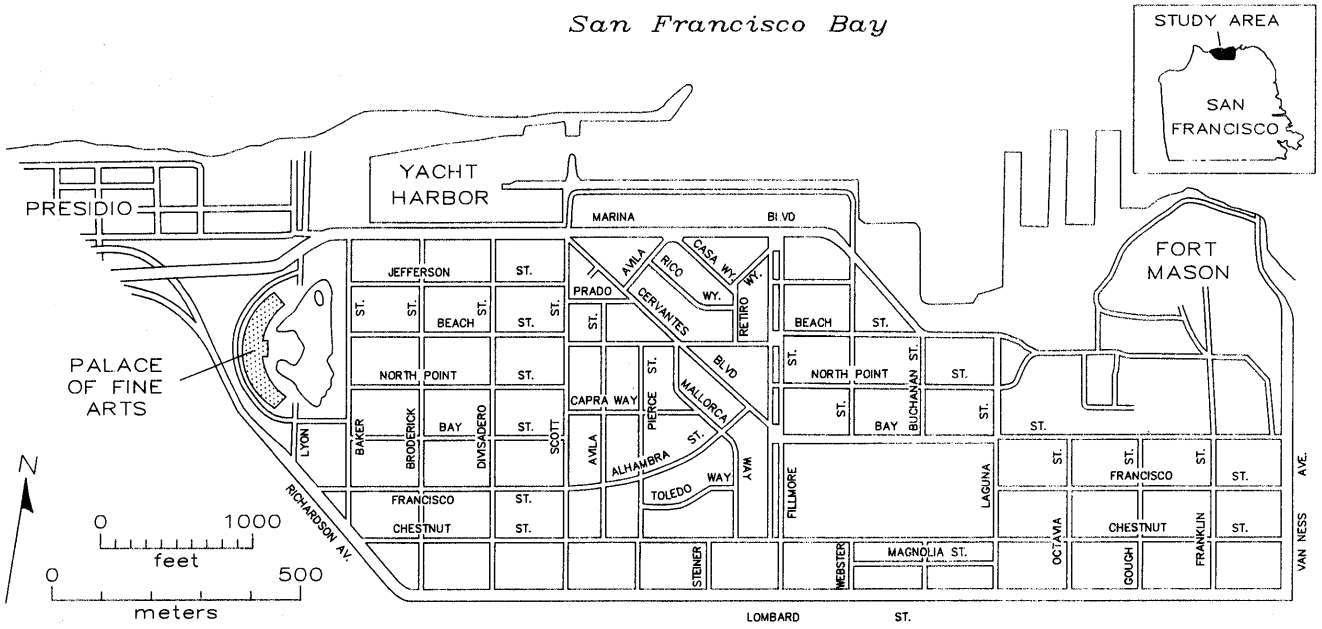


Base from U.S. Geological Survey San Francisco North 7.5' quadrangle, photorevised in 1973

Figure 1.—Marina District of San Francisco, showing locations of features mentioned in text.

tions are in conflict with his map. Furthermore, some of Whitworth's descriptions are clearly wrong, such as giving distance west of an east-west-trending street; other distances and directions place a borehole in a different part of a given building than his text states. The map by Leurey (1914) accurately shows a few boreholes in relation to exposition buildings, and he stated that boreholes were drilled at the corners of the buildings; Whitworth's locations in relation to exposition buildings, if not incongruous with other information, are accepted here. The locations of exposition buildings as shown by Todd (1921) were plotted in relation to present-day streets by using as controls the Palace of Fine Arts and the centerline of Scott Street, the only exposition street that was centered on existing San Francisco streets (Markwart, 1915a, p. 75).

## BEDROCK

The bedrock underlying the Marina consists of Franciscan assemblage and serpentine. Nearby outcrops consist of sandstone and shale except to the west, where serpentine is also exposed (Schlocker, 1974). The locations of outcrops of Franciscan sandstone and shale in Fort Mason are shown in figure 2. A borehole near the south end of the Palace of Fine Arts (2G1, fig. 3) penetrated shale, but a U.S. Geological Survey (USGS) borehole (5E3) southeast of the intersection of Divisadero and Beach Streets penetrated serpentine.

Several maps show the configuration of the bedrock surface beneath the Marina. The map by Whitworth (1932, pl. 33) shows the surface at an elevation of 75 m (250 ft) below sea level in the southern and southeastern parts of the Marina. The maps by Schlocker (1962, 1974) and Schlocker and others (1954) show similar depths except in the western part of the Marina where they show elevations of 0 to −15 m (0 to −50 ft). The map by Schlocker and others (1954) relied on the boreholes reported by Whitworth (1932), but included a precautionary note: "Bedrock may be considerably deeper than shown; contours drawn on top of 'yellow hardpan' of drillers log." This note, however, was omitted from the later bedrock-surface maps by Schlocker (1962; 1974, pl. 3). Various post-1932 borehole logs show that the bedrock is indeed deeper than the

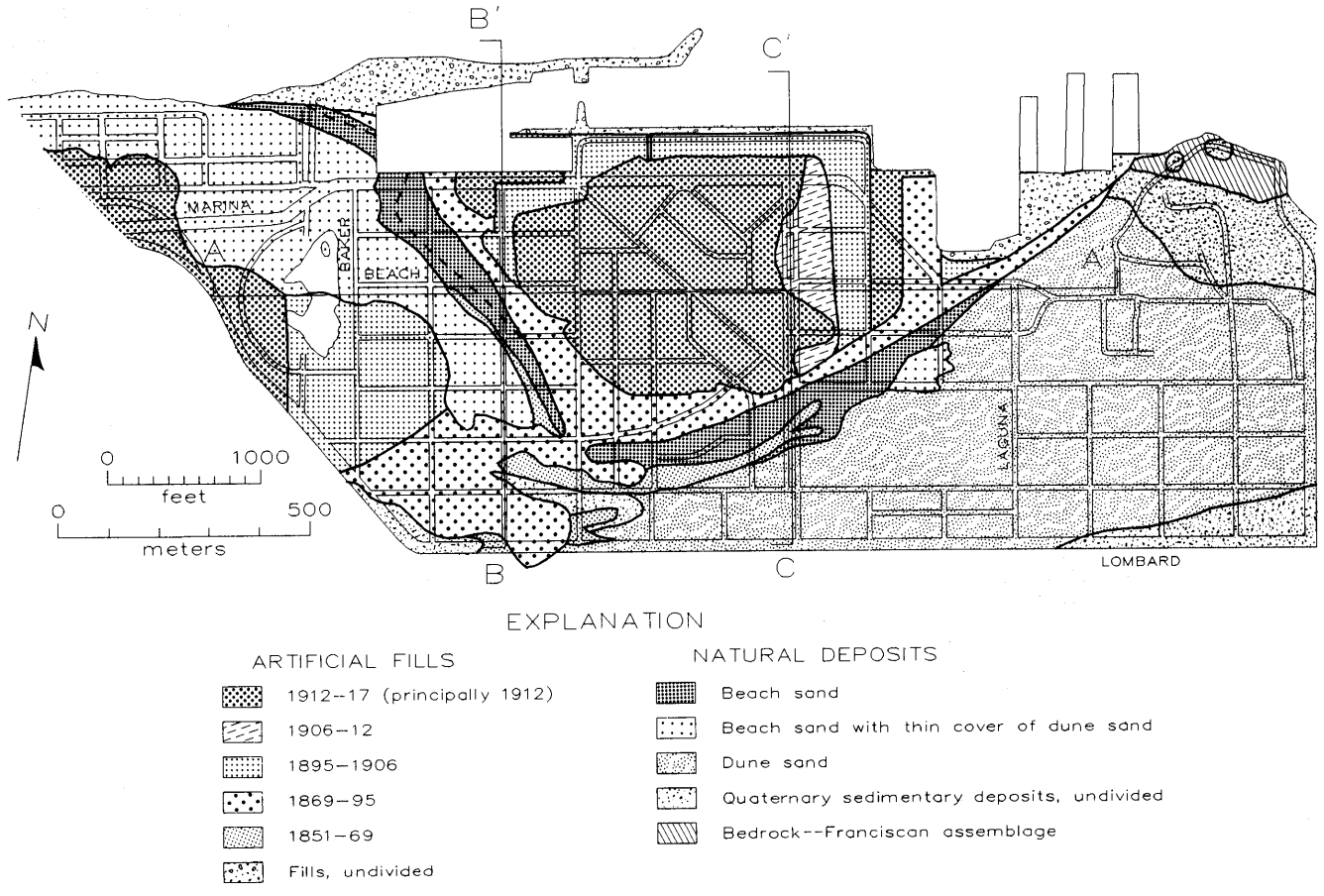


Figure 2.—Geologic map of the Marina District, showing locations of major artificial fills and cross sections *A–A'* through *C–C'* (see figs 5–7). Northwest-trending dashed curve on left designates part of 1851 shoreline. Undated fill near the Fort Mason docks was placed about 1910, and fills north of yacht harbor are post-1914. See text ("General Distribution, Age, and Composition of Artificial Fills") regarding accuracy of map.

yellow hardpan. A map showing the bedrock surface under part of the Marina and San Francisco Bay (Carlson and McCulloch, 1970) is based on the map by Schlocker (1962) and interpretation of offshore continuous subbottom acoustic profiling.

My interpretation of the configuration of the bedrock surface is shown in figure 4. Although more than 200 boreholes have been drilled in the Marina, few reach the bedrock surface; mapping of this bedrock surface therefore requires many inferences and interpretations. In preparing figure 4, I assumed that the bedrock surface was shaped by stream erosion rather than tectonic deformation and that the stream had its outlet through the Golden Gate, where bedrock is about 120 m (400 ft) below sea level (Carlson and McCulloch, 1970). The maps by Carlson and McCulloch (1978) and Schlocker (1974) show a bedrock basin in the Marina that opens to the north just west of Fort Mason. However, two boreholes considerably farther west (5E3, 2G1, fig. 3) that penetrated bedrock at elevations of –77 m (–252 ft) and –23 m (–75 ft) indicate that the bedrock basin may open to the northwest rather than the north. A stream flowing northwest would have a shorter path to the Golden Gate than one flowing northward and then westward, and so a northwest-flowing drainage was assumed. Using this basic model, the surface drainage shown on the old topographic maps was extrapolated, and contours were inferred from borehole data, outcrops, and the offshore geophysical survey of Carlson and McCulloch (1978).

The bedrock surface shown in the northwest corner of figure 4 is deeper than the onshore and near-offshore contours shown by Carlson and McCulloch (1970). Their interpretations onshore in the western part of the Marina were influenced by the erroneous contours on the yellow hardpan (Schlocker, 1962), and so they are discounted here. Offshore, Carlson and McCulloch show a –75-m (–250 ft) bedrock elevation where figure 4 shows an elevation of –90 m (–300 ft). Straight-line extrapolations of the bedrock surface between boreholes or between outcrops and boreholes indicate bedrock elevations of at least –90 m (–300 ft) well inland under the Marina, and so, if the stream-erosion model is correct, bedrock elevation must be less than –90 m in the northwest corner of figure 4. Owing to difficulty in identifying bedrock in the reflection profiles and unknown velocities in firm materials above bedrock, the bedrock surface may well be lower than shown on Carlson and McCulloch's map (P.R. Carlson, oral commun., 1990). Van Reenan (1966) also stated that identification of the bedrock surface by reflection methods is difficult in some places, and he noted on his profiles that refraction data locally show greater depths than do reflection data.

O'Rourke and others (1991, fig. 12; see O'Rourke and others, this chapter, fig. 14) independently prepared a map showing contours on the bedrock surface beneath the Ma-

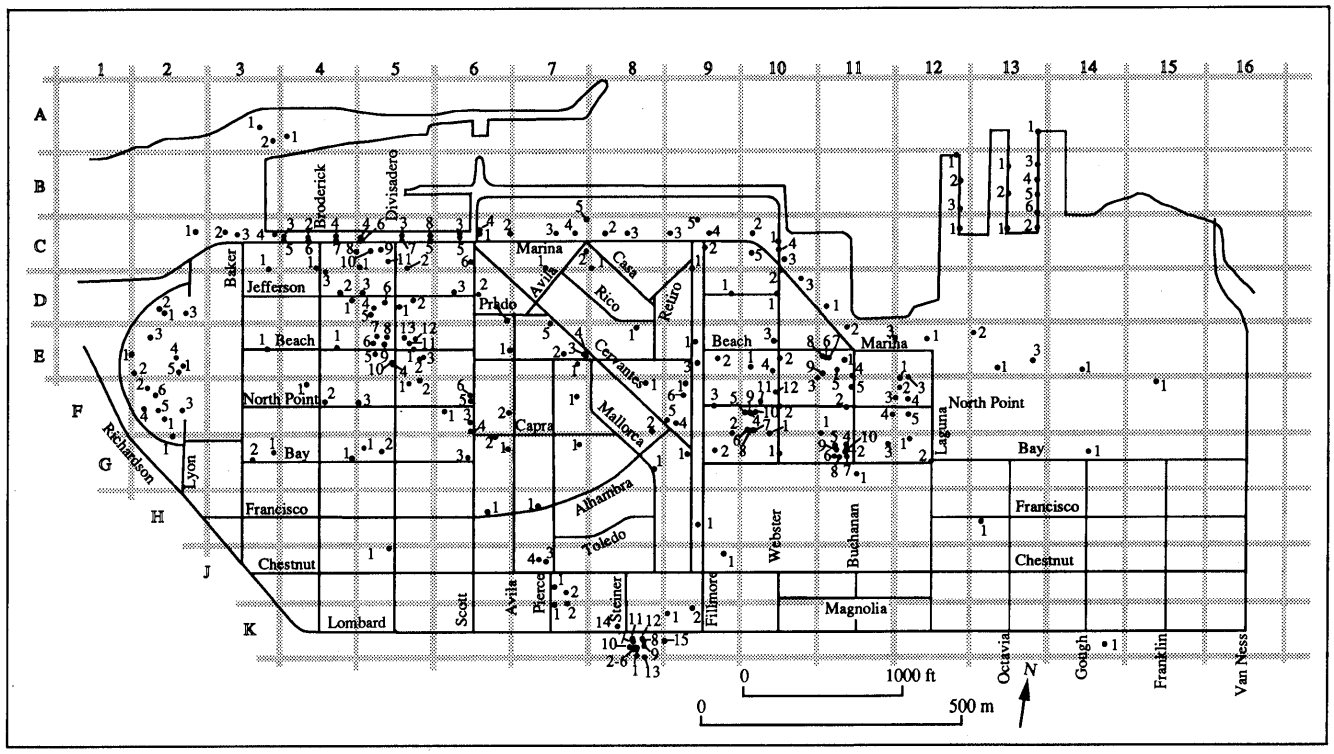


Figure 3.—Marina District, showing locations of boreholes (numbered dots). See text for explanation.

rina. They used bedrock outcrops farther to the southwest, south, and east than I did, but not Anita Rock or the offshore geophysical surveys. Their map, generated by computer software that uses a method called kriging, is similar to figure 4 in showing a northwest-trending valley in the bedrock surface, but differs in that the valley is about 15 m (50 ft) shallower and does not extend as far to the southeast.

## UNCONSOLIDATED NATURAL SEDIMENTARY DEPOSITS

The bedrock in the Marina is buried by a sequence of unconsolidated sedimentary deposits. The term "unconsolidated" is used here in the geologic sense (that is, not hard rock) rather than in the geotechnical sense. The complexity of these deposits can be partially understood by reviewing the recent geologic history of the San Francisco Bay estuary. During the past million years, at least four periods of deposition occurred in San Francisco Bay, separated by periods when sea level was lower because ocean water was incorporated into glaciers (Atwater, 1979). The lower sea levels during glacial periods resulted in erosion of valleys in the then-existing sedimentary deposits. Exposure of these deposits resulted in near-surface desiccation and oxidation, which made the sediment firmer and produced the brown colors commonly reported in boreholes. This geologic history produced various geologic units in the Marina and surrounding area, including bay, marsh, beach, and dune deposits.

### PLEISTOCENE BAY DEPOSITS

Several boreholes in the Marina penetrated silty to sandy clay at considerable depth. In USGS borehole WSS (5E3, fig. 3), south of Beach Street and east of Divisadero Street (Kayen and others, 1990), the clay is 58 m (189 ft) thick and extends from an elevation of −19 m (−63 ft) to the bedrock surface at an elevation of −77 m (−252 ft). The clay is probably correlative with one or more of the three pre-Holocene bay deposits that formed in San Francisco Bay during the past million years (Atwater, 1979). During the latest interglacial sea-level highstand about 100 ka, an extensive bay deposit formed in San Francisco Bay (Atwa-

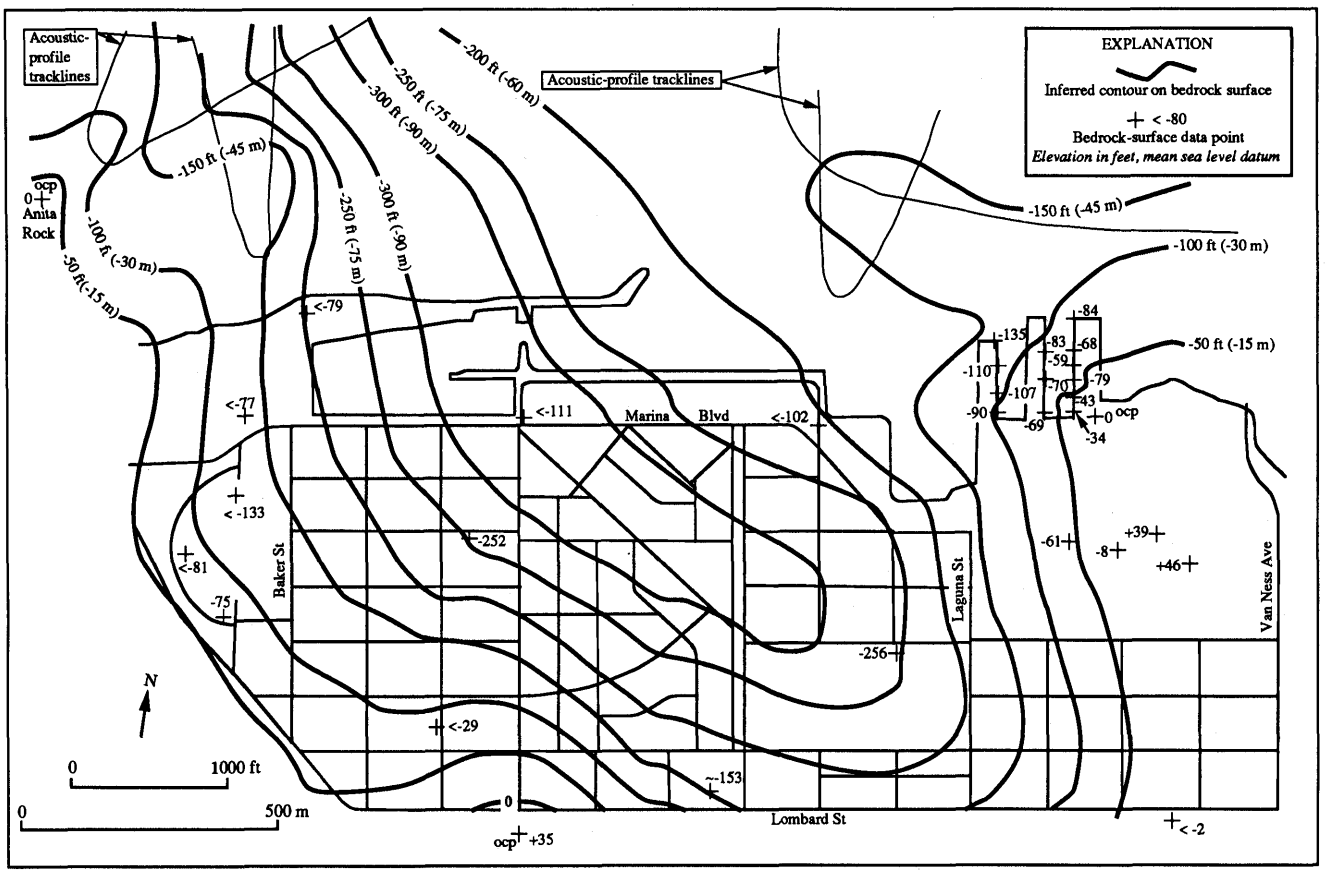


Figure 4.—Marina District, showing inferred contours on bedrock surface. ocp, data points at rock outcrops. Acoustic-profile tracklines from Carlson and McCulloch (1970).

ter and others, 1977; Atwater, 1979, fig. 3). The upper part of the thick clay penetrated in USGS borehole WSS (5E3, fig. 3) is probably this approximately 100,000-year-old bay deposit, but the lower part may be still-older bay deposits. The Pleistocene bay deposits are not exposed at the surface in the Marina, but their inferred extent and thickness in the area of figure 2 is shown on cross sections *A–A'*, *B–B'*, and *C–C'* (figs. 5, 6, and 7, respectively). When a plan-view sketch was made of the upper surface of the Pleistocene bay deposits, using the few borehole data, it became apparent that this surface has a broad depression, represented in figures 5 through 7, that apparently trends northeast. Treasher (1963) reported that valleys eroded into the older bay deposits are common in various parts of San Francisco Bay, and Atwater and others (1977) also recognized a major unconformity at that stratigraphic level. Whether this depression in the surface of the Pleistocene bay deposits in the Marina is a result of erosion is unclear.

## PLEISTOCENE SAND ZONE

Many boreholes penetrated a sand zone overlying the Pleistocene bay silty clay. Its thickness, as measured on the cross sections (figs. 5–7), ranges from 3 to 38 m. Two samples of the sand zone, from USGS borehole WSS (5E3, fig. 3) contain only 1 to 4 weight percent silt and clay (Kayen and others, 1990), suggesting a dune or beach origin. A third sample contains 26 weight percent silt and clay and could be of stream or estuarine origin. In some borehole logs, the sand zone is described as sand, silty sand, or clayey sand. Thick interbeds of clay (fig. 7) are probably estuarine, suggesting that the sand zone has had a varied history. A sand zone in the southeastern part of San Francisco has a similar stratigraphic position—under the Holocene bay clay and above the older bay clay—and in that area the lower part of the sand is interbedded with the older clay (Radbruch and Schlocker, 1958). The sand zone in the Marina is probably less than 100,000 years old because it overlies the Pleistocene bay deposits thought to be about 100,000 years old. As discussed in the next section, the upper part of this sand zone was apparently eroded by streams near the end of the latest glaciation, and so the zone is interpreted to be of Pleistocene age.

The sand zone lithologically resembles the Colma Formation and may be correlative with that formation. The Colma Formation, commonly a weathered sand, is thought to have originated primarily as a beach deposit (Schlocker, 1974). Information on the age of an ash bed in marine deposits beneath the Colma in the southwestern part of San Francisco (Meyer and others, 1980, 1991; Sarna-Wojcicki and others, 1985) indicates that the Colma must be considerably less than 400,000 years old and may correlate with one of the latest sea-level highstands between about 130 and 70 ka (Clifton and others, 1988).

## HOLOCENE BAY DEPOSITS

Sea level during the latest (Wisconsin) glaciation was 90 to 120 m (300–400 ft) lower than at present and the ocean shoreline was probably seaward of the Farallon Islands, about 50 km (30 mi) west of San Francisco. The Holocene bay deposits in the Marina accumulated during the sea-level rise that followed the latest glaciation. The rising sea is estimated to have entered the Golden Gate 11–10 ka (Helley and Lajoie, 1979, p. 18). The bay deposits in the Marina are generally soft silty clay or clayey silt, but locally they include fine sand. These deposits have been referred to by the term "bay mud and clay" (for example, Schlocker and others, 1958; Schlocker, 1974), but for brevity and in keeping with more common usage they are here referred to as "bay mud."

The bay mud formed the bottom of Marina Cove (see fig. 10) and underlies much of the Marina. This bay mud is not exposed at the ground surface, and so its extent must be inferred (fig. 8). The northern margin shown in figure 8 is based on a few borehole data on the west and on predevelopment lagoon-bottom contours, inferring that the edge of the estuarine mud coincides with the steep slope indicated by the contours in figure 9. The swift tidal currents in the deeper water do not permit deposition of mud, and sand is known to cover the bay bottom north of the Marina (Carlson and others, 1970, p. 106). These considerations and three boreholes to the west (3A1, 3A2, 4A1, fig. 3), each of which penetrated silty sand, are the basis for the inferred north contact of bay mud and silty sand shown in figure 6. Whether this contact is gradational or interfingering is unknown; the position of the margin of the bay mud west of the area of figure 8 is also unknown.

The configuration of the bottom of Marina Cove and of the surface of the bay mud in 1873 is shown in figure 9,

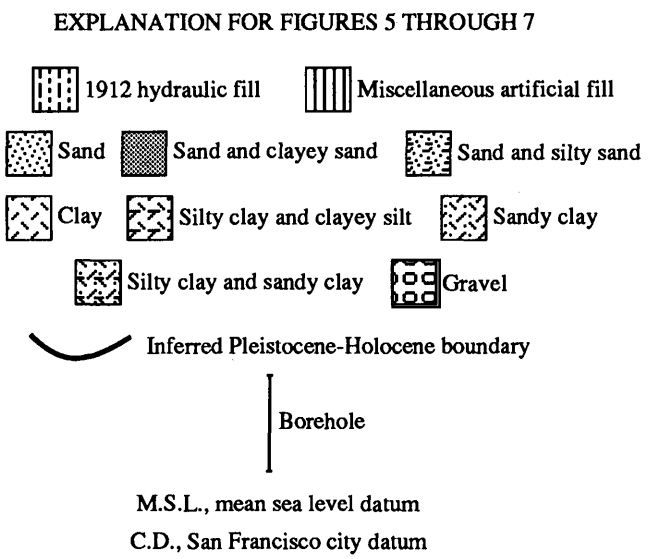


Explanation for figures 5 through 7.

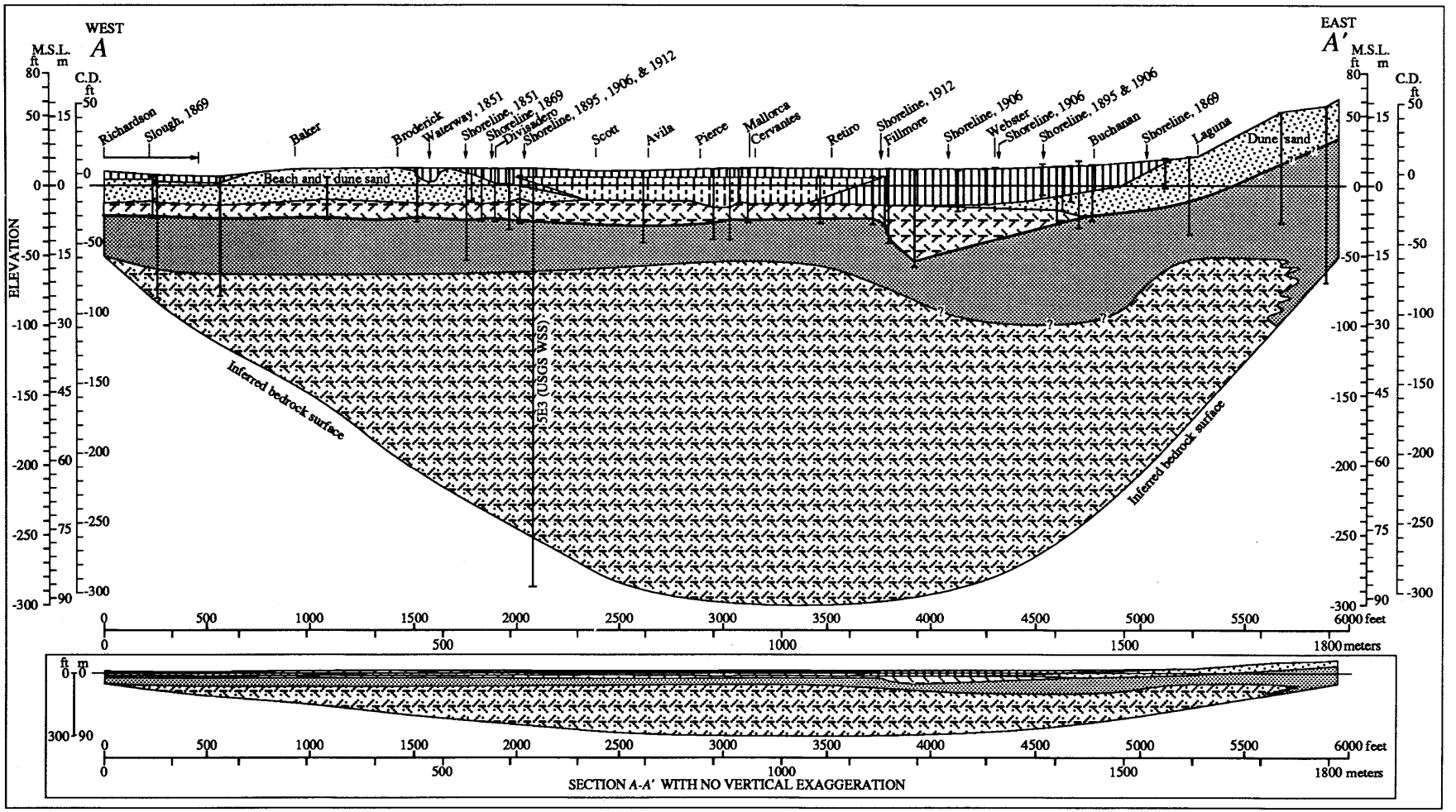


Figure 5.—East-west cross section *A–A'* along Beach Street (see fig. 2 for location). Sand fill, difficult to distinguish from natural sand, may locally overlie beach and dune deposits near Baker Street. Marsh deposits below artificial fills in western part of the cross section are too thin to be delineated. Queries indicate uncertainty in location. Interfingering of Pleistocene clay and Pleistocene sand in eastern part of cross section is schematic.

based on an 1873 map by the U.S. Coast Survey (register 1214a, scale 1:20,000), that shows soundings in feet below mean lower low water and contours of 6-, 12-, and 18-ft depth. These soundings and contours were transferred to a 1:10,000-scale base map, and the contours shown in figure 9 were drawn, interpolating between soundings and using the old shoreline and the three depth contours shown on the 1873 map as guides. The 1873 rather than earlier maps was used for contouring because the earlier maps are more difficult to match with modern maps and soundings are sparser. Both the top of the bay mud in 1873 and its present surface, modified by application of artificial fill (see O'Rourke and others, this chapter, fig. 16), show much less relief than its bottom does (see figs. 5–7). As discussed below, the bay mud was apparently deposited on a late Pleistocene erosional surface, a condition that accounts for its irregular bottom.

A layer of green sand and clay, commonly described as hard, was penetrated at the bottom or near the base of the bay mud in 70 percent of the boreholes made for the 1915 Panama-Pacific International Exposition, and most of the exposition piles were founded in this layer. A layer referred to in the borehole logs as "yellow hardpan" lies beneath the hard green sand and clay, and was reached by 85 percent of the exposition boreholes. Although descriptions vary, several 1989 and 1990 boreholes penetrated a similar zone containing hard or firm layers that produced high peaks on the cone-penetrometer-test records. The "yellow hardpan" is probably a soil zone that formed on an erosional surface developed during the low sea level of the

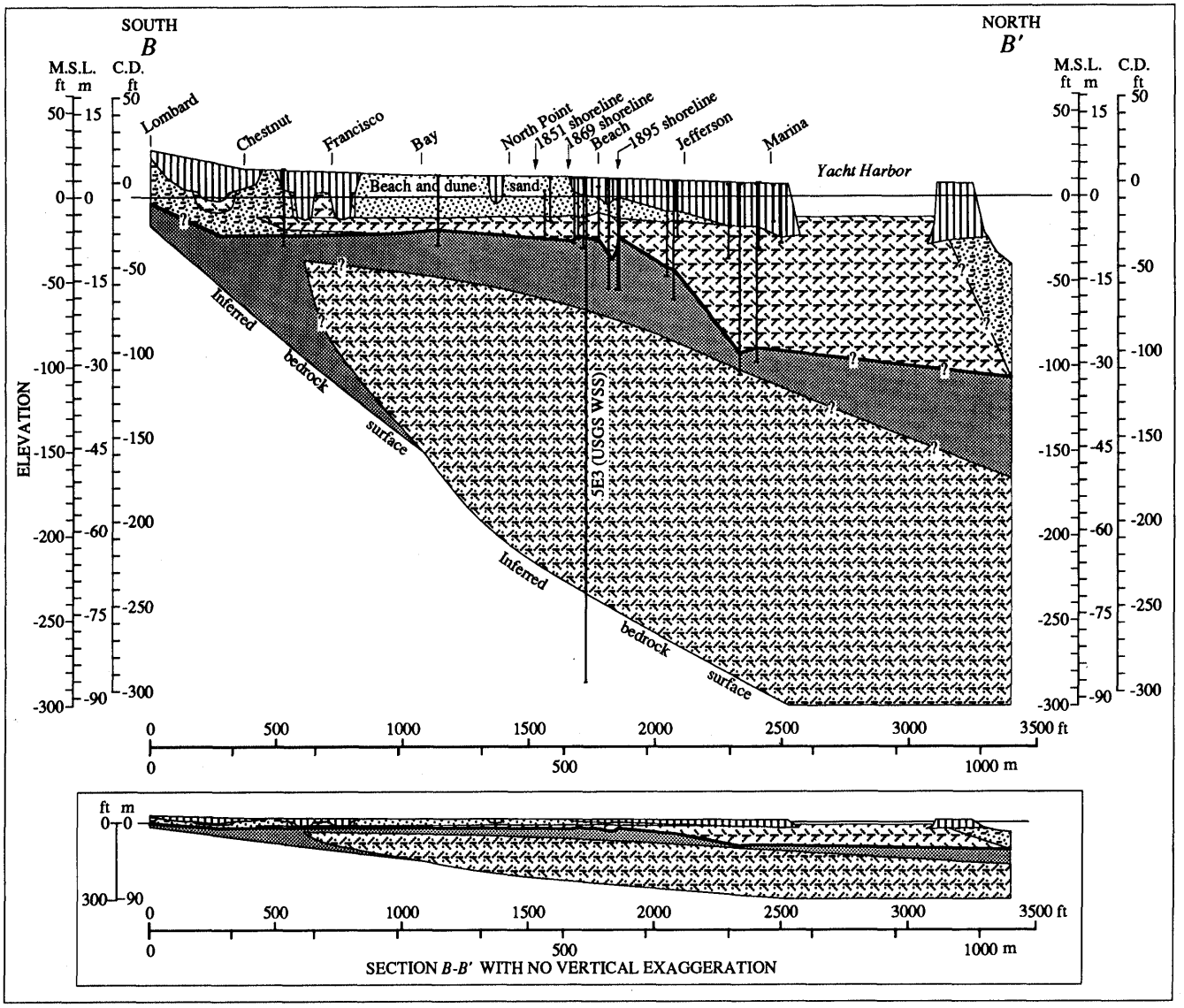


Figure 6.—North-south cross section *B–B'* along Divisadero Street (see fig. 2 for location). Sand fill, difficult to distinguish from natural sand, may locally overlie beach and dune deposits.

latest glaciation, and the green layer (sand and clay) formed during the early stages of bay deposition. Inclusion of the green layer within the bay deposits is supported by the fact that it is locally interbedded with bay deposits (Whitworth, 1932, boreholes 2, 11, and probably 14A). If this interpretation is correct, the hard zone (that is, the "yellow hardpan" and the hard green sand and clay) is near the local boundary between the Pleistocene and Holocene. In figures 5 through 7 the inferred Pleistocene-Holocene boundary is shown as a heavy line drawn above the yellow hardpan, where so identified in the borehole logs, or where hard zones of yellow or brown color are indicated in the logs. This boundary is at the top of the Pleistocene sand zone (described above), as shown in figures 5 through 7.

General descriptions of the bay mud were given by Schlocker (1974) and Helley and Lajoie (1979), and some of the geotechnical properties of the bay mud in the Marina were described by Kayen and others (1990) and are given in other reports in this chapter.

## HOLOCENE BEACH AND DUNE SAND

Holocene beach sand underlies the northwestern part of the Marina and forms a narrow strip in the southeastern

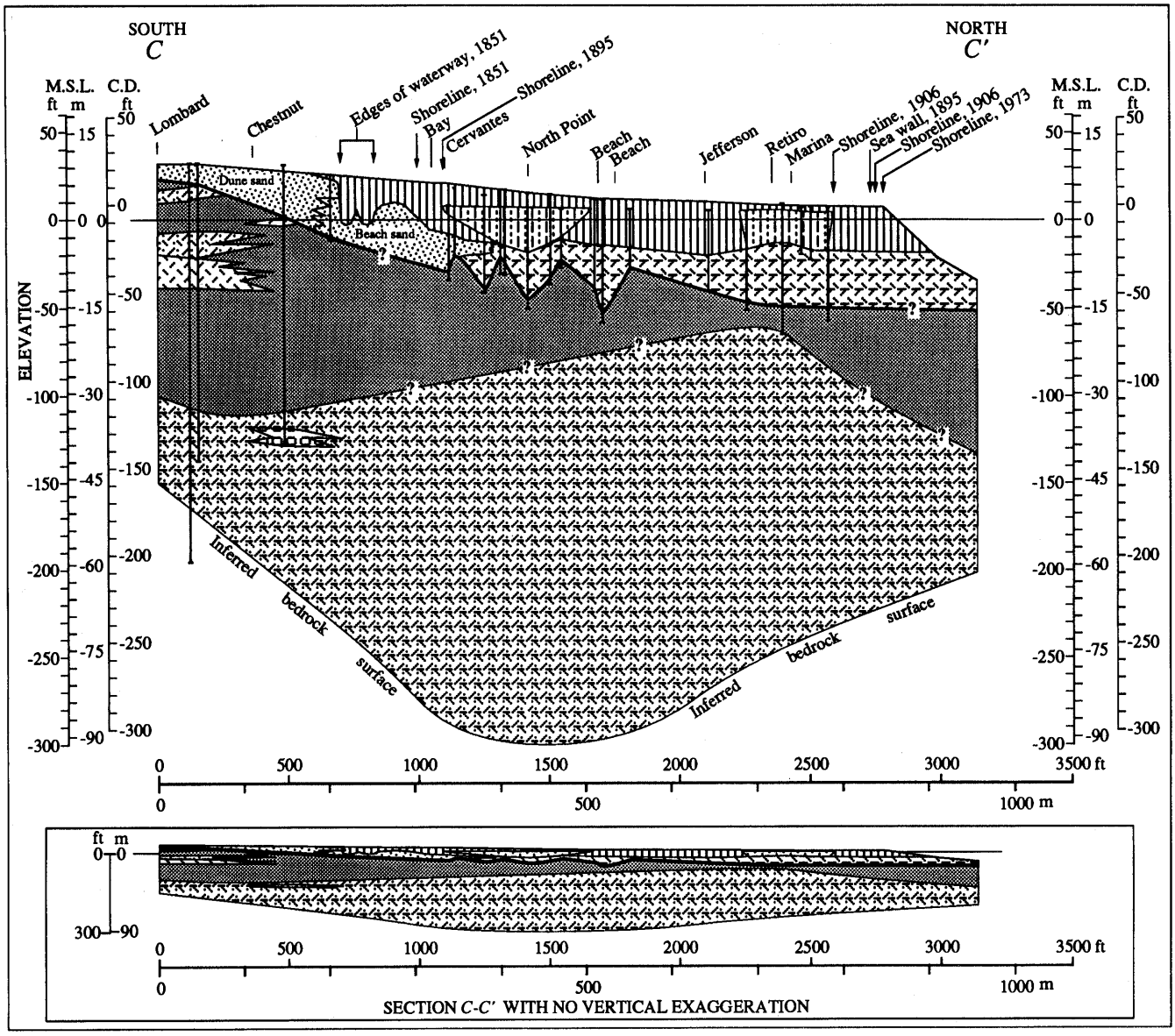


Figure 7.—North-south cross section *C–C'* along Fillmore Street (see fig. 2 for location).

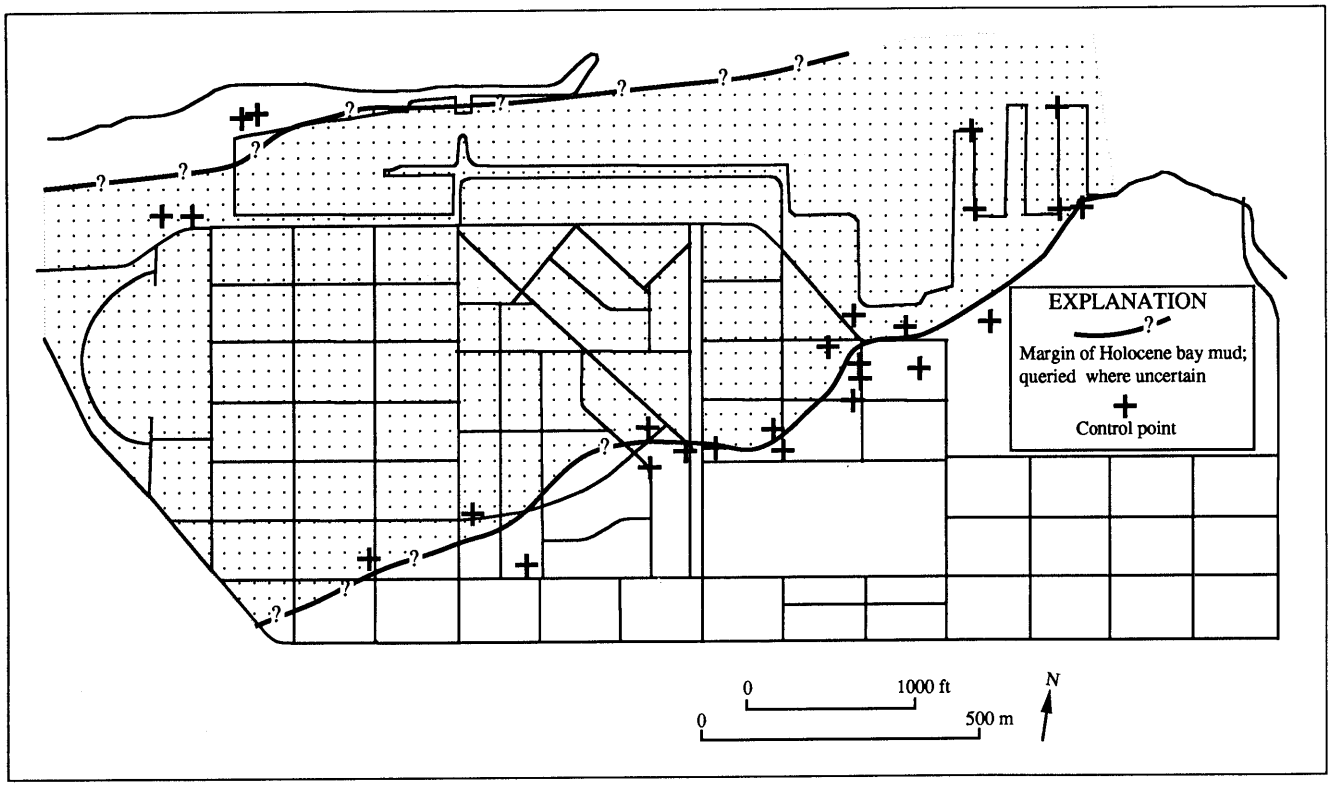


Figure 8.—Schematic map of the Marina District, showing areal extent of Holocene bay mud (dotted pattern) in subsurface. Small areas of thin marsh deposits lie outside boundary shown in southwestern part of the map area.

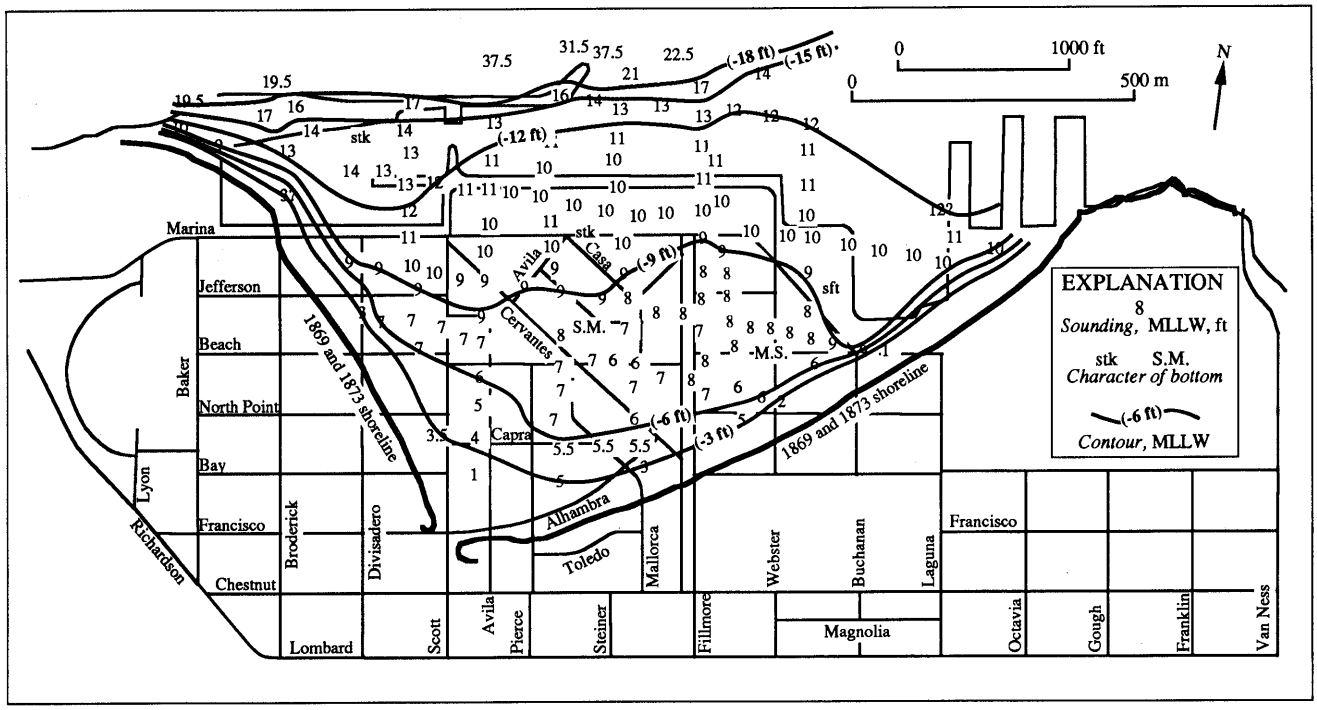


Figure 9.—Marina District, showing bottom of Marina Cove in 1873. Soundings from U.S. Coast Survey map 1214a, 1873, scale 1:20,000. MLLW, mean lower low water, approximately 0.9 m (3 ft) below mean sea level datum. Character of bottom: stk, sticky; S., sand; M., mud.

part (fig. 2). The sand deposits in the northwest form a spit formerly called Strawberry Island; comparison of maps dated 1851 and 1869 show that this spit was growing eastward before placement of artificial fill. On the basis of line patterns on old maps, and photographs taken in 1876, much of the beach sand had a thin, discontinuous cover of dune sand. The 1851 map shows a symbol that indicates "sand hills or dunes" (U.S. Coast and Geodetic Survey, 1942, fig. 189) for most of Strawberry Island and a small area southeast of Marina Cove (see fig. 10); these areas are shown in figure 2. Old maps, photographs, and historical accounts show that dune sand (wind-deposited sand) underlies the eastern and southeastern parts of the Marina.

The bulk of both the beach and dune deposits consists of clean, well-sorted sand. Detailed descriptions and analyses of the beach and dune sands were given by Schlocker (1974).

### HOLOCENE MARSH DEPOSITS

Tidal marsh deposits, now covered by artificial fill, underlie an area in the southwestern part of the Marina and continue westward into the Presidio; their original extent is shown on an 1851 map (fig. 10). A small part of the marsh was evidently covered by dune sand between 1851 and 1869; the marsh area east of the longest of the north-south segments of the tidal channel shown in figure 10 is indicated as sand on the 1869 map (fig. 11) and on the geologic map of Lawson (1908, map 17). This area is near the north central part of the block bounded by Bay, Divisadero, Francisco, and Broderick Streets.

The marsh deposits consist of clay and silt containing small amounts of marsh vegetation. They grade into the bay deposits that underlie the Marina, and in places interfinger with beach sand. General descriptions of the marsh deposits around San Francisco Bay were given by Helley and Lajoie (1979) and Atwater and others (1979).

### UNDIVIDED QUATERNARY SEDIMENTARY DEPOSITS

Small areas of undivided Quaternary sedimentary deposits are shown in the southwestern, southeastern, and northeastern parts of figure 2. In the southwest, near Chestnut and Scott Streets, figure 10 shows areas with map symbols that indicate bluffs, and "sand and gravel" or "stones and gravel" (U.S. Coast and Geodetic Survey, 1942, fig. 189). The origin of these deposits is unknown, but they could have been formed by storm waves. The undivided Quaternary sedimentary deposits shown in the southwest, southeast, and northeast corners of figure 2 are from Schlocker and others (1958) and Schlocker (1974). In the northeast

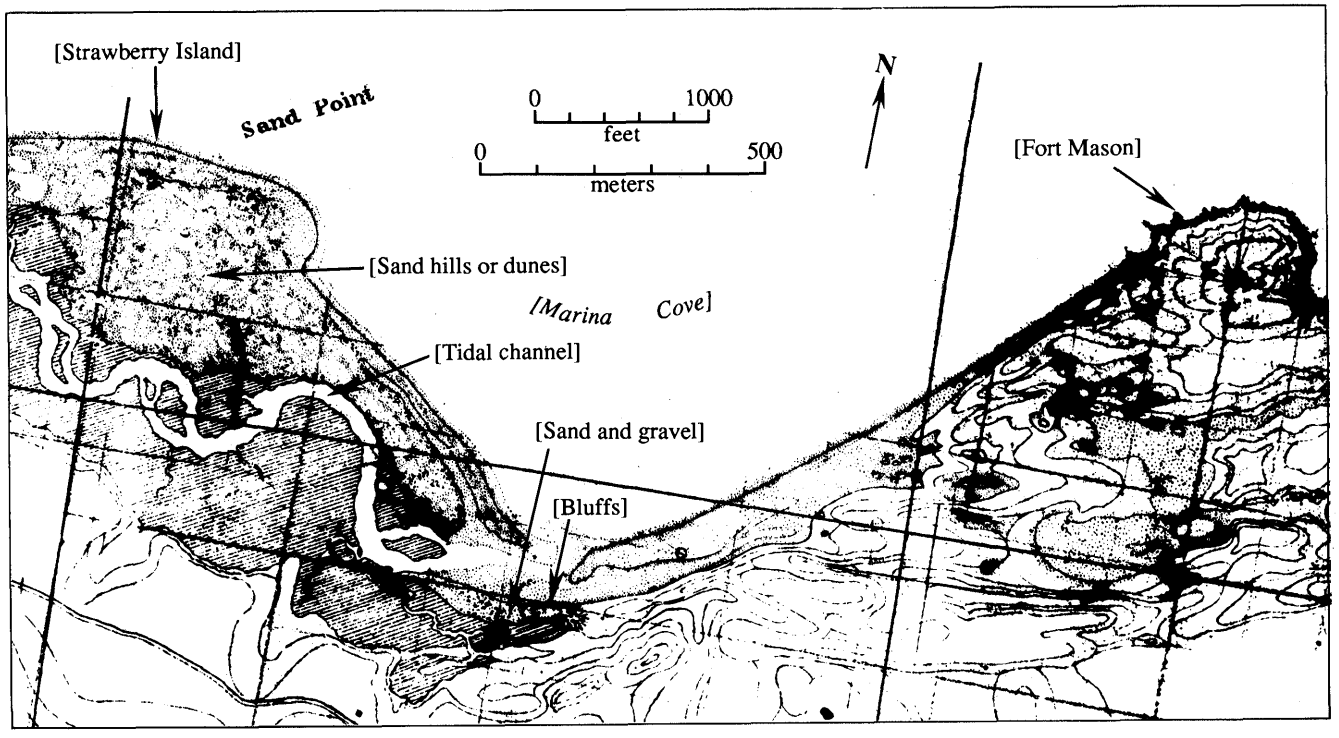


Figure 10.—Part of U.S. Coast Survey chart 314, dated 1851. Diagonal-lined area, marsh areas. Bracketed labels are not on original map, which is at 1:10,000 scale.

corner of figure 2, these deposits are primarily colluvium, and rest directly on bedrock.

## ARTIFICIAL FILLS

Human modification of the natural environment of the Marina, particularly by the emplacement of artificial fill, has had important effects on subsurface conditions there. To better understand both the environmental changes and the content of the fills, the development of the Marina is outlined.

### HISTORICAL DEVELOPMENT OF THE MARINA

The earliest accurate map of the Marina, dated 1851 (fig. 10), shows a small embayment (Marina Cove) west of the bedrock headland now occupied by Fort Mason, as well as a meandering tidal slough draining a marsh that extended west of the Marina. North of this principal slough was a broad sand spit, covered discontinuously by dune sand, referred to as Strawberry Island (Dow, 1973). The north edge of Strawberry Island is labeled "Sand Point" on the 1851 map. A narrow waterway extended northwestward of the mouth of the principal slough, just reaching the present position of Beach Street. Another small waterway, trending northeast, lay east of the principal slough. A narrow strip of beach sand was to the north, and a broad area of dune sand to the east of this waterway. The features shown on an 1857 U.S. Coast Survey map are almost the same, except for shortening of the narrow, northwest-trending waterway and an eastward shift in the positions of the mouth of the principal tidal slough and associated sand spits at the south end of Marina Cove. These changes were likely natural because no roads or structures are shown near the shoreline.

By 1869 (fig. 11), the mouth of the principal slough had shifted westward, probably by natural processes, and the narrow, northwest- and northeast-trending waterways mentioned above no longer existed. Probably both of these narrow waterways were artificially filled, at least in part, because roads are shown crossing their former sites. A roadway, evidently on fill, is shown partly crossing the principal slough along the present position of Divisadero Street at Francisco Street. The Fillmore Street wharf, built in 1863 and 120 m (400 ft) long (Dow, 1973, p. 95), is shown extending into Marina Cove north of the present

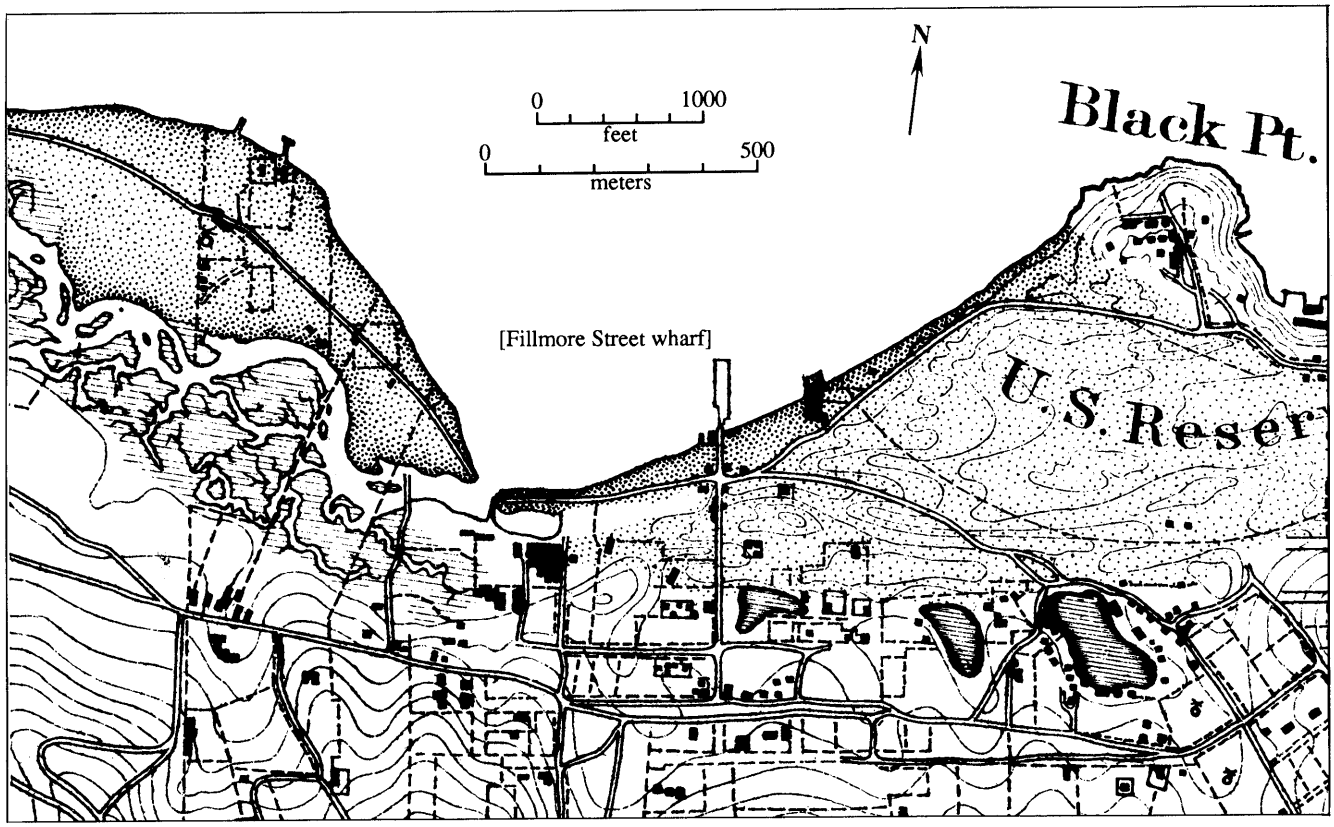


Figure 11.—Part of U.S. Coast Survey map 3055, dated 1869. Black Point is now part of Fort Mason. Intersection of Fillmore Street wharf and shoreline is approximately at present position of Bay Street-Fillmore Street intersection. Dotted patterns, sand areas; ruled pattern, marsh; ruled pattern with black borders, lake. Original map is at 1:40,000 scale and has a 20-ft contour interval. Surveys for this map were performed in 1850–57 and 1867–68.

position of Bay Street at Fillmore Street; presumably, this wharf was built on piles. East of the Fillmore Street wharf is an artificial fill, perhaps 30 m (100 ft) long, along the east side of the present position of Webster Street and south of the present position of North Point Street. The symbol used on the 1869 map suggests that this fill was of sand.

In the 1860's a hotel, shooting gallery, and other structures were built north of the present site of the Palace of Fine Arts. The Santa Cruz Power Co. had a small wharf in the same vicinity (Dow, 1973), probably one of the two wharves shown in figure 11 northwest of Marina Cove at a site north of the present-day Marina Boulevard. The Phelps Manufacturing plant, which made bolts, heavy forgings, railroad cars, and cable was built in 1882 in a triangular area bounded by present-day Fillmore, Bay, and Buchanan Streets (Dow, 1973, p. 95).

In 1891, the San Francisco Gas Light Co. Constructed a wharf extending 300 m (1,000 ft) north of Bay Street at its property east of the Phelps plant (fig. 12; Dow, 1973, p. 97). This wharf, which is referred to as an "earthen mole" on the map by the Sanborn Ferris Map Co. (1899), had a rock retaining wall around it (Olmsted and others, 1977, p. 667).

In the late 1800's, a seawall was built around property owned by J.G. Fair; it was built of rock dumped from cable-drawn railroad cars operating on a pile trestle (Olmsted and others, 1977, p. 716, pl. 20). According to Dow (1973, p. 96–101), this seawall was built in 1894, retained the hydraulic fill placed for the 1915 Panama-Pacific International Exposition, and was at or near the present seawall north of Marina Boulevard. The date of construction of Fair's seawall is problematic because it is not shown on the large-scale map of wharflines and pierheads surveyed in 1895 (fig. 12). The "seawall(?)" shown on the 1895 map only partly coincides with the present seawall and does not reach the east or west shores of the lagoon; however, an 1899 map shows the seawall reaching both shores (Sanborn Ferris Map Co., 1899).

At the time of the 1906 earthquake Marina Cove was enclosed by a rim of artificial fill except for a narrow opening to the north (fig. 13). Little historical information

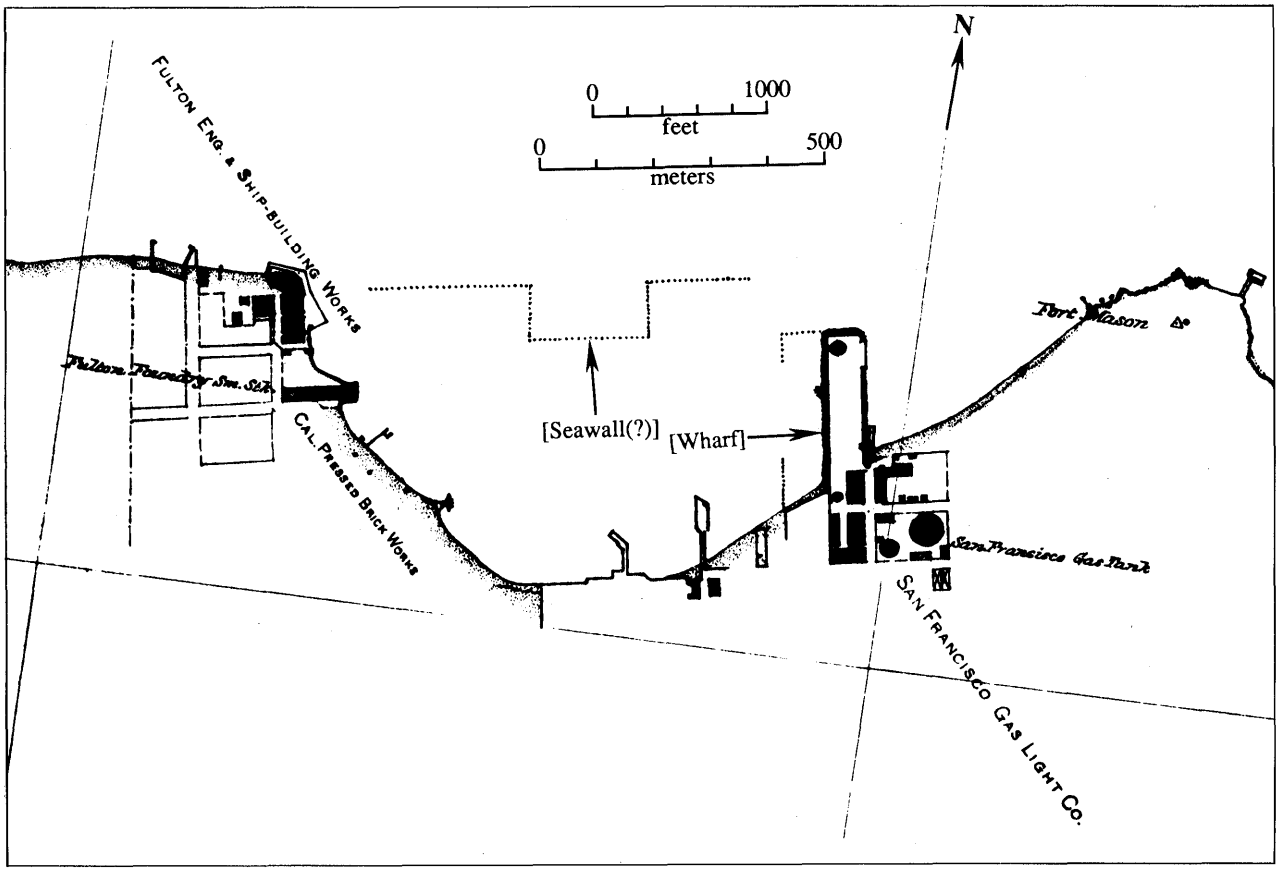


Figure 12.—Part of U.S. Coast and Geodetic Survey register 2205, surveyed in 1895. The intersection of North Point and Buchanan Streets is in center of San Francisco Gas Light Co. buildings. Building at southeast corner of intersection still exists and is called the Pacific Union Co. building. "Cal. Pressed Brick Works" is northeast of intersection of Jefferson and Broderick Streets. Dot-dashed line, boundary of the Presidio, which now curves to exclude the Palace of Fine Arts. Bracketed labels are not on original map, which is at 1:10,000 scale and is titled "Re-Survey of San Francisco Bay; City Water-Front Wharf-Lines and Pier-Heads."

is at hand as to the method of placement or composition of this fill, but segments of the assumed seawalls shown on the 1895 map and Fair's seawall must have been incorporated into it. Two boreholes drilled through the fill in 1975 penetrated sand containing some rock fragments, brick, and other rubble (Dames & Moore, 1976). Artificial fill had also been placed over the eastern part of the principal slough as far west as the present location of Lyon Street. A photograph of Marina Cove taken in 1912 before hydraulic filling (fig. 14) shows conditions similar to those shown on the 1908 map (fig. 13), except that the photograph shows a broader area of fill on the east side of the cove. The general outline of the west edge of this 1906–12 fill, as shown in figure 2, was interpreted from figure 3 of Leurey (1914) (fig. 15), which shows a contour line near mean high water, the conventional shoreline for most maps. How much debris from the 1906 earthquake and fire was incorporated into fills in the Marina is unknown, and, as described in the subsection below entitled "General Distribution, Age, and Composition of Artificial Fills," 1906 debris would be difficult to distinguish from the Panama-Pacific International Exposition debris. There was a refuse dump at the foot of Webster and Bay Streets in the 1900's (Khorsand, 1973, p. 35); from the context of the description, this dump probably predated the 1906 earthquake. Two historical accounts that cover the Marina (Dow, 1973; Khorsand, 1973) made no mention of any dumping of 1906 debris at Harbor View (present-day Marina). Two general reports on the 1906 earthquake stated that debris from the main part of San Francisco was dumped in Mission Bay (in the eastern part of San Francisco) and that some was hauled by barges to the vicinity of Mile Rock, west of the Golden Gate (Bronson, 1959, p. 170; Sutherland, 1959, p. 197). Considering its age, however, the 1906–12 fill could include debris from the 1906 earthquake. Logs of four boreholes (Whitworth, 1932,

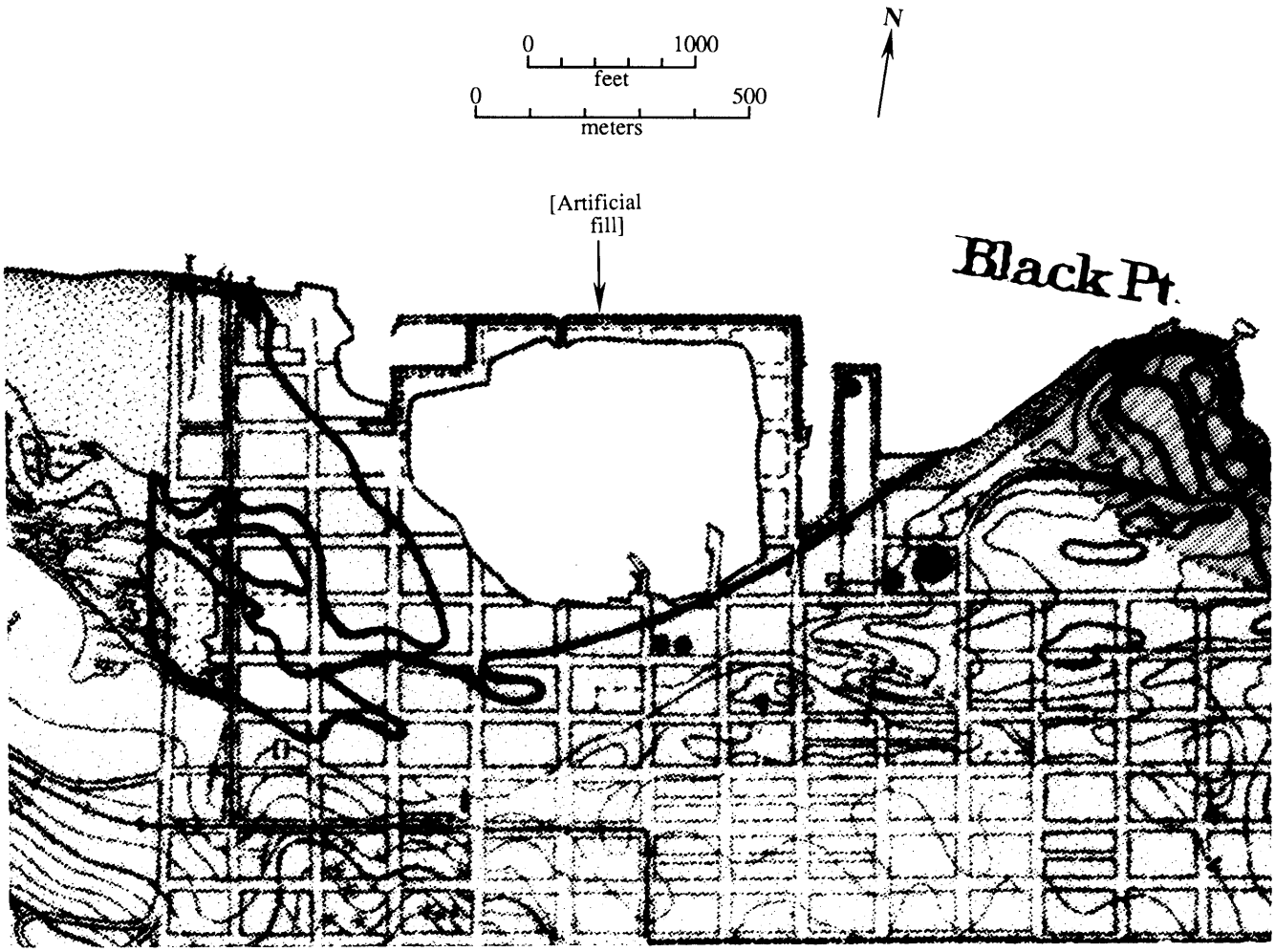


Figure 13.—Part of a geologic map published in the report on the 1906 earthquake (Lawson, 1908, map 17); original scale, 1:40,000. Bracketed label is not on original map, which identified by color the area of artificial fill surrounding Marina Cove.

boreholes 10A, 14A, 14B, 15) within this fill area do not mention debris, although the ambiguous term "fill" is used in one log. Another borehole, 9E3, on the border of the fill, penetrated a railroad tie and gravel in the upper 1 m (3 ft), and a boulder at a depth of 3 m (9.8 ft) (Bennett, 1990, p. D–34, borehole Marina 5). Probably, at least a small amount of 1906 debris is in the fills.

Large changes were made in the Marina in connection with the 1915 Panama-Pacific International Exposition. In 1912, large hydraulic fills were placed in the central part of the Marina and in adjacent parts of the Presidio. Smaller hydraulic and other fills were placed through 1917, during restoration of the site of the exposition; these changes are described in detail in the subsections that follow.

After restoration of the exposition site, the land was unused until about 1924, when sale of the land to developers quickly led to residential construction (Dow, 1973, p. 103–108). Various modifications were made in the yacht-harbor area, north of Marina Boulevard, including enlargement of the harbor, changes in breakwaters and seawalls, and the addition of some small fills.

### ARTIFICIAL FILLS RELATED TO THE PANAMA-PACIFIC INTERNATIONAL EXPOSITION

Changes made in the Marina in connection with the 1915 Panama-Pacific International Exposition were important, and so these changes are here described in detail. Hydraulic filling of what remained of Marina Cove was done from April 13 to September 7, 1912. The cove was "* * * 12 feet in depth to the mud at mean high tide, formed by a seawall running east and west along the line of what became the northern boundary of the grounds" (Markwart, 1915a, p. 63). A suction dredge was positioned about 90 m (300 ft) offshore and generally moved parallel to the shore. If the discharge contained too much fine material, the dredge was moved to get a larger proportion of sand. Marina Cove, which was being filled, contained semifluid sludge. A gate was left in the old seawall so that the sand, discharged on the landward side, would displace as much as possible of the soft material into the bay. To help remove mud from the bottom of the original basin, "* * * at times water was pumped instead of sand, and this carried out considerable mud in solution through the waste gate" (Markwart, 1915a, p. 64–65). The fill was about 70 percent sand and 30 percent mud (Todd, 1921, v. 1, p. 300).

Hydraulic fill was also placed west of Lyon Street in a low-lying area along the old marsh and tidal channel shown in figure 10. This fill did not exceed 1.8 m (6 ft) in depth, and was "* * * mostly sand with a slight percentage of mud and frequently large boulders * * *" (Markwart, 1915b).

Locally, nonhydraulic fill was placed for the exposition. "Six or eight acres, on part of which lay the eastern half

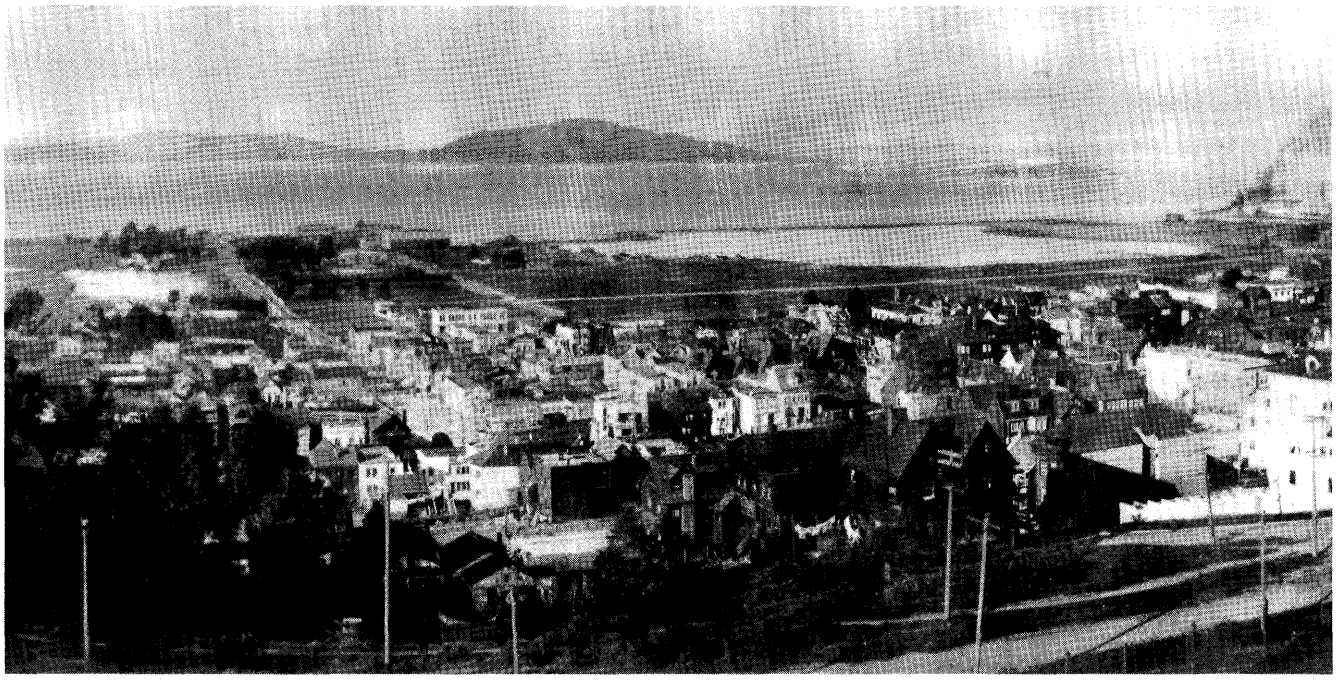

Figure 14.—Marina area in April(?) 1912. Shortly after this photograph was taken, cove in right center was hydraulically filled for the Panama-Pacific International Exposition. Sand was pumped from the bottom of the bay, transported by pipeline, and discharged into the cove. Pond to left is now part of lagoon at the Palace of Fine Arts. Next to pond is Baker Street and then Broderick Street. Photograph courtesy of Archives, San Francisco Main Library.

of the Court of the Four Seasons, had to be filled by scrapers to bring it up to grade" (Todd, 1921, v. 1, p. 162). The center of this court was southeast of the intersection of Beach and Broderick Streets, on the old sand spit formerly called Strawberry Island. The northwest-trending waterway mentioned above in connection with the 1851 map was in this area and may account for the need for a special fill. The east half of this court would cover only about 1 acre; this is probably the same fill described by Dow (1973, p. 101) as covering 12 acres. Dow logically inferred that the source of this fill was dune sand from the undeveloped land at the east end of the exposition grounds (Dow, 1973, p. 101–102).

The method of placement of the 1912–17 fill (fig. 2) in the zone half a block wide between the 1895–1906 fill and the 1891 San Francisco Gas Light Co.'s wharf is uncertain. The 1908 map (Lawson, 1908, map 17) shows a sand pattern without a definite boundary to the north, suggesting that natural sedimentation was taking place there. This strip was filled by the time of the Panama-Pacific International Exposition and evidently was filled for the exposition, but the information at hand does not indicate the method of filling.

## EXPOSITION PILES

Numerous wooden piles from the Panama-Pacific International Exposition probably still exist in the Marina. Whether these piles provided some resistance to long-term ground settlement and to earthquake-related liquefaction and vertical or horizontal ground displacements is unclear (Bonilla, 1990, 1991). More than 15,000 piles were used to support the principal buildings (Leurey, 1914), and piles supported some buildings not included in that total (Leurey, 1914, p. 254). The locations of buildings with pile foundations are shown in figure 16, and the number and average lengths of piles are listed in table 2.

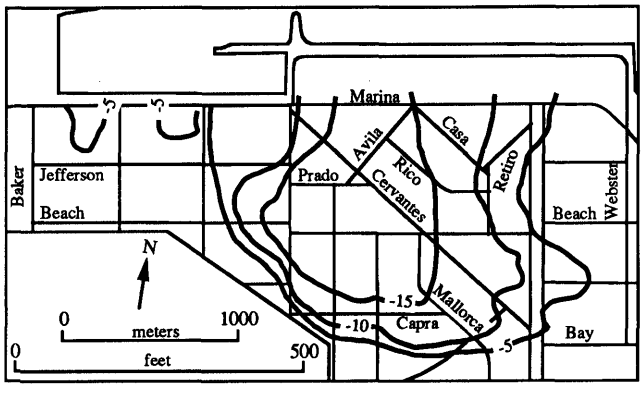


Figure 15.—Contours on bottom of Marina Cove in 1912, before modifications for the Panama-Pacific International Exposition, in relation to modern streets. Contours in feet, based on San Francisco city datum, which is approximately 8.6 ft above mean sea level datum. After Leurey (1914, fig. 3).

The spacing of the piles can be judged from specifications for the Mines Building and Varied Industries Building, which called for structural piles to be clustered in groups of 2 to 10, and the clusters to be about 9 m (28 ft) apart from north to south and 25 m (82 ft) apart from east to west (Markwart, 1915a, app. B). In addition to supporting structural frames of buildings, piles were used to support floors and to support columns for concrete firewalls (Markwart, 1913, 1915b; Leurey, 1914).

Piles were as much as 23 m (75 ft) long, and many were to be driven into the layer of green sand and clay (Markwart, 1913) described above in the subsection entitled "Holocene Bay Deposits." However, sand of preexposition artificial fill provided suitable support for piles of the Education Building (Leurey, 1914, p. 254). Figures 2 and 16 show that the Education Building site is underlain by fill placed in 1895–1906. One reason for the extensive use of piles for exposition buildings was greater safety in case of earthquakes (Markwart, 1913, p. 902; Leurey, 1914, p. 254).

Specifications for dismantling of the exposition include the statement that piles "* * * shall be cut off two (2) feet below the surface of the ground as it existed at the time the site was taken over" (Todd, 1921, v. 5, app. p. 134). However, the position of the ground surface referred to by Todd is unknown; as discussed below, the former exposition ground surface now has 1.5 m (5 ft) of artificial fill above it in some places. The exposition structures were designed for a lifespan of only a few years, and the piles were probably not treated with creosote. Thus, the parts of the piles above the water table may have deteriorated because of decay and termite action, but wooden piles that are submerged—that is, below the water table in the case of the Marina—last a long time. Borehole data indicate that the depth to the water table at exposition building sites ranges from about 2 to 3 m (7–10 ft).

Two boreholes drilled in 1923 encountered timbers, and the borehole sites had to be shifted to complete the holes; the reported timbers may have been remnants of piles. One borehole (10E2, fig. 3) was within the perimeter of the Machinery Building, and the other (9G2, fig. 3) was near but outside the perimeters of the Machinery and Varied Arts Buildings. I am not aware of any post-1923 boreholes or excavations that may have found pile remnants.

## DEMOLITION OF EXPOSITION BUILDINGS AND RESTORATION OF THE SITE

After the exposition closed in December of 1915, dynamite was used to bring down buildings and other struc-

tures, most of which were of wood. Wood that could not be economically salvaged was burned on the site on a daily basis by the fire department (Todd, 1921, v. 5, p. 246–247). Reinforced-concrete firewalls, foundations, and transformer vaults were dynamited and broken up by a pile hammer (Todd, 1921, v. 5, p. 246). As previously stated, piles were not removed, but foundation obstructions were removed to some unknown depth (Todd, 1921, v. 5, p. 247). Postexposition filling was also done, described as follows: "Some of the lands had not been filled up to the terms of the leases when they were built upon, and it was now necessary to carry out this part of the exposition's obligations. They were filled partly by the public dump method, but by September 1916, a suction dredge went to work pumping mud over them, and finished by January 1917" (Todd, 1921, v. 5, p. 247). One public dump was at Lobos Square, now the site of the Marina Junior High School and Moscone Recreation Center, southeast of the intersection of Bay and Webster Streets. The locations of other dumps were not given. The hydraulic fills in the postexposition period required construction of retaining levees, but their thickness and areal extent are unknown.

## CHANGES AFTER 1917

The land on which the exposition stood was unused until 1924, when residential construction began (Dow, 1973, p. 103–108). Any fills related to residential construction are probably very small. Some modifications have also been made in the yacht-harbor area, including enlargement of the harbor, changes in breakwaters and seawalls, addition of some small fills, and construction of a major sewerline under Marina Boulevard during the late 1970's.

## GENERAL DISTRIBUTION, AGE, AND COMPOSITION OF ARTIFICIAL FILLS

The areas of artificial fills of various ages are shown in figure 2. The fill boundaries are based on superimposing, on a 1973 map, shorelines shown on the maps of 1851, 1869, 1895, and 1908, supplemented by descriptions of the Panama-Pacific International Exposition fills. Shorelines and other features on the old maps cannot be precisely related to modern maps because the positions of many

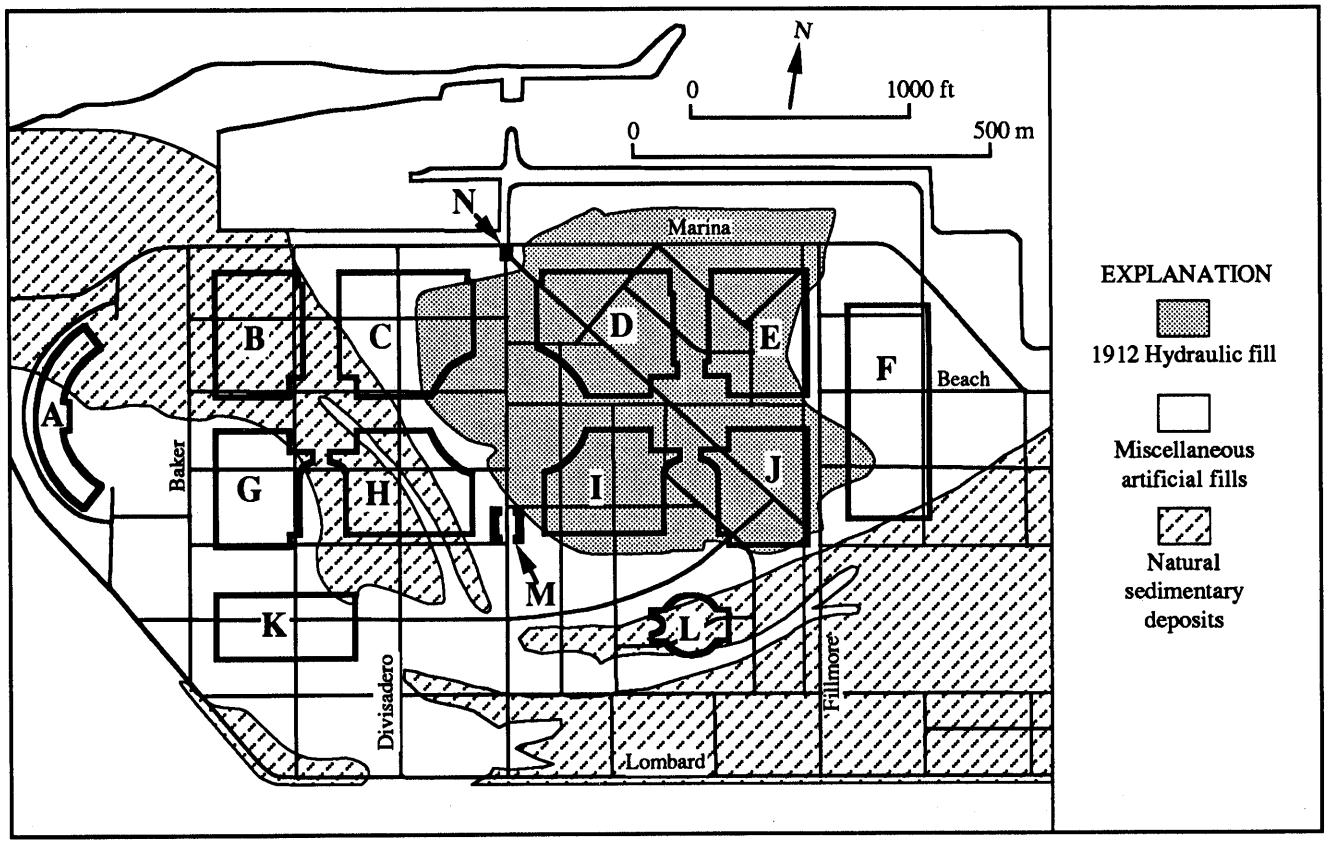


Figure 16.—Principal buildings of the 1915 Panama-Pacific International Exposition (letters; see table 2 for names), in relation to modern streets and simplified geology. Locations of exposition buildings from Todd (1921). Locations of buildings with respect to modern streets are based on location of Scott Street, the only exposition street that was centered on existing San Francisco streets (Markwart, 1915a, p. 75), and on location of the Palace of Fine Arts.

Table 2.—*Panama-Pacific International Exposition buildings and piles*

[Average length is below cutoff (from Leurey, 1914, table 1), which would have been at some unspecified height above the ground surface at that time]

| Symbol (fig. 16) | Building | Number of piles | Average length (ft) |
|---|---|---|---|
| A | Fine Arts | 1,051 | 25.6 |
| B | Food Products | 665 | 14.5 |
| C | Agriculture | 1,374 | 41.8 |
| D | Transportation | 4,541 | 63.2 |
| E | Mines | 2,026 | 46.1 |
| F | Machinery | 1,577 | 28.6 |
| G | Education | 634 | 15.7 |
| H | Liberal Arts | 751 | 13.0 |
| I | Manufactures | 1,591 | 35.7 |
| J | Varied Industries | 1,444 | 34.3 |
| K | Horticulture | (1) | --- |
| L | Festival Hall | (2) | --- |
| M | Tower of Jewels | (2) | --- |
| N | Tower of Progress | (2) | --- |

1 Unknown; under dome at east end.
2 Unknown.

natural and cultural landmarks are shown differently on the old and new maps, and so a best-fit compromise must be made by superimposing the maps at a common scale. Thus, the fill boundaries and other features shown may be in error by 30 m (100 ft) or more. The northeast-trending line in the southwestern part of the map separating the 1869–95 fill from the 1895–1906 fill is from the 1899 edition of a 1:62,500-scale topographic map that was surveyed in 1892–94 (Lawson, 1914); this line is less accurate than other boundaries. The major timespans during which the fills were emplaced are shown in figure 2, but each of the outlined areas may contain small fills younger than the designated ages. Some artificial fill also lies outside the fills delineated in figure 2. The shorelines on the maps, used to outline the fill, represent mean high water. Artificial fills were placed landward of the mapped shorelines to prevent flooding during higher tides, and so figure 2 shows only the minimum extent of the fills. Local fills were also placed at low points on land, such as in local drainageways and areas between sand dunes. Outside the principal fill areas, borehole data show fill thicknesses that generally range from 0 to 4.3 m (0–14 ft), but at a site on the east side of Pierce Street south of Chestnut Street, broken glass and other debris was penetrated at a depth of 7.6 m (25 ft).

Part of the 1851 shoreline is shown in figure 2 by a dashed curve that trends generally northwest. This shoreline is not shown as a fill boundary because the area between this line and the edge of the 1869–95 fill probably grew by natural sedimentation. The narrow, northwest- and northeast-trending 1851–69 fills may include naturally deposited material along waterways, as mentioned previously.

A general indication of the lower surface of the artificial fills is shown in figure 9. Only very minor fills had been placed in the cove by 1873: Except for a possible fill extending from near Chestnut Street along or just east of Scott Street as far north as Capra Way, the 1873 map shows no marked change in shoreline in comparison with the 1869 map, which shows essentially natural conditions. The artificial fills in the Marina probably sank only a short way into the soft upper surface of the bay mud shown in figure 9, which provides a good approximation of the minimum level of the bottom of the artificial fills. Even in the last remnant of Marina Cove, where the level of soft mud as indicated by bottom contours in 1912 (fig. 15) was several decimeters (feet) above the 1873 level, boreholes show that the hydraulic filling displaced or removed the softest mud down to approximately the 1873 level.

The 1869–95 fill probably consists mostly of sand, which was locally available from nearby beach and dune deposits. Levinsohn (1976, p. 34) stated that in filling the tidelands north of Lombard and Chestnut Streets during the 1890's, sand from the eastern sand hills (dune sand) was loaded by bucket conveyors to railroad cars which ran along tracks to the shoreline. In places, the 1869–95 fill contains riprap (large blocks of stone) placed for protection from wave action. For example, the rectangular, north-trending area in the northeastern part of the 1869–95 fill (fig. 2) is the site of the 1891 San Francisco Gas Light Co.'s wharf, which had a rim of riprap. The following description probably applies to the San Francisco Gas Light Co.'s mole: "A retaining wall was being built with rock brought to this site on barges and unloaded by a derrick barge around the three sides of this area. When the wall was completed, the interior was filled with earth and surfaced with a hard paving." (recollection of Howard Livingston, 1964, in Olmsted and others, 1977, p. 716). Locally, debris from factories and other sources probably is contained in the 1869–95 fill also.

The source and method of emplacement of the 1895–1906 fill are largely unknown. The fill evidently contains remnants of the assumed seawalls shown on the 1895 map, and Fair's seawall. As previously stated, Fair's seawall was built of rock dumped from railroad cars operating on a pile trestle. The 1906–1912 fill probably contains debris from the 1906 earthquake and fire, but exactly how much is problematical.

The 1912–17 fills were emplaced principally in 1912 for the Panama-Pacific International Exposition, using the hydraulic fill methods previously described. The general level of the top of the 1912 hydraulic fill before construction of the principal Panama-Pacific International exposition buildings was at an elevation of about –0.85 m (–2.75 ft) in relation to the San Francisco city datum (Leurey, 1914, p. 250). Its level can also be obtained from the elevations of boreholes that Leurey stated were drilled at the corners of the main buildings after the fill had settled somewhat, and those elevations were considered in drawing the upper surface of the hydraulic fill in figures 5 and 7.

The position of the bottom of the hydraulic fill is probably irregular and is poorly known. A map showing the approximate elevation of the lagoon bottom about 1912, before the filling (fig. 15; Leurey, 1914, fig. 3), indicates only its general position because Leurey (1914, p. 250) stated that the fill pushed its way 0.6 to 1.5 m (2–5 ft) into the soft ooze of the lagoon bottom, and postexposition borehole logs also show artificial fills extending below the 1912 bottom. As noted before, the area of 1912–17 fills also includes scraper fill, post-1915 hydraulic fill of unknown dimensions, and public dumps, all related to the exposition.

Several boreholes shown in figures 5 through 7 support the historical data indicating that fill was placed after the 1912 hydraulic fill. These boreholes were drilled in 1912, after placement of the main hydraulic fill. Since then about 1.5 m (5 ft) of fill has been placed above the 1912 surface at the sites of these boreholes, probably during restoration of the 1915 exposition site. The apparent fill over the borehole near 330 m (1,085 ft) on the horizontal scale of figure 5 (borehole 54 of Leurey, 1914) is unexplained; an unrecorded small fill may exist there.

A small body of artificial fill in the western part of cross section *A–A′* (fig. 5) was placed on a marsh area near the Palace of Fine Arts. Some of this fill was probably placed by hydraulic methods in 1912 for the exposition.

The artificial fills in the Marina are principally sand obtained from nearby sites on land or offshore. However, the varied history of development of the area, both cultural and physical, implies that a great variety of materials are locally incorporated into the fills. Borehole logs mention small amounts of timber, brick, pottery, glass, large rocks, coal, and wire rope.

### GROUND-WATER LEVELS

Depth to ground water is shown in figure 17. Because data are scarce, some water depths measured as long ago as 1923 are included; however, where both pre- and post-1980 depths are close together, they do not differ greatly, suggesting that water levels have changed very little. Pre-1980 measurements are identified in figure 17, which shows that ground-water depths are generally less than 2.7 m (9 ft) except in the southeastern part of the map area and a few other isolated areas.

## DISCUSSION AND CONCLUSIONS

Knowledge of site conditions is necessary for understanding the effects of past and future earthquakes. The Marina is worthy of study because much information is available on both site conditions and earthquake effects there. Site conditions vary. A deep, northwest-trending valley cut into bedrock is filled mostly by thick Pleistocene bay deposits overlain by an extensive Pleistocene sand zone. Above these are Holocene bay deposits, covered by Holocene sand in some places and various artificial fills in other places. The ground-water table in unconsolidated deposits is generally less than 2.7 m (9 ft) below the ground surface except in the dune-sand area, where it is generally more than 3 m (10 ft) deep. Liquefaction during the 1989 earthquake, as reported by Bennett (1990) and Benuska (1990), did not occur in some areas of very shallow ground water, illustrating again that suitable deposits as well as shallow ground water are necessary for liquefaction.

The effects of geology and historical development on earthquake damage in the Marina have been discussed by various authors, including Bonilla (1991). Although the damage in the Marina during the 1906 earthquake was high relative to nearby areas, not all of it was clearly related to fill (Lawson, 1908; Bonilla, 1991). High amplification of ground motion and severe damage to buildings in the 1989 earthquake sequence occurred on natural ground as well as on artificial fills (U.S. Geological Survey staff, 1990; Boatwright and others, 1990, 1991; Bonilla, 1991; Boatwright and others, 1991; Boatwright and others, this chapter). These facts suggest that the configuration, thickness, and composition of the natural materials had a strong influence on shaking. Liquefaction, settlement, and damage to foundations, streets, curbs, sidewalks, and pipelines during the 1989 earthquake, however, were largely confined to areas underlain by artificial fills (Bennett, 1990; Benuska, 1990, p. 89–114; O'Rourke and Roth, 1990; see O'Rourke and others, this chapter). Thus, the natural geologic conditions apparently were responsible for the greater shaking in the Marina relative to adjacent areas, but behavior of the artificial fills increased particular types of damage. More complete analysis of the available data and of new data should provide insights that can be used in anticipating and moderating the effects of inevitable future earthquakes, not only in the Marina but also in other places with similar conditions.

## ACKNOWLEDGMENTS

Substantial help in finding sources of information was provided by Jackie Freeberg of the U.S. Geological Survey's Library in Menlo Park, Calif.; by Roger Bonilla of the Palo Alto City Library; by Nicole Bouche of the University of California's Bancroft Library in Berkeley; and by Gladys Hanson and Patricia Akre of the San Francisco Archives, San Francisco Main Library. Jane Wegge of the California State Lands Commission, Sacramento, expedited the selection and duplication of out-of-print maps. F.L. Rollo of Treadwell Associates, Inc., San Francisco; Diane Sarmiento of Harding Lawson Associates, San Francisco; Don Fowler of Fowler and Associates; and Charles Ng,

City of San Francisco, provided access to unpublished data. R.V. Allen provided information on water depth at the yacht harbor, and Julius Schlocker identified the rock in USGS borehole WSS.

## REFERENCES CITED

Atwater, B.F., 1979, Ancient processes at the site of southern San Francisco Bay; movement of the crust and changes in sea level, *in* Conomos, T.J., Leviton, A.E., and Berson, Margaret, eds., 1979, San Francisco Bay; the urbanized estuary: American Association for the Advancement of Science, Pacific Division Annual Meeting, 58th, San Francisco, 1977, Proceedings, p. 31–45.

Atwater, B.F., Hedel, C.W., and Helley, E.J., 1977, Late Quaternary depositional history, Holocene sea-level changes, and vertical crustal movement, southern San Francisco Bay, California: U.S. Geological Survey Professional Paper 1014, 15 p.

Atwater, B.F., Conrad, S.G., Dowden, J.N., Hedel, C.W., Macdonald, R.L., and Savage, Wayne, 1979, History, landforms, and vegetation of the estuary's tidal marshes, *in* Conomos, T.J., Leviton, A.E., and Berson, Margaret, eds., 1979, San Francisco Bay; the urbanized estu-

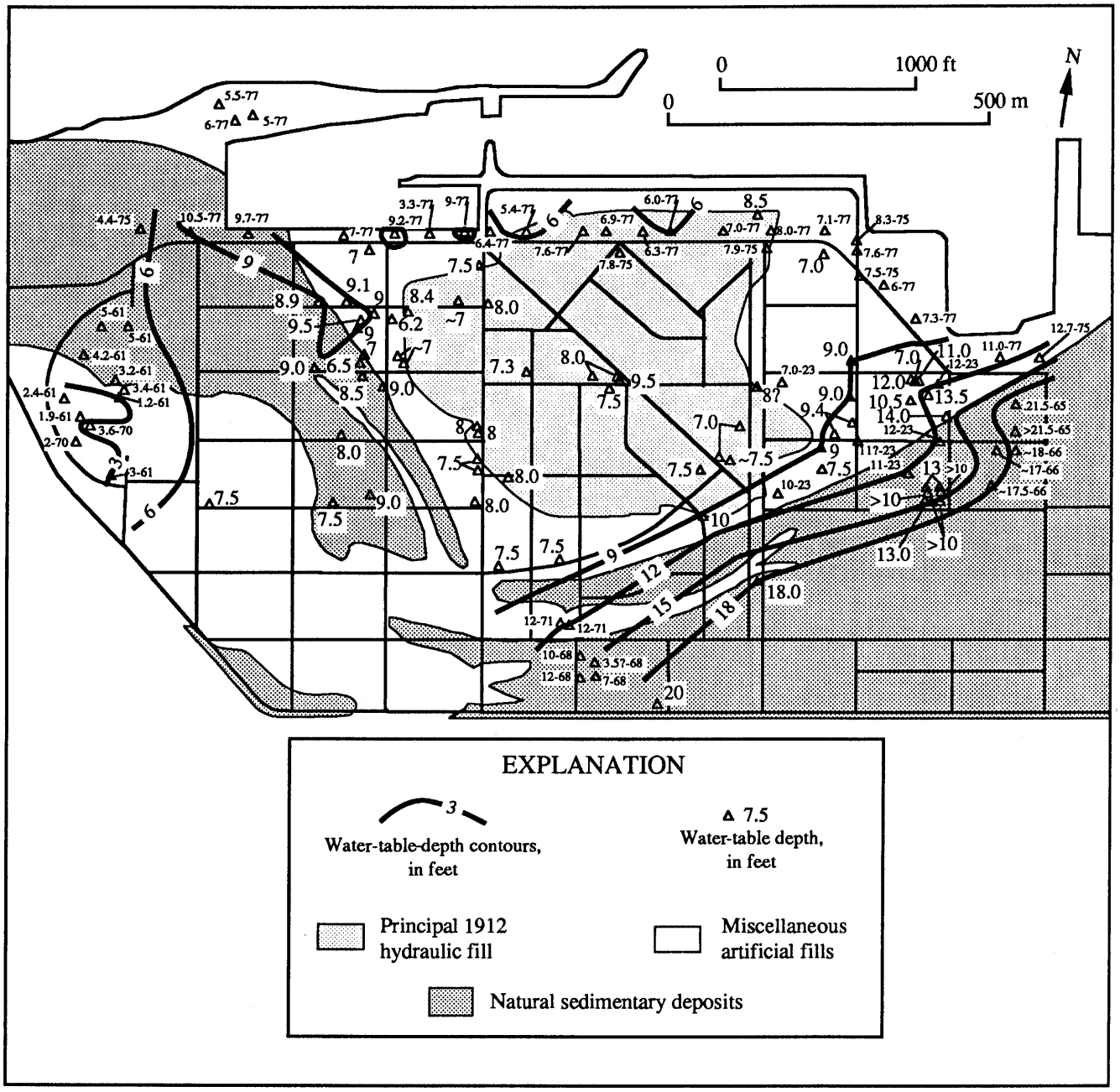


Figure 17.—Marina District, showing depth to water table. Depths measured before 1980 are in smaller type, with last two digits of year of measurement following hyphen.

ary: American Association for the Advancement of Science, Pacific Division Annual Meeting, 58th, San Francisco, 1977, Proceedings, p. 347–385.

Bennett, M.J., 1990, Ground deformation and liquefaction of soil in the Marina District, chap. D *of* Effects of the Loma Prieta earthquake on the Marina District, San Francisco, California: U.S. Geological Survey Open-File Report 90–253, p. D1–D11.

Benuska, Lee, ed., 1990, Loma Prieta earthquake reconnaissance report: Earthquake Spectra, v. 6, supp. 90–01, 448 p.

Boatwright, John, Seekins, L.C., and Mueller, C.S., 1990, Ground motion amplification in the Marina District, chap. F *of* Effects of the Loma Prieta earthquake on the Marina District, San Francisco, California: U.S. Geological Survey Open-File Report 90–253, p. F1–F24.

Boatwright, John, Seekins, L.C., Fumal, T.E., Liu, H.-P., and Mueller, C.S., 1991, Ground motion amplification in the Marina District: Seismological Society of America Bulletin, v. 81, no. 5, p. 1980–1997.

Bonilla, M.G., 1990, Natural and artificial deposits in the Marina District, chap. A *of* Effects of the Loma Prieta earthquake on the Marina District, San Francisco, California: U.S. Geological Survey Open-File Report 90–253, p. A1–A24.

———1991, The Marina District, San Francisco, California; geology, history, and earthquake effects: Seismological Society of America Bulletin, v. 81, no. 5, p. 1958–1979.

Bronson, William, 1959, The earth shook, the sky burned: Garden City, N.Y., Doubleday, 192 p.

Carlson, P.R., Alpha, T.R., and McCulloch, D.S., 1970, The floor of central San Francisco Bay: California Division of Mines and Geology Mineral Information Service, v. 23, no. 5, p. 97–107.

Carlson, P.R., and McCulloch, D.S., 1970, Bedrock-surface map of central San Francisco Bay, California: U.S. Geological Survey Open-File Map, scale approx 1:16,000 [San Francisco Bay Region Environment and Resources Planning Study Basic Data Contribution 10].

Clifton, H.E., Hunter, R.E., and Gardner, J.V., 1988, Analysis of eustatic, tectonic, and sedimentologic influences on transgressive and regressive cycles in the Upper Cenozoic Merced Formation, San Francisco, California, *in* Kleinspehn, K.L., and Paola, C., eds., New perspectives in basin analysis: New York, Springer-Verlag, p. 109–128.

Dames & Moore, 1976, Supplemental report; additional foundation investigation and tunnel design criteria, proposed consolidation sewer, North Shore Outfall Consolidation Project, San Francisco, California: report prepared for City and County of San Francisco.

Dow, G.R., 1973, Bay fill in San Francisco; a history of change: San Francisco, California State University, M.A. thesis, 116 p.

Helley, E.J., and Lajoie, K.R., 1979, Geology and engineering properties of the flatland deposits, *in* Helley, E.J., Lajoie, K.R., Spangle, W.E., and Blair, M.L., 1979, Flatland deposits of the San Francisco Bay Region, California—their geology and engineering properties, and their importance to comprehensive planning: U.S. Geological Survey Professional Paper 943, p. 14–68.

Kayen, R.E., Liu, H.P., Fumal, T.E., Westerlund, R.E., Warrick, R.E., Gibbs, J.F., and Lee, H.J., 1990, Engineering and seismic properties of the soil column at Winfield Scott School, San Francisco, chap. G *of* Effects of the Loma Prieta earthquake on the Marina District, San Francisco, California: U.S. Geological Survey Open-File Report 90–253, p. G1–G18.

Khorsand, S.L., ed., 1973, Marina memories, v. 16 *of* California History Center, Local history studies: Cupertino, Calif., DeAnza College, 73 p.

Lawson, A.C., chairman, 1908, The California earthquake of April 18, 1906; report of the State Earthquake Investigation Commission: Carnegie Institution of Washington Publication 87, 2 v.

———1914, San Francisco folio *of* Geologic atlas of the United States: Washington, D.C., U.S. Geological Survey, 24 p.

Leurey, L.F., 1914, Soft-ground foundations, Panama-Pacific International Exposition: Engineering News, v. 72, no. 5, p. 250–254.

Levinsohn, J.L., 1976, Cow Hollow; early days of a San Francisco neighborhood from 1776: San Francisco, Calif., San Francisco Yesterday, 46 p.

Markwart, A.H., 1913, The Panama-Pacific Exposition: Engineering News, v. 70, no. 19, p. 895–904.

———1915a, Building an exposition—report of the activities of the Division of Works of the Panama-Pacific International Exposition, covering the pre-exposition period, i.e., the period ending February 20, 1915: San Francisco, Panama-Pacific International Exposition, 751 p. [copy, without illustrations, in San Francisco Library Archives, Main Library; appendixes, also without illustrations, at Bancroft Library, University of California, Berkeley, bound volume 140].

———1915b, Engineering problems of the Panama-Pacific Exposition: Engineering News, v. 73, no. 7, p. 329–336.

Meyer, C.E., Sarna-Wojcicki, A.M., Hillhouse, J.W., Woodward, M.J., Slate, J.L., and Sorg, D. H., 1991, Fission-track age (400,000 yr) of the Rockland tephra, based on inclusion of zircon grains lacking fossil fission tracks: Quaternary Research, v. 35, p. 367–382.

Meyer, C.E., Woodward, M.J., Sarna-Wojcicki, A.M.,and Naeser, C.W., 1980, Zircon fission-track age of 0.45 million years on ash in the type section of the Merced Formation, west-central California: U.S. Geological Survey Open-File Report 80–1071, 9 p.

Olmsted, R., Olmsted, N., and Pastron, A., 1977, San Francisco waterfront; report on historical cultural resources: San Francisco, Calif., San Francisco Wastewater Management Program, 721 p.

O'Rourke, T.D., Gowdy, T.E., Stewart, H.E., and Pease, J.W., 1991, Lifeline and geotechnical aspects of the 1989 Loma Prieta earthquake: International Conference on Recent Advances in Geotechnical Earthquake Engineering and Soil Dynamics, 2d, St. Louis, Mo., 1991, Proceedings, v. 2, p. 1601–1612.

O'Rourke, T.D., and Roth, B.L., 1990, Performance of pipeline systems in the Marina, chap. E *of* Effects of the Loma Prieta earthquake on the Marina District, San Francisco, California: U.S. Geological Survey Open-File Report 90–253, p. E1–E8.

Radbruch, D.H., and Schlocker, Julius, 1958, Engineering geology of Islais Creek basin San Francisco, California: U.S. Geological Survey Miscellaneous Geologic Investigations Map I–264, scale 1:12,000.

Sanborn Ferris Map Co., 1899, Insurance maps, San Francisco, California: New York, v. 4.

Sarna-Wojcicki, A.M., Meyer, C.E., Bowman, H.R., Hall, N.T., Russell, P.C., Woodward, M.J., and Slate, J.L., 1985, Correlation of the Rockland ash bed, a 400,000-year-old stratigraphic marker in northern California and western Nevada, and implications for middle Pleistocene paleogeography of central California: Quaternary Research, v. 23, p. 236–257.

Schlocker, Julius, 1962, Bedrock-surface map of the San Francisco North quadrangle, California: U.S. Geological Survey Open-File Report, scale 1:18,000.

———1974, Geology of the San Francisco North quadrangle, California: U.S. Geological Survey Professional Paper 782, 109 p.

Schlocker, Julius, Bonilla, M.G., and Radbruch, D.H., 1958, Geology of the San Francisco North quadrangle, California: U.S. Geological Survey Miscellaneous Geologic Investigations Map I–272, scale 1:24,000.

Schlocker, Julius, Radbruch, D.H., and Bonilla, M.G., 1954, Preliminary bedrock-surface map of the San Francisco City area, California: U.S. Geological Survey Open-File Map, scale 1:24,000.

Sutherland, Monica, 1959, The damndest finest ruins: New York, Coward-McCann, 219 p.

Todd, F.M., 1921, The story of the Exposition: New York, G.P. Putnam's Sons, 5 v.

Treasher, R.C., 1963, Geology of the sedimentary deposits in San Francisco Bay, California, *in* Short contributions to California geology: California Division of Mines and Geology Special Report 82, p. 11–24.

U.S. Coast and Geodetic Survey, 1942, Hydrographic manual: Special Publication 143, 940 p.

U.S. Geological Survey staff, 1990, The Loma Prieta, California, earthquake; an anticipated event: Science, v. 247, no. 4940, p. 286–293.

Van Reenan, E.D., 1966, Final report [of] San Francisco Bay geophysical survey for State of California Division of Bay Toll Crossings, contract 1124: Bedford, Mass., EG&G International, Inc., Technical Report B–3437, 31 p.

Whitworth, G.F., ed., 1932, Subsidence and the foundation problem in San Francisco: San Francisco, American Society of Civil Engineers, San Francisco Section, Subsoil Committee, 107 p.

# TABLE 1

Table 1.—*Data on boreholes drilled in the Marina District of San Francisco*

[Where the date of drilling was not given in the log, another date, such as that of the accompanying report or the date when water level was measured, is listed as an approximation. Source firms have offices in San Francisco unless otherwise noted. PPIE, Panama-Pacific International Exposition; bldg, building; do., ditto]

| Borehole | Original No. | Location | Date | Source | Job No. |
|---|---|---|---|---|---|
| 1E1 | 1 | Palace of Fine Arts | 1912 | Whitworth (1932) | |
| 2C1 | 1 | Lyon St. projected, N. of Marina Blvd. | 6/4/75 | Dames & Moore | 185-109-03 |
| 2D1 | 2 | Palace of Fine Arts | 1912 | Whitworth (1932) | |
| 2D2 | 1 | do | 6/23/61 | Dames & Moore | 185-027-03 |
| 2D3 | 7 | do | 7/5/61 | do | 185-027-03 |
| 2E1 | 2 | do | 6/23/61 | do | 185-027-03 |
| 2E2 | 4 | do | 6/29/61 | do | 185-027-03 |
| 2E3 | 6 | do | 6/30/61 | do | 185-027-03 |
| 2E4 | 8 | do | 7/6/61 | do | 185-027-03 |
| 2E5 | 9 | do | 7/6/61 | do | 185-027-03 |
| 2F1 | 3 | do | 1912 | Whitworth (1932) | |
| 2F2 | 5 | do | 6/30/61 | Dames & Moore | 185-027-03 |
| 2F3 | 10 | do | 7/6/61 | do | 185-027-03 |
| 2F4 | 1 | do | 3/16/70 | do | 185-06-03 |
| 2F5 | 2 | do | 3/16/70 | do | 185-06-03 |
| 2F6 | 3 | do | 3/16/70 | do | 185-06-03 |
| 2G1 | 3 | do | 6/28/61 | do | 185-027-03 |
| 3A1 | 1 | St. Francis Yacht Club | 2/15/77 | Harding Lawson Associates | 9201001.04 |
| 3A2 | 3 | do | 2/17/77 | do | 9201001.04 |
| 3C1 | 2F | NW. corner Food Products bldg , PPIE | 1912 | Whitworth (1932) | |
| 3C2 | 1A | N. side Marina Blvd., W. of Baker St. projected | 7/25/75 | Dames & Moore | 185-109-03 |
| 3C3 | HSA-1 | NW. corner Baker St. & Marina Blvd. | 8/18/77 | do | |
| 3C4 | 185-L-1? | N. side Marina Blvd., E. of Baker St. | ? | do | 185-109-03? |
| 3E1 | 54 | SW. corner Food bldg, PPIE; Beach St. E. of Baker St. | 1912 | Leurey (1914) | |
| 3G1 | 5 | SW. corner Education bldg , PPIE | 1912 | Whitworth (1932) | |
| 3G2 | Marina 1 | N. side Bay St., 40 ft E. of Baker St. | 2/2/90 | Bennett (1990) | |
| 4A1 | 2 | St. Francis Yacht Club | 2/17/77 | Harding Lawson Associates | 9201001.04 |
| 4C1 | 4 | NE. corner Food bldg, PPIE | 1912 | Whitworth (1932) | |
| 4C2 | HSA-3 | N. side Marina Blvd., W. of Broderick St. | 8/18/77 | Dames & Moore | |
| 4C3 | HSA-2 | do | 8/19/77 | do | |
| 4C4 | HSA-4 | N. side Marina Blvd., E. of Broderick St. | 8/22/77 | do | |
| 4C5 | HSA-29 | N. side Marina Blvd., W. of Broderick St. | 8/26/77 | do | |
| 4C6 | HSA-28 | do | 8/26/77 | do | |
| 4C7 | HSA-27 | N. side Marina Blvd., E. of Broderick St. | 8/26/77 | do | |
| 4C8 | 2 | S. of Marina Blvd., between Broderick St. and Divisadero St. | 12/20/89 | Don Hillebrandt Associates | 2017-9 |
| 4D1 | 6A | W. side Agriculture bldg, PPIE | 1912 | Whitworth (1932) | |
| 4D2 | 1 | N. side Jefferson St., E. of Broderick St. | 12/19/89 | Treadwell & Associates | 1050A |
| 4D3 | 1 | E. side Broderick St., S. of Marina Blvd. | 7/2/90 | Don Hillebrandt Associates | 2017-9 |
| 4E1 | Marina 2 | N. side Beach St., E. of Broderick St. | 2/7/90 | Bennett (1990) | |
| 4F1 | 5A | NE. corner Education bldg PPIE; W. of Broderick St., N. of North Point St. | 1912 | Whitworth (1932) | |
| 4F2 | 101 | NE. corner North Point St. & Broderck St. | 11/1/89 | C.H. Hartsog & Associates, Mountain View, Calif. | --- |
| 4G1 | 1 | E. of Broderick St., N. side Bay St. | 1/31/90 | Treadwell & Associates | 1070A |
| 5C1 | 6 | NW. corner Agriculture bldg, PPIE; S. of Marina Blvd., W. of Divisadero St. | 1912 | Whitworth (1932) | |
| 5C2 | 58 | N. center Agriculture bldg, PPIE; E. of Divisadero St., S. of Marina Blvd. | 1912 | Leurey (1914) | |
| 5C3 | HSA-6 | N. side Marina Blvd., E. of Divisadero St. | 8/22/77 | Dames & Moore | |
| 5C4 | HSA-5 | N. side Marina Blvd., W. of Divisadero St. | 8/23/77 | do | |
| 5C5 | HSA-24 | N. side Marina Blvd., E. of Divisadero St. | 8/25/77 | do | |
| 5C6 | HSA-26 | N. side Marina Blvd., W. of Divisadero St. | 8/26/77 | do | |
| 5C7 | HSA-25 | N. side Marina Blvd., E. of Divisadero St. | 8/26/77 | do | |
| 5C8 | HSA-7 | do | 8/26/77 | do | |

Table 1.—*Data on boreholes drilled in the Marina District of San Francisco*—Continued

| Borehole | Original No. | Location | Date | Source | Job No. |
|---|---|---|---|---|---|
| 5C9 | --- | SW. corner Divisadero St. & Marina Blvd. | 11/4/89 | C.H. Hartsog & Associates, Mountain View, Calif. | --- |
| 5C10 | 1 | S. side Marina Blvd., W. of Divisadero St. | 12/21/89 | Don Hillebrandt Associates | 2015-2 |
| 5C11 | 2 | W. side Divisadero St., S. of Marina Blvd. | 12/21/89 | do | 2015-2 |
| 5D1 | 1 | E. sidewalk of Divisadero St., S. of Jefferson St. | 11/20/89 | Harlan Tait Associates | 964.01 |
| 5D2 | 2 | S. sidewalk Jefferson St., E. of Divisadero St. | 11/21/89 | Harlan Tait Associates | 964.01 |
| 5D3 | 1 | N. side Jefferson St., W. of Divisadero St. | 12/20/89 | Treadwell & Associates | 1063A |
| 5D4 | B-1 | S. of Jefferson St., W. of Divisadero St. | 3/8/90 | Harding Lawson Associates | 19870001.04 |
| 5D5 | B-2 | do | 3/9/90 | do | 19870001.04 |
| 5D6 | B-2 | do | 3/9/90 | do | 19856001.04 |
| 5E1 | 50 | SE. corner Agriculture bldg, PPIE; Beach St. E. of Divisadero St. | 1912 | Leurey (1914) | |
| 5E2 | 1 | NE. side of Winfield Scott School bldg. | 12/8/72 | Dames & Moore | 185-082-03 |
| 5E3 | WSS | do | 11/8/89 | Kayen and others (1990) | |
| 5E4 | 1 | W. side Divisadero St., S. of Beach St. | 11/21/89 | Harlan Tait Associates | 986.01 |
| 5E5 | 2 | S. sidewalk of Beach St., W. of Divisadero St. | 11/21/89 | do | 986.01 |
| 5E6 | 1 | Property at NW. corner Beach St. & Divisadero St. | 11/29/89 | Don Hillebrandt Associates | 2015-1 |
| 5E7 | 2 | do | 11/29/89 | do | 2015-1 |
| 5E8 | 3 | do | 11/30/89 | do | 2015-1 |
| 5E9 | 4 | do | 11/30/89 | do | 2015-1 |
| 5E10 | Marina 3 | W. curb of Divisadero St., 60 ft S. of Beach St. | 1/31/90 | Bennett (1990) | |
| 5E11 | 1 | NE. of Beach St. & Divisadero St. | 7/2/90 | Don Hillebrandt Associates | 103-43 |
| 5E12 | 2 | do | 7/2/90 | do | 103-43 |
| 5E13 | 3 | do | 7/3/90 | do | 103-43 |
| 5F1 | 7A | NE. side Liberal Arts bldg PPIE; E. of Divisadero St., N. of N. Point St. | 1912 | Whitworth (1932) | |
| 5F2 | 2 | Winfield Scott School bldg, E. side near center | 12/8/72 | Dames & Moore | 185-082-03 |
| 5F3 | B-1 | N. sidewalk of North Point St., W. of Divisadero St. | 12/27/89 | GeoResource Consultants | 1542-04 |
| 5G1 | 75 | SW. corner Liberal Arts bldg, PPIE; N. of Bay St., W. of Divisadero St. | 1912 | Leurey (1914) | |
| 5G2 | B-1 | W. of Divisadero St., N. of Bay St. | 12/26/89 | Harding Lawson Associates | 19738001.04 |
| 5J1 | 1 | W. side Divisadero St., between Chestnut St. & Francisco St. | 2/5/90 | Don Hillebrandt Associates | 2025-1 |
| 6C1 | 2 | N. side Marina Blvd., E. side Scott St. | 6/5/75 | Dames & Moore | 185-109-03 |
| 6C2 | HSA-9 | N. side Marina Blvd., E. of Scott St. | 8/9/77 | do | |
| 6C3 | HSA-8 | N. side Marina Blvd., W. of Scott St. | 8/17/77 | do | |
| 6C4 | HSA-23 | N. side Marina Blvd., E. side of Scott St. | 8/25/77 | do | |
| 6C5 | HSA-30 | N. side Marina Blvd., W. of Scott St. | 8/26/77 | do | |
| 6C6 | 2 | W. side Scott St., N. of Jefferson St. | 1/31/90 | Treadwell & Assoc | 1061A |
| 6D1 | 8 | SW. corner Transportation bldg, PPIE | 1912 | Whitworth (1932) | |
| 6D2 | 1 | Scott St., N. of Jefferson St. | 11/20/89 | Herzog Associates | 2813.01.00.1 |
| 6D3 | 1 | N. side Jefferson St., W. of Scott St. | 1/30/90 | Treadwell & Assoc | 1061A |
| 6E1 | 1 | W. side Avila St., N. of Beach St. | 3/12/90 | Herzog Associates | 2887.01.00.1 |
| 6F1 | 7 | E. side Liberal Arts bldg, PPIE | 1912 | Whitworth (1932) | |
| 6F2 | 9A | NW. side Manufactures Bldg, PPIE; W. side Avila St., N. of Capra Way. | 1912 | do | |
| 6F3 | 1 | W. side Scott St., N. of Capra Way | 11/28/89 | Herzog Associates | 2837.01.00.1 |
| 6F4 | 2 | do | 11/28/89 | do | 2837.01.00.1 |
| 6F5 | 1 | W. side Scott St., N. of North Point St. | 12/5/89 | do | 2846.01.00.1 |
| 6F6 | 2 | W. side Scott St., N. of North Point St. | 12/5/89 | do | 2846.01.00.1 |
| 6G1 | 42 | SW. corner Manufactures Bldg. PPIE; E. of Avila St., S. of Capra Way. | 1912 | Leurey (1914) | |
| 6G2 | 1 | N. side Bay St., W. of Scott St. | 11/20/89 | Treadwell & Associates | 1047A |
| 6G3 | 1 | S. side Capra Way, E. of Scott St. | 11/21/89 | Herzog Associates | 2813.01.00.1 |
| 6H1 | B-1 | N. of Alhambra St., E. of Scott St. | 12/13/89 | Harding Lawson Associates | 89 2316.04 |
| 7C1 | 104 | N. center Transportation bldg. PPIE; NW. of Avila St., S. of Marina Blvd. | 1912 | Leurey (1914) | |

Table 1.—*Data on boreholes drilled in the Marina District of San Francisco*—Continued

| Borehole | Original No. | Location | Date | Source | Job No. |
|---|---|---|---|---|---|
| 7C2 | 3 | S. side Marina Blvd. at Avila St. & Casa Way | 6/6/75 | Dames & Moore | 185-109-03 |
| 7C3 | HSA-10 | N. side Marina Blvd., W. of Avila St. | 8/9/77 | do | |
| 7C4 | HSA-11 | do | 8/9/77 | do | |
| 7C5 | Marina 9 | Marina Green, N. of Avila St.-Casa Way intersection | 8/15/90 | Bennett, 1991, Written commun. | |
| 7E1 | 1 | S. side Beach St., W. of Mallorca Way | 11/27/89 | Herzog Associates | 2831.01.00.1 |
| 7E2 | B-1 | N. side Beach St., W. of Cervantes Blvd. | 12/15/89 | do | 2853.01.00.1 |
| 7E3 | B-2 | do | 12/15/89 | do | 2853.01.00.1 |
| 7E4 | Marina 4 | NW. point Beach St. & Cervantes Blvd. | 1/31/90 | Bennett (1990) | |
| 7E5 | B-1 | SW. side Cervantes Blvd., SE. of Prado St. | 2/1/90 | Geospectra, Richmond, Calif. | 00141.004.01.01 |
| 7F1 | 76 | NE. corner Manufactures Bldg, PPIE; E. of Pierce St., S. of Beach St. | 1912 | Leurey (1914) | |
| 7G1 | 9 | SE. corner Manufactures Bldg, PPIE | 1912 | Whitworth (1932) | |
| 7H1 | 1 | N. side Alhambra St., W. of Pierce St. | 12/7/89 | Herzog Associates | 2853.01.00.1 |
| 7J1 | 2 | SE. of Pierce St. & Chestnut St. | 2/23/68 | Hawke Engineers | 601 |
| 7J2 | 4 | do | 2/26/68 | do | 601 |
| 7J3 | 1 | NW. of Pierce St. & Chestnut St. | 7/7/71 | Gribaldo Jones & Assoc. | E1-0314-S1 |
| 7J4 | 2 | do | 7/7/71 | do | E1-0314-S1 |
| 7K1 | 1 | SE. of Pierce St. & Chestnut St. | 2/21/68 | Hawke Engineering | 601 |
| 7K2 | 3 | do | 2/26/68 | do | 601 |
| 8C1 | 8A | NE.corner Transportation bldg PPIE; SW. of Casa Way, SE. of Avila St. | 1912 | Whitworth (1932) | |
| 8C2 | HSA-12 | N. side Marina Blvd., E. of Casa Way | 8/10/77 | Dames & Moore | |
| 8C3 | HSA-13 | do | 8/10/77 | do | |
| 8E1 | 64 | SW. corner Mines bldg, PPIE; S. side Rico Way, W. of Retiro Way. | 1912 | Leurey (1914) | |
| 8F1 | 11 | NW. corner Varied Industries bldg, PPIE | 1912 | Whitworth (1932) | |
| 8F2 | B-1 | NW. side Alhambra St., SW. side Mallorca Way | 12/13/89 | Harding Lawson Associates | 89 2316.04 |
| 8G1 | 1 | E. side Mallorca Way, SE. of Alhambra St. | 11/30/89 | Herzog Associates | 2845.01.00.1 |
| 8K1 | S-A | SE. side Steiner St. & Lombard St. | 10/26/87 | Pacific Environmental Group, Santa Clara, Calif. | 101.01.01 |
| 8K2 | S-B | do | 10/26/87 | do | 101.01.01 |
| 8K3 | S-C | do | 10/26/87 | do | 101.01.01 |
| 8K4 | S-D | do | 10/26/87 | do | 101.01.01 |
| 8K5 | S-E | do | 10/26/87 | do | 101.01.01 |
| 8K6 | S-F | do | 10/26/87 | do | 101.01.01 |
| 8K7 | SMW-1 | do | 1/19/88 | Woodward Clyde | 8820011A |
| 8K8 | SMW-2 | do | 1/19/88 | do | 8820011A |
| 8K9 | SMW-3 | do | 1/19/88 | do | 8820011A |
| 8K10 | MW-4 | E. side Steiner St., S. of Lombard St. | 7/6/89 | Harding Lawson Associates | 4022197.03 |
| 8K11 | MW-5 | SE. corner Steiner St. & Lombard St. | 7/6/89 | do | 4022197.03 |
| 8K12 | MW-6 | S. side Lombard St. E. of Steiner St. | 7/5/89 | do | 4022197.03 |
| 8K13 | MW-7 | SW. side Steiner St. & Lombard St. | 7/7/89 | do | 4022197.03 |
| 8K14 | MW-8 | NW. corner Steiner St. & Lombard St. | 12/27/89 | do | 4022197.03 |
| 8K15 | MW-9 | S. side Lombard St. E. of Steiner St. | 12/27/89 | do | 4022197.03 |
| 9C1 | 10 | NE. corner Mines bldg, PPIE; W. side Fillmore St., S. of Retiro Way. | 1912 | Whitworth (1932) | |
| 9C2 | 4 | S. side Marina Blvd., E. side Fillmore St | 6/9/75 | Dames & Moore | 185-109-03 |
| 9C3 | HSA-14 | N. side Marina Blvd., W. of Fillmore St. projected | 8/10/77 | do | |
| 9C4 | HSA-15 | NE. corner Fillmore St. & Marina Blvd. | 8/15/77 | do | |
| 9C5 | Marina 7 | Marina Green, N. of Marina Blvd., opposite Fillmore St. | 6/22/90 | M.J. Bennett (written commun., 1991) | |
| 9D1 | 14B | Jefferson St., E. of Fillmore St.; NW. corner Machinery bldg. bldg, PPIE. | 1912 | Whitworth (1932) | |
| 9E1 | 10A | SE. corner Mines bldg, PPIE; W. side Fillmore St., N. of Beach St. | 1912 | do | |
| 9E2 | 15 | S. of Beach St., E. of Fillmore St. | 1/24/23 | do | |
| 9E3 | Marina 5 | Fillmore St., due E. of S. curb Beach St. | 2/13/90 | Bennett (1990) | |

Table 1.—*Data on boreholes drilled in the Marina District of San Francisco*—Continued

| Borehole | Original No. | Location | Date | Source | Job No. |
|---|---|---|---|---|---|
| 9F1 | 11A | Varied Industries bldg, PPIE; SW. of Divisadero St. & Beach St. | 1912 | Whitworth (1932) | |
| 9F2 | 14A | SW. corner Machinery bldg., PPIE; S. of North Point St. | 1912 | do | |
| 9F3 | 16 | North Point St. E. of Fillmore St. | 1/24/23 | do | |
| 9F4 | B-1 | NE. of Cervantes Blvd. opposite Alhambra St. | 2/16/90 | Harding Lawson Associates | 4092007.04 |
| 9F5 | B-2 | NE. of Cervantes Blvd., NW. of Alhambra St. projected | 2/16/90 | do | 4092007.04 |
| 9F6 | B-1 | W. of Fillmore St., N. of North Point St. projected | 1/4/90 | do | 11504007.04 |
| 9G1 | 11B | Varied Industries bldg, PPIE; W. side Fillmore St., N. of Bay St. | 1912 | Whitworth (1932) | |
| 9G2 | 17 | E. of Fillmore St., N. of Bay St. | 1/24/23 | do | |
| 9H1 | Marina 6 | Fillmore St., N. of Chestnut St. | 1/29/90 | Bennett (1990) | |
| 9J1 | 18 | N. of Chestnut St. , E. of Fillmore St. | pre-1913 | Whitworth (1932) | |
| 9K1 | 12 | N. of Lombard St.,W. of Fillmore St. | 1912 | do | |
| 9K2 | 13 | W. of Fillmore St., N. of Lombard St. | pre-1913 | do | |
| 10C1 | 5A | N. side Marina Blvd. at Webster St. | 6/20/75 | Dames & Moore | 185-109-03 |
| 10C2 | HSA-16 | N. side Marina Blvd., W. of Webster St. | 8/11/77 | do | |
| 10C3 | HSA-18 | N. side Marina Blvd., E. of Webster St. | 8/11/77 | do | |
| 10C4 | HSA-17 | N. side Marina Blvd., at Webster St. | 8/16/77 | do | |
| 10C5 | 101 | S. side Marina Blvd. between Fillmore St. & Webster St. | 11/1/89 | C.H. Hartsog & Associates, Mountain View, Calif. | |
| 10D1 | 14C | NE. corner Machinery bldg. PPIE; Jefferson St. at Webster St. | 1912 | Whitworth (1932) | |
| 10D2 | 5 | S. side Marina Blvd. at Webster St. | 6/11/75 | Dames & Moore | 185-109-03 |
| 10D3 | HSA-19 | N. side Marina Blvd., E. of Webster St. | 8/12/77 | do | |
| 10E1 | 14D | Center Machinery bldg. PPIE; W. of Webster St., S. of Beach St. | 1912 | Whitworth (1932) | |
| 10E2 | 19 | S. side Beach St. at Webster St. | 1912 | do | |
| 10E3 | 2 | W. side Webster St., N. of Beach St. | 12/4/89 | Herzog Assoc | 2845.01.00.1 |
| 10E4 | 1 | N. of North Point St., W. side Webster St. | 12/19/89 | do | 2852.01.00.1 |
| 10F1 | 14 | SE. corner Machinery bldg., PPIE; W. of Webster St., S. of North Point St. | 1912 | Whitworth (1932) | |
| 10F2 | 20 | Webster St. & North Point St. | 1/24/23 | do | |
| 10F3 | 22 | E. of Webster St., N. of North Point St. | 1/24/23 | do | |
| 10F4 | 1 | W. of Webster St., S. of North Point St. | 12/17/65 | Harding Lawson Associates | 2827.1 |
| 10F5 | 1 | S. of North Point St., W. of Webster St. | 5/17/88 | L.B. Karp, Orinda, Calif. | 88023 |
| 10F6 | 2 | do | 5/17/88 | do | 88023 |
| 10F7 | 3 | do | 1/17/89 | do | 89018 |
| 10F8 | 4 | do | 1/17/89 | do | 89018 |
| 10F9 | 5 | do | 1/19/89 | do | 89018 |
| 10F10 | 6 | do | 1/19/89 | do | 89018 |
| 10F11 | 1 | N. side North Point St., W. of Webster St. | 11/20/89 | Treadwell & Associates | 1045A |
| 10F12 | 2 | W. side Webster St., N. of North Point St. | 11/21/89 | do | 1045A |
| 10G1 | 21 | N. side Bay St. at Buchanan St. | 1/24/23 | Whitworth (1932) | |
| 11D1 | HSA-20 | N. side Marina Blvd., W. of Buchanan St. | 8/12/77 | Dames & Moore | |
| 11E1 | 23 | S. of Beach St. , W. of Buchanan St. | 1/24/23 | Whitworth (1932) | |
| 11E2 | HSA-21 | N. side Marina Blvd., W. of Buchanan St. | 8/12/77 | Dames & Moore | |
| 11E3 | HSA-22 | N. side Marina Blvd., E. of Buchanan St. | 8/15/77 | do | |
| 11E4 | 2 | N. of North Point St., W. side Buchanan St. | 12/10/80 | Harding Lawson Associates | 12038001.04 |
| 11E5 | --- | S. of Marina Blvd., W. of Buchanan St. | 3/28/88 | do | 18613001.04 |
| 11E6 | 1 | S. side Beach St. , W. of Buchanan St. | 11/13/89 | Smith-Emery | 51421 |
| 11E7 | 2 | do | 11/13/89 | do | 51421 |
| 11E8 | B-1 | do | 12/1/89 | Harding Lawson Associates | 89-2327.04 |
| 11E9 | B-2 | do | 12/8/89 | do | 89-2327.04 |
| 11F1 | 24 | S. of North Point St., W. of Buchanan St. | 1/24/23 | Whitworth (1932) | |
| 11F2 | 25 | North Point St., W. of Buchanan St. | 1/24/23 | do | |
| 11F3 | 12 | N. of North Point St., W. of Laguna St. | 3/30/65 | Woodward Clyde | |
| 11F4 | 1 | W. of Laguna St., S. of North Point St. | 9/23/66 | Dames & Moore | 3384-022-03 |

Table 1.—*Data on boreholes drilled in the Marina District of San Francisco*—Continued

| Borehole | Original No. | Location | Date | Source | Job No. |
|---|---|---|---|---|---|
| 11F5 | 1 | N. of North Point St. at Buchanan St. | 12/9/80 | Harding Lawson Associates | 12038001.04 |
| 11G1 | 27 | S. side Bay St. opposite Buchanan St. | pre-1913 | Whitworth (1932) | |
| 11G2 | 26 | N. of Bay St., W. of Buchanan St. | 1/24/23 | do | |
| 11G3 | 2 | W. of Laguna St., N. of Bay St. | 9/23/66 | Dames & Moore | 3384-022-03 |
| 11G4 | 1 | NW. of Buchanan St. & Bay St. | 5/29/87 | Don Hillebrandt Associates | 1767-1A |
| 11G5 | 2 | do | 5/29/87 | do | 1767-1A |
| 11G6 | 3 | do | 5/29/87 | do | 1767-1A |
| 11G7 | 4 | do | 5/26/88 | do | 1767-1A |
| 11G8 | 5 | do | 5/26/88 | do | 1767-1A |
| 11G9 | 6 | do | 5/26/88 | do | 1767-1A |
| 11G10 | 7 | do | 5/26/88 | do | 1767-1A |
| 12B1 | 1-27D | Ft Mason, Pier 1 | 8/1949-1/1950 | U.S. Army Corps of Engineers | |
| 12B2 | 1-18E | do | 8/1949-1/1950 | do | |
| 12B3 | 1-9E | do | 8/1949-1/1950 | do | |
| 12C1 | 1-2E | do | 8/1949-1/1950 | do | |
| 12E1 | 6 | N. side Beach St. at Laguna St. | 6/10/75 | Dames & Moore | 185-109-03 |
| 12F1 | 10 | NW. of North Point St. & Laguna St. | 3/30/65 | Woodward Clyde | |
| 12F2 | 11 | do | 3/30/65 | do | |
| 12F3 | 13 | do | 3/30/65 | do | |
| 12F4 | 14 | do | 3/30/65 | do | |
| 12F5 | 3 | SW. of North Point St. & Laguna St. | 9/23/66 | Dames & Moore | 3384-022-03 |
| 12G1 | 4 | W. of Laguna St., N. of Bay St. | 9/23/66 | do | 3384-022-03 |
| 12G2 | 17 | SW. corner Laguna St. & Bay St. | 6/13/75 | do | 185-109-03 |
| 13A1 | 3-27W | Ft Mason, Pier 3 | 8/1949-1/1950 | U.S. Army Corps of Engineers | |
| 13B1 | 2-23E | Ft Mason, Pier 2 | 8/1949-1/1950 | do | |
| 13B2 | 2-14E | do | 8/1949-1/1950 | do | |
| 13B3 | 3-23W | Ft Mason, Pier 3 | 8/1949-1/1950 | do | |
| 13B4 | 3-18W | do | 8/1949-1/1950 | do | |
| 13B5 | 3-13W | do | 8/1949-1/1950 | do | |
| 13B6 | 3-7W | do | 8/1949-1/1950 | do | |
| 13C1 | 2-2E | Ft Mason, Pier 2 | 8/1949-1/1950 | do | |
| 13C2 | 3-2W | Ft Mason, Pier 3 | 8/1949-1/1950 | do | |
| 13E1 | 7 | Ft Mason, S. of Beach St. & W. of Octavia St. projected. | 6/12/75 | Dames & Moore | 185-109-03 |
| 13E2 | 30 | Ft Mason, N. of Beach St. projected, E. of Laguna St. | 10/20/75 | do | 185-109-03 |
| 13E3 | 34 | Ft Mason, S. of Beach St. & E. of Octavia St. projected. | 10/21/75 | do | 185-109-03 |
| 13H1 | 110 | S. of Francisco St., W. of Octavia St. | 11/1/89 | C.H. Hartsog & Associates, Mountain View, Calif. | |
| 14E1 | 8 | Ft Mason, S. of Beach St. & W. of Gough St. projected. | 6/13/75 | Dames & Moore | 185-109-03 |
| 14G1 | 18 | N. side Bay St. at Gough St. | 6/17/75 | do | 185-109-03 |
| 14K1 | 30 | SE. of Lombard St. & Gough St. | 1912 | Whitworth (1932) | |
| 15F1 | 9 | Ft Mason, S. of Beach St. & W. of Franklin St. projected. | 6/11/75 | Dames & Moore | 185-109-03 |

MARINA DISTRICT

# GROUND-MOTION AMPLIFICATION

By John Boatwright, Linda C. Seekins, Thomas E. Fumal, Hsi-Ping Liu, and Charles S. Mueller,
U.S. Geological Survey

## CONTENTS



ABSTRACT

After the earthquake, event-triggered seismographs were deployed in and around the Marina District to investigate site amplification. During the 3 weeks after the main shock, 23 aftershocks were recorded by two or more of these stations; two other stations, deployed in April 1990, recorded three earthquakes that occurred in Contra Costa County. By recasting the method of spectral ratios into a generalized inverse problem, we combine the shear-wave spectra from these 19 aftershocks to estimate the relative site amplification as a function of frequency. Ground motion at all five stations located in the central part of the Marina District were amplified by factors of 6 to 10 at 1 Hz and 2 to 4 at 3 Hz relative to a station located on Franciscan sandstone at Fort Mason, irrespective of whether they are sited on artificial fill or beach sand. Stations located on dune sand and Quaternary sedimentary deposits outside the central part of the Marina District were amplified by a factor of 2 to 4 at frequencies above 1 Hz. Four stations located on Franciscan sandstone in Pacific Heights, Nob Hill, Rincon Hill, and Diamond Heights show little amplification relative to Fort Mason.

Conditional estimates of the main-shock spectra can be determined at stations that recorded only aftershocks, if they can be linked to stations that recorded the main shock. These estimates are predicated on the assumption that the ground behaved linearly during the main shock, an assumption that is clearly violated for those sites where ground failure occurred. Using this method of extrapolation for a site in the Marina District that showed no evidence of ground failure yields an estimated main-shock spectrum that is slightly greater than the spectrum from the Outer Harbor Wharf in Oakland and that significantly exceeds the spectra from the free-field accelerograms located in San Francisco.

## INTRODUCTION

The extensive damage in the Marina District caused by the earthquake, as detailed in figure 1, suggests that the ground motion was significantly amplified relative to that in such nearby areas as Pacific Heights or Russian Hill. To investigate this amplification, the U.S. Geological Survey deployed seismometers with General Earthquake Observation System (GEOS) event recorders (Borcherdt and others, 1985) at 12 sites inside and just outside the Marina District for 3 weeks after the main shock. Despite the large epicentral distances (≈100 km) and the relatively noisy urban environment, 14 aftershocks ranging in local magnitude ($M_L$) from 3 to 5 were recorded in the Marina District; two smaller earthquakes were recorded at epicentral distances of 20 and 35 km.

This report analyzes these aftershock recordings to determine the relative site response as a function of frequency in the Marina District. By suitably combining the spectra of the recorded shear waves, we estimate the seismic amplification for five sites within the central part of the Marina District and for two sites outside this area, relative to a hard-rock site in Fort Mason. Our results indicate that ground motions within the central part of the Marina District are amplified by factors ranging from 6 to 10 for periods of about 1 s; the relative amplification decreases gradually to a factor of 3 for periods of about 0.3 s and to a factor of 2 for periods of about 0.2 s. We note that this amplification spans the approximate range of the fundamental periods (0.3–0.4 s) for three- to four-story wood-

frame structures (International Conference of Building Officials, 1985, p. 117), suggesting that seismic amplification contributed significantly to the earthquake damage in the Marina District.

No accelerographs were located in the Marina District before the earthquake. The extensive building damage and ground failure in the Marina District, however, encourage estimates of the main-shock ground motions. Conditional estimates or extrapolations of these ground motions can be made by using aftershock spectra from sites within the Marina District, together with aftershock and main-shock spectra from nearby sites in San Francisco that recorded the main shock. The closest site that recorded both main-shock and aftershock accelerograms was located at a fire station on Pacific Heights, approximately 1.5 km south of the Marina District.

The relative amplifications determined from aftershock recordings are explicitly appropriate only for weak levels of ground motion. Using these amplifications to estimate the strong ground motions in the Marina District during the main shock is problematic. The ground failure and liquefaction of hydraulic fill that occurred in parts of the Marina District conclusively demonstrate that the ground behaved nonlinearly and that the aftershock site amplifications cannot be used to estimate strong ground motions. In these areas, the extrapolated ground motions can be considered only as upper bounds for the main-shock ground motions.

One of our sites in the Marina District, however, lies outside the area of ground failure but within the concentration of building damage west of Divisadero Street (fig. 1). Although the absence of ground failure does not prove that the beach sand and older bay deposits underlying this site behaved linearly, the assumption of linearity is more reasonable for this station. Extrapolating the main-shock ground motions for this site yields spectral accelerations that are similar to those for the main shock recorded at the Outer Harbor Wharf in Oakland and that exceed those for the main shock recorded by all the free-field accelerographs in San Francisco.

## INSTRUMENT LOCATIONS

The locations of the six instruments deployed within the central Marina District are shown in figure 2*A*. In general,

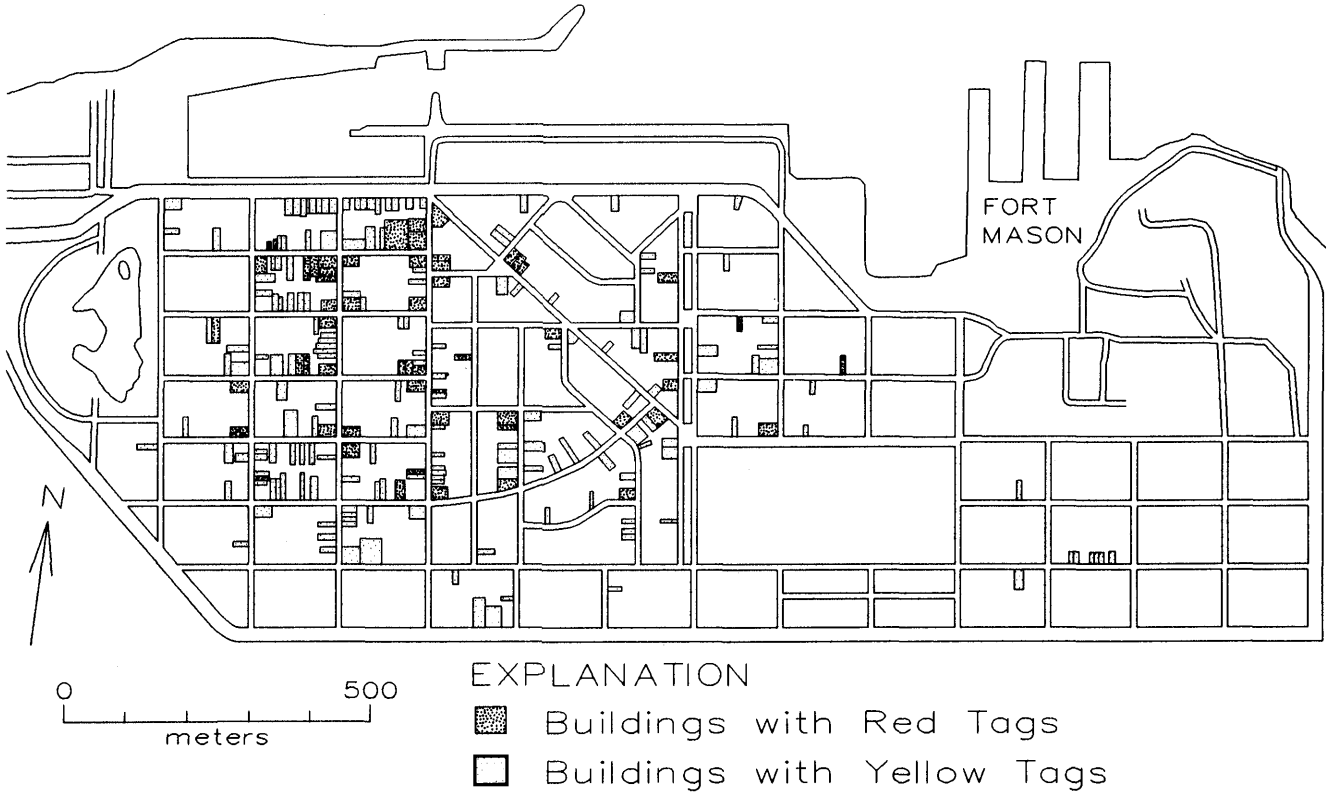


Figure 1.—Marina District of San Francisco, showing locations of red (unsafe for occupancy)- and yellow (dangerous)-tagged buildings. The set of tagged buildings was revised and updated by the City and County of San Francisco in fall 1990. Many red and yellow tags were originally issued to buildings for perceived danger from broken gas mains, asbestos, or possible collapse of a nearby building and were later upgraded; these buildings are plotted using the later tags. Red- and yellow-tagged buildings that were upgraded to yellow or green (no restriction on use) after repair work are plotted as originally tagged. A few demolished buildings are also included as red-tagged buildings.

Table 1.—*Aftershocks recorded at stations in San Francisco*

[Events are listed as arrival times by Julian day (first three digits) and Greenwich mean time (hours and minutes, last four digits); thus, the main shock, which occurred at 5:04 p.m. P.d.t. October 17, would be listed as event 2910004. Magnitudes from U.S. Geological Survey preliminary listing. Letters denote second when recording began: A, 0–2 s; B, 3–5 s; C, 6–8 s; and so on]

| Event | Magnitude | Station—LET | NPT | BEA | LMS | DEM | PUC | CAL | HHS | MAS | LEA | RIN | DIA |
|---|---|---|---|---|---|---|---|---|---|---|---|---|---|
| 2921014 | 5.0 | – | Q | – | – | – | – | – | – | – | – | Q | – |
| 2930018 | 3.9 | – | – | L | – | – | – | – | – | L | – | – | – |
| 2930813 | 3.6 | – | B | B | – | – | – | – | – | B | B | – | – |
| 2940049 | 4.3 | – | – | T | T | – | T | – | – | T | T | – | – |
| 2940832 | 2.7 | – | K | – | – | – | – | – | – | K | K | – | – |
| 2942215 | 4.6 | – | – | – | D | – | D | – | – | D | D | – | – |
| 2951424 | 3.7 | – | R | R | – | – | – | – | – | R | R | – | – |
| 2980127 | 4.5 | – | N | – | N | – | – | – | – | N | – | – | – |
| 2981301 | 3.7 | – | – | – | A | A | – | – | – | A | – | – | – |
| 2990901 | 3.6 | – | O | O | O | – | – | O | – | O | – | – | – |
| 3010835 | 2.5 | – | F | F | – | – | – | F | – | F | – | – | – |
| 3021311 | 2.9 | – | D | D | – | – | – | – | – | D | – | – | – |
| 3031117 | 3.6 | – | J | – | J | – | – | J | – | J | – | – | – |
| 3040835 | 3.4 | – | – | C | – | – | – | – | – | B | – | – | – |
| 3050803 | 3.7 | – | – | – | – | – | – | K | – | K | – | – | – |
| 3060550 | 4.5 | – | I | – | – | – | – | I | – | I | – | I | – |
| 3071048 | 3.0 | – | – | – | – | – | – | E | – | E | – | – | – |
| 3080716 | 3.6 | – | – | – | – | – | – | C | – | C | – | C | – |
| 3090130 | 3.7 | – | – | – | – | – | – | S | – | S | – | – | – |
| 3091337 | 3.8 | – | – | – | – | – | – | P | – | P | – | – | – |
| 3102337 | 2.9 | – | – | – | – | – | – | – | – | I | – | – | I |
| 3112342 | 4.0 | – | – | – | – | – | – | P | – | Q | – | – | P |
| 3121345 | 2.4 | – | – | – | – | – | – | I | – | I | – | – | I |
| 1180441 | 4.5 | A | – | – | – | – | – | – | S | R | – | – | – |
| 1180447 | 4.5 | P | – | – | – | – | – | – | P | P | – | – | – |
| 1180545 | 3.5 | – | – | – | – | – | – | – | C | C | – | – | – |

the site names are abbreviations for the street or building where the instruments were located; for example, stations NPT and BEA were located on North Point and Beach Streets, whereas station PUC was located at the Pacific Union Co. building, also known as the "Gas Light Building." Figure 2*A* also shows the location of station MAS, deployed on the knoll at Fort Mason.

The locations of other stations whose recordings are analyzed here are shown in figure 2*B*. Stations CAL and RIN, on Pacific Heights and Rincon Hill, respectively, were colocated with strong-motion accelerographs that recorded the main shock. A third station, DIA, was colocated with a strong-motion accelerograph on Diamond Heights, south of the map area. Station LEA is located on Nob Hill. These four stations, together with station MAS at Fort Mason, constitute a set of "hard rock" sites located on Franciscan sandstone in areas that sustained little or no damage during the main shock. Station CAL, colocated with a strong-motion accelerograph on Pacific Heights, is critical for estimating the main-shock ground motions in the Marina District. The 11 aftershocks recorded by both stations CAL and MAS ensure that the relative amplification at these two sites is well determined.

The aftershocks recorded at the various stations are listed in table 1. Station MAS recorded the largest number of aftershocks, probably as a result of its isolation from vehicular traffic and the relatively hard rock of its site. This instrument was deployed in a concrete ammunition bunker poured onto Franciscan sandstone. Station MAS provides a linchpin for comparing site amplifications throughout the city. The instruments that were deployed within the Marina District had to be retrieved about 2 weeks after the earthquake because the seismic noise from work of replacing the gas and water mains made it impossible to record aftershocks.

In April 1990, 5 months after the main shock, two additional stations, HHS and LET, were deployed at sites outside the central part of the Marina District. Station HHS was deployed on dune sand two blocks east of station PUC, and station LET was located in Letterman Army Medical Center within the Presidio, built on undivided Quaternary surficial deposits. Station LET was colocated

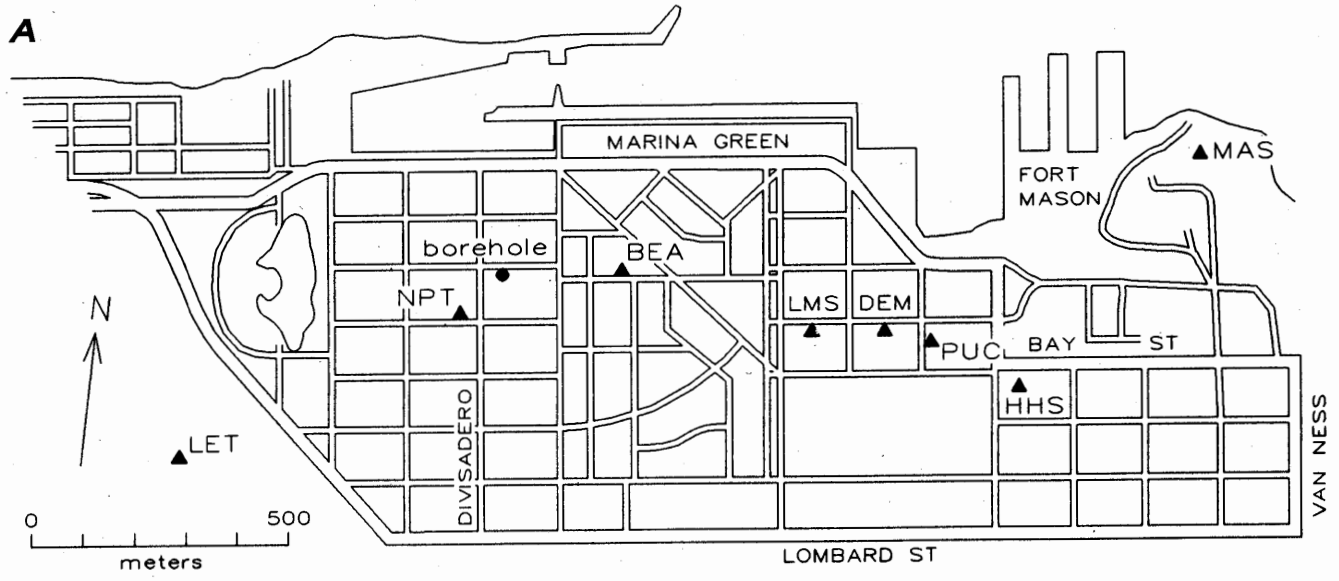
A
MARINA GREEN
FORT MASON
MAS
borehole
BEA
NPT
LMS
DEM
PUC
BAY
ST
HHS
N
LET
DIVISADERO
VAN NESS
0
500
meters
LOMBARD ST

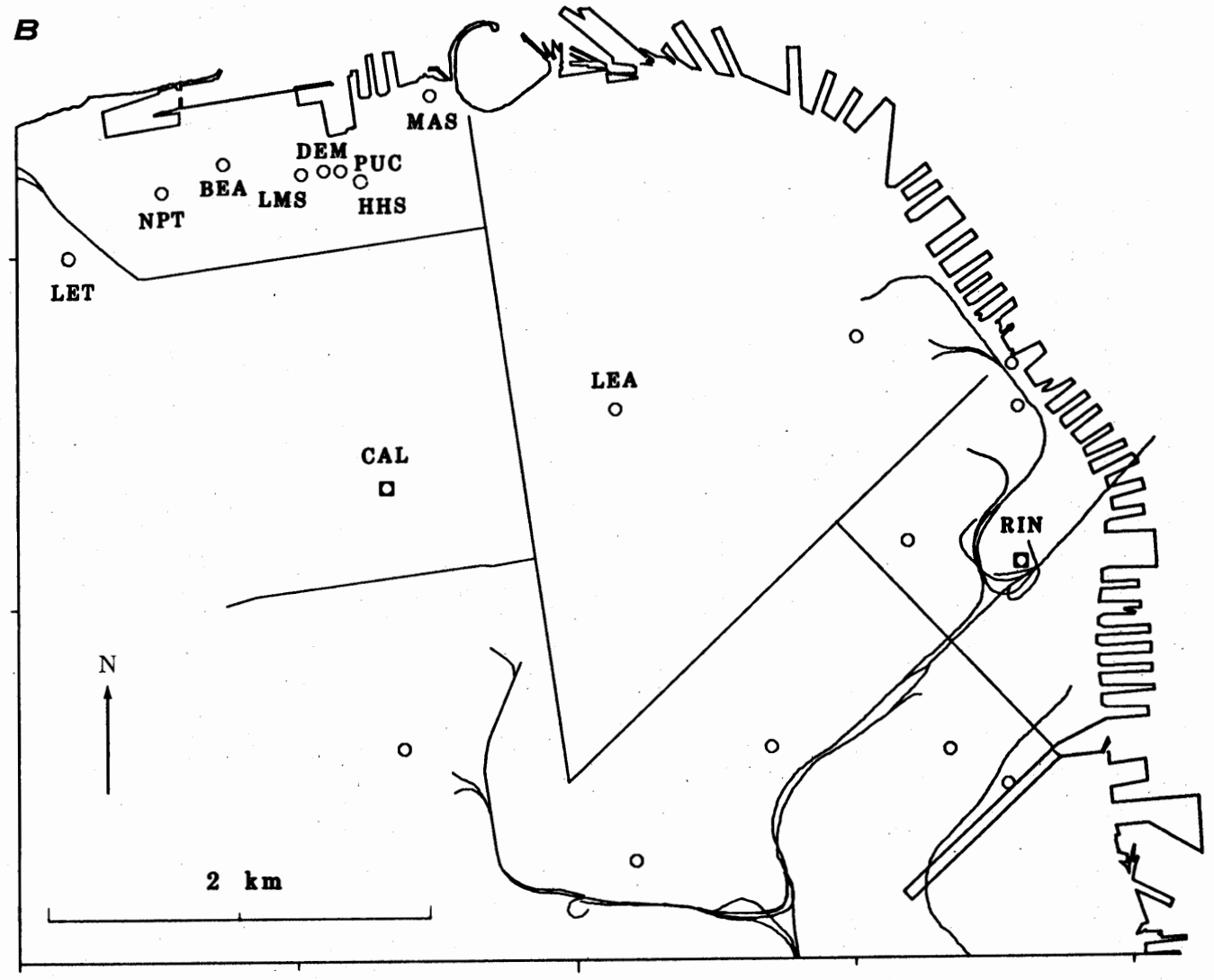
B
MAS
DEM
PUC
BEA
LMS
HHS
NPT
LET
LEA
CAL
RIN
N
2 km

with an accelerograph that recorded a peak acceleration of 0.14 *g* during the main shock. However, we were unable to obtain a digitizable copy of the main-shock accelerogram from the U.S. Army Corps of Engineers.

## AFTERSHOCK RECORDINGS

The east-west seismograms recorded at five stations during an $M_L$=3.6 aftershock are plotted in figure 3. This aftershock, which occurred 8 days after the main shock, was well recorded in the Marina District, largely because it occurred at 2:01 a.m. P.s.t. A cursory glance at the ground velocities indicates the severity of the ground amplification within the Marina District. At stations NPT, BEA, and LMS, located in the Marina District, the peak velocities range from 0.04 to 0.05 cm/s, whereas at stations MAS and CAL, located at relatively hard-rock sites, the peak velocities are 0.02 and 0.01 cm/s, respectively. The hypocentral distances to these stations range from only 97 to 99 km, and so we can reasonably assume that the wavefield incident at depth below these stations is the same.

The spectral amplitudes of the shear waves are plotted in figure 4. The relative seismic amplification apparent in figure 3 is clearly delineated in the frequency domain. In particular, the spectral amplitudes of the shear waves recorded at station CAL are consistently the smallest among the five stations. Station MAS exhibits spectral amplitudes intermediate to those at station CAL on Pacific Heights and at stations in the Marina District. Station BEA

◀ Figure 2.—Marina District (*A*) and northeastern part of San Francisco (*B*), showing locations of recording stations. In figure 2*A*, note that stations BEA and LMS lie within area of 1912 hydraulic fill (see Bonilla, this chapter) but stations NPT, DEM, and PUC lie outside it; station MAS is sited on an outcrop of Franciscan sandstone at Fort Mason. Circle labeled "borehole" indicates location of borehole described by Kayen and others (1990). In figure 2*B*, stations CAL and RIN were cosited with SMA–1 instruments that recorded the main shock on Pacific Heights and Rincon Hill, respectively; station LEA was sited at a fire station on Nob Hill. Unlabeled circles indicate temporary seismograph stations within the city whose recordings are not analyzed in this report.

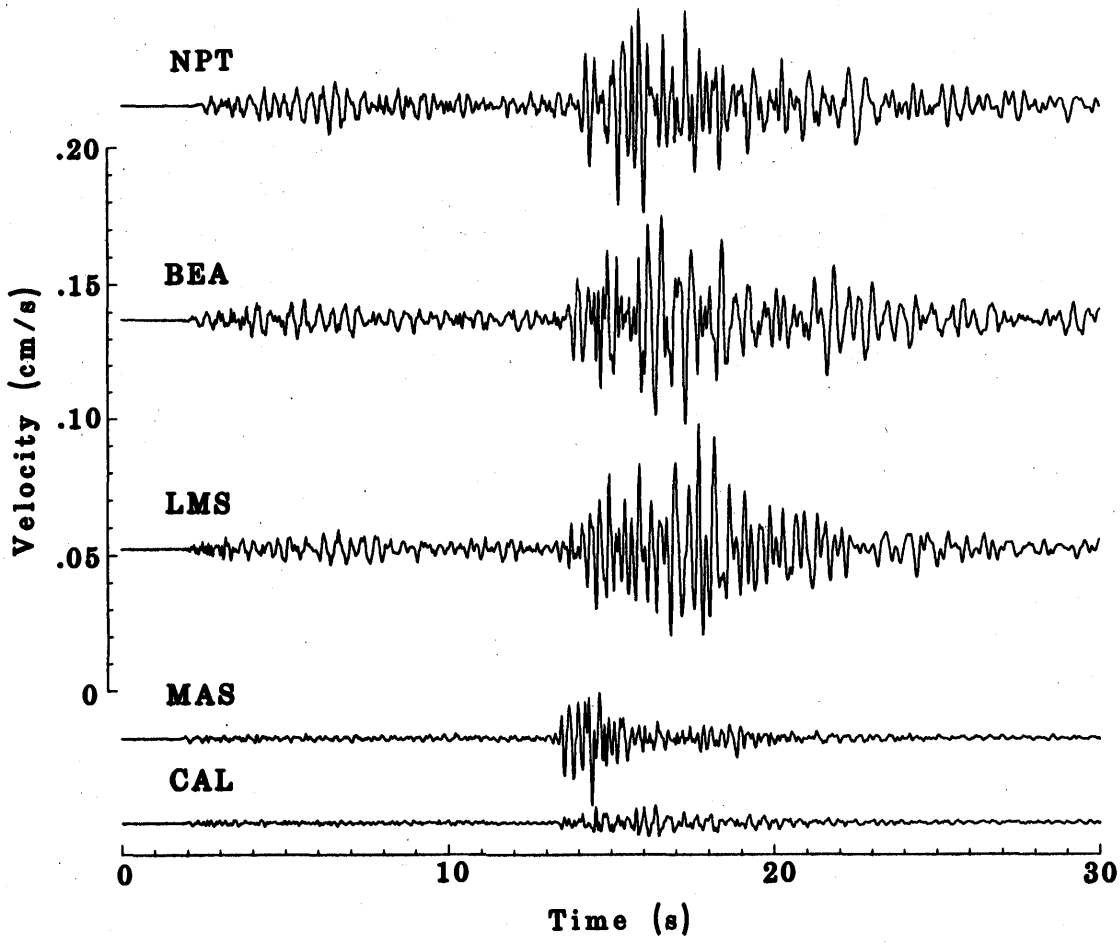


Figure 3.—East-west (EW) ground velocity for an $M_L$=3.6 aftershock (event 2990901, table 1) recorded at stations in the Marina District. *S* waves are strongest on east-west component, whereas *P* waves are weakest. Spectral amplitudes plotted in figure 4 are determined from 20-s samples starting approximately 2 s before *S*-wave arrival.

has a marked spectral peak at 2.2 Hz, whereas stations NPT and LMS have spectral peaks near 4.0 Hz, which is approximately the fundamental frequency for a three-story building with a wood frame.

In general, the relative spectral amplitudes recorded at these stations vary among events, depending on the component of ground motion, hypocentral distance, hypocentral depth, and the focal mechanism of the aftershock. To ensure that we obtained the least biased estimate of the seismic amplification, we used all the aftershock recordings together. We briefly describe this analysis in the next section.

## DECOMPOSITION FOR SOURCE AND SITE SPECTRA

Following Andrews (1986), we assume that each record spectrum is the product of a site-response spectrum and a source spectrum and may be written as

$$R_k(f) = \frac{1}{r_k} SR_i(f)\, ES_j(f), \qquad (1)$$

where the subscripts $k$, $i$, and $j$ refer to the recording, the station, and the earthquake, respectively; $SR_i(f)$ is the site-response spectrum for the $i$th station; and $ES_j(f)$ is the source spectrum for the $j$th earthquake. The geometric spreading factors $r_k = x_{ij}/2$ are set equal to half the hypocentral distance between the station and the earthquake; the factor of 2 compensates for the amplification of the free surface. Note that the decomposition in equation 1 does not explicitly describe attenuation as a function of distance and frequency, that is, $r_k(\omega)$. This description is unnecessary for the present data set because most of the aftershocks were recorded at similar epicentral distances.

This system of equations can be linearized by taking logarithms and solved by minimizing the error in the $k$=1, $K$ equations:

$$[\ln R_k(f) + \ln r_k - \ln SR_i(f) - \ln ES_j(f)]\,/\sigma_k^2(f) = 0 \ . \qquad (2)$$

The record spectra $R_k^2(f)$ are determined by summing the squares of the spectral amplitudes of the two horizontal components of the shear wave. The spectral amplitudes were resampled logarithmically to save space, with the

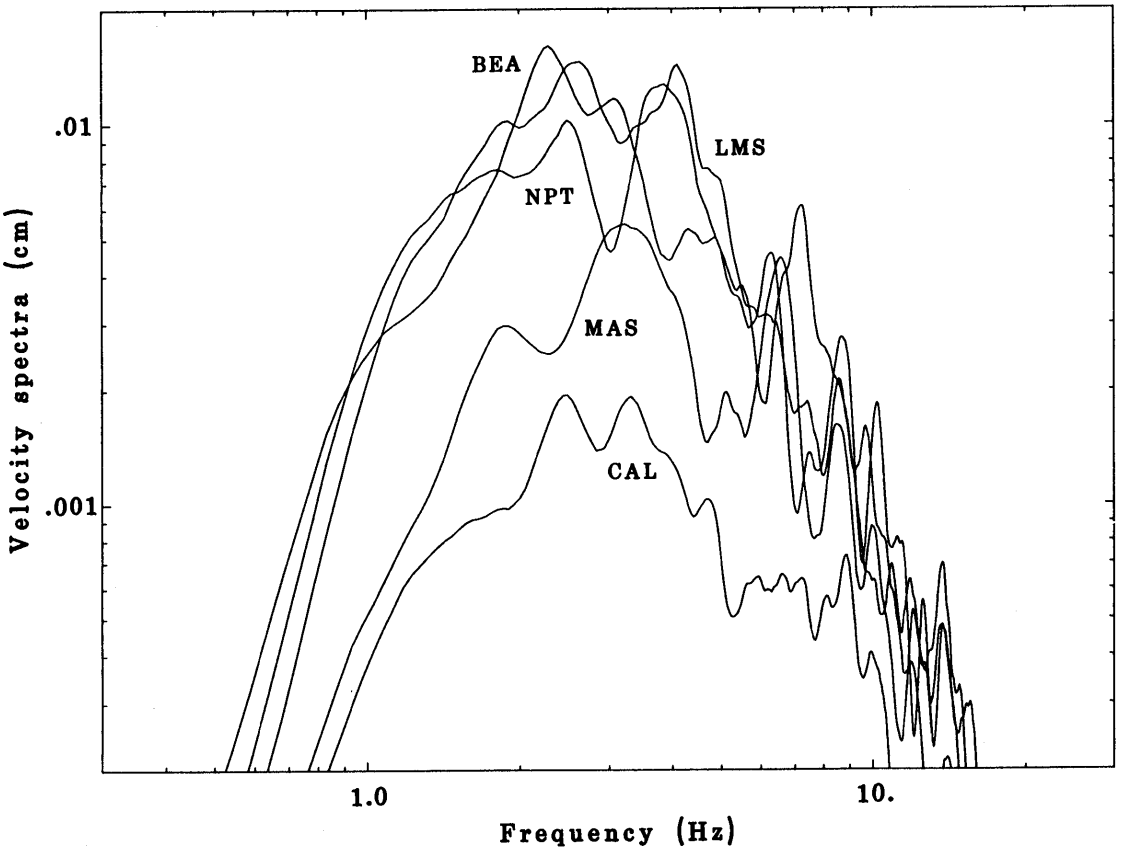


Figure 4.—Spectral amplitudes of shear waves plotted in figure 3. Note that the spectra from the Marina District stations (NPT, BEA, LMS) are similar in overall amplitude, as the relative amplitudes of the recorded velocities suggest. For this event and this component, station MAS is amplified by a factor of 3 at 3 Hz relative to station CAL.

frequencies from 0.1 to 100 Hz divided into 40 frequency bands that each span a factor of $2^{1/4}$=1.189 in frequency. This resampling effectively smooths the spectra at high frequencies.

The variances $\sigma_k^2(f)$ were determined by taking small samples of the *P*-wave coda before the shear-wave arrivals. Summing the squares of the noise spectra from the two horizontal components of ground motion yields the noise functions $N_k^2(f)$. The variances are constrained as (Andrews, 1986)

$$\sigma_k(f) = \max[(N_k(f)/R_k(f), 0.5], \quad (3)$$

which limits the signal-to-noise ratio of the data to less than a factor of 2. This conditioning is necessary because equation 1 represents an approximate decomposition and the *P*-wave-coda noise samples provide only weak estimates of the variation in the data.

For $K$ recordings, $I$ stations, and $J$ earthquakes, equation 2 describes a system of $K$ equations to determine $I+J$ unknowns. There is one undetermined degree of freedom associated with this system of equations. Physically, this undetermined degree of freedom means that we can estimate relative, but not absolute, site response and source spectra.

As a first constraint for the inversion, we set the site response for one station identically equal to 1 so that the site responses for the $I-1$ other stations are determined relative to this station (Bonamassa and Mueller, 1989). We use MAS as a reference station both because it recorded the most aftershocks and it has the most nearly "average" response among the hard-rock stations. This station constraint is simply written as $\ln SR_{MAS}(f)=0$. Inverting the resulting system of equations 2 yields the constrained "site" and "source" spectra,

$$\frac{SR_i(f)}{SR_{MAS}(f)} \quad \text{for } i = 1,I$$
$$\text{and} \qquad SR_{MAS}(f)\,ES_j(f) \quad \text{for } j = 1,J \qquad (4)$$

Dividing these constrained "source" spectra by the appropriate geometric spreading factors (that is, $x_{MAS_j}/2$) yields spectral estimates for the ground motion recorded at station MAS from the $j$th earthquake.

## RELATIVE SITE AMPLIFICATIONS

The site response at station NPT relative to station MAS is plotted in figure 5; station NPT is located within an area

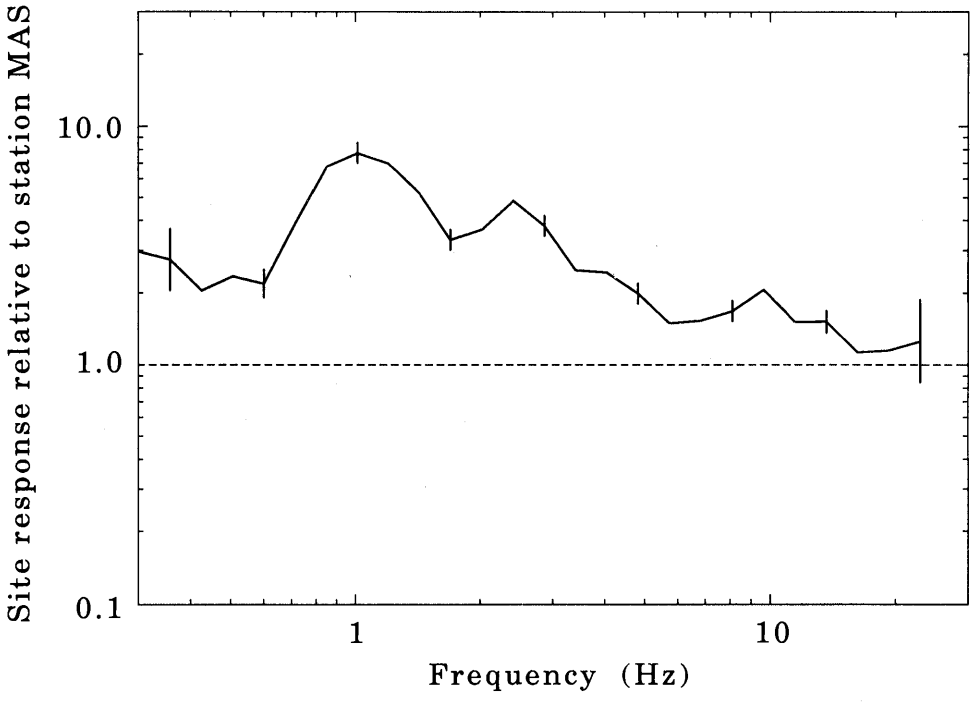


Figure 5.—Average site-response spectrum for shear waves at station NPT, relative to station MAS. Vertical bars show 68-percent-confidence interval for spectral estimates. Relative site response is well determined from 0.7 to 15 Hz. At low frequencies, relative amplification is slightly larger than a factor of 2; it peaks around 1 Hz and decreases gradually with increasing frequency up to 15 Hz, where there is little relative amplification.

that was heavily damaged during the main shock (fig. 1). The relative site response, which is well determined within the frequency band from 0.6 Hz (1.6 s) to 15 Hz, is amplified by a factor of 7 near 1 Hz and decreases gradually with increasing frequency up to 15 Hz. At the lowest frequencies, the amplification is approximately a factor of 2 but is poorly resolved.

The relative site response at all five stations located in the central part of the Marina District is plotted in figure 6. Although there is some variation among these five stations, the overall behavior is remarkably similar: a rapid increase to a peak amplification of 6 to 10 near 1 Hz, followed by a gradual decrease with increasing frequency up to 15 Hz. The frequency band from 0.7 to 3.0 Hz is significantly amplified for all the Marina District stations relative to station MAS. The logarithmic resampling interpolates, but does not smooth, the input record spectra; the absence of a marked peak-and-trough structure indicative of a modal site resonance is a consistent characteristic of these site-response spectra.

There is a slight variation among the site responses at high frequencies, where station PUC is more strongly amplified than the rest of the Marina District stations. The amplification at station PUC relative to station MAS is approximately a factor of 3 within the frequency band from 2.5 to 25 Hz. We note that station PUC is located to the east of the hydraulic fill (see Bonilla, this chapter); the thin (≈6 m thick) layer of hydraulic fill may attenuate the high-frequency motion at stations BEA and LMS.

The site response at the hard-rock stations (fig. 7) indicates the significance of the seismic amplification in the Marina District. On average, these stations show no relative amplification within the frequency band from 0.3 to 20 Hz. At 5.0 to 15 Hz, the amplification at station LEA increases to a factor of 2, whereas the amplification at station CAL is approximately half that at station MAS at 2.0 to 20 Hz. Overall, the median amplification at these five stations is remarkably close to 1, justifying the description of station MAS as an "average" hard-rock station. The increase in the relative site response at low frequencies at station DIA is the result of a malfunctioning recorder: Gary Glassmoyer (oral commun., 1990) identified, but could not correct, a baseline offset in the recording of event 3112342 (table 1).

The site response at stations HHS and LET is plotted in figure 8. Comparison with figure 6 indicates a pronounced difference in the response between these stations and the five stations in the central part of the Marina District: Stations HHS and LET, located on dune sand and sediment, respectively, show little relative amplification at low frequencies; the amplification increases to 2–4 above 1 Hz. We note that the difference in

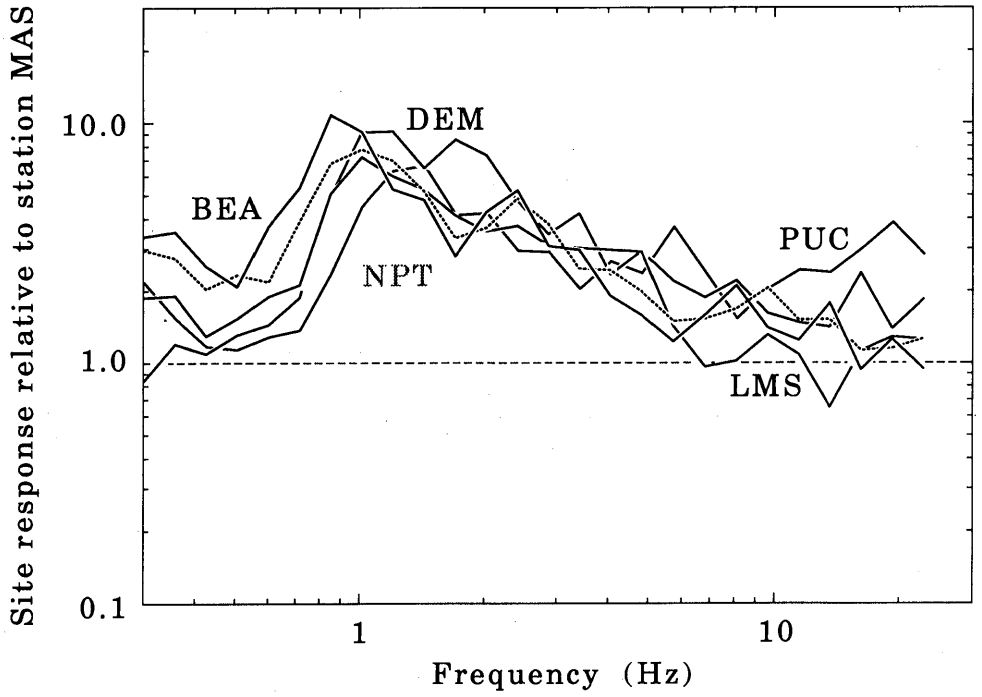


Figure 6.—Site-response spectra for shear waves at five stations in central part of the Marina District, relative to station MAS. Dotted line shows site response for station NPT. Although there is some variation between stations, the overall amplification is remarkably consistent, with a peak amplification of a factor of 7 to 10 near 1.0 Hz that gradually decreases with increasing frequency. Station PUC has the most amplification, and station LMS the least amplification, at high frequencies.

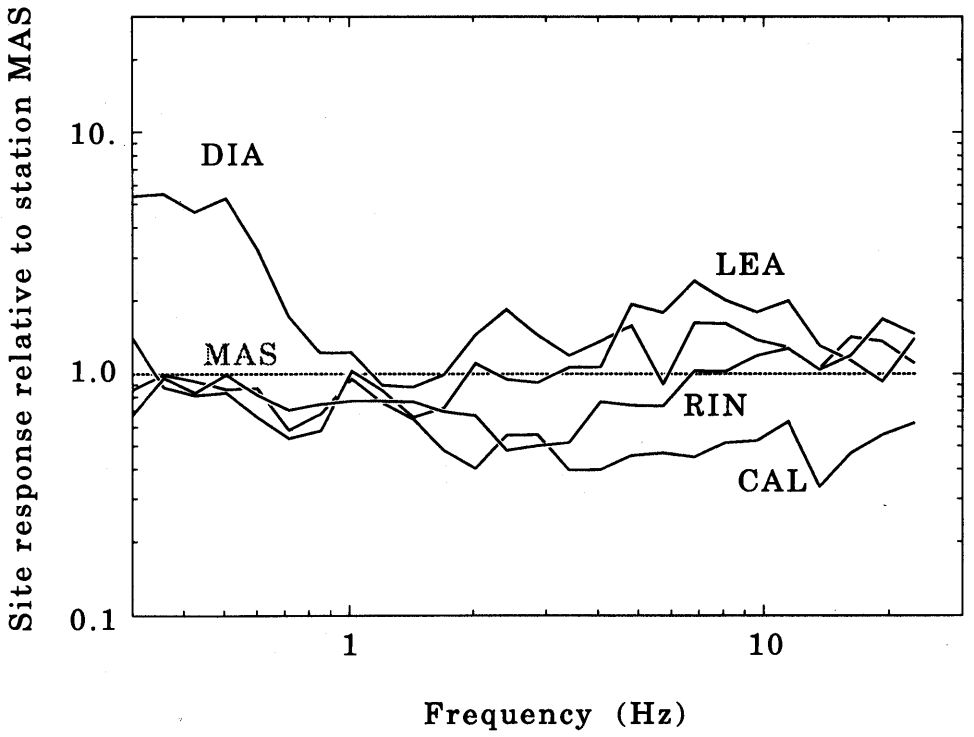


Figure 7.—Site-response spectra for shear waves at five hard-rock stations in San Francisco, relative to station MAS. Constraining station MAS yields a flat amplification of 1.0 (dotted line), close to the median site response for the other stations. Station CAL has the least amplification, and stations RIN and LEA the most amplification, reaching 2. Apparent amplification at low frequencies for station DIA is due to a malfunctioning recorder.

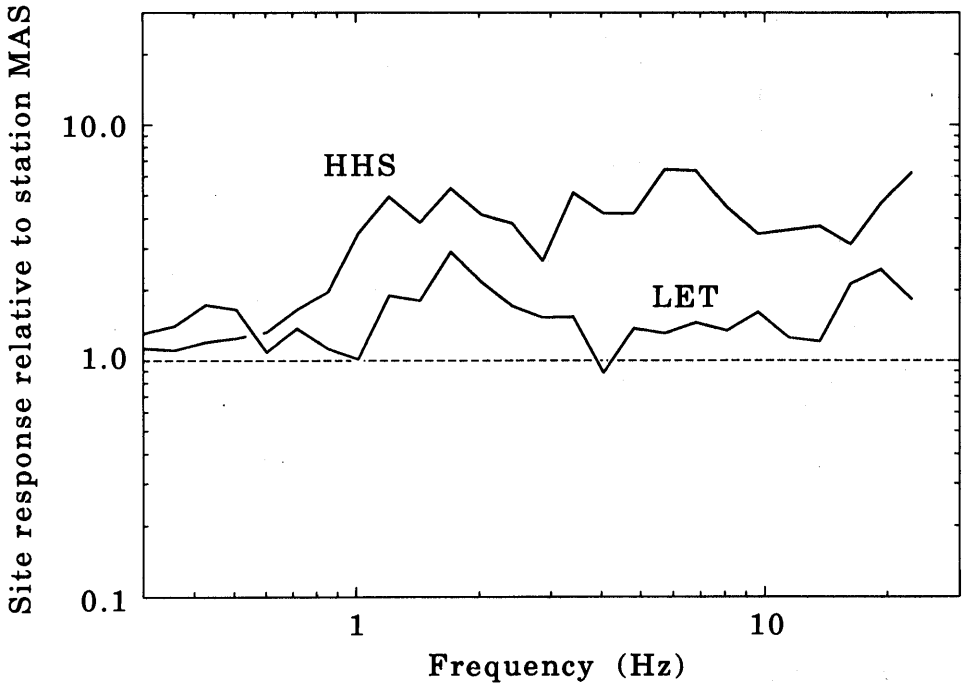


Figure 8.—Site-response spectra relative to station MAS for shear waves at two stations sited on dune sand and undivided sedimentary deposits inside and just outside the Marina District. Station LET is located at Letterman Army Medical Center in the Presidio, and station HHS in eastern part of the Marina District. Bedrock contours drawn by Bonilla (this chapter) indicate that the sedimentary basin underlying the Marina District is about 35 m thick beneath station HHS but does not extend westward beneath station LET.

relative amplification between stations HHS and LET correlates with the relative amount of damage in these two areas. There was little damage in the Presidio (LET), whereas the area near the Heritage House (HHS) sustained moderate damage (see fig. 1). Because Letterman Army Medical Center is a large (six story) building, the relative site response plotted in figure 8 is also conditioned by the building response.

## ONE-DIMENSIONAL MODEL FOR THE GROUND-MOTION AMPLIFICATION IN THE MARINA DISTRICT

The shear-wave velocities in the sedimentary deposits underlying the Marina District were determined by Kayen and others (1990) from a 91-m-deep borehole located near station NPT (see fig. 2*A*). The sedimentary column is largely made up of older bay mud, with a shear-wave velocity of approximately 300 m/s, overlying Franciscan serpentine. We investigate the amplification due solely to the vertical velocity structure, using the one-dimensional model of Haskell (1960) for the propagation of *SH* waves. The distributions of shear-wave velocity, density, and $Q$ are plotted in figure 9*A*. The estimated densities are assumed from results obtained in similar rock types, as are the shear-wave velocities for depths below 25 m (Fumal, 1991).

To model the amplification at station NPT relative to station MAS, we calculate the one-dimensional amplification for the velocity structure shown in figure 9*A* as the site amplification at station NPT, and use the velocity structure for depths below 80 m to calculate the site amplification at station MAS. Dividing the amplification at station NPT by the amplification at station MAS yields the model spectral ratio. The observed and model spectral ratios are plotted in figure 9*B*.

The one-dimensional model for the central part of the Marina District fits the observed amplification for frequencies above 2.5 Hz. Basically, this high-frequency fit is derived from the cumulative $Q$ structure shown in figure 9*A*. For frequencies between 1 and 2.5 Hz, however, the one-dimensional model substantially underestimates the observed amplification. In particular, the width of the low-frequency peak is poorly modeled. To first order, this peak represents the lowest mode of a quarter-wave resonance: The average shear-wave velocity of 300 m/s for 80 m of sediment yields a travel time of 0.27 s, a quarter of the period of the lowest resonance peak. The misfit of both the width of the spectral peak and the trough near 2 Hz (shaded area, fig. 9*B*) suggests that this quarter-wave resonance is modified by seismic-focusing effects. At these frequencies, the shape of the sedimentary basin underlying the Marina District (see Bonilla, this chapter, figs. 4, 5) may contribute significantly to the observed site amplification.

## EXTRAPOLATING MAIN-SHOCK GROUND MOTIONS

If we include the accelerograph recordings of the main shock in the record set that is decomposed into source and site spectra, equation 2 can be constrained to yield linear extrapolations of the main-shock ground motions at stations that recorded only aftershocks. Setting the source spectra of the main shock identically equal to 1 (that is, $\ln ES_o(f) = 0$, where "$o$" indicates the main shock) is mathematically similar to constraining one of the site spectra. Inverting the resulting set of equations yields the reconstrained "site" and "source" spectra

$$SR_i(f)\,ES_o(f) \quad \text{for } i = 1,I$$
$$\text{and} \qquad \frac{ES_j(f)}{ES_o(f)} \quad \text{for } j = 1,J \qquad (5)$$

Dividing these reconstrained "site" spectra by the geometric spreading factors ($x_{io}/2$) yields spectral estimates of the main-shock ground motions at the $I$ stations that recorded aftershocks. This method of reconstraining the inversion of equation 2 to extrapolate ground motion is more readily implemented than the explicit averaging

$$R_{io}(f) = \frac{1}{N}\sum_{n=1}^{N}\frac{x_{no}}{x_{io}}\frac{SR_i(f)}{SR_n(f)}R_{no}(f) \qquad (6)$$

determined from the $N$ main-shock recordings $R_{no}(f)$ and the relative site responses $SR_i(f)/SR_n(f)$ obtained through the constraints described in equation 4.

To test this procedure, we incorporate the main-shock spectrum at station CAL into the data set and extrapolate for station RIN. The recorded spectrum and the 68-percent-confidence limits for the extrapolated spectrum are plotted in figure 10. The recorded main-shock spectrum falls well within the confidence interval for this extrapolation, as determined from the variance defined in equation 3 and the number of main-shock accelerograms.

To extrapolate the ground motions in the central part of the Marina District for the main shock, we incorporate the main-shock spectra at stations CAL and RIN into the data set and extrapolate for station NPT. The extrapolated acceleration spectrum is plotted in figure 11. As shown in figure 5, the amplification at station NPT has a broad peak at 1 Hz and a "side lobe" at 2.3 Hz; these peaks are similarly evident in the extrapolated acceleration spectrum. Two main-shock acceleration spectra are also plotted in figure 11. The spectrum labeled "GGB" was obtained at a station located 2 km west of the Marina District, sited on Franciscan serpentine below the Toll Plaza of the Golden Gate Bridge. Station GGB recorded a peak ground acceleration of 0.25 $g$. The main-shock spectrum at station

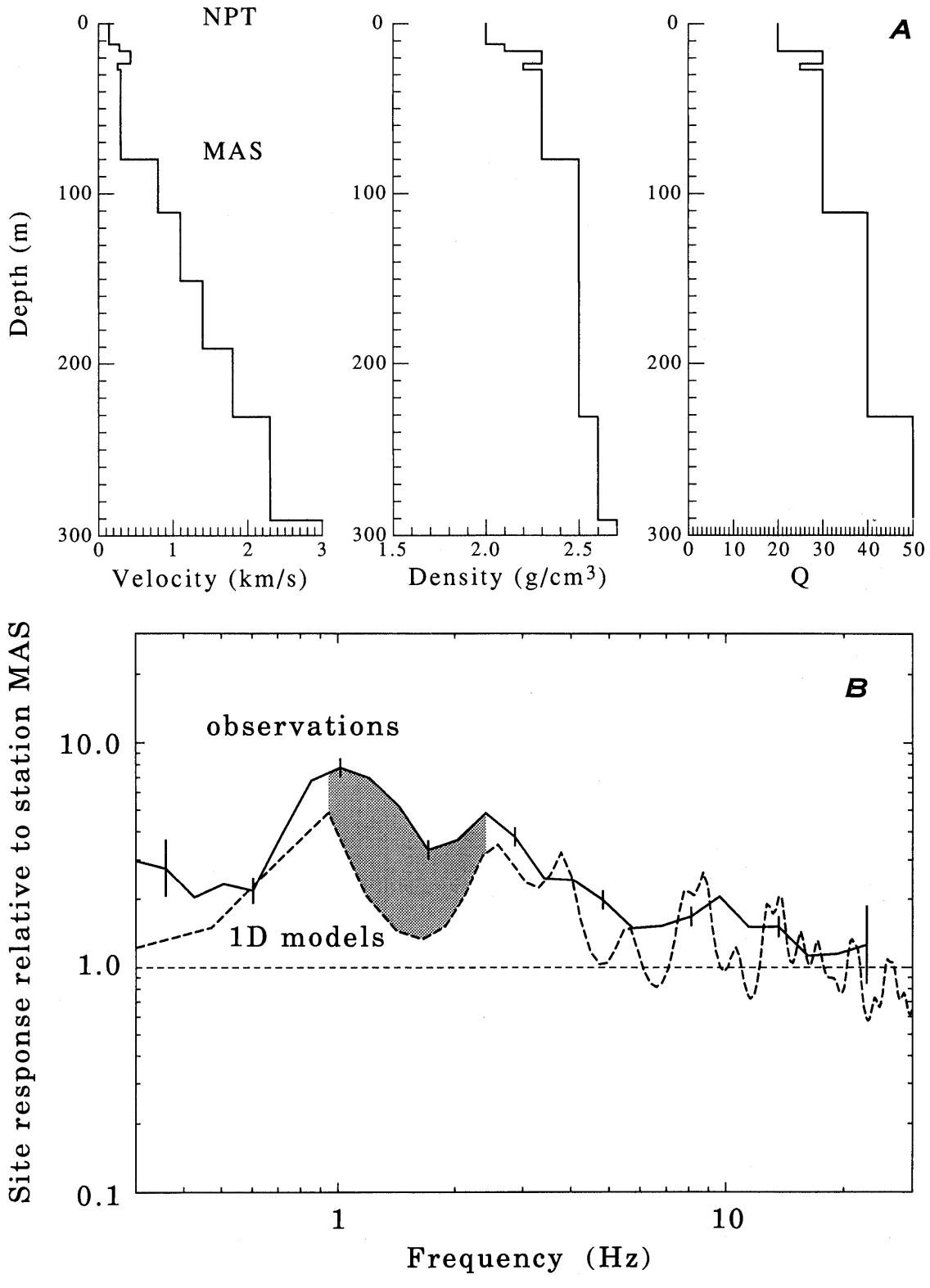


Figure 9.—One-dimensional model for ground-motion amplification. *A*, Distributions of shear-wave velocity, density, and *Q* values inferred for station NPT. Shear-wave velocity was logged by Kayen and others (1990) to a depth of 25 m, then extrapolated to Franciscan serpentine at 80 m, assuming a velocity of 300 m/s. Stepped increase in shear-wave velocity in the basement rock was chosen arbitrarily, as were the densities. *Q* structure was adjusted to fit observed spectral ratio at high frequencies. Velocity, density, and *Q* structure used to model station MAS were obtained by stripping the upper 80 m of structure used for station NPT. *B*, Observed spectral ratio compared to predicted amplification at station NPT, relative to station MAS. Fit at frequencies above 2.5 Hz was obtained by adjusting cumulative attenuation in the sedimentary deposits. Misfit between 1 and 2.5 Hz (shaded area) could be caused by seismic-focusing effects due to the shape of sedimentary basin; varying the velocity structure below 80-m depth does not improve this misfit.

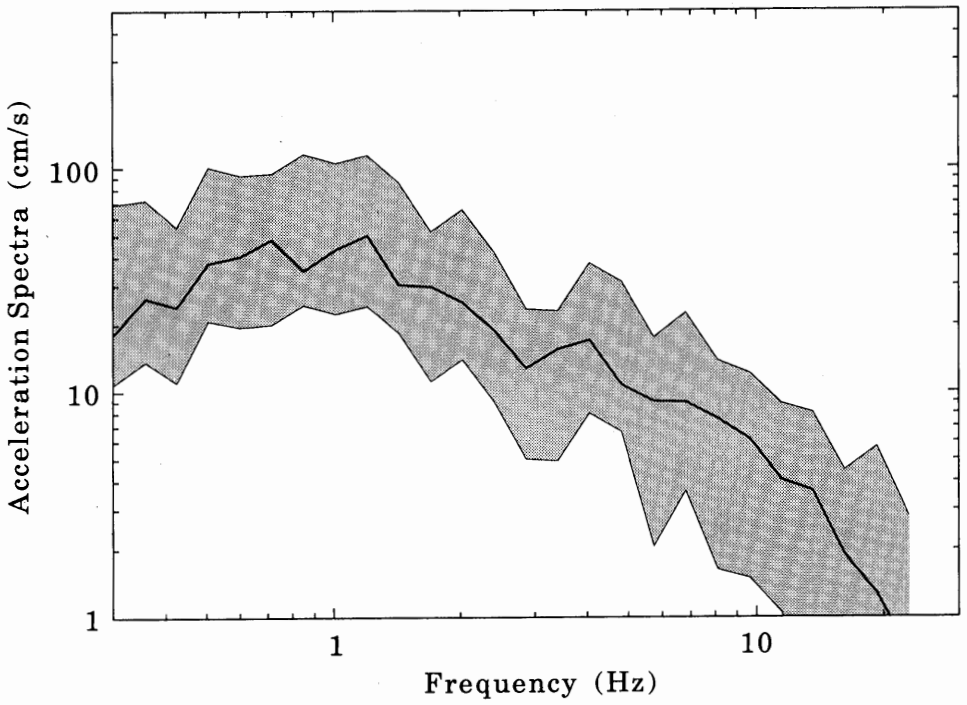


Figure 10.—Extrapolated acceleration spectrum, plotted as a 68-percent-confidence interval (shaded area), compared to acceleration spectrum for main shock from station RIN (heavy curve). Extrapolation was obtained using only the main-shock recording from station CAL, together with the set of aftershock recordings.

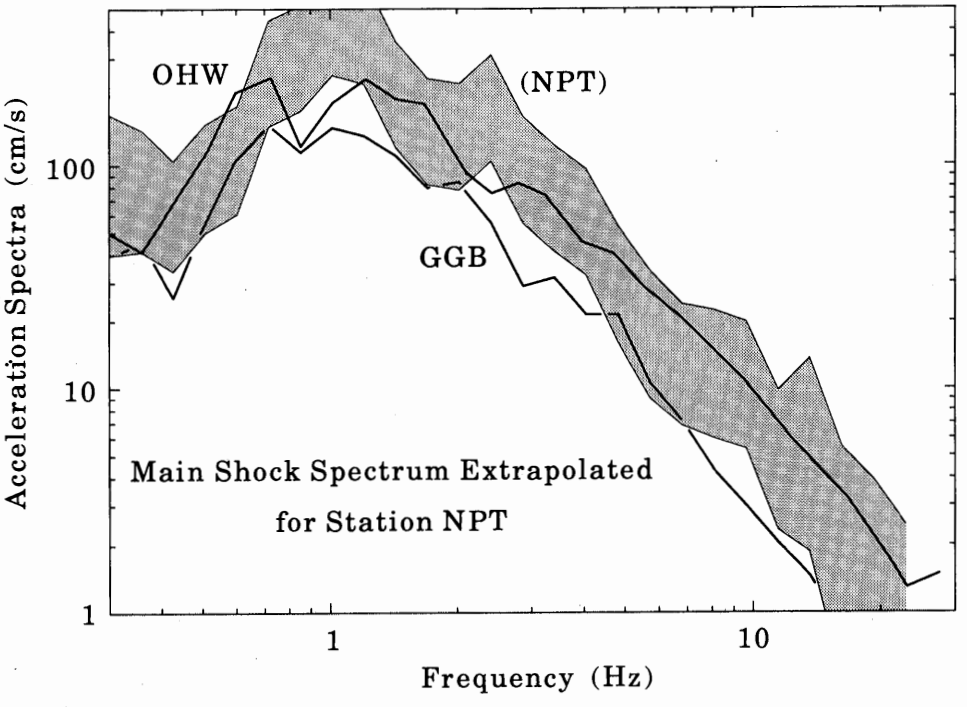


Figure 11.—Extrapolated acceleration spectrum, plotted as 68-percent-confidence interval (shaded area), for main shock at station NPT, compared to acceleration spectra from two accelerograph sites that recorded the main shock. Station GGB is sited on Franciscan serpentine below the Toll Plaza of the Golden Gate Bridge; station OHW is sited on older bay clay and sand at the Outer Harbor Wharf in Oakland. These two stations recorded peak accelerations of 0.25 and 0.29 *g*, respectively.

GGB is a factor of 3 smaller than the extrapolated spectrum for station NPT near 1 Hz, and a factor of 2 smaller at most other frequencies. The spectrum labeled "OHW" was obtained at a station sited on sand and older bay deposits near the Outer Harbor Wharf in Oakland. Station OWH recorded a peak ground acceleration of 0.29 *g*, the largest acceleration of any station north of the San Francisco Airport. The extrapolated spectrum for station NPT exceeds the main-shock spectrum for station OHW at 1 and 2 to 3 Hz; the two spectra are similar at frequencies above 4 Hz.

Although the spectral decomposition does not incorporate the phase information necessary for synthesizing acceleration time histories, the comparison of spectral amplitudes suggests a range ≥0.25 *g* in the extrapolated peak acceleration at station NPT, if the underlying sedimentary deposits responded linearly. This suggested range exceeds all the free-field peak accelerations recorded in San Francisco. Clearly, the assumption of linearity is critical: The extrapolated spectrum should be considered as an upper bound for the main-shock ground motion. The difference between the main-shock spectrum for station OWH and the extrapolated spectrum for station NPT could represent the nonlinearity of the response of the sedimentary deposits below station OHW. Station NPT lies one block outside the 1912 hydraulic fill (see Bonilla, this chapter). The ground settlement in this area was minimal, about 14 mm (Bennett, 1990). It cannot be determined after the fact whether nonlinear sediment response damped the main-shock ground motion near station NPT.

The suggested range in peak acceleration is commensurate, however, with modified Mercalli intensities (MMI's) of VIII and IX (Evernden and Thompson, 1985). An MMI of IX was assigned to the Marina District (Benuska, 1990, p. 69). It is useful to compare the damage in the Marina District with that in the Richmond District, which shares similar architectural styles and construction practices. The peak ground accelerations for the main shock recorded at the nearest stations, sited on undivided sedimentary deposits at Letterman Army Medical Center (0.14 *g*), on dune sand at Veterans' Administration Hospital (0.16 *g*), and on Franciscan serpentine at the Presidio (0.21 *g*), suggest that the peak ground acceleration in the Richmond District, underlain by dune sand, ranged from 0.10 to 0.20 *g*. The MMI assigned to the Richmond District ranged from VI to VII.

Extrapolating main-shock ground motions for areas that sustained ground failure generally overestimates the actual ground motions. Other than the two most northern blocks east of Scott Street, which sustained the largest ground

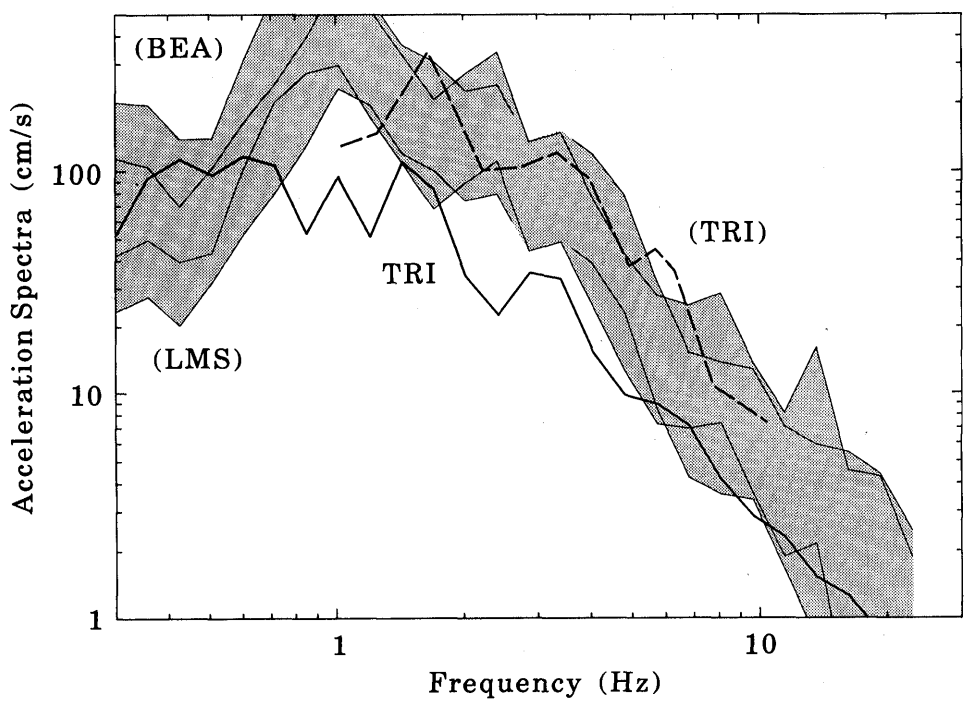


Figure 12.—Extrapolated acceleration spectra, plotted as 68-percent-confidence intervals (shaded area), for two sites within 1912 hydraulic fill, compared to recorded and extrapolated acceleration spectra at station TRI (dashed curve), located on hydraulic fill at Treasure Island. Extrapolation for station TRI was determined from relative amplification of north-south component of motion for seven aftershocks and from main-shock recording at station YBI on Yerba Buena Island. The recorded acceleration spectrum at station TRI is about a factor of 3 less than the extrapolated spectra, a difference due to nonlinearity of ground response.

settlement (Bennett, 1990), the area underlain by the 1912 hydraulic fill was less severely damaged than the blocks to the west and south (see fig. 1). This damage pattern contradicts the uniformity of relative amplification plotted in figure 6, which shows all the central Marina District stations to be similarly amplified in the frequency band 1–5 Hz, suggesting that the ground motions were smaller inside the area underlain by the 1912 hydraulic fill because the ground behaved nonlinearly during the main shock.

The extrapolated spectra for the main-shock ground motions at two stations underlain by the 1912 hydraulic fill in the Marina District are shown in figure 12. As in figures 10 and 11, these extrapolations are plotted using 68-percent-confidence intervals. The spectrum labeled "TRI" was obtained at the station on Treasure Island, which recorded a peak ground acceleration of 0.16 *g* at a site that sustained liquefaction. The dashed curve is an extrapolation of the main-shock spectrum at Treasure Island, obtained by multiplying the amplification at station TRI relative to the Yerba Buena Island station (YBI), determined from recordings of seven aftershocks by Jarpe and others (1990), by the main-shock spectrum at station YBI, according to equation 6.

The extrapolated spectrum for station TRI is similar to those for stations BEA and LMS, particularly at frequencies above 2 Hz. This comparison confirms one hypothesis of Hanks and Brady (1991), who suggested that the similarity of the geometric and geologic relations between stations TRI and YBI and stations CAL and BEA is indicative of a corresponding similarity of the relative amplification between these pairs of stations. We note, however, that the extrapolated spectrum overestimates the recorded spectrum at station TRI by a factor of 3 within the frequency band from 1 to 10 Hz. Hanks and Brady (1991) argued that the accelerogram recorded at station TRI approximates the ground acceleration in the area of the Marina District underlain by the 1912 hydraulic fill, although this assertion cannot be tested.

## CONCLUSIONS

Recordings of aftershocks indicate that weak ground motions in the Marina District were significantly amplified relative to sites in Fort Mason and Pacific Heights within the frequency band from 1 to 5 Hz. This frequency band spans the approximate range in the fundamental frequencies for two- to four-story wood-frame buildings. A one-dimensional model of the sedimentary structure in the Marina District yields an adequate fit to the amplification observed above 2.5 Hz but markedly underestimates the amplification observed from 1 to 2.5 Hz. This "additional" amplification may be associated with focusing of shear waves derived from the three-dimensional shape of the sedimentary basin underlying the Marina District.

The extensive shaking damage in the central part of the Marina District—that is, damage not directly associated with ground failure and liquefaction—suggests that the strong ground motions in parts of the Marina District were amplified during the main shock. Using the relative amplification obtained from aftershock recordings to extrapolate to main-shock spectra for the Marina District yields spectral estimates that exceed the spectra recorded at all other San Francisco sites. Both damage estimates and spectral extrapolations suggest that the peak accelerations in the Marina District reached or exceeded 0.25 *g*. This range is similar to the range of peak accelerations recorded at stations sited on sand and older bay deposits in Emeryville and Oakland (0.25–0.29 *g*).

The liquefaction of the hydraulic fill emplaced in 1912 in the Marina District can be reasonably expected to have attenuated the ground motions on the fill. The peak ground acceleration of 0.16 *g* recorded at Treasure Island, which also sustained liquefaction, appears markedly damped relative to both extrapolations and recordings at stations sited on older bay deposits that did not sustain ground failure. The distribution of damage shown in figure 1 indicates that the blocks to the west of the 1912 hydraulic fill sustained greater damage than the area within the 1912 fill, suggesting that the main-shock accelerations varied spatially within the Marina District. In contrast, there was relatively little variation in amplification of the weaker aftershock motions between the five sites in the central part of the Marina District.

## ACKNOWLEDGMENTS

We are indebted to Robert Bowen, Joseph Machi, David Katz, Al De Martini, the Pacific Union Co., the Heritage House, the Presidio of San Francisco, Jayne Shaeffer of the National Park Service, and Capts. John Herrington, James Groshong, and Douglas Goodin of the San Francisco Fire Department for allowing us to deploy GEOS recorders at the sites necessary to carry out this study. Thomas Hanks organized the deployment of seismographs in the Marina District. Christopher Deitel, Eugene Sembera, James Gibbs, Thomas Hanks, Thomas Noce, and Roger Borcherdt deployed and maintained the instruments, and Gary Glassmoyer was responsible for data playbacks and the consequent organization of the data (Mueller and Glassmoyer, 1990). The accelerograms from stations CAL, RIN, PRS, DIA, TRI, YBI, and OHW were gathered, processed, and distributed by the California Strong Motion Instrumentation Program of the California Division of Mines and Geology. The accelerogram from station GGB was gathered and processed by the National Strong Motion Network of the U.S. Geological Survey in Menlo Park, Calif. William Joyner, Robert Brown, Thomas Hanks, Gary Glassmoyer, Manuel Bonilla, and Tom

O'Rourke provided useful reviews of the manuscript; Carol Sullivan retyped it after the original file had been lost.

## REFERENCES CITED

Andrews, D.J., 1986, Objective determination of source parameters and similarity of earthquakes of different size, *in* Das, Shamita, Boatwright, John, and Scholz, C.H., Earthquake source mechanics: American Geophysical Union Monograph 37 (Maurice Ewing series, v. 6), p. 259–268.

Bennett, M.J., 1990, Ground deformation and liquefaction of soil in the Marina District, chap. D *of* Effects of the Loma Prieta earthquake on the Marina District, San Francisco, California: U.S. Geological Survey Open-File Report 90–253, p. D1–D36.

Benuska, Lee, ed., 1990, Loma Prieta earthquake reconnaissance report: Earthquake Spectra, v. 6, supp. 90–01, 448 p.

Bonamassa, Ornella, and Mueller, C.S., 1989, Source and site-response spectra from aftershock seismograms of the 1987 Whittier Narrows, California, earthquake [abs.]: Seismological Research Letters, v. 59, no. 1, p. 23.

Borcherdt, R.D., Fletcher, J.B., Jensen, E.G., Maxwell, G.L., Vanschaack, J.R., Warrick, R.E., Cranswick, Edward, Johnston, M.J.S., and McClearn, Robert, 1985, A general earthquake-observation system (GEOS): Seismological Society of America Bulletin, v. 75, no. 6, p. 1783–1825.

Evernden, J.F., and Thomson, J.M., 1985, Predicting seismic intensities, *in* Ziony, J.I., ed., Evaluating earthquake hazards in the Los Angeles region—an earth-science perspective: U.S. Geological Survey Professional Paper 1360, p. 151–202.

Fumal, T.E., 1991, Preliminary report on the geology and shear wave velocities at strong motion sites that recorded the Loma Prieta, California, earthquake: U.S. Geological Survey Open-File Report 91–311, 163 p.

Hanks, T.C., and Brady, A.G., 1991, The Loma Prieta earthquake, ground motion, and damage in Oakland, Treasure Island, and San Francisco: Seismological Society of America Bulletin, v. 81, no. 5, p. 2019–2047.

Haskell, N.A., 1960, Crustal reflections of plane *SH* waves: Journal of Geophysical Research, v. 65, no. 12, p. 4147–4150.

International Conference of Building Officials, 1985, Uniform building code: Whittier, Calif., 817 p.

Jarpe, S.P., Hutchings, L.J., Hauk, T.F., and Shakal, A.F., 1990, Selected strong- and weak-motion data from the Loma Prieta earthquake sequence: Seismological Research Letters, v. 60, no. 4, p. 167–176.

Kayen, R.E., Lui, H.-P., Fumal, T.E., Westerlund, R.E., Warrick, R.E., Gibbs, J.F., and Lee, H.J., 1990, Engineering and seismic properties of the soil column at Winfield Scott School, San Francisco, chap. G *of* Effects of the Loma Prieta earthquake on the Marina District, San Francisco, California: U.S. Geological Survey Open-File Report 90–253, p. G1–G18.

Mueller, C.S., and Glassmoyer, Gary, 1990, Digital recordings of aftershocks of the 17 October 1989 Loma Prieta, California, earthquake: U.S. Geological Survey Open-File Report 90–503, 147 p.

THE LOMA PRIETA, CALIFORNIA, EARTHQUAKE OF OCTOBER 17, 1989:
STRONG GROUND MOTION AND GROUND FAILURE

MARINA DISTRICT

# OBSERVATION OF LOCAL SITE EFFECTS AT A DOWNHOLE-AND-SURFACE STATION

By Hsi-Ping Liu, Richard E. Warrick, Robert E. Westerlund, Eugene D. Sembera, and Leif Wennerberg,
U.S. Geological Survey

## CONTENTS

[Figures 11–18 follow references]



## ABSTRACT

After the earthquake, the U.S. Geological Survey drilled a borehole at Winfield Scott School at Beach and Divisadero Streets; the borehole intersected bedrock surface at 79.5-m depth. Two three-component seismometers, one in bedrock at 88-m depth and one located at the surface, were installed at the site; each seismometer consists of one vertical and two orthogonally oriented horizontal geophones with a natural period of 0.5 s. Between August 1990 and January 1991, more than 50 earthquakes were recorded digitally; 8 of these earthquakes, ranging in magnitude from 2.8 to 3.6 and originating on the Calaveras, Franklin, Greenville, and Hayward Faults and on faults parallel and close to the San Andreas Fault, generated seismograms with high signal-to-noise ratios. Horizontal ground-motion amplification, expressed as spectral ratios between ground motions at the surface and in bedrock, was calculated for motions in two orthogonal directions (along Divisadero and Beach Streets), using entire seismograms. Except for the lowest-frequency spectral-ratio peak at about 1 Hz, the frequency of other peaks depends on earthquake location. The earthquakes were divided into two groups, comprising those with epicenters located east and south of San Francisco Bay. Within each group, spectral-ratio peaks from different earthquakes align with each other, thus showing consistency in spectral-ratio peaks as a function of earthquake location. The amplitude of spectral-ratio peaks varies, depending on ground-motion direction and earthquake location; for example, the amplitude of the 1-Hz spectral-ratio peak ranges from 7.2 to 12.7. The surface/downhole spectral ratio therefore provides only partial information on how ground motions are amplified by sedimentary deposits. If we use this ratio for earthquake engineering applications, the ratios for the eight earthquakes indicate the variation in spectral ratio to be expected from earthquakes with similar magnitudes and epicentral distances on various bay-area faults. Also noteworthy are observations that the two horizontal-component seismograms recorded by each seismometer have a similar coda amplitude and duration regardless of earthquake location, and that particle-motion polarization becomes complex shortly after the *P*- and *S*-wave onsets. This complex particle-motion polarization indicates that incident wavefields in the bedrock and at the surface are three dimensional; the bedrock topography underlying the site has been delineated previously to be three dimensional from drill-hole information. We suggest that three-dimensional effects need to be considered when modeling site amplification in the Marina District.

## INTRODUCTION

In comparison with other sites where the effects of near-surface sedimentary deposits on earthquake ground motions have been studied (for example, Seed and Idriss, 1970; Joyner and others, 1976; Johnson and Silva, 1981; Seale and Archuleta, 1989; Blakeslee and Malin, 1991), the

Marina District of San Francisco has several distinguishing features: (1) owing to a combination of liquefaction, differential ground settlement, and ground-motion amplification, extensive damage occurred during the earthquake (U.S. Geological Survey, 1990); (2) the soil column consists of a thick sequence of low-shear-wave-velocity clay and sand with a total depth of 79.5 m overlying bedrock; and (3) the three-dimensional bedrock topography underlying the site has been delineated from drill-hole and other information (Bonilla, 1991; O'Rourke and others, 1991).

After the earthquake, the U.S. Geological Survey (USGS) drilled a borehole (WSS, fig. 1) to 91-m depth on the Winfield Scott School playground at Beach and Divisadero Streets to obtain a detailed stratigraphy of the sedimentary deposits and to install a three-component seismometer below bedrock. Scientists could then study the three-dimensional characteristics of site amplification by comparing seismographic readings recorded below the bedrock with those recorded at the surface.

# METHODS

## SITE CHARACTERIZATION

A detailed description of the geology and history of artificial fill in the Marina District was given by Bonilla (1991). On the basis of borehole data and the assumption that the bedrock surface was shaped by stream erosion, the gross shape of this bedrock surface is inferred to be a half-basin deepening northwestward. Bonilla (1991, fig. 4) showed an east-west cross section of the Marina District intersecting USGS borehole WSS, located on the southwest side of the half-basin axis (lat 37°48′13″ N., long 122°26′30″ W.). Engineering and seismic properties of the soil column at the site were reported by Kayen and others (1990). To summarize, the soil column consists of 4.3 m of filled sand overlying another 3.3 m of natural-sand deposits near the surface. Below these deposits is an interbedded sequence of clayey sand and clay to a depth of 11.6 m interpreted to be the base of Holocene bay clay. A layer of dense sand between 11.6- and 22.9-m depth is characterized by a distinct yellow-brown color and high penetration resistance. The lower 56.6 m of the soil column consists of Pleistocene bay clay overlying hydrothermally altered serpentine bedrock. The shear-wave velocities are 130 m/s for the filled sand, 175 m/s for the natural sand, 145 m/s for the Holocene clay, 285 m/s for the upper section of dense sand, 435 m/s for the lower section of dense sand, and 260 m/s for the Pleistocene bay clay.

## TEST EQUIPMENT

### SEISMOMETERS

The surface seismometer, placed at a distance of 2 m from the borehole, is a Mark Products L–22–3D seismometer consisting of three orthogonally oriented Mark Products L–22D geophones, each with a natural period of 0.5 s. The horizontal components are designated "inline" and "perpendicular." Using a Brunton compass, the "inline" component is measured to orient at azimuth 353° after emplacement. The borehole seismometer, housed in a pressure-tight container, incorporates one verticall and two orthogonally oriented horizontal Mark Products L–22D geophones with the same specifications as those of the surface seismometer. The horizontal components of the borehole seismometer, designated "HG1" and "HG2," are leveled to within 0.1° after emplacement, using an internal gimbal device (Liu and others, 1991). The orientation of component "HG1" is determined to be 205.7±7.2°, using the nearly linearly polarized (linearity, ≥0.94) first-*P*-wave-arrival particle motions of eight earthquakes whose epicen-

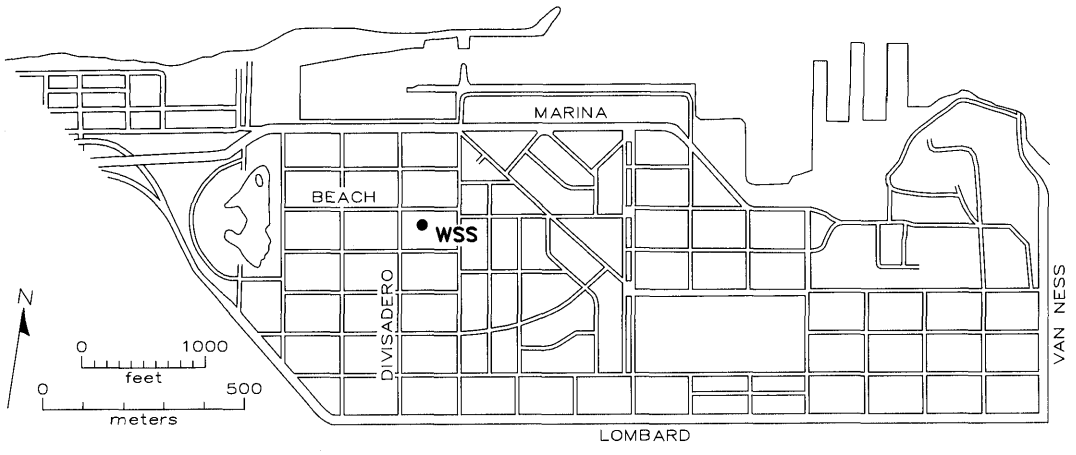


Figure 1.—Marina District of San Francisco, showing location of USGS borehole WSS.

ters were located by the USGS central California network (see supplementary section below entitled "Determination of Borehole Horizontal-Geophone Orientation"). The geophone amplitude and phase responses are calibrated by using the geophone-release test (Asten, 1977) and the phase-ellipse test (Liu and Peselnick, 1986). All geophones are adjusted to 0.7 of critical damping by shunt resistors. The effects on geophone response of the cable linking each seismometer to its recording instrument were analyzed and found to be negligible (Liu and others, 1991).

### RECORDING INSTRUMENT

One General Earthquake Observation System (GEOS) recorder (Borcherdt and others, 1985), set for six-channel digitization using 16-bit analog-to-digital conversion at a rate of 200 samples per second per channel, was used to record the earthquakes; the cutoff frequency of the anti-aliasing filter was set at 100 Hz. The gains were set at 18 dB for the surface seismometer and at 42 dB for the borehole seismometer. To reduce the possibility of false triggering by artificial noise, the recorder was triggered by a horizontal component of the borehole seismometer.

## SPECTRAL COMPUTATION

Horizontal ground-motion amplification, expressed as the spectral ratio between motion at the surface and that in the bedrock, was calculated from seismograms of high signal-to-noise ratio for two orthogonal directions. The spectra used in the spectral-ratio calculations were computed from the entire records, including preevent data. For example, the entire 45-s duration of the records shown in figure 4 was used for spectral computation, applying a fast Fourier transform (FFT) algorithm. One practical reason for using the entire record is that buildings and other structures respond to horizontal ground shaking regardless of wave type; another reason is that, by using the entire seismogram, accurate spectral estimates can be obtained. For low-noise seismograms, and for data windows that begin before the signal onset and end at the end of coda waves, the spectral-leakage problem associated with data truncation does not arise; only the possibility of aliasing error needs to be considered.

Corresponding to a sampling interval of 5 ms, the Nyquist frequency is 100 Hz. As shown by Papoulis (1977), the aliasing error is negligible if the spectral amplitude at frequencies above the Nyquist frequency is negligible in comparison with the peak spectral amplitude. This condition is, indeed, satisfied for all the seismograms analyzed in this report (see fig. 5).

Fluctuations in the FFT spectra were smoothed by using a truncated Gaussian window 0.61 Hz wide; the window decreases in height from 1 at the center to 0.21 at the edge.

# RESULTS

## DATA

Between August 1990 and January 1991, the station was maintained continuously, and more than 50 bay-area earthquakes were recorded during this period.

Seismograms generated by an $M_L$=3.4 earthquake on the San Andreas fault (epicentral distance, 74.2 km; backazimuth, 153.43°) are shown in figure 2. Because this earthquake occurred at 2:24 p.m. P.d.t., the first-*P*-wave-arrival ground motions at the surface seismometer were over-whelmed by artificial noise in the Marina District. In contrast, because surface-wave amplitude decreased exponentially with depth, this artificial noise was reduced considerably at 88-m depth, such that the impulsive first *P*-wave arrival was clearly recorded by the borehole seismometer.

Eight of the recorded earthquakes, however, occurred between 7 p.m. and 7 a.m. P.d.t.; both surface and bedrock ground motions were recorded with a high signal-to-noise ratio. These eight earthquakes, whose epicenters are plotted in figure 3 and whose parameters are listed in table 1, were analyzed for local ground-motion site amplification. Seismograms generated by the $M_L$=3.1 August 25, 1990, Berkeley, Calif., earthquake (2, table 1) are shown in figure 4. For all the seismograms analyzed for site amplification, the spectral amplitude at 50 Hz is negligible in comparison with the peak spectral amplitude. Smoothed FFT spectra of the horizontal-component seismograms in figure 4 are shown in figure 5. Spectral details differ for seismograms generated by different earthquakes. Seismograms generated by the $M_L$=3.0 September 23, 1990, Felt Lake, Calif., earthquake (3, table 1) are shown in figure 6, and smoothed FFT spectra of the horizontal-component seismograms are shown in figure 7. In comparison with the Berkeley earthquake, the Felt Lake earthquake generated higher frequency ground motions.

## SPECTRAL RATIO OF HORIZONTAL MOTIONS ALONG STREET DIRECTIONS

Because building response is strongly influenced by horizontal motions in an earthquake, and because most buildings in the Marina District respond differently to motions parallel and perpendicular to the street to which they front (Celebi, 1990), we calculated spectral ratios of horizontal motions parallel to Divisadero and Beach Streets by using the equation

$$X_s = \frac{\left| (X_{If}/I_{If}) \cos (A_I - A_s) - (X_{Pf}/I_{Pf}) \sin (A_I - A_s) \right|}{\left| (X_{Uf}/I_{Uf}) \cos (A_U - A_s) + (X_{Lf}/I_{Lf}) \sin (A_U - A_A) \right|}$$

where $X_{If}$ and $X_{Pf}$ are the Fourier transforms of the entire inline and perpendicular components, respectively, of the surface seismometer; $X_{Uf}$ and $X_{Lf}$ are the Fourier transforms of components HG1 and HG2, respectively, of the borehole seismometer; $I_{If}$, $I_{Pf}$, $I_{Uf}$, and $I_{Lf}$ are the corresponding geophone responses; and $A_I$, $A_P$, $A_U$, and $A_L$ are the azimuthal directions of positive movement of the geophone coils. For the surface seismometer, $A_I$=353° and $A_P$=083°; and for the borehole seismometer, $A_U$=205.7° and $A_L$=115.7°. The spectral ratio for motions parallel to Divisadero Street is calculated by substituting $A_S$=350.7° in the equation on the previous page, and for motions parallel to Beach Street by substituting $A_S$=080.7°.

The spectral ratios $R_S$ calculated for the eight earthquakes listed in table 1 are plotted in figure 8. The lowest frequency spectral-ratio peak, calculated for all eight earthquakes and for motions parallel to both Beach and Divisadero Streets, occurs coherently at about 1 Hz; the higher frequency spectral-ratio peaks are spread wider apart.

Two spectral ratios, one for motion parallel to Divisadero Street and the other for motion parallel to Beach Street, generated by earthquake 3 in table 1 are compared in figure 9. The peaks generally differ in position and amplitude; for example, both spectral ratios have a peak at 1.0 Hz, but the amplitude is 9.8 for motion parallel to Beach Street and 7.2 for motion parallel to Divisadero Street. The spectral ratios for motions in two orthogonal directions generated by earthquake 7 in table 1 are compared in figure 10.

The spectral ratios for motions generated by earthquakes 1 and 5 in table 1, which occurred close to each other on the Calaveras Fault (see fig. 3), are compared in figure 11. The spectral ratios for motion parallel to Beach Street (fig.

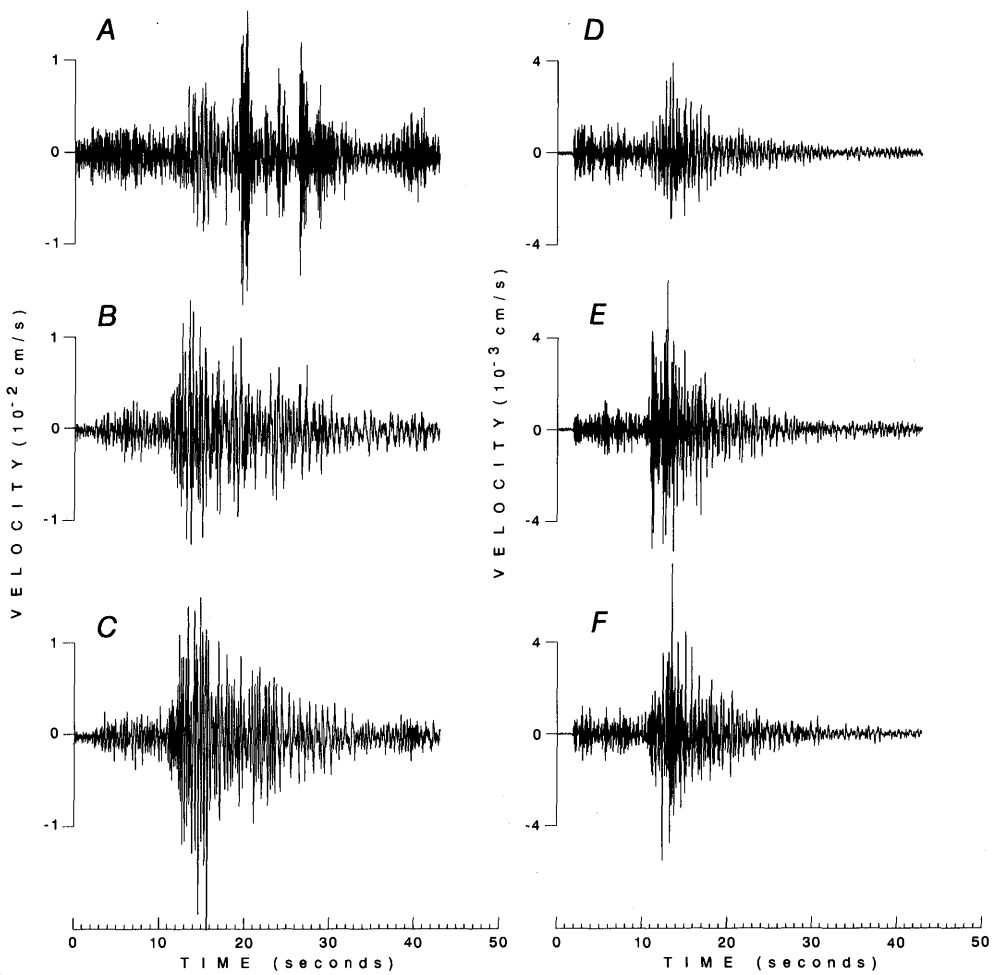


Figure 2.—Seismograms generated by an earthquake ($M_L$=3.4) on the San Andreas Fault and recorded by vertical component (*A*), inline horizontal component (*B*), and perpendicular horizontal component (*C*) of surface seismometer and by vertical component (*D*), horizontal component HG1 (*E*), and horizontal component HG2 (*F*) of borehole seismometer. Earthquake parameters: origin time, 1990:234:2124:5.62 G.m.t.; focal depth, 11.69 km; epicenter, lat 37°12.4′ N., long 122°4.01′ W.; epicentral distance, 74.2 km; backazimuth, 153.43°.

Table 1.—*1990 earthquakes used in analysis*

[Backazimuth is the angle measured from north to the line connecting the seismometer station and earthquake epicenter]

| Earthquake | Julian day | Time (G.m.t.) | Latitude (° N.) | Longitude (° W.) | Epicentral distance (km) | Backazimuth (°) | Depth (km) | $M_L$ | Fault |
|---|---|---|---|---|---|---|---|---|---|
| 1 | 229 | 0226: 16.77 | 37.293 | -121.665 | 89.1 | 129.46 | 7.2 | 3.6 | Calaveras |
| 2 | 237 | 1147: 29.71 | 37.873 | -122.230 | 20.1 | 067.17 | 8.7 | 3.1 | Hayward |
| 3 | 266 | 1335: 47.15 | 37.375 | -122.187 | 52.7 | 154.76 | 7.9 | 3.0 | Near San Andreas |
| 4 | 278 | 0604: 17.74 | 37.071 | -122.019 | 89.7 | 155.29 | 12.0 | 3.4 | Near San Andreas |
| 5 | 282 | 0413: 29.79 | 37.278 | -121.649 | 91.2 | 129.68 | 8.8 | 2.8 | Calaveras |
| 6 | 283 | 0659: 31.66 | 37.807 | -121.761 | 59.9 | 089.48 | 15.8 | 3.0 | Greenville |
| 7 | 287 | 0206: 20.98 | 38.050 | -122.233 | 33.0 | 033.86 | 12.0 | 3.3 | Franklin |
| 8 | 292 | 0208: 51.99 | 37.975 | -122.337 | 21.0 | 025.07 | 6.1 | 2.8 | Hayward |

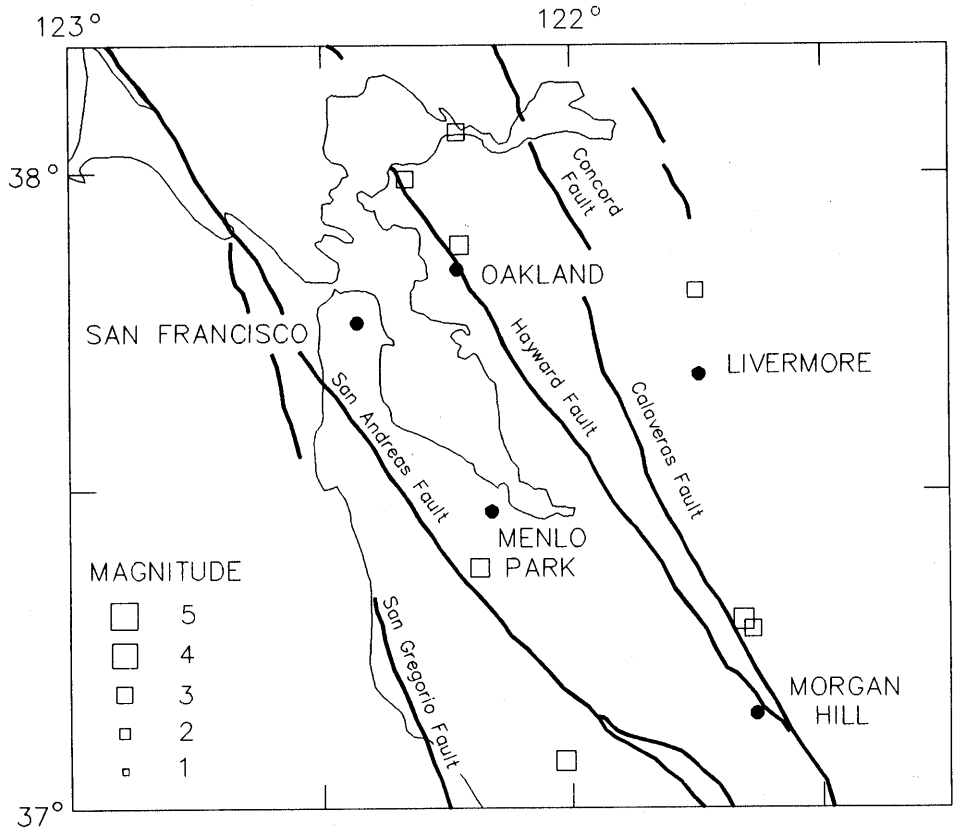


Figure 3.—Sketch map of San Francisco Bay area, showing locations of major faults and epicenters of earthquakes listed in table 1 (squares). Four earthquakes south of Menlo Park are grouped as "south bay"; other four earthquakes are grouped as "east bay."

11*B*) agree fairly well with each other, in that the first three major peaks at 1.0, 2.7, and 3.5 Hz are similar in amplitude; the agreement is less satisfactory for motions parallel to Divisadero Street (fig. 11*A*). Two spectral-ratio peaks, at 3.9 and 4.9 Hz, in response to the $M_L$=2.8 earthquake are missing from the spectral ratio in response to the $M_L$=3.6 earthquake; this discrepancy can be traced to differences in the spectra of the inline component of the surface seismometer, as shown in figure 12*A*. (The inline component of the surface seismometer, oriented at azimuth 353°, is nearly parallel to the orientation of Divisadero Street at azimuth 350.7°.) Smoothed FFT spectra of the perpendicular component of the surface seismometer, and of the two horizontal components of the borehole seismometer, generated by these two earthquakes are shown in figures 12*B* through 12*D*.

The eight earthquakes listed in table 1 can be divided into two groups by backazimuth. The four earthquakes (2, 6, 7, 8) whose backazimuths range from 025.07° to 089.48° can be grouped as "east bay" earthquakes; the other four earthquakes, whose backazimuths range from 129.46° to 155.29°, can be grouped as "south bay" earthquakes (see fig. 3). The epicentral distances of the south-bay earthquakes range from 20.1 to 59.9 km, and those of the east-bay earthquakes from 52.7 to 89.7 km. Spectral ratios in response to the four east-bay earthquakes are plotted in figures 13*A* and 13*B*. In contrast to figure 8, the second-lowest-frequency peak becomes coherent at 2.2 Hz for motions parallel to Divisadero Street (fig. 13*A*); and for motions parallel to Beach Street, the second- and third-lowest-frequency peaks become coherent at 2.4 and 3.4 Hz, respectively. In the plots of spectral ratios in response

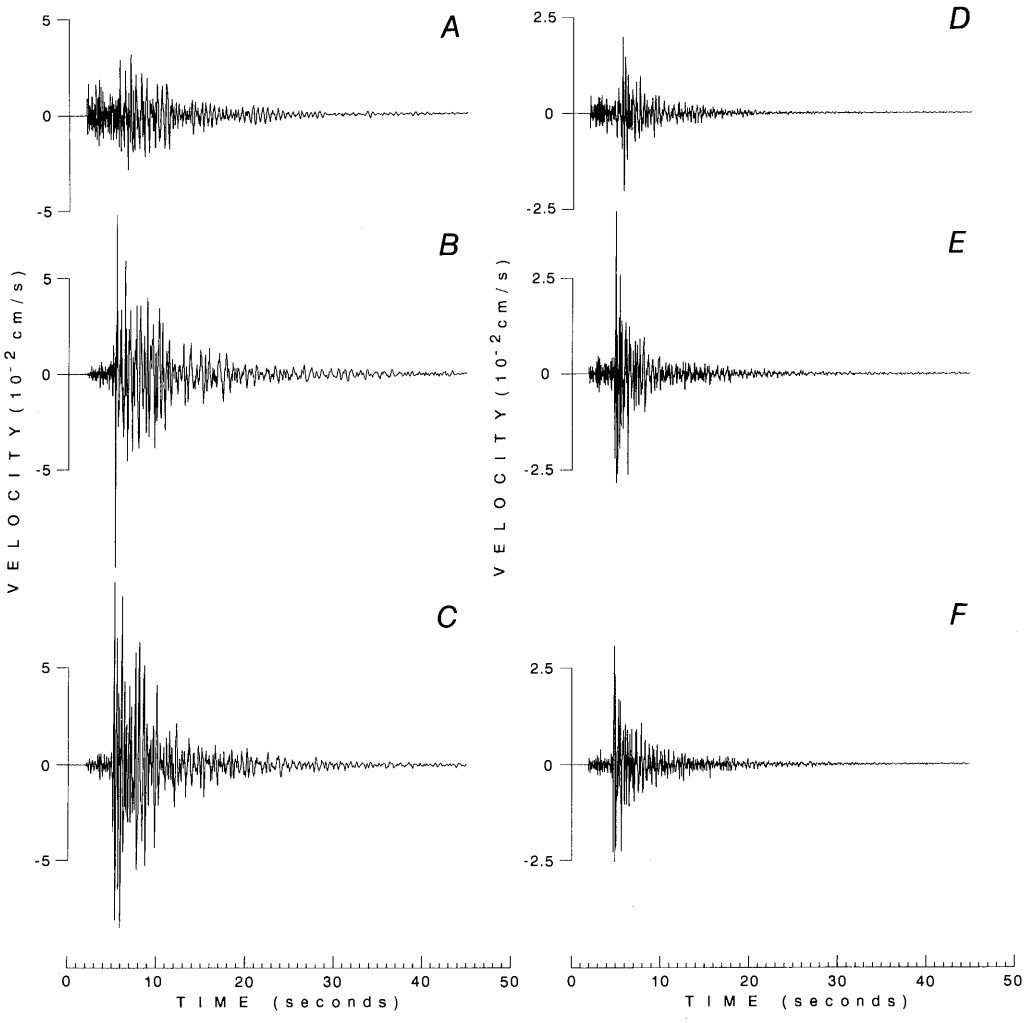


Figure 4.—Seismograms generated by August 25, 1990, Berkeley, Calif., earthquake ($M_L$=3.1), recorded by vertical component (*A*), inline horizontal component (*B*), and perpendicular horizontal component (*C*) of surface seismometer, and by vertical component (*D*), horizontal component HG1 (*E*), and horizontal component HG2 (*F*) of borehole seismometer. Earthquake parameters: origin time, 1990:237:1147:29.71 G.m.t.; focal depth, 8.72 km; epicenter, lat 37°52.42′ N., long 122°13.78′ W.; epicentral distance, 20.06 km; backazimuth, 067.17°.

to the four south-bay earthquakes (figs. 13*C*, 13*D*), the second-lowest-frequency peak becomes coherent at 2.7 Hz for motions parallel to Beach Street (fig. 13*D*). The locations and amplitudes of spectral-ratio peaks in response to an east-bay earthquake (fig. 10) and a south-bay earthquake (fig. 9) are listed in tables 2 and 3, respectively.

## PARTICLE MOTIONS

Comparison of two surface or downhole horizontal-component seismograms generated by any one of the eight earthquakes listed in table 1 (figs. 4*B* and 4*C*, 4*E* and 4*F*, 6*A* and 6*B*, and 6*C* and 6*D*) indicates that the two seismograms have similar coda amplitude and duration, an observation that holds true regardless of earthquake location. A reasonable conjecture for this similarity is that, in propagating from earthquake source to receiver, wave motions are randomized considerably by multiple reflections and scattering. To investigate this conjecture, surface particle motions, projected onto a horizontal plane as constructed from the horizontal-component seismograms in figures 4*B* and 4*C*, are plotted for successive 3-s intervals in figure 14. The first *P*-wave arrival (1, fig. 14*A*) is linearly polarized and aligns to within 011° of the earthquake backazimuth; however, this linear polarization is lost after half a cycle. Particle motions of the onset of a large-amplitude secondary arrival (fig. 14*B*), presumably of shear waves, are nearly linearly polarized and at an angle of about 117° to the earthquake backazimuth; again, linearity of secondary-arrival particle motions is lost after half a cycle. The other two particle-motion plots (figs. 14*C*, 14*D*) show an inconsistency in particle-motion polarization. Similar observations of short-period *P* waves propagating in the shallow crust of the Adirondack Mountains in New York State were reported by Menke and Lerner-Lam (1991).

## DISCUSSION AND CONCLUSIONS

Horizontal ground-motion amplification, expressed as the spectral ratio between motion at the surface and that directly below in the bedrock, $X_{2f}/X_{1f}$, was calculated for ground motions in two orthogonal directions, using entire seismograms. One reason for using the entire seismogram is that structures respond to all horizontal ground motions, regardless of wave type. As shown in figure 8, these spectral ratios are generally greater than 1 in the frequency interval of interest (0.5–20 Hz). The observed spectral ratios, however, provide only partial information on how ground motions are amplified by sedimentary deposits, as evidenced by variation in these ratios. For example, although the location of the lowest frequency spectral-ratio peak (at approx 1 Hz) is common to motions in two orthogonal directions (parallel to Divisadero and Beach Streets, respectively), its amplitude ranges from 7.2 to 12.7. At higher frequencies, $X_{2f}/X_{1f}$ depends on direction of ground motion as well as earthquake location. An analogy with a causal system in which $X_{1f}$ is the input, $X_{2f}$ is the

Table 2.—*Spectral-ratio peaks (below 10 Hz) in response to an east-bay ($M_L$=3.3 October 14, 1990, Martinez, Calif.) earthquake*

[Directions of motion: B, parallel to Beach Street; D, parallel to Divisadero Street]

| Direction of motion | Peak location (Hz) | Peak spectral-ratio amplitude |
|---|---|---|
| B | 0.92 | 7.8 |
| D | 1.09 | 10.6 |
| D | 2.23 | 6.8 |
| B | 2.51 | 6.1 |
| D | 2.94 | 4.7 |
| B | 3.41 | 6.9 |
| D | 3.64 | 5.3 |
| B | 4.39 | 3.2 |
| D | 5.03 | 2.9 |
| B | 5.97 | 3.5 |
| D | 6.68 | 1.6 |
| D | 7.42 | 2.4 |
| D | 8.64 | 2.8 |
| D | 9.48 | 3.8 |
| B | 9.57 | 3.3 |

Table 3.—*Spectral-ratio peaks (below 10 Hz) in response to a south-bay ($M_L$=3.0 September 23, 1990, Felt Lake, Calif.) earthquake*

[Directions of motion: B, parallel to Beach Street; D, parallel to Divisadero Street]

| Direction of motion | Peak location (Hz) | Peak spectral-ratio amplitude |
|---|---|---|
| D | 0.96 | 7.2 |
| B | .98 | 9.8 |
| D | 1.78 | 7.5 |
| D | 2.37 | 7.5 |
| B | 2.70 | 8.5 |
| D | 2.98 | 6.0 |
| D | 3.67 | 4.5 |
| B | 3.72 | 10.0 |
| B | 4.88 | 5.8 |
| D | 5.00 | 6.6 |
| B | 5.86 | 2.5 |
| D | 6.02 | 3.6 |
| B | 6.97 | 2.4 |
| D | 7.53 | 2.8 |
| B | 8.53 | 1.9 |
| D | 8.83 | 6.7 |
| D | 9.63 | 4.4 |
| B | 9.78 | 2.7 |

output, and $H_f = X_{2f}/X_{1f}$ is the system transfer function of the sedimentary deposits cannot be made because (1) upgoing as well as downgoing waves were recorded by the borehole seismometer, and only upgoing waves can be considered as input when investigating how site amplification is affected by sedimentary deposits overlying bedrock; (2) entire seismograms were used for spectral-ratio calculation, and some phases recorded by the surface seismometer—for example, higher frequency surface waves—may not be causally related to wave motions recorded by the borehole seismometer; and (3) the bedrock surface is curved, and so the input excitation must be characterized by bedrock motion at more than one point.

Boatwright and others (1991) calculated a model one-dimensional site amplification, using the shear-wave velocities determined at USGS borehole WSS by Kayen and others (1990), and estimated the shear-wave velocities of bedrock, as well as the density and shear-wave-absorption parameters of sedimentary deposits and bedrock. Their results agree qualitatively with our observations; in particular, the lowest frequency spectral-ratio peak is located at about 1 Hz.

The most interesting result of our study is establishment of the dependence of spectral ratio on earthquake location (fig. 13). Specifically, the coherency of some spectral-ratio peaks from different earthquakes is markedly improved when the earthquakes are broadly separated into two groups, east bay and south bay, in spite of the difference in epicentral distances within each group. (For example, the epicentral distances of the four east-bay earthquakes 2, 6, 7, and 8 are 20.1, 59.9, 33.0, and 21.0 km, respectively.) Other evidence that indicates an independence of spectral-ratio peaks from epicentral distance is shown in figure 15, which compares the spectral-ratio peaks of a south-bay earthquake (3, table 1; epicentral distance, 52.7 km) with those of an east-bay earthquake with a similar epicentral distance (6, table 1; epicentral distance, 59.9 km): The second- and third-lowest-frequency peaks from these two earthquakes do not align with each other.

Another significant result of our study is that the amplitude of spectral-ratio peaks varies with ground-motion direction. The surface/downhole spectral ratio therefore provides only partial information on how ground motions are amplified by sedimentary deposits. The spectral ratios from these eight earthquakes also indicate the variation in ground-motion amplification to be expected from earthquakes with similar magnitudes and epicentral distances on various bay-area faults.

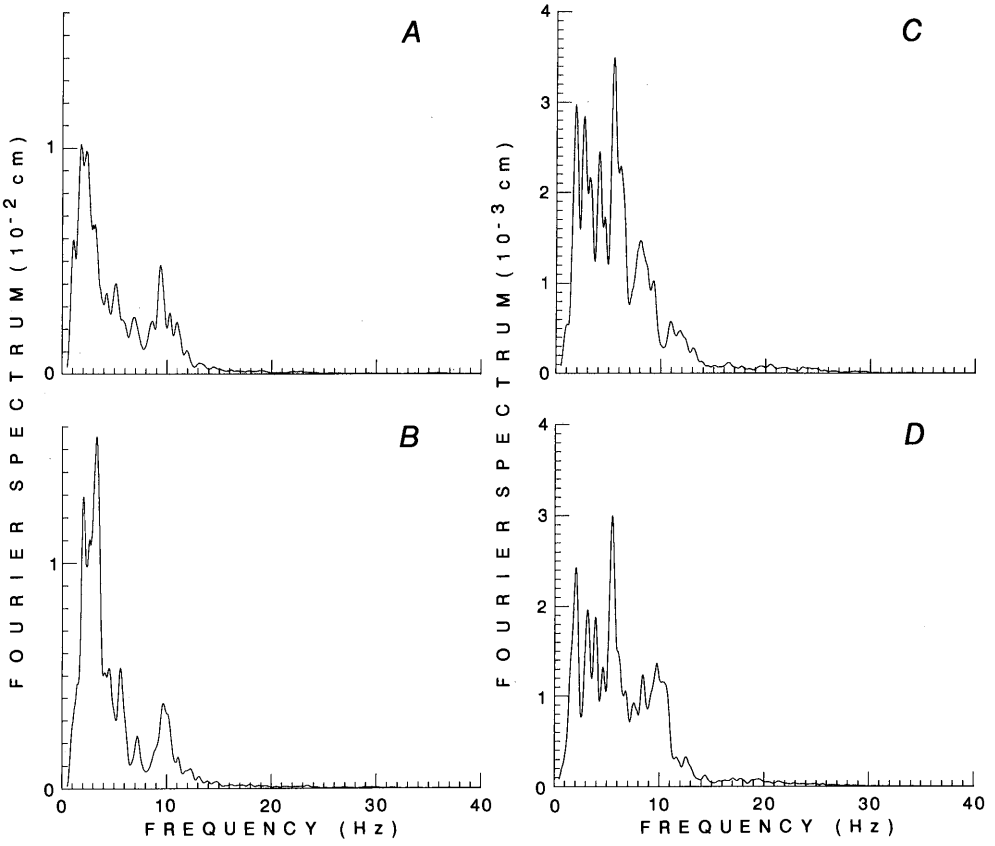


Figure 5.—Smoothed FFT spectra of horizontal-component seismograms in figure 4 for inline (*A*), and perpendicular (*B*) components of surface seismometer, and for components HG1 (*C*) and HG2 (*D*) of borehole seismometer. Spectral amplitude at 50 Hz is negligible in comparison with peak value in each plot.

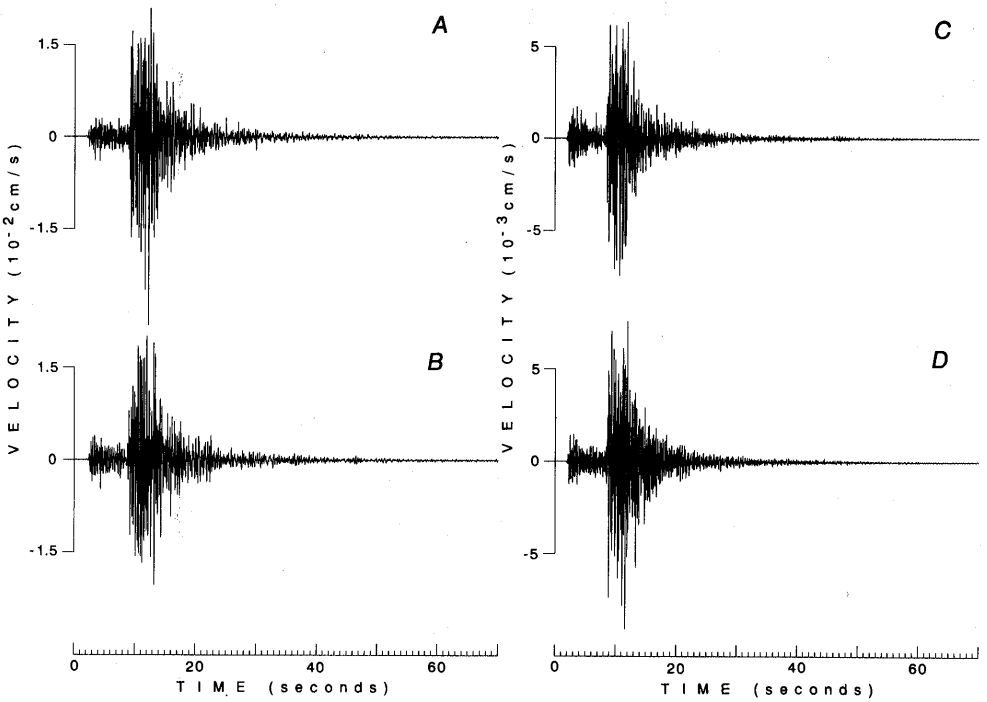


Figure 6.—Seismograms generated by September 23, 1990, Felt Lake, Calif., earthquake ($M_L$=3.0), as recorded by inline horizontal component (*A*), and perpendicular horizontal component (*B*) of surface seismometer, and by horizontal components HG1 (*C*) and HG2 (*D*) of borehole seismometer. Earthquake parameters: origin time, 1990:266:1335:47.15 G.m.t.; focal depth, 7.88 km; epicenter, lat 37°22.50′ N., long 122°11.23′ W.; epicentral distance, 52.71 km; backazimuth, 154.76°.

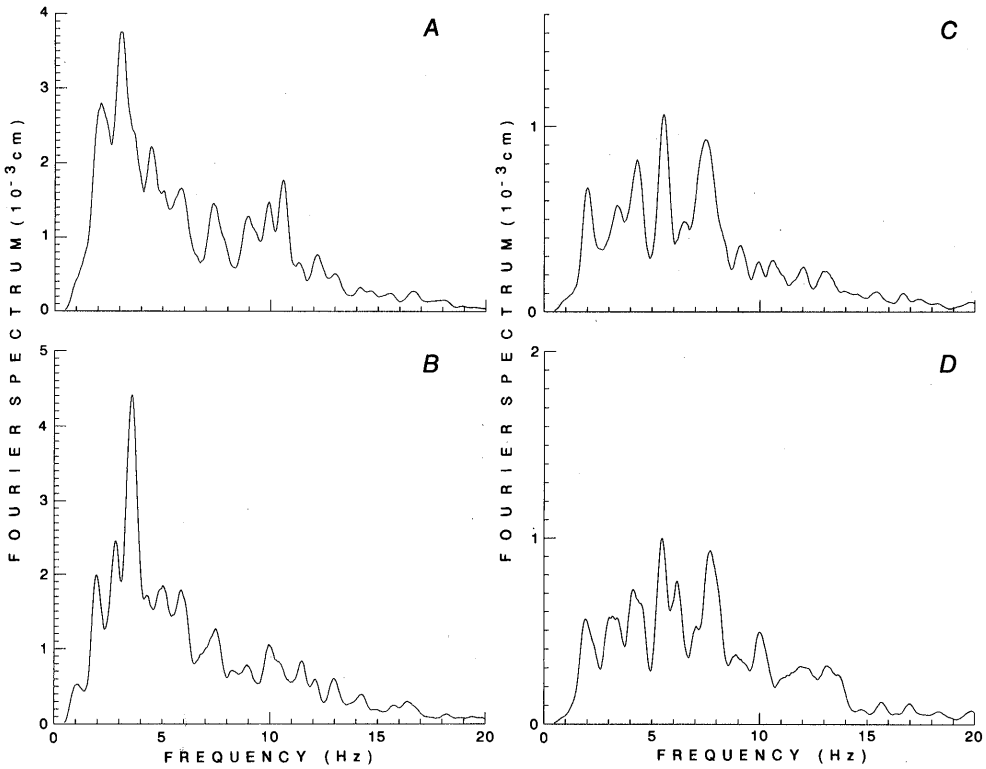


Figure 7.—Smoothed FFT spectra of horizontal-component seismograms in figure 6 for inline (*A*), and perpendicular (*B*) components of surface seismometer, and for components HG1 (*C*) and HG2 (*D*) of borehole seismometer.

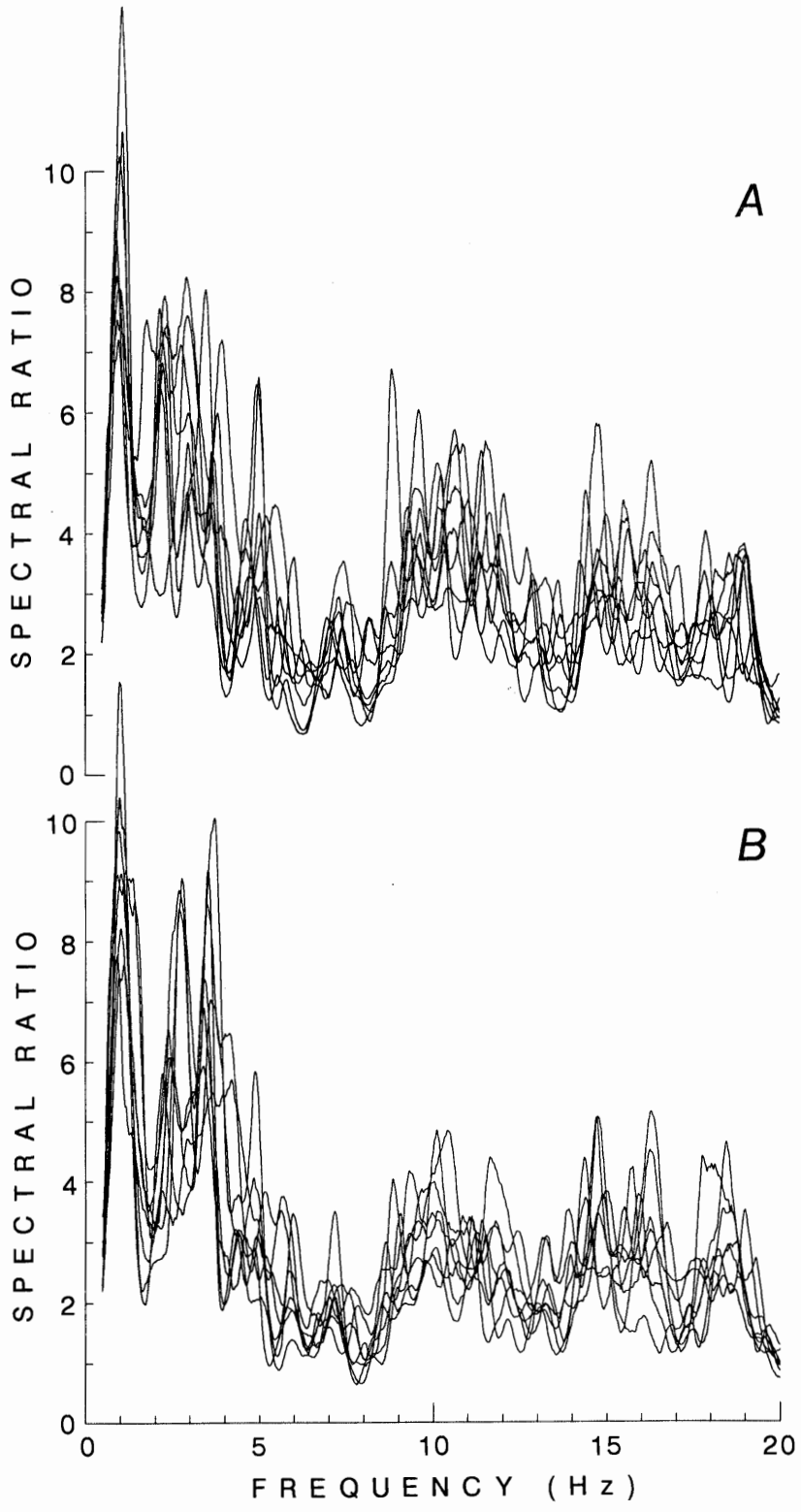


Figure 8.—Spectral ratios of horizontal motions at surface to those in bedrock in direction parallel to Divisadero Street (*A*) and Beach Street (*B*), calculated for eight earthquakes listed in table 1.

The observation that particle-motion polarization changes from linear to complex shortly after *P*- and *S*-wave onsets indicates that the incident wavefields in the bedrock and at the surface are three dimensional. The bedrock topography underlying the site has been delineated previously to be three dimensional from drill-hole information (Bonilla, 1991; O'Rourke and others, 1991). We suggest that such three-dimensional effects need to be considered when modeling site amplification in the Marina District.

To evaluate further the influence of bedrock topography on site response, we calculated spectral ratios for orthogonal-motion components parallel to the major and minor axes of the bedrock basin underlying the site using Bonilla's (1991) map. A notable difference in these results from those calculated for motions parallel to the street grid is that for a component of motion parallel to the major axis of the bedrock basin, spectral-ratio peaks are higher. Otherwise, the results (figs. 16, 17) are similar to those calculated for components of motion parallel to the main street-grid directions, in that except for the lowest frequency peak at about 1 Hz, the frequency of other peaks depends on earthquake location, and for east- or south-bay earthquakes, spectral-ratio peaks from different earthquakes align with each other. A quantitative understanding of the influence of bedrock topography on site amplification requires further numeric modeling.

The ground motions that generated the spectral ratios calculated in this study were small (peak acceleration, approx 0.002 *g*). Soil nonlinear effects, especially those associated with damping and shear-modulus degradation of Holocene bay clay and liquefaction in sand, are outside the scope of this report.

## ACKNOWLEDGMENTS

We thank Thomas Sammon and Claudia C. Jeung of the San Francisco Unified School District, who facilitated our work at Winfield Scott School; F.W. Lester, who provided us with the earthquake parameters determined by the U.S. Geological Survey's central California seismic network; and J.C. Savage, for helpful discussions.

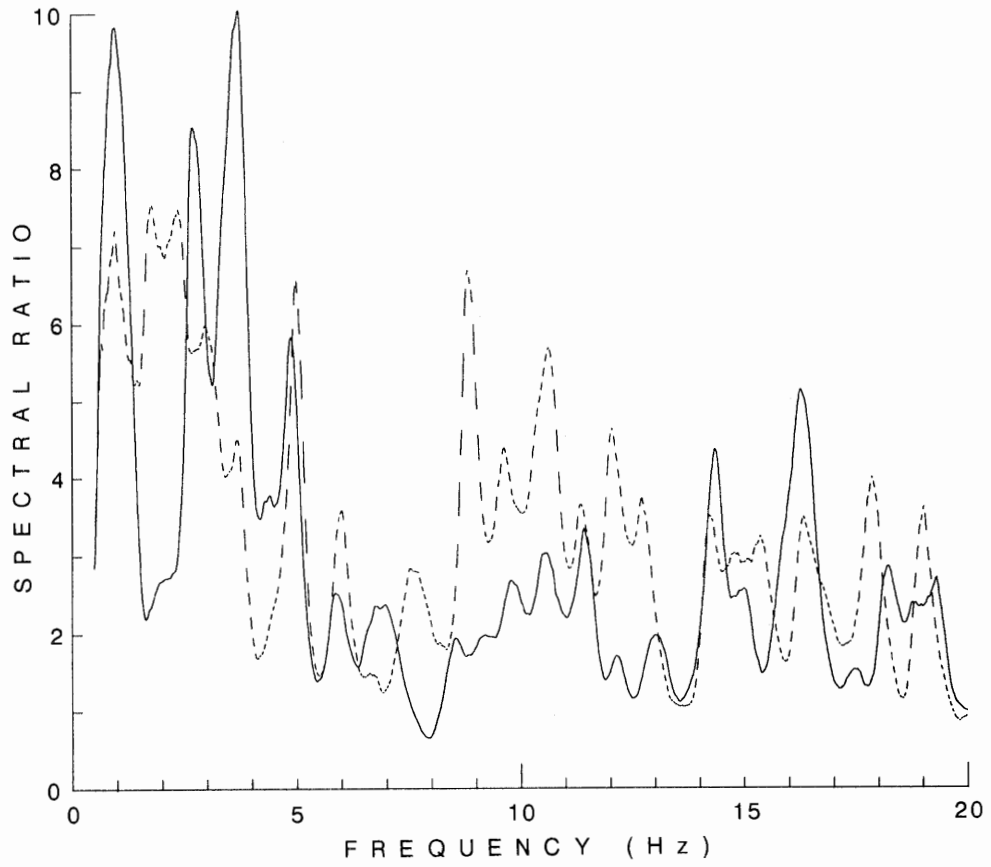


Figure 9.—Site response for motions parallel to Divisadero Street (dashed curve) and Beach Street (solid curve) generated by September 23, 1990, Felt Lake, Calif., earthquake ($M_L$=3.0). See figure 6 for seismograms.

## SUPPLEMENTARY INFORMATION: DETERMINATION OF BOREHOLE HORIZONTAL-GEOPHONE ORIENTATION

The orientation of the surface horizontal geophone was determined with a Brunton compass. Because no remote-reading compass was included in the borehole-seismometer package, the orientation of its horizontal geophones must be inferred indirectly. Using the nearly linearly polarized (linearity, ≥0.94) first-*P*-wave-arrival particle motions of eight earthquakes whose epicenters were located by the USGS' central California network, the orientation of horizontal component HG1 is determined to be 205.7±7.2°. Three criteria were used in selecting seismograms for borehole horizontal-geophone orientation: (1) the first-*P*-wave-arrival motion must be recorded with high signal-to-noise ratio, (2) the first half-cycle of first-*P*-wave-arrival particle motion must be nearly linearly polarized, and (3) the epicenter distribution of earthquakes that generated the seismograms should cover a wide range of backazimuths. The eight earthquakes used for borehole horizontal-geophone orientation are listed in table 4; four of these earthquakes are also listed in table 1. Following Aster and Shearer (1991) and using the variance-tensor method, we fit an ellipse to the first half-cycle of *P*-wave-arrival particle motions projected onto the horizontal plane. Orientations of the horizontal-component geophones can be determined to within ±180° if we assume that the semimajor axis of the ellipse aligns with the backazimuth. The ambiguity of 180° arises because it cannot be determined whether the first-*P*-wave-arrival motion is away from or toward the source by studying only borehole-seismometer data. Using seismograms recorded by the surface seismometer, the sense of the first-*P*-wave-arrival motion can be ascertained, thus eliminating this ambiguity. By averaging the results obtained from earthquakes whose epicenters cover a wide range of backazimuths, Aster and Shearer (1991) were able to determine the horizontal-geophone orientation of a surface seismometer in the San Jacinto fault zone to within 5.7°. (Because of the high surface noise in a city environment, we were unable to conduct a similar test on our surface seismometer.) To assess the uncertainty in the borehole horizontal-geophone orientation on spectral-ratio calculations, some

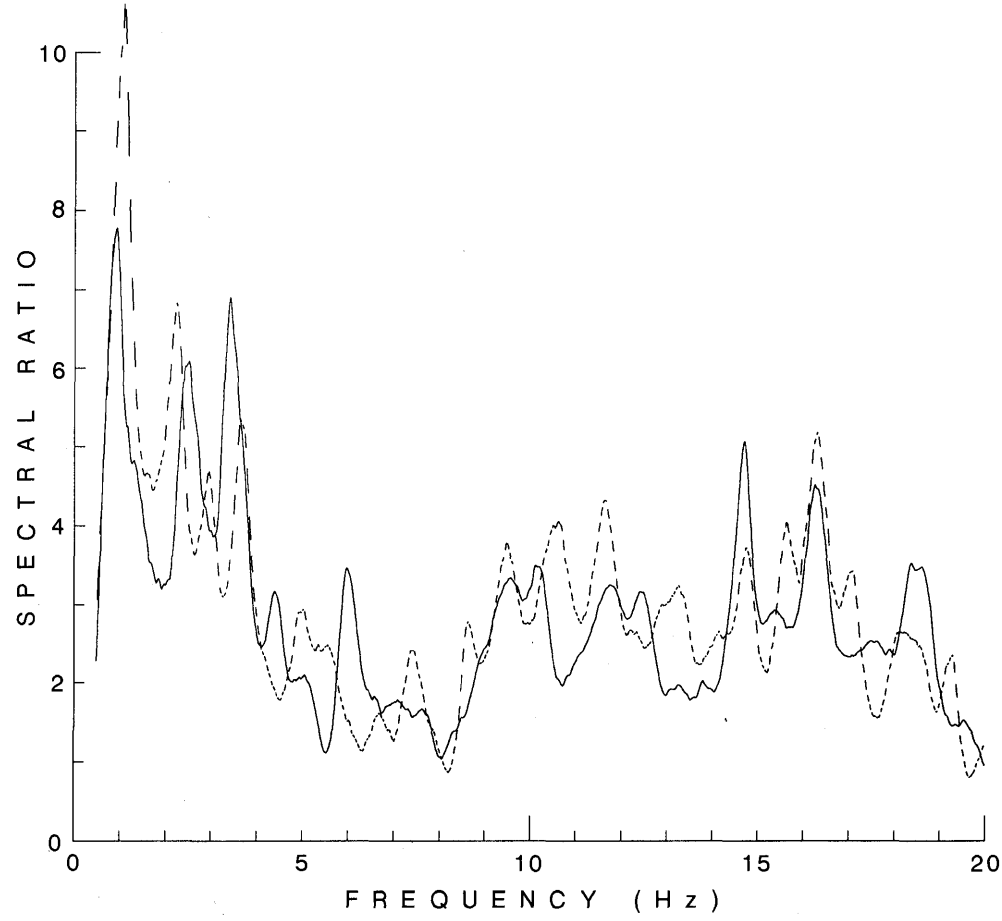


Figure 10.—Site response for motions parallel to Divisadero Street (dashed curve) and Beach Street (solid curve) generated by October 14, 1990, Martinez, Calif., earthquake ($M_L$=3.3) (earthquake 7, table 1).

Table 4.—*1990 earthquakes used in orienting borehole horizontal-component geophones*

[Backazimuth is the angle measured from north to the line connecting the seismometer station and earthquake epicenter]

| Julian day | Time (G.m.t.) | Latitude (° N.) | Longitude (° W.) | Epicentral Distance (km) | Back-azimuth (°) | Depth (km) | $M_L$ |
|---|---|---|---|---|---|---|---|
| 234 | 2124: 05.62 | 37.207 | -122.067 | 74.2 | 153.43 | 11.7 | 3.4 (Los Gatos) |
| 237 | 1147: 29.71 | 37.873 | -122.230 | 20.1 | 067.17 | 8.7 | 3.1 (Berkeley) |
| 266 | 0354: 06.32 | 37.872 | -122.221 | 20.8 | 068.43 | 11.0 | 2.1 (Berkeley) |
| 266 | 1335: 47.15 | 37.375 | -122.187 | 52.7 | 154.76 | 7.9 | 3.0 (Felt Lake) |
| 283 | 0659: 31.66 | 37.807 | -121.761 | 59.9 | 089.48 | 15.8 | 3.0 (N. of Liver-more) |
| 292 | 0208: 51.99 | 37.975 | -122.337 | 21.0 | 025.07 | 6.1 | 2.8 (San Pablo) |
| 297 | 0615: 18.06 | 38.056 | -119.128 | 292.3 | 083.46 | 13.0 | 5.7 (Mono Lake) |
| 355 | 1929: 53.82 | 37.763 | -122.562 | 11.4 | -113.54 | 11.4 | 1.7 (W. of Golden Gate Park) |

of the results plotted in figure 11 were calculated again for $A_U$=198.5° and $A_U$=212.9°. The results (fig. 18) show that such uncertainty mainly affects the amplitude, not the position, of spectral-ratio peaks.

## REFERENCES CITED


Asten, M.W., 1977, Theory and practice of geophone calibration in-situ using a modified step method: Institute of Electrical and Electronic Engineers Transactions on Geoscience Electronics, v. GE–15, no. 4, p. 208–214.

Aster, R.C., and Shearer, P.M., 1991, High-frequency borehole seismograms recorded in the San Jacinto fault zone, southern California: Seismological Society of America Bulletin, v. 81, no. 4, p. 1057–1100.

Blakeslee, Sam, and Malin, Peter, 1991, High-frequency site effects at two Parkfield downhole and surface stations: Seismological Society of America Bulletin, v. 81, no. 2, p. 332–345.

Boatwright, John, Fumal, T.E., Liu, H.-P., Mueller, C.S., and Seekins, L.C., 1991, Ground motion amplification in the Marina District: Seismological Society of America Bulletin, v. 81, no. 5, p. 1980–1997.

Bonilla, M.G., 1991, Geology and historical development of the Marina District, San Francisco, California: Seismological Society of America Bulletin, v. 81, no. 5, p. 1958–1979.

Borcherdt, R.D., Fletcher, J.B., Jensen, E.G., Maxwell, G.L., VanSchaack, J.R., Warrick, R.E., Cranswick, Edward, Johnston, M.J.S., and McClearn, Robert, 1985, A general earthquake-observation system (GEOS): Seismological Society of America Bulletin, v. 75, no. 6, p. 1783–1825.

Celebi, Mehmet, 1990, Types of structural damage, chap. B *of* Effects of the Loma Prieta earthquake on the Marina District, San Francisco, California: U.S. Geological Society Open-File Report 90–253, p. B1–B6.

Johnson, L.R., and Silva, Walt, 1981, Effects of unconsolidated sediments upon the ground motion during local earthquakes: Seismological Society of America Bulletin, v. 71, no. 1, p. 127–142.

Joyner, W.B., Warrick, R.E., and Oliver, A.A., 1976, Analysis of seismograms from a downhole array in sediments near San Francisco Bay: Seismological Society of America Bulletin, v. 66, no. 3, p. 937–958.

Kayen, R.E., Liu, H.-P., Fumal, T.E., Westerlund, R.E., Warrick, R.E., Gibbs, J.F., and Lee, H.J., 1990, Engineering and seismic properties of the soil column at Winfield Scott School, San Francisco, chap. G *of* Effects of the Loma Prieta earthquake on the Marina District, San Francisco, California: U.S. Geological Survey Open-File Report 90–253, p. G1–G18.

Liu, H.-P., and Peselnick, Louis, 1986, Improved phase-ellipse method for in situ geophone calibration: Geophysical Prospecting, v. 34, no. 4, p. 537–544.

Liu, H.-P., Warrick, R.E., Westerlund, R.E., and Fletcher, J.B., 1991, A three-component borehole seismometer for earthquake seismology: Seismological Society of America Bulletin, v. 81, no. 6, p. 2458–2485.

Menke, William, and Lerner-Lam, Arthur, 1991, Observations of the transition from linear polarization to complex polarization in short-period compressional waves: Seismological Society of America Bulletin, v. 81, no. 2, p. 611–621.

O'Rourke, T.D., Gowdy, T.E., Stewart, H.E., and Pease, J.W., 1991, Life line and geotechnical aspects of the 1989 Loma Prieta earthquake: International Conference on Recent Advances in Geotechnical Engineering and Soil Dynamics, 2d, St. Louis, Mo., 1991, Proceedings, v. 2, p. 1601–1612.

Papoulis, Athanasios, 1977, Signal analysis: New York, McGraw-Hill, 431 p.

Seale, S.H., and Archuleta, R.J., 1989, Site amplification and attenuation of strong ground motion: Seismological Society of America Bulletin, v. 79, no. 6, p. 1673–1696.

Seed, H.B., and Idriss, I.M., 1970, Analyses of ground motions at Union Bay, Seattle, during the earthquakes and distant nuclear blasts: Seismological Society of America Bulletin, v. 60, no. 1, p. 125–136.

U.S. Geological Survey, 1990, Effects of the Loma Prieta earthquake on the Marina District, San Francisco, California: Open-File Report 90–253.

# FIGURES 11–18

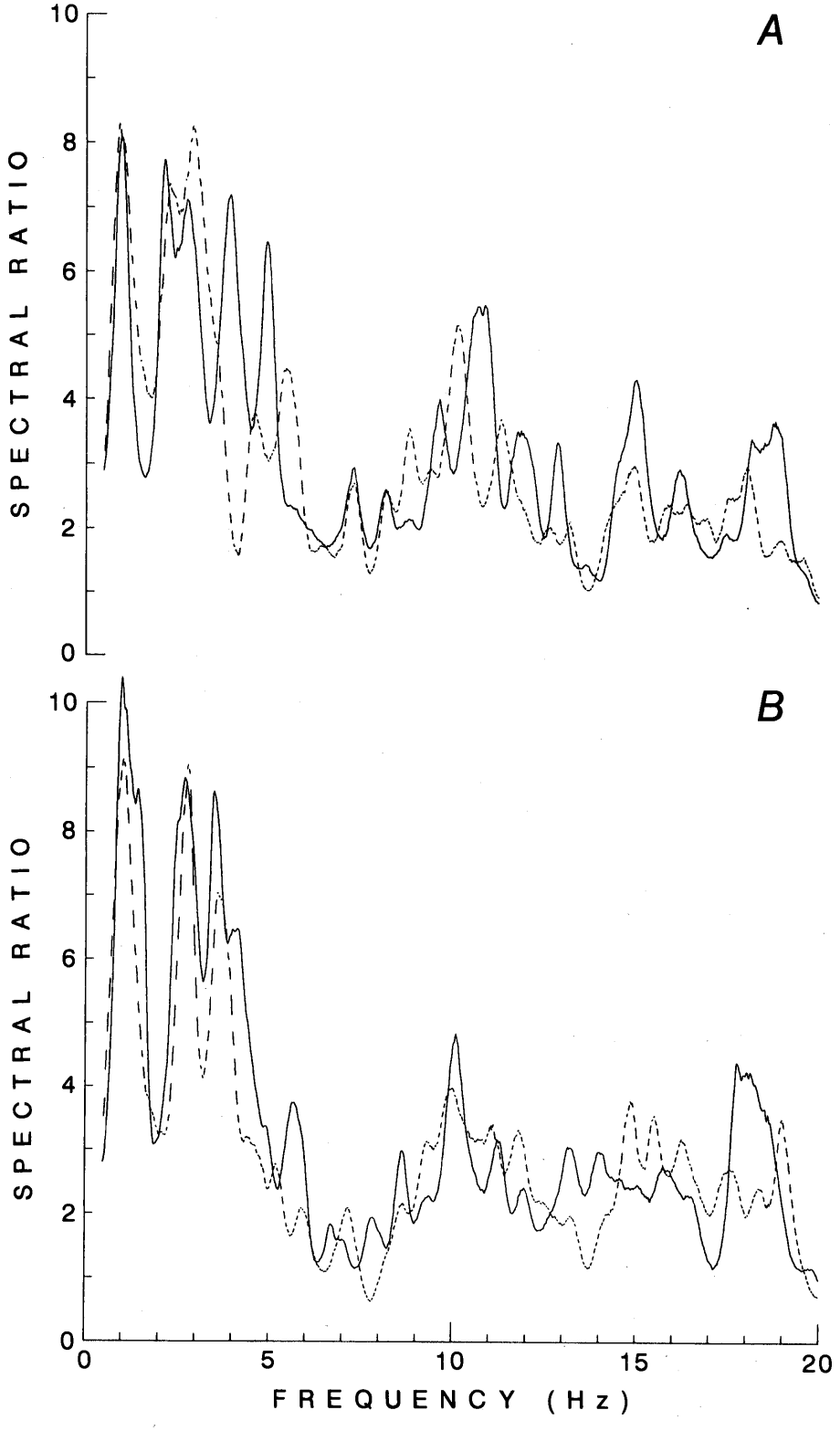


Figure 11.—Site response to two earthquakes (1, 5, table 1) that occurred close to each other on the Calaveras Fault for motions parallel to Divisadero Street (*A*) and Beach Street (*B*). Dashed curves, earthquake 1, solid curves, earthquake 5.

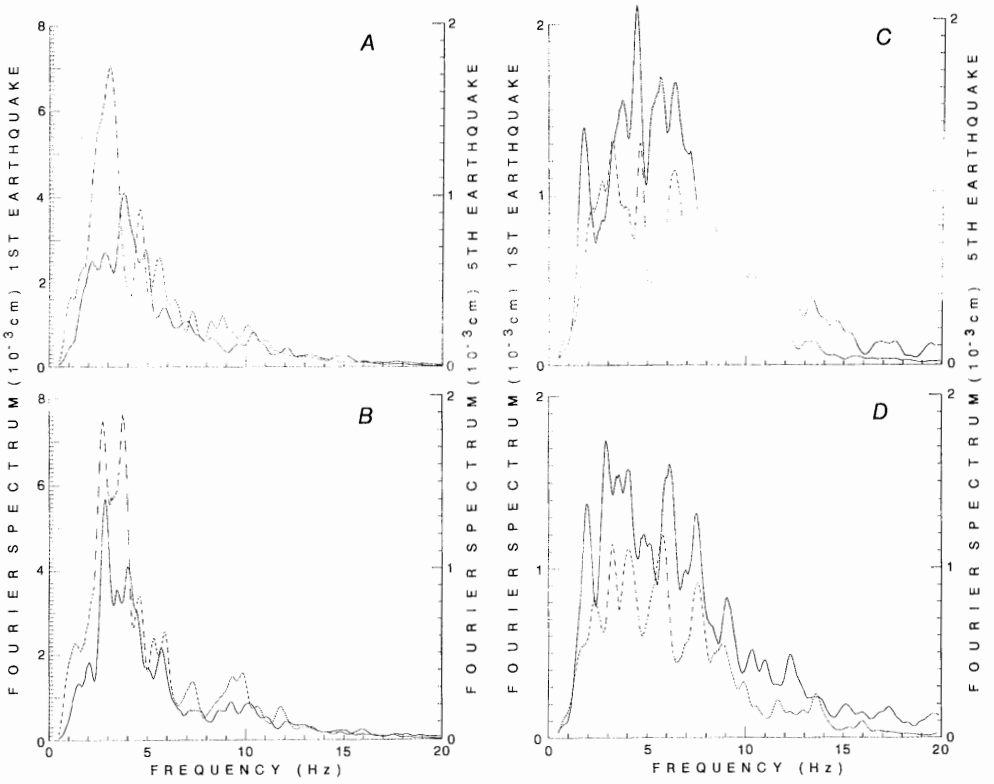


Figure 12.—FFT spectra of ground motion generated by two earthquakes (1, 5, table 1) that occurred close to each other for inline horizontal component (*A*) and perpendicular horizontal component (*B*) of surface seismometer, and for horizontal components HG1 (*C*) and HG2 (*D*) of borehole seismometer. Dashed curves, earthquake 1; solid curves, earthquake 5.

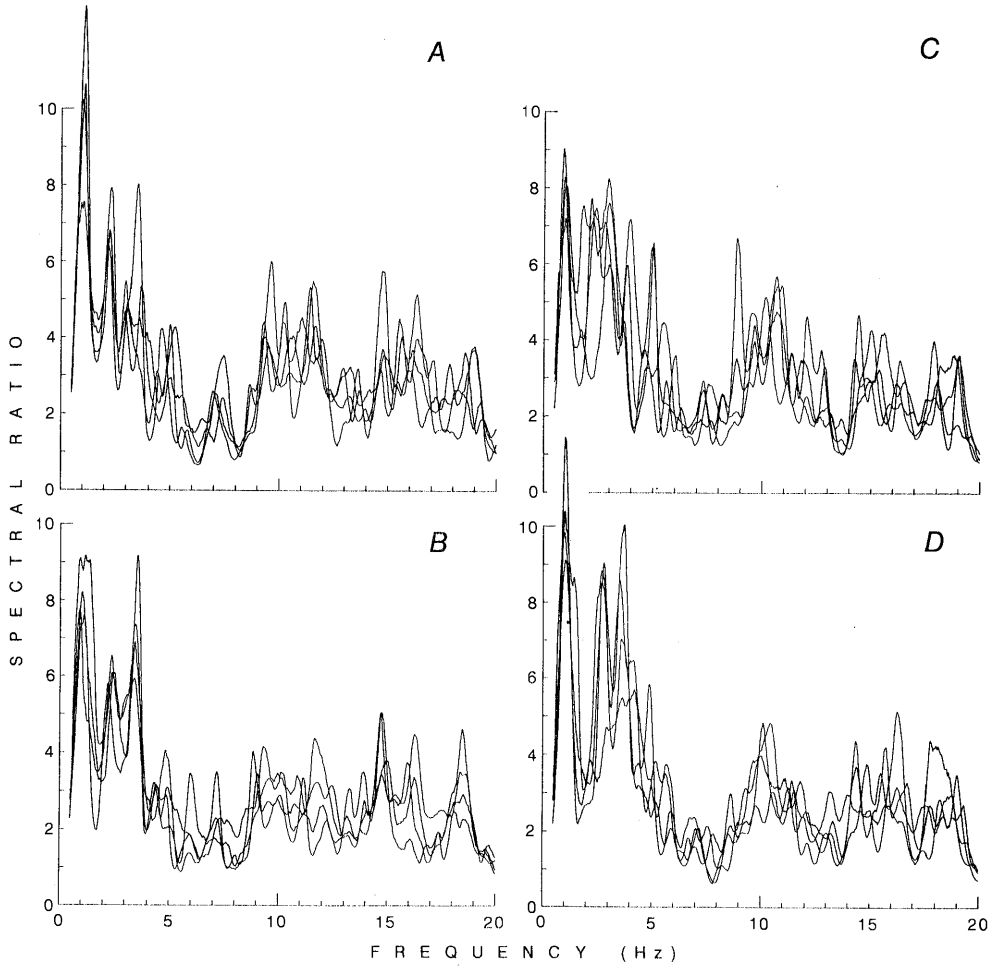


Figure 13.—Spectral ratios in response to east-bay (*A*, *B*) and south-bay (*C*, *D*) earthquakes for motions parallel to Divisadero Street (*A*, *C*) and Beach Street (*B*, *D*).

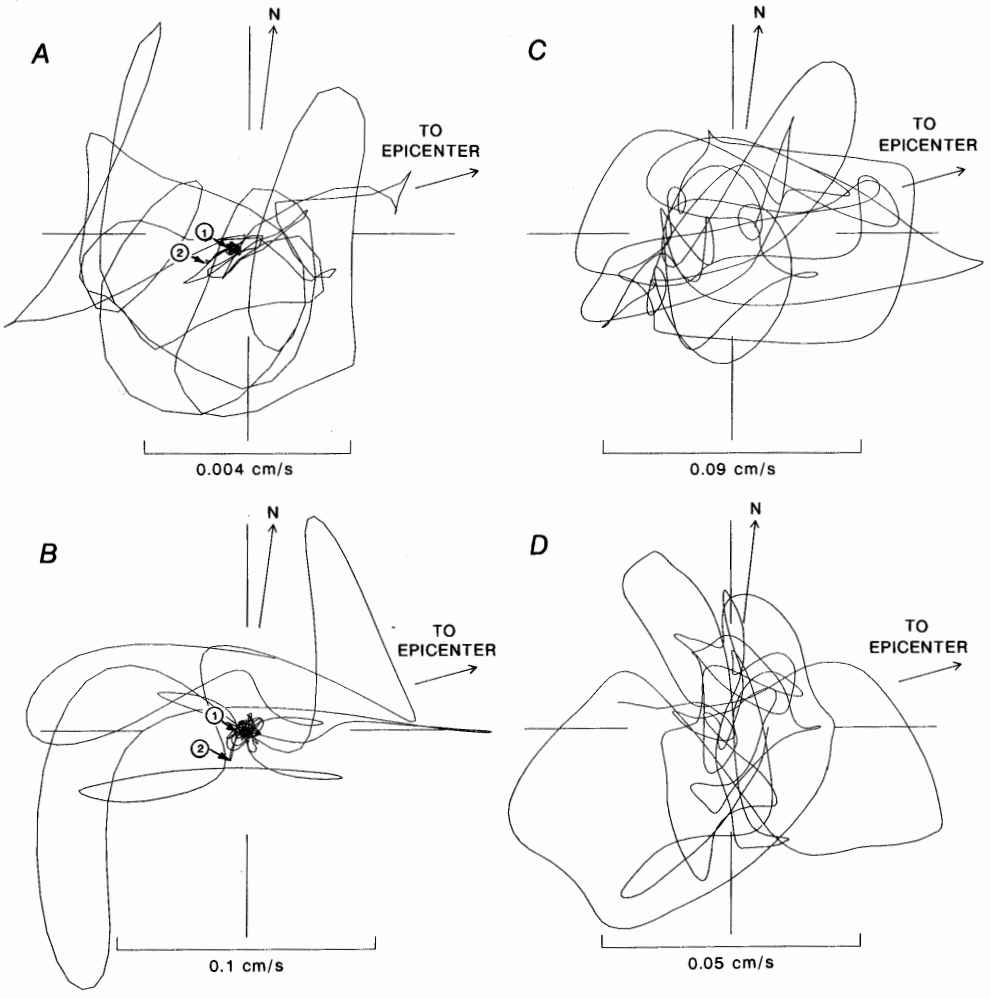


Figure 14.—Surface particle motions projected onto a horizontal plane, as constructed from horizontal-component seismograms in Figures 3*B* and 3*C*. *A*, 0 to 3 s. 1, onset of *P*-wave arrival; 2, maximum of *P*-wave arrival. *B*, 3 to 6 s. 1, onset of *S*-wave arrival; 2, maximum of *S*-wave arrival. *C*, 6 to 9 s. *D*, 9 to12 s.

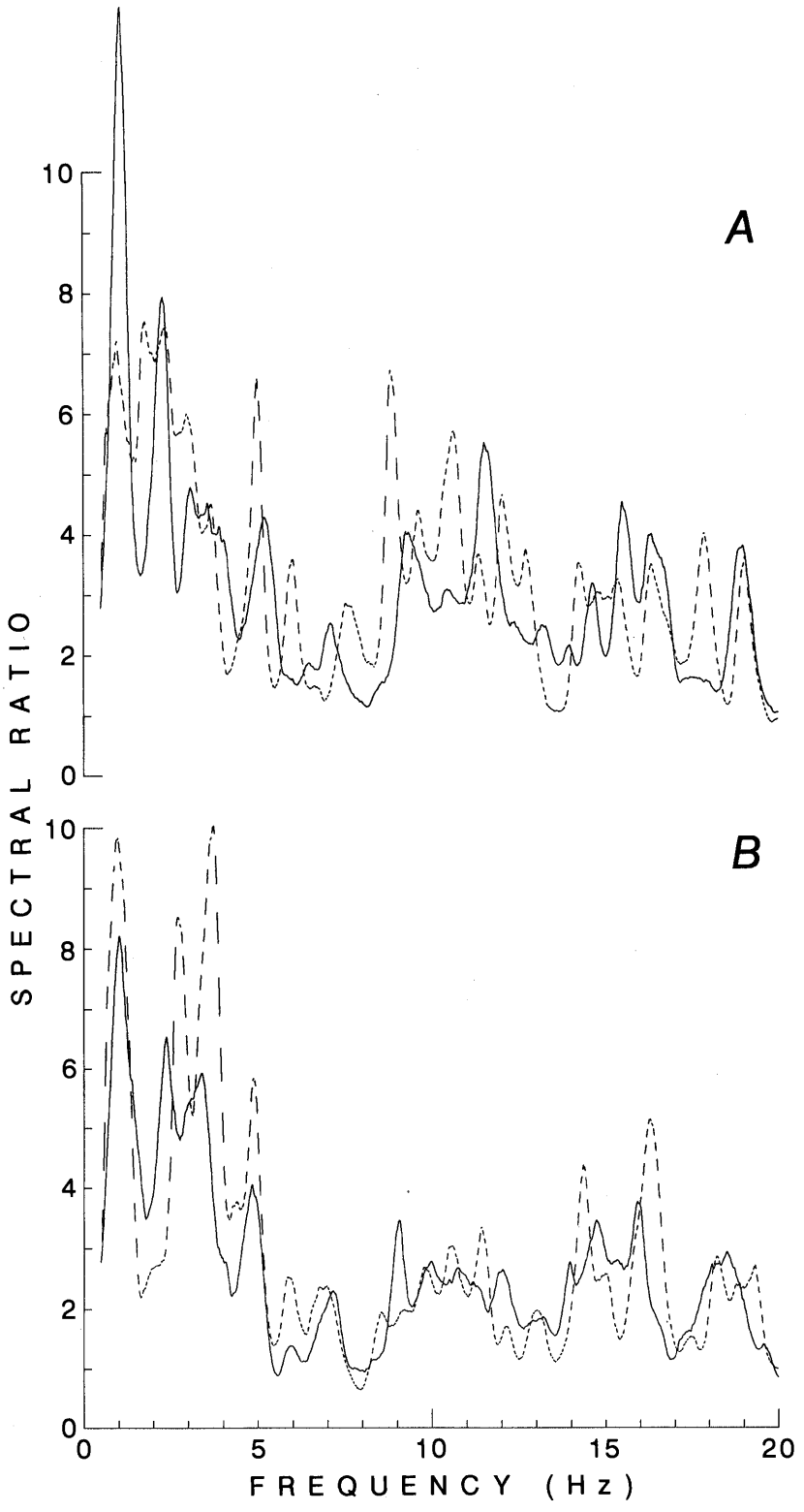


Figure 15.—Spectral ratios calculated for an east-bay earthquake (6, table 1) and a south-bay earthquake (3, table 1) for motions parallel to Divisadero Street (*A*) and Beach Street (*B*). Dashed curves, earthquake 3; solid curves, earthquake 6.

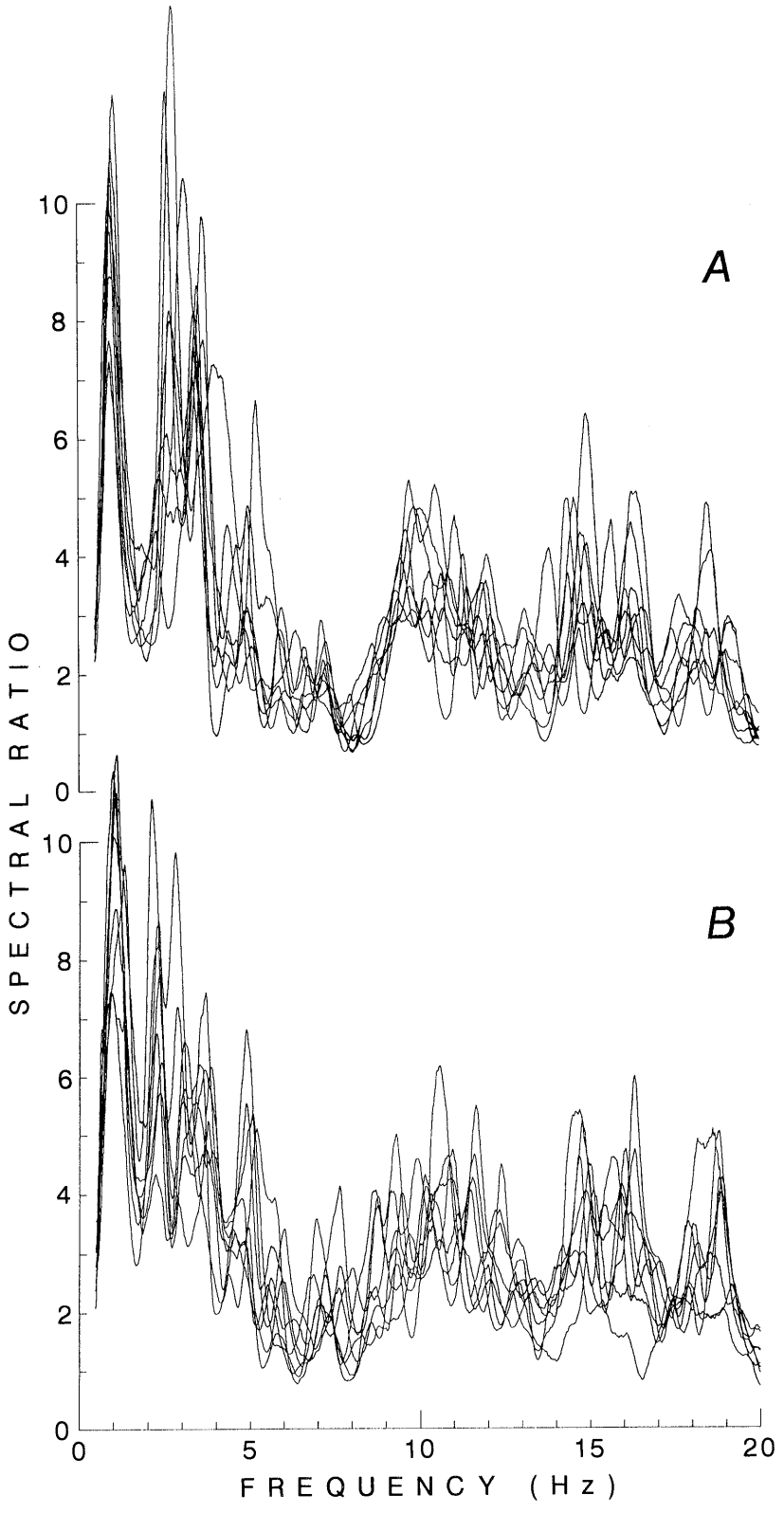


Figure 16.—Spectral ratios of horizontal motions at surface to those in bedrock parallel to major (*A*) and minor (*B*) axes of bedrock basin underlying the Marina District, calculated for eight earthquakes listed in table 1.

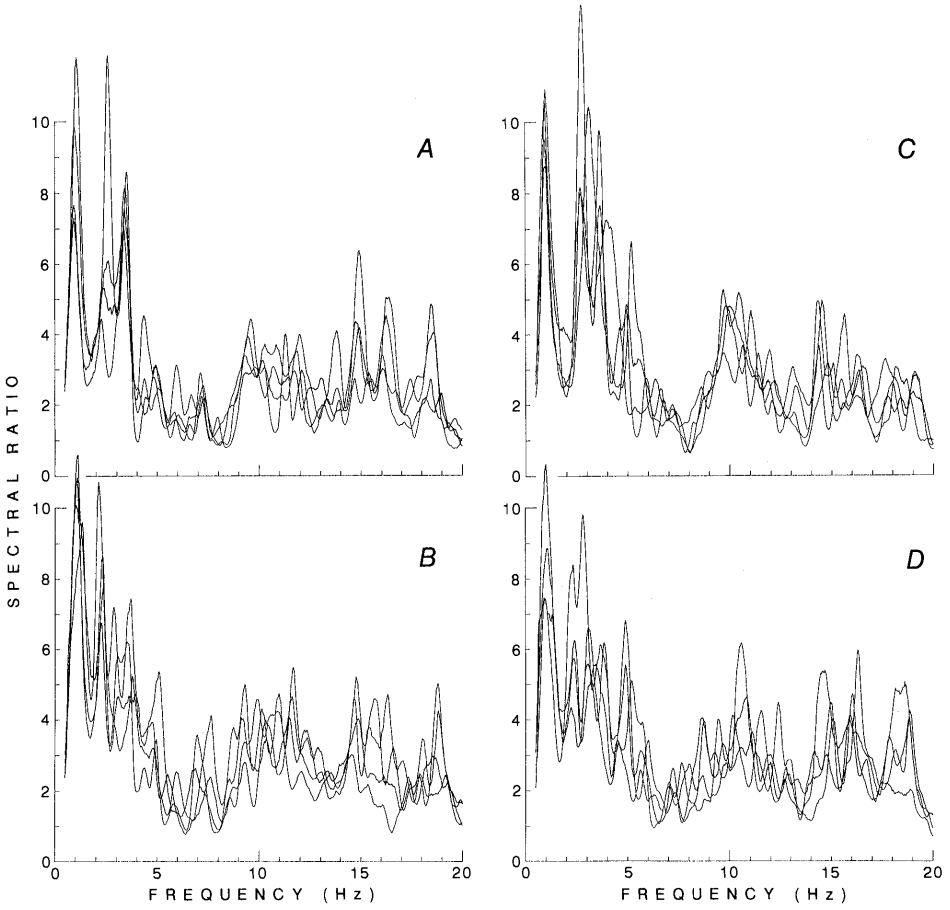


Figure 17.—Spectral ratios in response to east-bay (*A, B*) and south-bay (*C, D*) earthquakes for motions parallel to major (*A, C*) and minor (*B, D*) axes of bedrock basin underlying the Marina District.

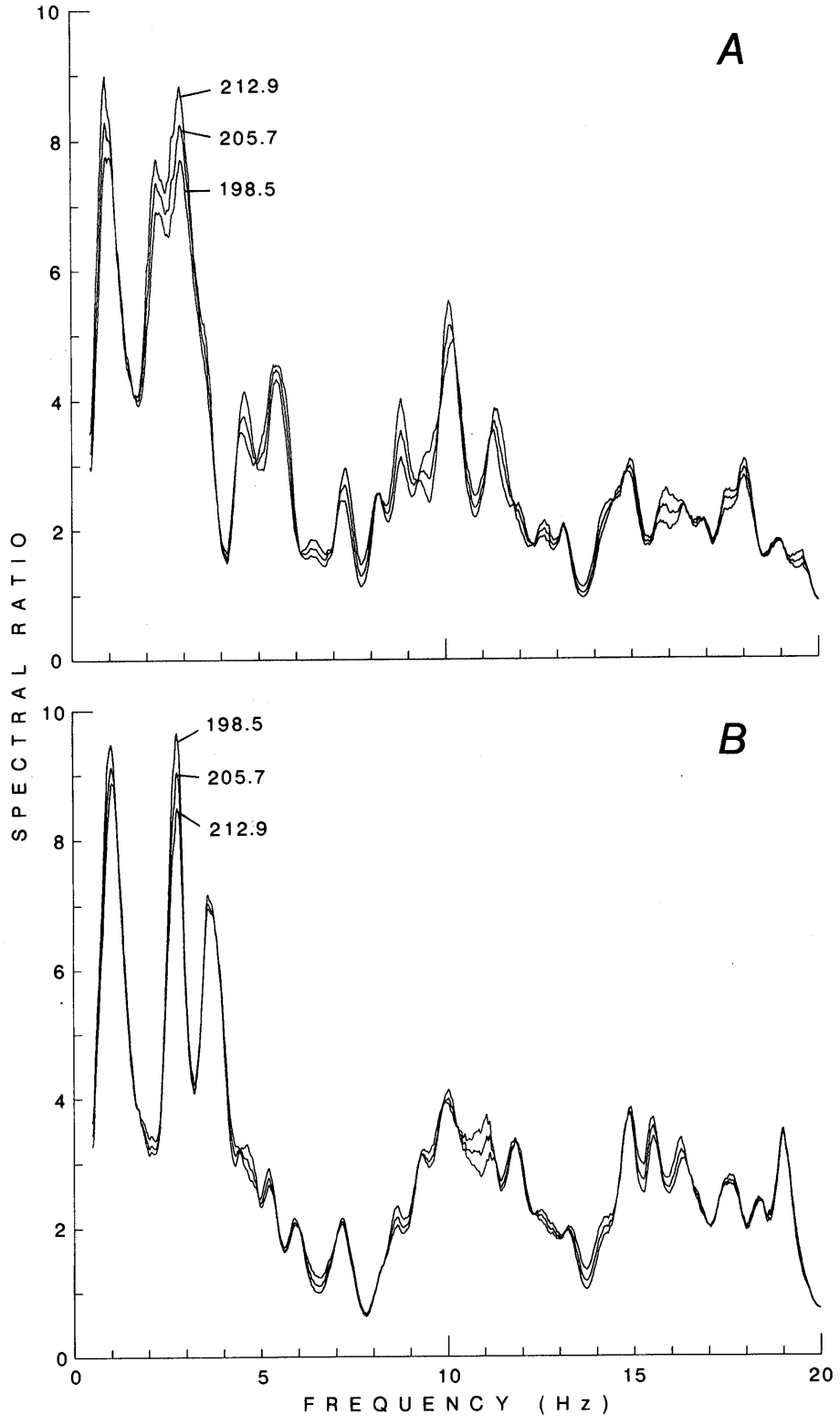


Figure 18.—Site response for motions parallel to Divisadero Street (*A*) and Beach Street (*B*) generated by earthquake 1 in table 1, showing effects of uncertainty in borehole horizontal-geophone orientation $A_U$ on calculated site response.

MARINA DISTRICT

# DETERMINATION OF THE DYNAMIC SHEAR MODULUS OF HOLOCENE BAY MUD FOR SITE-RESPONSE ANALYSIS

By Harry E. Stewart and Ashraf K. Hussein,
Cornell University

## CONTENTS



ABSTRACT

The earthquake caused severe damage in many parts of San Francisco that are underlain by deposits of soft Holocene bay mud. The damage was partly due to the amplification of bedrock motions through the soft deposits. Site-response analyses can be used as aids in understanding the interactions between local site conditions and earthquake motions, but such analyses depend on an accurate characterization of the dynamic soil properties. One of the critical aspects of soil modeling is the relation between dynamic shear modulus and shear strain.

We performed a series of laboratory tests on specimens of Holocene bay mud recovered from depths of approximately 10 to 20 m below the ground surface, near the intersection of Mission Street and the Embarcadero Skyway. We conducted one-dimensional consolidation tests, using instrumented lateral-stress membranes to determine the relationship between the coefficient of horizontal soil stress ($K_o$) and overconsolidation ratio (OCR), so that specimens later could be consolidated anisotropically in a resonant-column/torsional-shear (RC/TS) system while maintaining zero lateral strain. Large specimens of bay mud then were consolidated anisotropically in the RC/TS system to OCR's of 1, 2, and 4. The stress ratios used to maintain zero lateral strain were determined from the $K_o$–OCR relation. The shear moduli then were evaluated, using both RC methods for small strains and TS methods for larger strains. We present data for evaluating the low-amplitude shear modulus ($G_{max}$) on the basis of void ratio ($e$), OCR, and mean effective stress. The shear-modulus-reduction curves obtained in this study agree reasonably well with previously reported results for OCR=1 and OCR=2; shear moduli were found to decrease more rapidly for OCR=4.

## INTRODUCTION

The aim of this study is to develop relations for the normalized shear modulus of Holocene bay mud for stress states representative of those in situ. Specimens of bay mud were consolidated one-dimensionally to determine the overconsolidation ratio (OCR), and to evaluate the coefficient of horizontal soil stress ($K_o$) as a function of the OCR. Specimens were $K_o$-consolidated over a range of OCR's, and the dynamic shear moduli were determined, using a resonant-column/torsional-shear (RC/TS) system. The $K_o$–OCR relation for Holocene bay mud is presented here, along with laboratory values of the small-strain shear modulus ($G_{max}$). Simplified relations are presented to estimate $G_{max}$ on the basis of readily obtainable soil and site properties. Finally, modulus-reduction curves are presented for bay mud. The shear-modulus-reduction curves are compared with those obtained by other workers.

The Holocene bay mud used in this study was recovered from a boring made near the intersection of Mission Street and the Embarcadero Skyway near the northeast end of Market Street. The samples were obtained from 76.2-mm-diameter Shelby tubes with an Osterberg sampler. The soil tested is classified as clay of low plasticity (CL) in the Unified Soil Classification System, with a liquid limit of 35 percent, a plastic limit of 22 percent, and a plasticity index of 13 percent. The average natural water content (by

weight) was 47 percent. The average bulk unit weight was 17.08 kN/m$^3$, and the specific gravity was 2.70.

## EVALUATION OF $K_o$

The in situ coefficient of horizontal soil stress, $K_o$, depends on the loading and unloading sequences, or stress history, that the soil has undergone. In general, $K_o$ is difficult to determine in situ because the stress history of the soil may be unknown or complex. For level ground, the effective vertical stress ($\overline{\sigma}_v$) is equal to the total overburden stress minus the pore pressure. This $\overline{\sigma}_v$ value can be quite easily and accurately determined from in situ measurements of density and level of the water table. However, the effective horizontal stress ($\overline{\sigma}_h$) depends on the stress history of the deposit and cannot be measured directly without special field equipment or laboratory testing.

The variation in effective vertical and horizontal stresses for soil beneath level ground subjected to a simplified stress history that includes primary loading, primary unloading, and primary reloading is illustrated in figure 1. For primary or virgin loading, the soil is normally consolidated, and $K_o$=$K_{onc}$. This $K_o$ value generally is assumed to be constant over a wide range of stresses, represented by the segment O–A–B. Unloading from the normally consolidated state, termed "primary unloading," is represented by the concave-downward segment B–C–D. Upon unloading, both $\overline{\sigma}_v$ and $\overline{\sigma}_h$ decrease, and the soil becomes increasingly overconsolidated. However, since the soil element is confined laterally by the surrounding soil, these stresses do not decrease in direct proportion to each other, or by the same ratio, as in primary loading. For primary unloading $K_o$=$K_{opu}$, and $K_o$ increases with increasing overconsolidation. Upon reloading, $\overline{\sigma}_v$ and $\overline{\sigma}_h$ increase again, and the soil approaches a normally consolidated state. Reloading from the minimum stress state, termed "primary reloading," is represented by the concave-upward segment D–E.

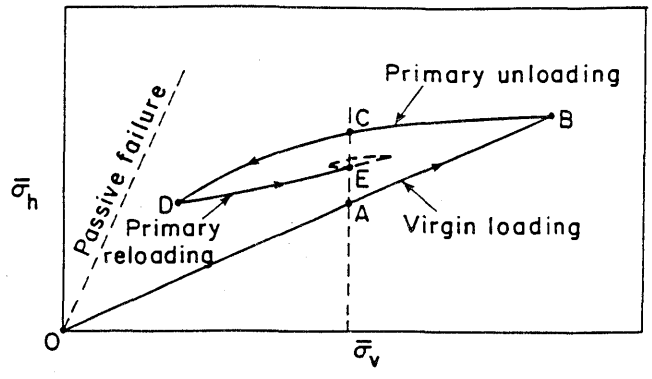


Figure 1.—Effective horizontal stress ($\overline{\sigma}_h$) versus effective vertical stress ($\overline{\sigma}_v$), showing stress paths for simple stress histories (after Mayne and Kulhawy, 1982). See text for explanation.

Table 1.—*Characteristics of wire-reinforced membranes*

| | |
|---|---|
| **Membrane:** | |
| Cross-sectional specimen area (cm$^2$) | 35 |
| Length (mm) | 65 |
| **Wire reinforcement:** | |
| Wire diameter (mm) | 0.15 |
| Center-to-center spacing between wires (mm) | 0.5 |
| Height of wire windings (mm) | 30 |
| Young's modulus of Constantan (kPa) | $1.52 \times 10^8$ |
| Tensile strength of Constantan (kPa) | $5.7 \times 10^5$ |
| **Instrumentation:** | |
| Electrical resistance (Ω) | ≈138 |
| Maximum excitation voltage (V) | 2 |

For primary reloading, $K_o$=$K_{opr}$, and $K_o$ decreases with decreasing overconsolidation. Beyond point B, the soil becomes normally consolidated again, and $K_o$=$K_{onc}$. The reloading curve is expected to join the virgin-loading curve at point B.

## $K_o$ TESTING OF HOLOCENE BAY MUD

Horizontal stresses are directly measurable in the laboratory with a direct-simple-shear (DSS) device, using a calibrated, wire-reinforced rubber membrane that acts on a strain-gage principle. This method was used by Dyvik and others (1981) to measure horizontal stresses in soft marine clays. The measurements of horizontal stress obtained during consolidation loading and unloading were used to determine the $K_o$–OCR relation.

In this procedure, a Constantan wire-reinforced membrane was calibrated by applying known air pressures to the instrumented membrane and measuring the resulting change in the electrical resistance of the wires. The specifications for the calibrated wire-reinforced membranes used with the Norwegian Geotechnical Institute (NGI) DSS device are listed in table 1. The radial stiffness of the membranes generally is regarded as high enough that lateral expansion can be ignored, although it has been argued (Saada, 1984) that the reinforcement is insufficient to maintain a $K_o$ condition. The pressure was applied to the membrane through an aluminum cylinder surrounded by a rubber bladder that was used to disperse the concentrated flow of air released from the holes. The membrane was secured to the rubber bladder and cylinder with rubber strips and hose clamps placed adjacent to the wire reinforcement. A mechanical air-pressure regulator was used to manually cycle the pressure over a 5-minute timespan; the pressure was cycled between ambient pressure and ap-

proximately 140 kPa several times to define any difference in behavior due to unloading or reloading.

The amplifier system used was a Measurements Group, Inc., model 2130 strain-gage-conditioning amplifier. The bridge system included a two-arm Wheatstone bridge composed of an active membrane, a passive membrane, and two precision resistors (within the amplifier) to complete the bridge, as shown in figure 2. The membrane used to measure horizontal stress is the active membrane; the passive membrane is an identical membrane used to complete the circuit and provide temperature compensation. A typical membrane-calibration curve is shown in figure 3. The curve is nearly a straight line, but the zero-pressure reading does not coincide with the origin, as shown by the intercept, because an initial pressure is required to seat the bladder against the membrane. The slope, not the intercept, is important for the calibration; the slope was determined by linear regression.

Each calibration consisted of a loading followed by at least one unloading-reloading cycle. The difference between the slopes of the unloading and reloading segments was less than 1 percent. However, the slope of the loading portion differed slightly; this behavior during initial loading was attributed to seating of the membrane. The calibration value used for the consolidation tests, called $K_o$ tests, was the average value between the curves.

Additional calibrations were performed after $K_o$ tests to identify any change in membrane performance due to testing. No significant differences were observed. In addition, there was no evidence of creep or drift in the horizontal stress measurements over time. To minimize temperature effects, the passive membrane was placed within a few centimeters of the specimen, a temperature-compensating circuit was used, and constant laboratory temperature was maintained.

A specimen was trimmed from a 76.2-mm-diameter Shelby tube sample recovered from a depth of 10.7 to 11.4 m. The specimen was then consolidated incrementally. Beyond the maximum past pressure ($\bar{\sigma}_{vm}$), unload-reload-unload cycles were applied. The variations in effective horizontal and vertical stresses measured during a $K_o$ test are plotted in figure 4. When the soil was removed from the ground, the confining stresses were released, and the soil underwent unloading. Recompression occurred during the initial stages of consolidation until the preconsolidation pressure was reached. This recompression is shown in figure 4 by the concave-upward segment from the origin to point A. Beyond the preconsolidation pressure, segment A–B represents primary loading. Along this stress path, the soil is normally consolidated (OCR=1), and the horizontal-stress coefficient is $K_{onc}$. Along segment B–C, which represents primary unloading, the OCR is increasing, and the horizontal-stress coefficient is $K_{opu}$. Along segment C–B′, which represents primary reloading, the OCR is decreasing, and the horizontal-stress coefficient is

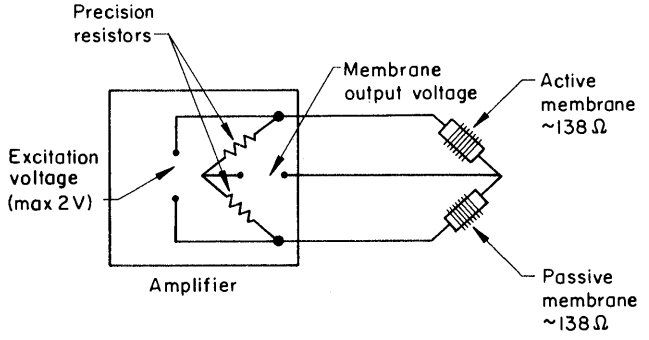


Figure 2.—Schematic diagram of bridge amplifier system.

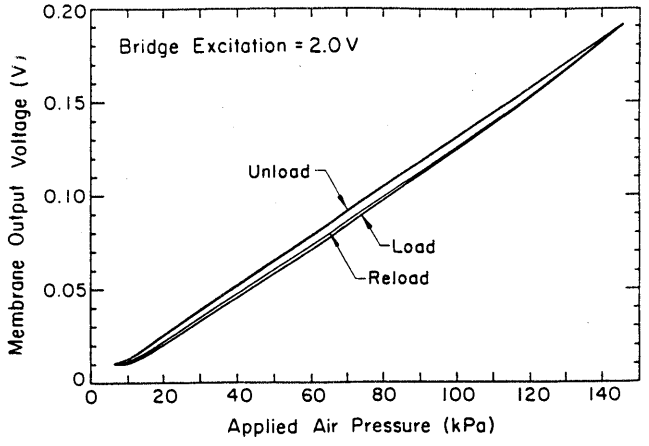


Figure 3.—Membrane output voltage versus applied air pressure, showing calibration curve.

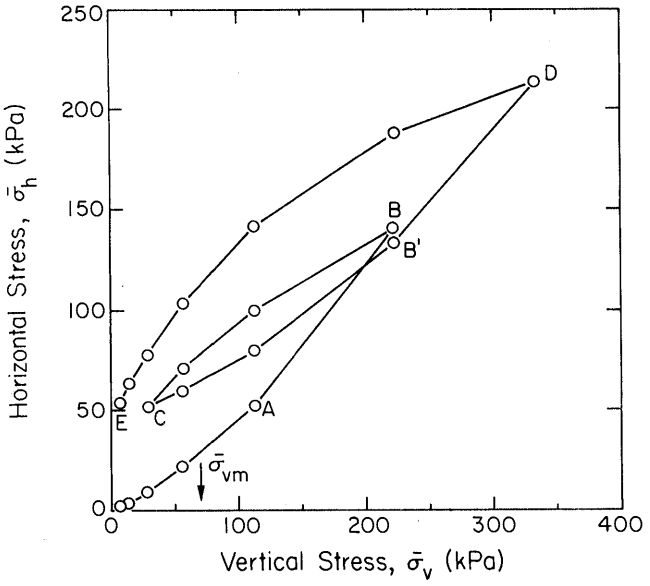


Figure 4.—Effective horizontal versus effective vertical stress during $K_o$ loading and unloading. See text for explanation.

$K_{opr}$. Note that $K_{opu}$ and $K_{opr}$ are changing continuously as the OCR changes. After point B′, segment B′–D followed the primary-loading curve. The specimen finally was unloaded to point E.

The relation between the effective horizontal and vertical stresses for primary loading during a $K_o$ test is shown in figure 5. Using linear regression through the origin, the equation of the curve is:

$$\bar{\sigma}_h = 0.62\bar{\sigma}_v \qquad (r^2 = 0.971), \qquad (1)$$

where $\bar{\sigma}_h$ is the effective horizontal stress and $\bar{\sigma}_v$ is the effective vertical stress. Equation 1 indicates that $K_{onc}$= 0.62.

The $K_{opu}$–OCR relation (fig. 6) can be expressed by

$$K_{opu} = 0.62\text{OCR}^{0.58} \qquad (r^2 = 0.983). \qquad (2)$$

The general form of equation 2 has been used frequently by other workers (for example, Schmidt, 1966).

The regression intercept in equation 2 represents the $K_o$ value for OCR=1. The agreement between the two fitted data sets for OCR=1 indicates that $K_{onc}$=0.62 for Holocene bay mud and that equation 2 is reasonable for evaluating $K_o$ for primary unloading. The tests conducted in this study did not generate sufficient data to develop equations for $K_{opr}$.

## OEDOMETER TESTS

The purpose of the oedometer tests was to determine the maximum past pressure ($\bar{\sigma}_{vm}$) for a specimen before testing in the RC/TS system, to ensure that the RC/TS specimens would be consolidated to stresses greater than $\bar{\sigma}_{vm}$ and then rebounded to controlled OCR's. The oedometer specimens were trimmed from the tube sample directly above the RC/TS specimen. The original plan was to perform an oedometer test for each RC/TS specimen; however, the results from six oedometer tests indicated little variation in the results, and so additional testing was discontinued. Specimen depth, initial void ratio ($e_o$), OCR, compression ratio (CR), and recompression ratio (RR) from these oedometer tests are listed in table 2.

## RESONANT-COLUMN/ TORSIONAL-SHEAR APPARATUS

RC/TS tests were conducted separately to measure the dynamic soil properties over a wide range of shear strain. The use of two types of equipment requires two different specimens, which may have different properties. When using two separate systems, it may be difficult to obtain overlap between the results from the low-strain RC tests and the higher strain TS tests. This limitation is significant when investigating the reduction in shear modulus as a function of strain amplitude, or in determining the strain level at which pore pressure begins to build up. These drawbacks led to the design of a hybrid device, combining RC and TS, that allows the determination of dynamic properties over the entire range of shear strain that is of engineering interest.

The RC/TS apparatus used in this study was designed by Soil Dynamics Instruments, Inc. This apparatus, shown schematically in figure 7, can test solid or hollow speci-

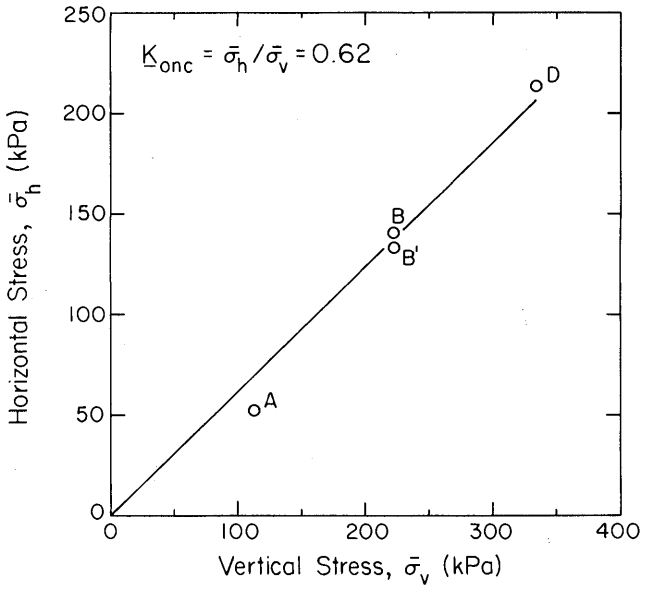


Figure 5.—Effective horizontal versus effective vertical stress for primary loading. See text for explanation.

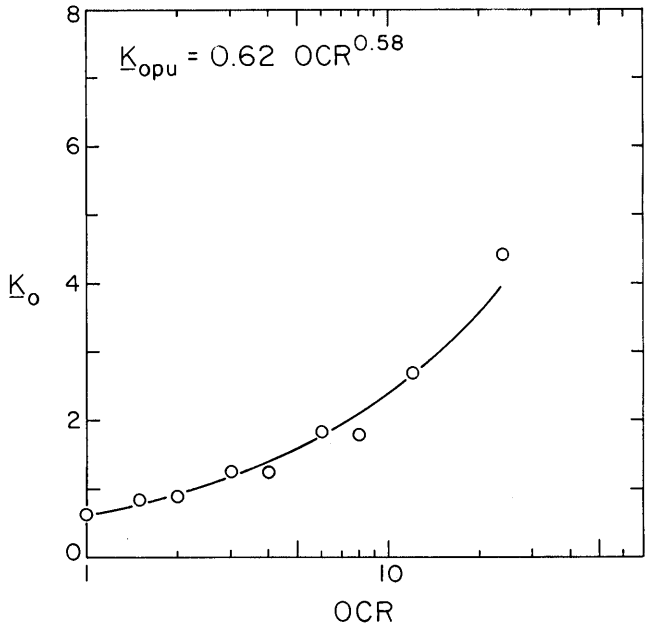


Figure 6.—$K_o$ versus overconsolidation ratio (OCR) for primary unloading.

Table 2.—*Results of oedometer tests on Holocene bay mud*

[CR, compression ratio; $e_o$; initial void ratio; OCR, overconsolidation ratio; RR, recompression ratio; $\bar{\sigma}_{vm}$, maximum past pressure; $\bar{\sigma}_{vo}$, in situ effective vertical stress]

| Sample depth (m) | $\bar{\sigma}_{vo}$ (kPa) | $e_o$ | $\bar{\sigma}_{vm}$ (kPa) | OCR | CR | RR |
|---|---|---|---|---|---|---|
| 9.90 | 82.1 | 1.289 | 90.3 | 1.10 | 0.199 | 0.024 |
| 10.67 | 89.5 | 1.274 | 94.5 | 1.08 | .198 | .025 |
| 11.43 | 92.9 | 1.301 | 106.9 | 1.15 | .210 | .024 |
| 18.29 | 141.5 | 1.243 | 147.2 | 1.04 | .207 | .023 |
| 19.05 | 146.9 | 1.230 | 157.1 | 1.07 | .212 | .024 |
| 19.81 | 152.2 | 1.218 | 159.9 | 1.05 | .218 | .025 |
| Average | | | | | 0.207 | 0.024 |
| Coefficient of variation (percent) | | | | | 3.7 | 3.1 |

mens, consolidated either isotropically or anisotropically. The dynamic and quasi-static loadings are controlled independently and may be applied simultaneously. Quasi-static loading may be monotonic or cyclic, using strain or stress control. The pneumatic axial loader was added so that anisotropic consolidation stresses could be controlled more accurately.

A Hardin oscillator was used to apply sinusoidal torsional vibrations. The large inertia mass of the oscillator provides a fixed reaction. The maximum shear strain that can be generated in the RC is approximately $1.5\times10^{-2}$ percent, depending on specimen geometry.

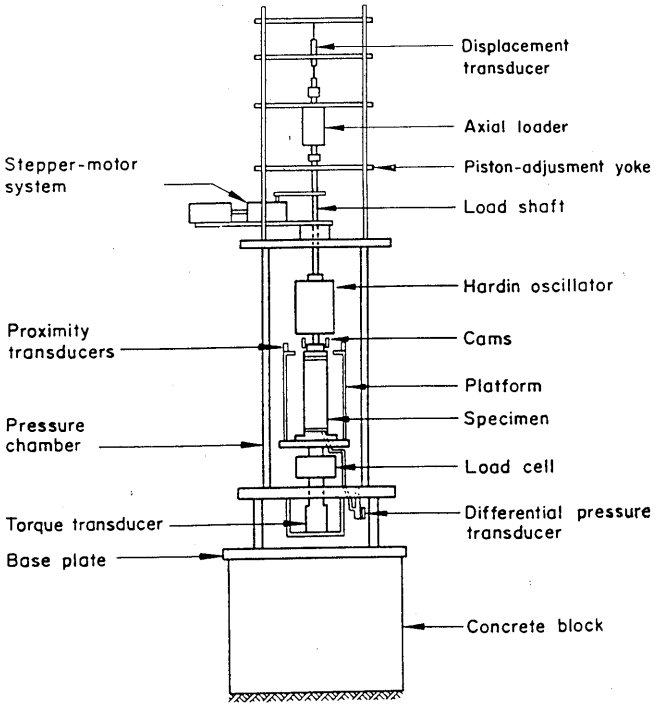


Figure 7.—Schematic diagram showing resonant-column/torsional-shear apparatus.

A quasi-static torsional load can be applied to the specimen by a torque motor system mounted on the pressure-chamber lid. The motor system consists of a stepper motor, rotary table, and sprockets located on the top of the rotary table and on the piston, which are linked by two plastic-coated wire chains. The piston passes through the chamber lid and is fixed rigidly to the Hardin oscillator, which is fastened to the top platen by a special coupling. The applied torsion passes through a cam assembly, the upper platen, the specimen, and axial-load transducer, and is measured with a torque transducer mounted under the pressure-chamber base. The relative rotation between the bottom and top of the specimen is measured by two noncontacting displacement transducers located on a cylindrical platform. The maximum rotation is approximately 30° in either direction.

## TESTING PROCEDURES

Undrained RC/TS $K_o$ tests were performed to study the dynamic properties of Holocene bay mud. A total of 18 RC and 24 TS tests were carried out on undisturbed specimens for this study. Typical testing procedures were as follows.

1. Undisturbed specimens were trimmed from the Shelby tubes.
2. Backpressure was used to ensure full saturation of the specimens. While maintaining the effective confining pressure at 50 kPa, both cell pressure and backpressure were increased in 35-kPa increments, allowing time for equalization at each stage. Full saturation was assumed to be achieved when the value of Skempton's *B* parameter was at least 0.96 or greater; a backpressure in the range 300–400 kPa generally was required to satisfy this condition.
3. After saturation at $\bar{\sigma}_v=\bar{\sigma}_h=50$ kPa, the specimens were consolidated anisotropically to the required effective vertical stress ($\bar{\sigma}_v$) and effective horizontal stress ($\bar{\sigma}_h$)

(effective confining pressure). Each specimen initially was normally consolidated (OCR=1), with $\bar{\sigma}_h/\bar{\sigma}_v$=0.62. During this consolidation phase, the axial loads were adjusted by using the pneumatic loader mounted above the load shaft. Overconsolidation was achieved by increasing $\bar{\sigma}_v$ and $\bar{\sigma}_h$ with $K_o$=0.62 (OCR=1) and then reducing these stresses to achieve the desired OCR. The results from the $K_o$ tests were used to determine $\bar{\sigma}_v$ and $\bar{\sigma}_h$ during unloading to the desired OCR's. A value of $\bar{\sigma}_h/\bar{\sigma}_v$=0.93 was used for unloading to OCR=2, and of $\bar{\sigma}_h/\bar{\sigma}_v$=1.40 for further unloading to OCR=4; these values were determined from the test results given by equation 2. The stress paths used for obtaining different OCR's under $K_o$ conditions are shown in figure 8.

4. The changes in the axial length and the volume of the specimens were monitored during consolidation. During consolidation and rebound, $\bar{\sigma}_v$ and $\bar{\sigma}_h$ were adjusted to the $K_o$ values for primary loading and primary unloading determined from the tests made with the lateral-stress membranes in the DSS device. If the true $K_o$ values were achieved in the RC/TS system, then the axial strains should equal the volumetric strains. The axial and volumetric strains measured from the RC/TS consolidation and rebound phases are shown in figure 9. The excellent agreement of the results indicates that the $K_o$–OCR relation determined by using the lateral-stress membranes is appropriate.
5. After the end of primary consolidation, the drainage lines were closed, and the shear modulus was determined by using the RC. These tests provided shear moduli at single-amplitude shear strains ranging from $2\times10^{-5}$ to $7\times10^{-3}$ percent.
6. After the RC tests, one cycle of strain-controlled TS testing was carried out at a higher strain level, with a constant strain rate of 0.3 percent/min. The data from this test were used to determine the shear modulus at this higher shear-strain level.
7. Finally, the apparatus was disassembled, final specimen dimensions were measured, and the water content was determined.

## TEST RESULTS

The test results are summarized in table 3. The data were reduced using the equations recommended by Chen and Stokoe (1979) and Isenhower and others (1987), which take into account nonlinear stress-strain behavior. In table 3, $G_{max}$ is the modulus for a shear strain of about$10^{-4}$ percent.

## DETERMINATION OF $G_{max}$

Hardin and Drnevich (1972) proposed the following equation to calculate the low-amplitude shear modulus, $G_{max}$, for cohesive soils:

$$G_{max}/p_a=321[(2.97-e)^2/(1+e)]OCR^K(\bar{\sigma}_o/p_a)^{0.5}, \quad (3)$$

where $K$ is a parameter related to the plasticity index, OCR is the overconsolidation ratio, $\bar{\sigma}_o$ is the effective mean stress, $e$ is the void ratio (not to exceed 2), and $p_a$ is atmospheric pressure. However, the shear moduli calculated from this equation with K=0.13 (plasticity index, 13

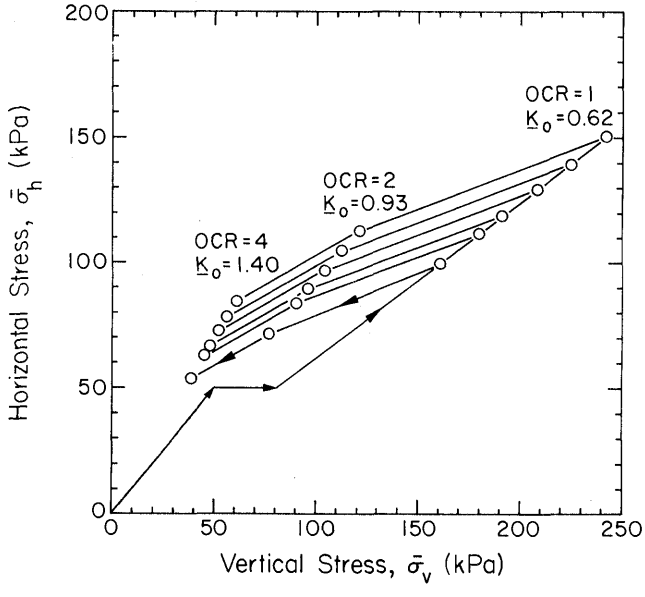


Figure 8.—Effective horizontal versus effective vertical stress for various OCR's in resonant-column/torsional-shear tests.

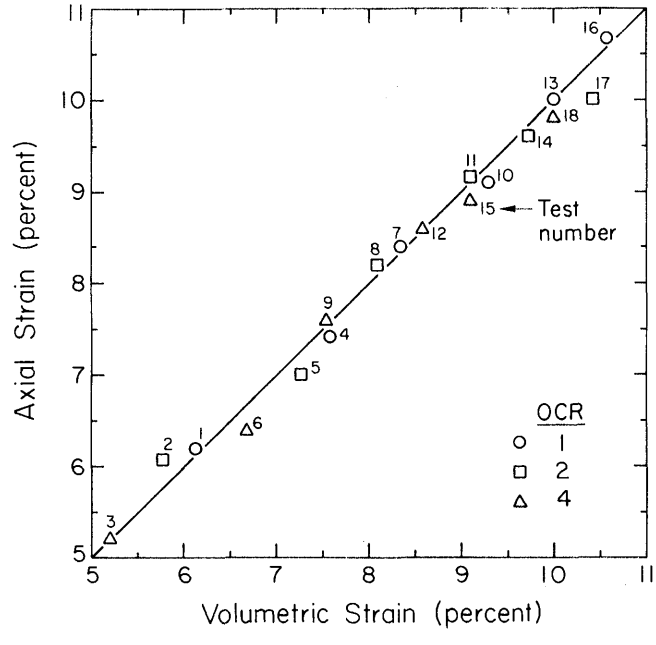


Figure 9.—Axial and volumetric strain from consolidation and rebound.

Table 3.—*Results of resonant-column/torsional-shear tests*

[*e*, void ratio; *G*, shear modulus; $G_{max}$, low-amplitude shear modulus; OCR, overconsolidation ratio; $\gamma_{cy}$, cyclic shear strain; $\bar{\sigma}_h$, effective horizontal stress; $\bar{\sigma}_v$, effective vertical stress]

| Test | OCR | $\bar{\sigma}_v$ (kPa) | $\bar{\sigma}_h$ (kPa) | e | $G_{max}$ (MPa) | $\gamma_{cy}$ (percent) | G (MPa) |
|---|---|---|---|---|---|---|---|
| 1 | 1 | 160.6 | 100.0 | 1.133 | 32.2 | 0.156 | 13.9 |
| 2 | 2 | 76.8 | 71.7 | 1.150 | 27.8 | .159 | 10.8 |
| 3 | 4 | 38.5 | 53.9 | 1.167 | 17.9 | .156 | 7.4 |
| 4 | 1 | 179.8 | 112.0 | 1.119 | 36.8 | .320 | 11.0 |
| 5 | 2 | 89.9 | 84.0 | 1.129 | 31.0 | .312 | 9.4 |
| 6 | 4 | 45.0 | 63.0 | 1.147 | 20.0 | .316 | 7.1 |
| 7 | 1 | 191.1 | 119.0 | 1.108 | 39.5 | .079 | 23.1 |
| 8 | 2 | 95.9 | 89.5 | 1.118 | 37.6 | .079 | 19.7 |
| 9 | 4 | 47.7 | 66.8 | 1.136 | 30.7 | .081 | 13.5 |
| 10 | 1 | 207.9 | 129.5 | 1.092 | 43.0 | .518 | 10.5 |
| 11 | 2 | 104.0 | 97.1 | 1.101 | 36.1 | .511 | 9.0 |
| 12 | 4 | 52.0 | 72.8 | 1.118 | 33.6 | .510 | 6.4 |
| 13 | 1 | 224.5 | 139.8 | 1.081 | 45.2 | .035 | 35.3 |
| | | | | | | .051 | 32.0 |
| | | | | | | .068 | 29.7 |
| 14 | 2 | 112.2 | 104.8 | 1.090 | 39.2 | .032 | 31.2 |
| | | | | | | .051 | 27.6 |
| | | | | | | .066 | 26.7 |
| 15 | 4 | 56.1 | 78.5 | 1.106 | 33.9 | .033 | 22.9 |
| | | | | | | .049 | 21.2 |
| | | | | | | .067 | 19.5 |
| 16 | 1 | 241.8 | 150.6 | 1.070 | 50.4 | 1.055 | 7.4 |
| 17 | 2 | 121.0 | 113.0 | 1.075 | 39.7 | 1.061 | 6.4 |
| 18 | 4 | 60.5 | 84.7 | 1.090 | 34.6 | 1.061 | 5.0 |

percent) were found to be 30 to 40 percent higher than those measured in the RC tests. Regression was used to fit an empirical equation to the measured values. The general form of the predictive equation was kept the same so that comparisons between the two equations would be clearer. The results of this regression on the Holocene bay mud data are given by

$$G_{max}/p_a=601[(2.18-e)^2/(1+e)]OCR^{0.13}(\bar{\sigma}_o/p_a)^{0.5}. \quad (4)$$

The coefficient of determination ($r^2$) for this regression is 0.95, indicating that this equation fits the measured values very well. The relation between the backcalculated values of $G_{max}$ for bay mud, using equation 4 and the measured values of $G_{max}$, is plotted in figure 10.

In equation 4, $\bar{\sigma}_o$ is the mean effective stress, which can be written as

$$\bar{\sigma}_o=\bar{\sigma}_v(1+2K_o)/3. \quad (5)$$

By substituting the relations for $K_o$ presented previously, equation 4 can be expressed as

$$G_{max}/p_a=347[(2.18-e)^2/(1+e)]OCR^{0.13} \cdot [(\bar{\sigma}_v/p_a)(1+1.24OCR^{0.58})]^{0.5} \quad (6)$$

Note that equations 4 and 6 represent laboratory test results. In the field, the effects of secondary compression or aging must be taken into consideration, as explained by Anderson and Stokoe (1978).

## SHEAR-MODULUS REDUCTION

The relation between the normalized shear modulus, $G/G_{max}$, from the RC/TS tests and the cyclic shear strain

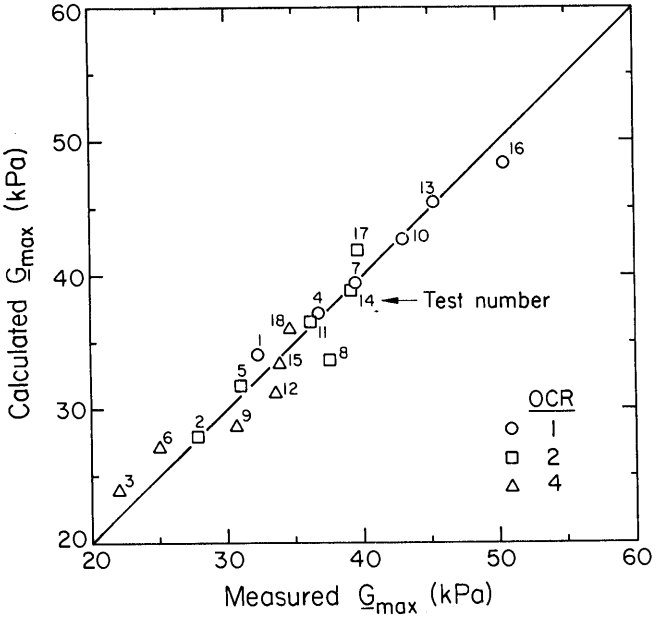


Figure 10.—Calculated versus measured $G_{max}$ value.

($\gamma_{cy}$) is shown in figure 11. For OCR=1 and OCR=2, $G/G_{max}$≈1.0 until the cyclic shear strain exceeds 0.001 percent. At OCR=4, the apparent threshold cyclic-shear-strain level is approximately 0.0001 percent.

The normalized shear moduli are nearly the same for OCR=1 and OCR=2, but lower for OCR=4. This increased degradation for OCR=4 is at variance with the results for the effects of stress history obtained by Kokusho and others (1982) and Dobry and Vucetic (1987), possibly because of the differences in material structure and composition of the other soils.

For purposes of comparison, Isenhower and Stokoe's (1981) normalized shear-modulus-reduction curve for San Francisco bay mud at Hamilton Air Force Base, and that of Stokoe and Lodde (1978) at the Dumbarton Bridge, are plotted along with the curves obtained in this study in figure 12. The results of this study indicate smaller threshold strain limits than those reported by other workers.

## CONCLUDING REMARKS

We have presented laboratory test data on the values of $K_o$, $G_{max}$, and $G/G_{max}$ for Holocene bay mud. The $K_o$ values are consistent with trends identified for general stress-history effects. The specific $K_o$ values determined for various OCR's were used to control the anisotropic-consolidation stresses in the RC/TS tests. Measurements of axial and volumetric strains during primary loading and unloading confirmed that the $K_o$ values determined from the calibrated lateral-stress membranes are reasonable.

Laboratory measurements of $G_{max}$, using RC/TS techniques, indicate that, for a given strain level and OCR, the shear modulus increases with increasing effective mean stress. However, the effective mean stress has a negligible effect on the $G/G_{max}$-strain relation. For tests in which the effective mean stress was approximately the same, the shear modulus increased with increasing OCR. The laboratory test results were compared with the frequently used formulation of Hardin and Drnevich (1972) for cohesive soils, which predicts shear moduli about 30 to 40 percent higher than the measured values. An empirical relation for bay mud was developed that accounts for stress-history effects by including $K_o$ as dependent on the OCR. The $G_{max}$ value determined from these laboratory tests will be substantially smaller than the in situ value because of aging effects, which were not evaluated in this study, but are recognized as significant for San Francisco bay mud (Lodde, 1979). The modulus-reduction curves obtained in this study agree reasonably well with previously reported results for bay mud but indicate that the effects of the OCR may be significant.

## ACKNOWLEDGMENTS

This study was sponsored in part by National Science Foundation grant BCS–9011458. A. Avcisoy and K.J. Stewart, who prepared the drawings and manuscript, respectively, are duly recognized for their skills and contributions.

## REFERENCES CITED

Anderson, D.G., and Stokoe, K.H., II, 1978, Shear modulus; a time-dependent soil property, *in* Dynamic geotechnical testing: American

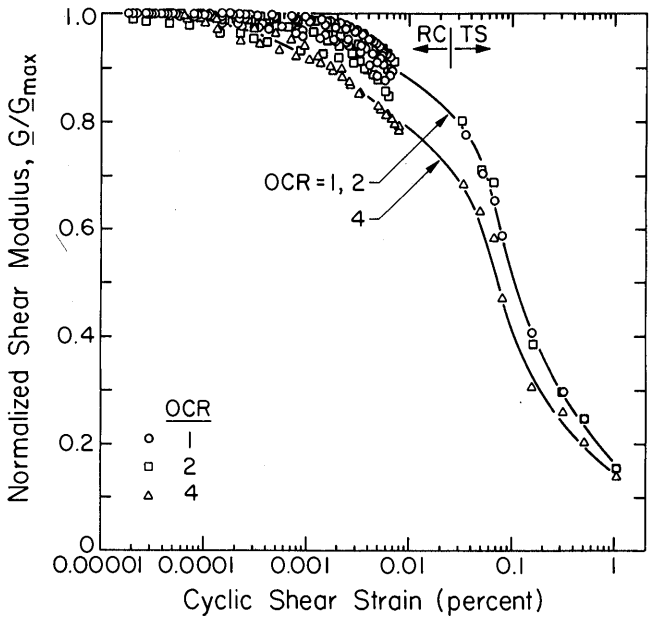


Figure 11.—Normalized shear modulus versus cyclic shear strain.

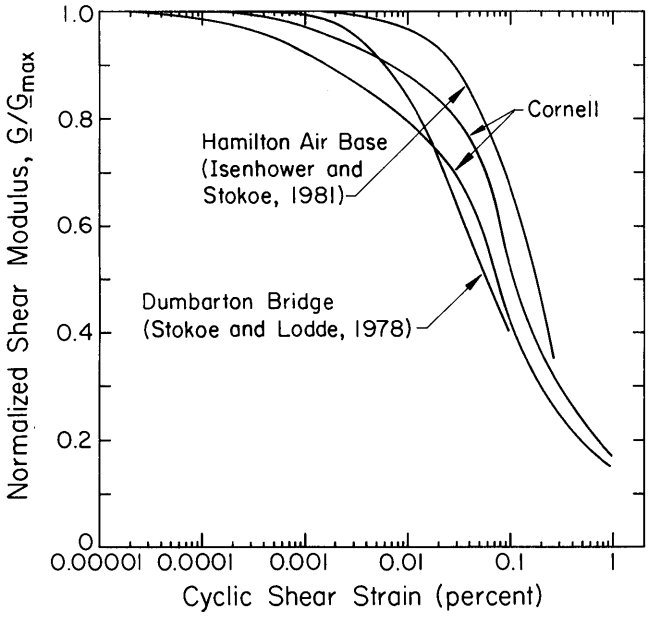


Figure 12.—Curves of normalized shear modulus versus cyclic shear strain obtained in this study in comparison with those from previous studies.

Society for Testing and Materials Special Technical Publication 654, p. 66–90.

Chen, A.T.F., and Stokoe, K.H., II, 1979, Interpretation of strain-dependent modulus and damping from torsional soil tests: Menlo Park, Calif., U.S. Geological Survey Report USGS–GD–79–002 (NTIS–PB–298749/AS), 45 p.

Dobry, Ricardo, and Vucetic, Mladen, 1987, State-of-the-art report; dynamic properties and response of soft clays: International Symposium on Geotechnical Engineering of Soft Soils, 1987, Proceedings, v. 2, p. 51–87.

Dyvik, Rune, Zimmie, T.F., and Floess, C.H.L., 1981, Lateral stress measurements in direct simple shear device, *in* Laboratory shear strength of soil: American Society for Testing and Materials Special Technical Publication 740, p. 191–206.

Hardin, B.O., and Drnevich, V.P., 1972, Shear modulus and damping in soils: design equations and curves: American Society of Civil Engineers Proceedings, Soil Mechanics and Foundations Division Journal, v. 98, no. SM7, p. 667–692.

Isenhower, W.M., and Stokoe, K.H., II, 1981, Strain rate-dependent modulus of San Francisco Bay Mud: International Conference on Recent Advances in Geotechnical Earthquake Engineering and Soil Dynamics, St. Louis, Mo., 1981, Proceedings, v. 2, p. 597–602.

Isenhower, W.M., Stokoe, K.H., II, and Allen, J.C., 1987, Instrumentation for torsional shear/resonant column measurements under anisotropic stresses: Geotechnical Testing Journal, v. 10, no. 4, p. 183–191.

Kokusho, Takeji, Yoshida, Yasuo, and Esashi, Ysuyuki, 1982, Dynamic properties of soft clay for wide strain range: Soils and Foundations, v. 22, no. 4, p. 1–18.

Lodde, P.F., 1979, Shear moduli and material damping of San Francisco Bay Mud: Austin, University of Texas, M.S. thesis.

Mayne, P.W., and Kulhawy, F.H., 1982, $K_o$–OCR relationships in soil: American Society of Civil Engineers Proceedings, Geotechnical Engineering Division Journal, v. 108, no. GT6, p. 851–872.

Saada, A.S., 1984, Discussion; specimen size effect in simple shear test: Journal of Geotechnical Engineering, v. 110, no. 3, p. 445–447.

Schmidt, Birger, 1966, Discussion; earth pressures at rest related to stress history: Canadian Geotechnical Journal, v. 3, no. 4, p. 239–242.

Stokoe, K.H., II, and Lodde, P.F., 1978, Dynamic response of San Francisco Bay Mud: American Society of Civil Engineers Conference on Earthquake Engineering and Soil Dynamics, Pasadena, Calif., 1978, Proceedings, v. 2, p. 940–959.

THE LOMA PRIETA, CALIFORNIA, EARTHQUAKE OF OCTOBER 17, 1989:
STRONG GROUND MOTION AND GROUND FAILURE

MARINA DISTRICT

# SITE-RESPONSE ANALYSES

By J.-P. Bardet, M. Kapuskar, G.R. Martin, and J. Proubet,
University of Southern California

## CONTENTS

[Figures 19–23, 28–35, and 38–53 follow references]




### ABSTRACT

We have analyzed the site response of the Marina District of San Francisco during the earthquake, using numerical-modeling techniques that encompass the conventional methods used in engineering practice, as well as advanced techniques capable of accounting for three-dimensional geometry and wave propagation. Our models are based on a synthesis of the geology of the Marina District with data from various site investigations.

Nonlinear one-dimensional analyses with the computer programs DETRAN and LINOS predict peak ground-surface accelerations of 0.12 and 0.15 *g* in the Marina District for the Yerba Buena accelerogram with bedrock peak accelerations of 0.067 *g* (original) and 0.15 *g* (scaled), respectively. The program SHAKE predicts a larger amplification, reflecting the use of an equivalent linear material model that does not consider complete failure. The Yerba Buena Island accelerogram was assumed to be the most realistic input record because its peak acceleration of 0.067 *g* agrees with the accelerations recorded on bedrock sites in the San Francisco Bay area. The amplification of bedrock acceleration resulted mainly from deep deposits of older bay mud. The accelerations reaching the layer of yellow hardpan were truncated by yielding of the overlying layers composed of artificial fills and younger bay mud. A

simplified liquefaction analysis clearly indicated that the artificial fills would liquefy during the earthquake.

For comparison with the one-dimensional analyses, we also performed two types of two-dimensional site-response analyses using numerical methods that are not commonly used in engineering practice. The first type assumed a uniform input for the ground motion along the model boundary, whereas the second type assumed nonuniform inputs along the model boundary in an attempt to account for the effects of wave propagation on the dynamic response of the Marina District. These two-dimensional analyses predicted peak ground-surface accelerations of 0.20 and 0.23 *g* for peak bedrock accelerations of 0.067 and 0.15 *g*, respectively. The two-dimensional analyses predicted larger peak accelerations than the one-dimensional analyses, indicating that the one-dimensional site-response analyses used in engineering practice may not necessarily be conservative.

Our analyses indicate that two-dimensional effects are important in the site response of the Marina District. These two-dimensional effects resulted mainly from the irregular geometry of the bedrock and the yellow hardpan. Inclusion of wave-propagation effects into the site-response analyses substantially complicates the dynamic-response analyses; however, these effects were more noticeable in linear than in nonlinear analyses. The present study shows the complexity of site-response analyses for three-dimensional geologic structures and clearly indicates that future research is needed on this topic.

## INTRODUCTION

The 1989 earthquake was the largest to occur in the San Francisco Bay area since the catastrophic San Francisco

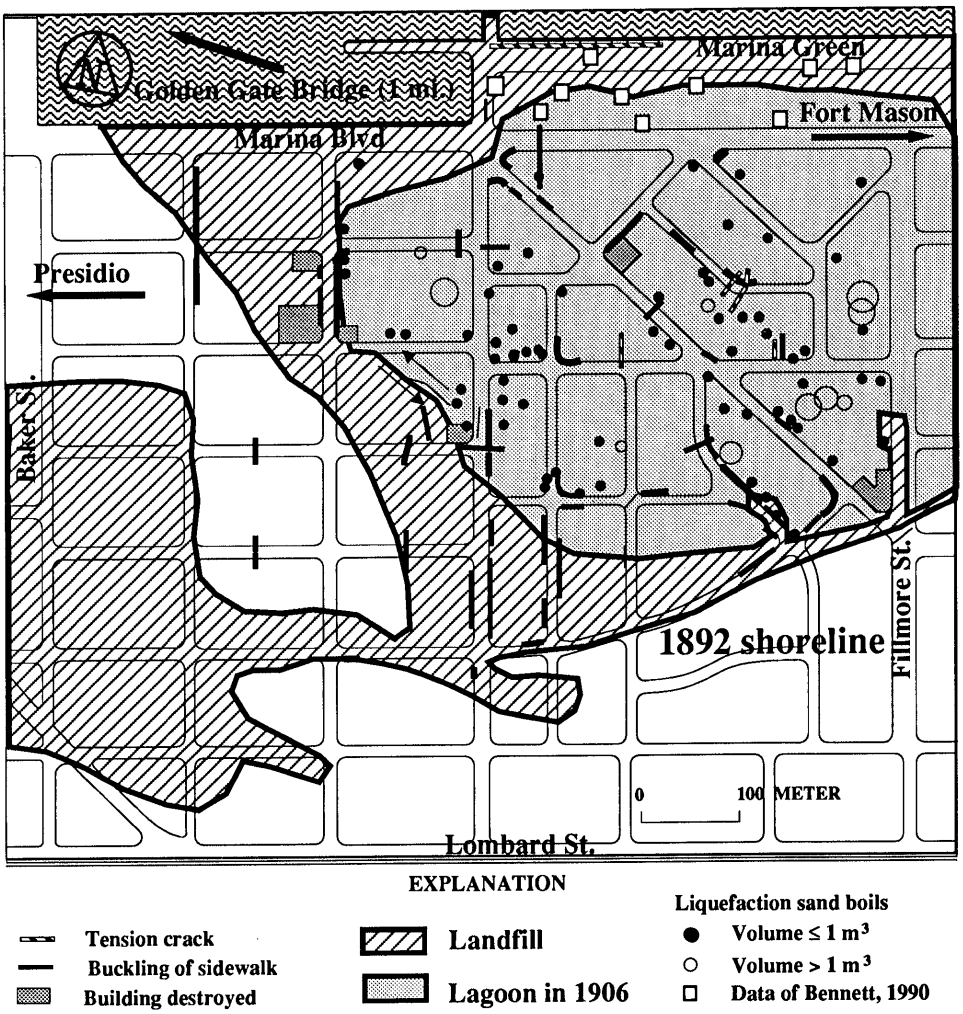


Figure 1.—Sketch map of study area in the Marina District, showing results of field investigation of October 1989.

earthquake of 1906. About 40 buildings were destroyed or condemned in the Marina District, 108 km away from the epicenter. Disruption of the ground underlying the Marina District caused vertical settlement and lateral displacement of most buildings, as well as buckling of sidewalks, cracking of asphalt pavements, and breakage of underground pipes (Bardet and Kapuskar, 1991c and in press).

This report investigates the site response of the Marina District during the 1989 earthquake by using numerical-modeling techniques of site response, including conventional analyses and advanced nonlinear finite-element methods. Our objectives are to describe the dynamic response of the Marina District by applying the site-response analyses used in engineering practice, and to complete these analyses by using advanced techniques capable of accounting for two- and three-dimensional geometry and wave-propagation effects.

## OBSERVATIONS ON SAND BOILS AND STRUCTURAL DAMAGE

Besides structural collapse, one of the most striking phenomena recorded in the Marina District during the earthquake was the abundant ejection of water and fine-grained sand from the ground. These observations are only briefly described here; a more complete description was given by Bardet (1990a) and Bardet and Kapuskar (1991c and in press).

A few days after the earthquake, a reconnaissance team from the University of Southern California (USC) visited the Marina District and collected data on sand boils. The study area (fig. 1) is bounded by Baker Street, Fillmore Street, Marina Boulevard, and Lombard Street. Sand boils were highly visible on the concrete floors of buildings and on sidewalks. A few days after the main shock, access to the study area was still limited, a circumstance that was unintentionally beneficial to our research: The police protection preserved perishable sand boils that otherwise would have been cleaned up by Marina District residents.

One of the largest sand boils covered a 29-$m^2$ area (fig. 2). It emerged through a backyard lawn, flowed through a wooden fence, and completely covered a neighboring backyard. The sand-water mixture, which emerged through two large craters, must have been under high pressure to have created such large orifices. A large volume of water also was evidently expelled from the ground so as to transport the large amount of deposited sediment. Abundant mud and silt littered the periphery of the sand volcanoes.

We recorded a total of 74 sand boils in the study area (fig. 1). Bennett (1990) reported 10 additional sand boils north of the study area (squares, fig. 1); 42 percent of

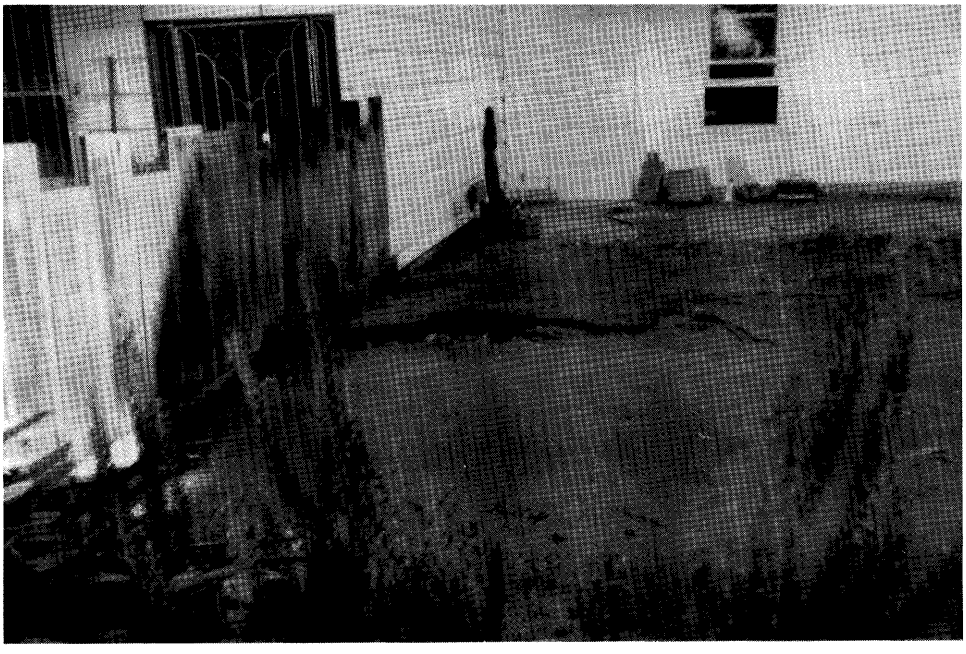

Figure 2.—Large sand boils that covered two backyards in the Marina District during the earthquake (approx scale, 1 in.=2 m).

these sand boils were smaller than 0.2 $m^3$ in volume. The cumulative volume of sand ejected during the earthquake exceeded 37 $m^3$. The largest sand boil (3.5-$m^3$ volume) completely flooded the backyard of an apartment building; the ejected sand was fine, dark gray, odorless, and accompanied by bay mud. In some places, sand seeped through the lawn and littered the grass and flowerbeds. Contrary to common belief, the sand boils were not caused by breakage of waterpipes or sewerpipes but by liquefaction of underlying soils.

The sand boils did not completely cover the Marina District but surfaced mainly in the northeastern part, over a 350- by 600-m area near the corner of Fillmore Street and Marina Boulevard (fig. 1). Without exception, all of the sand boils occurred over the site of a 1906 lagoon that was filled in 1915 to host the Panama-Pacific International Exposition. Lawson (1908, p. 404–405) reported severe ground shaking around this lagoon during the 1906 earthquake, even before the Marina District was built. In addition to sand boils, our survey also mapped evidence of superficial ground displacements, such as buckling of concrete sidewalks, rupture of curbs, and tension cracks in asphalt pavement. Our observations of ground displacements and major structural damage to buildings are summarized in figure 1.

A superficial crack about 300 m long was observed in the middle of the Marina District, along the southeast side of the liquefied area. The lateral ground displacement was estimated to reach 30 cm, according to our measurements. Along this superficial crack, a major fire was ignited, and three apartment buildings located at street corners collapsed. Surprisingly, the collapsed buildings and large ground displacement were not close to the sand boils but about 100 m away (fig. 1). The damage was not directly caused by liquefaction of the sand underlying the foundation of the buildings, as was observed during the 1964 Niigata, Japan, earthquake (Seed, 1970). The ripples and undulations in the ground surface suggest that the liquefied sandy fills of the Marina District spread laterally and were forced down a gentle slope by gravity. The most severe structural damage took place along the edges of the liquefied area and resulted from differential displacements between the liquefied and nonliquefied soils (Bardet and Kapuskar, 1991c and in press).

## GEOLOGY OF THE MARINA DISTRICT

We first summarize the geology of the Marina District because it is used to construct the model for site-response analysis (see Bonilla, this chapter, for details). The Marina District is located on the north waterfront of San Francisco, 1 mi east of the Golden Gate Bridge, between the Presidio and Fort Mason (see fig. 1). The soils beneath the Marina District are divided into natural deposits and artificial fills.

### NATURAL DEPOSITS

During the last 1 m.y. of the late Cenozoic glacial episode (3,500–15 ka), at least three glacial-interglacial cycles occurred in San Francisco Bay, each marked by a period of material deposition during high sea levels, followed by a period of desiccation and erosion due to lower sea levels (W.H. Hensolt, written commun., 1988).

Between 1.8 and 0.7 Ma, when sea level was more than 90 m lower than today, the Golden Gate channel was formed, and San Francisco Bay came into existence. As suggested by Schlocker (1974), the bedrock underlying the Marina District is composed of Franciscan assemblage eroded by waters of the ancient Sacramento and San Joaquin Rivers flowing through the Golden Gate channel about 1.5 Ma.

The earliest stage of development of the Golden Gate channel and San Francisco Bay took place during the glacial-interglacial cycle that occurred between 1.0 and 0.5 Ma, when unconsolidated estuarine sandy materials were deposited during high sea levels. These older materials consist of firm, orange to light-brown sand.

During the most recent interglacial interval, the Sangamon stage of the Pleistocene Epoch (125–75 ka), thick, gray estuarine clay deposits containing interbeds of sand and shells were formed (Schlocker, 1974; Bonilla, 1990). These materials (also referred to as the older bay mud) cover virtually all of the deep soils and bedrock underlying the Marina District.

Borehole logs from as early as 1912 (Schlocker, 1961) and more recent investigations (for example, Bennett, 1990) have indicated that beds of dense sand cover the older clay deposits under the Marina District. These firm materials, the uppermost part of which are called the yellow hardpan, are assumed to be eolian deposits formed during the early part of the Altonian Glaciation (40–30 ka) that were subjected to surface erosion during the low sea level of the Wisconsin Glaciation. These hard strata, referred to as Pleistocene sand zones (Bonilla, 1990), are considered to be at least 10 ka old.

After the Wisconsin Glaciation that ended some 10 ka, deposition of estuarine materials began on the site of the Marina District, owing to high sea levels flooding the Golden Gate channel. These materials (commonly referred to as the younger bay mud) consist of semiconsolidated, olive-gray, fine sand and clay that cover most the Marina District.

### ARTIFICIAL FILLS

The shoreline of the Marina District is shown in figure 1. By 1906, Marina Cove was enclosed by a seawall. The Panama-Pacific International Exposition of 1915 had the largest environmental impact on the Marina District. A.H.

Markwart, assistant director of works for the exposition, wrote in 1915 that the filling started on April 13, 1912, along the shoreline to create solid land for the exhibition. The filling of the tidelands continued for 5 months, and by September 1915, 1 million $m^3$ of sand and mud had been pumped into the area. Sand containing silt, gravel, debris, and organic waste mainly composed the material used for fill. According to Markwart, the fill was about 70 volume percent sand and 30 volume percent mud. A total of 46 ha (114 acres) of marshlands on the grounds of the Presidio were also filled for the exposition. "The fills proved satisfactory," Markwart wrote, "as the installation of roads and gardens, the work of pile driving, and construction of the Exhibition Palaces took place immediately upon completion of the fill, a procedure which was unusual (in 1912) in the case of many new fills." After the exposition closed, the area remained unused until the 1920's, when real estate development began in the Marina District.

## THREE-DIMENSIONAL SOIL MODEL

The study area covers about 1.2 $km^2$ between Lyon, Lombard, and Laguna Streets and the northern waterfront, including the St. Francis Yacht Club Harbor (fig. 3).

Data on stratigraphy and soil properties were compiled to construct a three-dimensional soil model of the Marina District. On the basis of data compiled from 86 borehole logs, 10 geologic units were distinguished: Franciscan assemblage, serpentine (of the Franciscan assemblage), Colma Formation, late Pleistocene bay clay, Holocene bay clay, shells, beach sand, dune sand, tidal-marsh deposits,

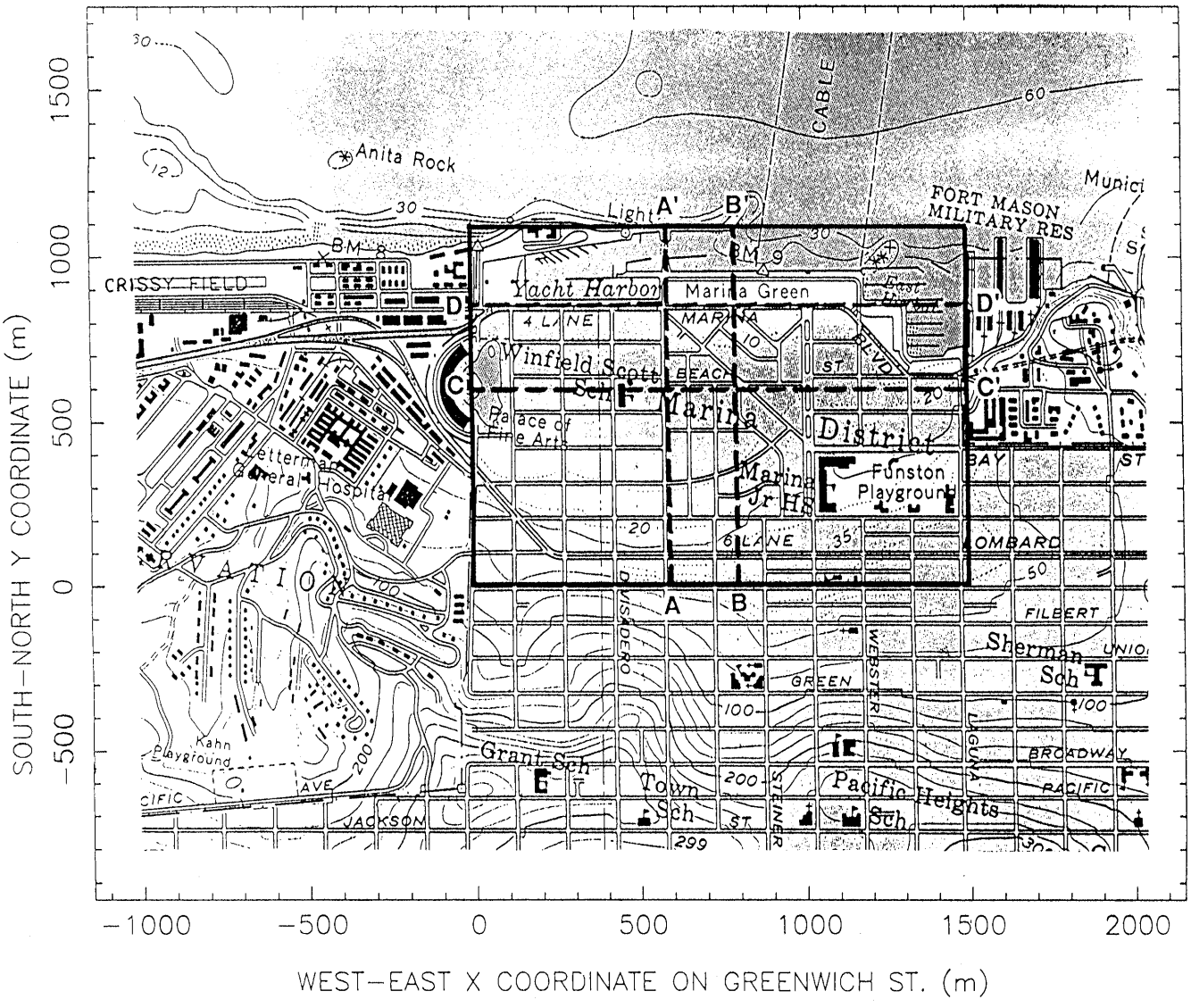


Figure 3.—Marina District, showing location of study area (box) and orientation of cross sections *A–A'* through *D–D'* in three-dimensional soil model.

and artificial fills. These units were grouped into four layers: (1) the late Pleistocene bay clay, above a bedrock surface of Franciscan assemblage; (2) the yellow hardpan; (3) Holocene bay clay, with traces of Holocene green sand; and (4) an upper layer of mixed silt-sand-gravel, beach sand, and dune sand.

## SITE INVESTIGATION IN SEPTEMBER 1990

Deep-borehole logs were too scarce to provide sufficient information on the depth, thickness, and soil properties of the yellow hardpan and older bay mud, and so the purpose of the site investigation was to collect additional soil profiles and soil properties. The investigation included nine cone penetration tests (CPT's) and three downhole seismic CPT's. The CPT investigation was performed in September 1990 by Earth Technology Corp. (1990), using a 20-ton system.

To delineate the subsurface strata to the north of the study area, two CPT soundings were located on the Marina waterfront (boreholes C–1, C–5, fig. 4). Two downhole seismic CPT's were performed in borehole C–1. To aid interpretation of the CPT results, an additional CPT sounding C–2 was performed in borehole C–2 in the center of the old Marina Cove, next to U.S. Geological Survey (USGS) borehole M4. The third seismic CPT, in borehole C–17, was located on the 1857 shoreline, where surficial dune sand occurs.

Six soil columns interpreted from the CPT results are illustrated in figure 5. These columns were obtained after comparing the CPT results obtained in borehole C–2 against the soil column in USGS borehole M4 (U.S. Geological Survey, 1990). Our interpreted soil columns in other places were found to match the borehole logs obtained by Dames & Moore (1977) and Harding Lawson Associates (written commun., 1990).

The yellow hardpan was penetrated in boreholes C–1 and C–5, where it was found to be less than 1.2 m thick. It was penetrated in borehole C–1 at a depth of 31 m, and in borehole C–3 at a depth of 27.7 m, 5 m below the depth predicted by Dames & Moore (1977).

During the CPT investigation, problems arose with the sticky older bay mud. At borehole C–1, the CPT was ter-

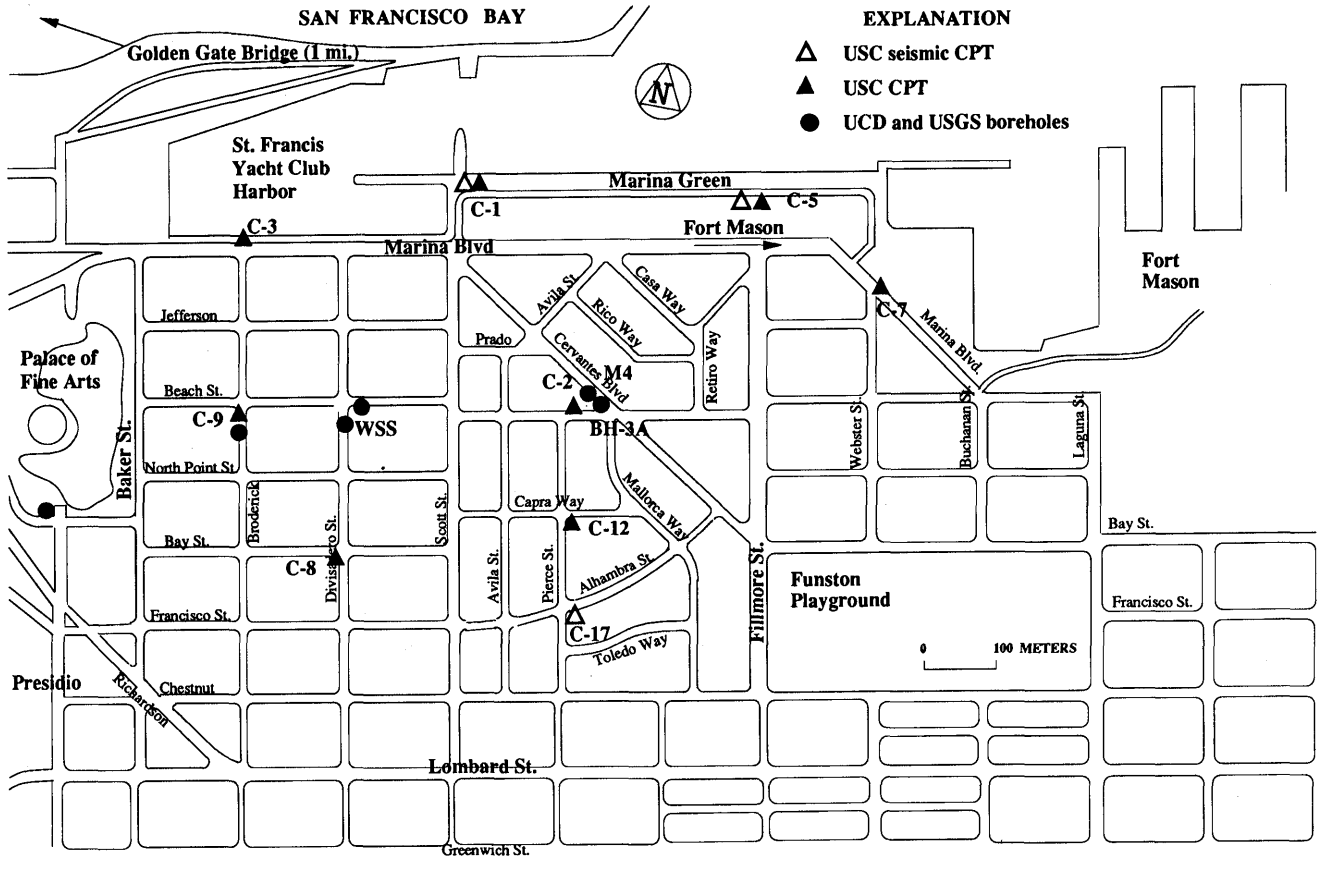


Figure 4.—Marina District, showing locations of boreholes and CPT soundings during site investigation of September 1990.

minated 12 m below the yellow hardpan, owing to excessive sleeve friction; and in boreholes C–2, C–8, and C–12, penetration failed owing to rod buckling and high tip bearing resistance. In all the other boreholes, the dense sand layer was not reached, owing to sleeve friction in the hydraulic fill and (or) excessive probe inclination.

## UNDRAINED SHEAR STRENGTH

The undrained shear strength $S_u$ in the older and younger bay muds was calculated from the tip resistance measured from the CPT soundings of the site investigation, using the method of Schmertmann (1975) with a bearing-capacity factor of 6, based on shear-strength correlations between CPT and vane shear tests (Denby, 1961; Martin and Tsai, 1981). The calculated $S_u$ values (fig. 6) were correlated with additional data from Schlocker (1974), Dames and Moore (1977), Denby (1978), Bonaparte and Mitchell (1979), Seed and Sun (1989), and Kayen and others (1990). The calculated profile of un-drained shear strength (fig. 6) is complex and varying; the $S_u$ value tends to increase with depth and jumps abruptly in the yellow hardpan and in the top 5 m, owing to the presence of debris. A highly simplified shear-strength profile was used in the site-response analyses (fig. 6) to reduce the number of elements required in the two-dimensional models. For nonlinear site-response analyses, the $S_u$ values plotted in figure 6 were increased to account for rapid-loading effects. The values of undrained shear strength $\tau_{max}$ in dynamic analyses were assumed to be 40 percent greater than the $S_u$ values in all soil layers except the top layer. An average $S_u$ value of 20 kPa was assumed for the saturated cohesionless fill and the younger bay mud above the yellow hardpan. $S_u$ was set to 160 kPa in the yellow hardpan, as in the deeper layers of the older bay mud, and to 100 kPa in the 30-m-thick layer of late Pleistocene bay clay underlying the yellow hardpan.

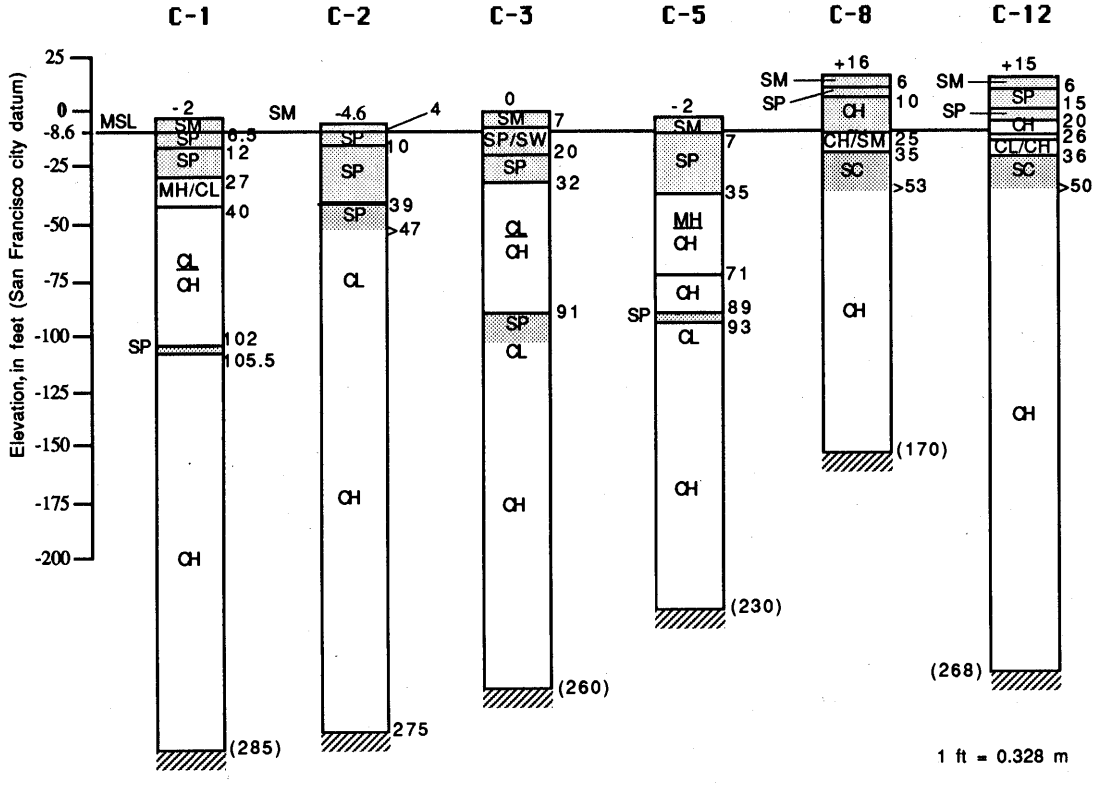


| location | 3899 Scott St. | 101 Cervantes | 701 Marina Blvd (Broderick St.) | Marina Green Drive (extension of Fillmore St.) | 3495 Divisadero St. | 3481 Pierce St. |
|---|---|---|---|---|---|---|
| soil-column calibration | HSA-23 (Dames & Moore, 1977) | M4 (USGS,90) BH-3A (UCD,90) | HSA-3 (Dames & Moore, 1977) | HSA-15 (Dames & Moore, 1977) | Job 19738,001.04 (Harding Lawson Associates) | Hole 78 (Schlocker, 1961) |

Figure 5.—Soil columns interpreted from CPT results in boreholes, with references used for comparison. Soils are identified by symbols in Unified Soil Classification.

## WAVE VELOCITY

Shear- and compressional-wave velocities were determined from three seismic CPT's performed in boreholes C–1, C–5, and C–17. As plotted in figure 7, four zones can be distinguished from the interpreted shear-wave velocities.

1. In the loose, unsaturated and unconsolidated, sandy and gravelly artificial fill, the velocities of shear and compressional waves are $v_s$=290–415 m/s and $v_p$=580–870 m/s, respectively. The large variation in these velocities is attributed to the inhomogeneity of the artificial fill, which ranges widely in composition from silty sand and debris (borehole C–17, fig. 4), through clayey sand and scattered rock fragments near Fair's seawall (boreholes C–1, C–5, fig. 4), to wooden piles left over from the exposition.
2. In the saturated, sandy artificial fill, the natural-sand deposits, and the Holocene bay clay, $v_s$=120–225 m/s and $v_p$=1,520–1,650 m/s. The lower range is confirmed by measurements (Kayen and others, 1990) in USGS borehole WSS (fig. 4), where $v_s$=128–160 m/s. The higher $v_s$ value applies to more consolidated Holocene bay clay.
3. In the yellow hardpan, $v_s$=290–460 m/s. These velocities were measured in USGS borehole WSS in a layer of the yellow hardpan 11 m thick. The average $v_s$ value of 366 m/s is similar to the values of 335 and 365 m/s selected in the dynamic analyses of Seed and Sun (1989).
4. Below the yellow hardpan, $v_s$>225 m/s and $v_p$=1,740 m/s. In borehole C–1, seismic CPT's were performed down to a depth of 43 m, about 10 m into the late Pleistocene bay clay. The $v_s$ values were found to be identical to those in the lowest parts of the Holocene bay clay. In the absence of other deep measurements of $v_s$ in the Marina District, the shear-wave velocities were supplemented by measurements in three other places: USGS borehole WSS (fig. 4), the Southern Pacific Building (approx 1.5 km southeast of the Marina District), and the Embarcadero Center (Seed and Sun, 1989). In USGS borehole WSS, $v_s$ =265 m/s. At the Southern Pacific Building, where soil conditions are similar to those in the Marina District; $v_s$ was estimated at 335 m/s for a layer of stiff, consolidated (Pleistocene) clay 30 m thick.

The shear-wave velocities measured in these other places and the velocity profile selected in our analysis are plotted in figure 7. This velocity profile was used to calculate the low-strain elastic-shear modulus $G_{max}$ in the site-response analyses.

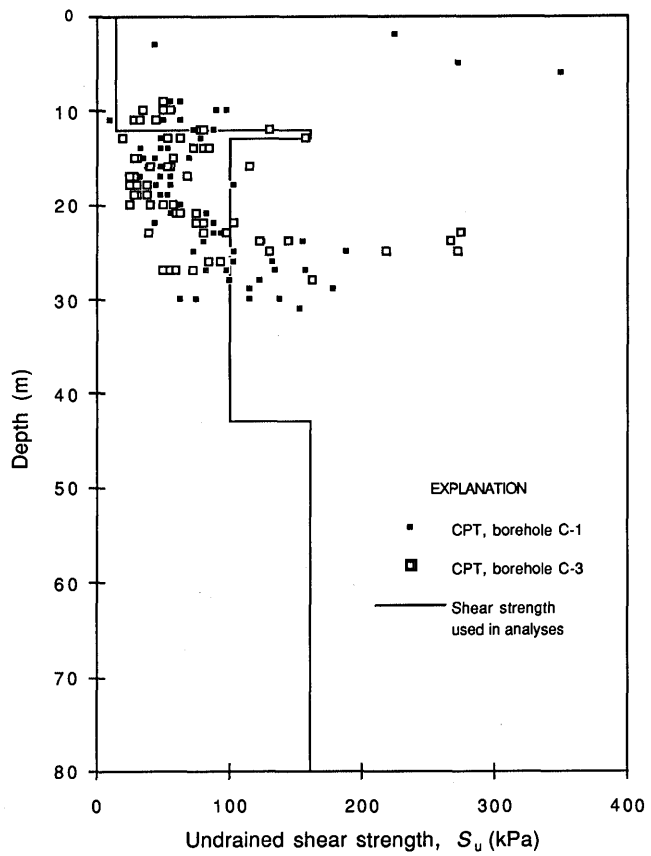


Figure 6.—Depth versus undrained shear strength in the study area.

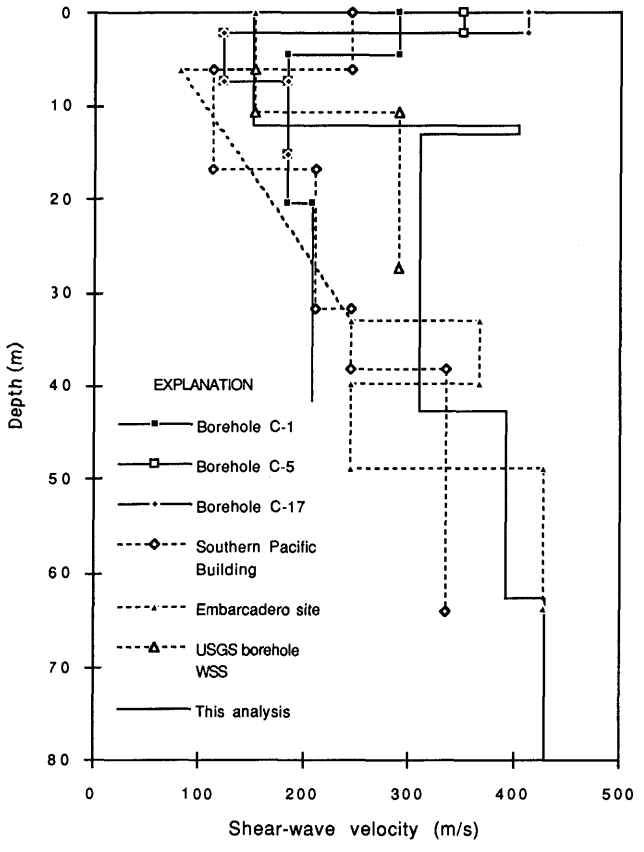


Figure 7.—Depth versus shear-wave velocity in the study area.

## CONSTRUCTION OF THREE-DIMENSIONAL SOIL MODEL

On the basis of a compilation of the borehole data, a four-layer model was constructed to represent the soils in the Marina District. Later, these basic material layers are further divided into elements when defining the finite-element meshes. This degree of accuracy is believed to be adequate for evaluating site-response characteristics.

The three-dimensional model was developed from discrete borehole logs. It covers a horizontal area 1,500 by 1,100 m and is composed of 1,152 nodes. It was constructed by identifying the top and bottom surfaces and three interfaces—that is, five surfaces—in all the available borehole logs. Each surface was generated by the elevation of nodes on a uniform grid of 16 by 12 nodes. Delaunay triangulation was used to interpolate the elevations of these evenly spaced nodes from the scattered data of borehole logs. In the process, erroneous identifications of soils were filtered, and the interface positions were smoothed. The layers were stacked in sandwich fashion without intersecting one another. The elevation of gridpoints was slightly adjusted by trial and error until interfaces stopped intersecting. Each surface and layer in the model are described below.

### GROUND SURFACE

The ground surface constitutes the upper surface of the three-dimensional model. It was defined by 650 scattered elevation points digitized from USGS topographic maps (U.S. Geological Survey, 1973) inside a rectangular 4,000-by 3,000-m frame. A three-dimensional model of the Marina District and its surroundings is shown in figure 8.

### BEDROCK SURFACE

The bedrock surface constitutes the lower surface of the three-dimensional model. In geotechnical engineering, the definition of bedrock is generally subjective, closely dependent on the particular problems to be solved. In the Marina District, the bedrock was rather easily identified because a significant discontinuity could be located between superficial and deep sedimentary deposits. The bedrock underlying the Marina District is made up of serpentine and of sandstone and weathered shale of the Franciscan assemblage. A bedrock depression was inferred from (1) the distribution, size, and shape of nearby outcrops; (2) a few reliable deep boreholes; and (3) geologic considerations.

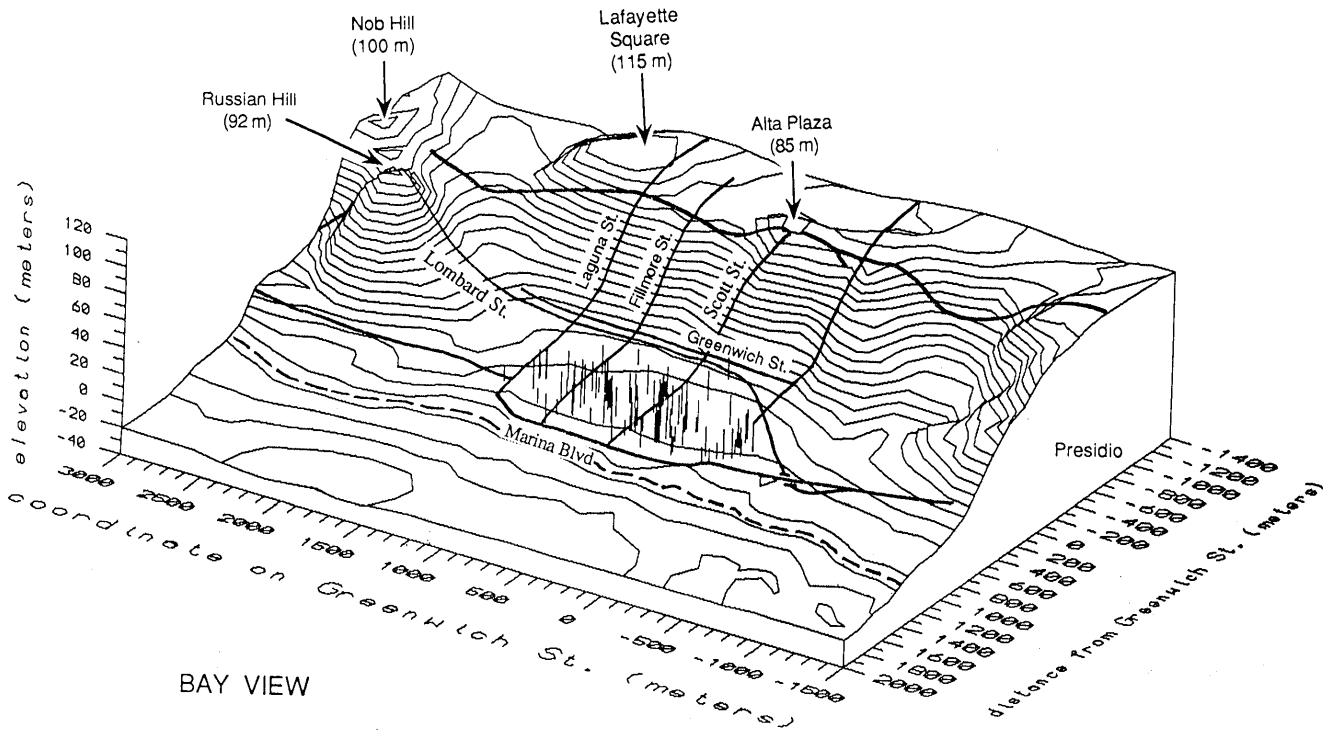


Figure 8.—Three-dimensional model of ground surface in the study area. Short vertical segments represents boreholes used to generate model.

Our construction of the three-dimensional bedrock surface was made difficult by the absence of deep borehole data. At this date, only three boreholes have reached bedrock. High-resolution profiling based on geophysical seismic reflection would have been an appropriate technique to define the exact position of the bedrock; however, the limitations of this type of investigation in the presence of deep sedimentary deposits in a heavily urbanized area ruled out its use.

Construction of the bedrock surface was also complicated by the presence of a layer of yellow hardpan 60 m above the true bedrock. This hard layer was misinterpreted as bedrock by several investigators (for example, Schlocker, 1961) who based their definition of bedrock on available geotechnical soundings. The error was discovered in the USGS map (Schlocker, 1974) after noting the anomaly in the bedrock contours east of Webster Street.

The outcrops noted on the geologic map of Schlocker (1961) were useful in reconstructing the bedrock surface in the Marina District (fig. 9). The following bedrock outcrops surrounding the Marina District were included: at Fort Mason, on Russian Hill, on Nob Hill, around Lafayette Square (Fillmore Hill), at the intersection of Scott and Greenwich Streets, at Alta Plaza east of the Presidio, in the central part of the Presidio, and at Crissy Field. The bedrock depths determined in USGS borehole WSS and in UCD borehole BH–3A (at USGS borehole M4, fig. 4) were extremely useful to calibrate the bedrock depth. Old drillholes at the center of Funston Playground (fig. 3; U.S. Geological Survey, 1990) and south of the Palace of Fine Arts (fig. 3; Dames & Moore, 1962) were also included.

Bedrock-elevation contours were obtained by interpolating (with a Delaunay triangulation) the scattered data of 130 known and about 20 hypothetical elevations. The hypothetical elevations were obtained on the basis of geologic considerations, such as the gradients of bedrock drainage paths toward the Golden Gate channel, as shown in figure 9 (Schlocker, 1974; W.H. Hensolt, written commun., 1990). The bedrock surface is assumed to be a half-basin surrounded by bedrock outcrops; it opens toward the bay on a northwestward trend. Under the Marina waterfront, the depression is bounded by the bedrock outcrops

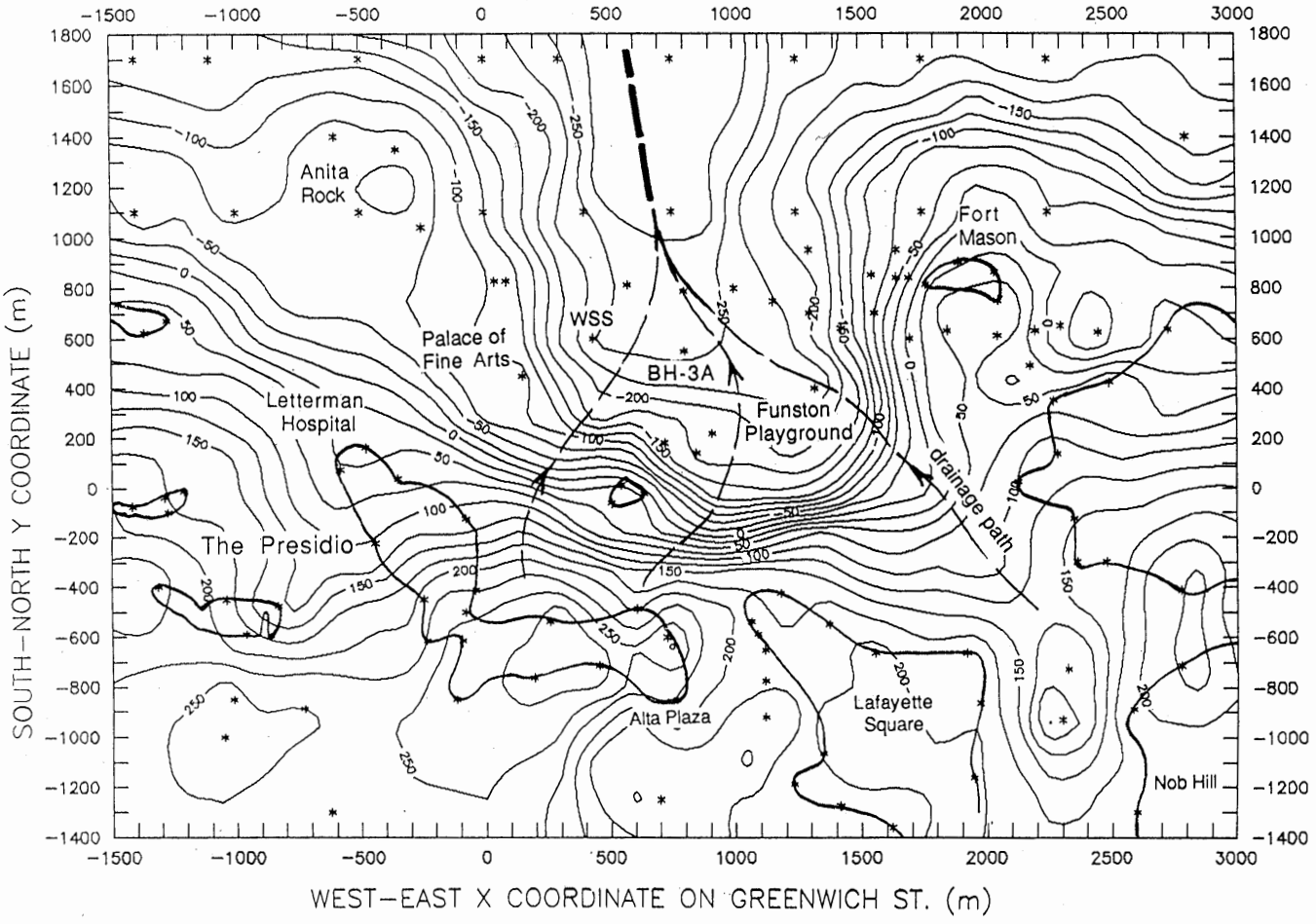


Figure 9.—Estimated bedrock contours and drainage paths in the Marina District. Coordinate system is defined in figure 3. Asterisks represent points (hypothetical or measured) used to draw contour lines.

at Forts Mason and Scott. The depression is assumed to reach 87-m depth under Marina Boulevard. Offshore, the basin is bounded by the outcrop of Alcatraz Island to the far northeast (Schlocker, 1961), which is less than 2 mi from the Marina District, and by an underwater outcrop called Anita Rock (fig. 3; Carlson and McCulloch, 1970).

#### LATE PLEISTOCENE BAY CLAY (OLDER BAY MUD)

The late Pleistocene bay clay covers the bedrock under the Marina District; it reaches a thickness of about 60 m under Marina Boulevard between Scott and Fillmore Streets. Only a few deep boreholes were available to yield reliable information on this layer, which is assumed to be continuous and overlain by the yellow hardpan throughout the Marina District.

#### YELLOW HARDPAN

The top of the yellow hardpan was modeled on the basis of 74 borehole logs, and its bottom from 35 borehole logs; 39 boreholes did not penetrate this layer. The yellow hardpan deepens toward the waterfront and rapidly dips down to below 28-m depth at borehole C–3 and to below 31-m depth at borehole C–1 (fig. 4). In comparison with other layers, the yellow hardpan generally is very thin (0.3–1.2 m thick), although it thickens considerably (11 m) under the Palace of Fine Arts (fig. 3; Dames & Moore, 1962).

#### HOLOCENE BAY CLAY (YOUNGER BAY MUD)

The layer of Holocene bay clay was constructed from 87 borehole logs. It extends landward past the 1869 shoreline from Fort Mason across Funston Playground (fig. 3) and under Lombard Street toward the Presidio. This layer has a fairly smooth top that could be explained by the absence of erosion since its deposition. A layer of hard green sand underlies the Holocene bay clay under most of the Marina District.

#### TOP LAYER

The top layer is composed of tidal-marsh deposits, beach sand, dune sand, and artificial fills. A band of tidal-marsh deposits occurs under the Presidio (at Crissy Field, fig. 3) and southwest of the Marina District between Scott and Fillmore Streets as far south as Lombard Street. These deposits contain organic clay and silt and some Holocene materials, such as bay mud and beach sand. The natural-sand deposits along the present shoreline east of the Golden Gate between Fort Point and Telegraph Hill are now overlain by artificial materials that were used for landfill during the 1980's. These deposits, which underlie the western part of the Marina District, formed old Strawberry Island, a sand spit in the northwest corner of the district. A small band of beach sand is situated south of Alhambra Street (fig. 4). Dune sand that probably covered the western beach deposits occurs mainly between Webster Street and Fort Mason.

### THREE-DIMENSIONAL MODEL

A three-dimensional model of the ground and bedrock surfaces as seen from the waterfront is shown in figure 10. The elevation of the ground surface rises from 0 to about 15 m (San Francisco city datum) near the shoreline in the southwestern part of the Marina District; southeast of the Presidio, the bedrock surface meets the ground surface.

Soil profiles along four cross sections through the three-dimensional model of figure 10 are shown in figure 11. Cross sections *A–A′* and *B–B′*, which run north-south, have not been extended northward because of the absence of borehole logs in San Francisco Bay. The northern part of the three-dimensional model is therefore only approximately defined. Cross section *C–C′*, which contains Beach Street, is used in a two-dimensional analysis of the site response. The bedrock eventually emerges at the ground surface if the widths of cross sections *C–C′* and *D–D′* are extended.

Our three-dimensional soil model of the Marina District reveals that the bedrock and soil layers are not horizontal and uniform but have a complex three-dimensional configuration. Because the methods for treating multidimensional site response are still in a relatively early stage of development and evaluation, the three-dimensional model was not directly analyzed. However, two one-dimensional soil columns (in boreholes M4 and WSS, fig. 4) and one two-dimensional cross section (*C–C′*, fig. 11) were extracted from the three-dimensional model and subjected to several types of site-response analyses.

## ONE-DIMENSIONAL SITE-RESPONSE ANALYSES

We first examine the site response of the Marina District by using conventional one-dimensional analyses.

### PROGRAMS FOR ONE-DIMENSIONAL ANALYSIS

Several computer programs for one-dimensional analysis of the effects of local soil conditions on ground response during earthquakes are presently available, for example, SHAKE (Schnabel and others, 1972), DETRAN (Chen and Joyner, 1974), DYSAC2 (Muraleetharan and others,

1990), DYNA1D (Prevost, 1989), LASS II (Ghaboussi and Dikmen, 1977), DESRA2 (Lee and Finn, 1978), and LINOS (Bardet, 1989). Some of these computer programs were described by the National Research Council (1985). The numerical methods are based on the assumption that the soil deposits are homogeneous layers of infinite horizontal extent and that earthquake response arises from upward propagation of shear waves from the underlying rock formations. Analytical procedures based on this concept and the inclusion of nonlinear soil behavior are being increasingly used in earthquake engineering for predicting site response and the characteristics of ground-surface motions. We used the programs SHAKE, DETRAN, and LINOS in this study.

The program SHAKE (Schnabel and others, 1972) is based on a one-dimensional lumped-mass model of the soil-layer system connected by linear shear springs and dashpot elements. The nonlinearity of the shear modulus is accounted for by the use of equivalent linear soil properties (Seed and Idriss, 1970). An iterative procedure is used to obtain values for modulus and damping compatible with the effective shear strains in each soil layer.

The program DETRAN (a version of NONLI3, developed by Chen and Joyner, 1974) is based on a one-dimensional lumped-mass model of the soil-layer system connected by multilinear shear springs and dashpot elements. The multilinear springs are made of a series of linear springs in parallel with frictional elements (Iwan, 1967). In contrast to SHAKE, the program DETRAN uses a true hysteretic formulation of the stress-strain relation and can therefore handle nonlinear strain-softening material with hysteretic damping. The stress-strain behavior of the springs satisfies Masing's (1926) criterion.

The program LINOS (Bardet, 1989) is a three-dimensional, nonlinear, finite-element code that includes dynamic capabilities and a library of various nonlinear material models. The program may also be used to simulate one- and two-dimensional problems. The material models may be formulated in terms of either total or effective stress.

## INPUT MOTION

As summarized in table 1, 11 strong-motion accelerograms were recorded (Shakal and others, 1989) within 7 km of the Marina District. The peak acceleration ranges from 0.05 to 0.21 *g* in the horizontal direction; these extremes were measured in Pacific Heights and the Presidio, respectively 1.7 and 2.2 km from the Marina District. Surprisingly, both extremes were in the records closest to the

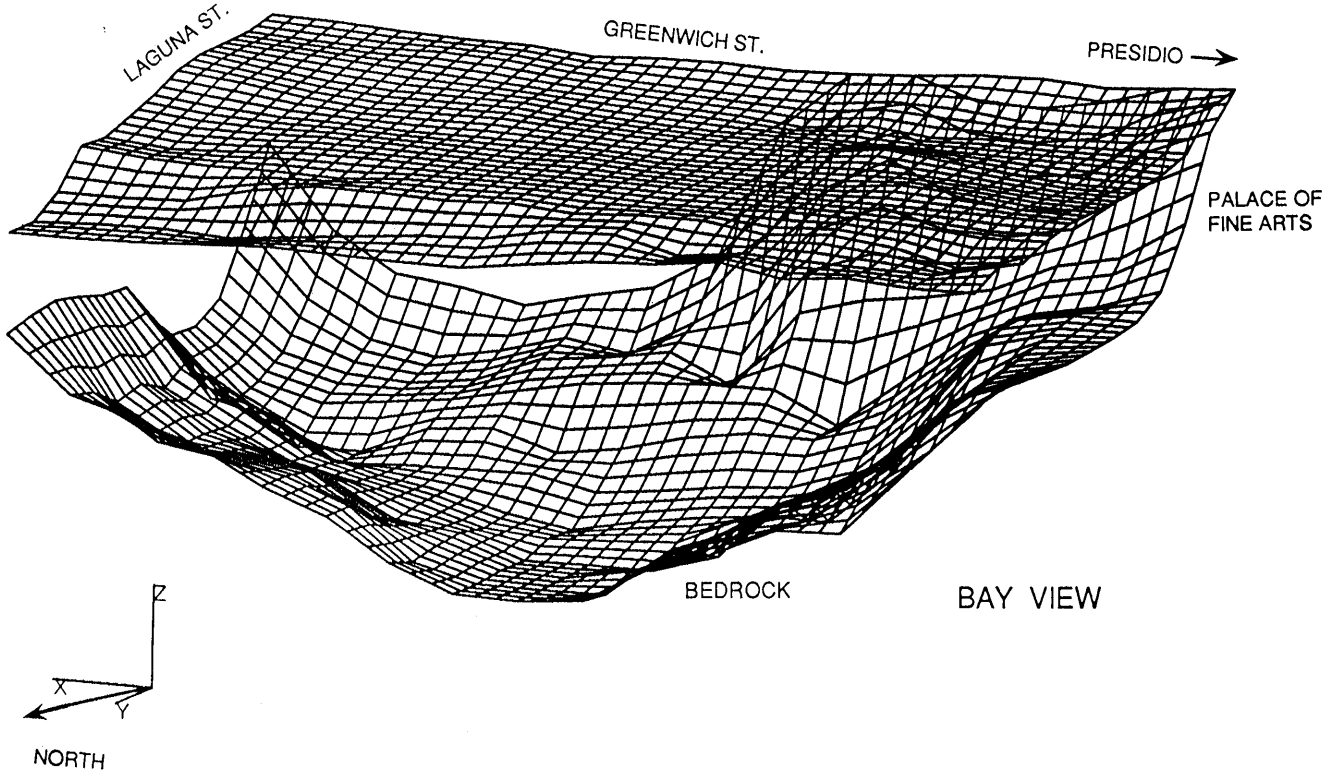


Figure 10.—Isometric view of three-dimensional soil model.

Table 1.—*Accelerograms recorded during the earthquake in the vicinity of the Marina District*

| Accelero-gram | Location | Distance (km) | Maximum acceleration | | Site subsoils |
|---|---|---|---|---|---|
| | | | Horizontal (*g*) | Vertical (*g*) | |
| 532 | 47-story office building | 4.1 | 0.13 | 0.08 | Artificial fill. |
| 151 | Rincon Hill | 4.9 | .09 | .03 | Franciscan assemblage (sandstone, shale). |
| 480 | 18-story building | 3.9 | .17 | .04 | Artificial fill over bay muds. |
| 131 | Pacific Heights | 1.7 | .05 | .03 | Franciscan assemblage (sandstone, shale). |
| 133 | Telegraph Hill | 2.7 | .08 | .03 | Franciscan assemblage (shale, sandstone). |
| 222 | Presidio | 2.2 | .21 | .06 | Serpentine. |
| 132 | Cliff House | 6.7 | .11 | .08 | Franciscan assemblage (sandstone, shale). |
| 479 | 6-story building, University of California, San Francisco. | 4.9 | .09 | .04 | ----- |
| 130 | Diamond Heights | 7.0 | .12 | .05 | Franciscan (chert). |
| 117 | Treasure island | 6.6 | .16 | .02 | Artificial fill. |
| 163 | Yerba Buena Island | 7.0 | .06 | .03 | Franciscan assemblage (sandstone). |

district. Among the accelerograms listed in table 1, the record from Yerba Buena Island, 7 km east of the Marina District, was thought to be best representative of the accelerations that probably took place in the bedrock of the Marina District during the earthquake. The original record has a peak acceleration of 0.067 *g* and a duration of 39.8 s in an east-west direction. Yerba Buena Island is primarily built on sandstone of the Franciscan assemblage. The peak acceleration on bedrock sites versus epicentral distance *d* is plotted in figure 12. The peak accelerations corresponding to *d*=80 km (Marina District) range from 0.03 to 0.15 *g*. The peak acceleration of 0.067 *g* on the original Yerba Buena accelerogram is a mean of the peak accelerations plotted in figure 12. Those accelerograms listed in table 1 that were recorded in the basements of buildings were not considered in this study because they were influenced by building structural responses. The accelerograms recorded on Treasure Island and in the Presidio also were not considered: The Treasure Island station is located on soft soils, and the strong motion recorded in the Presidio, although this station is located on serpentine bedrock, was much higher than the average recorded on bedrock in the San Francisco Bay area. The accelerograms recorded on Treasure Island and in the Presidio, although they correspond to the same distance *d* as the Marina District, fall outside the range of bedrock accelerations plotted in figure 12. A similar conclusion may be drawn from the response spectra of five accelerograms recorded in the vicinity of the Marina District (fig. 13). All of these response spectra were calculated by assuming 5-percent critical damping. The Telegraph Hill, Pacific Heights, and Yerba Buena Island accelerograms, which were recorded on bedrock, clearly differ from the Treasure Island and Presidio accelerograms recorded on soft soils.

Two input acceleration-time histories were considered in the one- and two-dimensional analyses: the original Yerba Buena Island accelerogram (east-west and vertical components) and a scaled Yerba Buena Island accelerogram. The scaled horizontal acceleration has a peak of 0.15 *g*, which corresponds to the upper bound of peak acceleration for *d*=80 km in figure 12. The scaled vertical acceleration has a peak of 0.061 *g*, which preserves the ratio between the horizontal and vertical components of the original motion. The east-west and vertical components of the original Yerba Buena Island accelerogram are plotted in figures 14*A* and 14*B*, respectively. As shown in the response spectra (fig. 14*C*), the dominant period of bedrock acceleration is about 0.6 s.

## ONE-DIMENSIONAL LINOS MODEL

The soil column used in the one-dimensional analyses represents the soil profile at the center of the liquefaction zone shown in figure 1. This soil column consists of five layers, including four clay layers and a 1-m-thick layer of the yellow hardpan at the transition between the older and younger bay muds (fig. 15). The finite-element model consists of plane-strain, four-noded, isoparametric elements with two degrees of freedom per node. The analyses were carried out by assuming that the deformation remained undrained during earthquake shaking. The term "undrained" refers to zero volume change. This incompressibility, which was ensured by using a penalty formulation,

is justified in view of the low permeability coefficient of the older and younger bay muds, which prevents rapid consolidation. This assumption does not significantly influence the numerical model because the material model used in the analyses does not depend on the mean effective pressure.

## MODELING OF NONLINEAR SOIL PROPERTIES

The parameters required for the nonlinear material model in the numerical analysis could not be calibrated directly from laboratory test results, owing to the absence of data. The model parameters were calibrated from the site-investigation data and from independent studies on the older and younger bay muds. The only field measurements during the site investigation were shear-wave velocity and CPT results. The shear-wave velocity measurements were used to derive the distribution of initial low-strain shear modulus versus depth, whereas the CPT results were used to evaluate the shear strength. The variations in normalized shear modulus $G/G_{max}$ versus shear strain $\gamma$ and in equivalent viscous damping ratio $D$ versus $\gamma$ were known from a previous laboratory study of the older and younger bay muds (Isenhower, 1979).

The results of laboratory and site investigations were combined in a two-step calibration procedure. In the first step, nonlinear backbone curves (assuming Masing behavior) were generated to reproduce the curves of $G/G_{max}$ and $D$ versus $\gamma$ for the older and younger bay muds. In the

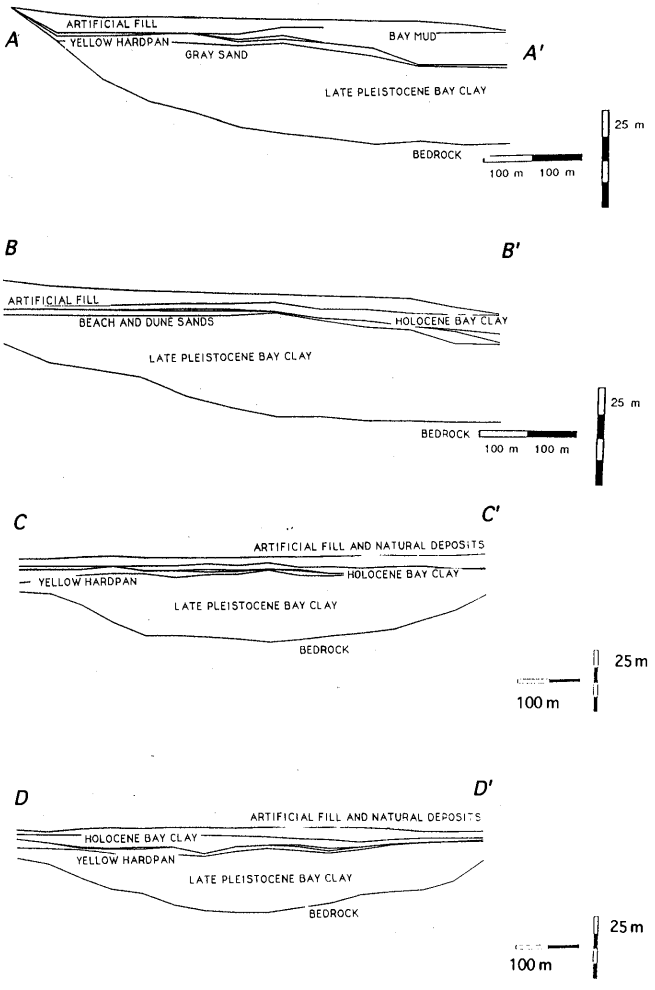


Figure 11.—Cross sections *A–A'* through *D–D'* in three-dimensional soil model (see fig. 3 for locations). Vertical exaggeration, 2×.

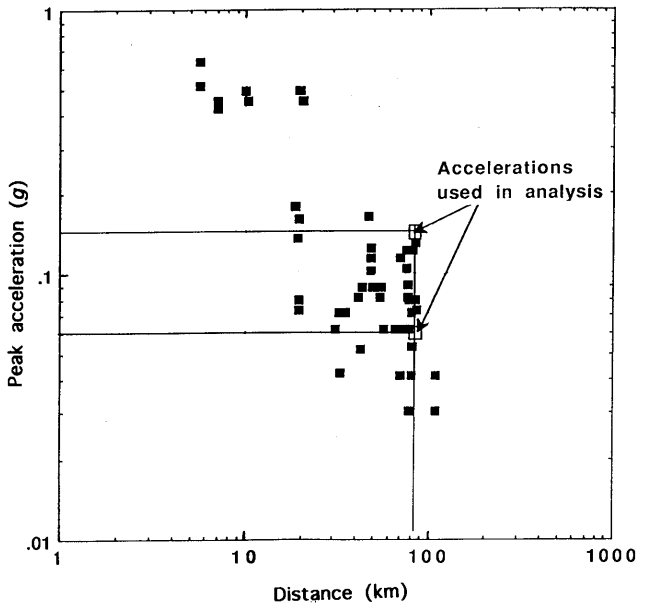


Figure 12.—Peak acceleration versus distance for accelerograms recorded at bedrock sites during the earthquake (data from Housner and Penzien, 1990).

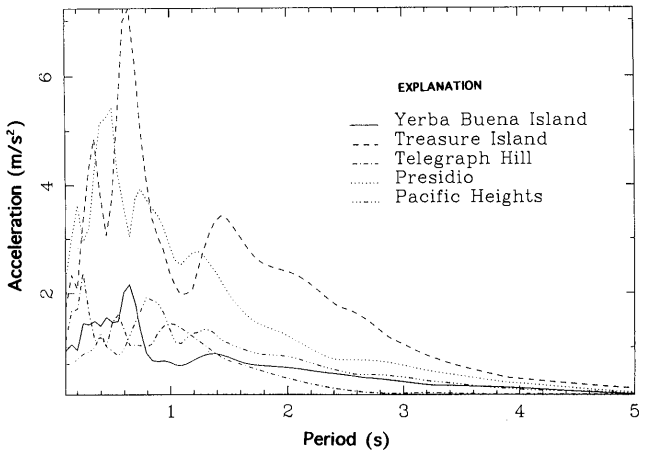


Figure 13.—Response spectra of accelerograms from five stations in the vicinity of the Marina District.

second step, these synthesized backbone curves were used to calibrate the material parameters of a three-dimensional constitutive model for soils. An elastoplastic model with multiple yield surfaces (Prevost, 1978) was selected to represent the soil behavior in the one- and two-dimensional analyses.

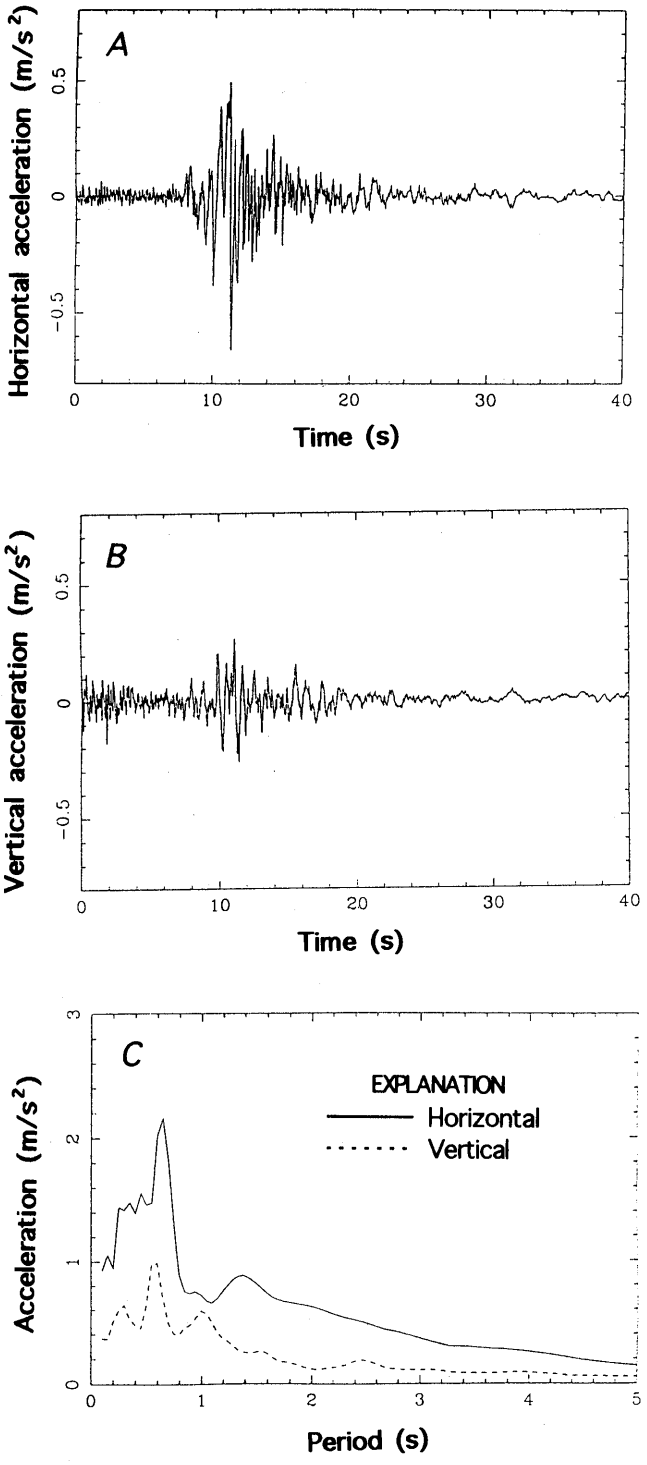


Figure 14.—Acceleration-time history of horizontal (*A*) and vertical (*B*) components of ground motion, with corresponding response spectra (*C*), for original Yerba Buena Island accelerogram (peak acceleration, 0.067 *g*).

## GENERATION OF BACKBONE CURVES

The stress-strain response of soils during cyclic simple-shear tests is commonly described by using a backbone curve and the Masing effect. The best known and most widely used backbone curve is of the hyperbolic type (Hardin and Drnevich, 1972). Backbone curves were generated by three models in this study: a bilinear model, a modified hyperbolic model, and a power-law model.

### BILINEAR MODEL

The stress-strain response in the bilinear model during simple shear is given by

$$\tau = \begin{cases} G_{max}\gamma & \text{for } \gamma < \gamma_r \\ \tau_{max} & \text{for } \gamma > \gamma_r, \end{cases} \quad (1)$$

where $\tau$ is the shear stress, $\tau_{max}$ is the maximum allowable shear stress, $G_{max}$ is the elastic initial shear modulus, and

| Depth (m) | | $\gamma_{sat}$ (kN/m³) | $G$ (MPa) | $\tau_{max}$ (kN/m²) | $v_s$ (m/s) | $n$ |
|---|---|---|---|---|---|---|
| 0.0 | HOLOCENE BAY CLAY | 17.6 | 40.5 | 19.4 | 305<br>183<br>234<br>152<br>207 | .4 |
| 12.0 | YELLOW HARDPAN | 20.8 | 345.0 | 225.0 | 366 | .4 |
| 13.0 | HOLOCENE AND LATE PLEISTOCENE BAY CLAY | 17.9 | 175.0 | 140.0 | 213<br>230<br>245<br>260 | .6 |
| 42.7 | LATE PLEISTOCENE BAY CLAY WITH INTERBEDS OF SHELLS | 18.4 | 287.5 | 225.0 | 275<br>300 | .6 |
| 62.5 | LATE PLEISTOCENE BAY CLAY | 18.4 | 345.0 | 225.0 | 335 | .6 |
| 84.0 | BEDROCK | 25.0 | -- | -- | 3,000 | -- |

Figure 15.—Soil column near borehole M4 (fig. 4), showing corresponding soil properties. $\gamma_{sat}$, saturated unit weight; $G$, shear modulus; $\tau_{max}$, undrained shear strength; $v_s$, shear-wave velocity; $n$, porosity.

$\gamma_r = \tau_{max}/G_{max}$ is the shear strain at failure. The secant shear modulus, $G$, is given by

$$G = \begin{cases} G_{max} & \text{for } \gamma < \gamma_r \\ \dfrac{\tau_{max}}{\gamma} & \text{for } \gamma > \gamma_r. \end{cases} \quad (2)$$

The equivalent viscous damping, $D$, is given by

$$D = \frac{2}{\pi}\left(\frac{W_1}{W_2}\right), \quad (3)$$

where the work $W_1$ is defined as the area under the stress-strain curve

$$W_1 = \int_0^{\gamma} \tau d\gamma \quad (4)$$

and $W_2$ is the work under the secant line:

$$W_2 = \frac{1}{2}\gamma\tau. \quad (5)$$

In the bilinear model, equations 4 and 5 become

$$\begin{cases} W_1 = W_2 & \text{for } \gamma < \gamma_r \\ W_1 = W_2 + \dfrac{1}{2}(\gamma - \gamma_r)\tau_{max} & \text{for } \gamma > \gamma_r. \end{cases} \quad (6)$$

The bilinear model was applied to reproduce the curves of $G/G_{max}$ and $D$ versus $\gamma$ for the older bay mud at 28-m depth. At this depth, we selected $\tau_{max}=S_u=140$ kPa and $G_{max}=175{,}000$ kPa on the basis of the results of the site investigation plotted in figures 6 and 7. As shown in figure 16, the bilinear model predicts that $G=G_{max}$ until $\gamma=0.08$ percent, and then $G<G_{max}$ as $\gamma$ increases. The bilinear model cannot simulate hysteretic damping at low strain ($\gamma<\gamma_r$) and overestimates $D$ for $\gamma>0.1$ percent. This model is of only limited interest for site-response analyses; it does not provide any flexibility to fit the experimental data plotted in figure 16 because it has only two parameters, $\tau_{max}$ and $G_{max}$.

## MODIFIED HYPERBOLIC MODEL

The stress-strain response in modified hyperbolic model (Prevost, 1989) is given by

$$\tau = \tau_1 \frac{\gamma}{\dfrac{\tau_1}{G_{max}} + \gamma} - \tau_1 \frac{\dfrac{\tau_1}{G_{max}}}{\left(\dfrac{\tau_1}{G_{max}} + \gamma_{max}\right)^2} \frac{1}{\gamma_{max}^m} \frac{\gamma^{m+1}}{m+1} \quad (7)$$

where $G_{max}$, $\gamma_{max}$, $\tau_1$, and $m$ are all real, positive material parameters. Equation 7 ensures that

$$\tau = 0 \quad \text{and} \quad \frac{\partial\tau}{\partial\gamma} = G_{max} \quad \text{at } \gamma = 0$$
$$\text{and} \quad \frac{\partial\tau}{\partial\gamma} = 0 \quad \text{at } \gamma = \gamma_{max} \quad (8)$$

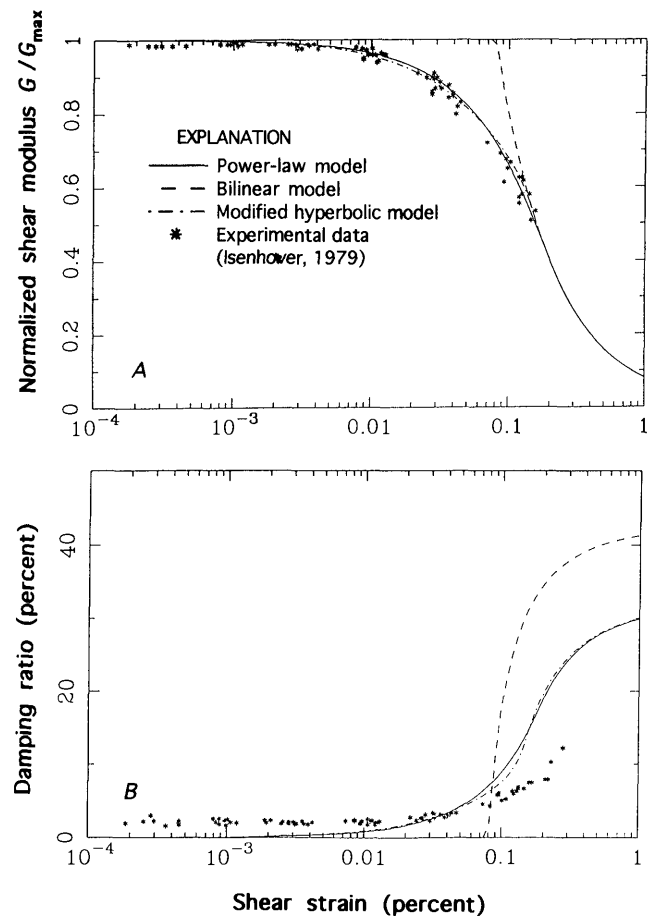


Figure 16.—Normalized shear modulus (*A*) and damping ratio (*B*) versus shear strain for older and younger bay muds (modified from Isenhower, 1979), fitted to curves generated by power-law, bilinear, and modified hyperbolic models.

$\tau=\tau_{max}$ at $\gamma=\gamma_{max}$ when the following relation is satisfied:

$$\tau_1 = G_{max}\gamma_{max}\frac{y_{max}-\frac{1}{2}+\sqrt{\frac{1}{4}-\frac{y_{max}}{m+1}}}{\frac{m}{m+1}-y_{max}}, \quad (9)$$

where $y_{max}=\tau_{max}/(G_{max}\gamma_{max})$. Equation 7 is calibrated from experimental data by fitting only two material parameters, $m$ and $\gamma_{max}$, since $G_{max}$ and $\tau_{max}$ are given from experimental results. The secant shear modulus $G$ is computed by dividing $\tau$ in equation 7 by $\gamma$. The equivalent damping ratio $D$ is calculated by using equation 3 specified in the following expressions for $W_1$ and $W_2$:

$$W_1 = G_{max}\gamma_{max}^2\left[yx - y^2\ln\left(\frac{y+x}{y}\right) - \frac{y^2}{y+1^2}\frac{x^{m+2}}{(m+1)(m+2)}\right] \quad (10)$$

$$\text{and } W_2 = \frac{1}{2}G_{max}\gamma_{max}^2\left[y\frac{x^2}{x+y}-\frac{y^2}{(y+1)^2}\frac{x^{m+2}}{m+1}\right], \quad (11)$$

where $x=\gamma/\gamma_{max}$ and $y=\tau_1/(G_{max}\gamma_{max})$.

The experimental curves of $G/G_{max}$ versus $\gamma$ and $D$ versus $\gamma$ were fitted by choosing $m$=5 and $\gamma_{max}$=0.0015 (fig. 16). $G$ is simulated accurately, whereas $D$ is underestimated for small values of $\gamma$ and overestimated for $\gamma$>0.1 percent. The discrepancy between experimental and simulated results at small values of $\gamma$ is expected because the material model generates only structural damping and neglects viscous damping.

## POWER-LAW MODEL

As an alternative to the modified hyperbolic model, a simpler, power-law model was also used (Bardet, 1990c). In this model, the tangent shear modulus $G_t$ varies as a power function of the distance between $\tau$ and the line $\tau=\tau_{max}$:

$$\begin{cases} G_t = \dfrac{\partial\tau}{\partial\gamma} = G_{max}\left(\dfrac{\tau_{max}-\tau}{\tau_{max}}\right)^n & \text{for } \tau<\tau_{max}, \\ G_t = 0 \quad \text{for } \tau>\tau_{max} \end{cases} \quad (12)$$

where $n$ is the material parameter. After integrating equation 12, the backbone curve becomes

$$\begin{cases} \tau = \tau_{max}\left\{1-\left[1-\left(1-n\right)\dfrac{G_{max}}{\tau_{max}}\gamma\right]\right\}^{\frac{1}{1-n}} & \text{for } \gamma<\gamma_r \\ \tau = \tau_{max} \quad \text{for } \gamma>\gamma_r \end{cases} \quad (13)$$

where $\gamma_r=\tau_{max}/[G_{max}(1-n)]$. The secant shear modulus $G$ is computed by dividing $\tau$ in equation 13 by $\gamma$. The equivalent damping ratio $D$ is calculated by using equation 3 specified in the following expressions for $W_1$ and $W_2$:

$$\begin{cases} W_1 = \tau_{max}\gamma + \dfrac{\tau_{max}^2}{G_{max}(2-n)}\left\{\left[1-\dfrac{G_{max}\gamma(1-n)}{\tau_{max}}\right]^{\frac{2-n}{1-n}}-1\right\} \\ \qquad\qquad \text{for } \gamma<\gamma_r \\ W_1 = \tau_{max}\gamma - \dfrac{\tau_{max}^2}{G_{max}(2-n)} \quad \text{for } \gamma>\gamma_r \end{cases} \quad (14)$$

In contrast to the modified hyperbolic model, the power-law model has only one material parameter $n$, which was set equal to 0.6 to fit the experimental data on the older and younger bay muds. As shown in figure 16, both the modified hyperbolic and power-law models are capable of describing the experimental points, whereas the bilinear model is too approximate. Therefore, we selected the power-law model to generate the backbone curves of the older and younger bay muds because its formulation and calibration are simpler than those of the modified hyperbolic model.

## ELASTOPLASTIC MODELING OF THE BEHAVIOR OF THE OLDER AND YOUNGER BAY MUDS

The backbone curves describe soil behavior only for one-dimensional loading and cannot be directly used for generalized multidimensional loadings, such as those used in two-dimensional analyses or even one-dimensional site-response analyses allowing for vertical motion. In the LINOS analyses, the elastoplastic constitutive equation for multiple yield surfaces (Prevost, 1978) was used to simulate the nonlinear behavior of the older and younger bay muds under generalized loadings. This elastoplastic model, which was available within the program LINOS, provided a piecewise linear simulation of the power-law model (assuming Masing behavior) fitted to the experimental data.

## ELASTOPLASTIC MODEL

The pressure-independent elastoplastic model was used successfully to simulate the hysteretic response of clays during cyclic loading (Prevost, 1978). The yield surfaces may be expressed by the equation

$$\frac{3}{2}(s_{ij}-\alpha_{ij}^{m})(s_{ij}-\alpha_{ij}^{m})-k_m^2=0 \qquad (15)$$

where $\alpha_{ij}^{m}$ is the center of the $m$th yield surface, $k_m$ is the size of the $m$th yield surface, and $s_{ij}$ is the deviatoric stress, given by

$$s_{ij}=\sigma_{ij}-p\delta_{ij}, \qquad (16)$$

where $\sigma_{ij}$ is the effective stress tensor, $p=\frac{1}{3}\sigma_{kk}$ is the effective mean pressure, and $\delta_{ij}$ is Kronecker's delta. The yield-surface evolution is controlled by kinematic hardening; the yield surfaces may translate, but they do not change in size. The largest yield surface is fixed in stress space and defines the failure surface.

## CALIBRATION OF MATERIAL CONSTANTS

The elastoplastic model predicts that the stress-strain response is piecewise linear. If the initial values of all the coefficients $\alpha_{ij}^{m}$ are assumed to be zero, then the increments of shear stress $d\tau$ and shear strain $d\gamma$ during simple shear with an initially isotropic stress are linearly related through

$$d\gamma = d\tau\left(\frac{1}{G}+\frac{2}{H_m}\right), \qquad (17)$$

where $H_m$ is the plastic modulus associated with the $m$th yield surface. Equation 17 applies, provided that $k_m/\sqrt{3}<\tau<k_{m+1}/\sqrt{3}$. When $\tau$ is inside the smallest yield surface—that is, when $\tau<k_1/\sqrt{3}$ —equation 17 becomes

$$d\gamma = \frac{d\tau}{G}. \qquad (18)$$

As shown in figure 17, the continuous backbone curves may be fitted by piecewise linear curves defined by discrete points ($\gamma_m$, $\tau_m$). Three to seven points were found to be sufficient to accurately fit the continuous backbone curves for the older and younger bay muds. Once these discrete points have been selected, the surface radius $k_m$ is related to $\tau_m$ by

$$k_m = \sqrt{3}\tau_m, \qquad (19)$$

where $\tau_m$ is the ordinate of the $m$th point on the stress-strain curve in figure 17. The elastic-shear modulus $G$ is the initial slope of the stress-strain curve:

$$G=\frac{\tau_1}{\gamma_1}. \qquad (20)$$

The elastoplastic modulus $H'_m$ associated with the $m$th yield surface is given by

$$H'_m = 2\frac{\tau_{m+1}-\tau_m}{\gamma_{m+1}-\gamma_m}, \qquad (21)$$

where $H'_m$ is related to the plastic modulus $H_m$ through

$$\frac{1}{H'_m} = \frac{1}{H_m}+\frac{1}{2G}. \qquad (22)$$

The plastic modulus associated with the largest yield surface is set equal to zero. The material parameters calibrated for the four layers of the older and younger bay muds and the yellow hardpan are listed in table 2.

The layer of yellow hardpan was modeled by using the same type of model as for the older and younger bay muds. On the basis of the CPT results, the yellow hardpan was assigned a large shear strength, 160 kPa, equal to the largest shear strength selected for the older bay mud. Because no laboratory data were available on the yellow hardpan, this layer was assigned the same material properties as the older bay mud at 70-m depth. Because the thin

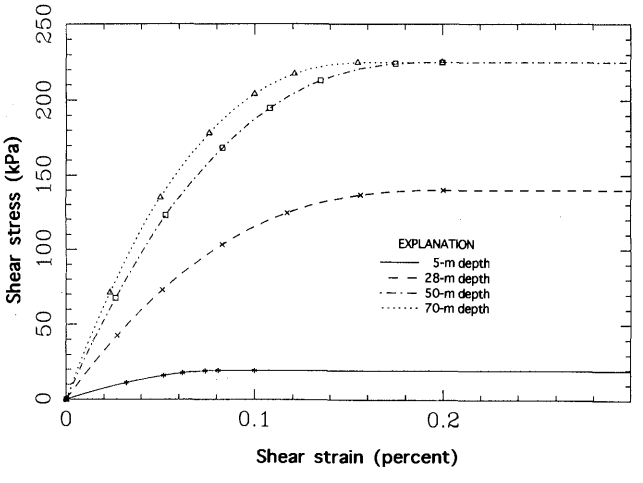


Figure 17.—Stress-strain relation during simple shear, as predicted by multiple-yield-surfaces model at various depths for older and younger bay muds and yellow hardpan.

Table 2.—*Material parameters of multiple-yield-surfaces model*

[*G*, shear modulus; *n*, Poisson ratio; m, number of yield surface; *k*, size of yield surface; *H'*, elastoplastic modulus]

| *G* (MPa) | ν | *m* | *k* (kPa) | *H'* (MPa) |
|---|---|---|---|---|
| | | layer 1 | (depth, 5 m) | |
| 34.8 | 0.3 | 1 | 19.3 | 49.1 |
| | | 2 | 27.8 | 35.1 |
| | | 3 | 30.8 | 22.5 |
| | | 4 | 33.2 | 7.08 |
| | | 5 | 33.6 | 0.00 |
| | | layer 2 | (depth, 13 m) | |
| 309.4 | 0.3 | 1 | 123.2 | 472.5 |
| | | 2 | 233.7 | 332.3 |
| | | 3 | 308.6 | 216.1 |
| | | 4 | 353.5 | 126.9 |
| | | 5 | 376.6 | 43.96 |
| | | 6 | 389.5 | 0.54 |
| | | 7 | 389.7 | 0.00 |
| | | layer 3 | (depth, 28 m) | |
| 157.7 | 0.3 | 1 | 73.7 | 253.0 |
| | | 2 | 126.3 | 190.1 |
| | | 3 | 179.0 | 124.2 |
| | | 4 | 215.6 | 63.36 |
| | | 5 | 237.0 | 14.45 |
| | | 6 | 242.5 | 0.00 |
| | | layer 4 | (depth, 50 m) | |
| 259.5 | 0.3 | 1 | 116.9 | 410.4 |
| | | 2 | 212.8 | 303.6 |
| | | 3 | 291.7 | 211.0 |
| | | 4 | 337.4 | 134.7 |
| | | 5 | 368.9 | 56.12 |
| | | 6 | 388.3 | 6.52 |
| | | 7 | 389.7 | 0.00 |
| | | layer 5 | (depth, 70 m) | |
| 309.4 | 0.3 | 1 | 123.2 | 472.5 |
| | | 2 | 233.7 | 332.3 |
| | | 3 | 308.6 | 216.1 |
| | | 4 | 353.5 | 126.9 |
| | | 5 | 376.6 | 43.96 |
| | | 6 | 389.5 | 0.54 |
| | | 7 | 389.7 | 0.00 |

layer of surficial sand was not expected to significantly influence the overall site response, its behavior was not simulated with accuracy. Instead, it was modeled by using the same elastoplastic model as for clay, but calibrated with the 20-kPa shear strength estimated from the CPT results.

The backbone curves generated by the power-law model for the older and younger bay muds at four depths ranging from 5 to 70 m are plotted in figure 17. The initial shear modulus $G_{max}$ and maximum stress $\tau_{max}$ were computed based on results of field investigation. The power law model provides a smooth and gradual change of slope from elastic to perfectly plastic behavior.

The curves of $G/G_{max}$ versus $\gamma$ and $D$ versus $\gamma$ generated by the elastoplastic model at four different depths are plotted in figure 18. As in figure 15, this model accounts well for the shear modulus, although it slightly overestimates the damping properties at larger strain amplitudes. The damping ratio is also underestimated at low strain because the material model neglects viscous damping. The quality of fit depends on the depth because the backbone curve (eq. 13) predicted by the power-law model depends on $G_{max}$ and $\tau_{max}$, which vary with depth.

## RESULTS OF ONE-DIMENSIONAL LINOS ANALYSES

The one-dimensional analyses were carried out, first, by assuming elastic properties for the underlying soils and, second, by using the elastoplastic model. The linear analysis, though of limited interest in practice, was carried out first to provide a means of qualitatively assessing the effect of material nonlinearity on the dynamic response of the Marina District. Only the scaled Yerba Buena Island accelerogram was used in the elastic one- or two-dimensional analyses. The results of linear analyses at 0.15 *g* can be scaled linearly down to 0.067 *g* for the original Yerba Buena Island accelerogram. The damping, which was of the Rayleigh stiffness type, was adjusted to provide a 1-percent critical damping ratio at the fundamental peri-

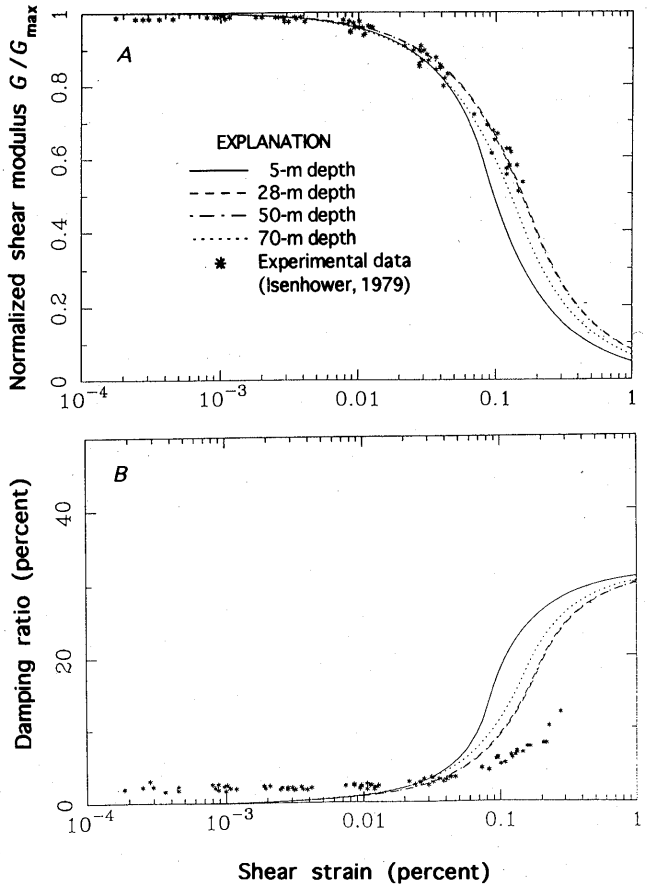


Figure 18.—Normalized shear modulus (*A*) and damping ratio (*B*) versus shear strain at various depths for older and younger bay muds.

od. This damping ratio, which is slightly smaller than the value of 2 percent observable in the low-strain laboratory test results of Isenhower (1979), corresponds to the damping ratio predicted by the power law at 0.01-percent shear strain.

The elastic response of the ground surface to the scaled bedrock input motion on Yerba Buena Island is plotted in figure 19. The peak acceleration is 0.4 and 0.07 *g* in the horizontal and vertical directions, respectively. The acceleration is practically unchanged in the vertical direction (fig. 19*A*), whereas it is amplified 2.6 times in the horizontal direction (fig. 19*B*).

The acceleration-time history and response spectra of ground-surface acceleration at borehole M4 (fig. 4), as predicted by linear and nonlinear analyses for the scaled Yerba Buena Island accelerogram (peak acceleration, 0.15 g) are plotted in figure 20. The predicted peak acceleration is not amplified; it is about 0.15 *g* in the horizontal direction and 0.06 *g* in the vertical direction. As shown in figure 20*A*, the peak horizontal acceleration is truncated, owing to yielding of the soft top layer (fig. 20*E*) that reaches a maximum shear strength of 19.4 kPa (as specified in fig. 15). The response spectrum of horizontal acceleration shows two distinct peaks at 0.6 and 1 s; the second peak corresponds to the fundamental mode of the elastic soil deposit. The structural damping, as illustrated by the hysteretic stress-strain curve in figure 20*E*, lowers the spectral peaks obtained in the linear analysis. The response spectra in the vertical direction are almost identical in the nonlinear and linear analyses.

The acceleration-time history and response spectra of ground-surface acceleration at borehole M4 (fig. 4), as predicted by nonlinear and linear analyses for the original Yerba Buena accelerogram (peak acceleration, 0.067 *g*), are plotted in figure 21. In contrast to the figure 20, the predicted peak acceleration (0.12 *g*) is amplified by a factor of 2 in the horizontal direction. The stress-strain curves at 9- and 6-m depth are plotted in figures 21*E* and 21*F*, respectively. The soft top layer does not yield as much as in figure 20*E*; however, the yielding at 9-m depth controls the peak acceleration at the ground surface, which is the same as that predicted for 0.15 *g* in figure 20*E*. The vertical accelerations predicted in the linear and nonlinear analyses coincide. The lower accelerations and reduced yielding also account for the greater similarity of the response spectra in the nonlinear and linear analyses.

The acceleration-time history at the ground surface, at 4-m depth, and at the top of the yellow hardpan is plotted in figure 22. The yellow hardpan sustained the same acceleration as the ground surface. The soft layers just above the yellow hardpan did not amplify the acceleration further because they yielded at this acceleration level. Figure 22 suggests that most of the site amplification in the Marina District during the earthquake was caused by the thick layers of older bay mud underlying the yellow hardpan.

## RESULTS FROM THE PROGRAMS SHAKE AND DETRAN

The site response at borehole M4 (fig. 4) was analyzed by using the programs DETRAN and SHAKE. The same geometry and backbone curves were defined for the soil layers (see figs. 15, 16). The ground motion in the SHAKE and DETRAN analyses is limited to the horizontal east-west component of the Yerba Buena Island accelerogram. In the SHAKE analysis, we used the curves of $G/G_{max}$ versus $\gamma$ and $D$ versus $\gamma$ of Isenhower (1979) for the older and younger bay muds. The 40-percent increase in undrained shear strength $S_u$ was not considered in the SHAKE analysis. A 1-percent viscous damping was also considered in the DETRAN analysis in addition to the hysteretic structural damping.

The response spectra of the horizontal component of the ground motion at borehole M4 (fig. 4) calculated by using the programs DETRAN, SHAKE, and LINOS are plotted in figure 23. All the response spectra are similar in shape but differ in amplitude; they predict similar dominant periods but different amplifications. The spectral amplitude calculated by using the program LINOS falls between those predicted by the programs DETRAN and SHAKE. The DETRAN analysis predicts the lowest amplitude because it includes a 1-percent viscous damping in addition to the same structural damping, as in the LINOS analysis. The SHAKE analysis predicts the highest spectral amplitudes, reflecting the use of an equivalent material model that does not include complete failure. Similar conclusions were drawn by Arulanandan and Yogachandran (1990) after comparing the results of the programs SHAKE and DYSAC2. Provided with the same input ground motion, soil-layer geometry, and properties for the Marina District, the programs DETRAN and LINOS gave comparable results, whereas the program SHAKE tends to give higher spectral amplifications.

## SIMPLIFIED LIQUEFACTION ANALYSIS OF ARTIFICIAL FILL

Equivalent SPT blow counts were determined from the CPT results, on the basis of correlations with normalized tip bearings and friction ratios (Douglas and Olsen, 1981; Earth Technology Corp., 1990; Martin, 1991). Within the bounds of Marina Cove, the equivalent SPT blow count $N_1$ was found to range from 5 to 20 in the artificial fill (top 2.75 m) and to average 5 for the lower natural-sand deposits (Bardet and Kapuskar, 1991b). The properties of the soils above the yellow hardpan at borehole M4 are listed in figure 24*A*. The average earthquake-induced shear stress $\tau_{ave}$ in the hydraulic fill was obtained by the simplified method of Seed and Idriss (1971; see Seed and others, 1983):

$$\tau_{ave} = 0.65\frac{\gamma h}{g} r_d a_{max}, \quad (23)$$

where $a_{max}$ is the peak ground acceleration, $g$ is the acceleration due to gravity, $\gamma$ is the soil unit density, $h$ is the height of soil shaken, and $r_d$ is a depth factor that accounts for the variation in ground acceleration with depth. In view of the shallow thickness $h$ of the column considered in figure 24*A*, no depth correction was considered ($r_d$=1). The estimated average stress ratio $\tau_{ave}/\sigma'_v$ (where $\sigma'_v$ is the effective overburden pressure) calculated for a peak acceleration of 0.15 $g$ is listed in table 3. Because ground accelerations were not measured in the Marina District, the value of 0.15 $g$ was chosen to represent a reasonable estimate on the basis of the results of site-response analyses.

The liquefaction potential of the sand above the yellow hardpan was assessed by using the empirical procedure of Seed and others (1983) that is commonly used in engineering practice today. From field correlations between SPT tests and the observed liquefaction characteristics of sand over a range of earthquake magnitudes, cyclic liquefaction-strength curves ($\tau_{cyc}/\sigma'_v$ versus number of cycles $N_L$ to cause liquefaction) were derived. The liquefaction-strength curves obtained for $N_1$=5, 10, and 20 by using this procedure are plotted in figure 24*B*. $\tau_{cyc}$ is the average stress ratio to achieve liquefaction after a representative "significant" number of cycles associated with a given earthquake magnitude. The average shear-stress ratios $\tau_{cyc}/\sigma'_v$ listed in table 3 fall well above the liquefaction-strength curves, indicating that the sand deposits in the Marina District should liquefy under the acceleration predicted at borehole M4.

Using the liquefaction-strength curves in figure 24*B*, a DESRA2 analysis (Lee and Finn, 1978) could have been performed to demonstrate the acceleration-time histories of pore-pressure buildup in the layers of saturated sand. However, this additional analysis would not have contributed significantly to our understanding of the site response of the Marina District. In view of the relative proportion of clay and sand in the subsoils of the Marina District, the site response (leading to liquefaction of the saturated sand) was largely controlled by the underlying older and younger bay muds.

Table 3.—*Summary of liquefaction analyses for sands at borehole M4 (fig. 4) by a simplified evaluation procedure*

| Parameter | (Units) | Compacted sandy fill (depth, 2.75 m) | Sand deposit (depth, 7.5 m) |
|---|---|---|---|
| $a_{max}$ | ($g$) | 0.15 | 0.15 |
| $\gamma$ | (kN/m$^3$) | 18.5 | 17.6 |
| $\tau_{ave}$ | (kPa) | 5.0 | 12.87 |
| $\sigma'_{vo}$ | (kPa) | 12.0 | 29.2 |
| $N_1$ | (blows/ft) | 10 | 5 |
| $\tau_{ave}/\sigma'_{vo}$ | applied | 0.4 | 0.44 |
| $\tau_{cyc}/\sigma'_{vo}$ | required to withstand liquefaction for $N_L$=10 | .2 | .06 |

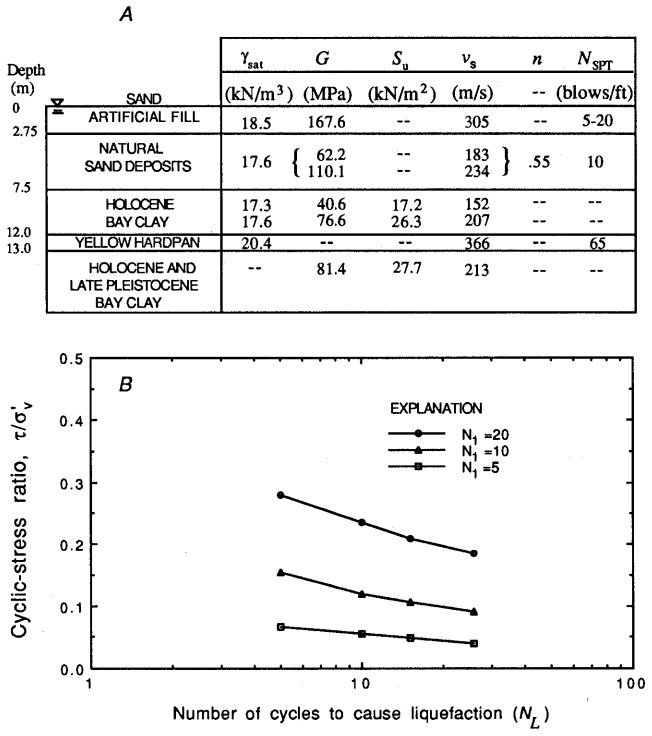


Figure 24.—Soil column in borehole M4 (fig. 4) (*A*) and liquefaction strength curve (*B*) for artificial fill, as estimated from CPT results. $\gamma_{sat}$, saturated unit weight; $S_u$, undrained shear strength; $G$, shear modulus; $v_s$, shear-wave velocity; $n$, porosity; $N_{SPT}$, SPT blow count.

# TWO-DIMENSIONAL SITE-RESPONSE ANALYSES

## TWO-DIMENSIONAL MODEL

A cross section of the three-dimensional model in figure 10 that is used hereafter in two-dimensional analyses of the Marina District is shown in figure 25. This east-west cross section contains Beach Street (see fig. 3) and intersects the liquefied zone. The cross section is 1,500 m long and as much as 90 m high: It is discretized into 250 plane-strain elements, arranged in 50 columns of five elements each. The model has five layers: The top layer is composed of surficial materials that are either the younger bay mud or artificial fill; the second layer from the top represents the thin, dense sand layer at the transition between the surficial layer and the older bay mud; and the underly-

ing layers are composed of overconsolidated older bay mud. As shown in figure 25, the thickness and depth of these layers are not constant but vary in an east-west direction. The lateral boundaries of the two-dimensional model were defined sufficiently far away from the region of interest to attenuate undesirable boundary effects. The optimal model width was defined by eigenvalue analysis.

## EIGENVALUE ANALYSIS

The 10 vibrational modes of the selected cross section, which correspond to the lowest natural frequencies ranging from 1.16 to 1.93 Hz, are illustrated in figure 26. The elastic properties of the one-dimensional analyses were assumed in these eigenvalue calculations. The first mode, with a natural frequency of 1.16 Hz, is essentially similar to the first mode of a shear beam. The vertical columns lean in the same direction and have a maximum amplitude at the center and zero amplitude on the extremities; there is a slight surface wave, the wavelength of which is equal to the model width. The second mode has a natural frequency (1.23 Hz) close to the fundamental frequency. In the second mode, the vertical columns do not lean in the same direction, and the surface wave has a wavelength equal to half the model width. The soil elements in the center of the model do not undergo cycles of simple shear loading but are subjected to cycles of lateral tension-compression. The other modes display an increasing importance of the surface modes. Starting from the third mode, the surface modes exhibit a common focal point on the east side of the Marina District; the ninth mode exhibits the strongest surface amplification in the vicinity of this focal point. This particular mode should, however, be interpreted with some caution because the wavelength has reached the spacing of the discretized systems. The common focal point is located east of the region where the yellow hardpan layer is thinnest.

A wider model was constructed to estimate lateral boundary effects. This larger model included bedrock that crops out on the east at Nob Hill (approx 1,500 m east) and is very shallow in the west under the Presidio. Because its eigenvalues and eigenvectors were found to coincide approximately with those of the model in figure 26, we concluded that this first model was wide enough for the purposes of our analysis.

To compare the natural modes of the one- and two-dimensional analyses, the natural modes of a one-dimensional model selected at the center of the two-dimensional model are plotted in figure 27. The first five modes range in natural frequency from 1.12 to 7.95 Hz. The lowest frequency of the one-dimensional model is slightly smaller than that of the two-dimensional model. The corresponding mode shapes coincide in the one- and two-dimensional analyses; however, the second natural frequency (2.87 Hz) of the one-dimensional model is higher than the 10th natural frequency of the two-dimensional model. The compressional modes are not plotted in figure 27 because the column was assumed to be composed of incompressible material. In contrast to the soil elements of the two-dimensional model that may undergo tension-compression, the soil elements of the one-dimensional model undergo only simple shear loading.

From this comparison, it is apparent that two-dimensional effects could significantly influence the dynamic response of the Marina District. These effects are caused by thinning of the hard sand layer and the slope of the bedrock surface. The modal deformations in the two-dimensional analyses are also more complex than in the one-dimensional analyses. The soils undergo not only simple shear versus depth but also much more complex loadings involving tension-compression and combined shear/normal-loading cycles. These complex loadings observed in linear mode shapes may be also influenced by nonlinear soil behavior.

## INPUT MOTIONS

As in the one-dimensional analyses, the earthquake motion was characterized by two input accelerations: from the original (0.067 *g*) and the scaled (0.15 *g*) Yerba Buena

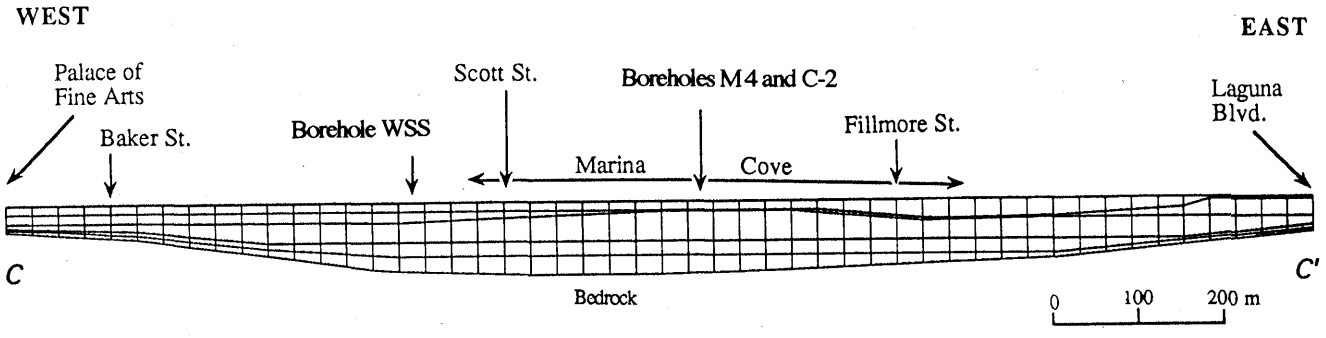


Figure 25.—Two-dimensional model of the Marina District (cross sec. *C–C'*, fig. 3).

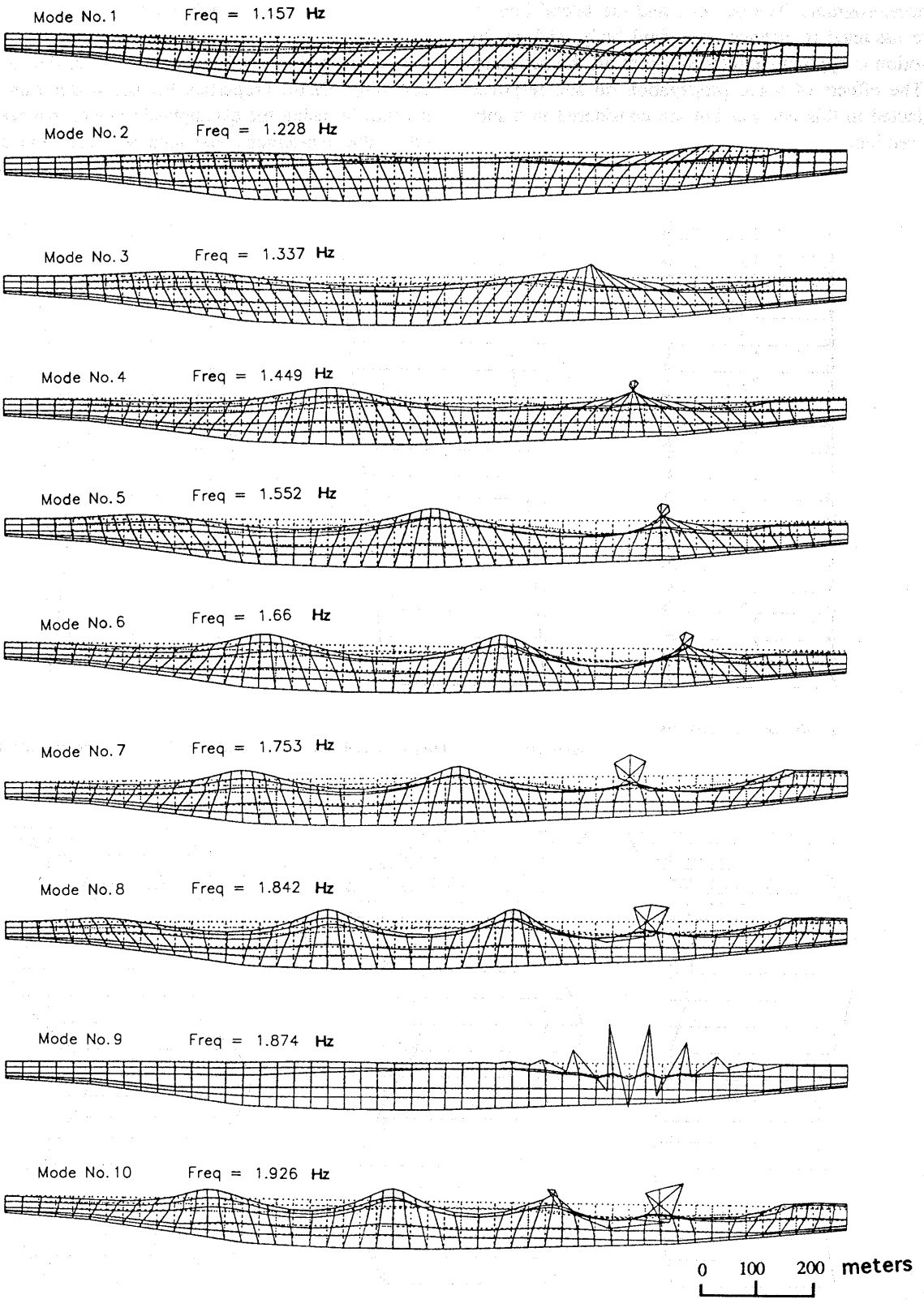


Figure 26.—Eigenmodes of two-dimensional model (fig. 25).

Island accelerograms. The bedrock and the lateral boundaries are assumed to behave as a rigid body, and so the input motion is applied simultaneously to all the boundary nodes. The effects of wave propagation on site response are neglected in this analysis but are considered in a subsequent section.

## RESULTS

The two-dimensional analyses were carried out, first, by assuming elastic properties for the underlying soils and, second, by using the elastoplastic model that was calibrated in the one-dimensional analyses. Like the one-dimen-

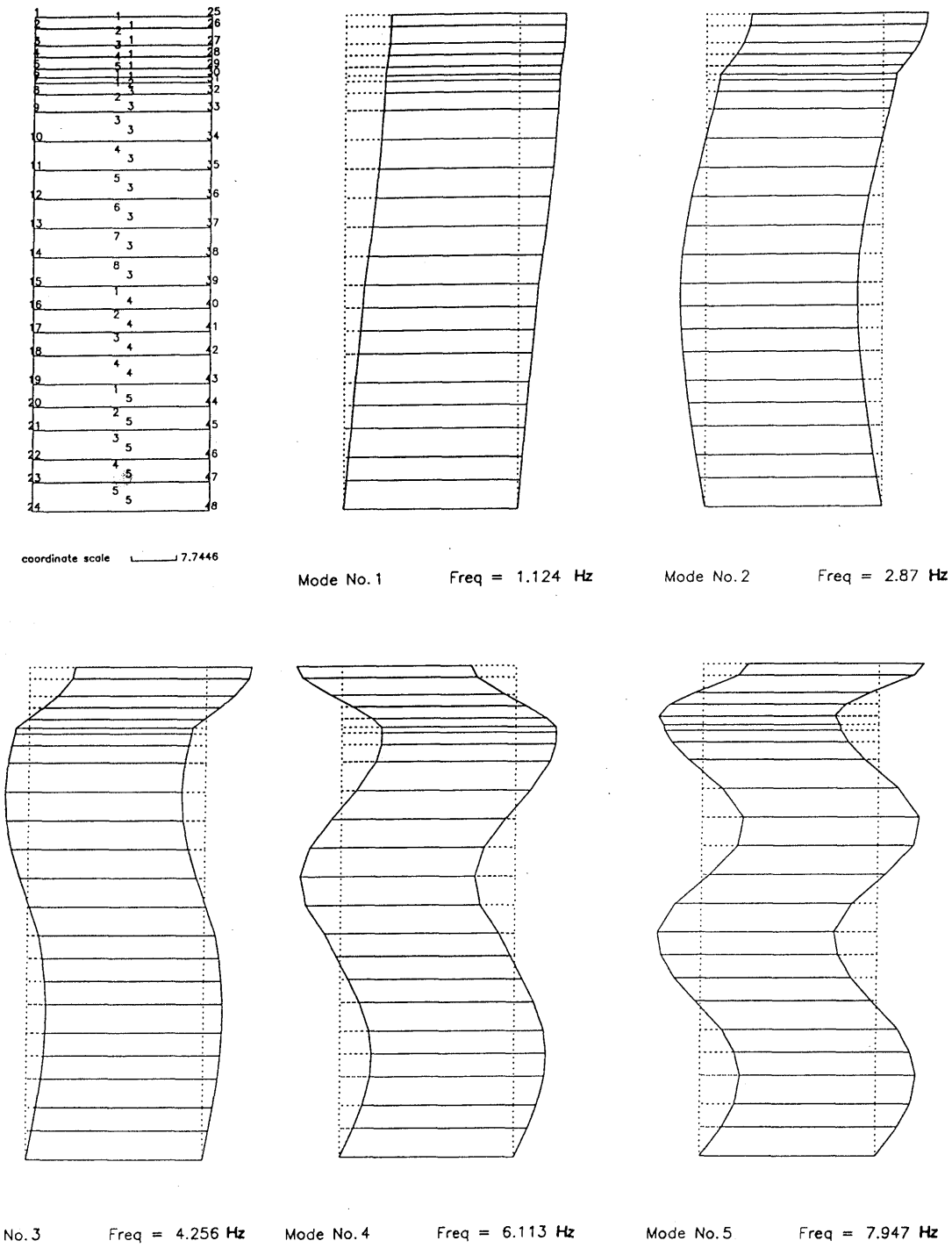


Figure 27.—Eigenmodes of one-dimensional model at borehole M4 (fig. 4).

sional analyses, linear two-dimensional analyses are of limited interest in practice. They were carried out mainly to evaluate the effects of material nonlinearity on the dynamic response of the Marina District and to compare two- versus one-dimensional elastic response.

## LINEAR ANALYSES

Only the scaled Yerba Buena Island accelerogram was used in the elastic two-dimensional analyses. The results of the linear analyses were scaled down linearly to give results corresponding to the original Yerba Buena Island accelerogram. The acceleration-time history and response spectra at borehole M4 (fig. 4), in the center of the artificially filled Marina Cove that liquefied in 1989, are plotted in figure 28. The peak horizontal acceleration reaches 0.58 *g* in the two-dimensional analyses, in comparison with 0.40 *g* in the one-dimensional analyses. The acceleration-time histories are comparable in both analyses but show a larger amplitude in the two-dimensional analyses. In both analyses, the dominant period is 0.7 s; the corresponding frequency (1.43 Hz) is close to the fourth natural frequency (1.45 Hz) of the two-dimensional model shown in figure 26.

The response spectra of predicted ground motion at boreholes M4 and WSS (fig. 4) in comparison with those of bedrock motions are shown in figure 29. The bedrock motion exhibits a small peak acceleration at a period of 0.6 s; this peak is amplified about 5 times at borehole M4, whereas it is amplified about 4 times at borehole WSS. The amplification of ground motion at 0.6 and 0.7 s results from the presence of 0.6- to 0.7-s motion in the input bedrock motion that activates the fourth and fifth modes shown in figure 26 (1.45 and 1.55 Hz, respectively).

## NONLINEAR ANALYSES

The acceleration-time history and response spectra of predicted ground motion at boreholes M4 and WSS (fig. 4) for the scaled Yerba Buena Island accelerogram are shown in figures 30 and 31, respectively. In the nonlinear analyses, the peak accelerations at boreholes M4 and WSS are identically equal to 0.23 *g*, in comparison with 0.58 *g* in the linear analyses. The peak acceleration is amplified 1.5 times for the horizontal component and 1.6 times for the vertical component. The response spectra emphasize the difference in response between boreholes M4 and WSS: The peak at borehole M4 is smaller and broader than at borehole WSS. Wider peaks in the response spectra are generally attributable to material nonlinearity because material softening shifts the fundamental period. This nonlinear effect is observed by comparing the response spectra in the linear and nonlinear analyses plotted in figures 30*C* and 31*C*. The wide peak in figure 30*C* implies that the soils at borehole M4 underwent larger strain than at borehole WSS, as corroborated by comparison of the stress-strain curves in figure 30*E* and 31*E*. The energy dissipated, which corresponds to the area underneath the stress-strain curve, is larger at borehole M4 than at borehole WSS. The peak acceleration at borehole M4 predicted in the two-dimensional analyses (0.23 *g*, fig. 30*A*) is larger than that predicted in the one-dimensional analyses (0.12 *g*, fig. 20*A*). As shown in figure 30*F*, in the two-dimensional analyses, the soil elements in the upper layer undergo not only cyclic simple-shear loading but also cycles of tension-compression. These changes in loading direction cause an increase in acceleration that may be transmitted through soils. The stress states in the two-dimensional analyses, however, are more complex than in the one-dimensional analyses, ruling out a calculation of peak acceleration from shear strength by using relations similar to equation 23.

Similarly, the acceleration-time history and response spectra of predicted ground motion at boreholes M4 and WSS (fig. 4) for the original Yerba Buena Island accelerogram are shown in figures 32 and 33, respectively. The peak acceleration is 0.20 *g* at both boreholes in the two-dimensional analyses, larger than the peak acceleration of 0.12 *g* predicted at borehole M4 by the one-dimensional analyses but agreeing well with the peak acceleration of 0.21 *g* measured in the Presidio, 2 km from the Marina District (see table 1). The stress-strain curves at 9-m depth indicate that the soft top layer failed at borehole M4 but barely yielded at borehole WSS, an observation that is corroborated by comparing figures 32*C* and 33*C*: The peak of spectral acceleration in figure 32*C* is wider and lower than that in figure 33*C*, implying larger material nonlinearity.

The bedrock accelerations are amplified 3 times on the original Yerba Buena Island accelerogram, in comparison with 1.5 times on the scaled accelerogram. The stress-strain curves for the soft top layer plotted in figures 32*E* and 33*E* show less yield that those in figures 30*E* and 31*E*, implying that the accelerations in the yellow hardpan are not truncated by the soft top layer on the original Yerba Buena Island accelerogram. The response spectra in figures 30*C* and 32*C* clearly indicate the contribution of the fundamental mode (1.15 Hz) to the ground motion at borehole M4 (fig. 4).

The amplification of the horizontal and vertical components of ground motion along the surface of the two-dimensional model is plotted in figures 34 and 35, respectively. The linear results are for the scaled Yerba Buena Island accelerogram (peak acceleration, 0.067 *g*), whereas the nonlinear results are for both the original and scaled accelerograms (peak acceleration, 0.067 and 0.15 *g*, respectively). In the linear analyses, the amplification of ground motion reaches a maximum of 4 between points H

and I and is constant at 2.5 between points B and G. Modal deformation was observed to be concentrated within segment HI (see fig. 26). The nonlinear analyses for the original accelerogram predict the same amplification as does the linear analyses between points B and G; however, between points H and I, the nonlinear analyses predict a minimum, whereas the linear analyses predict a maximum. The nonlinear analyses for the scaled accelerogram predict an amplification lower in value but similar in shape to that for the original accelerogram. This decrease in amplification for the scaled accelerogram results from nonlinear effects. The nonlinear analyses predict a minimum amplification between points H and I as a result of the concentration of deformation and nonlinear effects. The vertical component (fig. 34) follows trends similar to those of the horizontal component (fig. 35).

The importance of two-dimensional effects on the site-response of the Marina District is clearly shown in figures 28 through 35. These two-dimensional effects were characterized for a particular type of stress-strain relation derived from conventional dynamic testing. The two-dimensional analyses predict an overall-stronger horizontal component of ground motion. Comparison of the one- and two-dimensional analyses at boreholes M4 and WSS in the Marina District indicates that the one-dimensional analyses give acceptable, but not necessarily conservative, predictions for the acceleration at the ground surface.

## WAVE-PROPAGATION ANALYSIS OF SITE RESPONSE

In the preceding section, we studied the response of the Marina District by assuming a uniform acceleration on the boundary nodes, therefore neglecting the influence of wave propagation on site response, as well as the effects of the overlying soil layers on bedrock motion. However, the model is 1,500 m long; that is, shear waves traveling horizontally at a velocity of 3 km/s in the underlying bedrock take 0.5 s to cross the model. Thus, the assumption of constant in-phase input acceleration needs to be investigated. The previous analyses also neglected the refraction of waves at the soil-bedrock interface. This assumption is reasonably justifiable because the overconsolidated older bay mud is much softer than the underlying bedrock, and so the wave energy may be expected to remain trapped inside the soil layer without dissipation through refraction.

### CALCULATION OF INPUT ACCELERATION

The inclusion of wave-propagation effects in finite-element analysis complicates the problems of site response. The influence of wave propagation has been investigated for elongate structures, such as suspended cable bridges, but has received little attention for earth structures and soil deposits.

We accounted for the influence of wave propagation on the dynamic response of the Marina District by prescribing nonuniform acceleration-time histories along the bedrock. Joyner (1975) adopted a similar approach to account for wave propagation in two-dimensional problems. However, our calculation of the prescribed acceleration used a more rigorous method developed by X. Wu and V.W. Lee (unpub. data, 1991). A simpler method had earlier been proposed by Mooeen-Vaziri and Trifunac (1988), and similar methods were also used by Todorovska and Lee (in press) in analyzing the site response of valleys.

First, Wu and Lee calculated fast Fourier transforms (FFT's) of the free-field-accelerogram data in the horizontal and vertical directions. These FFT's were then considered as incident waves to the arbitrary-shape canyon. They were multiplied by the corresponding transfer functions at each point of the canyon in the frequency domain to obtain FFT's of the resulting waves after scattering and diffraction from the canyon. An inverse FFT was then taken to calculate the resulting wave in the time domain. At each frequency and point of the canyon, the value of the complex transfer function is calculated as the solution of a boundary condition involving zero stress at the surface of the canyon and half-space:

$$\sigma_{nn} = \sigma_{nt} = 0, \tag{24}$$

where $\sigma_{nn}$ and $\sigma_{nt}$ are the normal and tangential components of stress, respectively, at the surface of the canyon and half-space. The resulting waves are the sum of the incident and scattered waves. The scattered waves are composed of both longitudinal (*P*) and shear (*S*) waves satisfying Sommerfeld's radiation conditions. Scattering

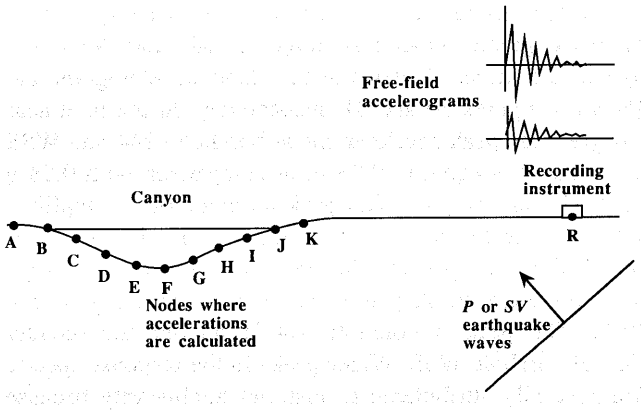


Figure 36.—Calculation of input acceleration from free-field input in two-dimensional model (fig. 25).

and diffraction will cause the resulting waves to differ in both amplitude and phase at each point of the canyon, which is no longer undergoing uniform motion.

The calculation of bedrock accelerations is illustrated in figure 36. Station R (Yerba Buena Island) measures the free-field accelerogram at the surface of the half-space composed of bedrock. The acceleration at station R, which results from the incoming and reflected earthquake waves, is assumed not to be influenced by surface geometry, such as valleys or soft-soil layers. On the basis of the free-field accelerogram, this method gives the acceleration along points located on the surface of the canyon.

Three types of earthquake waves are independently considered in the wave-propagation analysis: longitudinal (*P*), vertical shear (*SV*), and Rayleigh (*R*). The free-field accelerogram is assumed to result from only one type of wave, either *P*, *SV*, or *R*. This assumption is simplistic, however, because earthquake accelerations result from a combination of *P*, *SV*, and *R* waves. As yet, no method exists to combine these various types of *R* waves.

The wave-propagation analysis assumes that free stress conditions exist along the bedrock surface; it therefore neglects the weight of soils above bedrock and any interaction between soils and bedrock. This assumption may be justified by the relatively small thickness of the soil deposits and the difference between wave velocity in soils and bedrock.

## INPUT MOTIONS

In a rigorous sense, the boundary nodes should undergo different accelerations due to the effects of wave propagation. Because each digitized input-acceleration record has a duration of 40 s and a time increment of 0.02 s, there are 2,000 data points for each component of acceleration. If all the nodes were independent, 244,000 data points would be required to specify the acceleration on the model boundary. For practical reasons, the boundary nodes were assembled into 11 groups labeled A through K (fig. 37), reducing the input from 244,000 to 44,000 data points.

The inclusion of wave-propagation effects in the site-response analysis also raises the problem of specifying the direction and type of waves that hit the Marina District. Because this more complete determination is not yet possible, only a few wave types and orientations are considered here. These types include a *P* wave traveling vertically or at a 20° inclination to the vertical, an *SV* wave traveling vertically or at a 20° inclination, an *R* wave, and, finally, an arbitrary combination of *P*, *SV*, and waves.

The record used to generate the acceleration along the boundary is the original Yerba Buena Island accelerogram (peak acceleration, 0.067 g). The input accelerations at the model boundary resulting from *P*, *SV*, and *R* waves are plotted in figures 38 through 46.

The acceleration-time history of the horizontal and vertical components of ground motion in groups A through K for a vertical *P* wave is plotted in figures 38 and 39, respectively, and the corresponding response spectra in figure 40. In comparison with the Yerba Buena Island accelerogram (fig. 14), the vertical component varies slightly along the model boundary and is practically equal to the original vertical component, whereas the horizontal component varies spatially, reaching a minimum at the center of the model and a maximum at the extremities. The response spectra indicate that the dominant period (initially 0.6 s in fig. 14) decreases to 0.4 s in groups B through E and remains constant at 0.6 s in group A. Because the P wave travels vertically in the far field, only the vertical component influences the acceleration in the model boundary, explaining the presence of the dominant period of 0.4 s noticed in the vertical component on the original Yerba Buena Island accelerogram.

The acceleration-time history of the horizontal and vertical components of ground motion in groups A through K for a vertical *SV* wave is plotted in figures 41 and 42, respectively, and the corresponding response spectra in figure 43. The horizontal component is practically uniform along the model boundary and is equal to the original horizontal component, whereas the vertical component is smaller and varies spatially, increasing with the inclination of the boundary. The response spectra indicate that the horizontal component along the model boundary has the same dominant period as on the original accelerogram, whereas the vertical component displays two dominant periods, at 0.5 and 0.9 s.

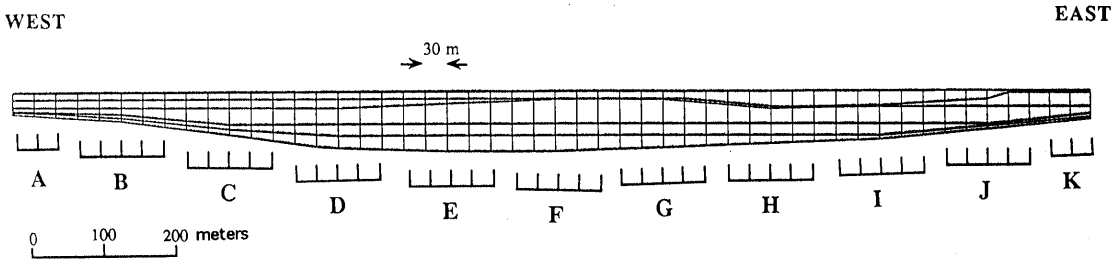


Figure 37.—Groups (A–K, fig. 36) of boundary nodes in two-dimensional model (fig. 25) assembled for inclusion of wave-propagation effects.

Four additional sets of input acceleration, not shown here, were also calculated. Two of these sets correspond to the cases of a *P* wave and an *SV* wave traveling at an inclination of 20°, an angle arbitrarily chosen to represent a deviation from the vertical propagation assumed in the one-dimensional analyses. No seismologic data were available on wave paths from the earthquake epicenter to the Marina District. The third set corresponds to the case of an R wave traveling horizontally from east to west. The fourth set corresponds to an arbitrary weighted sum of the accelerations caused by *P*-, *SV*-, and *R*-wave motions; the weighting coefficients were set to 20, 70, and 10 percent, respectively.

### RESULTS

Most of the wave-propagation analyses of site response were carried out by assuming elastic properties for the underlying soils. Only two nonlinear analyses were carried out, by using an *SV* wave inclined at 20°.

#### LINEAR ANALYSES

The response spectra of the horizontal and vertical components of ground motion predicted at borehole M4 for various types of waves are plotted in figure 44. The input accelerations along the model boundary were generated by using the scaled Yerba Buena Island accelerogram (peak acceleration, 0.15 *g*). These response spectra may be compared to those in figure 28 for the case of uniform acceleration. The dominant period is 0.7 s in both directions, independent of wave type and propagation direction. However, the peak of the spectral amplitude depends strongly on wave type and propagation direction. The largest amplitude, obtained for a *P* wave inclined at 20°, is almost twice that obtained with uniform input acceleration. The other types of waves and inclinations produce smaller amplitudes. Both *SV* and *R* waves have similar response spectra. Vertical *SV* waves produce the same response as uniform input acceleration. The lowest amplitude is obtained for a vertical *P* wave, underlining the importance of *P*-wave inclination on the response spectra. This effect is emphasized in figure 45, which compares the response spectra for two *P*-wave inclinations of 20° and −20°.

The amplification of the horizontal and vertical components of ground motion along the surface of the two-dimensional model is plotted in figures 46 and 47, respectively. The amplification is a maximum (approx 7) at point H for a *P* wave traveling at 20°, and a minimum (0.4) at point F for a vertical *P* wave. The other types of waves produce an amplification ranging from 2 to 4, always with a maximum amplification in the segment HI, where modal deformations were concentrated. Except for a *P* wave inclined at 20°, uniform input acceleration produces an upper bound for site-response amplification.

As shown in figure 47, the vertical component is not so strongly influenced by wave type: The vertical component is amplified by a factor ranging from 1 to 3, with a peak of 5 at point I for a *P* wave inclined at 20°.

#### NONLINEAR ANALYSES

The acceleration-time history and response spectra of the horizontal and vertical components of ground motion at borehole M4 and the stress-strain relation at 9-m depth, as predicted by two-dimensional nonlinear analyses for uniform input acceleration and an *SV* wave inclined at 20°, are plotted in figure 48. The stress-strain relation predicted by the analyses with uniform input acceleration and with an inclined *SV* wave are similar (fig. 48*F*). In both analyses, the peak acceleration is truncated at 0.12 *g*, owing to yielding of the soft top layer.

The amplification of the horizontal and vertical components of ground motion along the surface of the two-dimensional model for the scaled Yerba Buena Island accelerogram is plotted in figures 49 and 50, respectively. The amplification factors coincide perfectly in the nonlinear analyses, whereas they differ in the linear analyses. From figures 48 through 50, we conclude that nonlinear behavior decreases the influence of wave propagation on the site amplification.

Results similar to those in figures 48 through 50 for the original Yerba Buena Island accelerogram are shown in figures 51 through 53, respectively. The similarity of response with uniform input acceleration and with wave-propagation effects included shows that the influence of wave propagation is unimportant in this nonlinear analysis. Future research is needed to establish the effects of wave propagation in the presence of material nonlinearity.

## CONCLUSIONS

We have analyzed the site response of the Marina District during the earthquake by using numerical modeling techniques, which encompass the conventional analyses used in engineering practice and advanced techniques capable of accounting for three-dimensional geometry and wave propagation.

The one-dimensional analyses predict peak ground-surface accelerations of 0.12 and 0.15 *g*, for peak bedrock accelerations of 0.067 and 0.15 *g*, respectively. The amplification of bedrock acceleration resulted mainly from thick deposits of the older bay mud. The acceleration reaching the yellow hardpan was truncated by yielding of the soft top layer composed of artificial fill and the younger bay mud. The programs SHAKE and DETRAN, which are used to analyze one-dimensional site response in engineer-

ing practice, yielded results in agreement with those of the program LINOS. However, the program SHAKE predicted a larger amplification, reflecting the limitation of an equivalent linear material model that does not consider complete failure. A simplified liquefaction analysis based on these acceleration values clearly indicates that the artificial fills liquefied during the earthquake. The Marina District was constructed in 1915 on landfill that was predisposed to ground amplification. Liquefaction of the sand filling the 1906 lagoon was therefore triggered by amplification of the earthquake motion by natural deposits of the older bay mud.

Two types of two-dimensional analyses were performed to complete the one-dimensional analyses. The first type assumed uniform input ground motion on the model boundary, whereas the second type attempted to account for the effects of wave propagation on the site response of the Marina District. The two-dimensional analyses predicted peak ground-surface accelerations of 0.20 and 0.23 *g* for peak bedrock accelerations of 0.067 and 0.15 *g*, respectively. The two-dimensional analyses therefore predicted a larger peak acceleration than did the one-dimensional analyses, indicating that the one-dimensional site-response analyses used in engineering practice are not necessarily conservative.

The two-dimensional analyses indicated that two-dimensional effects are important in modeling the site response of the Marina District. These two-dimensional effects, which resulted mainly from the irregular geometry of the bedrock surface and the layer of yellow hardpan, provide a better understanding of the deformational modes of the Marina District. The effects of wave propagation were found to be important but could not be completely characterized. The complex input acceleration generated along the model boundary tends to excite many other vibrational modes within the soft-soil deposits than the first fundamental mode used in one-dimensional models. Inclusion of wave-propagation effects in the site-response analysis substantially complicates the dynamic response of the soft soils. Material nonlinearity was observed to decrease these effects. The present study shows the complexity of site-response analyses for three-dimensional geologic structures and clearly indicates the need for future research in seismic site-response analysis.

## ACKNOWLEDGMENTS

We thank V.W. Lee and his graduate research assistant X. Wu of the Department of Civil Engineering of the University of Southern California, Los Angeles, for their contribution to the wave-propagation analysis, and T.D. O'Rourke of Cornell University, Ithaca, N.Y., for sharing his site-investigation data. This research was supported by National Science Foundation grant BCS9003656.

## REFERENCES CITED

Arulanandan, K., and Yogachandran, G., 1990, A preliminary analysis of ground response and soil liquefaction of sites in the Marina District of San Francisco subjected to the Loma Prieta earthquake of October 17, 1989: Davis, University of California, Department of Civil Engineering Report 1990–1.

Bardet, J.-P., 1990a, LINOS; a nonlinear finite element program for geomechanics and geotechnical engineering: Los Angeles, University of Southern California, Department of Civil Engineering, 117 p.

———1990b, Damage at a distance: Nature, v. 346, no. 6287, p. 799.

———1990c, Hypoplastic model for sands: Journal of Engineering Mechanics, v. 116, no. 9, p. 1973–1994.

Bardet, J.-P., and Kapuskar, M., 1991a, Collection and interpretation of data on the liquefaction sand boils in the San Francisco Marina District after the 1989 Loma Prieta earthquake: Los Angeles, University of Southern California, Department of Civil Engineering report to National Science Foundation, 46 p.

———1991b, Site investigation of the Marina District of San Francisco in September 1990: Los Angeles, University of Southern California, Department of Civil Engineering report to National Science Foundation, 94 p.

———1991c, The liquefaction sand boils in the Marina District of San Francisco, California: International Conference on Recent Advances in Geotechnical Engineering and Soil Dynamics, 2d, St. Louis, Mo., 1991, Proceedings, v. 2, p. 1687–1691.

———in press, An analysis of the sand boils due to liquefaction in the San Francisco Marina District during the 1989 Loma Prieta earthquake: Journal of Geotechnical Engineering.

Bennett, M.J., 1990, Ground deformation and liquefaction of soil in the Marina District, chap. D *of* Effects of the Loma Prieta earthquake on the Marina District, San Francisco, California: U.S. Geological Survey Open-File Report 90–253, p. D1–D36.

Bonaparte, R., and Mitchell, J.K., 1979, The properties of San Francisco bay mud at Hamilton Air Force Base: Berkeley, University of California, Civil Engineering Department.

Bonilla, M.G., 1990, Natural and artificial deposits in the Marina District, chap. A *of* Effects of the Loma Prieta earthquake on the Marina District, San Francisco, California: U.S. Geological Survey Open-File Report 90–253, p. A1–A24.

Carlson, P.R., and McCulloch, D.S., 1970, Bedrock-surface map of central San Francisco Bay, California: U.S. Geological Survey Open-File Map, scale approx 1:16,000.

Chen, A.T.F., and Joyner, W.B., 1974, Multi-linear analysis for ground motion studies of layered systems: U.S. Geological Survey report, 49 p. [available from National Technical Information Service, U.S. Department of Commerce, Springfield, VA 22161, as report PB–232 704/AS].

Dames & Moore, 1962, Main building rehabilitation, Palace of Fine Arts: San Francisco, report on job 185–033–03.

———1977, North Shore Outfalls Consolidation Project. Supplementary: San Francisco, report on job 185–118–03.

Denby, G.M., 1978, Self-boring pressure meter study of San Francisco bay mud: Stanford, Calif., Stanford University, Department of Civil Engineering Technical Report CE–232.

Douglas, B.J., and Olsen, R.S., 1981, Soil classification using electric cone penetrometer: St. Louis, Mo., American Society of Civil Engineers, Geotechnical Engineering Division.

Earth Technology Corp., 1990, Seismic velocity profiles determined from CPT soundings near the Marina Blvd., San Francisco, California: Huntington Beach, Calif., report on project 91–8000–01.

Ghaboussi, J., and Dikmen, S.U., 1977, LASS II, computer program for analysis of seismic site response and liquefaction of horizontally layered sands: Urbana-Champaign, University of Illinois, Department of Civil Engineering Report UILU–ENG–77–2010.

Hardin, B.O., and Drnevich, V.P., 1972, Shear modulus and damping in soils; design equations and curves: American Society of Civil Engineers Proceedings, Soil Mechanics and Foundations Division Journal, v. 98, no. 7, p. 667–692.

Housner, G.W., and Penzien, J., 1990, Competing against time; report of the Governor's Board of Inquiry on the 1989 Loma Prieta Earthquake: Sacramento, Calif., 264 p.

Idriss, I.M., and Seed, H.B., 1968, Seismic response of horizontal layers: American Society of Civil Engineers Proceedings, Soil Mechanics and Foundations Division Journal, v. 94, no. SM4, p. 1003–1031.

Isenhower, W.M., 1979, Torsional simple shear/resonant column properties of San Francisco bay mud: Austin, University of Texas, M.S. thesis.

Iwan, W.D., 1967, On a class of models for the yielding behavior of continuous and composite systems: Journal of Applied Mechanics, p. 612–617.

Joyner, W.B., 1975, A method for calculating nonlinear seismic response in two-dimensions: Seismological Society of America Bulletin, v. 65, no. 5, p. 1337–1357.

Kayen, R.E., Liu, H.P., Fumal, T.E., Westerlund, R.E., Warrick, R.E., Gibbs, J.F., and Lee, H.J., 1990, Engineering and seismic properties of the soil column at Winfield Scott School, San Francisco, chap. G *of* Effects of the Loma Prieta earthquake on the Marina District, San Francisco, California: U.S. Geological Survey Open-File Report 90–253, p. G1–G18.

Lawson, A.C., 1908, The California earthquake of April 18, 1906; report of the State Earthquake Investigation Commission: Carnegie Institution of Washington Publication 87, 2 v.

Lee, M.K.W., and Finn, W.D.L., 1978, DESRA–2—dynamic effective stress response analysis of soil deposits with energy transmitting boundary including assessment of liquefaction potential: Vancouver, British Columbia, Canada, University of British Columbia.

Martin, G.R., 1991, Site investigation using the CPT and CPT/SPT correlations; short course on the evaluation and mitigation of earthquake induced hazards: Los Angeles, 22 p.

Martin, G.R., and Tsai, C.F., 1981, Nonlinear response of soft clay sediments to high-strain earthquake ground motions: Long Beach, Calif., Earth Mechanics Corp. report on contract USGS–14–08–0001–19106, p. 29–46.

Masing, G., 1926, Eigenspannungen und Verfestigung beim Messing [Fundamental stresses and strengthening with brass]: Inter-national Congress of Applied Mechanics, 2d, Zürich, 1926, Proceedings.

Mooeen-Vaziri, Nasser, and Trifunac, M.D., 1988, Scattering and diffraction of plane *P* and *SV* waves by two-dimensional inhomogeneities; part II: Soil Dynamics and Earthquake Engineering, v. 7, no. 4, p. 189–200.

Muraleetharan, K.K., Mish, K., and Arulanandan, K.K., 1990, DYSAC2; user's manual: Davis, University of California, Department of Civil Engineering.

National Research Council, 1985, Liquefaction of soils during earthquakes: Washington, D.C., National Academy Press, p. 137–143.

Prevost, J.H., 1978, Anisotropic undrained stress-strain behavior of clays: American Society of Civil Engineers Proceedings, Geotechnical Engineering Division Journal, v. 104, no. GT8, p. 1075–1090.

———1989, DYNA1D; a computer program for nonlinear seismic site response analysis—technical documentation: Buffalo, N.Y., National Center for Earthquake Engineering Research Technical Report NCEER–89–0025, p. 6–1 to 6–13.

Schlocker, Julius, 1961, Geological topographic bedrock map of the San Francisco North quadrangle, California: U.S. Geological Survey Open File Map, scale 1:31,680.

———1974, Geology of the San Francisco North quadrangle, California: U.S. Geological Survey Professional Paper 782, 109 p.

Schmertman, J.H., 1975, Measurement of in situ shear strength: ASCE Conference on In Situ Measurement of Soil Properties, Raleigh, N.C., 1975, Proceedings, v. 2, p. 79–99.

Schnabel, P.B., Lysmer, J., and Seed, H.B., 1972, SHAKE—a computer program for earthquake response analysis of horizontally layered sites: Berkeley, University of California, Earthquake Engineering Research Center Report EERC 72–12.

Seed, H.B., 1970, Soil problems and soil behavior, *in* Wiegel, R.L., ed., Earthquake engineering: Englewood Cliffs, N.J., Prentice-Hall, p. 227–252.

Seed, H.B. and Idriss, I.M., 1971, Simplified procedure for evaluation of soil liquefaction potential: American Society of Civil Engineers Proceedings, Soil Mechanics and Foundations Division Journal, v. 97, no. SM9, p. 1249–1273.

Seed, H.B., Idriss, I.M., and Arango, Ignacio, 1983, Evaluation of liquefaction potential using field performance data: Journal of Geotechnical Engineering, v. 109, no. 3, p. 458–482.

Seed, H.B., and Idriss, I.M., 1970, Soil moduli and damping factors for dynamic response analysis: Berkeley, University of California, Earthquake Engineering Research Center Report EERC 70–10.

Seed, H.B. and Sun, J.I., 1989, Implications of site effects in the Mexico City earthquake of Sept. 19, 1985 for earthquake-resistant design criteria in the San Francisco Bay area of California: Berkeley, University of California, Earthquake Engineering Research Center Report UCB/EERC–89–03, p. 27–40.

Shakal, A., Huang, M., Reichle, M., Ventura, C., Cao, T., Sherburne, R., Savage, M., Darragh, R., and, Petersen, C., 1989, CSMIP strong-motions records from the Santa Cruz Mountains (Loma Prieta), California earthquake of 17 October 1989: California Division of Mines and Geology, Office of Strong Motion Studies Report OSMS 89–06, 196 p.

Todorovska, M.I., and Lee, V.W., in press, Surface motion of circular alluvial valleys of variable depth for incident plane *P*-waves—analytical solution: Royal Astronomical Society Geophysical Journal.

U.S. Geological Survey, 1973, San Francisco North quadrangle, California: special topographic map, scale 1: 24,000.

———1990, Effects of the Loma Prieta earthquake on the Marina District, San Francisco, California: Open-File Report 90–253.

# FIGURES 19–23, 28–35, AND 38–53

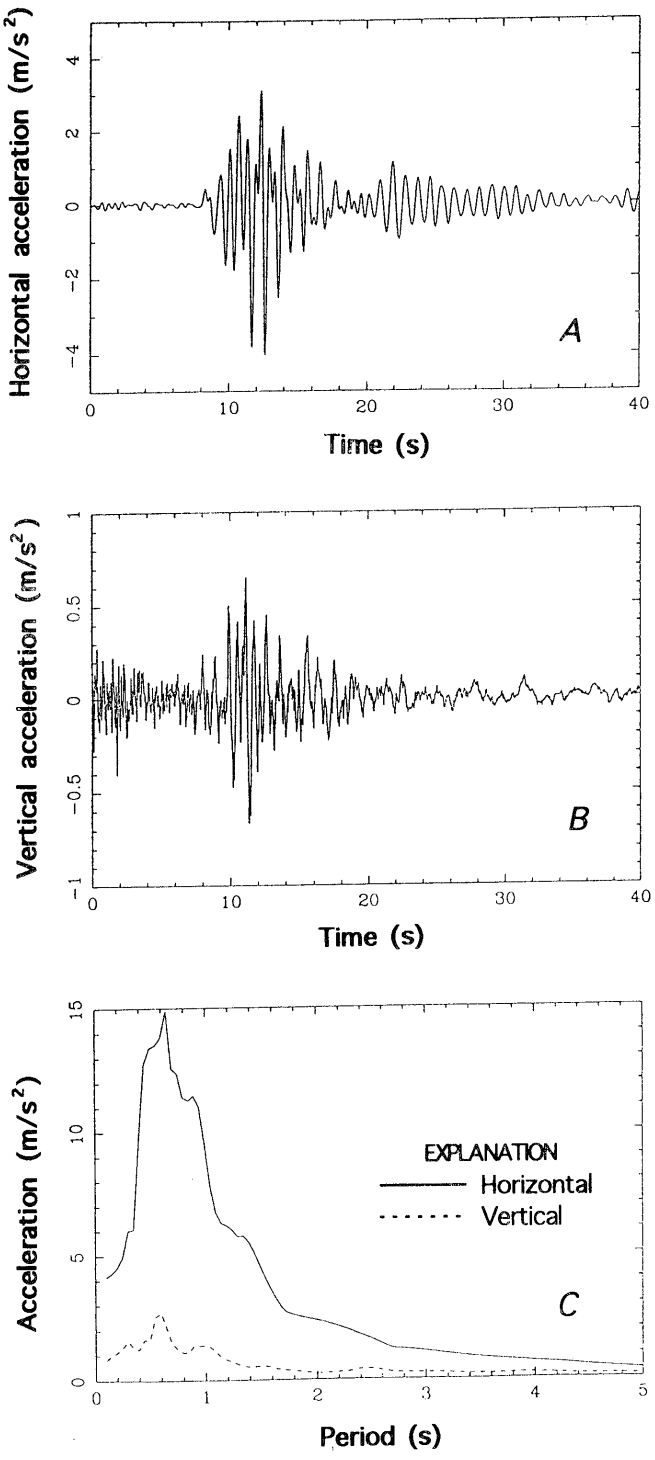


Figure 19.—Acceleration-time history of horizontal (*A*) and vertical (*B*) components of ground motion, with response spectra (*C*) of horizontal (solid curve) and vertical (dashed curve) components, at borehole M4 (fig. 4), as predicted by one-dimensional linear analyses for scaled Yerba Buena Island accelerogram (peak acceleration, 0.15 *g*). Curves in figure 19*C* are plotted with 5-percent damping.

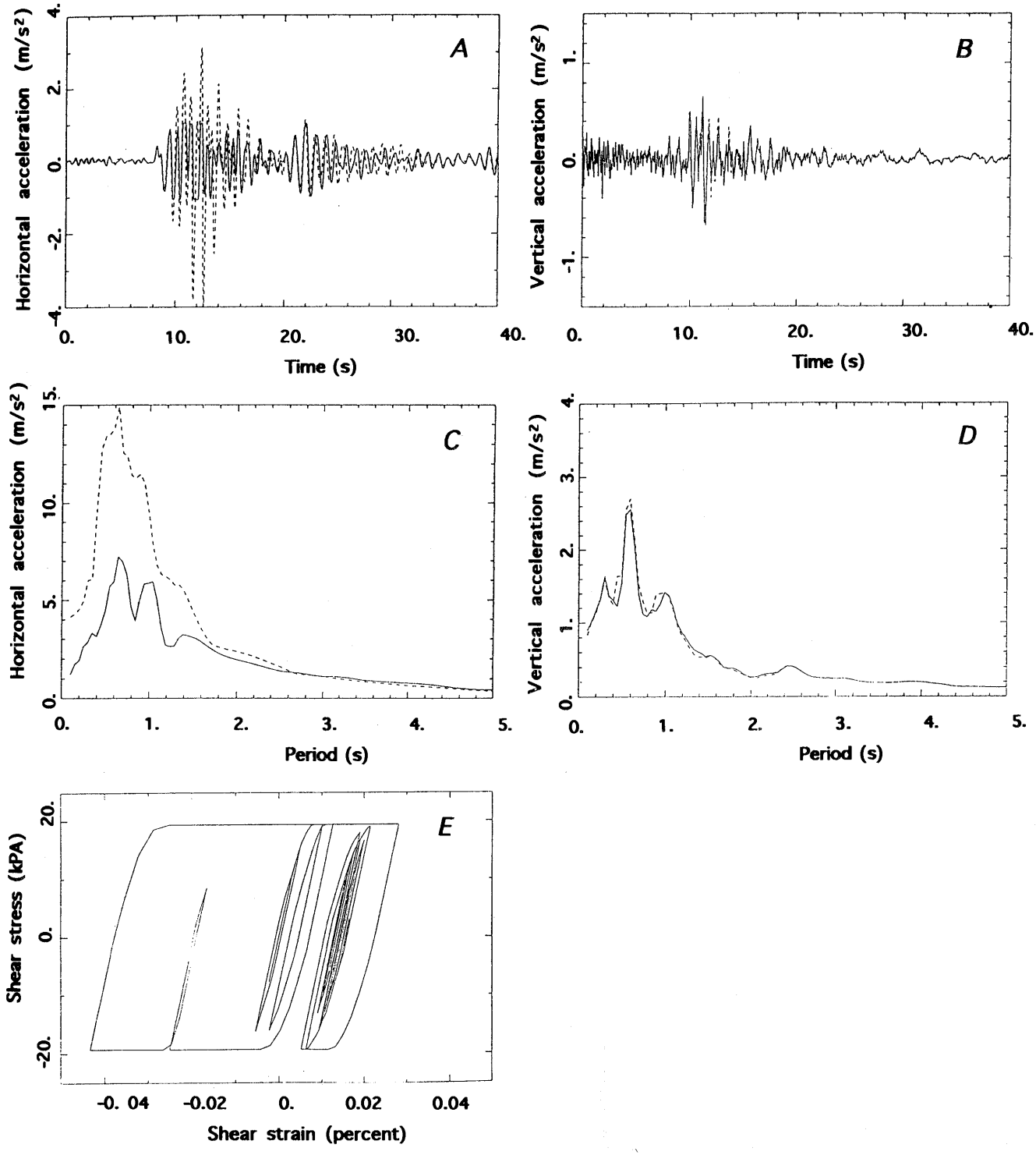


Figure 20.—Acceleration-time history of horizontal (*A*) and vertical (*B*) components of ground motion, with corresponding response spectra (*C*, *D*), at borehole M4 (fig. 4), and stress-strain relation (*E*) at 6-m depth, as predicted by nonlinear (solid curves) and linear (dashed curves) one-dimensional analyses for scaled Yerba Buena Island accelerogram (peak acceleration, 0.15 *g*). Curves in figures 20*C* and 20*D* are plotted with 5-percent damping.

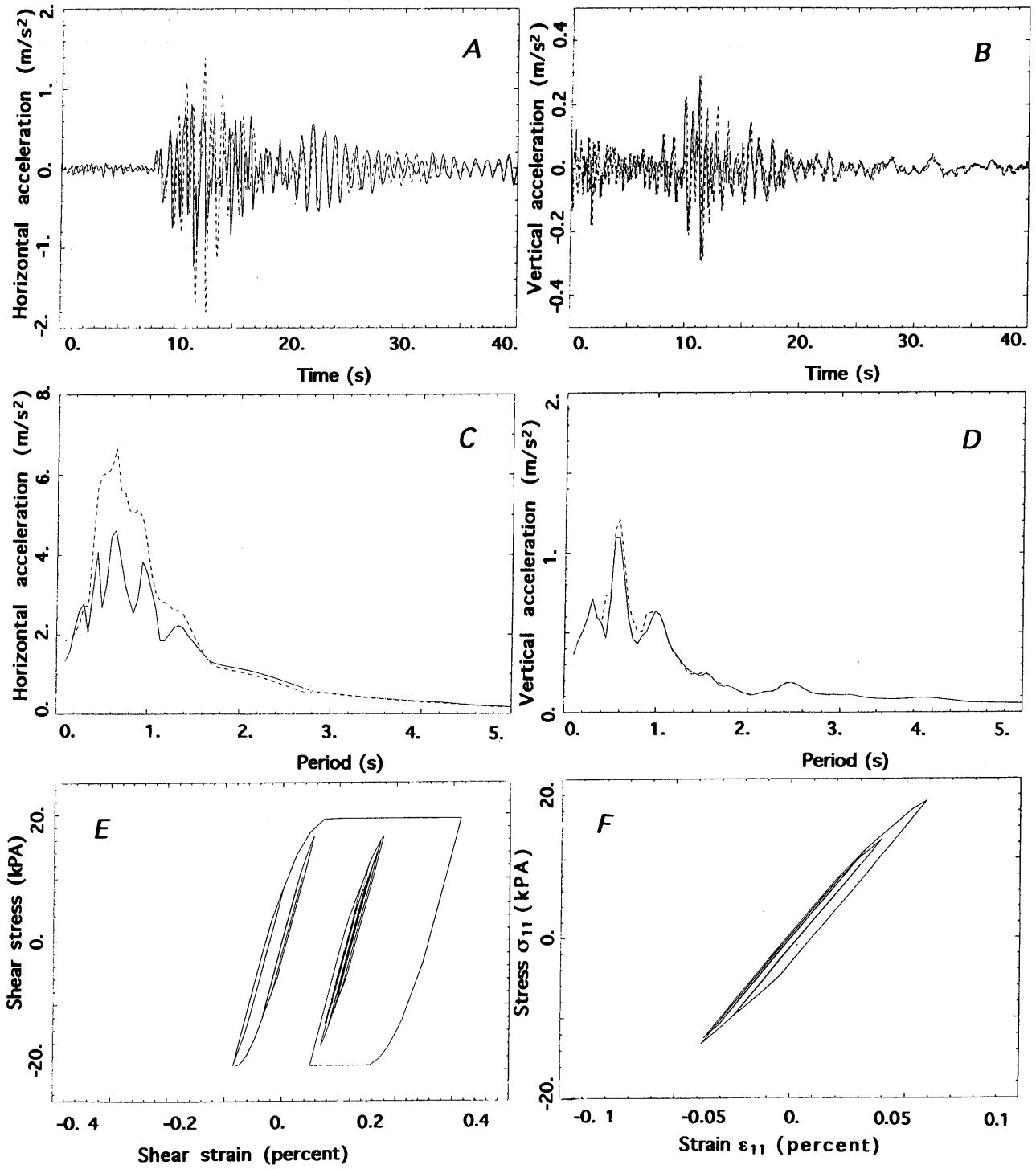


Figure 21.—Acceleration-time history of horizontal (*A*) and vertical (*B*) components of ground motion, with corresponding response spectra (*C*, *D*) at borehole M4 (fig. 4), and stress-strain relation at 9 (*E*)- and 6 (*F*)-m depth, as predicted by nonlinear (solid curves) and linear (dashed curves) one-dimensional analyses for original Yerba Buena Island accelerogram (peak acceleration, 0.067 *g*). Curves in figures 21*C* and 21*D* are plotted with 5-percent damping.

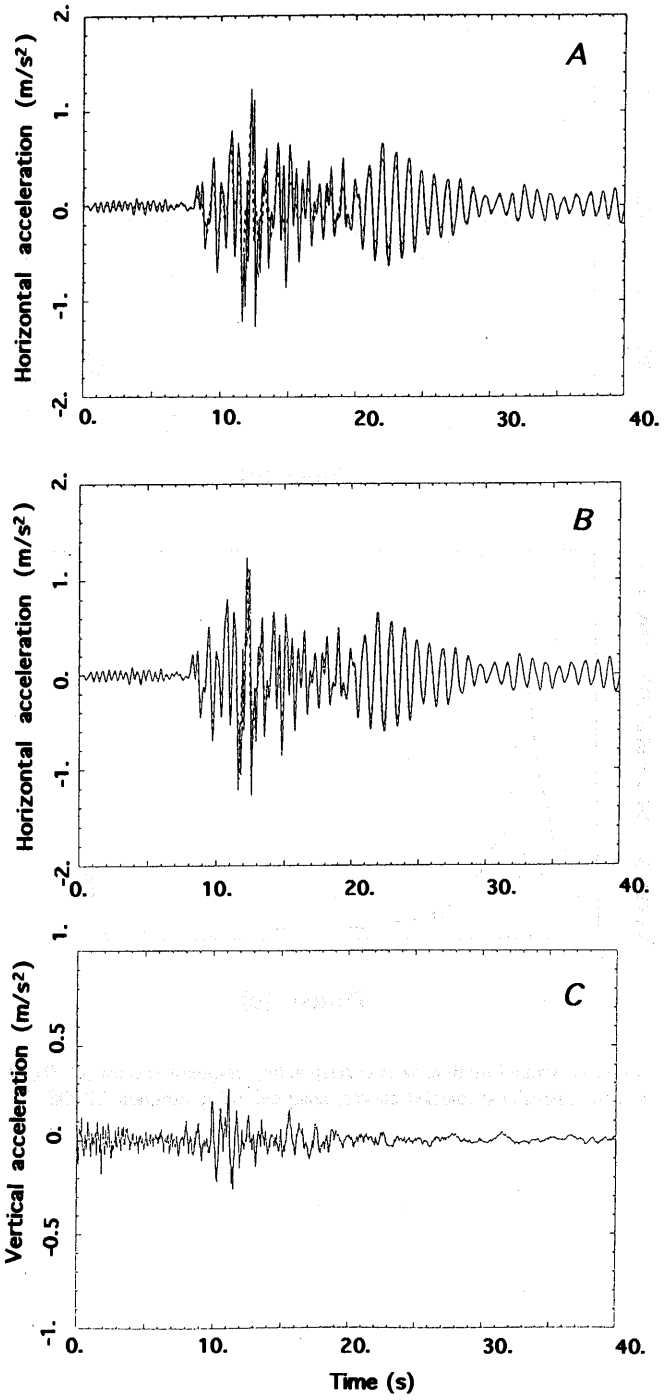


Figure 22.—Acceleration-time history of horizontal (*A*, *B*) and vertical (*C*) components of ground motion at surface (solid curves), at top of yellow hardpan (dashed curves, figs. 22*A*, 22*C*), and at 4-m depth (dashed curve, fig 22*B*) at borehole M4 (fig. 4), as predicted by nonlinear one-dimensional analyses for original Yerba Buena Island accelerogram (peak acceleration, 0.067 *g*).

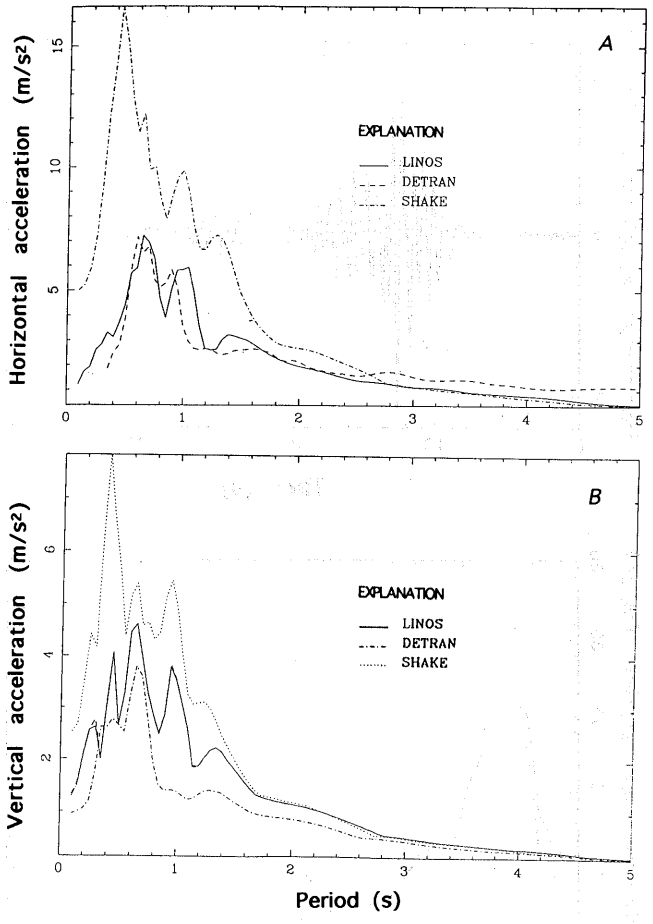


Figure 23.—Response spectra of horizontal acceleration at borehole M4 (fig. 4), calculated by using three computer programs of site-response analysis for scaled (*A*; peak acceleration, 0.15 *g*) and original (*B*; peak acceleration, 0.067 *g*) Yerba Buena Island accelerograms.

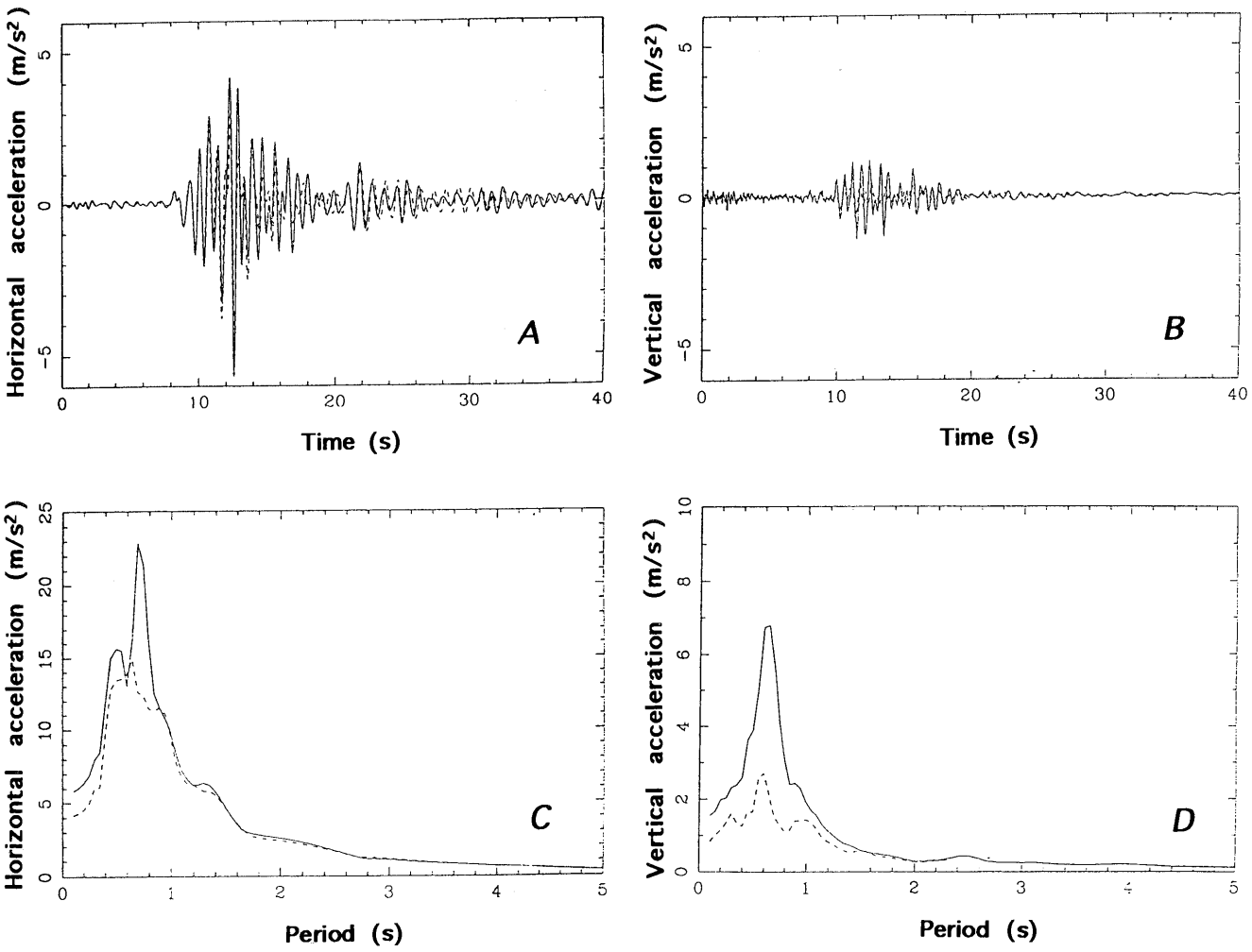


Figure 28.—Acceleration-time history of horizontal (*A*) and vertical (*B*) components of ground motion, with corresponding response spectra (*C*, *D*), at borehole M4 (fig. 4), as predicted by linear two-dimensional (solid curves) and one-dimensional (dashed curves) analyses, using program LINOS, for scaled Yerba Buena Island accelerogram (peak acceleration, 0.15 *g*).

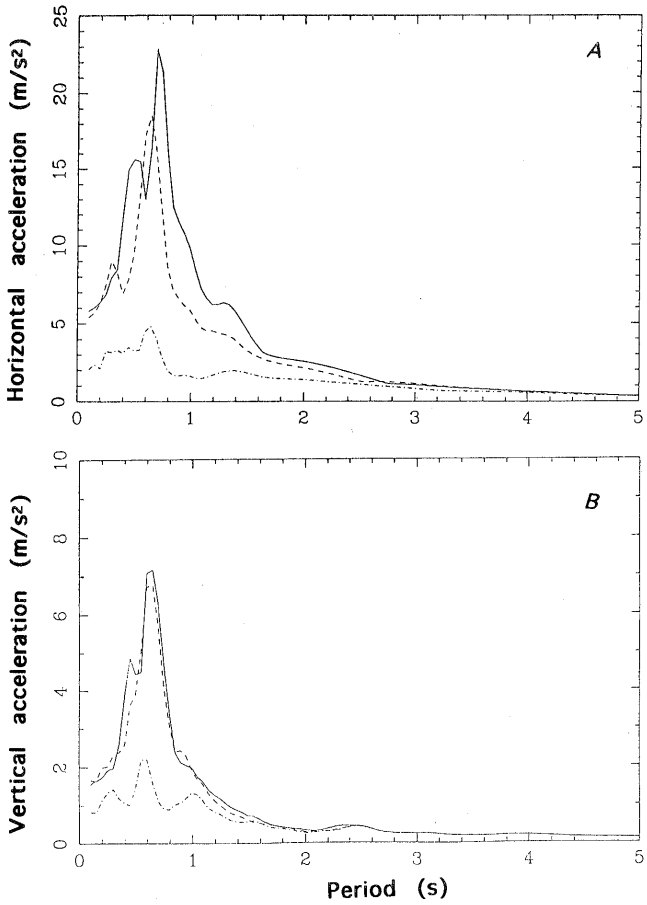


Figure 29.—Response spectra of horizontal (*A*) and vertical (*B*) components of ground motion at borehole M4 (solid curves), at borehole WSS (dashed curves), and on bedrock (dot-dashed curves), as predicted by linear two-dimensional analyses for scaled Yerba Buena Island accelerogram (peak acceleration, 0.15 *g*).

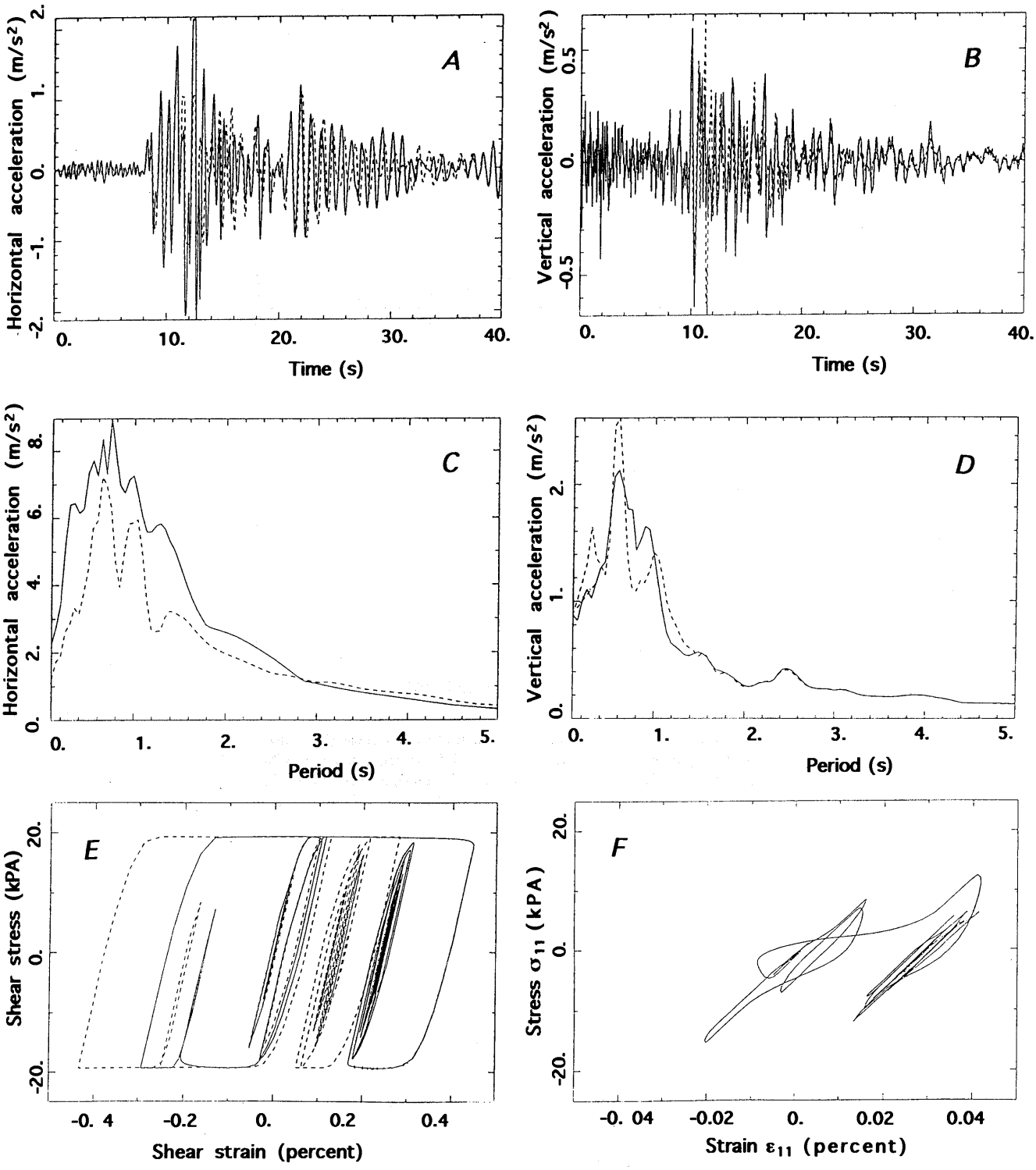


Figure 30.—Acceleration-time history of horizontal (*A*) and vertical (*B*) components of ground motion, with corresponding response spectra (*C*, *D*), at borehole M4 (fig. 4), and stress-strain relation (*E*, *F*) at 9-m depth, as predicted by two-dimensional (solid curves) and one-dimensional (dashed curves) nonlinear analyses, using the program LINOS, for scaled Yerba Buena Island accelerogram (peak acceleration, 0.15 *g*).

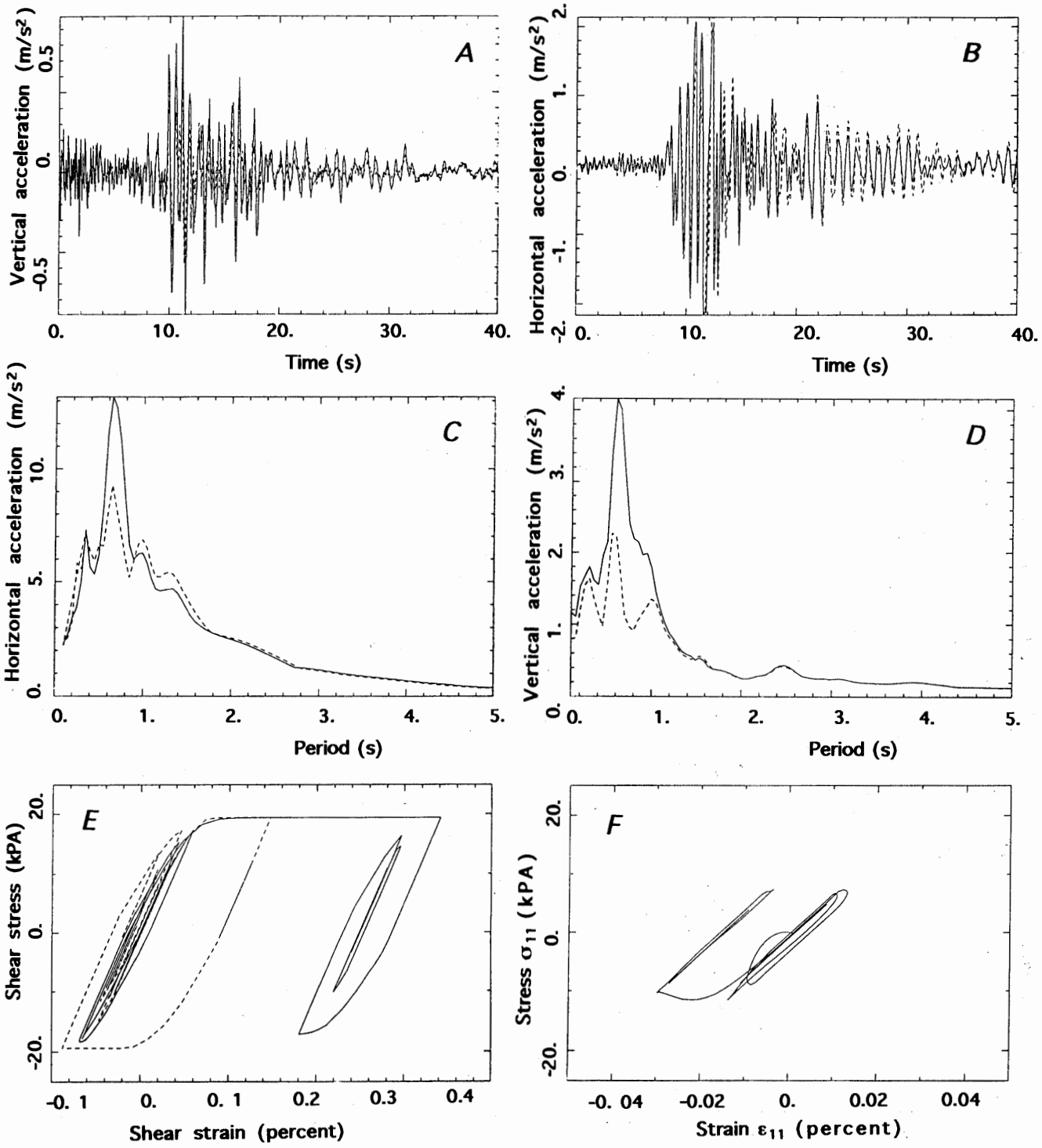


Figure 31.—Acceleration-time history of horizontal (*A*) and vertical (*B*) components of ground motion, with corresponding response spectra (*C*, *D*), at borehole WSS (fig. 4), and stress-strain relation (*E*, *F*) at 9-m depth, as predicted by two-dimensional (solid curves) and one-dimensional (dashed curves) nonlinear analyses, using the program LINOS, for scaled Yerba Buena Island accelerogram (peak acceleration, 0.15 *g*).

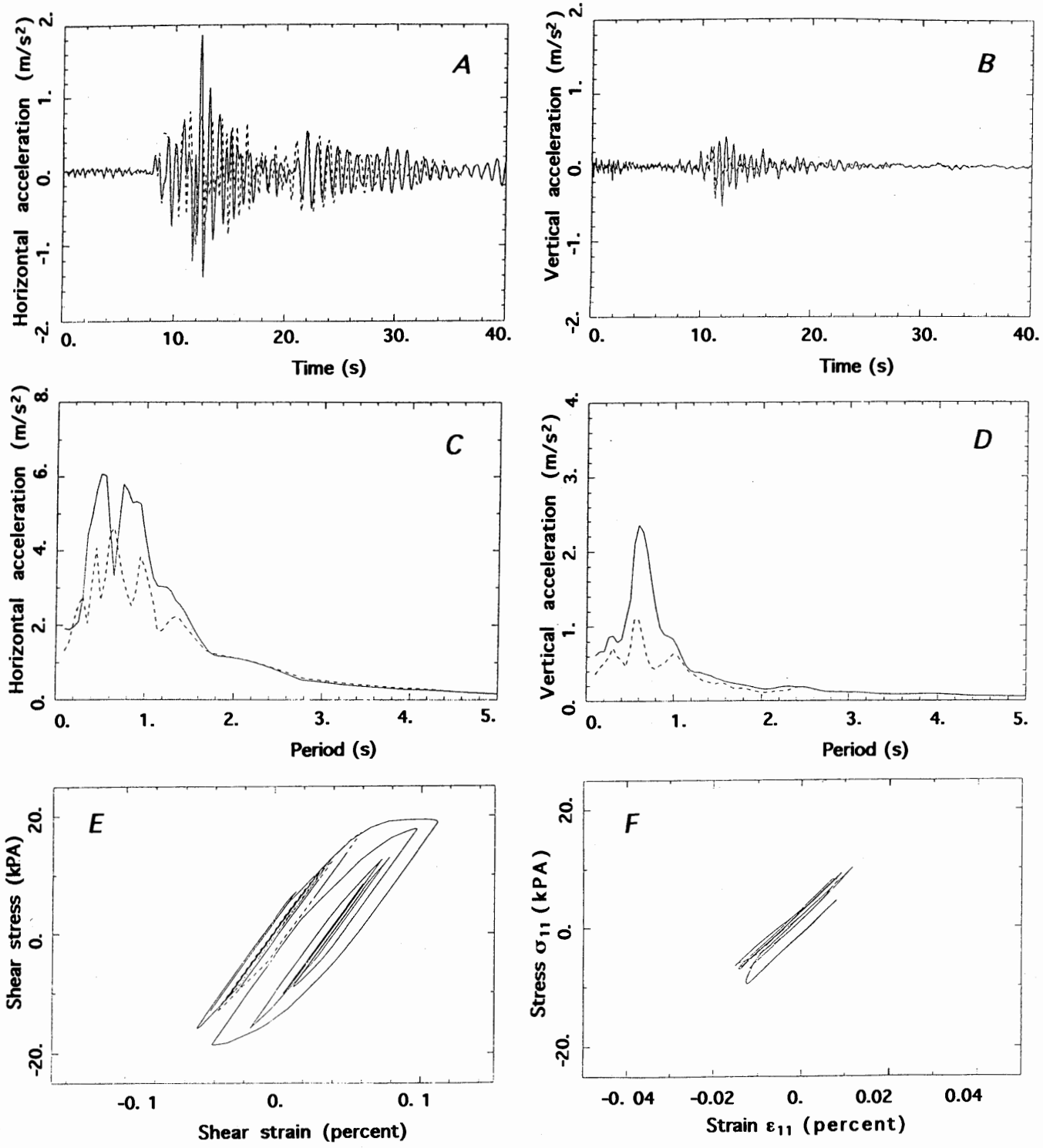


Figure 32.—Acceleration-time history of horizontal (*A*) and vertical (*B*) components of ground motion, with corresponding response spectra (*C*, *D*), at borehole M4 (fig. 4), and stress-strain relation (*E*, *F*) at 9-m depth, as predicted by two-dimensional (solid curves) and one-dimensional (dashed curves) nonlinear analyses, using the program LINOS, for original Yerba Buena Island accelerogram (peak acceleration, 0.067 *g*).

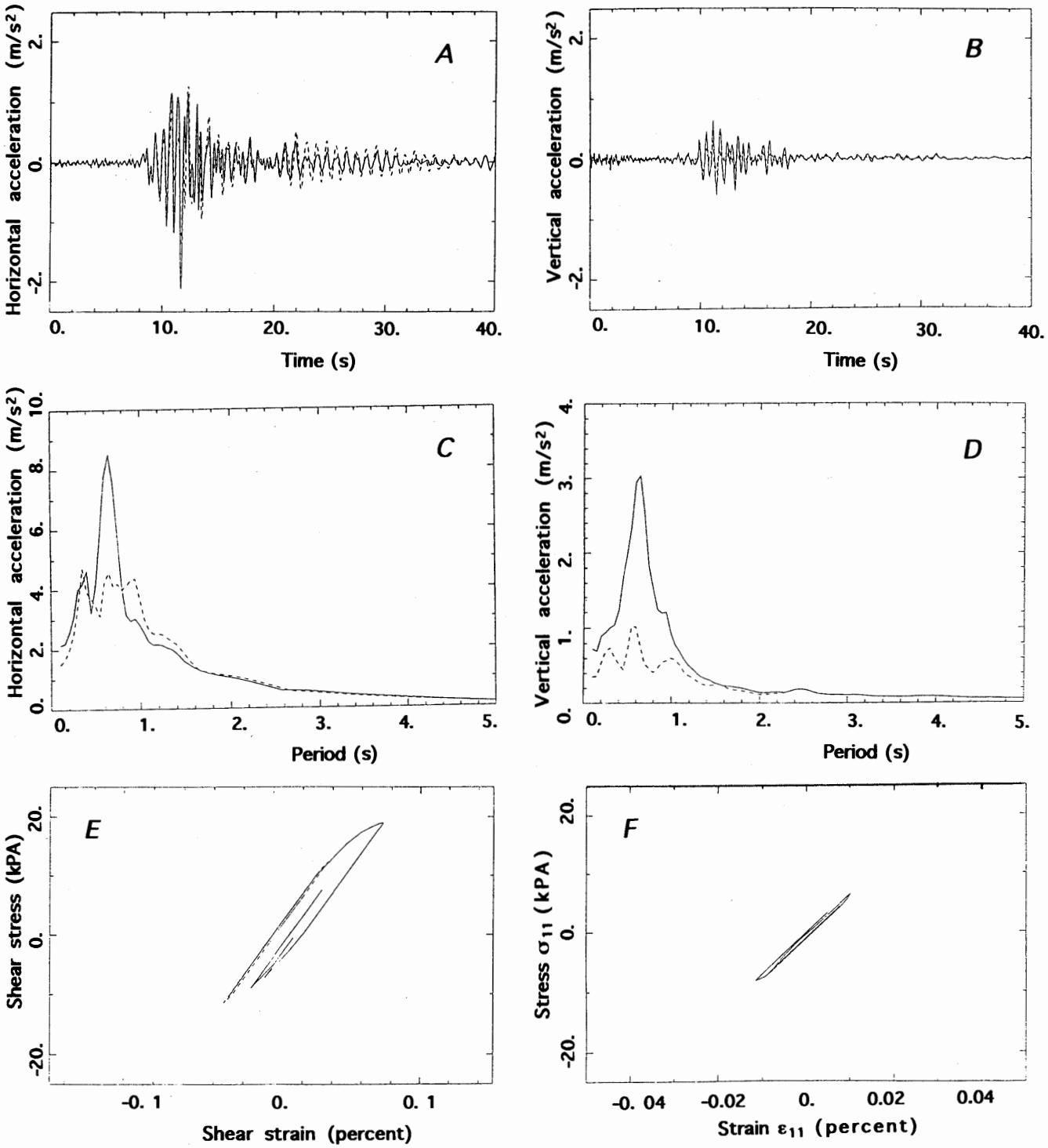


Figure 33.—Acceleration-time history of horizontal (*A*) and vertical (*B*) components of ground motion, with corresponding response spectra (*C*, *D*), at borehole WSS (fig. 4), and stress-strain relation (*E*, *F*) at 9-m depth, as predicted by two-dimensional (solid curves) and one-dimensional (dashed curves) nonlinear analyses, using the program LINOS, for original Yerba Buena Island accelerogram (peak acceleration, 0.067 *g*).

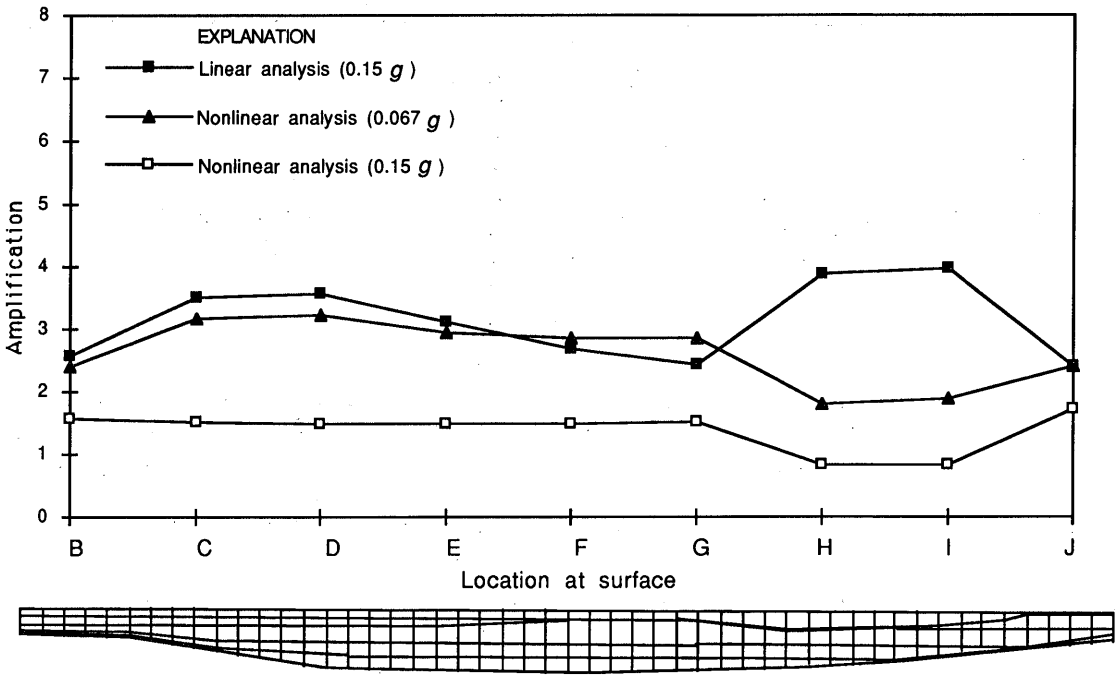


Figure 34.—Amplification of horizontal component of ground motion along surface of two-dimensional model (fig. 25), as predicted by two-dimensional nonlinear and linear analyses. Letters refer to groups of boundary nodes in figure 37.

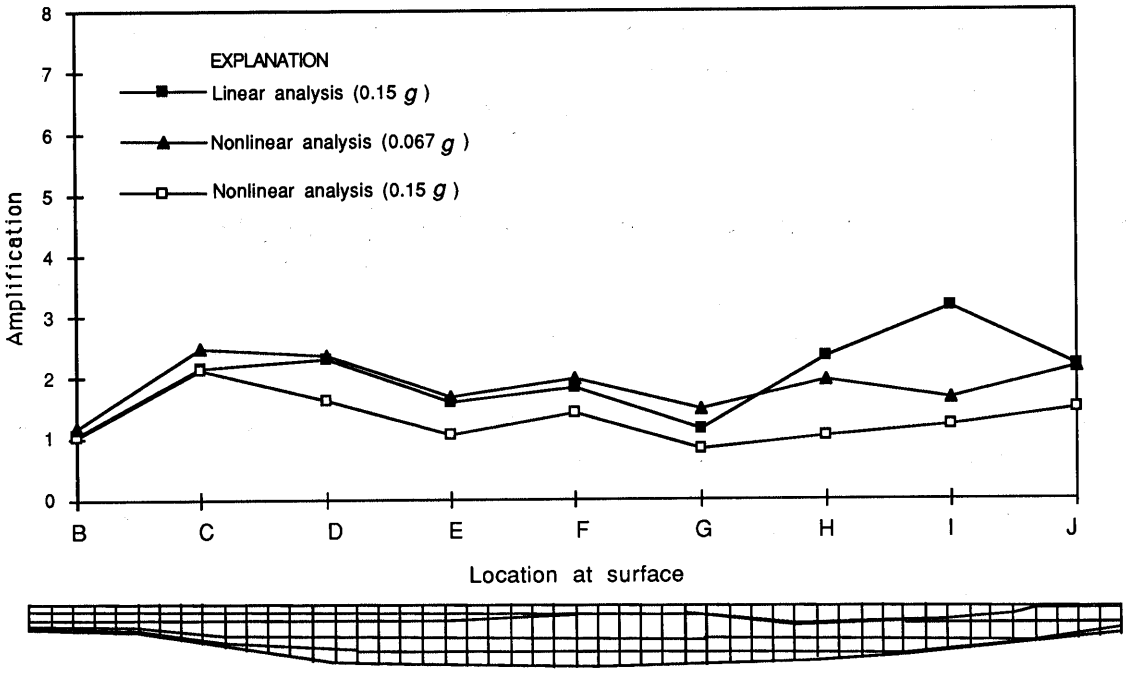


Figure 35.—Amplification of vertical component of ground motion along surface of two-dimensional model (fig. 25), as predicted by two-dimensional nonlinear and linear analyses. Letters refer to groups of boundary nodes in figure 37.

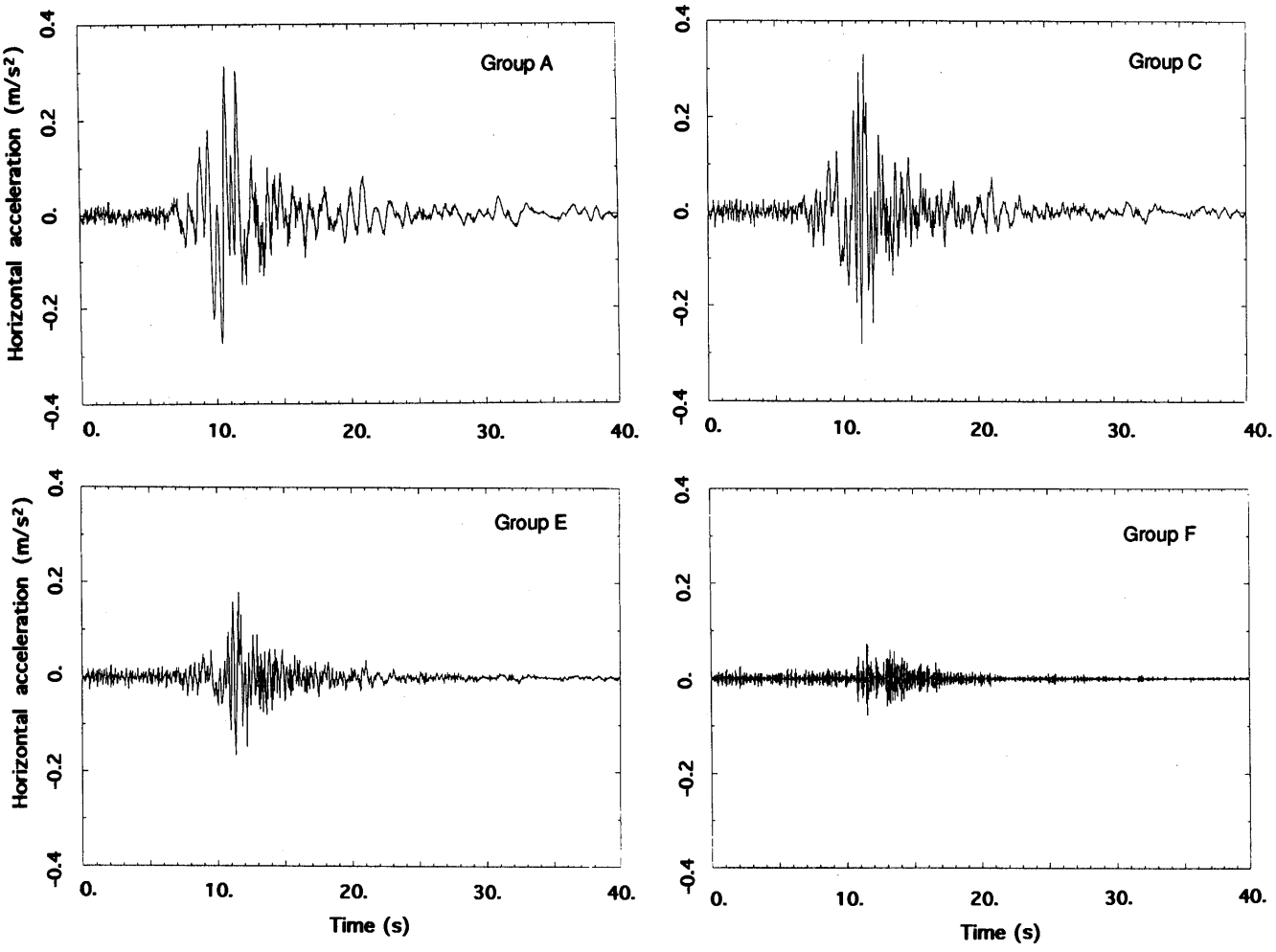


Figure 38.—Acceleration-time history of horizontal component of ground motion in bedrock for a vertical *P* wave (groups A, C, E, and F, fig. 37).

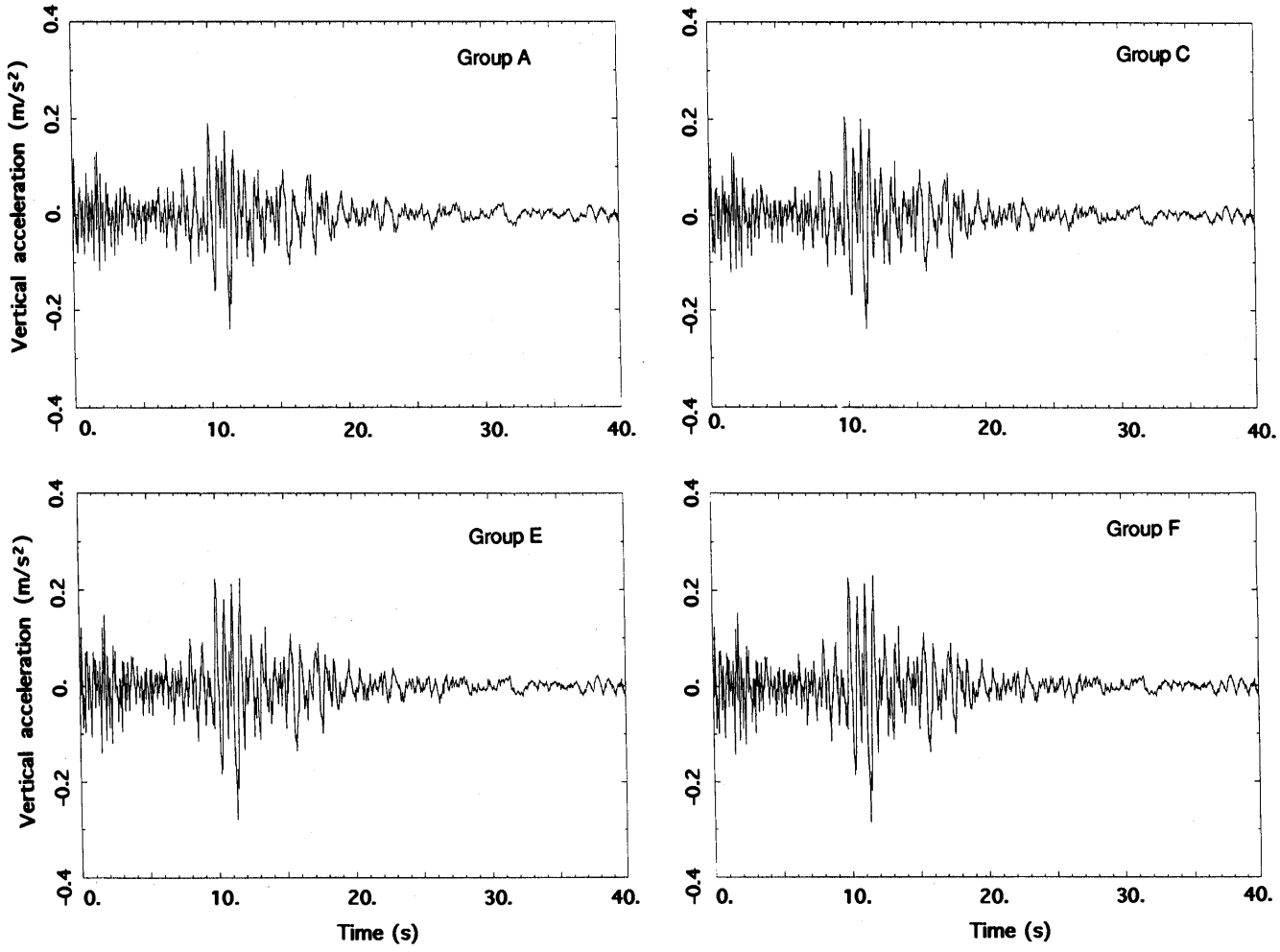


Figure 39.—Acceleration-time history of vertical component of ground motion in bedrock for a vertical *P* wave (groups A, C, E, and F, fig. 37).

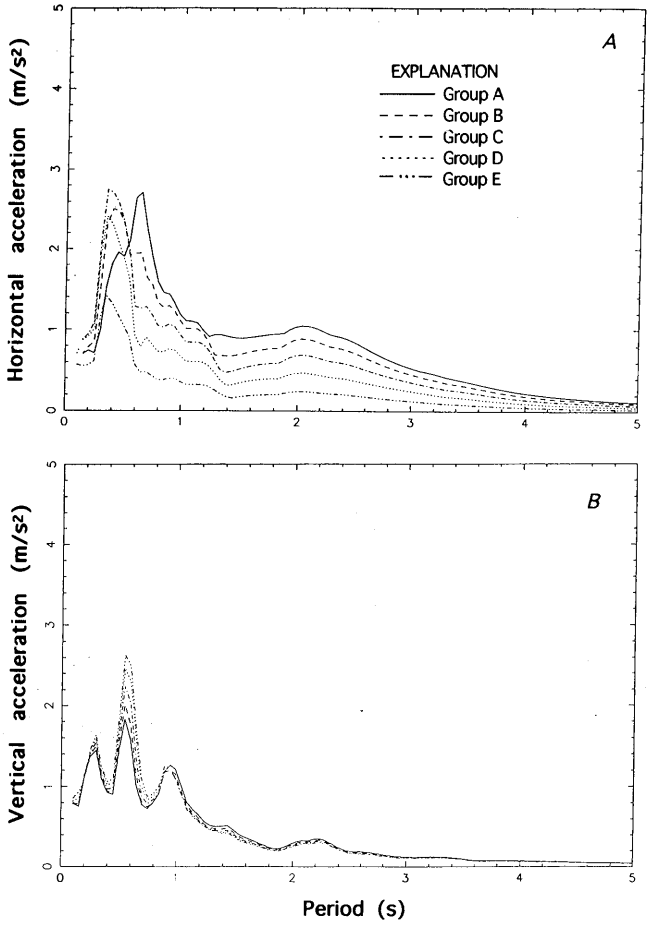


Figure 40.—Response spectra of horizontal (*A*) and vertical (*B*) components of ground motion in bedrock for a vertical *P* wave on original Yerba Buena Island accelerogram (peak acceleration, 0.067 *g*).

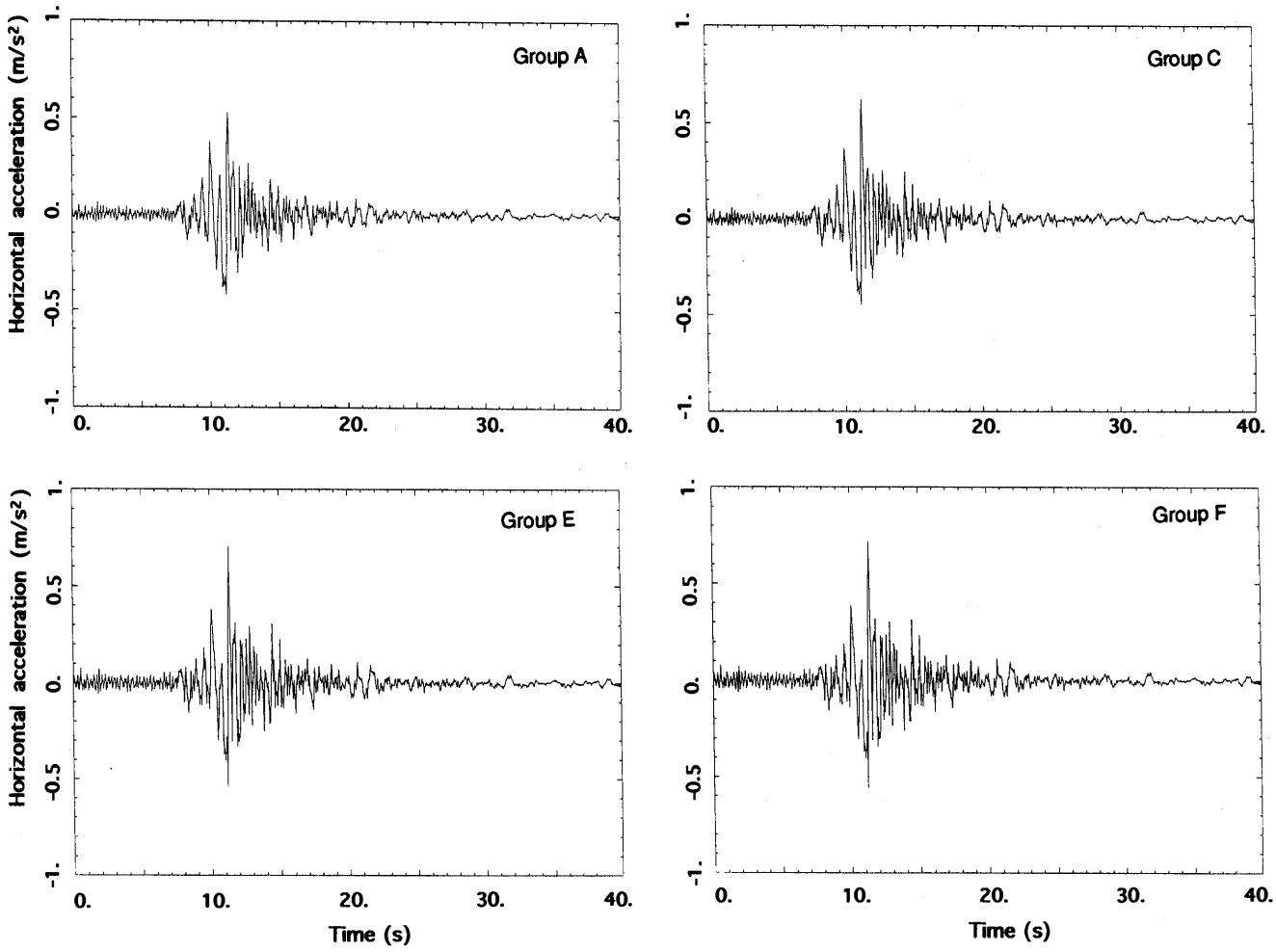


Figure 41.—Acceleration-time history of horizontal component of ground motion in bedrock for a vertical *SV* wave (groups A, C, E, and F, fig. 37).

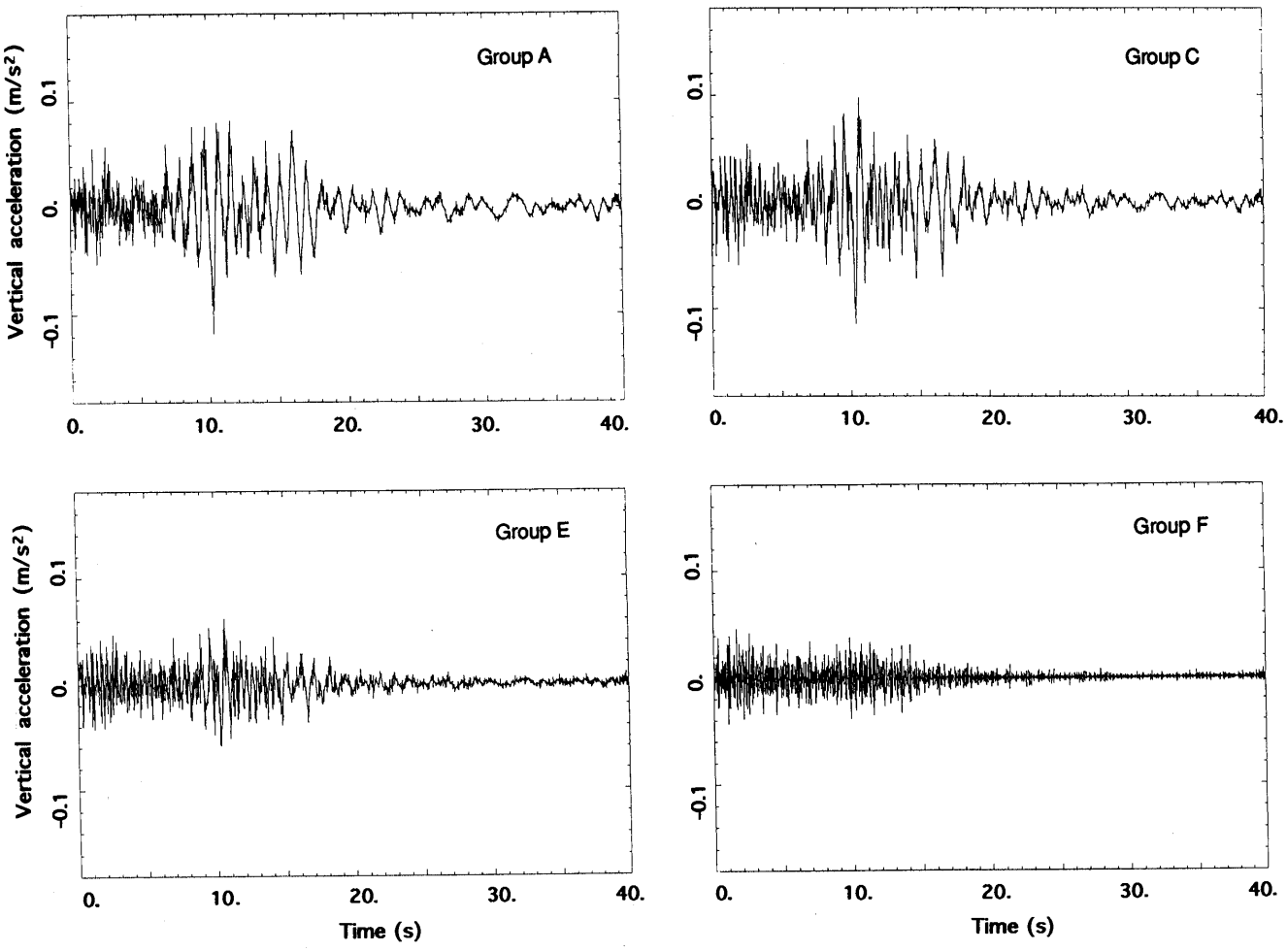


Figure 42.—Acceleration-time history of vertical component of ground motion in bedrock for a vertical *SV* wave (groups A, C, E, and F, fig. 37).

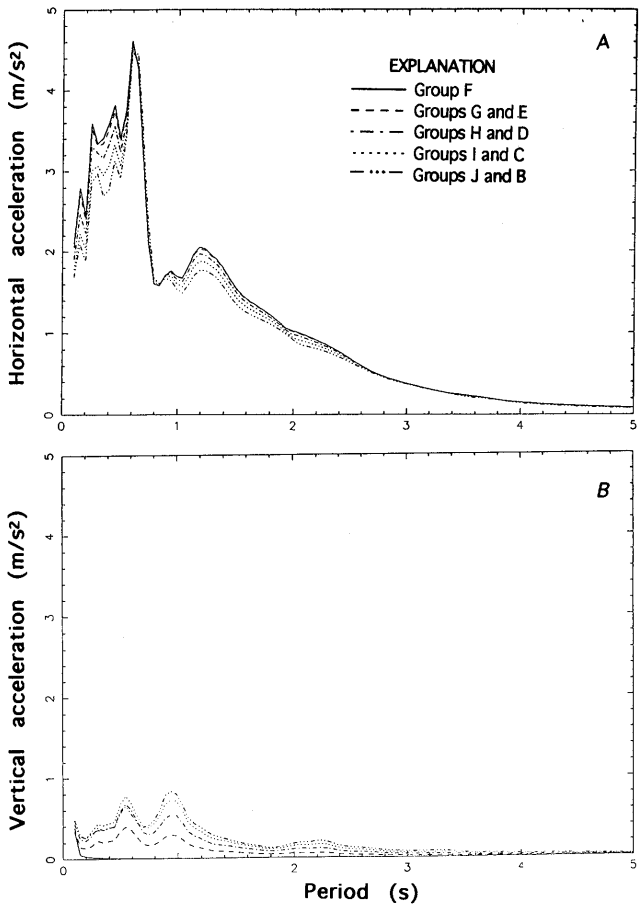


Figure 43.—Response spectra of horizontal (*A*) and vertical (*B*) components of ground motion in bedrock for a vertical *SV* wave on original Yerba Buena Island accelerogram (peak acceleration, 0.067 *g*).

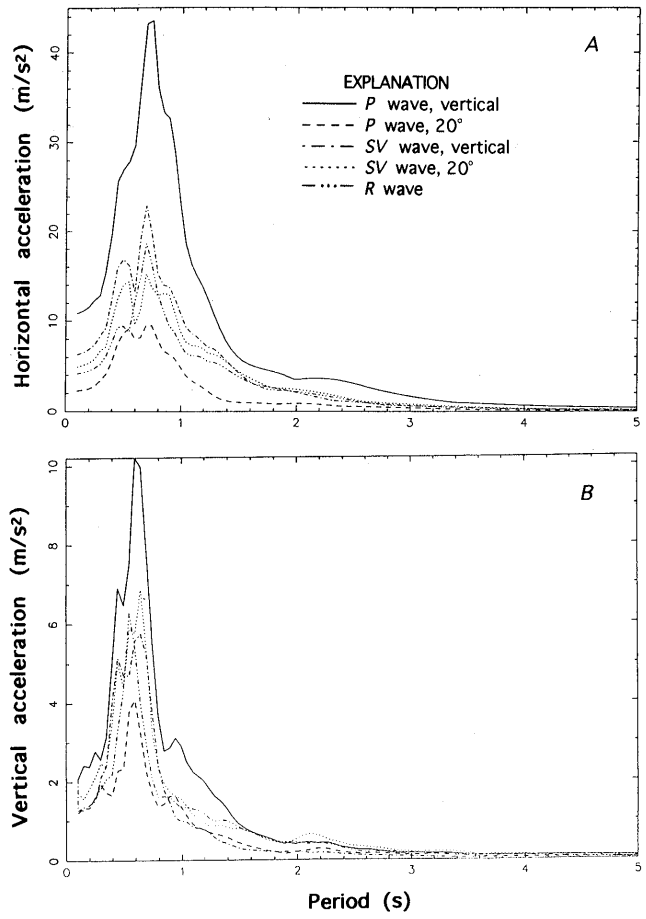


Figure 44.—Response spectra of horizontal (*A*) and vertical (*B*) components of ground motion at borehole M4 (fig. 4), as predicted by linear analyses for different types of waves on scaled Yerba Buena Island accelerogram (peak acceleration, 0.15 *g*).

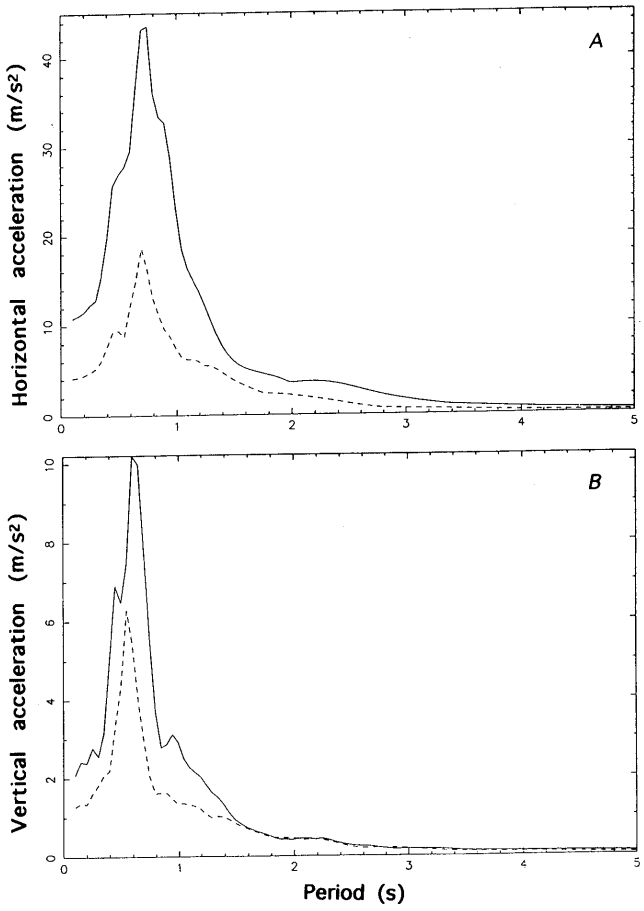


Figure 45.—Response spectra of horizontal (*A*) and vertical (*B*) components of ground motion at borehole M4 (fig. 4), as predicted by linear analyses for *P* waves traveling at 20° (solid curves) and −20° (dashed curves).

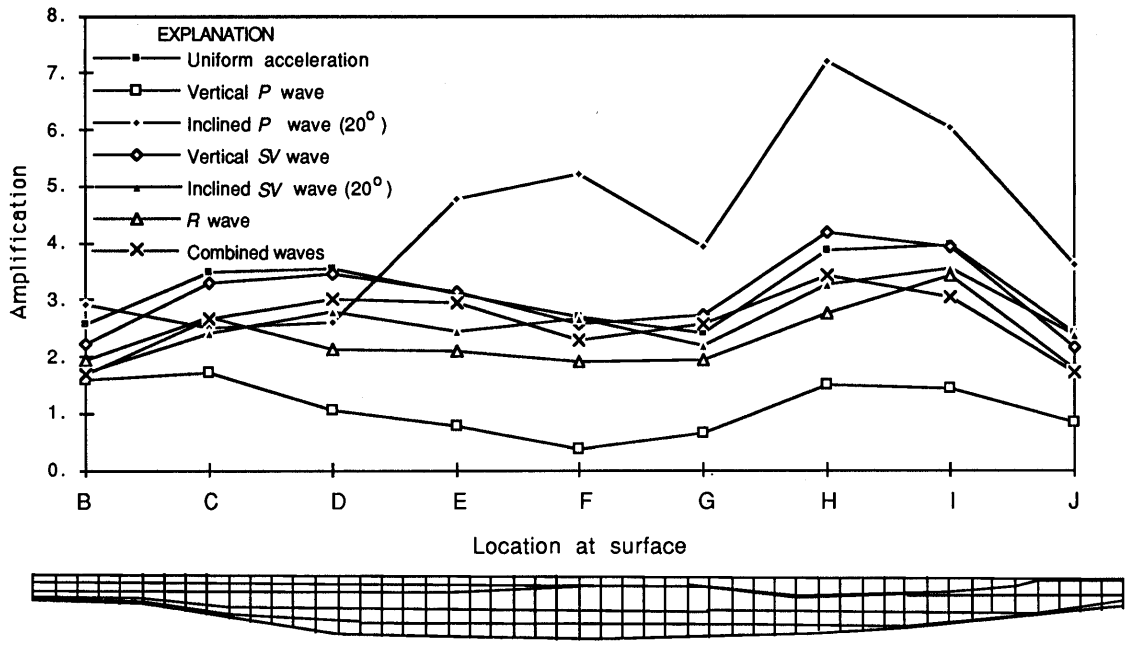


Figure 46.—Amplification of horizontal component of ground motion along surface of two-dimensional model (fig. 25), as predicted by linear analyses for different types of waves. Letters refer to groups of boundary nodes in figure 37.

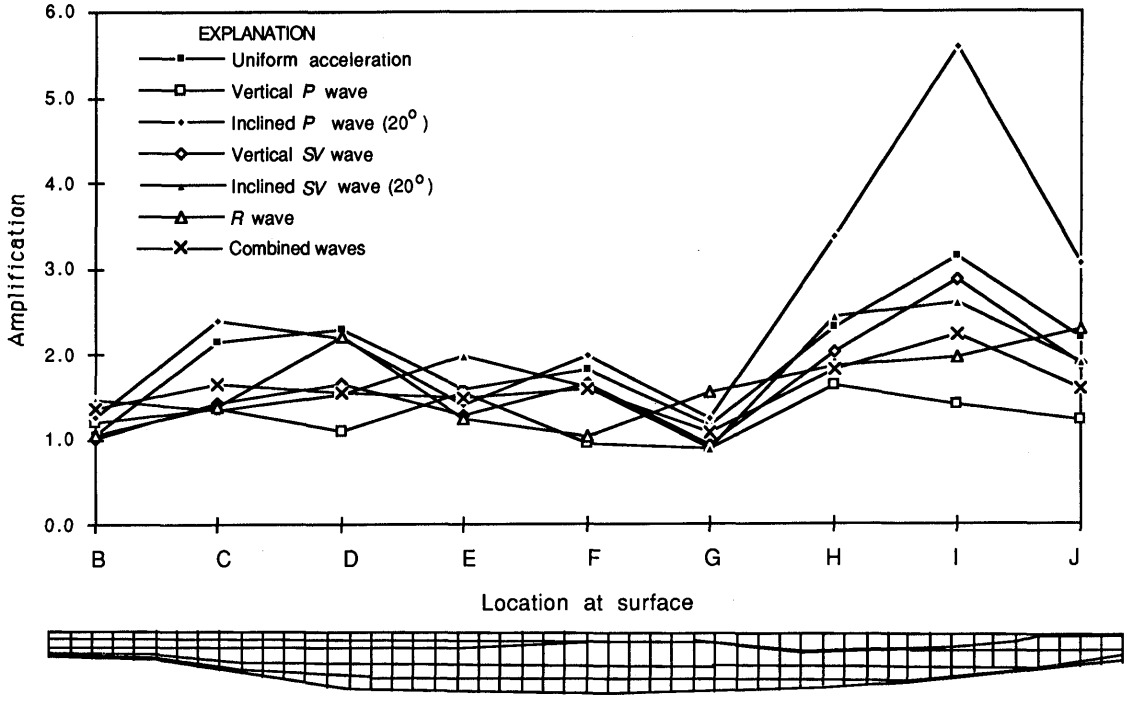


Figure 47.—Amplification of vertical component of ground motion along surface of two-dimensional model (fig. 25), as predicted by linear analyses for different types of waves. Letters refer to groups of boundary nodes in figure 37.

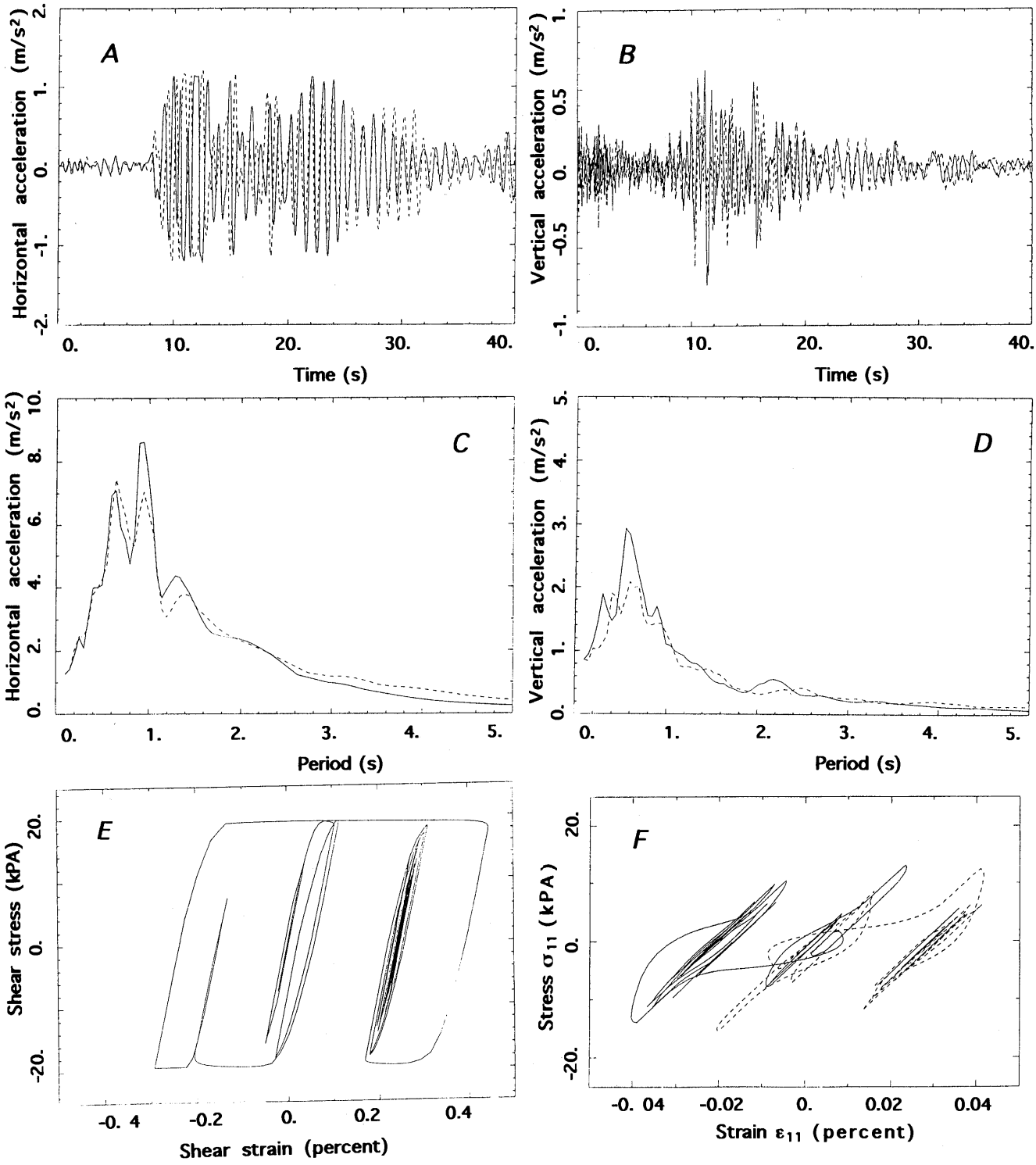


Figure 48.—Acceleration-time history of horizontal (*A*) and vertical (*B*) components of ground motion, with corresponding response spectra (C, *D*), at borehole M4 (fig. 4), and stress-strain relation (*E*, *F*) at 9-m depth, as predicted by two-dimensional nonlinear analyses for *SV* waves inclined at 20° (solid curves) and uniform acceleration (dashed curves) on scaled Yerba Buena Island accelerogram (peak acceleration, 0.15 *g*).

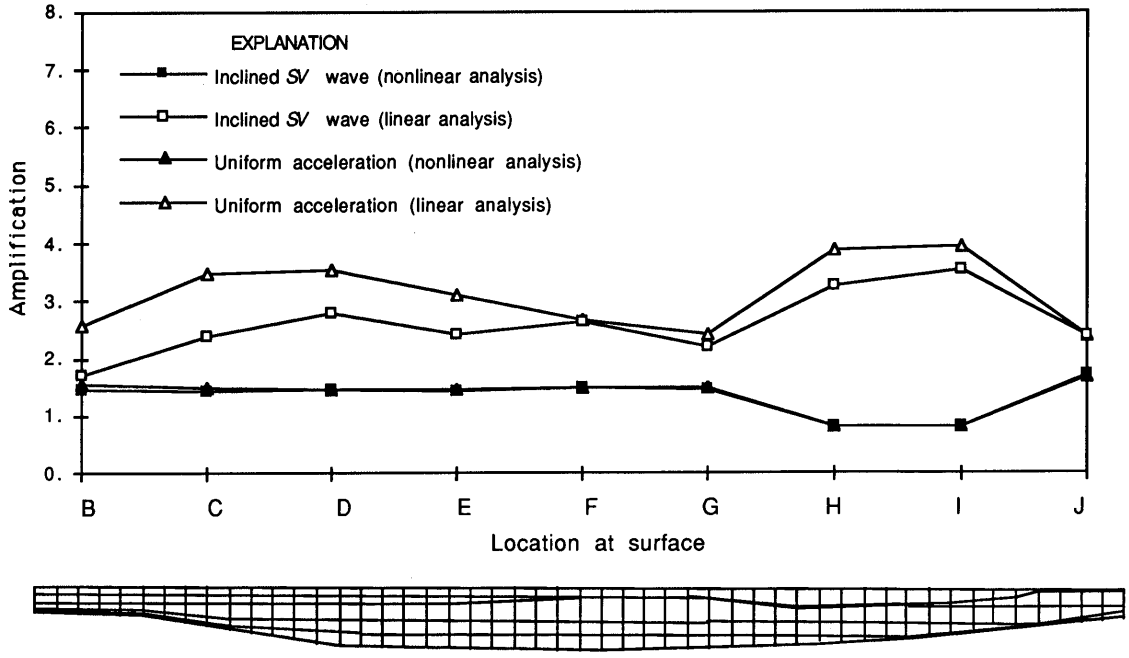


Figure 49.—Amplification of horizontal component of ground motion along surface of two-dimensional model (fig. 25), as predicted by two-dimensional nonlinear analyses with wave-propagation effects included for scaled Yerba Buena Island accelerogram (peak acceleration, 0.15 *g*). Letters refer to groups of boundary nodes in figure 37.

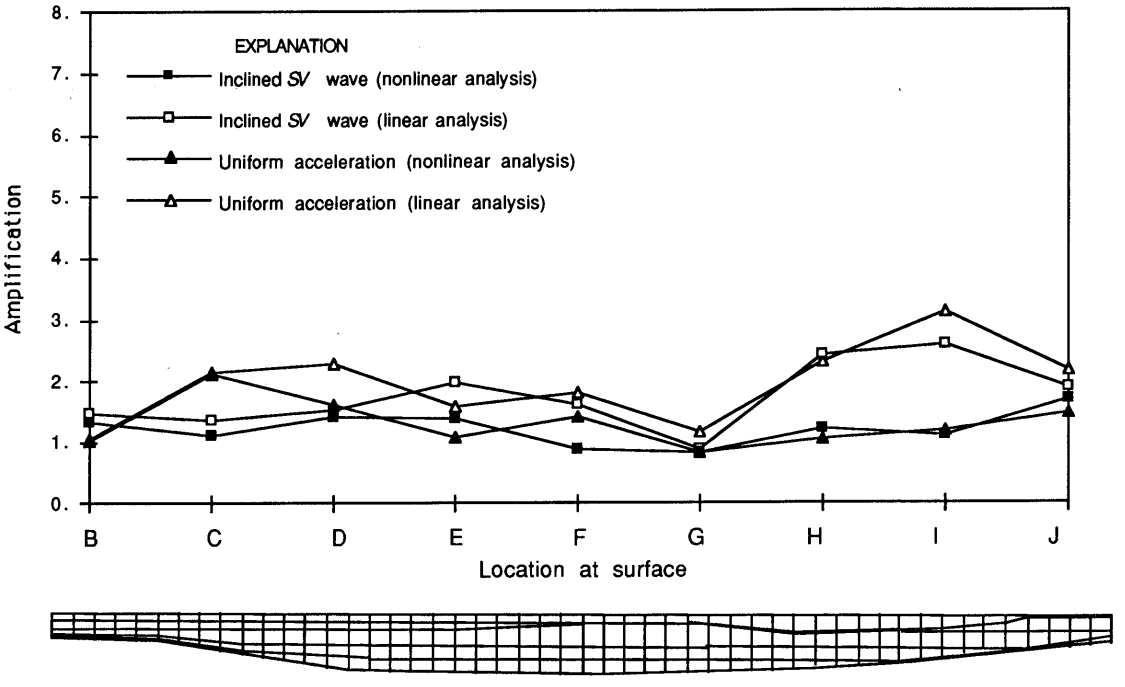


Figure 50.—Amplification of vertical component of ground motion along surface of two-dimensional model (fig. 25), as predicted by two-dimensional nonlinear analyses with wave-propagation effects included for scaled Yerba Buena Island accelerogram (peak acceleration, 0.15 *g*). Letters refer to groups of boundary nodes in figure 37.

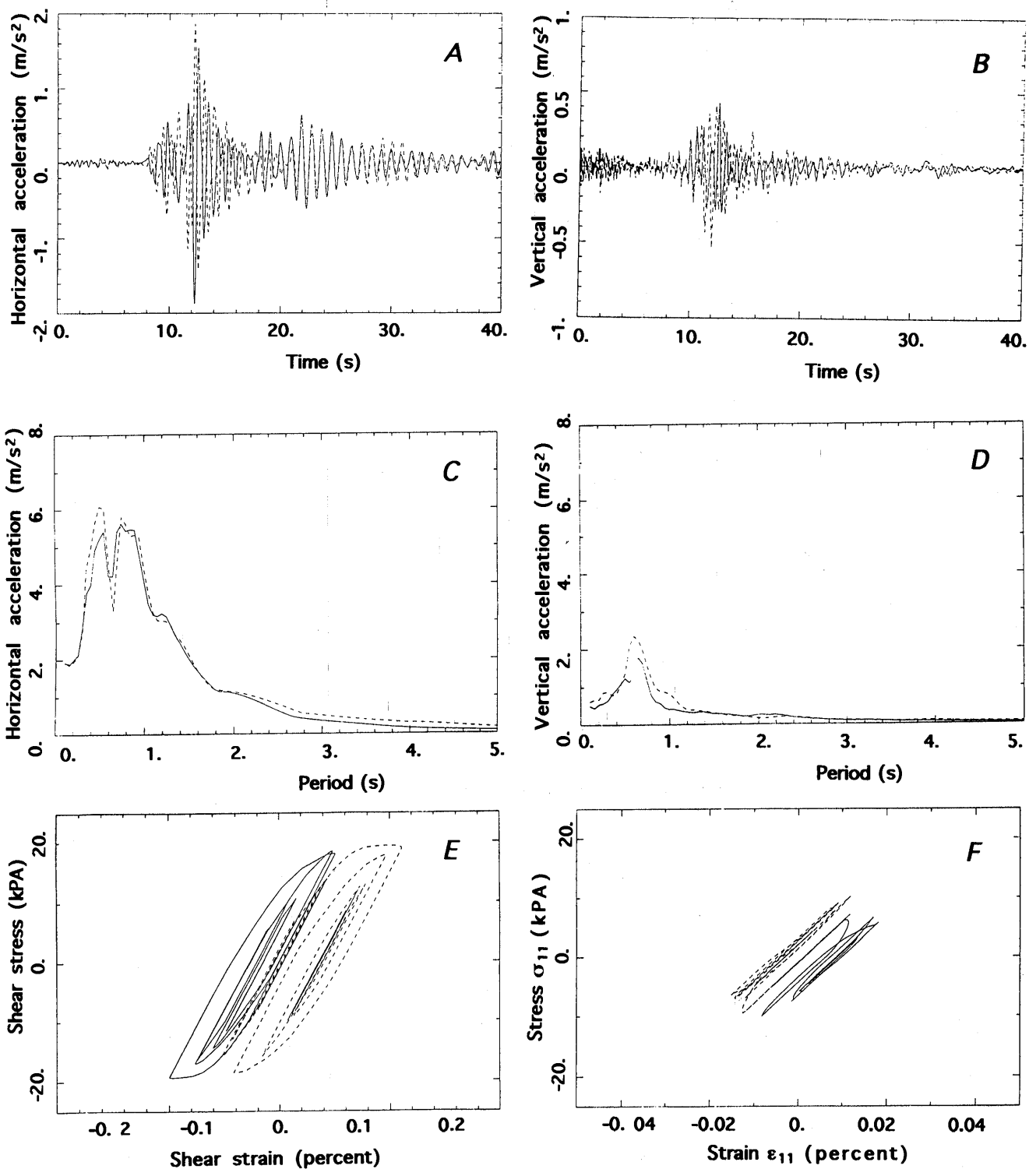


Figure 51.—Acceleration-time history of horizontal (*A*) and vertical (*B*) components of ground motion, with corresponding response spectra (*C*, *D*), at borehole M4 (fig. 4), and stress-strain relation (*E*, *F*) at 9-m depth, as predicted by two-dimensional nonlinear analyses for *SV* waves inclined at 20° (solid curves) and uniform acceleration (dashed curves) on original Yerba Buena Island accelerogram (peak acceleration, 0.067 *g*).

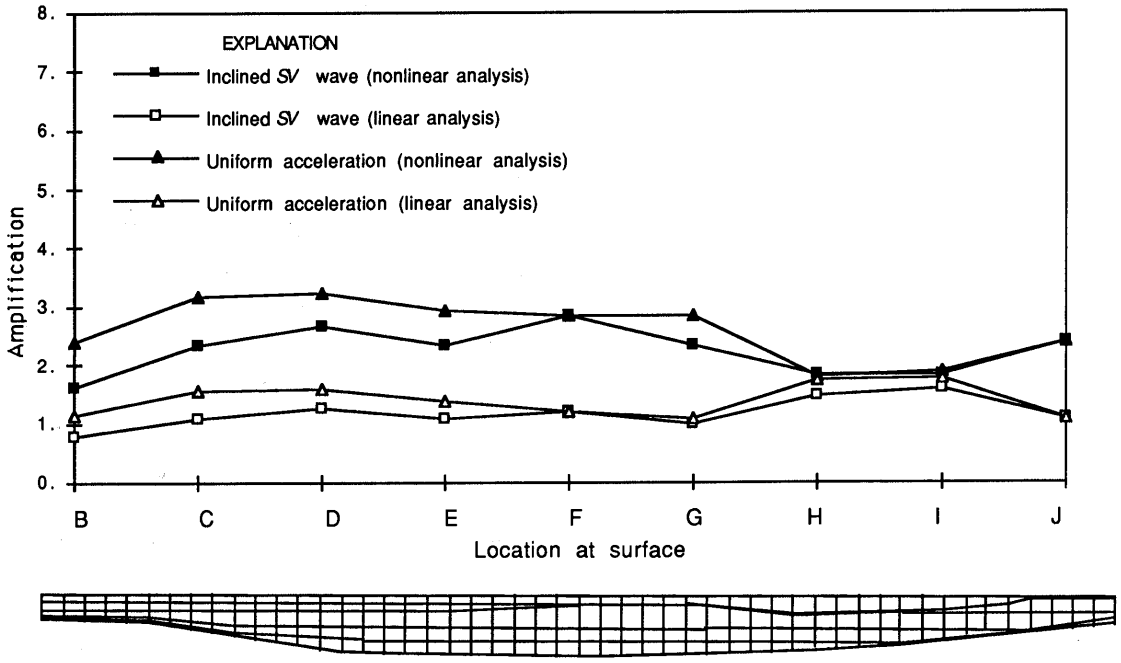


Figure 52.—Amplification of horizontal component of ground motion along surface of two-dimensional model (fig. 25), as predicted by two-dimensional nonlinear analyses with wave-propagation effects included for original Yerba Buena Island accelerogram (peak acceleration, 0.067 *g*). Letters refer to groups of boundary nodes in figure 37.

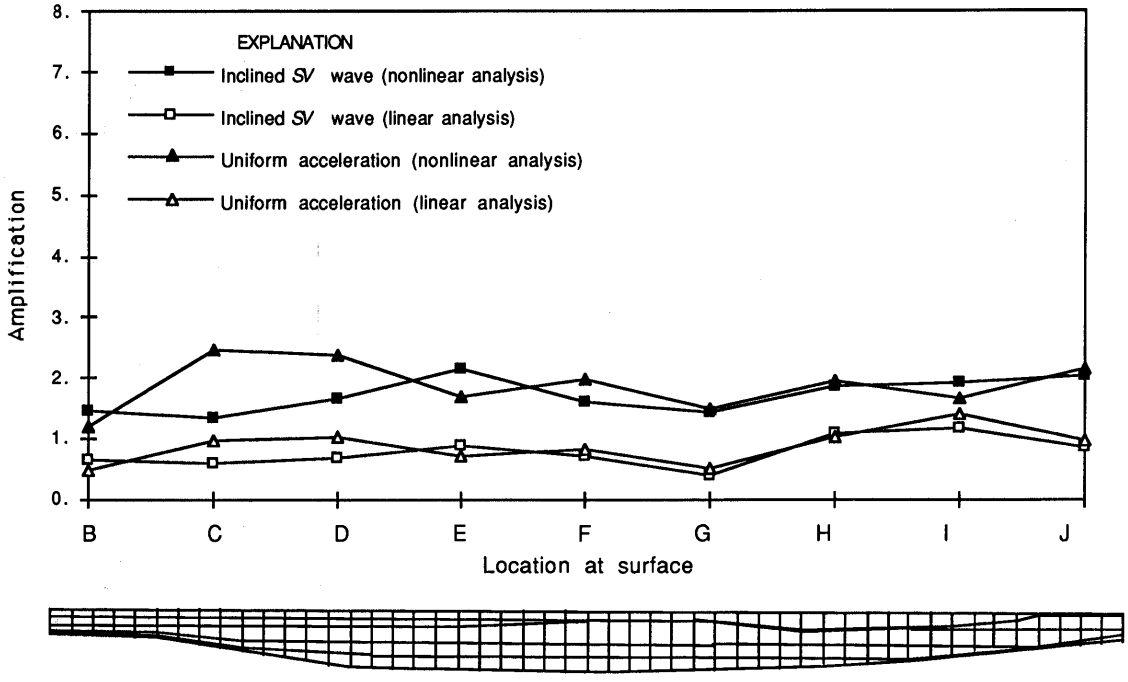


Figure 53.—Amplification of vertical component of ground motion along surface of two-dimensional model (fig. 25), as predicted by two-dimensional nonlinear analyses with wave-propagation effects included for original Yerba Buena Island accelerogram (peak acceleration, 0.067 *g*). Letters refer to groups of boundary nodes in figure 37.

MARINA DISTRICT

# BEHAVIOR OF THE SEAWALLS AND SHORELINE DURING THE EARTHQUAKE

By H.T. Taylor, J.T. Cameron, S. Vahdani, and H. Yap,
Harding Lawson Associates

## CONTENTS



ABSTRACT

Deformations resulting from the earthquake occurred in the seawalls that surround the St. Francis Yacht Club Harbor, in the seawall north of the St. Francis Yacht Club along the shore of San Francisco Bay, and in the seawall north of the Marina Green. Although the deformations were as great as 2 ft, damage to the walls was relatively light. This report describes the subsurface conditions, including the history of filling this reclaimed land; records the approximate deformations; and estimates the magnitude of ground shaking. The study area is north of Marina Boulevard, east of the Presidio, and includes Fort Mason.

## INTRODUCTION

This study records the earthquake-related deformations (both settlement and lateral displacement) that were observed, reported, and measured in the area north of Marina Boulevard. The study area includes the Marina Green, Fort Mason, Gas House Cove, and the St. Francis Yacht Club Harbor (fig. 1).

We first describe the fill history and subsurface conditions; then the major structures, including Fair's seawall, the Marina Boulevard seawall, and the Marina Boulevard box sewer; and finally, the estimated ground shaking during the earthquake.

## SUBSURFACE CONDITIONS

### FILL HISTORY

Most of the present Marina District is founded on fills of various types that were constructed to provide greater land area above water.

A map by the U.S. Coast Survey dated 1851 shows a small bay, herein referred to as Marina Cove, and a tidal slough draining a marsh that extended westward from the present location of Scott Street into the Presidio. A broad area of beach sand, perhaps with some discontinuous cover of dune sand, that existed west of Marina Cove is referred to as Strawberry Island.

By 1894, a seawall known as Fair's seawall had been built along the alignment shown in figure 1. This seawall was reportedly built of rock from the San Bruno Mountain quarry (Olmstead and others, 1977); the rock was dumped from a pile-supported trestle. A narrow band of fill was placed by 1906 behind Fair's seawall; this seawall was later used to retain the hydraulic fill that formed the land for the Panama-Pacific International Exposition of 1915.

The area east of Webster Street and one arm of Fair's seawall had been filled for a gas plant before 1903. This filled area was described as "earthen fill surrounded by a rock retaining wall." A pile-supported bulkhead and transport docks were constructed at Fort Mason in 1910; the area behind this bulkhead was filled with sand. In 1962, the Gashouse Cove Yacht Harbor was created, and a driven concrete-sheet-pile wave barrier was installed.

A small boat harbor was created by the Fulton Shipbuilding Works in the area of St. Francis Spit before 1900. This harbor was utilized during the 1915 exposition;

the California Building was supported on fill that occupied the west end of what is now the St. Francis Yacht Club Harbor. After the San Francisco Port Commissioners acquired these properties, the yacht harbor was improved about 1920; improvements included dredging the fill that had formerly supported the California Building. The original St. Francis Yacht Club building was constructed on a pier about 1928 and was accessible by a road. The filling of this spit area continued during the 1930's, and a wall was built in 1935 by the Works Progress Administration. In 1958, the yacht-harbor entrance was moved from the north side to the east side, and the spit was further extended. Repairs and maintenance were performed on the seawalls surrounding the yacht harbor during the period from 1952 through the 1980's. There is no evidence that the existing seawalls on either side of the spit are pile supported.

## SITE CONDITIONS

The ground surface in the Marina District slopes downward very gently toward the bay, at an average grade of about 0.4 percent.

The soil profile along Divisadero Street (fig. 2) shows that (1) the fill thickness is 20 to 30 ft and (2) the bay mud is as much as 80 ft thick near Marina Boulevard. However, bay mud was not present in the boreholes drilled near the St. Francis Yacht Club, where the subsurface consists of about 20 ft of medium-dense sand fill, 20 ft of medium-dense beach sand underlain by loose to medium-dense silty sand to a depth of 80 ft, and dense silty sand to a depth of 90 ft. The ground-water level is approximately 8 ft below the ground surface.

The subsurface beneath Fort Mason (fig. 1) consists of 0 to 35 ft of loose to medium-dense sandy fill containing a few silt and clay zones. Below the sandy fill is 0 to 10 ft of bay mud consisting of soft to medium-stiff silt and clay. This bay mud is underlain by medium-dense to dense sand and silty sand that extends to bedrock at a depth of about 100 ft. The hydraulically placed sand fill is generally fine grained, with a mean grain size of 0.15 to 0.20 mm (Bennett, 1990). It is generally loose to medium dense, with blow counts generally less than 10 (O'Rourke and others, 1990a) and a fines content of 3 to 21 percent[1] (Bennett,

[1]Borehole data indicate that the fines content is a high as 35 percent.

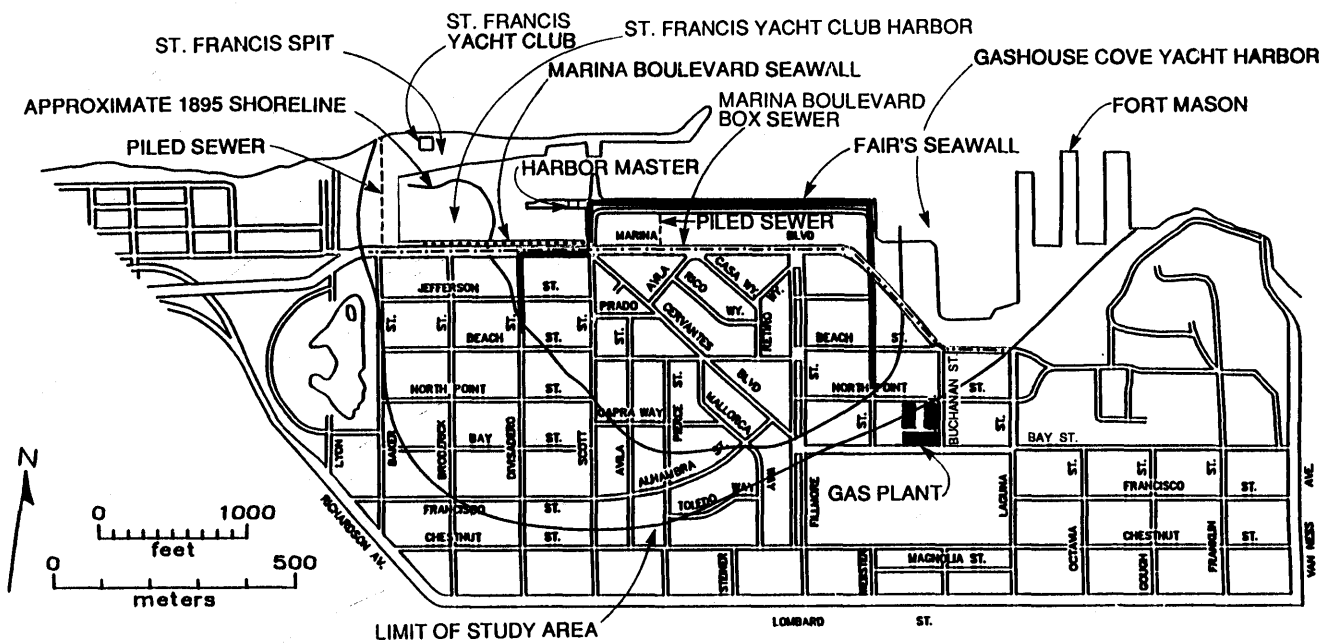


Base from U.S. Geological Survey San Francisco North 7.5' quadrangle, photorevised in 1973

EXPLANATION

Approximate Alignment of Fair's Seawall

Approximate Alignment of Marina Boulevard Seawall

Approximate Alignment of Marina Boulevard Box Sewer

Figure 1.—Marina District of San Francisco, showing locations of features referred to in text. Base from U.S. Geological Survey (1990).

1990). The bay mud is generally soft to medium stiff and is normally consolidated (O'Rourke and others, 1990b); the old bay clay underlying the bay mud is generally stiff to very stiff.

The slopes along the shoreline typically range from 3:1 to 6:1 (horizontal to vertical).

## FAIR'S SEAWALL

Olmstead and others (1977) described the construction of Fair's seawall (fig. 1), which was built about 1894 by James G. Fair to fill approximately 15 blocks of tidelands and 21 blocks of shoreline property for commercial and industrial development. The seawall (of undocumented height) was built of rock that was brought to the site in cars on barges from the San Bruno Mountain quarry. The cars were unloaded from the barges by hoisting engines onto a pile-supported trestle constructed approximately parallel to the proposed alignment of the seawall. The rock was then dumped from the cars at various points along the alignment, to construct the seawall. A masonry seawall was built on top of Fair's seawall in 1935.

## MARINA BOULEVARD SEAWALL

The Marina Boulevard seawall (fig. 1) was built between 1933 and 1934 through collaborative efforts of the San Francisco Board of Supervisors and the State Emergency Relief Administration. The Marina Boulevard seawall is a cantilever concrete wall with basalt block facing supported by wood piles. This seawall is about 30 ft north of the Marina Boulevard box sewer. The seawall is 5 ft wide at the base and approximately 9.5 ft high.

## MARINA BOULEVARD BOX SEWER

The Marina Boulevard box sewer (fig. 1) is part of the Northshore Outfalls Consolidation Project, a high-capacity, gravity-flow, consolidating sewer designed to collect the dry- and wet-weather flows from all existing outfall sewers in the northshore area. The box sewer runs along the northern curbline. It was constructed in the late 1970's by open-cut techniques, and the excavation was temporarily shored by sheet piles, which we understand were removed at the end of construction.

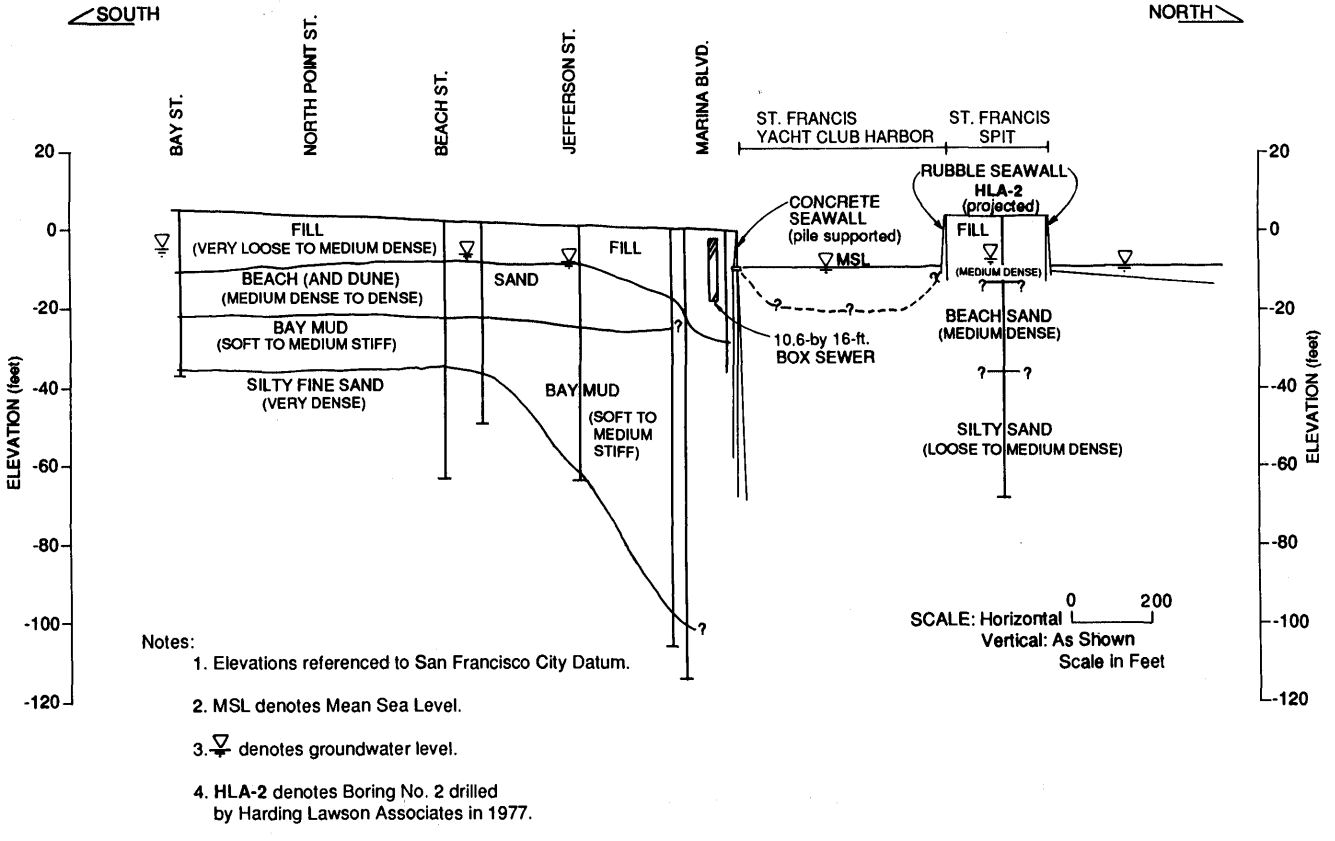


Figure 2.—Subsurface profile along Divisadero Street.

The top of the box sewer is approximately 2 ft below the ground surface. The dimensions of the box sewer increase from west to east, from approximately 11 ft wide by 12 ft high at Baker Street to approximately 21 ft wide by 23 ft high at Buchanan Street. The box sewer is underlain by a 1-ft-thick layer of drain rock, and the 1-ft-wide space between the sheet pile and its sides was also filled with drain rock. The drain-rock backfill was intended to reduce any uplift pressure that may develop below the box sewer, should the underlying fills liquefy during a major earthquake.

## DEFORMATION OF THE MARINA SHORELINE

### SETTLEMENT

Ground-surface settlement of the Marina shoreline resulting from the earthquake was determined by comparing a November 1987 topographic map (1:600 scale) of the San Francisco Marina with surveying information obtained between October and December 1990. Although some minor consolidation settlement may have occurred within this period, we can reasonably assume that any differences in elevation between these two surveys indicate the amount of settlement caused by the earthquake.

The approximate amounts of settlement along the shoreline between the two surveys are shown in figures 3 and 4. From 0.5 to almost 2 ft of settlement seems to have occurred in the vicinity of the St. Francis Yacht Club. On the basis of information obtained from the contractors who repaired the St. Francis Yacht Club, the maximum settlement of the ground at the yacht club was 0.5 to 1.0 ft. The pile-supported building, however, settled less than 1 in. In addition, visual inspection of those areas where large settlement is indicated does not appear to correlate with these high values. We cannot explain the discrepancies between the observed and calculated amounts of settlement in the vicinity of the St. Francis Yacht Club.

From 0.5 to 0.7 ft of settlement occurred along the sidewalk immediately north of Marina Boulevard between Baker and Scott Streets. This amount of settlement appears to be consistent with that reported by Bennett (1990) for settlements measured along the south side of Marina Boulevard.

The survey information indicates that 1 to 2 ft of settlement occurred in the vicinity of the Harbor Master building near the north end of Scott Street (fig. 1). The pavement surface slumped approximately 0.6 to 1.0 ft immediately north of a buried concrete box culvert near the bayward tip of Scott Street. In addition, it appears that approximately 1 ft of slumping occurred at the south edge of the pavement surface in the seawall that runs east-west immediately south of the Harbor Master building. The seawalls and the Harbor Master building itself appear to have undergone little or no differential settlement. As with the relatively large amounts of settlement calculated near the St. Francis Yacht Club, those calculated near the Harbor Master building do not appear consistent with visual inspection.

Approximately 0.5 to 1 ft of settlement occurred at the northeast corner of the Marina shoreline (fig. 4). The calculated settlements in this part of the Marina District are consistent with estimates made by visual inspection.

Measurements near the outfall location of the pile-supported sewerline that is aligned with the projection of Pierce Street (fig. 1) indicate that approximately 6 to 8 in. of differential settlement occurred between the sewer and the surrounding soils. Figure 4 does not include settlements calculated for this area because it was not included in the 1990 survey. Similar measurements at the outfall location of the pile-supported sewerline that exits near the west edge of the St. Francis Yacht Club indicate approximately 0.8 ft of differential settlement between the sewer and the surrounding soil surface (fig. 5). These measurements are consistent with the amount of settlement indicated by comparison of the survey data obtained in 1987 and 1990.

Fort Mason (fig. 1), immediately east of the Marina Green, is composed of a combination of three pile-supported piers and five adjacent pile-supported buildings with slab-on-grade floors. Each of the buildings is 200 to 370 ft long by 50 ft wide and oriented lengthwise in a north-south direction. Four of the five buildings have perimeter loading docks supported on shallow footings that extend 3 to 5 ft away from the building face. The loading docks range from 1.5 to 3.5 ft in height, with a concrete slab-on-grade at the dock surface. As a result of the earthquake, the loading docks settled differentially with respect to the buildings by as much as 0.6 ft. Similar amounts of differential settlement occurred between the floor slabs and the building walls inside the buildings. The greater amount of settlement occurred at the north end of the buildings, where the underlying fill and bay mud are thickest. In addition to settling of the loading docks, the buildings also underwent separation of exterior metal stairways from the tops of the loading dock and some separation of utility lines that were connected to the outside of the buildings. There were no noticeable signs of differential movement between the base of the loading docks and the adjacent pavement; they appear to have settled together.

### LATERAL SPREADING

The 1987 topographic map, which was obtained by aerial photography before the earthquake, is not sufficiently accurate to measure the lateral movements that occurred as a result of the earthquake. Therefore, lateral spreading

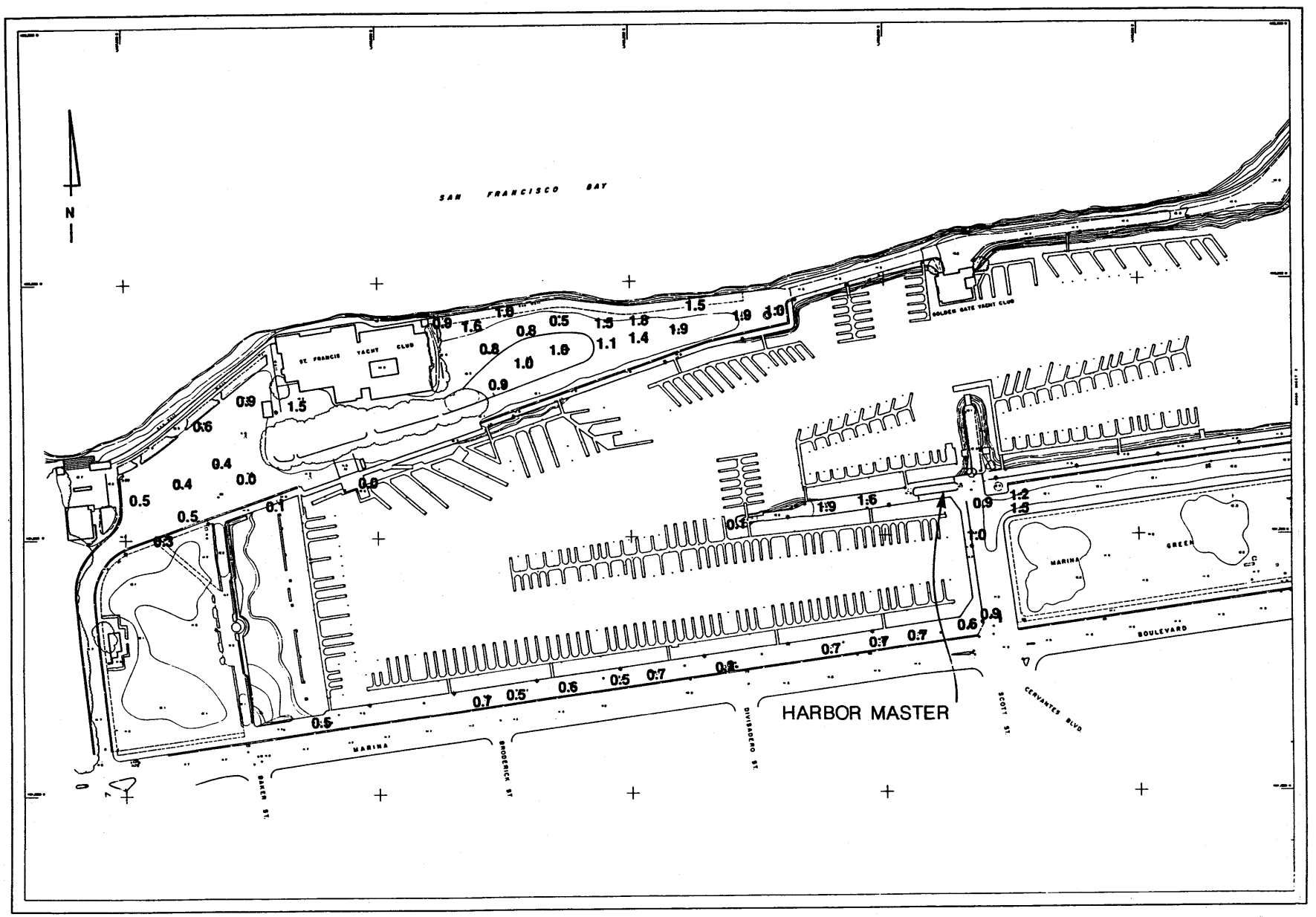


Figure 3.—Computed settlements of west side of Marina shoreline (in feet) between November 1987 and December 1989 surveys.

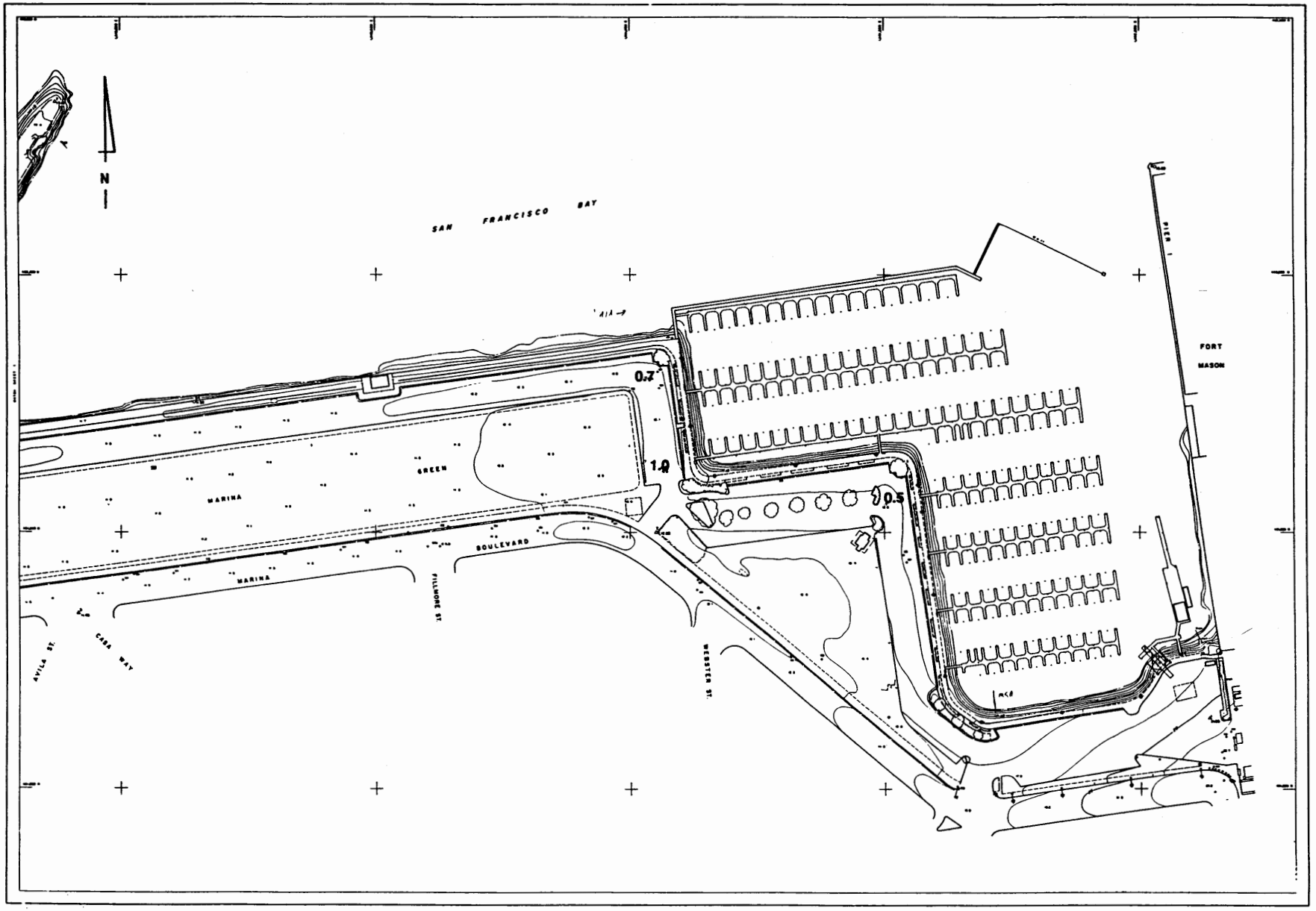


Figure 4.—Computed settlements of east side of Marina shoreline (in feet) between November 1987 and December 1989 surveys.

was determined by visual inspection or by discussing movements with knowledgeable people present immediately after the earthquake. The greatest apparent lateral spreading was in the parking area and seawall west of the St. Francis Yacht Club (fig. 6). Summing up the cracks in the pavement indicates a movement of approximately 2 ft between San Francisco Bay to the north and the San Francisco Yacht Club Harbor to the south, whereas the separations in the masonry landscape wall perpendicular to the shore and west of the St. Francis Yacht Club indicate a total displacement of about 1 ft (fig. 7). Lateral movements of the seawall and parking area east of the St. Francis Yacht Club appeared to be somewhat smaller. Deformation in the seawalls directly north and south of

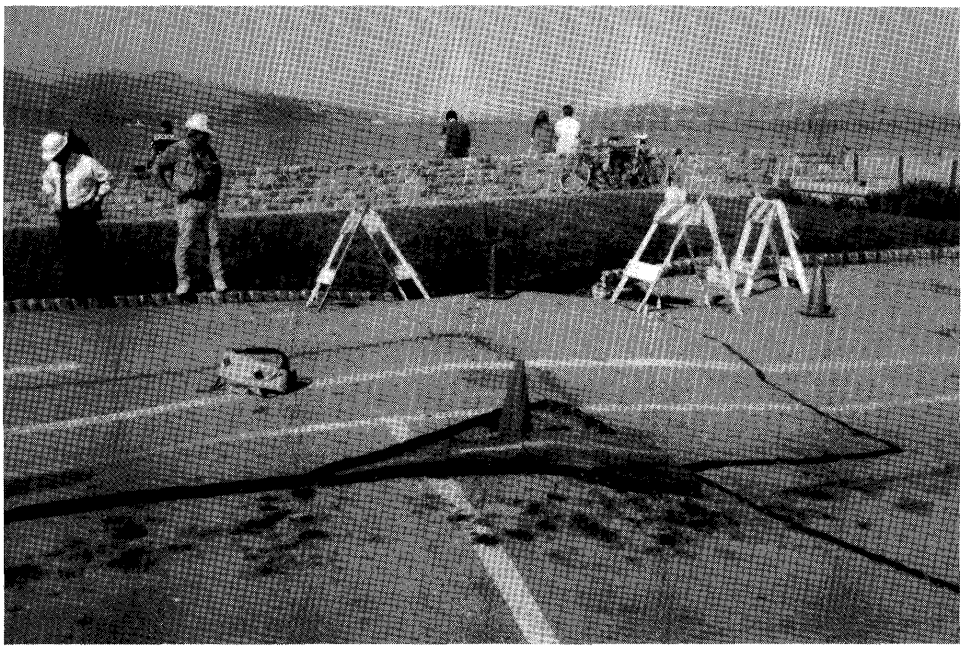

Figure 5.—Storm sewer outlet immediately west of the St. Francis Yacht Club. Photograph taken in October 1989.

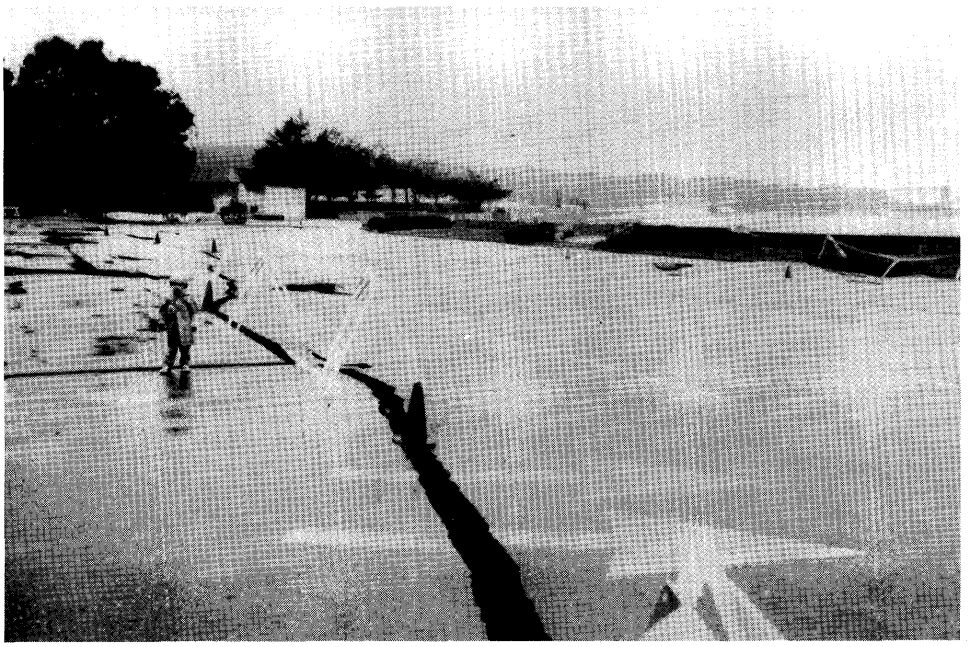

Figure 6.—Cracks in asphalt pavement southwest of the St. Francis Yacht Club. Photograph taken in October 1989.

the St. Francis Yacht Club is discussed in the next section. No evidence exists that any of the seawalls are supported on pilings instead of on spread footings on sand fill. The cobblestone seawall located at the west end of the St. Francis Yacht Club Harbor was considerably damaged, owing to both lateral movement and settlement (fig. 8). The pile-supported seawall located along the south side of the St. Francis Yacht Club Harbor just north of Marina Boulevard showed no evidence of any significant horizontal movement. The masonry seawall along San Francisco Bay just north of the Marina Green is believed to be supported on spread-footing foundations on top of Fair's seawall. This masonry seawall showed no evidence of uneven lateral movement or settlement (fig. 9), but there was a crack a few inches wide parallel to, and about 30 to 50 ft behind, the seawall. There was no evidence of lateral

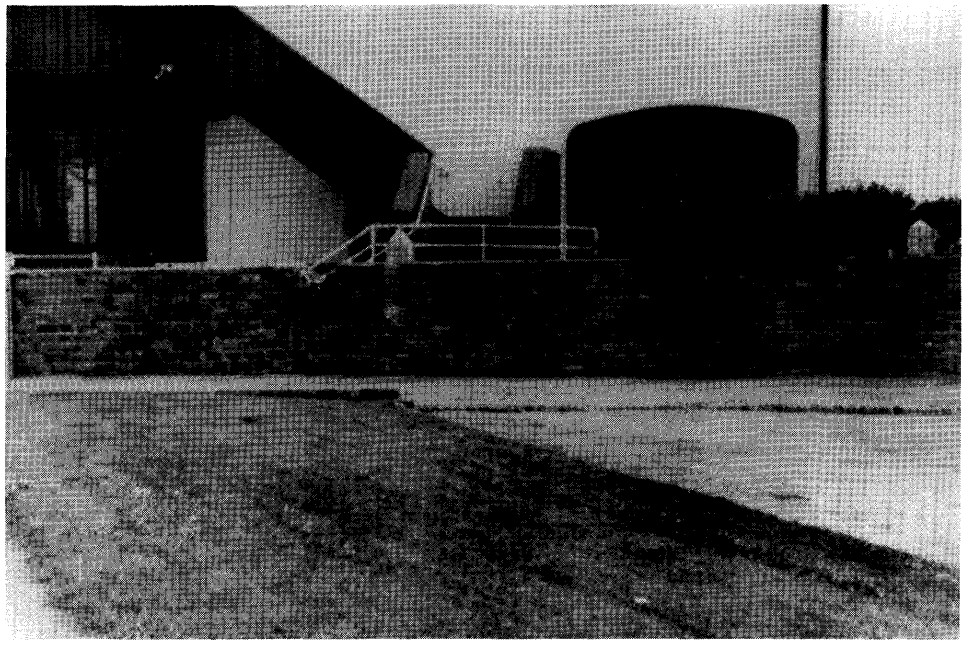

Figure 7.—Earthquake-caused cracks in masonry wall on west side of the St. Francis Yacht Club. Photograph taken in 1991.

Figure 8.—Seawall at west end of the St. Francis Yacht Club Harbor. Photograph taken in 1991.

movement of the seawalls around Gashouse Cove or in the Fort Mason area.

## ST. FRANCIS YACHT CLUB

Because most of the St. Francis Yacht Club building is a relatively new structure supported on long concrete pilings, it is a reference point for judging both lateral spreading and vertical settlement. Observed movements are mapped in figure 10 and detailed below:

*Location (fig. 10)* — *Comments*

A ----- Paved parking lot (fig. 6). Horizontal movement toward San Francisco Bay, about 2 ft; vertical settlement, generally less than 1 ft.

B------ Masonry wall separated into 12 segments, 8 to 12 ft long, with gaps of as much as 2 in; total of gaps, about 12 in. (fig. 7).

C------ Open deck supported on wood piles reportedly less than 60 ft long moved northward away from west wing 3 in. and settled about 8 in.

D ----- Open deck supported on wood piles moved northward 12 in. and settled about 8 in. sloping down toward north. Upper 2 ft of piles under east wing visible, with slight lean toward north. Soil craters around piles (fig. 11).

E------ Concrete-block wall on spread footings settled and shifted toward San Francisco Bay (fig. 12).

F------ Parking lot and seawall settled and shifted toward San Francisco Bay (fig. 13).

G------ West wing built in 1977 after original building was destroyed by fire. New 16-in.-square prestressed piles 85 to 90 ft long were driven. Floor slab was poured on top of old wood-pile-supported deck, leaving about 2 ft of clearspace above ground surface. Moderate damage to utilities supported on ground. Building within 1 in. of level but estimated to have shifted northward 2 to 4 in.

H------ East wing built in 1985 on 90-ft-long, 16-in.-square prestressed piles, including courtyard. No visible signs of movement in building but extensive damage to underground utilities. Utilities were embedded in fill, which had been used as a form to pour floor slab. Underground tunnels dug to repair utilities. About 6 in. of settlement observed in ground surface, and pipes displaced that same amount (fig. 14).

I ------ South wing built in 1929 and survived 1977 fire, so it was not rebuilt; was either supported on short wood piles or on spread footings. Settled 6 to 12 in. with structural damage. A 4-in. gap between south wing and 1977 west wing caused by lateral spreading. Demolished; new two-story building built on new 90-ft-long, 16-in.-square prestressed piles.

J ------ Slabs on ground settled about 4 in. more than adjacent building and moved southward from building 4 to 6 in.

K------ Soil adjacent to pile-supported entrance slab indicated 6 to 8 in. of vertical and lateral movement.

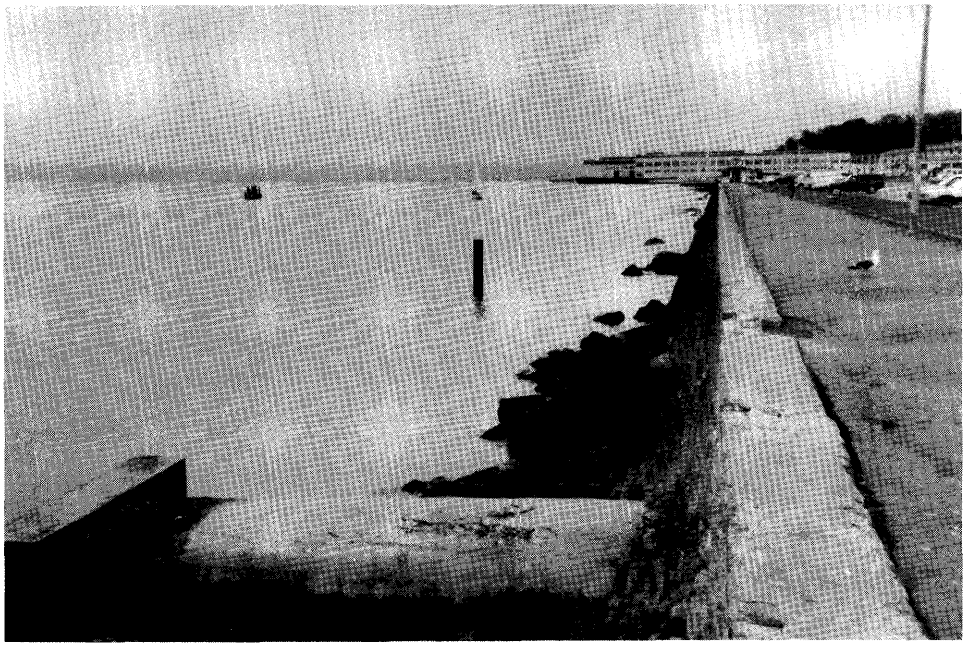

Figure 9.—Masonry wall above Fair's seawall. Note storm-sewer outfall in foreground. Photograph taken in 1991.

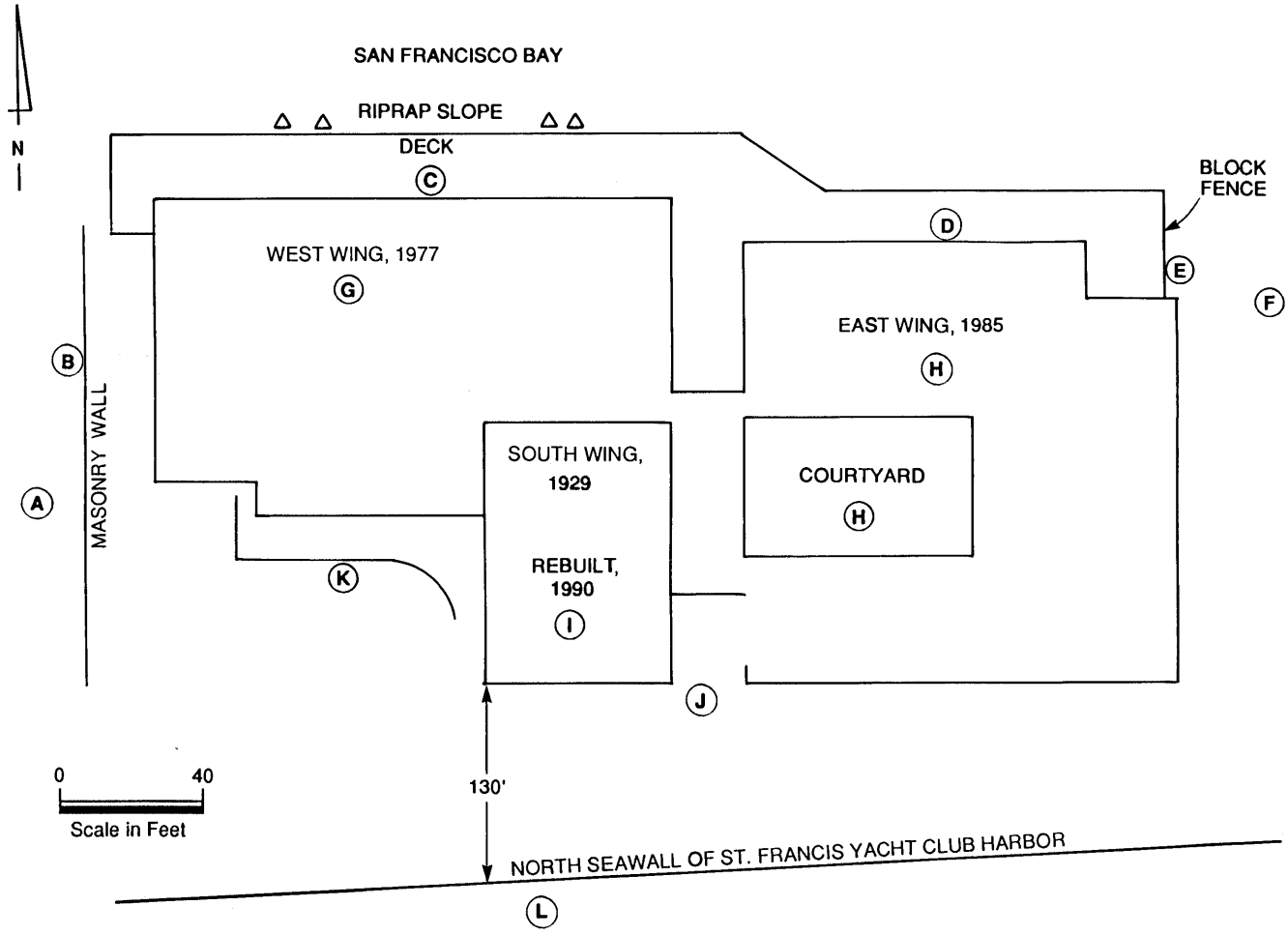


Figure 10.—Sketch plan of the St. Francis Yacht Club. Letters denote locations referred to in text.

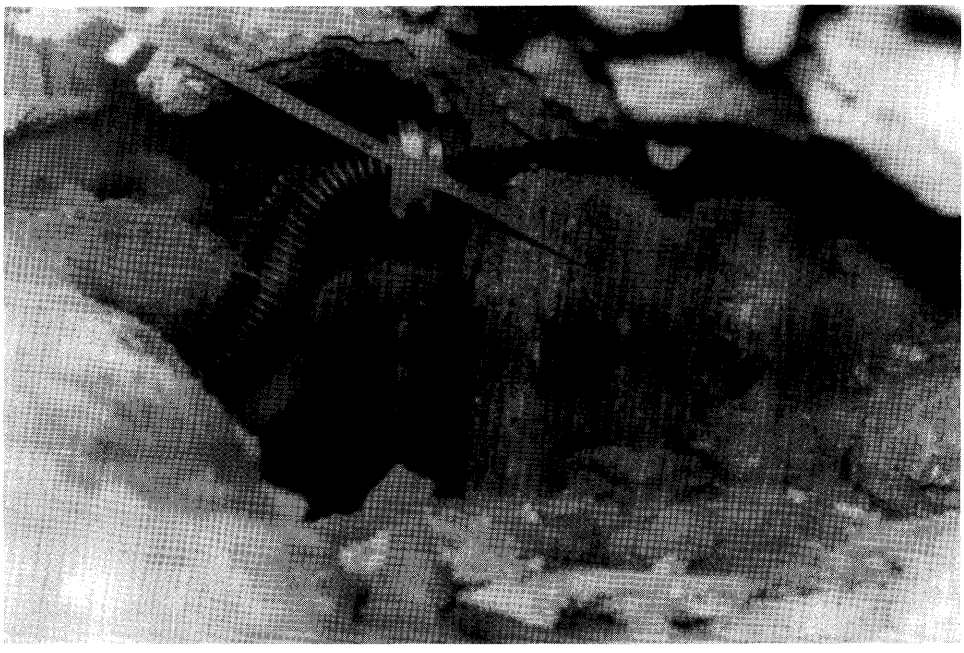

Figure 11.—Approximate 8-in. gap between concrete pile and adjacent soil caused by ground settlement below the St. Francis Yacht Club. Photograph taken in October 1989.

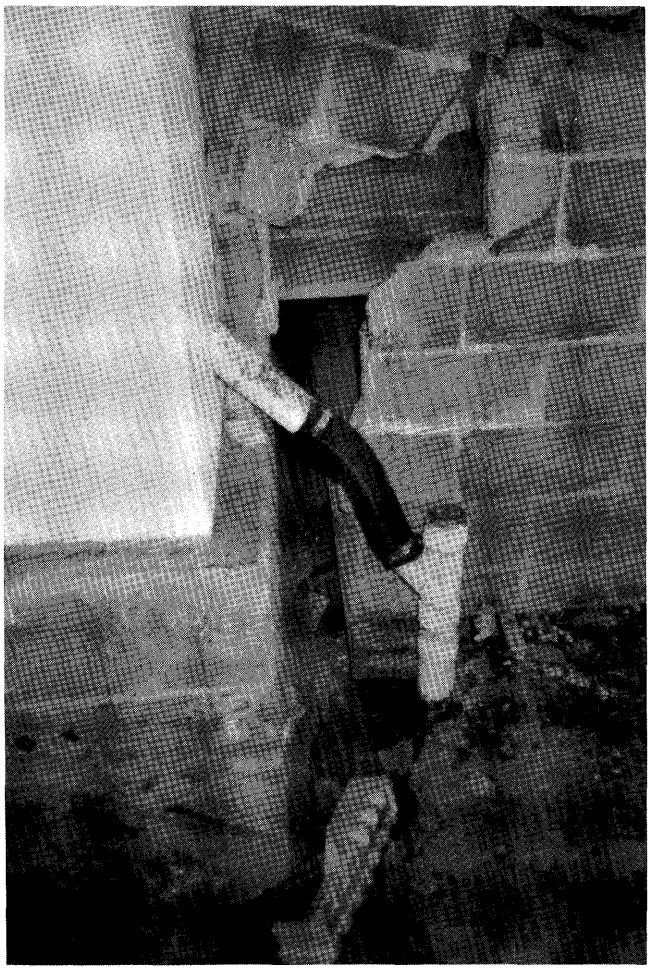

Figure 12.—Separation between concrete-block wall and east building wall of the St. Francis Yacht Club. View westward; photograph taken in October 1989.

L ------ Yacht-harbor edge about 130 ft south of St. Francis Yacht Club is masonry wall, not pile supported, and is at top of riprapped 4:1 (horizontal to vertical) slope about 15 ft high. No visible cracking or displacement of masonry wall. Short wood piles that support hoist platform and guide floats leaned toward south. Piles under hoist also settled a few inches.

## SEISMIC GROUND SHAKING

Because there were no accelerographs in the Marina District at the time of the main shock, recorded motions are not available for the area. The extensive building damage and ground failure in the Marina District suggest a significant amplification of bedrock motion in that area relative to such nearby undamaged areas as Pacific Heights or Russian Hill. Because of the collapse and widespread structural damage to buildings in the Marina District, and because some of these structures were severely damaged with no apparent evidence of ground failure, a modified Mercalli intensity of IX has been assigned to this area (Benuska, 1990)

The closest accelerograph that recorded the main shock was located at a fire station in Pacific Heights, approximately 1.5 km south of the Marina District. The recorded motions at this station and on Telegraph Hill, about 2 km east of the Marina District indicate that the average of the two horizontal components of peak bedrock acceleration in the Marina District was about 0.07 *g*. The frequency content of average bedrock motions recorded in the San Francisco Bay area, including those recorded at Pacific

Figure 13.—Parking-lot deformation east of the St. Francis Yacht Club. Photograph taken in 1991.

Heights and on Telegraph Hill, indicate that bedrock motion had significant energy in the period range 0.25–1.0 s (Office of Strong Motion Studies, 1989; Housner and Penzien, 1990). Also, recordings of aftershocks in the Marina District, including data from stations immediately south of the Marina Green, indicate that ground motions were significantly amplified (relative to bedrock sites) in the same period range (see Boatright and others, this chapter).

The subsurface along Fair's seawall (north of the Marina Green) in the Marina District consists of an average of about 25 ft of sand fill and dune sand, 55 ft of Holocene bay mud, 4 ft of dense sand (hardpan), and 180 ft of old bay clay, with estimated low-strain shear-wave velocities of 600, 550, 1,200, and 1,000 ft/s, respectively (Kayen and others, 1990; Bardet and others, 1991). The site period, estimated from a weighted-average shear-wave velocity of 870 ft/s and a depth to bedrock of 270 ft, was about 1.25 s.

On the basis of a one-dimensional wave-propagation analysis (Bardet and others, 1991; Dickenson and Seed, 1991) and the recorded motion at Treasure Island under similar soil conditions, the average of the two horizontal ground-surface accelerations during the earthquake is estimated at 0.17 *g*. At the St. Francis Yacht Club, where sand fill is underlain by natural sand, the amplification factor is estimated to be less than along Fair's seawall. Neglecting the effects of liquefaction on ground-motion parameters, the average of the two horizontal ground-surface accelerations near the St. Francis Yacht Club during the earthquake is estimated at 0.12 *g*.

## CONCLUSIONS

The hydraulically placed sand fill and loose natural-sand deposits near the shoreline of the Marina District in San Francisco underwent liquefaction during the earthquake, resulting in ground settlements and lateral spreading of as much as 2 ft. Earlier studies (John A. Blume & Associates, 1974) predicted that liquefaction could occur in the Marina District. The greatest apparent lateral spreading was in the parking area and seawall west of the St. Francis Yacht Club.

The pile-supported Marina Boulevard seawall showed no evidence of any significant lateral movement. Fair's seawall, a rock dike with a masonry seawall on top, moved a few inches.

We performed a deformation analysis of Fair's seawall, using the method of Newmark (1965), the acceleration-time history recorded on Treasure Island (with peak acceleration scaled to 0.17 *g*), and a yield acceleration of 0.05 *g* (Harding Lawson Associates and others, 1991). The results of this analysis indicate movement of Fair's seawall by about 6 in., which agrees with the observed movement.

## REFERENCES CITED

Bardet, M.K., Martin, G.R., and Proubet, J., 1991, Preliminary results of the dynamic response of the Marina District of San Francisco during the Loma Prieta earthquake: Japan-U.S. Workshop on Earthquake Resistant Design of Lifeline Facilities and Countermeasures

Figure 14.—Separated 3-in.-diameter utility line beneath the St. Francis Yacht Club. Bottom of slab-on-grade is at top. Photograph taken in 1990.

for Soil Liquefaction, 3d, San Francisco, 1990, Proceedings, p. 109–128.

Bennett, M.J., 1990, Ground deformation and liquefaction of soil in the Marina District, chap. D *of* Effects of the Loma Prieta earthquake on the Marina District, San Francisco, California: U.S. Geological Survey Open-File Report 90–253, p. D1–D36.

Benuska, Lee, ed., 1990, Loma Prieta earthquake reconnaissance report: Earthquake Spectra, v. 6, supp. 90–01, 448 p.

Dickenson, S.E., and Seed, R.B., 1991, Correlations of shear wave velocity and engineering properties for soft soil deposits in the San Francisco Bay Region: Berkeley, University of California, Earthquake Engineering Research Center Report UCB/EERC–AL/XX, 105 p.

Harding Lawson Associates, Dames & Moore, Kennedy/Jenks/Chilton, and EQE Engineering, 1991, Liquefaction study, Marina District and Sullivan Marsh area, San Francisco, California; final report prepared for San Francisco Department of Public Works: San Francisco, 144 p.

Housner, G.W., and Penzien, J., 1990, Competing against time; report of the Governor's Board of Inquiry on the 1989 Loma Prieta Earthquake: Sacramento, Calif., 264 p.

John A. Blume & Associates, 1974, San Francisco seismic safety investigation; report prepared for San Francisco Department of City Planning: San Francisco, 124 p.

Kayen, R.E., Liu, H.-P., Fumal, T.E., Westerlund, R.E., Warrick, R.E., Gibbs, J.F., and Lee, H.J., 1990, Engineering and seismic properties of the soil column at Winfield Scott School, San Francisco, chap. G *of* Effects of the Loma Prieta earthquake on the Marina District, San Francisco, California: U.S. Geological Survey Open-File Report 90–253, p. G1–G18.

Newmark, N.M., 1965, Effects of earthquakes on dams and embankments: Geotechnique, no. 2, p. 139–160.

Office of Strong Motion Studies, 1989, Plots of the processed data for the interim set of 14 records from the Santa Cruz Mountains earthquake of October 17, 1989: Sacramento, California Division of Mines and Geology, 133 p.

Olmstead, R., Olmstead, N., and Pastron, A., 1977, San Francisco Waterfront; report on historical cultural resources for the north shore and channel outfalls consolidation projects: San Francisco, Wastewater Management Program, 728 p.

O'Rourke, T.D., Gowdy, T.E., Stewart, H.E., and Peese, J.W., 1990a, Lifeline performance and ground deformations in the Marina during the 1989 Loma Prieta Earthquake: U.S.-Japan Workshop on Earthquake Resistant Design of Lifeline Facilities and Countermeasures for Soil Liquefaction, 3d, San Francisco, 1990, Proceedings, p. 129–146.

O'Rourke, T.D., Stewart, H.E., Blackburn, F.T., and Dickerman, T.S., 1990b, Geotechnical and lifeline aspects of the October 17, 1989 Loma Prieta earthquake in San Francisco: Buffalo, N.Y., National Center for Earthquake Engineering Research Technical Report 90–001.

U.S. Geological Survey, 1990, Effects of the Loma Prieta earthquake on the Marina District, San Francisco, California: Open-File Report 90–253.

THE LOMA PRIETA, CALIFORNIA, EARTHQUAKE OF OCTOBER 17, 1989:
STRONG GROUND MOTION AND GROUND FAILURE

MARINA DISTRICT

# LIFELINE PERFORMANCE AND GROUND DEFORMATION DURING THE EARTHQUAKE

By Thomas D. O'Rourke, Jonathan W. Pease, and Harry E. Stewart,
Cornell University

## CONTENTS



ABSTRACT

We describe the subsurface conditions and settlements associated with soil liquefaction in the Marina District as a result of the earthquake, and evaluate the earthquake performance of the water-supply, gas-distribution, and wastewater-conveyance systems. The response of the Municipal Water Supply System depended strongly on pipe diameter; moreover, strong correlations exist for each diameter of pipe between the repair rate per unit length of pipe and the angular distortion, a measure of the local slope of the settlement profile. The close correspondence between the settlement distribution and the pattern of damage to buried utilities emphasizes the critical role of subsurface conditions in the performance of lifeline systems.

The vertical strains inferred from surface settlements in various sandy soils agree closely with the strains predicted by means of existing simplified procedures, provided that the presence of nonliquefiable soils is accounted for properly. The postliquefaction consolidation of hydraulic fill in the Marina District apparently was influenced by layers of fine-grained sedimentary deposits. The resolution in delineating subsurface conditions with cone-penetration-test measurements is important for estimating the magnitude and extent of postliquefaction consolidation in the hydraulic fill. Hydraulic fill, because it may be interstratified with fine-grained soils, is likely to require a more detailed evaluation for assessing postliquefaction settlement than can be supplied by the widely used standard penetration test and split-spoon sampling.

## INTRODUCTION

The Marina District is a microcosm of the types of site response and damage patterns that can be sustained in the most vulnerable settings of the San Francisco Bay area. During the earthquake, the deep alluvial basin and thick deposits of Holocene bay mud underlying the Marina District amplified accelerations and altered the natural period of ground motions transmitted from bedrock to surface structures. Liquefaction of loose sandy fill led to settlement and lateral movement of the ground. Especially important was the influence of ground deformation on buried utilities. Damage to the water-distribution system in the Marina District cut off critical water resources that were needed during the outbreak of fire which followed the earthquake.

Various reports have already been written about the earthquake in the Marina District (for example, U.S. Geological Survey, 1990; Mitchell and others, 1990; O'Rourke and others, 1991a, b; Bardet and others, 1991; Bonilla, 1991). In addition, a detailed study of geotechnical conditions and underground public facilities in areas of potential ground deformation from liquefaction, including the Marina District, has been performed for the city of San Francisco (Harding Lawson Associates and others, 1991).

This report concentrates on two aspects of earthquake response in the Marina District. First, we summarize the damage to buried lifeline systems and evaluate it in the context of the historical and geotechnical factors contributing to the disruption of these systems. Second, we examine the soil characteristics affecting postliquefaction consolidation, and draw conclusions with respect to the ground deformations that occurred in natural and fill materials. We

show that postliquefaction consolidation played a critical role in lifeline performance, and we develop relations between the magnitude of settlement and the proportion of pipeline system damaged.

## HISTORICAL DEVELOPMENT OF THE MARINA DISTRICT

The Marina District is bounded by San Francisco Bay on the north, the Presidio on the west, and Lombard Street and Van Ness Avenue on the south and east, respectively. In this report, we focus on that part of the district to the west of Laguna Street. As discussed by Bonilla (this chapter), this area overlies the deepest part of an underlying bedrock basin and includes loose fills. Furthermore, the area includes virtually all locations of lifeline damage and pipeline replacements as a result of the earthquake.

Like several other sites in the San Francisco Bay area, the Marina District has been developed by placing sandy fills on soft clay and silt. A plan view of the Marina District on which is superimposed the 1857 shoreline, as mapped by the U.S. Coast Survey (1857), is shown in figure 1. Along its west boundary was a narrow sand spit known as Strawberry Island, with adjacent saltwater marshes. Sand dunes, 6 to 12 m high, were situated south of the shoreline in the southeastern part of the area.

To aid in the construction of industrial facilities, a seawall was built during the 1890's (Olmsted and others, 1977). The seawall was constructed by dumping rock, which had been hauled to the site on barges, and backfilling in places behind the rock embankment with sand taken primarily from the dunes. Similar construction was performed by the San Francisco Gas and Light Co. to establish an earthen mole. The locations of the seawall and earthen mole (Sanborn Ferris Map Co., 1905), which represent the waterfront and extent of filling at the time of the 1906 earthquake, are shown in figure 2. This configuration of seawall, embankment, and artificial fill remained essentially unchanged until 1912, when construction on the site was started for the 1915 Panama-Pacific International Exposition.

Although the Marina District was not developed extensively in 1906, there are nevertheless several historical accounts of damage in this area (Jones, 1906; Gilbert and others, 1907; Lawson, 1908), some of which are summarized in figure 2. Lawson (1908), for example, drew attention to evidence of severe ground shaking in the area extending from North Point Street between Lyon and Broderick Streets to the shoreline (diagonal-lined area, fig. 2). In this area, timber structures were thrown out of vertical, reminiscent of the shear deformation sustained by four-story timber buildings during the 1989 earthquake. Moreover, damage to the Baker Street sewer implies that permanent ground deformation occurred in this area.

The most comprehensive observations of damage are associated with the coal-gasification plants that were located in the southeastern part of the Marina District in 1906. Gilbert and others (1907) reported that all the buildings at the San Francisco Gas and Electric (renamed from the original San Francisco Gas Light Co.) plant sustained damage and that the ground settled "very considerably" in this place. Jones (1906) reported from 600 to 900 mm of settlement adjacent to the principal gas holder at the North Beach Station. The settlement ruptured the 600-mm-diameter outlet connections of the holder, causing all the stored gas to escape.

In 1912, the lagoon enclosed by the seawall was filled with dredged soil pumped from bay deposits approximately 90 m offshore. Pumping of the fill material was relatively strictly controlled. The opening along the north line of the seawall was used to sluice out fine-grained and organic materials during hydraulic filling. An estimated 70 percent of the fill placed in this way was sand (Olmsted and others, 1977).

In summary, the placement of fill and development in the Marina District may be simplified as having occurred in two stages. The first stage was associated with the placement of land-tipped, or end-dumped, fills. Most of these soils were placed until about 1900 adjacent to both the original shoreline and Strawberry Island, and as part of the seawall. The second stage was in 1912, when sandy deposits were dredged and pumped into the lagoon bounded by the old seawall. On the basis of historical development, three general types of soils are distinguishable in the Marina District: (1) natural soils associated with the original beach and sand spit deposits, (2) land- and barge-tipped fills, and (3) hydraulic fill. Areas underlain by each of these soil types behaved differently during the 1989 earthquake, as analyzed below.

## WATER-SUPPLY SYSTEM

Water to the Marina District is supplied by two systems of pipelines: the Municipal Water Supply System (MWSS) and the Auxiliary Water Supply System (AWSS). The MWSS supplies potable water for domestic and commercial uses, as well as for firefighting via hydrant and sprinkler systems; the AWSS supplies water exclusively for firefighting purposes.

Within the Marina District, in an area bounded by the 1857 shoreline on the south (U.S. Coast Survey, 1857) and the current shoreline on the north, there is approximately 11,300 m of pipelines belonging to the MWSS and 2,300 m of pipelines belonging to the AWSS. The MWSS mains are 100, 150, 200, and 300 mm in diameter, whereas the AWSS mains are predominantly 250 and 300 mm in diameter. The pipelines in both systems are composed of pit-cast iron, and many were installed between late 1924 and

1925. The MWSS pipelines were built predominantly with cement-caulked, bell-and-spigot couplings, whereas the AWSS pipelines were built with special couplings, as described below. All the pipelines were buried at nominal depths to top of pipe between 0.9 and 1.2 m.

The locations of MWSS pipelines and repairs relative to the current street system, 1906 waterfront, and 1857 shoreline are shown in figure 3. Repairs were made at points of sheared or disengaged service connections with mains, flexural round cracks in mains, and longitudinally split sections of mains. In some places, damage was concentrated at or near gate valves, which tend to anchor the pipelines and therefore may contribute to locally pronounced deformation and stresses.

The locations of the MWSS mains that were replaced after initial repair are shown in figure 4. These mains were most heavily damaged in areas of greatest surface settlement and so are most likely to be subject to continuing rupture and maintenance difficulties in the future. Approximately 2.7 km of mains was replaced, primarily in or immediately adjacent to areas underlain by hydraulic fill.

Even though the MWSS was substantially damaged in the Marina District, the AWSS was repaired at only one place, at a leaking joint at Scott and Beach Streets (fig. 5). The MWSS pipeline damage reported by the San Francisco Water Department as of November 1, 1989, is summarized in table 1. Service connections typically are made with pipe substantially smaller than the main, and in many places, the performance of service connections cannot be linked directly with the diameter of the main. Thus, the service repairs listed in table 1 are omitted from the repair rate based on pipe diameter but are included in the total

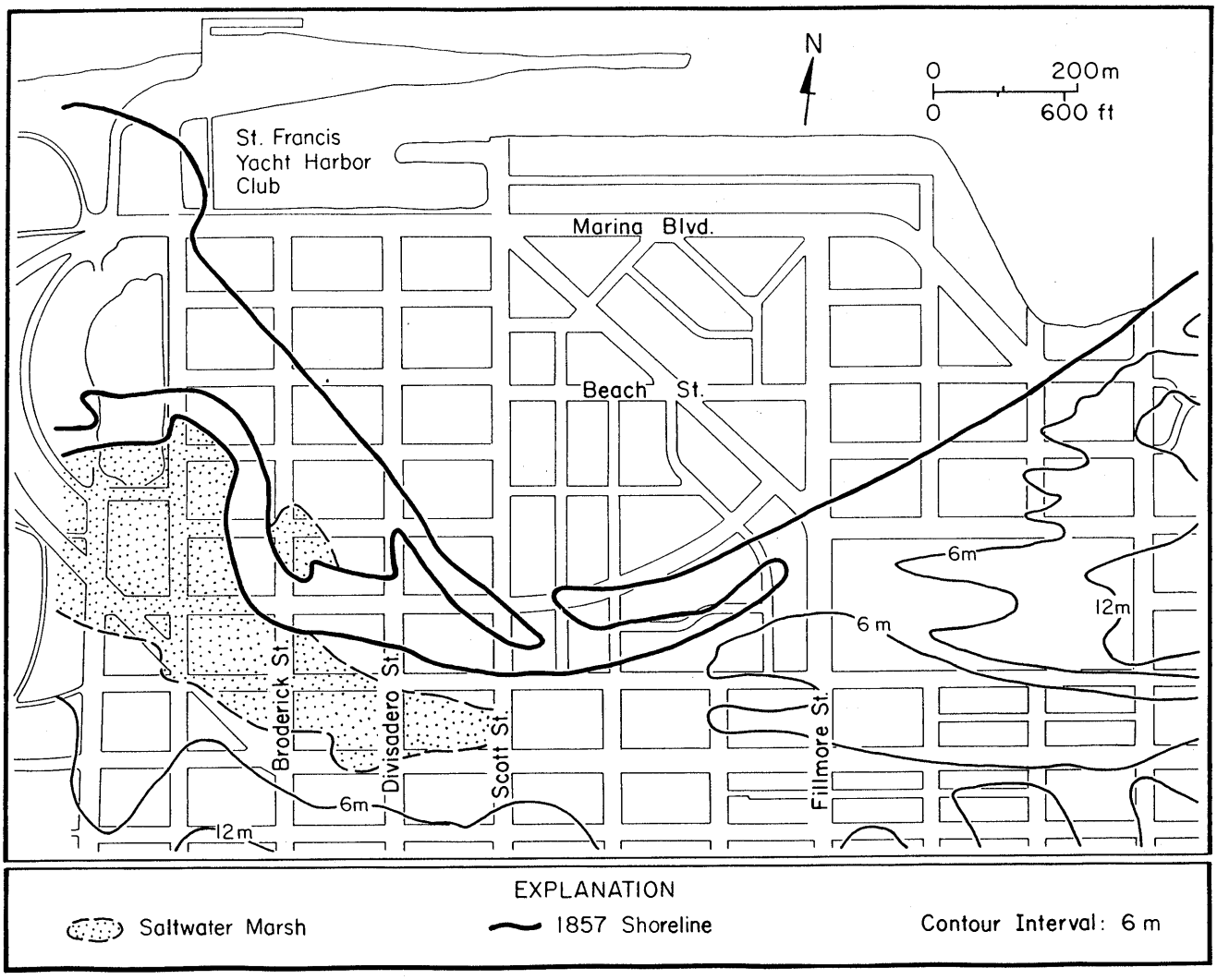


Figure 1.—Marina District, showing location of 1857 shoreline.

Table 1.—*Municipal Water Supply System pipeline damage*

| Pipeline diameter (mm) | Main repairs | Repairs at or near gate valves | Service-line repairs | Length of pipe (m) | Repair rate (per kilometer) |
|---|---|---|---|---|---|
| 100 | 16 | 2 | | 1,250 | 14.40 |
| 150 | 33 | 8 | | 5,600 | 7.32 |
| 200 | 7 | 2 | | 3,300 | 2.73 |
| 300 | 1 | - | | 1,200 | 0.83 |
| TOTAL | 57 | 12 | 54 | 11,350 | [1]10.84 |

[1]Includes mains and service lines.

repair rate, because they contribute to an overall assessment of system damage. The repair statistics pertain to the area of MWSS pipeline damage bounded by Baker Street, Marina Boulevard, and Buchanan Street on the west, north, and east, respectively, and by Bay and Chestnut Streets on the south.

A total of 123 repairs were made to the MWSS mains and service lines in the Marina District, more than three times the number in the entire MWSS elsewhere. A total of 69 repairs were made to mains, including those at or near gate valves; more than 80 percent of these repairs were attributed to flexural round cracks. In contrast, only one leaking joint was found in a 300-mm-diameter AWSS pipeline out of 2,290 m of 250- and 300-mm-diameter pipelines within the area of MWSS damage described above, resulting in a repair rate of only 0.43 per kilometer.

The repair rates for MWSS and AWSS pipelines are plotted on a logarithmic scale as a function of nominal pipe diameter in figure 6. The slope of the linear regression is approximately −3, implying that pipeline repair was inversely proportional to the cube of the pipe diameter. Because the moment of inertia of a given pipe is a function of the cube of its diameter, the regression analysis indicates that damage was influenced strongly by the longitudinal bending resistance of the pipelines. Thus, it appears that bending stress caused by differential settlement of the underlying soil was the main cause of pipe failure and that resistance to such stress, resulting from

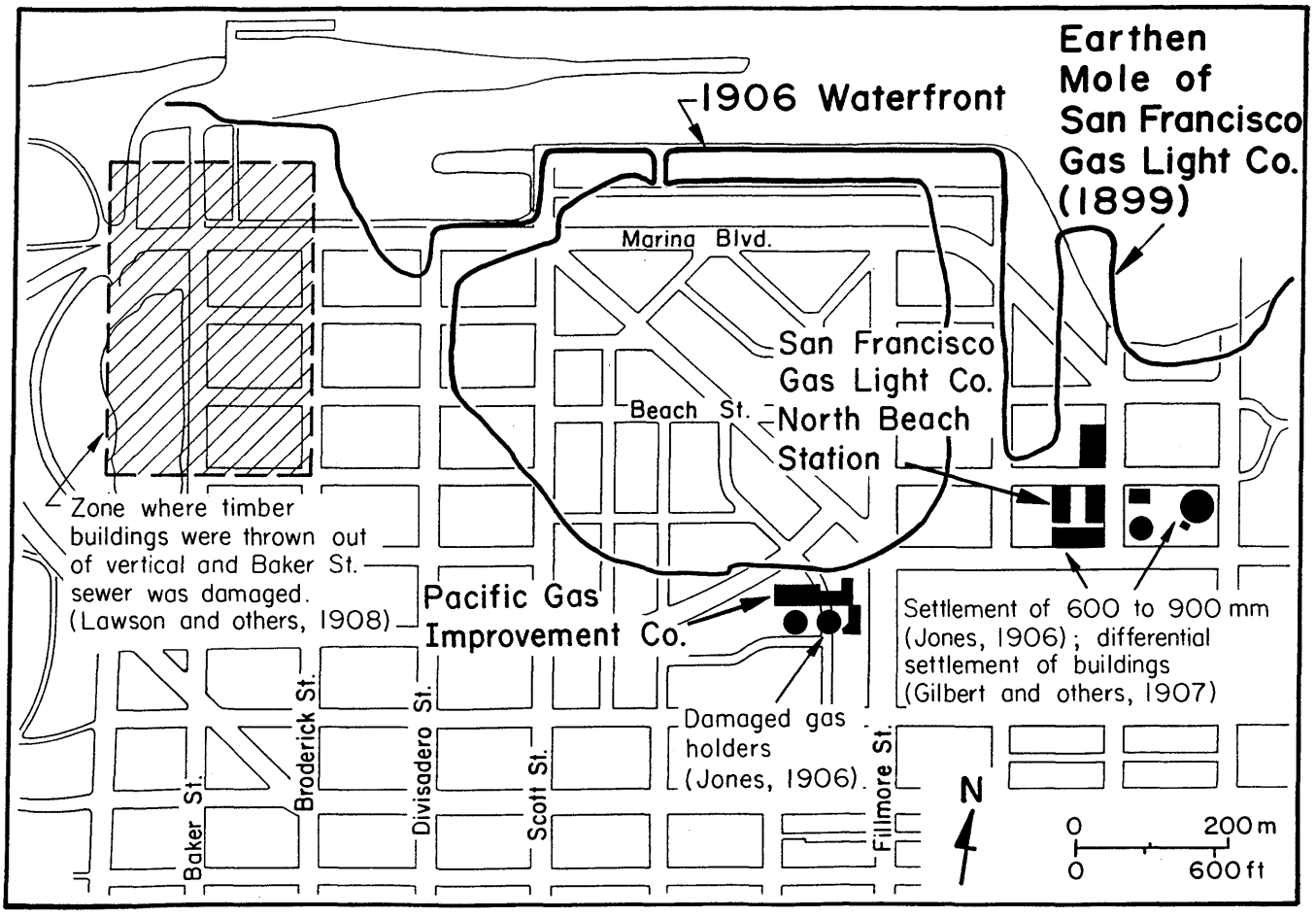


Figure 2.—Marina District, showing locations of 1906 waterfront and of damage and ground movements observed after 1906 San Francisco earthquake.

flexible AWSS joints and increasing pipe diameter, was responsible for the lowest repair rates.

## GAS-DISTRIBUTION SYSTEM

The high pressure gas-distribution lines in the Marina District were damaged in only one place, at a miter joint near the boundary of hydraulic fill and the 1857 shoreline. The high-pressure mains were constructed mostly of Grade B steel with electric-arc girth welds.

In contrast to the high-pressure (approx 200 kPa) lines, the low-pressure (approx 2 kPa) gas-distribution mains were substantially damaged. Approximately 13.6 km of steel and cast-iron mains, ranging from 100 to 300 mm in diameter, was replaced within the area bounded by Laguna, Lombard, and Lyon Streets and San Francisco Bay (Phillips and Virostek, 1990). A little more than half this length was replaced with medium-density polyethylene (MDPE) piping inserted within existing steel and cast-iron pipes; the rest was replaced by direct burial of MDPE piping. The replacement pipes ranged from 50 to 150 mm in nominal diameter; about 90 percent were 50 mm in diameter.

## WASTEWATER-CONVEYANCE SYSTEM

In San Francisco, wastewater is collected, transported, and treated under the Clean Water Program. The wastewater-conveyance system consists of 1,159 km of collector sewers, ranging in diameter from 200 to 600 mm; 241 km of transport sewers, ranging in diameter from 0.9 to 2.3 m; and a series of storage culverts to hold water during heavy runoff for later transport and treatment. Approximately 77 percent of the collection and transport sewers are more than 50 years old.

Three types of sewage conduit in the Marina District were affected by the earthquake: (1) collector sewers, ranging in diameter from 200 to 600 mm; (2) outfall sewers, ranging in diameter from 1.5 to 2.3 m; and (3) a 3- to 5-m-wide reinforced-concrete box sewer along Marina Boulevard. The collector sewers are composed mainly of vitrified-clay pipe in sections nominally 1.5 to 1.8 m long,

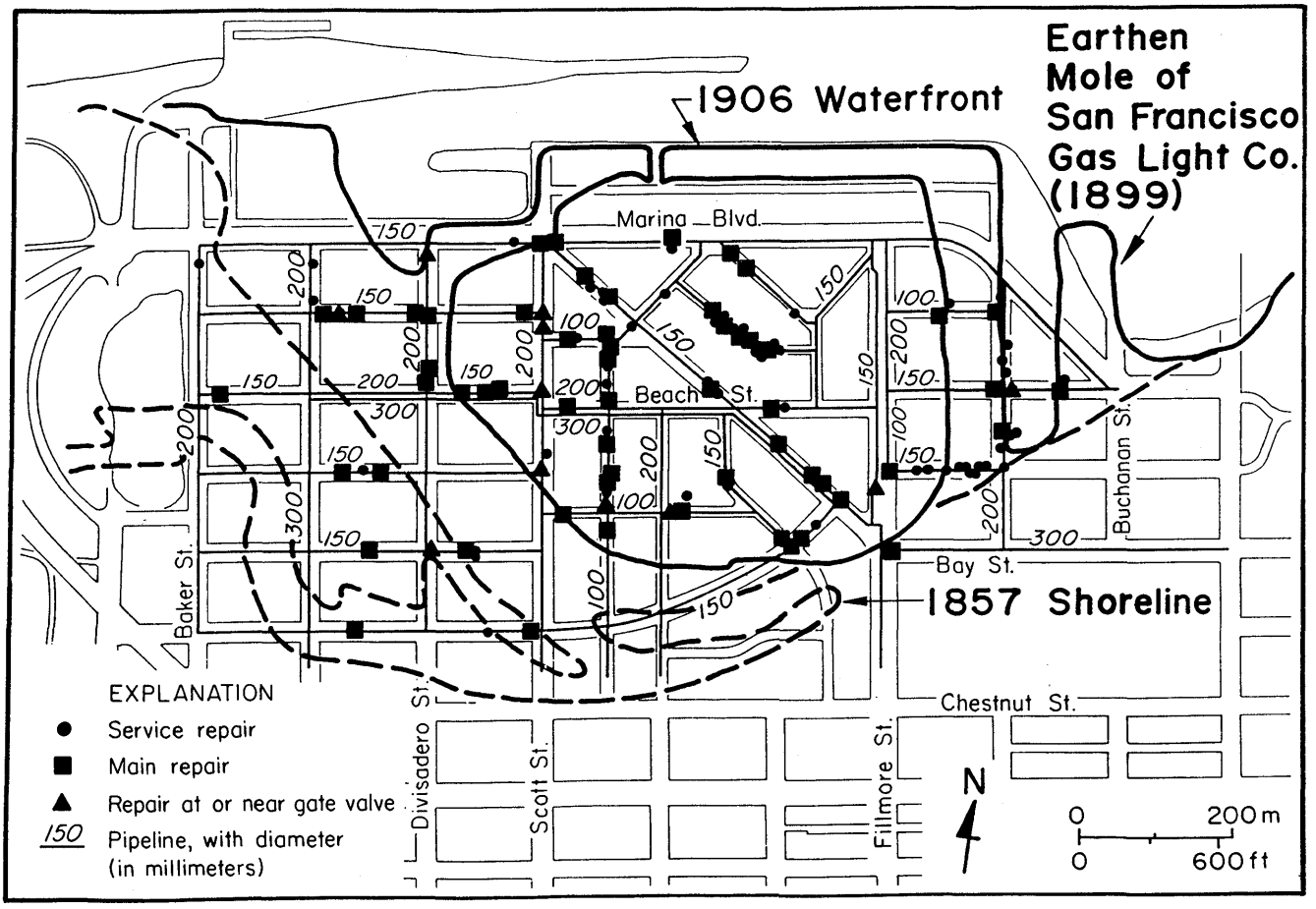


Figure 3.—Marina District, showing locations of repairs to MWSS mains, service lines, and sections at or near gate valves as of November 1, 1989.

with mortared joints. This type of pipe is relatively weak and brittle. Since about 1960, the Clean Water Program has been installing stronger vitrified-clay pipe, equipped with polyethylene gaskets at the joints to promote flexibility.

The locations of damage to the wastewater-conveyance system are shown in figure 7. Damage at the outfall sewers occurred primarily because of broken connections between the pile-supported outfalls and collector sewers, which settled differentially relative to the outfalls. The outfall sewer along Pierce Street was a circular reinforced-concrete structure, ranging in diameter from 1.8 to 2.3 m, supported on timber piles, with an invert depth about 3 m below the ground surface. It was heavily damaged north of the seawall on the Marina Green. The 1.5-m-diameter Baker Street outfall, of similar construction, was cracked and fractured at a turning point (triangle, fig. 7) where a joint connects it to an overflow weir. Minor cracking was observed along the invert of the Marina Boulevard sewer.

Within the area bounded by Marina Boulevard and Baker, Chestnut, and Buchanan Streets is 9.8 km of vitrified-clay-pipe collector sewers, of which approximately 2 km were replaced or repaired as a result of the earthquake. The lengths of pipeline in which repairs and replacements were made are shown in figure 7 on the basis of records provided by the Clean Water Program. Much of the damage was in the form of cracked and crushed joints. Approximately 1.4 km of vitrified-clay pipe was replaced with stronger clay pipe, utilizing gasketed joints. Nearly 73 percent of the replaced or repaired pipes were located in or immediately adjacent to (within half a block of) areas of hydraulic fill.

The repair-and-replacement statistics for collector sewers are summarized in table 2. In contrast to the MWSS damage, the collector-sewer damage does not correlate with nominal pipe diameter. Except for the 250- and 600-mm-diameter pipes, from 15 to 28 percent of the collector sewers were replaced; overall, 20 percent of the collector sewers within the area of damage were replaced.

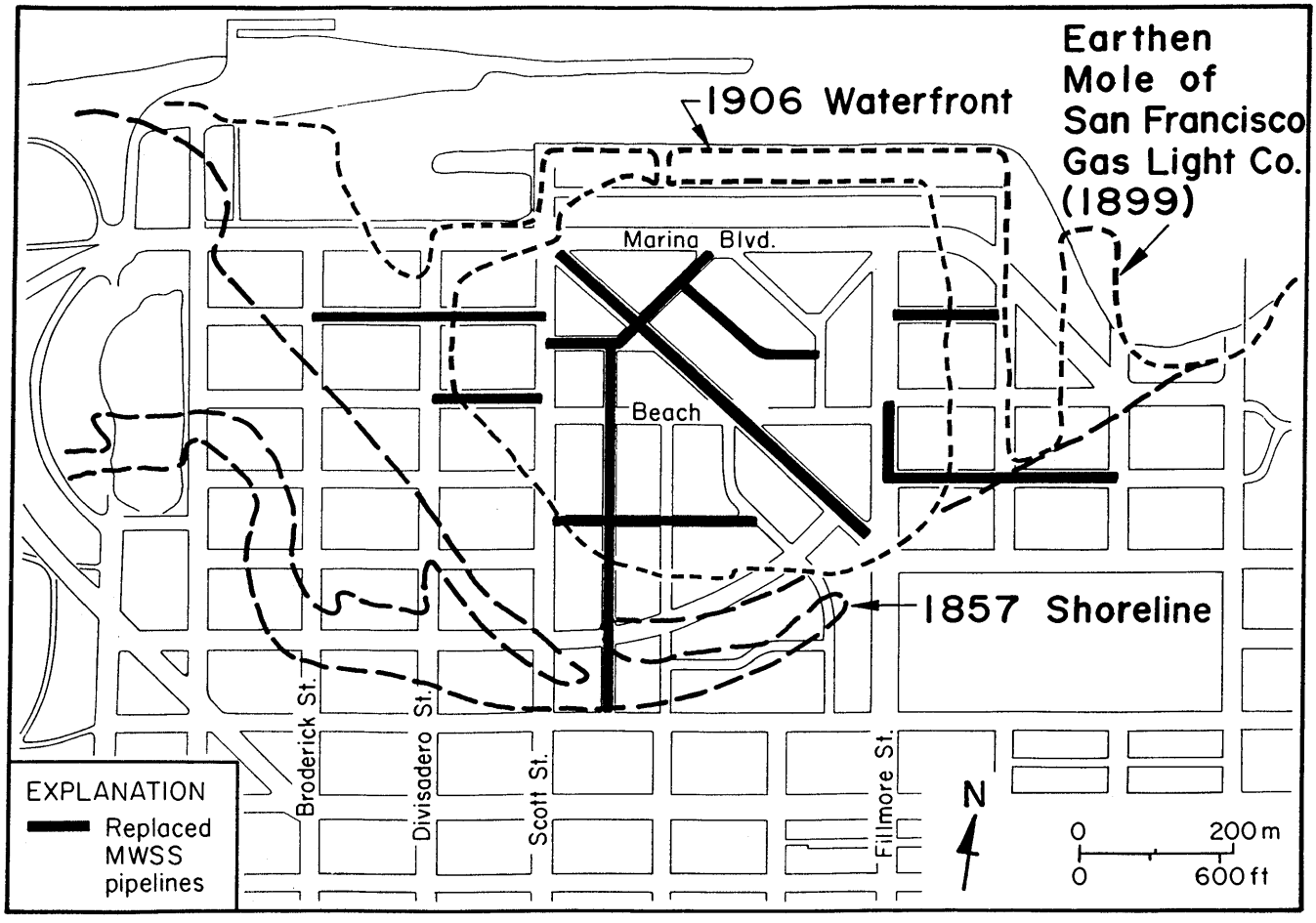


Figure 4.—Marina District, showing locations of MWSS pipelines replaced about 6 months after initial repairs illustrated in figure 3.

Table 2.—*Repair-and-replacement statistics for collector sewers*

| Diameter (mm) | Length (m) | Length replaced or repaired (m) | Percentage replaced or repaired |
|---|---|---|---|
| 200 | 5,345 | 1,127 | 21 |
| 250 | 300 | 143 | 48 |
| 300 | 875 | 152 | 17 |
| 375 | 950 | 175 | 18 |
| 450 | 580 | 87 | 15 |
| 525 | 930 | 258 | 28 |
| 600 | 805 | 0 | 0 |
| TOTAL | 9,785 | 1,942 | 20 |

## GROUND DEFORMATION AND PIPELINE REPAIR

Settlement caused by the earthquake was evaluated on the basis of survey data collected in 1961, 1974, and 1989 and published by Bennett (1990), and a detailed evaluation of subsurface conditions in the Marina District was presented by O'Rourke and others (1991b). Settlement data were confined to street intersections.

It was assumed that the settlement from 1961 to 1974 was caused principally by secondary compression of Holocene bay mud. From the survey data base, the incremental secondary compression, $\Delta S$, was regressed relative to the thickness of Holocene bay mud, $H$, to obtain the best linear fit of the data with slope $\Delta S/H$=0.0011, which is related to soil properties in the form

$$\frac{\Delta S}{H} = C_{\alpha\varepsilon} \log (t_2/t_1) \tag{1}$$

where $C_{\alpha\varepsilon}$ is the coefficient of secondary compression, defined as the ratio of the change in one-dimensional vertical strain to the change in the logarithm of time since the end of primary consolidation; and $t_1$ and $t_2$ are the times since the placement of hydraulic fill in 1974 and 1912–61, respectively.

A value of $C_{\alpha\varepsilon}$=0.011 was calculated with equation 1, which compares favorably with the $C_{\alpha\varepsilon}$ value determined

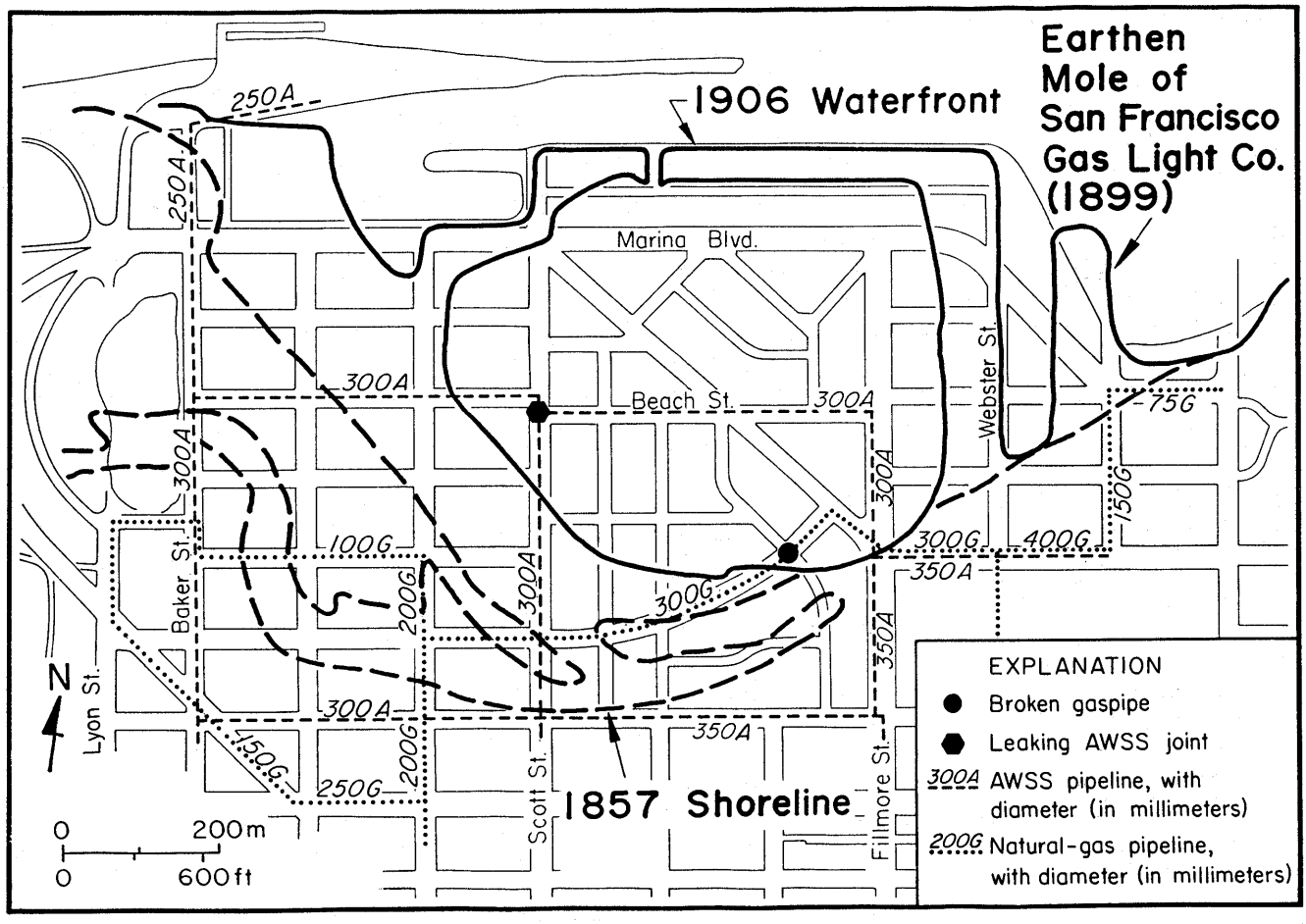


Figure 5.—Marina District, showing locations of damage to AWSS and high-pressure gas-distribution system. Approximately 13.6 km of low-pressure gas-distribution mains that were replaced after the earthquake is omitted for simplicity.

for Holocene bay mud on the basis of one-dimensional consolidation tests (Dames & Moore, 1989). On the basis of 42 test results with stress increments to levels of 1.2 to 2.5 times the preconsolidation pressure, the mean $C_{\alpha\varepsilon}$ value was 0.011, with a standard deviation of 0.004.

The value of $C_{\alpha\varepsilon}$=0.011 was used to calculate the incremental secondary compression for each survey point between 1974 and 1989. These values were subtracted from the difference in actual survey measurements to yield "corrected" settlements that would best represent the amount of vertical movement caused by liquefaction-associated consolidation of the fills underlying the Marina District. Settlement contours were calculated from these corrected measurements with Golden Software, Inc.'s computer program "Surfer," using a procedure referred to as kriging, in which contours are computed with minimal estimation variance from a statistical evaluation of the input data (Ripley, 1981).

The resulting settlement contours are mapped in figure 8. The maximum settlements occurred in the hydraulic fill, with decreasing amounts of vertical deformation in the land- and barge-tipped fills and in areas underlain by natural beach and sand-bar deposits.

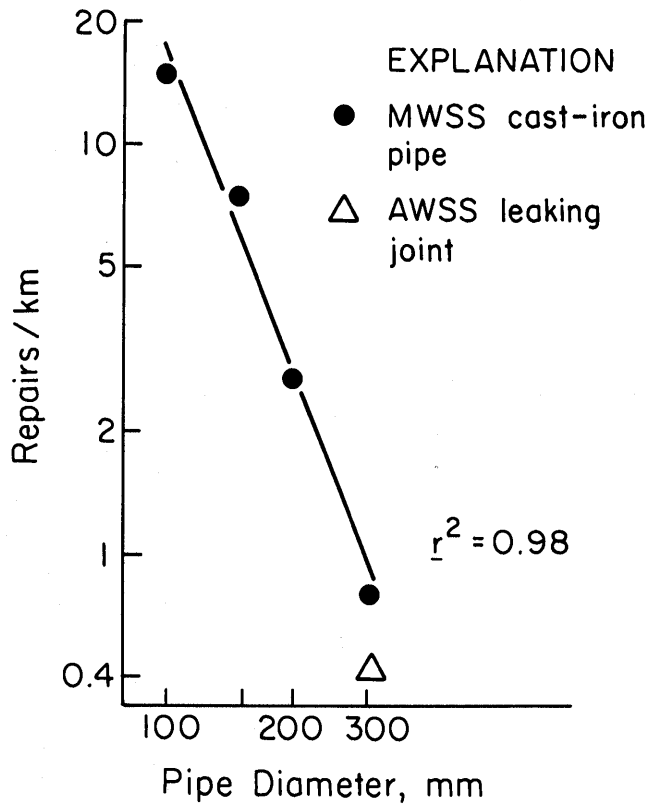


Figure 6.—Linear regression of repair rate versus nominal pipe diameter for MWSS and AWSS mains in the Marina District. Only repairs to MWSS mains, including sections at or near gate valves, were used in regression analysis.

To represent the distribution of MWSS damage, the Marina District was divided into a grid of approximately 40 cells, and the number of repairs in each cell was counted. The repairs then were normalized with respect to a reference length of 300 m to provide a consistent basis for evaluation. Contours of equal repair rates were drawn and superimposed on the street system and previous shorelines, as shown in figure 9. These repair-rate contours are closely related to the settlement contours and to the locations of hydraulic fill and the 1857 shoreline. Inspection of figures 8 and 9 shows that the closely spaced settlement contours, indicating the largest local settlement slopes, correspond to the highest repair-rate contours. High concentrations of pipeline repair fall within the area of hydraulic fill. The heaviest repair concentration occurs at the junction of the hydraulic fill, seawall, and 1857 shoreline, except for an isolated area on Rico Way, where unusual stresses were generated as a result of pipeline construction along the curved street.

We note that settlement before the earthquake, caused by primary consolidation and secondary compression of Holocene bay mud, could have affected the vulnerability of existing pipelines. Because such settlement would have been largest over the thickest parts of bay mud, we would expect pipeline damage to be locally high near these places. The relative absence of concentrated pipeline damage in places of thick Holocene bay mud implies that any vulnerability caused by preearthquake consolidation was not sufficiently pronounced to influence damage when other factors, such as postliquefaction consolidation, were involved.

To explore further the relation between pipeline damage and settlement pattern, MWSS repair rates were correlated with both the magnitude of settlement and the slope of the local settlement profile. The MWSS pipeline repairs within half a block in all street directions from each intersection were divided by the total length of pipe within this area and correlated with the settlement measured at each intersection. In addition, the MWSS pipeline repairs along each block were divided by the total length of pipeline along the block and correlated with the angular distortion, defined as the differential settlement across each block divided by the block length, or the local slope of the settlement profile. In geotechnical engineering practice, angular distortion is the parameter most commonly used to evaluate potential damage to buildings from differential foundation settlement (Tomlinson, 1986).

In calculating the correlations, the pipelines on Rico Way and Pierce Street were deleted from the data base. Because the water main on Rico Way had been laid along a relatively sharp curve in the street, it is believed to have been especially vulnerable to damage because of installation stresses and constraints imposed by such construction. The water main along Pierce Street was underlain by a pile-supported sewer.

Only a weak correlation was found between repair rate and the magnitude of settlement. Relatively good correlations were found between repair rate and angular distortion. The relation between the MWSS repair rate per 300 m of pipe and the angular distortion is plotted in figure 10. Note that the data in figure 10 do not include damage to service lines and connections but only to mains. Because of the strong correlation between repair rate and nominal pipe diameter illustrated in figure 6, regressions were developed for each diameter of cast-iron main. An equation and coefficient of determination, $r^2$, are given for each regression curve in figure 10. The slopes of these curves increase in inverse proportion to the nominal pipe diameter. For 200-mm-diameter mains, a bilinear plot (dashed curve, fig. 10*C*) also conforms with the data.

The spatial patterns of damage mapped in figures 7 and 9 and their close relation to the pattern of settlement mapped in figure 8 indicate a strong link between pipeline damage and differential movement that is corroborated further by the correlations plotted in figure 10. Differential movement and angular distortion were most heavily concentrated at the boundaries among the fills, natural soils, and old seawalls. Note that damage to the relatively large, 300-mm-diameter MWSS main (see fig. 3) and 300-mm-diameter gas pipeline (see fig. 5) both occurred very close to the boundary between hydraulic fill and the 1857 shoreline, where there was substantial differential settlement and angular distortion.

The amount of differential settlement also depends on the properties and relative thickness of the soil susceptible to liquefaction, as discussed in the following sections.

## SOIL CONDITIONS

The locations of boreholes and soundings for which data were collected to evaluate subsurface conditions in the Marina District are shown in figure 11. The boreholes were drilled for engineering projects both before and after the earthquake, although most were drilled to clarify foundation conditions beneath buildings during repair and reconstruction after the earthquake (O'Rourke and others,

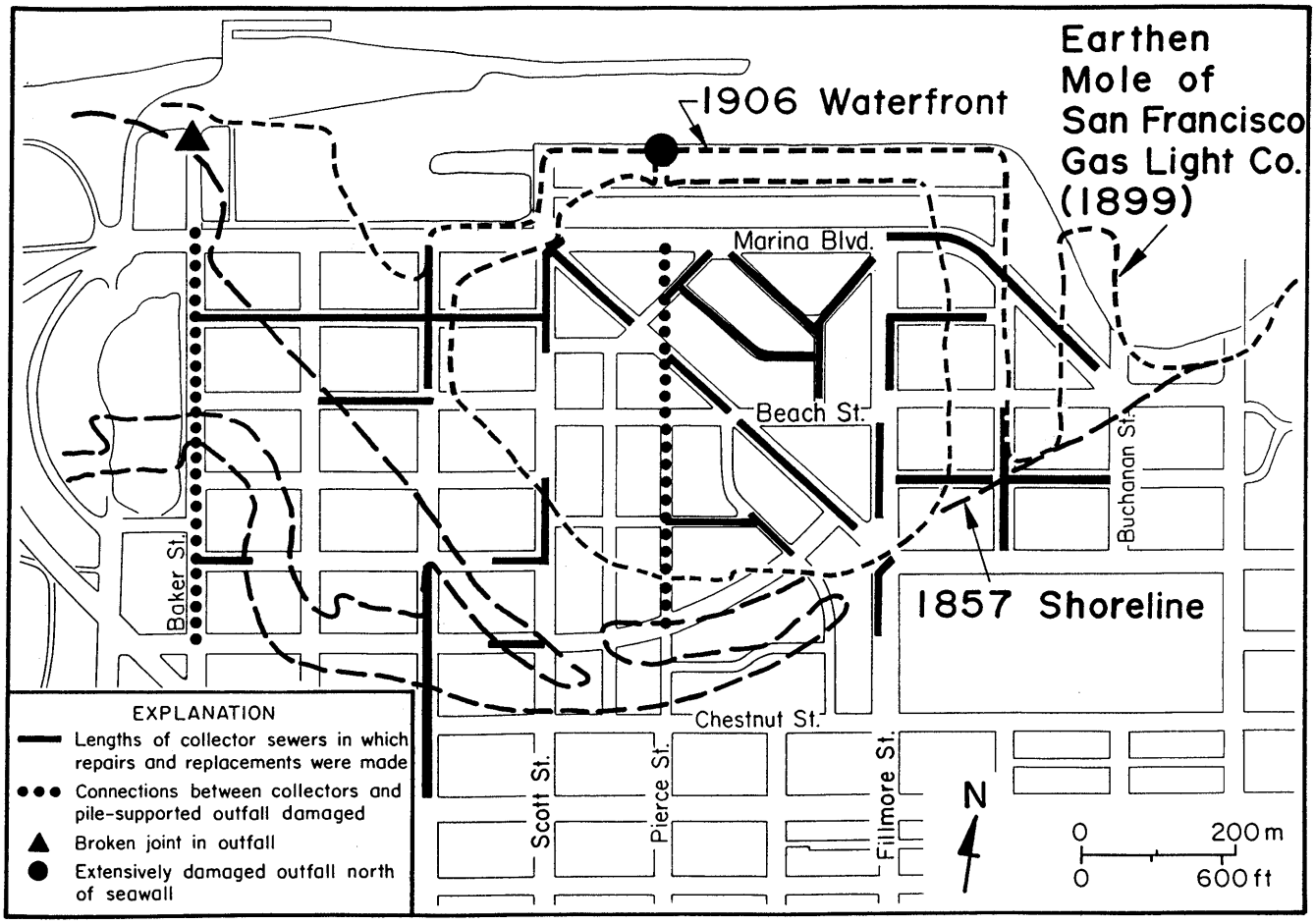


Figure 7.—Marina District, showing locations of damage to wastewater-conveyance pipelines.

1991a; Bonilla, this chapter). A total of 144 conventional boreholes and 14 cone-penetration-test soundings were used in the evaluation.

On the basis of borehole and sounding data, two cross sections (*A–A'*, *B–B'*, fig. 11) providing information about the type of soil, water level, fines content, plasticity, and approximate undrained shear strength of soft to medium clays. Standard penetration tests (SPT) were performed in conjunction with many of the conventional borings, and selected uncorrected SPT values are given.

Cross section *A–A'* (fig. 12) shows loose fill extending along Marina Boulevard from approximately Baker Street to Buchanan Street, with a maximum depth of about 9 m. This distance correlates well with the distance between locations of the 1857 shoreline shown in figures 1 and 11. The depth to water table is approximately 2.5 m. Underlying the loose fills and natural-sand deposits is Holocene bay mud, which ranges in thickness along Marina Boulevard from 9 to 32 m. Underlying the Holocene bay mud are dense sand and stiff to hard clay.

Cross section *B–B'* (fig. 13) trends northwest through the hydraulic fill, which is characterized by low SPT values. Holocene bay mud increases rapidly in thickness toward the bay from about two blocks from the Marina waterfront.

Borehole and outcrop information were analyzed with a geostatistics procedure, embodied in Golden Software, Inc.'s computer program "Surfer." This method of analysis is the same as that employed for generating the contours of surface settlement in figure 8. Contours of the bedrock surface and the bottom and top of the Holocene bay mud underlying the Marina District are shown in figures 14 through 16. Similar subsurface-contour plots have been discussed elsewhere (O'Rourke and others, 1991a), and so they are only briefly described here.

Figure 14 shows that the Marina District is underlain by an oblong bedrock basin, with its long axis oriented west by northwest. The basin is more than 75 m deep below Marina Boulevard.

Figure 15 shows that the Holocene bay mud thickens rapidly toward the bay and that its steepest bottom surface

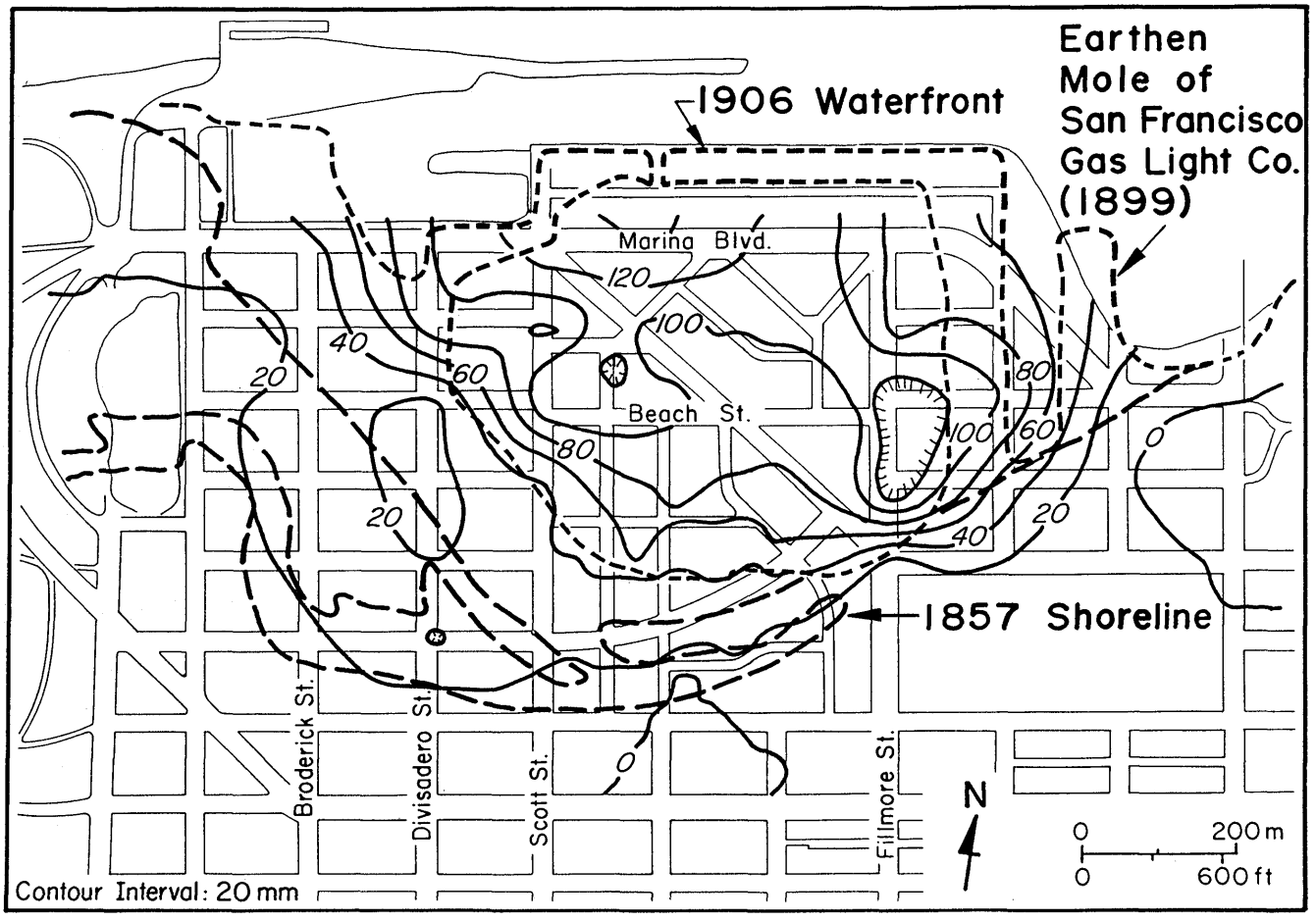


Figure 8.—Marina District, showing contours of settlement caused by the earthquake, calculated from 1961, 1974, and 1989 survey data reported by Bennett (1990). Settlements were adjusted for secondary compression between 1974 and 1989 of underlying Holocene bay mud, as inferred from 1961–74 settlement measurements. Hachures indicate area of closed low.

extends from Broderick Street to Scott Street between Marina Boulevard and Jefferson Street. Slopes of the bottom of the bay mud in this area are locally as steep as 10°.

Figure 16 shows that the underlying surface of the fills is irregular, especially beneath the hydraulic fill, and that it takes the form of a hummocky surface with mounds and depressions. Such an irregular surface is consistent with the method of filling whereby sand was pumped into various parts of the lagoon, causing local bearing failures and associated mounding of displaced fine-grained sedimentary deposits. Across the rest of the area, the top of the Holocene bay mud is in contact with natural sand and does not show disturbed features. Note that the contours of the top of the Holocene bay mud are a good representation of the fill thickness because the elevation of the ground surface is relatively uniform throughout much of the Marina District.

A three-dimensional view of the Marina District in which the street surface, fill and natural-sand deposits, and Holocene bay mud are superimposed on the underlying bedrock basin is shown in figure 17.

## LIQUEFACTION POTENTIAL FROM SPT MEASUREMENTS

Given a general understanding of the bedrock and soil conditions in the Marina District, we next examine the various soil deposits with respect to their liquefaction potential. It is well known that contraction of loose granular soils is associated with liquefaction, resulting in volume reduction and settlement. Differential settlement in the Marina District significantly affected buried-lifeline response. Accordingly, the liquefaction characteristics of the Marina District soils and their contribution to ground movement are of critical importance in evaluating and planning for future lifeline performance.

As mentioned previously, the Marina District provides an excellent opportunity to examine the characteristics and liquefaction response of three different soil types: (1) hydraulic fill, (2) land-tipped fills, and (3) natural-sand deposits. The locations of these deposits in the Marina District can be delineated with reasonable accuracy on the

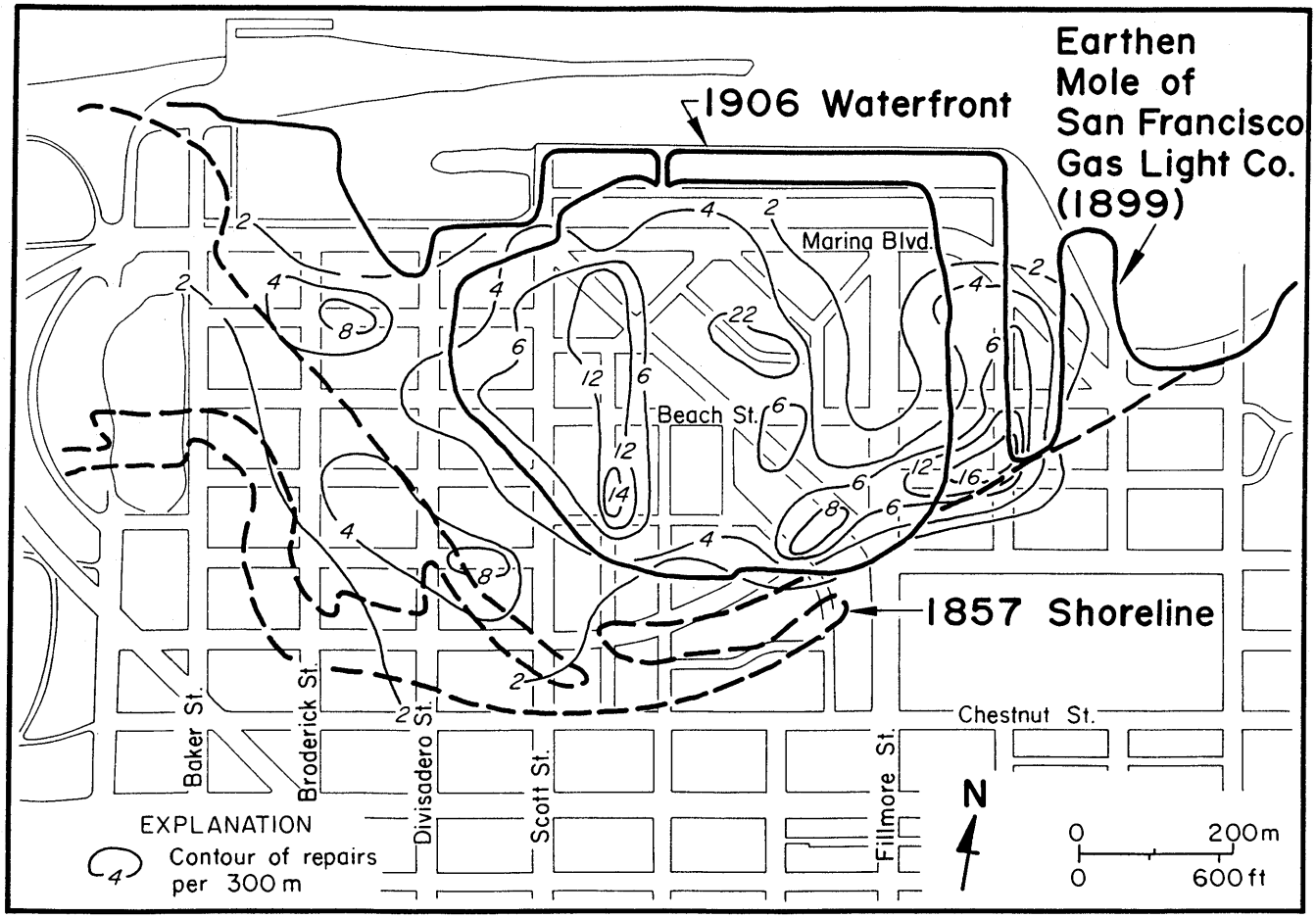


Figure 9.—Marina District, showing contours of MWSS repair rates per 300 m, including damage to mains, service lines, and sections at or near gate valves. Anomolously high contour of 22 per 300 m represents a pipeline installed along a relatively sharp curve on Rico Way, thus vulnerable to earthquake effects because of installation stresses and constraints imposed at joints.

basis of historical records and many boreholes and soundings.

Liquefaction-potential analyses were performed for each soil type, using the empirical relation between cyclic-stress ratio and corrected SPT value developed by Seed and others (1983, 1985). The SPT values were obtained from 75 boreholes in which tests were performed in accordance with the specifications of the American Society for Testing and Materials (1991a). The SPT values were corrected for such factors as in situ confining stress and energy losses, according to the recommendations of Seed and others (1983, 1985). The cyclic-stress ratio for various depths was calculated by assuming a peak acceleration of 0.2 *g*, a value consistent with the peak horizontal component of acceleration recorded at the nearby Presidio (Benuska, 1990). The results are plotted in figure 18.

The most striking feature of the plots in figure 18 is the relatively high liquefaction potential of the hydraulic fill. The corrected SPT values for at least half of the measurements in the sample are less than 6, implying that the hydraulic fill would have a very low undrained residual shear strength, perhaps lower than 5 kPa, based on the empirical relations suggested by Seed (1987). In contrast, both the land-tipped fills and natural-sand deposits show increasing resistance to liquefaction, as well as a successively wider range of in situ densities, as reflected by the SPT values. About half the data for land-tipped fills plot to the left of the 5-percent-fines curve, whereas only about 15 percent of the data for natural-sand deposits plot in the same zone. The land-tipped fills show the widest variation with respect to corrected SPT values, with a coefficient of variation of 0.65 for $(N_1)_{60}$.

The relation between depth and corrected SPT value for the hydraulic fill, land-tipped fills, and natural-sand deposits with regard to liquefaction potential is plotted in figure 19. Although these plots provide only a general picture of subsurface conditions because they lump all the data into a single cross section, they nevertheless show some interesting trends. A relatively uniform distribution of low in situ density with depth is indicated for the hydraulic fill, whereas density tends to increase markedly with depth for areas underlain by land-tipped fills. The natural-sand deposits vary widely in in situ density with depth; most densities fall outside the range of susceptibility to liquefaction during the earthquake.

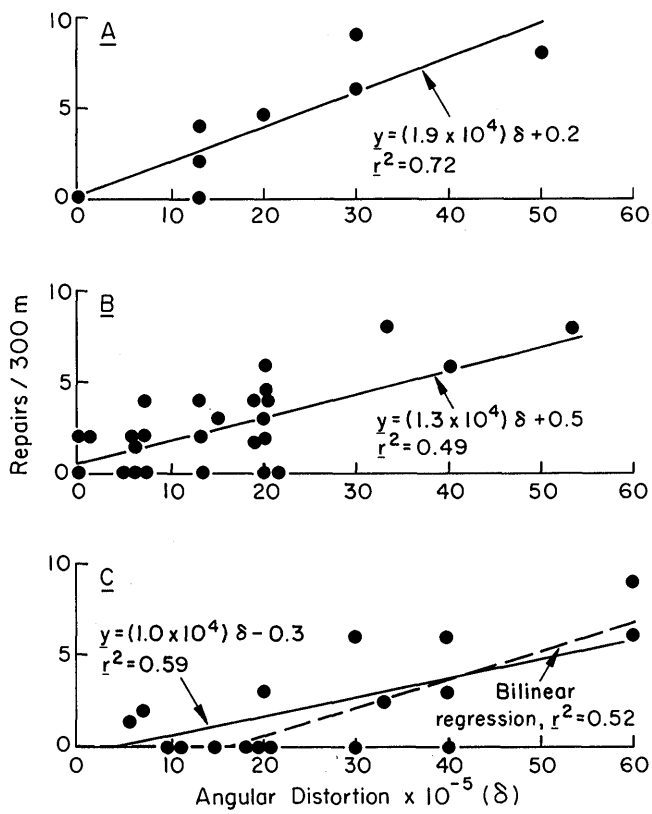


Figure 10.—Linear regressions of MWSS repair rate versus angular distortion (local slope of settlement profile) for water mains 100 (*A*), 150 (*B*), and 200 mm in diameter (*C*).

## LIQUEFACTION POTENTIAL FROM CPT MEASUREMENTS

As illustrated in figure 11, 14 CPT soundings were used in this study of the Marina District, most of which had been reported by Bennett (1990) and Bardet and Kapuskar (1991). The CPT measurements were performed in accordance with the specifications of the American Society for Testing and Materials (1991b). CPT soundings can resolve subsurface conditions in considerably more detail than SPT measurements, and so they provide a more accurate picture of the variations in in situ density and soil type.

Liquefaction-potential analyses were performed for all CPT soundings in areas of hydraulic fill, using the empirical correlations between cyclic-stress ratio and modified cone-tip resistance, $q_{c1}$, proposed by Seed and de Alba (1986). Calculation of the modified cone-tip resistance involves normalizing the measured tip resistance with respect to an effective overburden stress of about 100 kPa, according to the recommendations of Seed and de Alba (1986). The cyclic-stress ratios for various depths were calculated similarly to those for the corrected SPT values by assuming a peak acceleration of 0.2 *g*.

As an illustration of this analysis, consider the normalized CPT profiles shown in figure 20, in which liquefaction-potential curves are plotted for three combinations of fines content and mean grain size chosen to be consistent with the composition of the fills and natural-sand deposits in the Marina District. The CPT data for each sounding were first analyzed to identify the soil type at each depth, according to the recommendations of Robertson and Campenella (1983) and Olsen and Farr (1986). On the

basis of this soil identification, the appropriate liquefaction-potential curve was used to evaluate whether the soil type at a given depth was susceptible to liquefaction during the earthquake.

The CPT profiles for three soundings in the hydraulic fill, from north to south designated as C–8, C–4, and C–15 (see fig. 11), are shown in figures 20*B* through 20*D*, respectively. For example, sounding C–8 indicates liquefiable sand and silty sand between depths of 3 and 4.5 m and again at 5.5 to 6.5 m. Between 4.5 and 5.5 m, the cone penetrated silt and silty clay, which can be interpreted as not susceptible to liquefaction, and so no heavy curve is drawn for this depth interval. Sounding C–4 (fig. 20*C*) shows liquefiable sand and silty sand generally between depths of 2.6 to 7 m, with thin intervening layers of clayey silt that can be interpreted as not susceptible to liquefaction. Sounding C–15 (fig. 20*D*) shows only a few thin seams of sand and silty sand that are clearly susceptible to liquefaction.

In general, the liquefaction potential deduced from CPT measurements corroborates the average trends shown by the SPT measurements for hydraulic fill, land-tipped fills, and natural-sand deposits. The advantage of the CPT soundings is the precision to which potentially liquefiable and nonliquefiable layers can be delineated. This precision permits an additional degree of detail in evaluating the postliquefaction consolidation at various places in the Marina District, as discussed in the next section.

## VERTICAL STRAINS AND SETTLEMENT

Simplified methods for predicting the vertical strain caused by postliquefaction consolidation were proposed by Tokimatsu and Seed (1987) and Ishihara and Yoshimine (1990). These methods permit an estimation of the vertical strain, given either corrected SPT values or relative densities. This approach is similar to that used for evaluating liquefaction potential, in that the cyclic-stress ratio is required as an input parameter. Ishihara and Yoshimine's method requires an estimation of the factor of safety against liquefaction, $FS_L$, defined as the ratio of the cyclic-

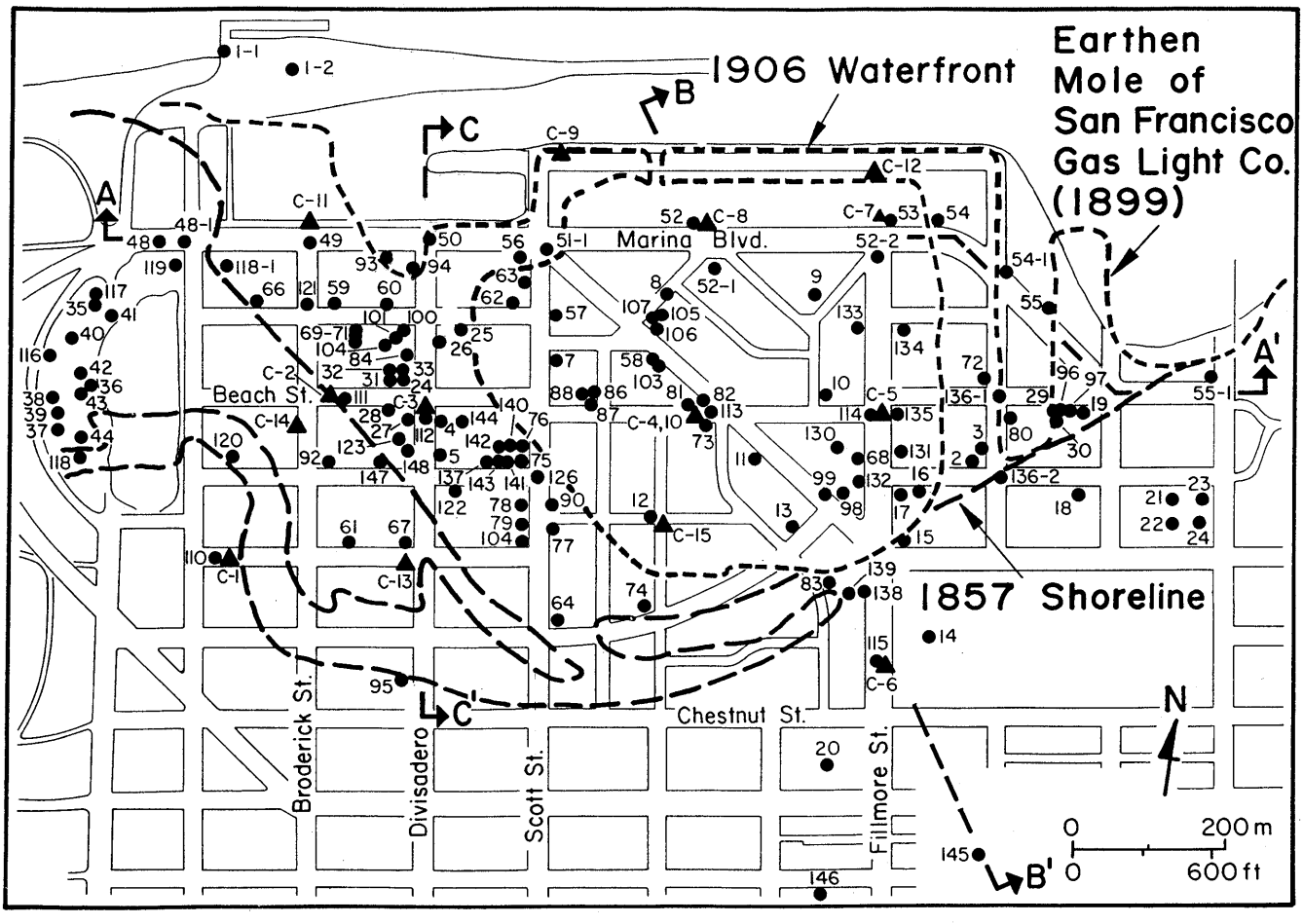


Figure 11.—Marina District, showing locations of conventional boreholes (dots), cone-penetration-test soundings (triangles), and cross sections *A–A'*, *B–B'*, and *C–C'* (figs. 12, 13, 22).

stress ratio required to initiate liquefaction, $CSR_L$, to the cyclic-stress ratio that actually affects the soil layer of interest, CSR ($FS_L=CSR_L/CSR$). We evaluate the cyclic-stress ratio to initiate liquefaction, according to the liquefaction-potential curves in figure 18, as the intercept between the appropriate curve and the average corrected SPT value for the soil. Once the vertical strain has been estimated, we multiply it by the thickness of soil below the water table to estimate the magnitude of settlement.

Although it is beyond the scope of this report to discuss strain-estimation methods in detail, it is nonetheless instructive to illustrate the application of at least one method. The relation between the cyclic-stress ratio and the corrected SPT value for the various soil types in the Marina District relative to the simplified estimation of earthquake-induced vertical strain in saturated sand proposed by Tokimatsu and Seed (1987) is plotted in figure 21. The predicted strains are lowest for natural-sand deposits, with strains of about 0.1 to 0.2 percent corresponding to the average corrected SPT value. Likewise, strains of about 2 and 4 percent are associated with the average corrected SPT values of land-tipped fills and hydraulic fill, respectively.

Vertical strains were estimated from the observed settlements at different sites above land-tipped fills and hydrau-

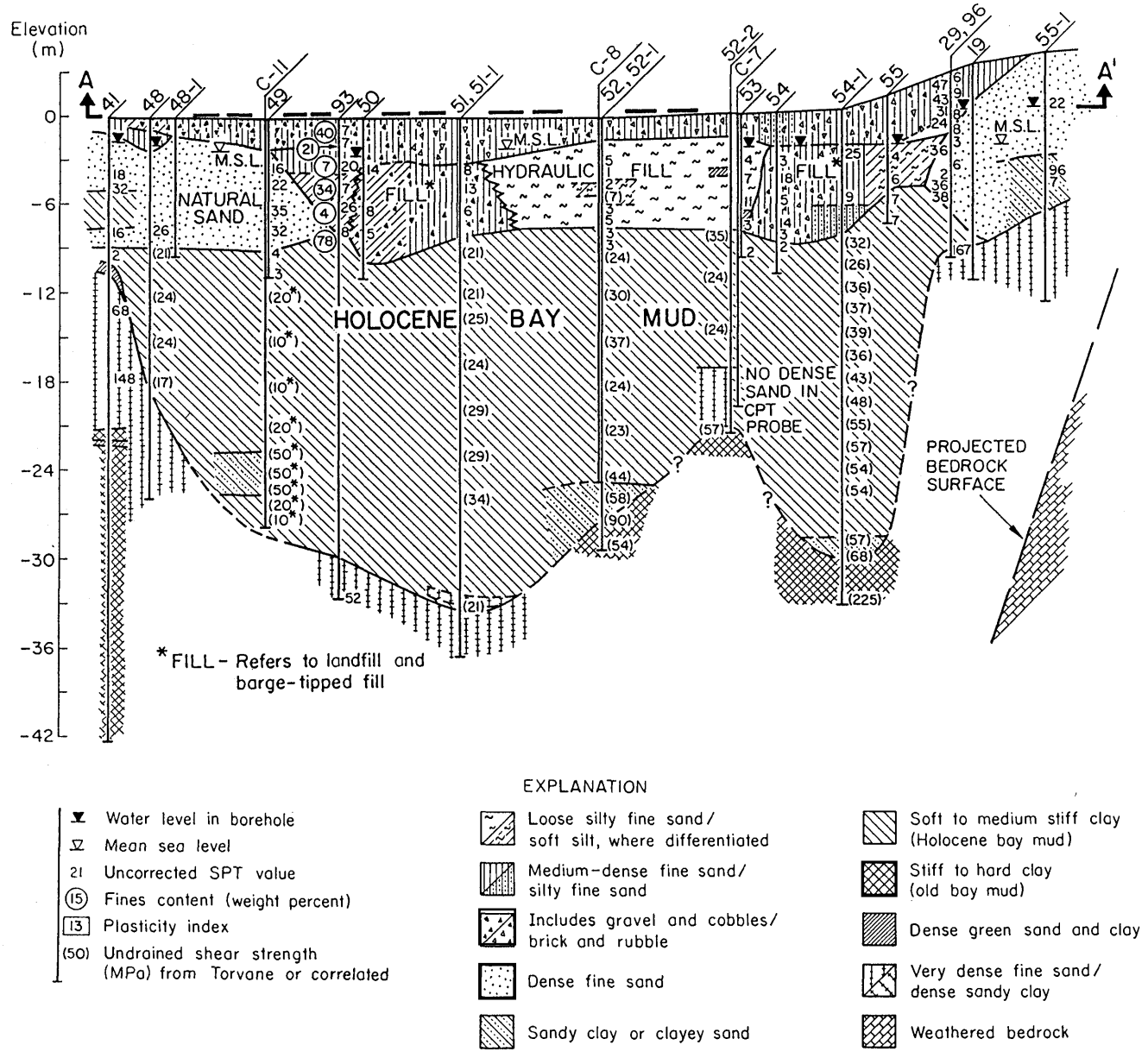


Figure 12.—Cross section *A–A'* along Marina Boulevard. Elevation refers to San Francisco city datum. See figure 11 for location.

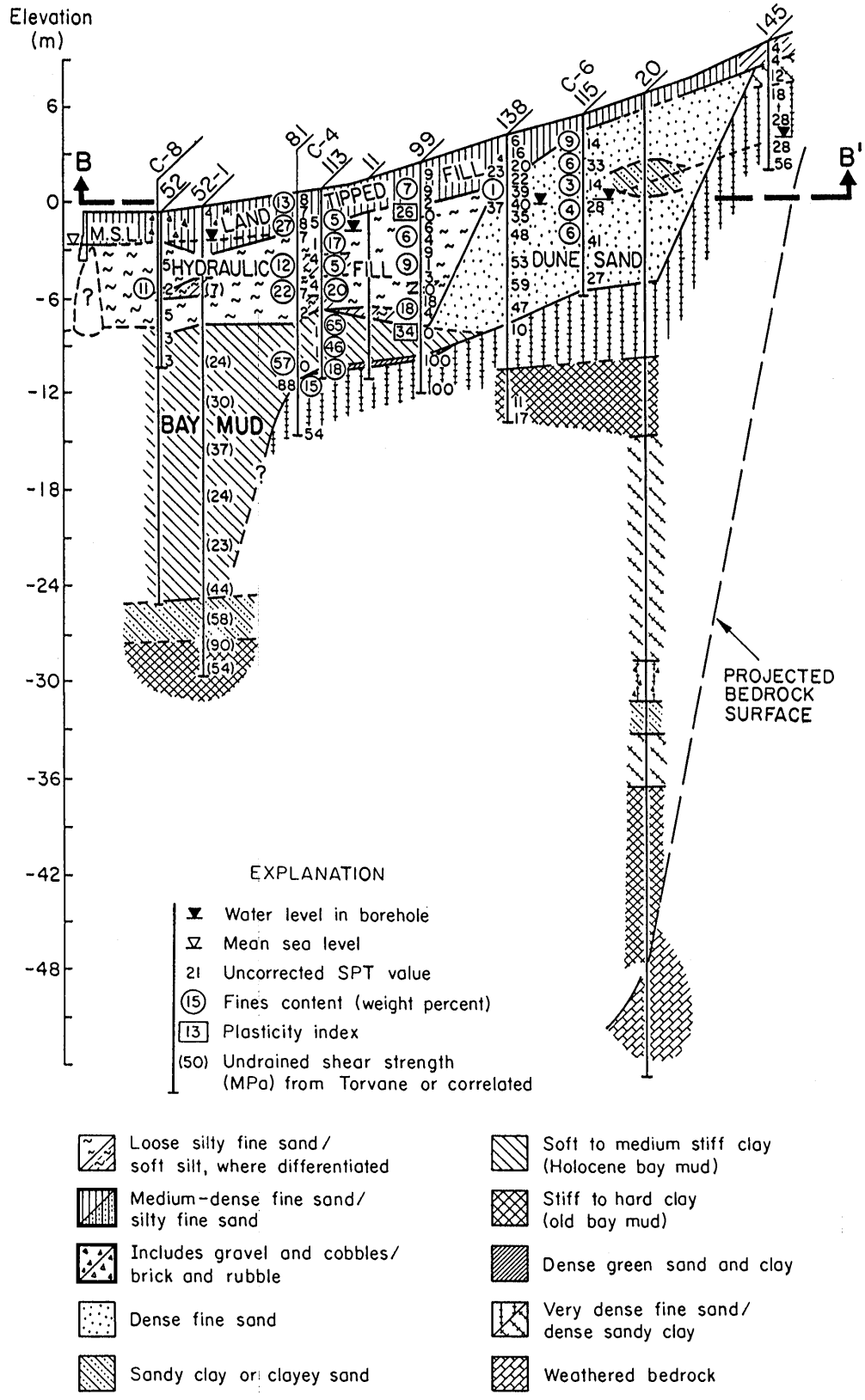


Figure 13.—Cross section *B–B'* trending northwest through hydraulic fill. Elevation refers to San Francisco city datum. See figure 11 for location.

lic fill. At each site, the settlement was divided by the thickness of fill below the water table to give the vertical strain. The data for land-tipped fills and hydraulic fill are summarized in tables 3 and 4, respectively. The weighted-average vertical strain is 2.1 percent for land-tipped fills and hydraulic fill.

Areas of the Marina District where little damage occurred were not explored extensively. As a result, more detailed information about the subsurface stratigraphy at sites of measured settlement is available for land-tipped fills and hydraulic fill than for natural-sand deposits. Data from a few sites, summarized in table 5, indicate that vertical strains of about 0.1 to 0.2 percent occurred in natural-sand deposits. Note that the sites included in table 5 were selected in part because of their proximity to the areas of strongest ground shaking.

Strains were evaluated on the basis of the data listed in tables 3 through 5 by assuming that surface settlements were caused by postliquefaction consolidation throughout the entire depth of fill or natural sand below the water table. The natural-sand deposits and land-tipped fills are relatively consistent in composition with depth; their fines content is less than 5 percent, and their median grain size ranges from 0.2 to 0.4 mm. Because silty and clayey layers are scarce or absent, it seems reasonable to estimate strains in these materials directly from the submerged thickness. Such is not the case with hydraulic fill, however, whose average fines content has been shown to be

Table 3.—*Average settlement and vertical strain for land-tipped fills*

| Average settlement (mm) | Number of locations | Average depth of fill (m) | Average depth of fill below water table (m) | Vertical strain (percent) |
|---|---|---|---|---|
| 5 | 16 | 2.2 | --- | --- |
| 30 | 22 | 4.0 | 1.4 | 2.2 |
| 60 | 14 | 5.6 | 3.0 | 2.0 |
| 100 | 9 | 7.2 | 4.6 | 2.2 |
| | | | Weighted average | 2.1 |

Table 4.—*Average settlement and vertical strain for hydraulic fill*

| Average settlement (mm) | Number of locations | Average depth of fill (m) | Average depth of fill below water table (m) | Vertical strain (percent) |
|---|---|---|---|---|
| 60 | 5 | 6.5 | 3.9 | 1.5 |
| 100 | 25 | 7.1 | 4.5 | 2.2 |
| 125 | 5 | 8.5 | 5.9 | 2.1 |
| | | | Weighted average | 2.1 |

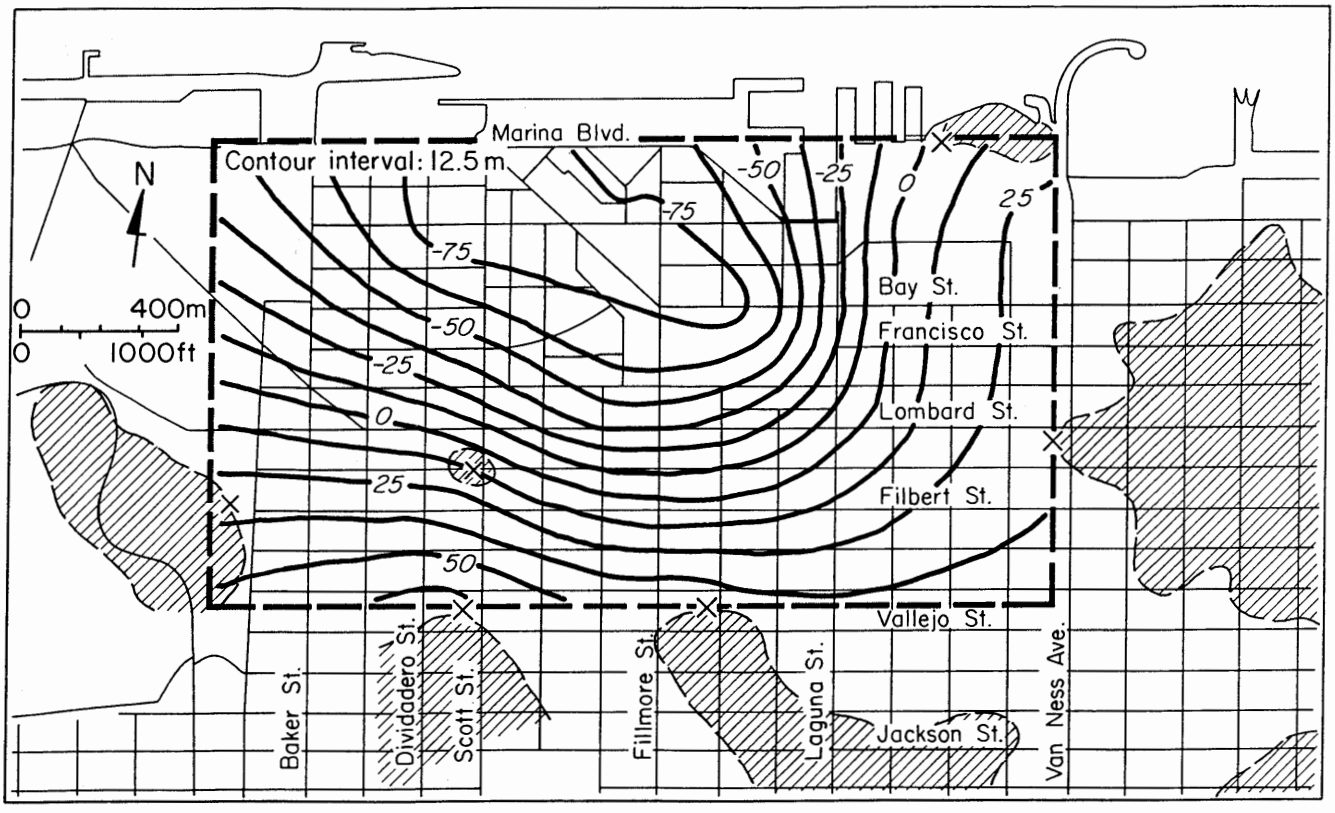


Figure 14.—Contours of equal elevation, relative to San Francisco city datum, of bedrock surface underlying the Marina District. Diagonal-lined areas, bedrock-outcrops from Schlocker (1974).

Table 5.—*Settlement and vertical strain for natural-sand deposits*

| Settlement (mm) | Location | Thickness of natural sand below water table (m) | Vertical strain (percent) |
|---|---|---|---|
| 11 | Divisadero Street between Beach and North Point Streets (2 locations) | 4.5 | 0.2 |
| 7 | Bay Street near Baker Street. | 4.2 | .2 |
| 5 | Fillmore Street near Chestnut Street. | 8.7 | .1 |

generally at least 15 percent (O'Rourke and others, 1991b).

O'Rourke and others (1991b) suggested that the average fines content of the hydraulic fill results in soil conditions not fully consistent with those for relatively clean sand and the median grain sizes of soils on which the simplified strain-estimation procedures of Tokimatsu and Seed (1987) are based. They suggested that an increase in the corrected SPT values would account for the influence of fines content on diminishing the vertical strains resulting from postliquefaction consolidation. These increased SPT values could then be used in Tokimatsu and Seed's diagram (fig. 21) to estimate the vertical strain. Their reasoning, however, was based on the assumption that the hydraulic fill has a relatively consistent, silty-sand composition. This type of soil characterization emerges from an evaluation of borehole data that utilize SPT measurements and split-spoon sampling.

We examined the characteristics of the hydraulic fill in greater detail by means of the CPT soundings. As explained previously, CPT measurements can be used to distinguish relatively thin layers of silty and clayey soils that would not be expected to liquefy. Moreover, in soil types that are susceptible to liquefaction, the modified cone-tip resistance, $q_{c1}$, can be used to assess the liquefaction potential.

The settlements observed near five CPT soundings in hydraulic fill are summarized in table 6. The net liquefiable thickness was determined by subtracting the cumulative thickness of silty and clayey soils as well as soils with

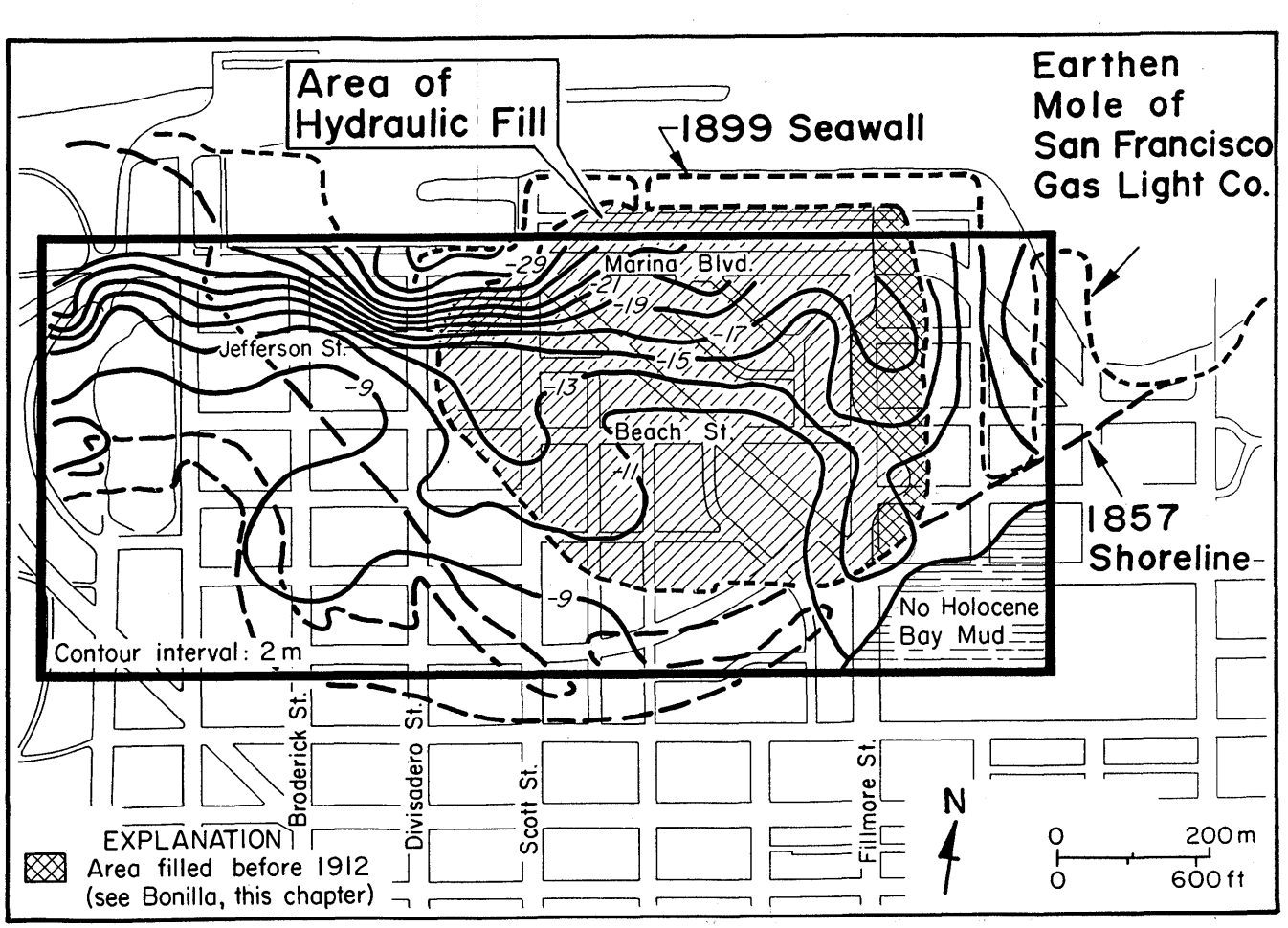


Figure 15.—Contours of equal elevation, relative to San Francisco city datum, of bottom of Holocene bay mud.

Table 6.—*Settlement and vertical strain deduced from CPT soundings*

| CPT sounding (fig. 11) | Settlement (mm) | Fill thickness below water table (m) | Net liquefiable thickness (m) | Vertical strain (percent) |
|---|---|---|---|---|
| C-4 | 95 | 4.5 | 2.4-3.2 | 3.0-4.0 |
| C-7 | 80 | 5.3 | 2.4 | 3.3 |
| C-8 | 135 | 5.0 | 2.9 | 4.7 |
| C-10 | 95 | 4.5 | 2.4-3.9 | 2.4-4.0 |
| C-15 | 60 | 5.1 | 2.0 | 3.0 |
| | | | Average | 3.5 |

Table 7.—*Comparison of observed and predicted vertical strains*

| Soil type | Observed vertical strain (percent) | | Predicted vertical strain (percent) | |
|---|---|---|---|---|
| | With CPT adjustment | Without CPT adjustment | Tokimatsu and and Seed (1987) | Ishihara and and Yoshimine (1992) |
| Natural-sand deposits. | --- | 0.2 | 0.3 | 0.2 |
| Land-tipped fill: | | | | |
| <3.5 m deep | --- | 2.2 | 2.2 | 2.7 |
| >3.5 m deep | --- | 2.1 | 1.3 | 1.8 |
| Hydraulic fill. | 3.5 | 2.1 | 3.7 | 4.5 |

a high $q_{c1}$ value relative to their liquefaction threshold from the total submerged thickness. For some soundings, such as C–10, there was uncertainty regarding the soil composition at a particular depth. At these sites, the net liquefiable thickness was estimated as an upper and lower bound. The vertical strain was computed by dividing the settlement by the net liquefiable thickness.

The observed and predicted vertical strains for the various soil types in the Marina District are compared in table 7. Predictions were made on the basis of corrected SPT values, using the techniques of Tokimatsu and Seed (1987) and Ishihara and Yoshimine (1992). Because of the increase in in situ density with depth for the land-tipped fills (see fig. 19), the vertical strains in these soils were evaluated for depths less than and greater than 3.5 m. The predicted and observed vertical strains agree closely for natural-sand deposits and land-tipped fills, whereas the

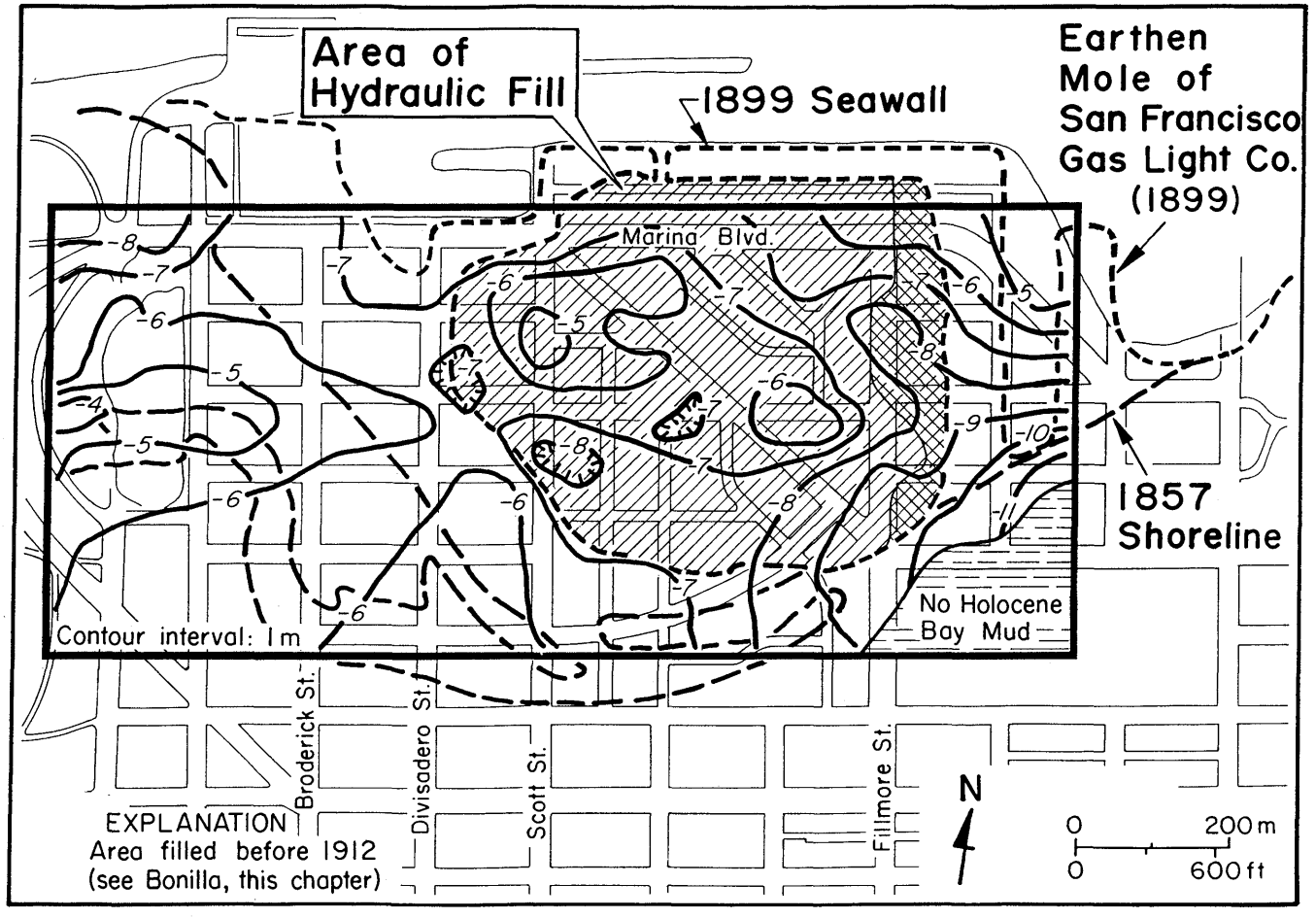


Figure 16.—Contours of equal elevation, relative to San Francisco city datum, of top of Holocene bay mud.

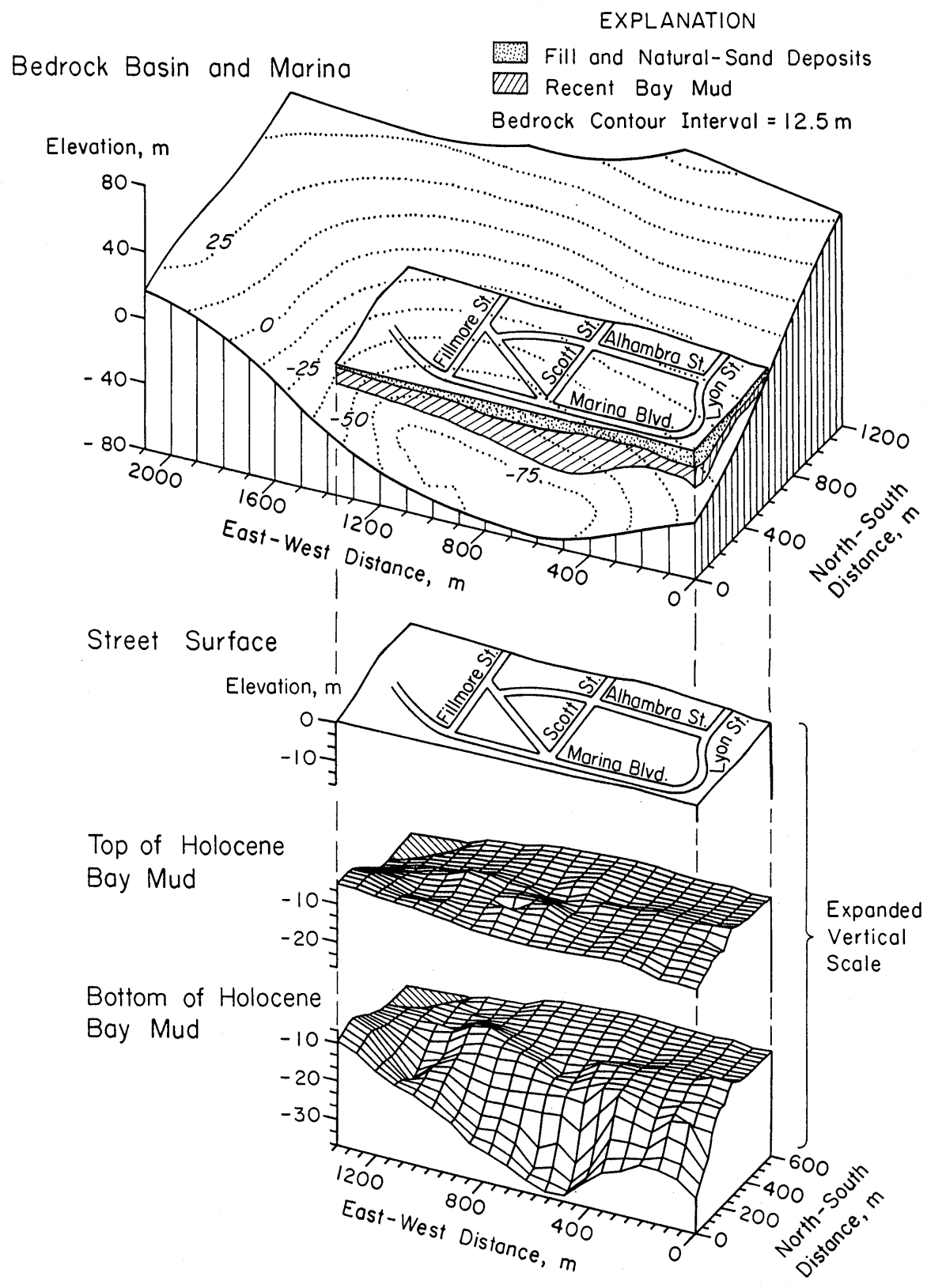


Figure 17.—Block diagram of the Marina District, generated by computer on the basis of borehole and CPT logs. View southeastward.

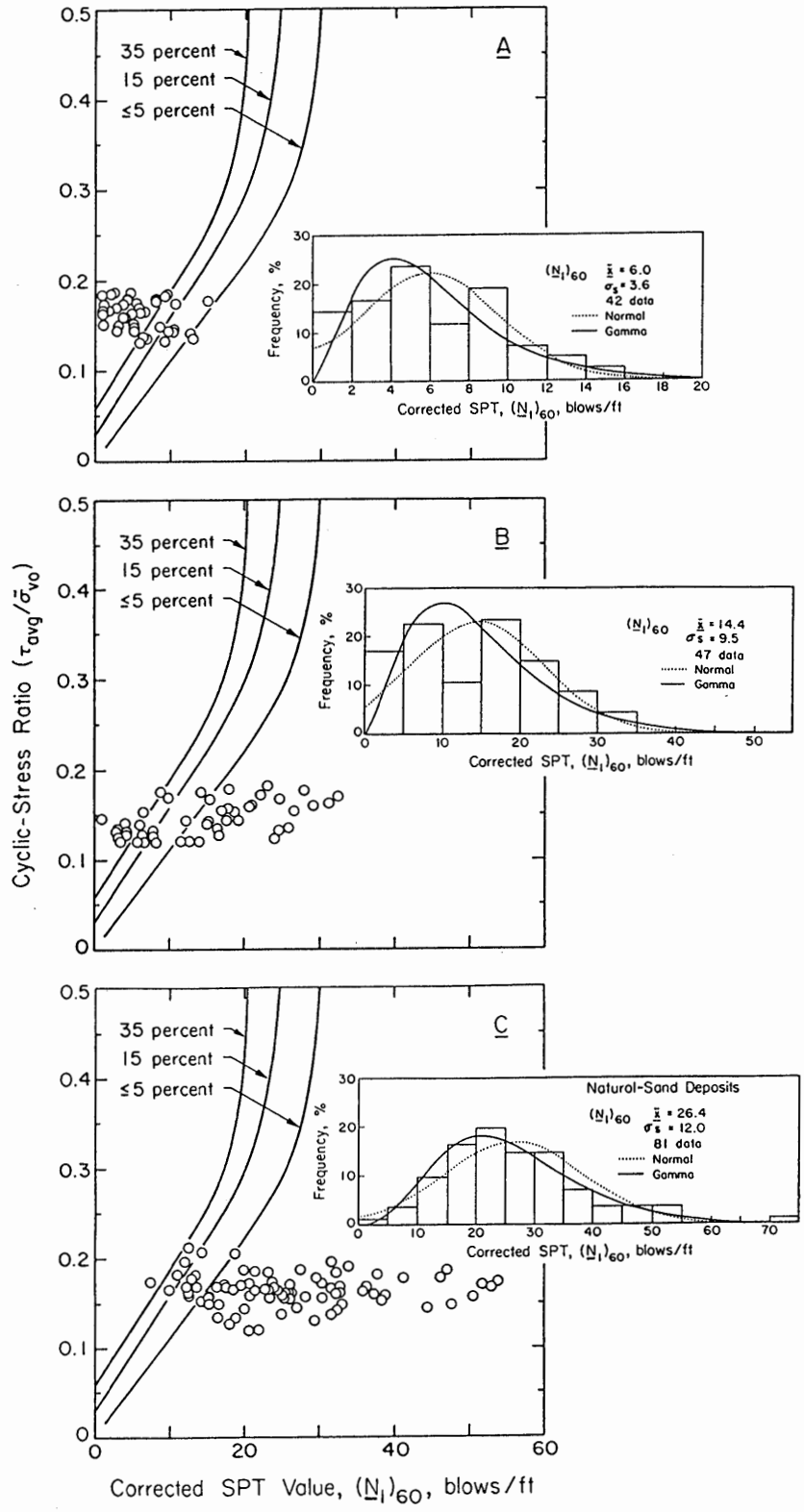


Figure 18.—Cyclic-stress ratio versus corrected SPT value at different fines contents for hydraulic fill (*A*), land-tipped fills (*B*), and natural-sand deposits (*C*). Fines content is defined as proportion (in weight percent) of soil that is silt size or smaller (≤0.075 mm). Curves show boundaries of liquefaction potential for an $M$=7.1 earthquake, according to procedure of Seed and others (1985); data points to left of curves indicate increasing susceptibility to liquefaction. Histograms, showing normal and gamma frequency distributions of corrected SPT values, provide a measure of variation in soil density. $\bar{x}$, mean; σ, standard deviation.

predicted strains are from 75 to 114 percent higher than those observed for the hydraulic fill, using the total fill thickness. When the net liquefiable thickness is adjusted on the basis of CPT measurements, the vertical strains inferred from observed settlements compare quite favorably with the predicted strains.

Note that the vertical strains in the hydraulic fill predicted solely on the basis of corrected SPT values will be influenced by the relatively low SPT values associated with layers of silt and clay. Even though these fine-grained layers are discounted when estimating the net liquefiable thickness, there is no direct way to remove the associated SPT values from data on the hydraulic fill. An alternative approach for predicting the vertical strain is to use CPT measurements directly in conjunction with the technique of Ishihara and Yoshimine (1992). The potential vertical strain for each increment of cone penetration can be determined from charts developed by Ishihara and Yoshimine, using the $q_{c1}$ value to estimate the relative density and the $FS_L$ value. The vertical strains determined in this way for each increment of thickness can be averaged to provide an average strain, or integrated over the full

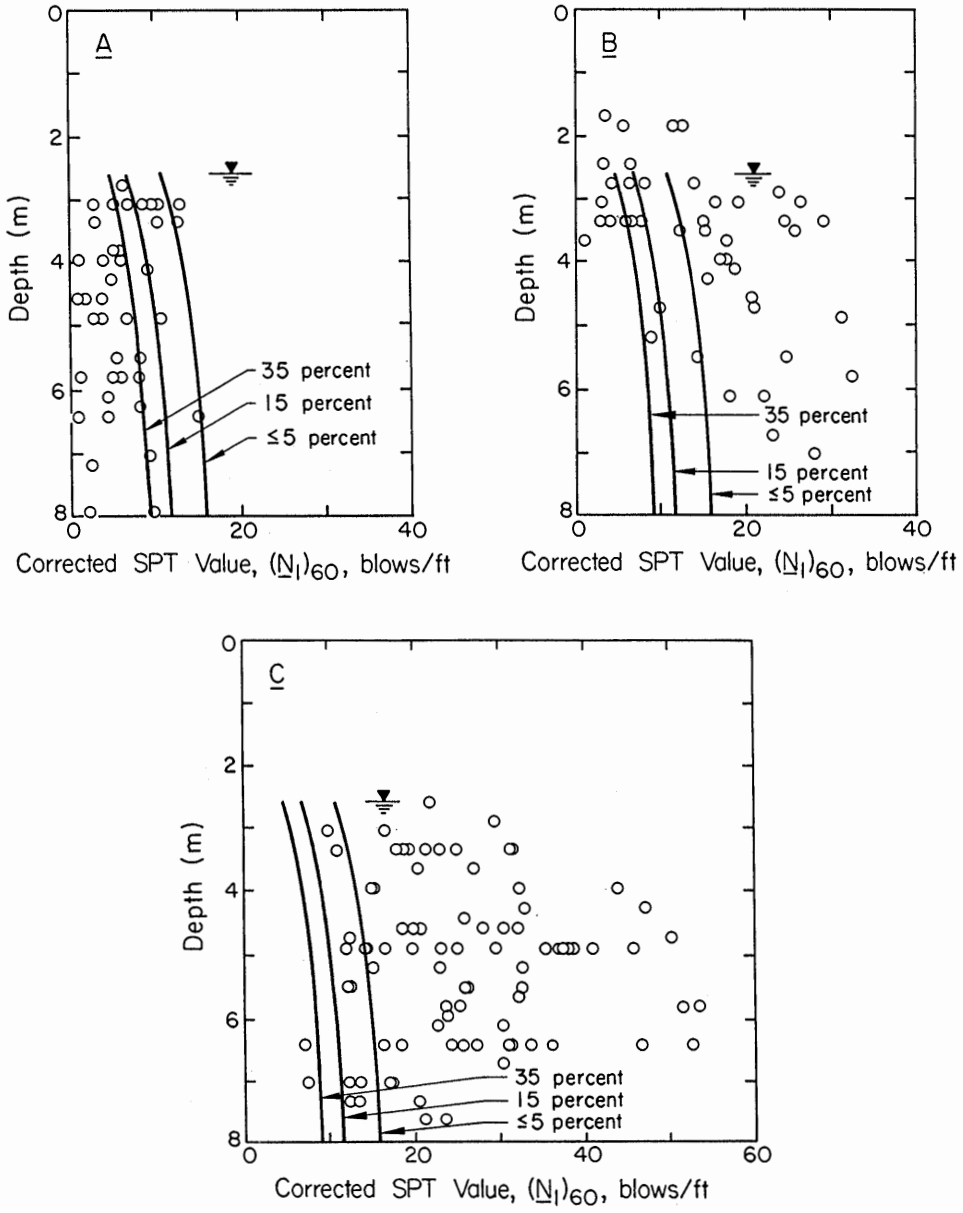


Figure 19.—Depth versus corrected SPT value at different fines contents for hydraulic fill (*A*), land-tipped fills (*B*), and natural-sand deposits (*C*). Fines content is defined as proportion (in weight percent) of soil that is silt size or smaller (≤0.075 mm). Curves show boundaries of liquefaction potential for an $M$=7.1 earthquake, according to procedure of Seed and others (1985); data points to left of curves indicate increasing susceptibility to liquefaction. Inverted triangles denote depth to water table.

thickness to yield an estimated settlement. Although the details are beyond the scope of this report, this approach nonetheless represents a potentially useful area for further study and evaluation.

Strong evidence exists that the liquefaction behavior of the hydraulic fill is influenced by the presence of fine-grained soil layers. When the net thickness of sand and silty sand most susceptible to liquefaction is assessed, the agreement between the observed and predicted vertical strains is good. This result indicates that the resolution provided by CPT measurements is an important factor in estimating the magnitude and extent of postliquefaction consolidation for these and similar soils. Investigations by Martin and others (1991) on the practical assessment of liquefaction effects also emphasize the importance of CPT characterization. The hydraulic fill, because it may contain relatively thin fine-grained soil layers, is likely to require more detailed evaluation for assessing postliquefaction settlement than can be supplied by SPT measurements.

## DISTRIBUTION OF SETTLEMENT

As discussed above, the highest concentrations of differential settlement and, thus, of damage to buried utilities depend on the boundaries among the fills, natural-sand de-

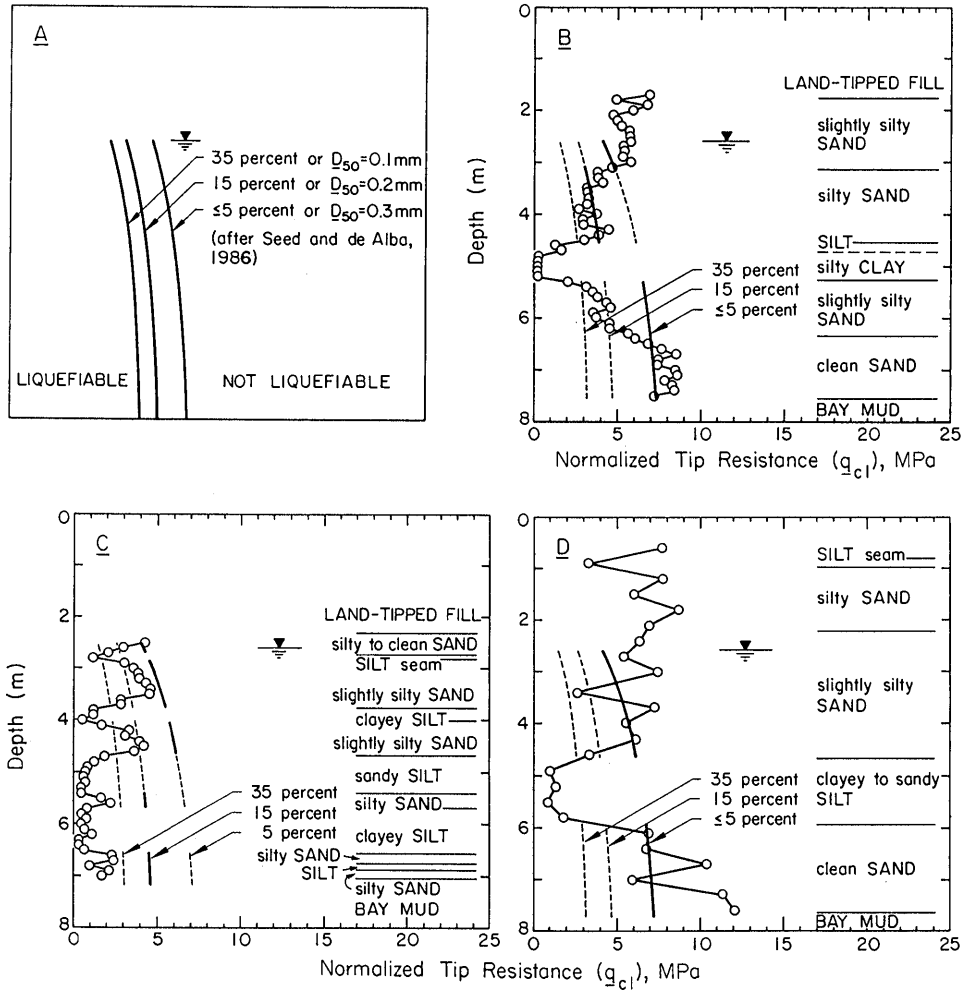


Figure 20.—Depth versus normalized tip resistance at different fines contents for hydraulic fill (*A*) and for CPT soundings C–8 (*B*), C–4 (*C*), and C–15 (*D*) (see fig. 11 for locations). Fines content is defined as proportion (in weight percent) of soil that is silt size or smaller (≤0.075 mm). Profiles in figure 20*A* were calculated for an $M$=7.1 earthquake, according to procedure of Seed and others (1985); profiles in figures 20*B* through 20*D* were plotted according to procedure of Seed and de Alba (1986). In figures 20*B* through 20*D*, solid curves denote appropriate liquefaction potential for specific depths and soil types, and dashed curves are shown for reference. Data points to left of curves indicate increasing susceptibility to liquefaction; breaks in curves indicate that a particular soil layer is not readily susceptible to liquefaction. Inverted triangles denote depth to water table.

posits, and old seawalls, as well as on the properties and thicknesses of soils susceptible to liquefaction. Given that existing simplified methods provide reasonably good estimates of the vertical strain from postliquefaction consolidation, accurate prediction of buried-lifeline damage will also require an assessment of differential settlement and, thus, a knowledge of the variation in fill thickness.

The relation between settlement and fill thickness is illustrated in figure 22, which shows a simplified cross section along Divisadero Street (*C–C'*, fig. 11). Note that some of the most extensive damage to pipelines and the heaviest concentration of building damage were on Divisadero Street, primarily in the area from Beach Street to Marina Boulevard.

Cross section *C–C'* shows that the settlement profile along Divisadero Street is closely related to the thickness of land-tipped fills. The locations of maximum settlement coincide with increasing fill thickness from Beach Street to Marina Boulevard, as well as with increasing fill thickness in a zone once occupied by a tidal marsh south of old Strawberry Island. The zone of minimum settlement coincides with Strawberry Island and its associated natural-sand deposits. As shown in figures 3 and 7, the locations of maximum settlement and angular distortion between Beach Street and Marina Boulevard and near Francisco Street are also the locations of greatest damage to MWSS pipelines and collector sewers along Divisadero Street.

## CONCLUDING REMARKS

Information obtained from our investigations in the Marina District has provided insight critically important for the design and planning of lifeline systems in relation to local geology and soil conditions. Because the historical development of the Marina District is well understood, at least three different local soil types can be identified with reasonable accuracy: (1) hydraulic fill; (2) fills tipped from the shoreline or during seawall construction, herein referred to as land-tipped fills; and (3) natural beach, dune, and sand-spit deposits. Comparisons of the observed vertical strains in each of these three soil types with those predicted on the basis of simplified procedures indicate that the predicted and observed vertical strains agree closely for the natural-sand deposits and land-tipped fills, whereas the predicted strains are substantially higher than the observed strains in hydraulic fill, using only SPT measurements. When the net liquefiable thickness is adjusted on the basis of CPT measurements, the vertical strains inferred from observed settlements compare quite favorably with the predicted strains.

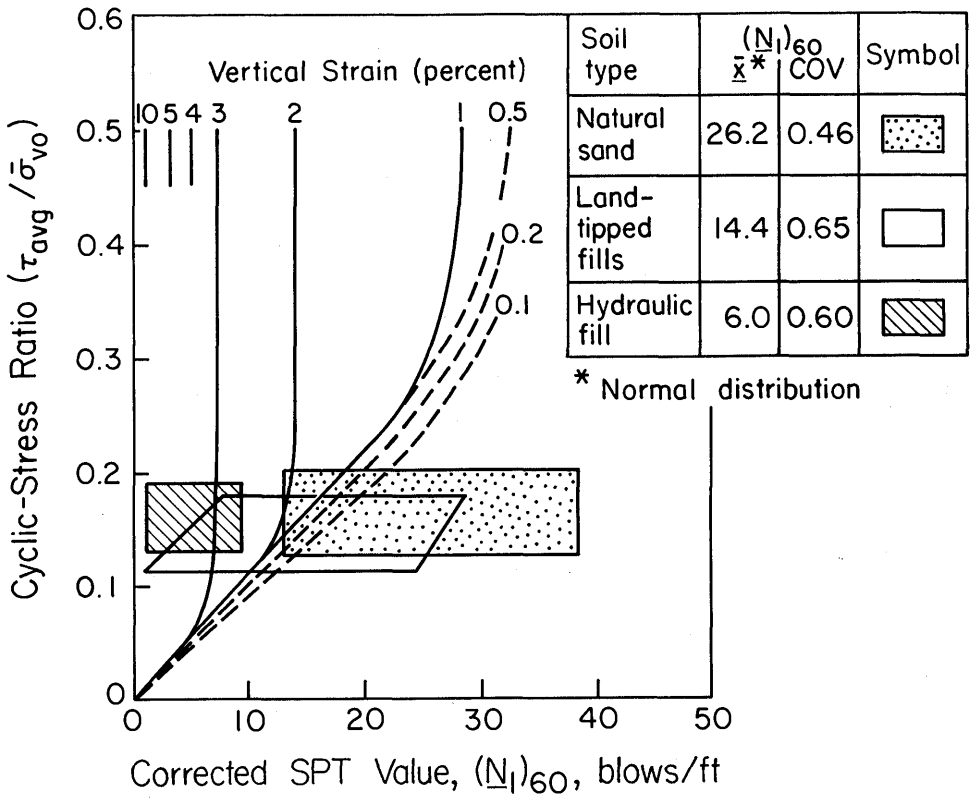


Figure 21.—Cyclic-stress ratio versus corrected standard-penetration-test value for hydraulic fill, land-tipped fills, and natural-sand deposits, superimposed on chart of Tokimatsu and Seed (1987) for estimating vertical strain caused by postliquefaction consolidation. COV, coefficient of variation; $\bar{x}$, mean.

The liquefaction behavior of the hydraulic fill in the Marina District was apparently influenced by the presence of fine-grained soil layers. The resolution in delineating subsurface conditions by CPT measurements is shown to be an important factor in estimating the magnitude and extent of postliquefaction consolidation in the hydraulic fill. Hydraulic fill, because it may be interstratified with fine-grained soils, is likely to require more detailed evaluation for assessing postliquefaction settlement than can be supplied by the widely used methods of SPT measurements and split-spoon sampling.

## ACKNOWLEDGMENTS

This study was sponsored by the National Center for Earthquake Engineering Research, Buffalo, N.Y., under project 893008, and by the National Science Foundation grant BCS–90 11458. We especially thank T. Dickerman of the San Francisco Water Department, F. Blackburn and A. Nielsen of the San Francisco Fire Department, J. Clark of the Pacific Gas and Electric Co., and P.T. Law and S. Yu of the Clean Water Program, all for their help in gathering lifeline data; and T.L. Holzer and M.J. Bennett of the U.S. Geological Survey, R. Darragh and D. Koutsoftas of Dames & Moore, H. Taylor of Harding Lawson Associates, and M. Power of Geomatrix for their help in gathering geotechnical data. We appreciate the assistance of Ted Gowdy, who helped prepare data bases and performed three-dimensional computer analyses, A. Avcisoy, who drafted the illustrations, and L. Mayes and K.J. Stewart, who typed the manuscript.

## REFERENCES CITED

American Society for Testing and Materials, 1991a, Standard test method for deep, quasi-static, cone and friction-cone penetration tests of soil, *in* 1991 annual book of standards: Philadelphia, v. 4.08, p. 439–444.

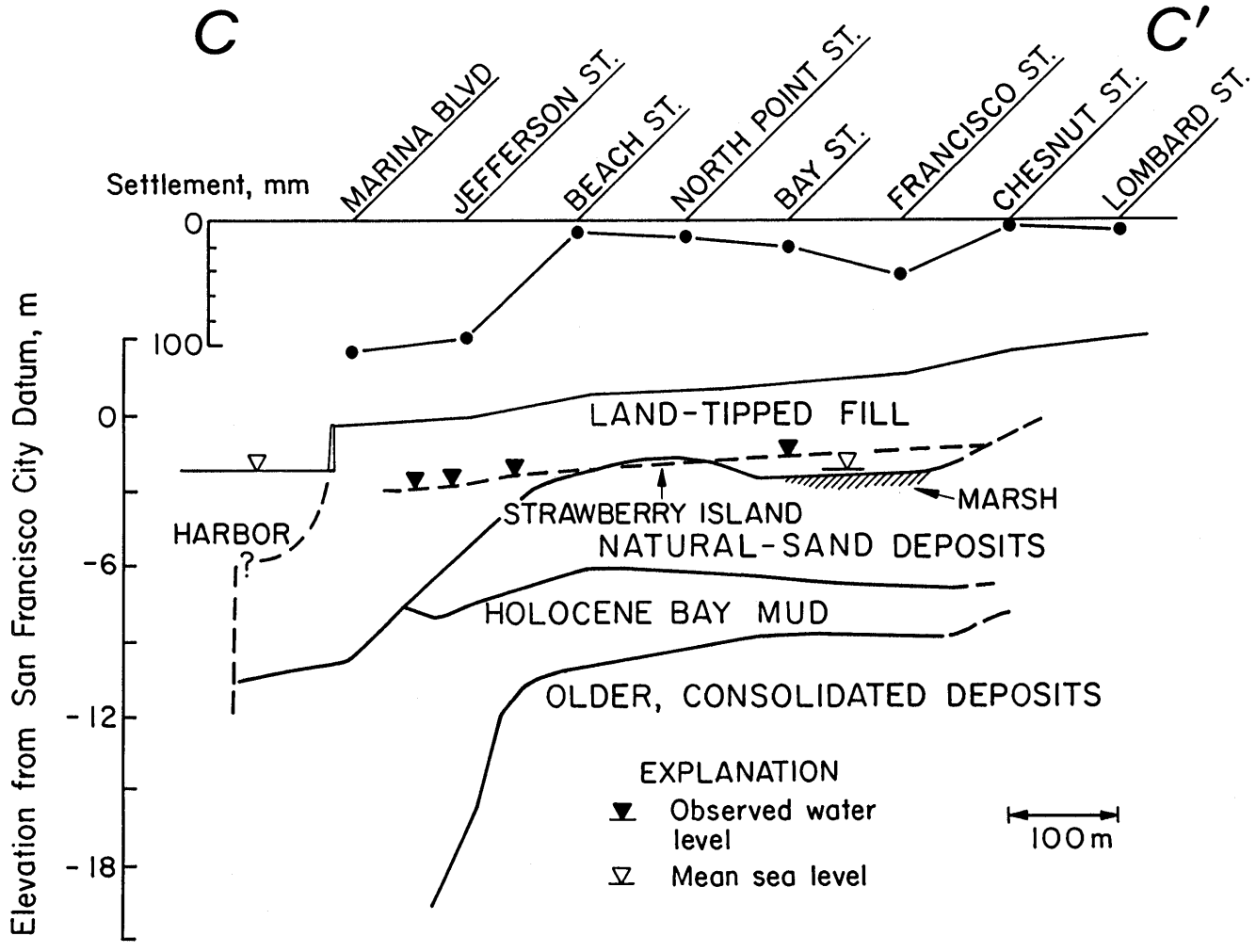


Figure 22.—Cross section *C-C′* along Divisadero Street, showing settlement profile, water table, and stratification of underlying soils. See figure 11 for location.

———1991b, Standard test method for penetration test and split-barrel sampling of soils, *in* 1991 annual book of ASTM standards: Philadelphia, v. 4.08, p. 232–239.

Bardet, J.P., and Kapuskar, M., 1991, Site investigation of the Marina District of San Francisco in September 1990, *in* report to National Science Foundation: Los Angeles, University of Southern California, Civil Engineering Department, 93 p.

Bardet, J.P., Kapuskar, M., and Martin, G.R., 1991, Dynamic response of the Marina District of San Francisco during the 1989 Loma Prieta earthquake, *in* Japan-U.S. Workshop on Earthquake-Resistant Design of Lifeline Facilities and Countermeasures for Soil Liquefaction, 3d, San Francisco, 1991, Proceedings: Buffalo, N.Y., National Center for Earthquake Engineering Research, Report NCEER–91–0001, p. 109–128.

Bennett, M.J., 1990, Ground deformation and liquefaction of soil in the Marina District, *in* Effects of the Loma Prieta earthquake on the Marina District, San Francisco, California: U.S. Geological Survey Open-File Report 90–253, p. D1–D36.

Benuska, Lee, ed., 1990, Loma Prieta earthquake reconnaissance report: Earthquake Spectra, v. 6, supp. 90–01, 448 p.

Bonilla, M.G., 1991, The Marina District, San Francisco, California—geology, history, and earthquake effects: Seismological Society of America Bulletin, v. 81, no. 5, p. 1958–1979.

Dames & Moore, 1989, Factual report, site investigation for completion of preliminary design—phase I, Muni Metro Turnaround Facility; report for Bechtel National, Inc., Job 185–215–03: San Francisco, v. 2.

Gilbert, G.K., Humphrey, R.L., Sewell, J.S., and Soulé, F., 1907, The San Francisco earthquake and fire of April 18, 1906, and their effects on structures and structural materials: U.S. Geological Survey Bulletin 324, 170 p.

Harding Lawson Associates, Dames & Moore, Kennedy/Jenks/Chilton, and EQE Engineering, 1991, Liquefaction study, Marina District and Sullivan Marsh area, San Francisco, California: final report prepared for San Francisco Department of Public Works: San Francisco, 144 p.

Ishihara, Kenji, and Yoshimine, M., 1992, Evaluation of settlements in sand deposits following liquefaction during earthquakes: Soils and Foundations, v. 32, no. 1, p. 1–22.

Jones, E.C., 1906, The story of the restoration of the gas supply in San Francisco after the fire, *in* Pacific Gas Association Annual Meeting, 14th, San Francisco, 1906, Proceedings, p. 350–364.

Lawson, A.C., chairman, 1908, The California earthquake of April 18, 1906; report of the California State Earthquake Investigation Commission: Carnegie Institution of Washington Publication 87, 2 v.

Martin, G.R., Tsai, C.-F., and Arulmoli, K., 1991, A practical assessment of soil liquefaction effects and remediation needs: International Conference on Recent Advances in Geotechnical Earthquake Engineering and Soil Dynamics, 2d, St. Louis, Mo., 1991, Proceedings, v. 1, p. 411–418.

Mitchell, J.K., Tahir, M., Kayen, R.E., and Seed, R.B., 1990, Soil conditions and earthquake hazard mitigation in the Marina District of San Francisco; report to mayor of San Francisco: San Francisco, 59 p.

Olmsted, R., Olmsted, N., and Pastron, A., 1977, San Francisco waterfront—report on historical cultural resources for the north shore and channel outfalls consolidation projects: San Francisco, Wastewater Management Program, 728 p.

Olsen, R.S., and Farr, J.V., 1986, Site characterization using the cone penetrometer test, Clemence, S.P., ed., *in* Use of in-situ tests in geotechnical engineering: American Society of Civil Engineers Geotechnical Special Publication 6, p. 854–868.

O'Rourke, T.D., Gowdy, T.E., Stewart, H.E., and Pease, J.W., 1991a, Lifeline and geotechnical aspects of the 1989 Loma Prieta earthquake: International Conference on Recent Advances in Geotechnical Earthquake Engineering and Soil Dynamics, 2d, St. Louis, Mo., 1991, Proceedings, v. 2, p. 1601–1612.

———1991b, Lifeline performance and ground deformation in the Marina during 1989 Loma Prieta earthquake, *in* Japan-U.S. Workshop on Earthquake-Resistant Design of Lifeline Facilities and Countermeasures for Soil Liquefaction, 3d, San Francisco, 1991, Proceedings: Buffalo, N.Y., National Center for Earthquake Engineering Research, Report NCEER–91–0001, p. 129–146.

Phillips, S.H., and Virostek, J.K., 1990, Natural gas disaster planning and recovery—the Loma Prieta earthquake: San Francisco, Pacific Gas and Electric Co., 39 p.

Ripley, B.D., 1981, Spatial statistics: New York, Wiley, 252 p.

Robertson, P.K., and Campanella, R.G., 1983, Interpretation of cone penetration tests, part I—sand: Canadian Geotechnical Journal, v. 20, no. 4, p. 718–733.

Sanborn Ferris Map Co., 1899 [1905], Insurance maps: San Francisco, 4 v.

Schlocker, Julius, 1974, Geology of the San Francisco North quadrangle, California: U.S. Geological Survey Professional Paper 782, 109 p.

Seed, H.B., 1987, Design problems in soil liquefaction: Journal of Geotechnical Engineering, v. 113, no. 8, p. 827–845.

Seed, H.B., and de Alba, Pedro, 1986, Use of SPT and CPT tests for evaluating the liquefaction resistance of sands, *in* Clemence, S.P., ed., Use of in situ tests in geotechnical engineering: American Society of Civil Engineers Geotechnical Special Publication 6, p. 281–302.

Seed, H.B., Idriss, I.M., and Arango, Ignacio, 1983, Evaluation of liquefaction potential using field performance data: Journal of Geotechnical Engineering, v. 109, no. 3, p. 458–482.

Seed, H.B., Tokimatsu, Kohji, Harder, L.F., and Chung, R.M., 1985, Influence of SPT procedures in soil liquefaction resistance evaluations: Journal of Geotechnical Engineering, v. 111, no. 12, p. 1425–1445.

Tokimatsu, Kohji, and Seed, H.B., 1987, Evaluation of settlements in sands due to earthquake shaking: Journal of Geotechnical Engineering, v. 113, no. 8, p. 861–878.

Tomlinson, M.J., 1986, Foundation design and construction (5th ed.): Harlow, U.K., Longman, 842 p.

U.S. Coast Survey, 1857, Topographic map of city of San Francisco and its vicinity, California: scale 1:10,000.

U.S. Geological Survey, 1990, Effects of the Loma Prieta earthquake on the Marina District, San Francisco, California: Open–File Report 90–253.

THE LOMA PRIETA, CALIFORNIA, EARTHQUAKE OF OCTOBER 17, 1989:
STRONG GROUND MOTION AND GROUND FAILURE

MARINA DISTRICT

# EFFECTS OF GROUND CONDITIONS ON THE DAMAGE TO FOUR-STORY CORNER APARTMENT BUILDINGS

By Stephen K. Harris, EQE Engineering and Design; and
John A. Egan, Geomatrix Consultants

## CONTENTS



ABSTRACT

Damage in the Marina District from the earthquake was concentrated in one class of building: four-story, wood-frame corner apartment buildings, which accounted for six of the seven building collapses. Construction in the district is quite uniform in configuration and material; however, ground conditions vary widely, from firm, competent sand, through soft natural clay and silt, to liquefaction-susceptible hydraulic fill.

On the basis of postearthquake observations of ground-failure phenomena and borehole data, the Marina District was divided into three soil-profile zones: a ground-failure zone, bayward of the old (1851) shoreline and characterized by thick recent (post-1906) fill underlain by deep bay mud, within which substantial ground-failure effects were observed; a "soft"-soil-profile zone, also bayward of the old shoreline, characterized by older (pre-1906) fill underlain by dense natural-sand deposits and deep, old bay mud; and a "firm"-soil-profile zone, landward of the old shoreline, characterized by competent natural-sand deposits overlying relatively thin or no bay mud. We expect that ground shaking in the Marina District varied considerably among these three zones.

Estimated response spectra indicating amplified spectral ordinates of approximately 5 for the "soft"-soil-profile zone were calculated from ground motions recorded on bedrock in Pacific Heights. Using these response spectra, a simplified, single-degree-of-freedom dynamic analysis of the corner buildings was undertaken. Building weights ranging from 400 to 500 kips (1,800–2,200 kN), and wall stiffnesses of 0.67 kips/in. per foot of wall (385 kN/m per meter of wall), were estimated. Building periods ranging from 0.8 to 1.25 s were computed. Correlations were made between spectral displacement and observed damage, indicating a maximum spectral displacement for the heavily damaged buildings approximately equal to the observed permanent lateral deformation, and between structural base shear and observed damage, suggesting a damage threshold of approximately 15 to 20 kips/ft (225–300 kN/m). Results indicate that the severe damage to this class of buildings in the Marina District was due to a combination of factors, particularly the near-coincidence of the fundamental building period with the maximum spectral displacement.

## INTRODUCTION

The Marina District of San Francisco was one of the most heavily damaged areas in the earthquake. Damage included building collapse, underground-pipe breakage, and road and sidewalk damage due to ground shaking and liquefaction-related ground failure. Of the more than 1,400 buildings in the Marina District, 7 collapsed, and another 65 were moderately to severely damaged. Damage was concentrated in one class of building: four-story, wood-frame corner apartment buildings; the 74 buildings in this class accounted for 6 of the 7 collapses. Because of the great uniformity in construction of these buildings, it is reasonable to question the nonuniformity in their apparent damage. Ground conditions throughout the district vary widely, from firm, competent sand, through soft natural clay and silt, to liquefaction-susceptible hydraulic fill. This report discusses the effects of ground conditions on the response and performance of these buildings.

## DESCRIPTION OF BUILDINGS

The Marina District was built in the late 1920's and early 1930's, after the 1915 Panama-Pacific International Exposition. Construction until 1930 was all wood frame; after 1930, the large garages under apartment buildings were built of noncombustible materials (masonry or concrete) instead of wood frame. Most of the buildings are single-family dwellings or flats. About 5 percent of the total Marina District building stock consists of pre-1930, wood-frame corner apartment buildings (Harris and others, 1990), which are the focus of this report.

All the corner buildings are four-story structures, with three residential levels over a parking garage. Although several of these buildings were built on acute-angle corners and are triangular in plan, most (50 of 74) are rectangular, with plan dimensions of approximately 50 by 75 ft (15 by 23 m). Of these buildings, nearly all are oriented with their 50-ft (15 m) dimension oriented north-south. The distribution of years of construction (79 percent of the buildings were built between 1926 and 1928; Real Estate Data, Inc., 1991) is plotted in figure 1 and the distribution of building area (68 percent of the buildings are from 10,000 to 14,000 ft$^2$ [900 and 1,300 m$^2$] in area; Real Estate Data, Inc., 1991) is plotted in figure 2.

Because of the garages at their bottom levels, the corner buildings have many garage-door openings on both street sides. In general, the two street sides of the buildings are completely open, except for 10 to 20 ft (3–6 m) on one side near the corner. A typical garage-level building plan is shown in figure 3.

## GEOTECHNICAL ASPECTS

The land of the present Marina District consists of areas of native soil deposits (beach, dune, and older alluvium) and artificial fills created during several periods of filling from about 1851 to 1917. Areas adjacent to the original shoreline (U.S. Coast Survey, 1851) and sloughs that meandered inland from the old shoreline were filled before 1894. At that time, a seawall was constructed that partly enclosed the Marina lagoon and, over the next decade, small amounts of fill were placed adjacent to the seawall. After the great 1906 San Francisco earthquake, principally in 1912, the enclosed lagoon area was hydraulically filled with sand and silt in preparation for the Panama-Pacific International Exposition held in 1915; this hydraulically filled area is now the central part of the Marina District. Minor filling, grading, and leveling were performed after the exposition, but in general the land in the Marina District was little modified between 1917 and 1989. (See Bonilla, this chapter, for a more detailed account of the Marina District's development.

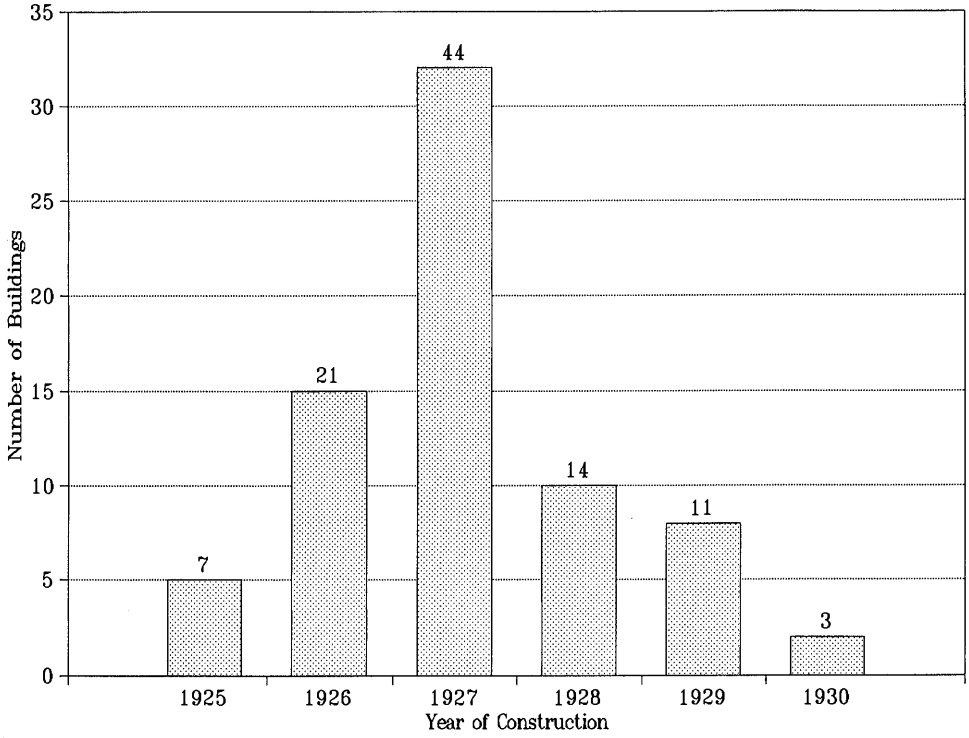


Figure 1.—Number of buildings in the Marina District versus year of construction. Numbers at top of bars indicate percentage of total.

After the 1989 earthquake, effects of strong ground shaking and liquefaction could be observed throughout the Marina District. Liquefaction and ground failure were manifested by sand boils; subsurface voids; horizontal and vertical spreading cracks in pavements, sidewalks, and soil; areal subsidence; settlement; distortion of residential buildings; compressional buckling of sidewalks and curbs; and utility-line breaks. Street-by-street mapping of geotechnical effects was conducted, and the more significant of these observations are summarized in figure 4, with the

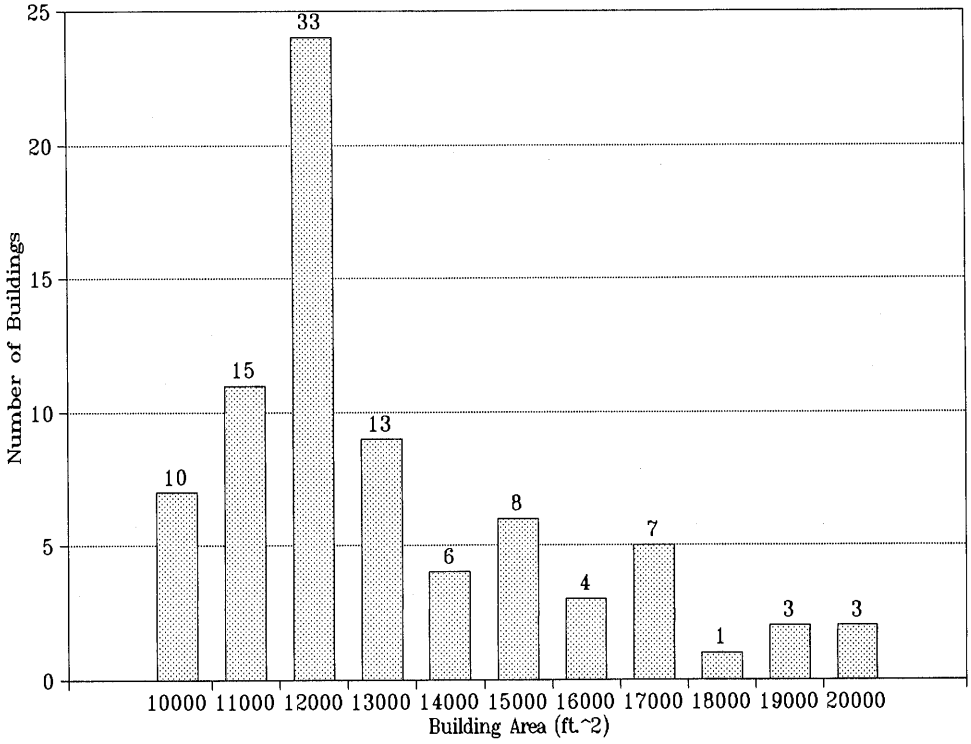


Figure 2.—Number of buildings in the Marina District versus building area. Numbers at top of bars indicate percentage of total.

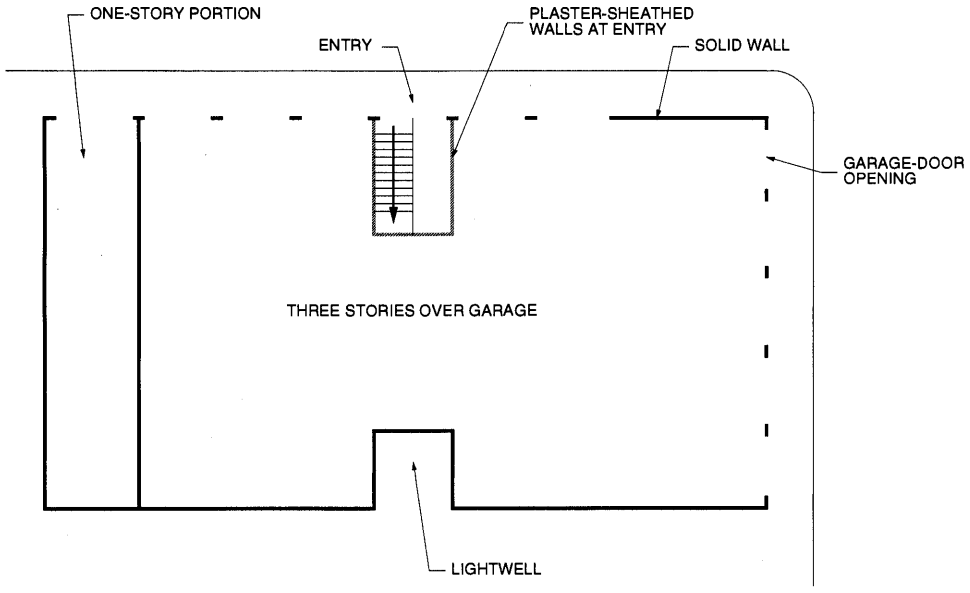


Figure 3.—Typical garage-level building plan, showing solid-wall construction of brick veneer or stucco over straight wood sheathing over wood studs. Not to scale.

location of the original shoreline (U.S. Coast Survey, 1851) drawn for reference. Examination of the pattern of observations shown in figure 4 indicates that the areas of lateral-spreading cracks, liquefaction sand boils, settlement, and buckling coincide well and define what may be considered as the ground-failure zone. This zone lies bayward of the old shoreline, extending about 3,000 ft (900 m) along Marina Boulevard between Webster and Broderick Streets and inland as far as about the intersection of Alhambra and Avila Streets. Note that a close spatial correlation exists between the ground-failure zone identified in figure 4 and the area of fill placed after 1906. Geotechnical effects did occur outside of the postulated ground-failure zone but appeared to consist primarily of differential building settlements and local subsidence near the old shoreline and in the filled slough channel (fig. 4). For example, a house on Francisco Street near Divisadero Street sustained 1.7 ft (0.5 m) of differential settlement; and farther west along Francisco Street, near Broderick Street, sidewalks and backyard soils exhibited cracks with horizontal widths as large as half an inch (0.01 m) and vertical offsets as large as 1.25 in. (0.03 m). In areas landward of the old shoreline and former slough boundaries, negligible geotechnical effects were observed.

No ground-motion recordings were obtained in the Marina District during the main shock, and so actual ground motions there are unknown. Peak horizontal ground accelerations at nearby bedrock strong-motion-recording stations in Pacific Heights and on Telegraph Hill were 0.06 and 0.08 *g*, respectively, but liquefaction and ground-failure observations indicate that higher levels of ground motion were probably sustained in the Marina District.

Sand boils erupted throughout the ground-failure zone. In most places, ejected sand was dark gray, indicative of the sandy fill dredged from the bay bottom. Results of liquefaction analyses using simplified procedures (Seed and others, 1985) indicate that liquefaction during the main shock was confined primarily to the loose hydraulic fill.

Settlement damage to buildings occurred in many places, mainly along Marina Boulevard. Between Broderick and Scott Streets, several houses settled as much as 6 to 12 in. (0.15–0.3 m), as manifested by unclosable garage doors, buckling of downspouts, and distortion of walls, as well as by cracking of garage slabs. Between Fillmore and Webster Streets, at the other end of the ground-failure zone, houses settled differentially, listing against each other in their final positions. Bearing deformation (punching) of column footings and wall foundations was observed in many places. Lateral spreading was most evident in the vicinity of Winfield Scott School, where movements of as much as 8 in. (0.2 m) were observed. Spreading could be traced easily across the schoolyard to North Point Street near Scott Street, and through the garage of the corner building at Scott and North Point Streets. Several houses

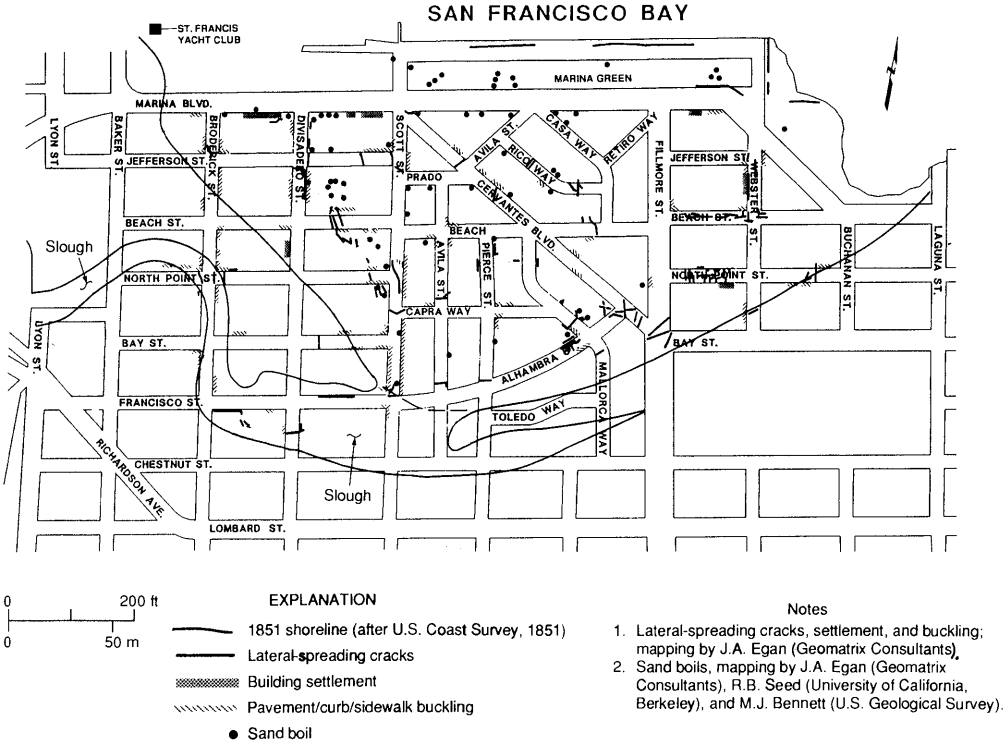


Figure 4.—Marina District, showing locations of earthquake-related liquefaction and ground failure and of 1851 shoreline.

in this area were racked by settlement and lateral movement. Horizontal displacement was also evident along Beach and North Point Streets near Webster Street, where cracks as much as 3 in. (0.08 m) wide opened in the street, and separations between curb and street pavement as great as 5 in. (0.15 m) developed. Several inches of areal subsidence occurred within the ground-failure zone. Subsidence of as much as 5 in. (0.15 m) was observed around a 60-ft (18 m)-diameter inground pump station on the Marina Green near Avila Street. Such vertical and lateral displacements caused broken waterlines and fractured manholes throughout the Marina District; near the seawall and at the St. Francis Yacht Club, lateral-spreading cracks and deformation were quite evident. At the yacht club, differential settlement of 8 in. (0.2 m) was observed between the pile-supported part of the structure and that part supported on spread footings. Finally, a phenomenon observed throughout the ground-failure zone was buckling of sidewalks and curbs, including heave and override of driveway and sidewalk slabs. Although some of this buckling was associated with lateral spreading, we believe that much of it was caused by large, spatially nonuniform displacements.

In examining the ground performance mapped in figure 4, three soil-profile zones can be defined (fig. 5): first, the ground-failure zone; second, a zone between the ground-failure zone and the old shoreline within which relatively minor ground-failure effects were observed; and third, a zone landward of the old shoreline within which ground-failure effects were essentially absent. Ground conditions in these three zones were evaluated by examining the logs of numerous boreholes drilled throughout the Marina District both before and after the earthquake.

The first soil-profile zone is generally characterized by approximately 25 to 30 ft (7.6–9.1 m) of loose to very loose hydraulic fill (sand and silt) overlying Holocene natural sand and soft bay sedimentary deposits, hardpan (older sand), and deep, old bay clay. After the earthquake, the U.S. Geological Survey drilled an exploratory borehole in the Winfield Scott School yard near Beach and Divisadero Streets (within this first soil-profile zone) to investigate subsurface geologic/geotechnical conditions (Kayen and others, 1990). The borehole penetrated about 25 ft (7.6 m) of loose sandy fill overlying Holocene bay mud and natural sand to a depth of about 40 ft (12 m), where a firm material described as "hardpan" was penetrated. Bedrock-contour maps by Schlocker (1974) indicate bedrock at approximately this depth. The borehole continued into and through the hardpan and penetrated clay at a depth of about 75 ft (23 m). The clay stiffens with depth until bedrock is penetrated at a depth of 265 ft (81 m).

The second soil-profile zone is generally characterized by older, medium-dense, surficial fill materials overlying generally dense natural beach sand and, in turn, deep, old bay clay. Given the deep, relatively soft conditions in the ground-failure zone and this "soft"-soil-profile zone, site amplification of ground motions in the Marina District during the main shock may have occurred analogously to that at similar sites of deep, soft sedimentary deposits around the margins of San Francisco Bay, notably

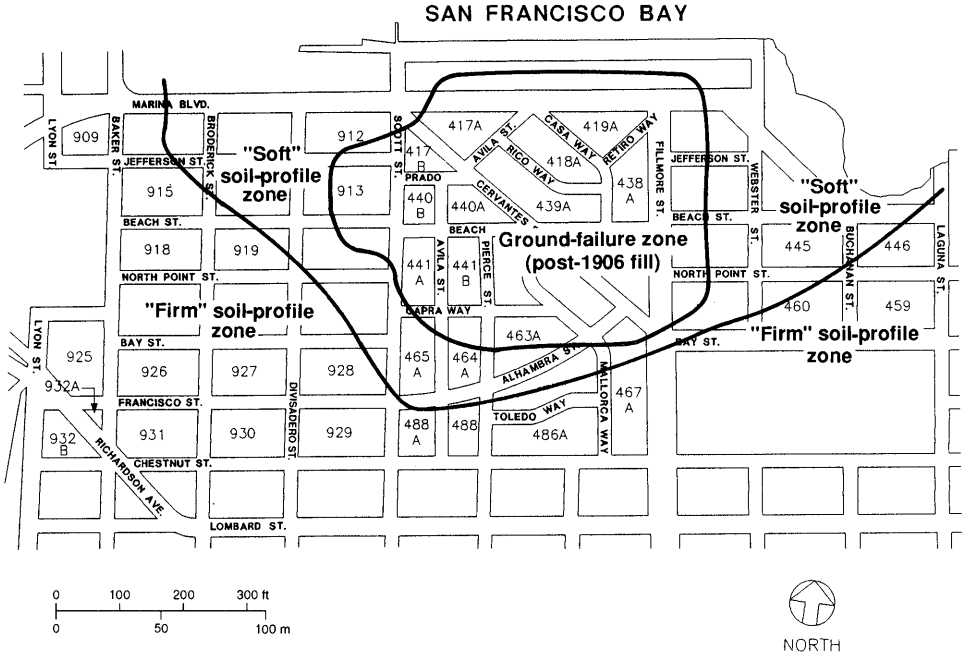


Figure 5.—Marina District, showing locations of three soil-profile zones differentiating relative ground performance during the earthquake. Numbers shown are city block numbers, which are referenced in table 2.

Treasure Island, Emeryville, and Oakland. Aftershock recordings obtained at temporary stations established in the Marina District indicate significant site-amplification effects for low-amplitude bedrock motions nearby (see Boatwright and others and Liu and others, this chapter).

The third soil-profile zone is generally characterized by firm, competent natural beach and (or) dune sand underlain by a considerably lesser thickness or even absence of bay clay. Thus, the ground motions during the earthquake in this "firm"-soil-profile zone landward of the old shoreline are not expected to have been as great as in the "soft"-soil-profile zone bayward of the old shoreline.

## OBSERVED PERFORMANCE

Given their eccentric building plan, we expected that the corner buildings would behave in a highly torsional manner. In general, however, torsion was not exhibited by the damaged buildings: They were seen to lean at the first story, parallel to the street (some leaned in two directions). This nontorsional behavior may be explained by the presence of short, plaster-sheathed walls on each side of the buildings' main-entry doors (see fig. 3); these stiff but brittle walls were able to resist some of the forces generated by the eccentricity. The lightwell walls opposite the main entry also contributed to the buildings' torsional resistance.

The Marina District buildings are built immediately adjacent to each other, without space to allow for lateral drift. Thus, pounding has been identified as one of the main causes of damage to the corner buildings. (The thinking is that the last building in a line gets pushed over.) Although pounding must have been a contributing factor, at least one corner apartment building (1801 Beach Street) failed that was not immediately adjacent to another building, suggesting that pounding was not everywhere required for corner-building failure.

Damage to the wood-frame, corner apartment buildings in the Marina District varied; the average damage to these buildings was more than 3 times higher than for any other building type. However, more than 50 percent of these corner buildings were assessed during a postearthquake survey as having sustained a maximum of 10 percent damage (Harris and others, 1990). Clearly, then, there was a great deal of disparity in the damage within a fairly uniform class of buildings. Some differences exist in construction between the corner buildings, but not so much as to explain the variation in damage observed. The distribution of damage to corner buildings in the three soil-profile zones described above is plotted in figures 6 through 8; the damage states are defined in table 1.

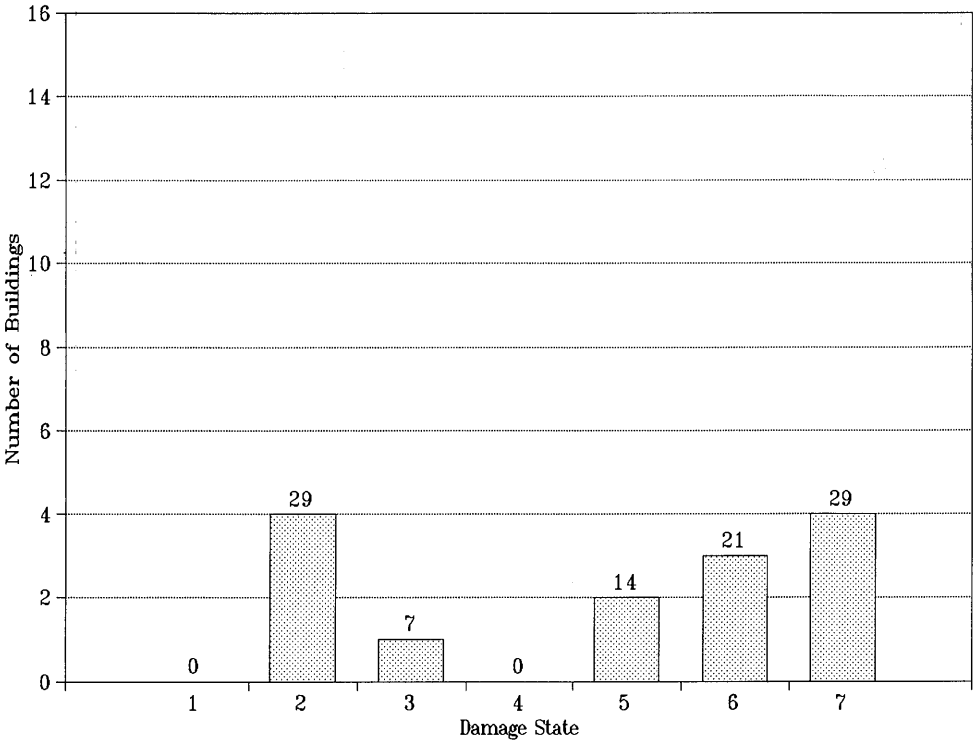


Figure 6.—Number of buildings in "soft"-soil-profile zone versus damage state. Most (64 percent of) buildings were assigned to damage states 5 (heavy) through 7 (destroyed). Numbers at top of bars indicate percentage of total.

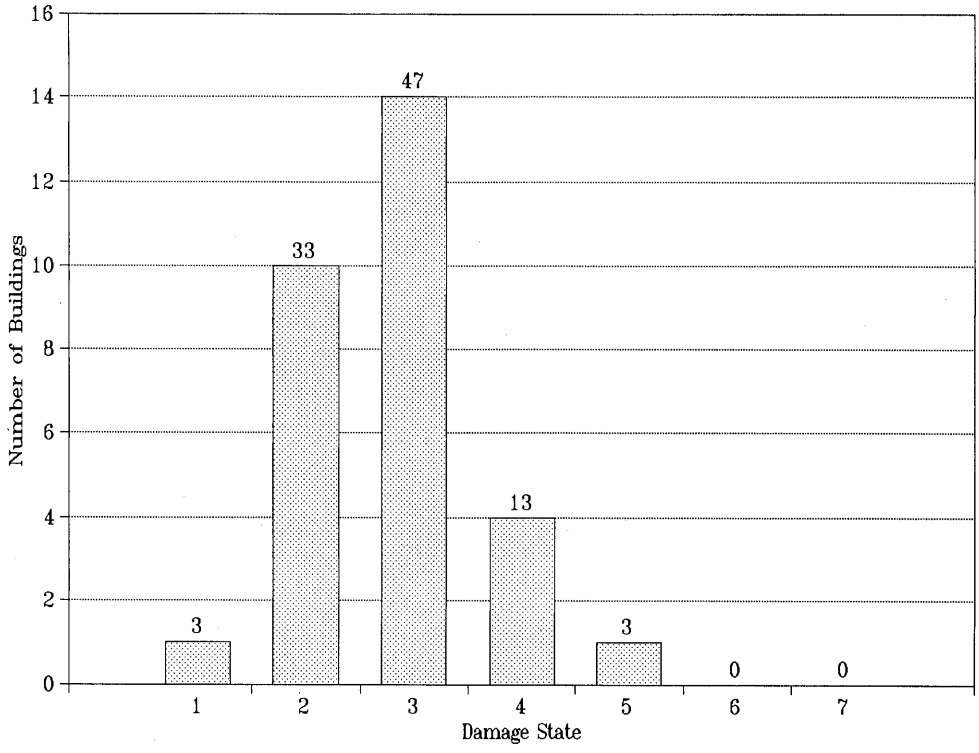


Figure 7.—Number of buildings in "firm"-soil-profile zone versus damage state. All buildings except one were assigned to damage states 4 (moderate) and below. Numbers at top of bars indicate percentage of total.

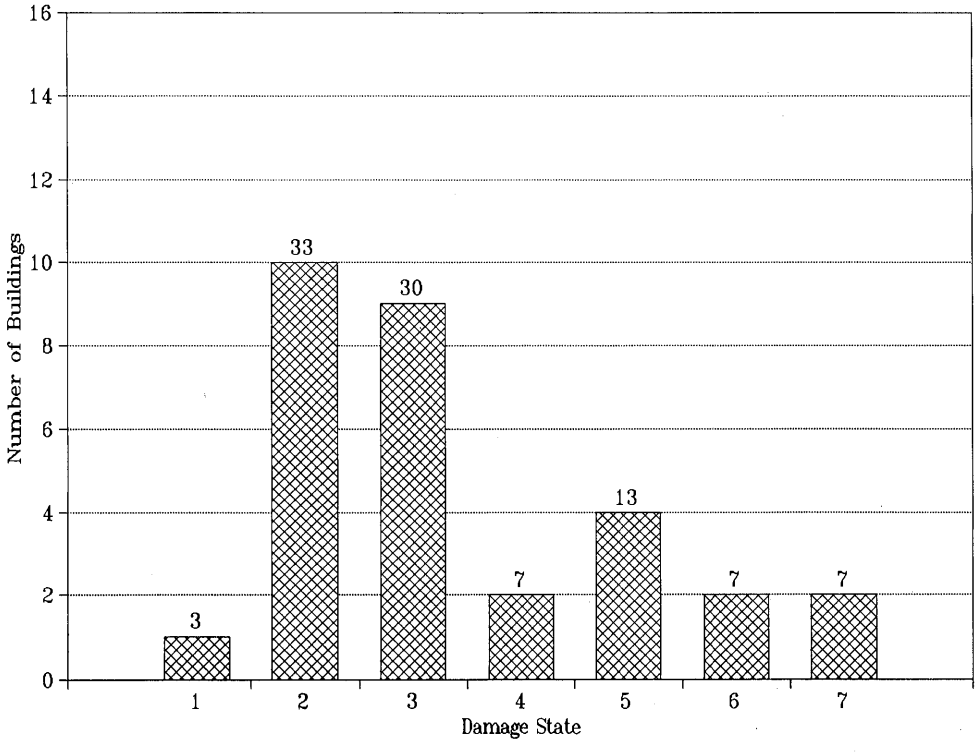


Figure 8.—Number of buildings in ground-failure zones versus damage state. Buildings are spread across all damage states but are concentrated at lower end. Numbers at top of bars indicate percentage of total.

Table 1.—*Definition of damage states*

[From Applied Technology Council (1986)]

| Damage state | Description of damage | Damage factor (percent) | Central damage factor (percent) |
|---|---|---|---|
| 1 | None | 0 | 0.0 |
| 2 | Slight | 0–1 | .5 |
| 3 | Light | 1–10 | 5.5 |
| 4 | Moderate | 10–30 | 20.0 |
| 5 | Heavy | 30–60 | 45.0 |
| 6 | Major | 60–100 | 80.0 |
| 7 | Destroyed | 100 | 100.0 |

Damage states for each building were estimated by engineers during an extensive field survey immediately after the earthquake (Harris and others, 1990). Figures 6 through 8 indicate a definite correlation of damage state with soil-profile zone. Only one of the buildings on firm, native soil (albeit marshland) was damaged beyond state 4. Buildings on soft soil, however, were damaged more severely; 64 percent of these buildings were assigned to damage states 5 through 7. The buildings in the ground-failure zone showed a mixed performance: 73 percent were assigned to damage states 1 through 4, and the rest to damage states 5 through 7.

## ANALYSIS AND METHODOLOGY

To quantify further the correlation of damage state with soil-profile zone, a simplified dynamic structural analysis was performed on the corner buildings, as described below.

### RESPONSE SPECTRA

As mentioned previously, no ground-motion recordings of the main shock were obtained in the Marina District. The closest strong-motion data were recorded by the California Division of Mines and Geology (Shakal and others, 1989) in Pacific Heights (sta. 58131), approximately 1.5 mi (2.5 km) south of the Marina District. The Pacific Heights station is founded on bedrock. To estimate the ground motions in the Marina District, we decided to relate the recorded Pacific Heights bedrock motions to Marina District ground motions through simple period-dependent amplification-transfer functions. For the "soft"-soil-profile zone, we considered that the pair of stations on Treasure Island (sta. 58117) and Yerba Buena Island (sta. 58163), both islands in San Francisco Bay, would provide an appropriate transfer function, given their similarity in distance and azimuth from the fault rupture, their subsurface site conditions and depth to bedrock, and their site geometry. To account for possible differences between direction of shaking, north-south and east-west amplification-transfer functions were evaluated separately. These functions were then used to scale the respective directional components of the Pacific Heights record to calculate ground motions for the "soft"-soil-profile zone. The resulting spectra are plotted in figure 9, with components of the Pacific Heights bedrock record shown for comparison.

For the "firm"-soil-profile zone, no similar soil-bedrock site pairs existed within reasonable proximity to the Marina District, and so an amplification-transfer function was developed from the soil and bedrock attenuation relation of Sadigh and others (1986). Because this attenuation relation does not differentiate shaking direction, only an average function was utilized to scale the Pacific Heights bedrock record, and an average bedrock spectrum was cal-

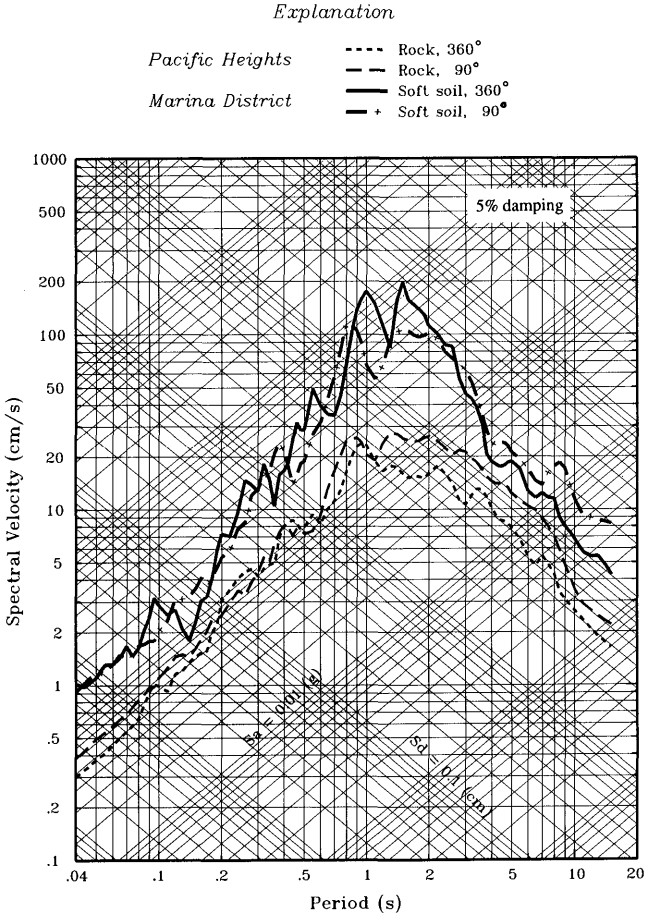


Figure 9.—Estimated "soft"-soil-profile-zone tripartite response spectra of orthogonal horizontal north-south (360°) and east-west (90°) ground-motion components in the Marina District derived from respective components recorded at bedrock station in Pacific Heights (California Division of Mines and Geology sta. 58131), which are shown for comparison.

culated from components of this record. The resulting spectrum is plotted in figure 10, with the corresponding Pacific Heights bedrock spectrum shown for comparison.

## BUILDING MODELS

Earthquake deformations in the corner buildings were concentrated in the weak first stories. Even heavily damaged buildings commonly showed little evidence of deformation above the first story, and so the buildings were assumed to behave essentially as structures with a single degree of freedom in each major axis, and to be rigid above the first story. Using these assumptions, the estimation of building response becomes a straightforward task. (For simplicity, buildings with irregular plans were omitted from the analysis.) The steps involved were (1) estimation of the total building mass tributary to the first story and above, (2) estimation of the stiffness of the first story in the building's two principal directions, (3) calculation of the building's fundamental period of vibration in its two principal directions, and (4) application of the appropriate response spectra to the fundamental periods to determine spectral amplitudes.

Building mass was estimated by using average unit weights based on construction typical of the 1920's, as indicated below:

| *Part of building* | *Unit weight (lb/ft² [kPa])* |
|---|---|
| Roof | 21 (1.0) |
| Floor (including 5 lb/ft² [0.239 kPa] for partitions) | 22 (1.1) |
| Wood-sheathed exterior walls | 12 (0.6) |
| Exterior stucco over wood-sheathed exterior walls | 20 (1.0) |
| Exterior 4-in.-thick brick veneer over wood-sheathed exterior walls | 52 (2.5) |

Using these unit weights, total building weights were calculated, mostly in the range 400–500 kips (1,800–2,200 kN). The estimated building weights and building dimensions are listed in table 2.

Building stiffnesses in each principal direction were estimated by using a unit shear stiffness derived from testing of wood-sheathed diaphragms (ABK Joint Venture, 1981). One of the diaphragms tested was an unchorded, straight-sheathed diaphragm intended to represent the roof of a typical unreinforced-masonry (URM) building; this construction is quite similar to the exterior walls of the corner buildings. Because the diaphragm was unchorded, it deformed almost exclusively in shear, not in flexure. The same shear deformation (mostly due to nail slip) was evident in damaged Marina District buildings. The absence of flexural stiffness in the building walls also allows the addition of wall-pier stiffnesses along a line without regard to the piers' relative flexural rigidity. Total wall stiffness was based on the total length of available wall.

From the results of these tests, a unit shear stiffness of 0.67 kips/in. per foot of wall (385 kN/m per meter of wall) was calculated on the basis of the preyield stiffness of the test diaphragm. Postyield tests show that considerable softening occurs after repeated load cycles. However, since the building periods under consideration are quite long and the earthquake was of short duration, the number of postyield cycles that any building underwent is likely to have been small, and so only the preyield stiffness was used in our analyses.

The distribution of building stiffnesses, as represented by the fundamental period of vibration, in east-west and north-south directions is plotted in figure 11. Note that the buildings are generally stiffer in the east-west direction, because most of them are oriented with their longest dimension oriented east-west.

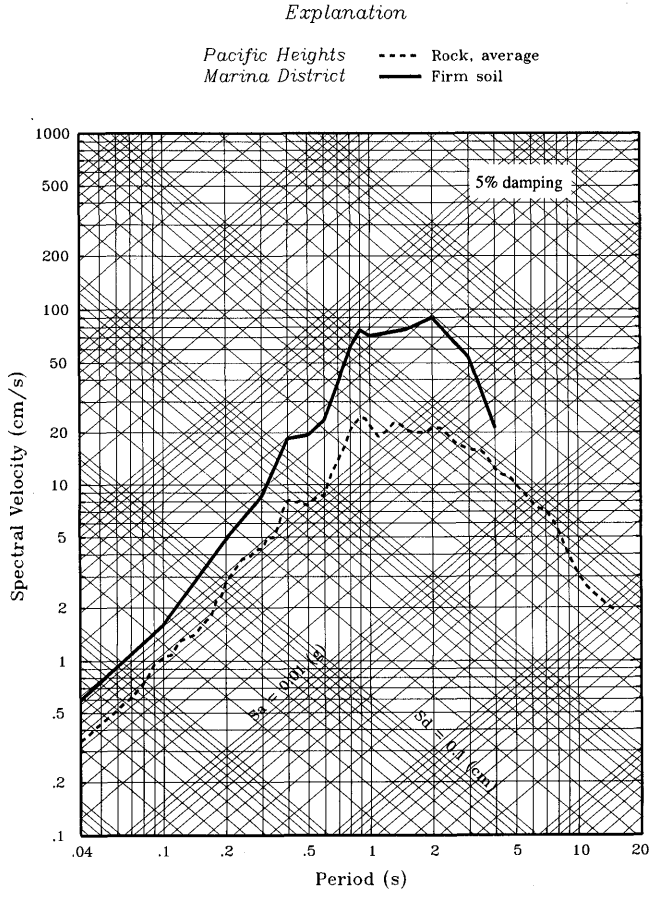


Figure 10.—Estimated "firm"-soil-profile-zone tripartite response spectrum of average horizontal-motion component in the Marina District, derived from average of horizontal components recorded at bedrock station in Pacific Heights (California Division of Mines and Geology sta. 58131), which is shown for comparison.

Table 2.—*Data on corner buildings*

| Location | Block | Year | Area (ft2) | Units | N-S Dimension (ft) | N-S Walls (ft) | EW Dimension (ft) | EW Walls (ft) | Facade | Weight (kips) |
|---|---|---|---|---|---|---|---|---|---|---|
| 2 Alhambra Street | 462A | 1927 | 13,310 | 18 | -- | -- | -- | -- | -- | -- |
| 90 Alhambra Street | 462A | 1927 | 13,940 | 18 | -- | -- | -- | -- | -- | -- |
| 190 Alhambra Street | 463A | 1926 | 10,720 | 18 | -- | -- | -- | -- | -- | -- |
| 200 Alhambra Street | 464A | 1925 | 16,480 | 21 | -- | -- | -- | -- | -- | -- |
| 290 Alhambra Street | 465A | 1925 | 12,600 | 15 | 50 | 20 | 85 | 30 | Stucco | 455 |
| 400 Avila Street | 439A | 1929 | 14,830 | 18 | 65 | 6 | 85 | 20 | Stucco | 529 |
| 2100 Bay Street | 921 | 1927 | 11,100 | 15 | 50 | 30 | 75 | 17 | Stucco | 404 |
| 2101 Bay Street | 928 | 1927 | 11,250 | 15 | 50 | 30 | 75 | 11 | Stucco | 409 |
| 2185 Bay Street | 928 | 1926 | 12,430 | 24 | 50 | 20 | 75 | 28 | Stucco | 443 |
| 2190 Bay Street | 921 | 1926 | 11,820 | 18 | 50 | 14 | 75 | 10 | Brick | 485 |
| 2285 Bay Street | 927 | 1929 | 11,420 | 12 | 50 | 20 | 75 | 25 | Stucco | 414 |
| 2300 Bay Street | 923 | 1927 | 10,800 | 15 | 50 | 6 | 75 | 20 | Stucco | 396 |
| 2301 Bay Street | 926 | 1927 | 11,100 | 18 | 50 | 6 | 75 | 18 | Brick | 464 |
| 1700 Beach Street | 438A | 1927 | 14,722 | 20 | 50 | 25 | 100 | 30 | Stucco | 526 |
| 1701 Beach Street | 443A | 1926 | 12,890 | 18 | 50 | 20 | 75 | 10 | Brick | 516 |
| 1740 Beach Street | 438A | 1927 | 9,750 | 12 | 50 | 6 | 62.5 | 23 | Brick | 411 |
| 1750 Beach Street | 439A | 1927 | 11,420 | 15 | 50 | 20 | 75 | 30 | Brick | 474 |
| 1801 Beach Street | 442A | 1928 | 12,210 | 15 | 50 | 20 | 75 | 10 | Stucco | 437 |
| 1901 Beach Street | 441B | 1928 | 6,430 | 9 | -- | -- | -- | -- | -- | -- |
| 2000 Beach Street | 913 | 1927 | 11,200 | 18 | 50 | 6 | 75 | 20 | Stucco | 407 |
| 2090 Beach Street | 913 | 1927 | 11,200 | 15 | 50 | 6 | 75 | 20 | Stucco | 407 |
| 2101 Beach Street | 919 | 1927 | 11,250 | 18 | 50 | 6 | 75 | 20 | Stucco | 409 |
| 2190 Beach Street | 914 | 1927 | 14,110 | 21 | 50 | 6 | 75 | 40 | Stucco | 492 |
| 2195 Beach Street | 919 | 1957 | 15,550 | 18 | -- | -- | -- | -- | -- | -- |
| 3255 Broderick Street | 931 | 1928 | 17,100 | 18 | 75 | 22 | 75 | 40 | Stucco | 595 |
| 3301 Broderick Street | 926 | 1928 | 11,380 | 12 | 50 | 24 | 75 | 10 | Stucco | 413 |
| 3465 Broderick Street | 923 | 1928 | 11,700 | 12 | 50 | 22 | 75 | 10 | Stucco | 422 |
| 3555 Broderick Street | 918 | 1927 | 11,970 | 15 | 75 | 30 | 50 | 6 | Stucco | 430 |
| 3650 Broderick Street | 914 | 1929 | 14,500 | 15 | 90 | 10 | 65 | 35 | Stucco | 523 |
| 10 Capra Way | 442A | 1926 | 13,940 | 18 | -- | -- | -- | -- | -- | -- |
| 50 Capra Way | 442A | 1927 | 11,490 | 18 | 50 | 6 | 75 | 30 | Brick | 476 |
| 75 Capra Way | 463A | 1926 | 12,000 | 18 | 37.5 | 12 | 75 | 10 | Stucco | 422 |
| 101 Capra Way | 464A | 1928 | 11,760 | 15 | 37.5 | 12 | 75 | 10 | Stucco | 415 |
| 2 Casa Way | 419A | 1930 | 16,350 | 15 | -- | -- | -- | -- | -- | -- |
| 2 Cervantes Boulevard | 443A | 1927 | 31,940 | 30 | -- | -- | -- | -- | -- | -- |
| 25 Cervantes Boulevard | 467A | 1927 | 14,690 | 18 | -- | -- | -- | -- | -- | -- |
| 95 Cervantes Boulevard | 462A | 1926 | 8,620 | 15 | -- | -- | -- | -- | -- | -- |
| 98 Cervantes Boulevard | 443A | 1925 | 11,550 | 12 | -- | -- | -- | -- | -- | -- |
| 101 Cervantes Boulevard | 440A | 1927 | 24,450 | 33 | -- | -- | -- | -- | -- | -- |
| 2050 Chestnut Street | 486A | 1927 | 10,770 | 15 | -- | -- | -- | -- | -- | -- |
| 2390 Chestnut Street | 929 | 1927 | 15,160 | 27 | -- | -- | -- | -- | -- | -- |
| 2490 Chestnut Street | 930 | 1928 | 10,240 | 18 | 50 | 5 | 75 | 30 | Stucco | 379 |
| 2500 Chestnut Street | 931 | 1928 | 10,050 | 15 | 50 | 6 | 65 | 25 | Brick | 423 |
| 3459 Divisadero Street | 927 | 1929 | 18,330 | 18 | 75 | 20 | 80 | 30 | Brick | 708 |
| 3501 Divisadero Street | 922 | 1926 | 14,350 | 14 | 65 | 10 | 75 | 30 | Brick | 576 |
| 3560 Divisadero Street | 921 | 1926 | 10,600 | 14 | -- | -- | -- | -- | -- | -- |
| 3701 Divisadero Street | 914 | 1927 | 16,120 | 21 | 50 | 6 | 75 | 25 | Stucco | 550 |
| 3755 Divisadero Street | 914 | 1927 | 16,120 | 21 | 50 | 6 | 75 | 25 | Stucco | 550 |
| 3789 Fillmore Street | 438A | 1921 | 9,190 | 9 | -- | -- | -- | -- | -- | -- |
| 2200 Francisco Street | 928 | 1926 | 10,740 | 15 | 50 | 40 | 75 | 10 | Stucco | 394 |
| 2201 Francisco Street | 929 | 1925 | 10,910 | 16 | 50 | 6 | 75 | 25 | Stucco | 399 |
| 2290 Francisco Street | 928 | 1927 | 12,690 | 18 | 50 | 15 | 75 | 10 | Stucco | 451 |
| 2295 Francisco Street | 929 | 1926 | 10,350 | 18 | 50 | 25 | 75 | 10 | Stucco | 383 |
| 2300 Francisco Street | 927 | 1926 | 12,000 | 18 | 50 | 6 | 75 | 25 | Stucco | 431 |
| 2301 Francisco Street | 930 | 1927 | 11,460 | 18 | 50 | 25 | 75 | 10 | Stucco | 415 |
| 2395 Francisco Street | 930 | 1927 | 10,800 | 18 | 50 | 6 | 75 | 25 | Stucco | 396 |
| 1801 Jefferson Street | 913 | 1927 | 12,230 | 18 | 50 | 15 | 75 | 10 | Stucco | 437 |
| 1895 Jefferson Street | 913 | 1927 | 11,200 | 18 | 50 | 15 | 75 | 10 | Stucco | 407 |
| 180 Mallorca Way | 467A | 1927 | 15,490 | 24 | -- | -- | -- | -- | -- | -- |
| 201 Mallorca Way | 463A | 1926 | 12,440 | 15 | -- | -- | -- | -- | -- | -- |
| 225 Mallorca Way | 463A | 1929 | 16,190 | 21 | -- | -- | -- | -- | -- | -- |
| 2100 North Point Street | 920 | 1928 | 11,100 | 15 | 50 | 6 | 75 | 25 | Stucco | 404 |
| 2101 North Point Street | 921 | 1927 | 11,100 | 18 | 50 | 15 | 75 | 10 | Stucco | 404 |
| 2200 North Point Street | 919 | 1927 | 11,380 | 15 | 50 | 20 | 75 | 35 | Stucco | 413 |
| 5 Rico Way | 439A | 1927 | 7,870 | 12 | 35 | 15 | 75 | 10 | Brick | 354 |
| 3360 Scott Street | 488A | 1925 | 5,820 | 12 | -- | -- | -- | -- | -- | -- |
| 3490 Scott Street | 465A | 1929 | 11,980 | 18 | 50 | 15 | 75 | 10 | Stucco | 430 |
| 3636 Scott Street | 441A | 1930 | 11,870 | 12 | 50 | 15 | 75 | 10 | Stucco | 427 |
| 3750 Scott Street | 440B | 1929 | 12,750 | 15 | -- | -- | -- | -- | -- | -- |
| 3800 Scott Street | 417B | 1929 | 10,390 | 12 | -- | -- | -- | -- | -- | -- |
| 3825 Scott Street | 912 | 1928 | 18,810 | 18 | -- | -- | -- | -- | -- | -- |
| 1 Toledo Way | 486A | 1926 | 7,260 | 12 | 35 | 4 | 75 | 25 | Stucco | 283 |
| 2 Toledo Way | 466A | 1926 | 12,520 | 15 | 50 | 6 | 75 | 25 | Stucco | 446 |
| 96 Toledo Way | 466A | 1927 | 13,550 | 18 | 50 | 6 | 75 | 25 | Brick | 535 |

On the basis of the soil-profile-zone map (fig. 5), each building was assigned to either the "soft"-soil-profile response spectrum or the "firm"-soil-profile response spectrum. Response parameters in each of the buildings' principal directions were calculated and are discussed in the next section.

## RESULTS AND DISCUSSION

### SPECTRAL DISPLACEMENT VERSUS DAMAGE RATIO

Using the simplified dynamic analysis described above, correlations were made between the damage ratio, defined as the repair cost divided by the replacement cost, and the estimated maximum spectral displacement for corner buildings in all three soil-profile zones (fig. 12) and for only those outside the ground-failure zone (fig. 13). Although the data in figure 13 do not show a strong correlation, they do illustrate the following points.

1. The maximum spectral displacement for buildings 80 percent damaged (which leaned over but did not collapse) is about 1 ft (0.3 m). The buildings 100 percent damaged show similar, if slightly more varied, results. Note that because these buildings collapsed, such detailed dimensions as wall length were only estimated. A spectral displacement of 1 ft (0.3 m) is approximately equal to the permanent lateral deformation observed in these buildings.
2. The data in figure 13 appear to suggest an upper bound for the damage ratio, given the spectral displacement, that may indicate the presence (in some buildings) of structural attributes invisible from the exterior, such as diagonal wall sheathing or first-story walls with interior stucco, that would significantly increase building strength and stiffness.

Examination of the "soft"-soil-profile response spectra in figure 9 indicates that the maximum spectral displacements occur in the period between 1.5 and 2.5 s, whereas the calculated fundamental building periods are in the range 0.8–1.25 s. Thus, if some decrease in building stiffness occurred during hysteresis, there would have been an accompanying increase in spectral displacement. Although this effect cannot be quantified at this time, some of the uncertainty evident in figure 13 may be due to decreases in building stiffness.

We also note the contrast in the response of the wood-frame corner buildings to that of the corner buildings with URM or concrete first stories. Harris and others (1990)

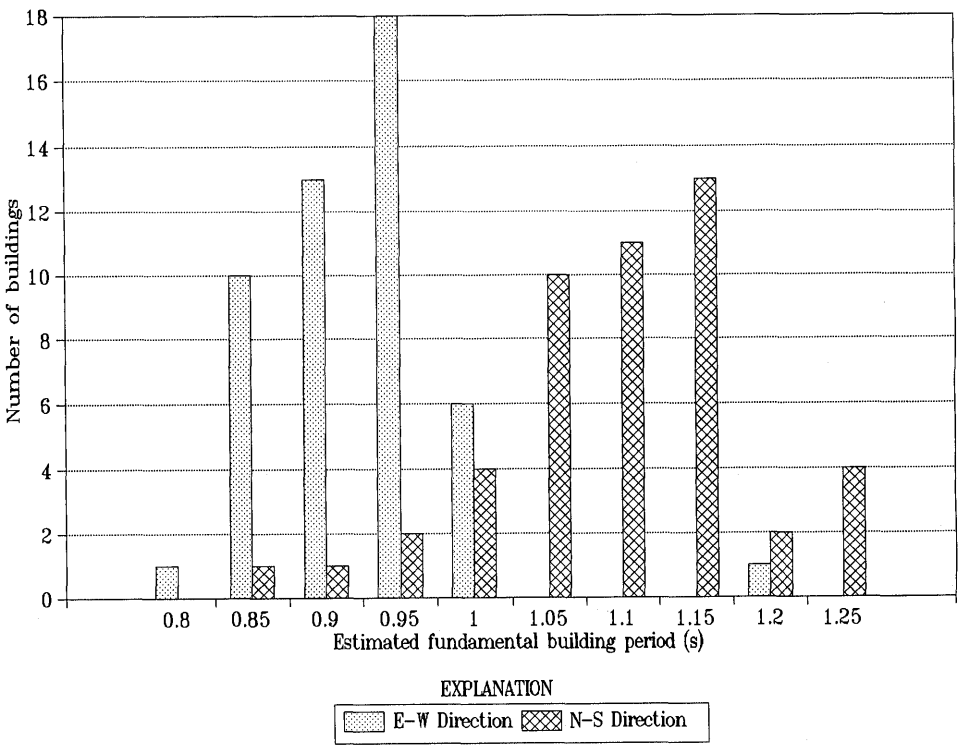


Figure 11.—Number of buildings versus estimated fundamental building period. Periods are spread across a narrow band from 0.8 to 1.25 s. East-west periods are generally shorter than north-south periods, owing to building orientation. Periods plotted are preyield estimates; actual periods may be somewhat longer because of postyield hysteresis.

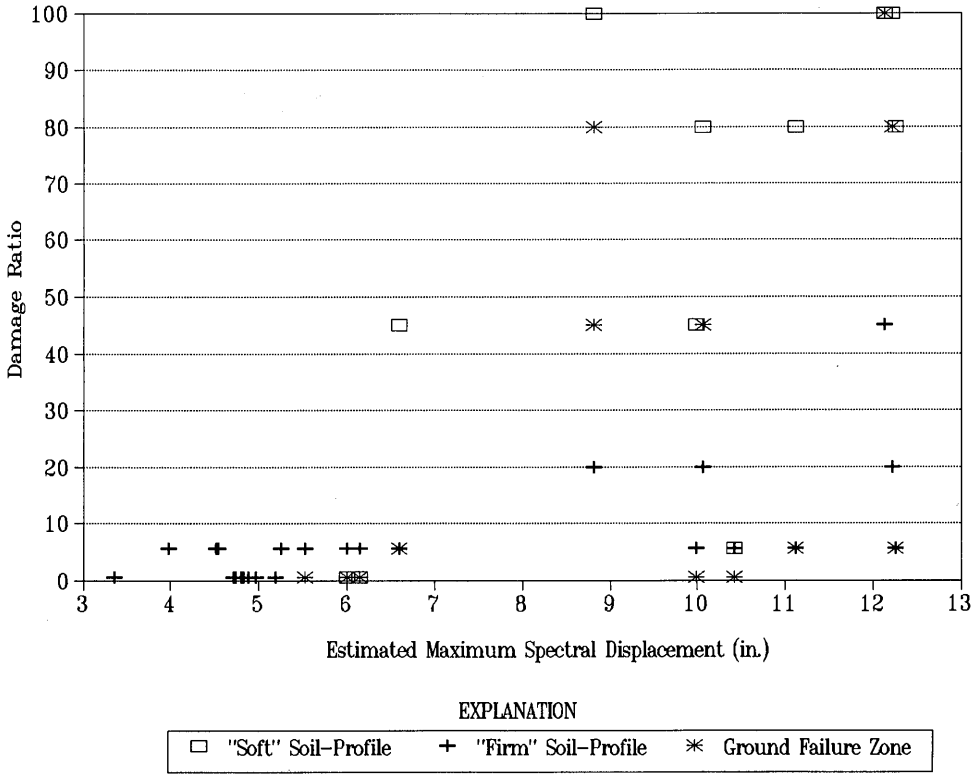


Figure 12.—Damage ratio versus estimated maximum spectral displacement for all corner buildings studied.

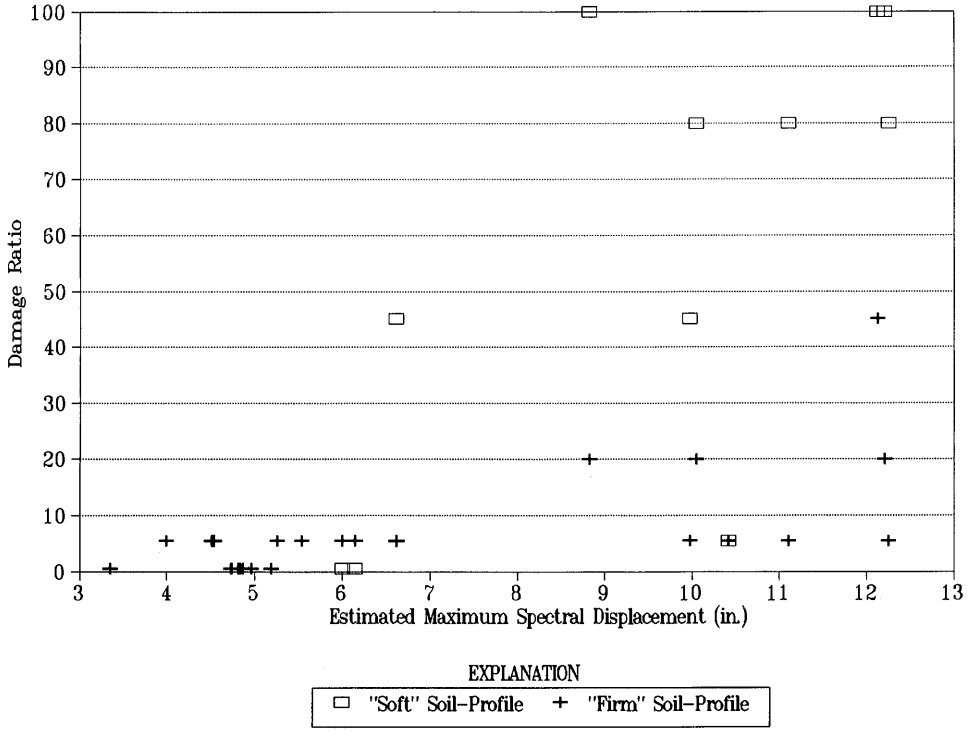


Figure 13.—Damage ratio versus estimated maximum spectral displacement for all corner buildings studied except those within ground-failure zone. Spectral displacements of buildings 80 to 100 percent damaged are about 1 ft (0.3 m), approximately equal to permanent lateral deformation observed in heavily damaged buildings that did not collapse.

reported that these buildings were damaged, on average, 10 times less severely than the (otherwise similar) wood-frame buildings. In addition, none of the URM- or concrete-first-story buildings was damaged beyond state 4 (moderate). The fundamental building periods of these stiffer structures may be estimated at about 0.3 s. Applied to the "soft"-soil-profile response spectra in figure 9, this building period results in a spectral displacement of approximately 0.4 in. (0.01 m). The decrease in response helps to explain the surprisingly good performance of URM construction in the Marina District, where the soft soils may be considered to have isolated these stiff but brittle buildings from damaging, high-frequency ground motions.

### BASE SHEAR VERSUS DAMAGE RATIO

Correlations were also made between the damage ratio and the estimated maximum structural base shear per foot of exterior wall (fig. 14). Again, owing to the approximations in these analyses, a well-defined correlation is not apparent, although a general positive slope is indicated for the "soft"-soil-profile zone. The following observations can be made.

1. The buildings in the "firm"-soil-profile zone generally indicate base shears less than about 15 to 20 kips/ft (225-300 kN/m), whereas those in the "soft"-soil-profile zone generally indicate a higher shear that appears to be an approximate lower bound for the large permanent lateral deformation observed in the heavily damaged corner buildings.
2. This correlation is somewhat clearer than that between damage ratio and maximum spectral displacement, indicating that the length of wall available for shear resistance is also an important factor affecting damage, as would be expected.

## SUMMARY AND CONCLUSIONS

The extremely poor performance of many of the wood-frame corner apartment buildings in the Marina District during the earthquake appears to be due to an infortuitous combination of factors, among the most important of which is the near-coincidence of the fundamental building period with the maximum spectral displacement. The ground failure in the central part of the filled area appears to have mitigated much of the potential damage by dissipating seismic energy through liquefaction. From these and the above observations, we draw two main conclusions.

First, in future large earthquakes that affect the Marina District, the energy dissipation from ground failure may

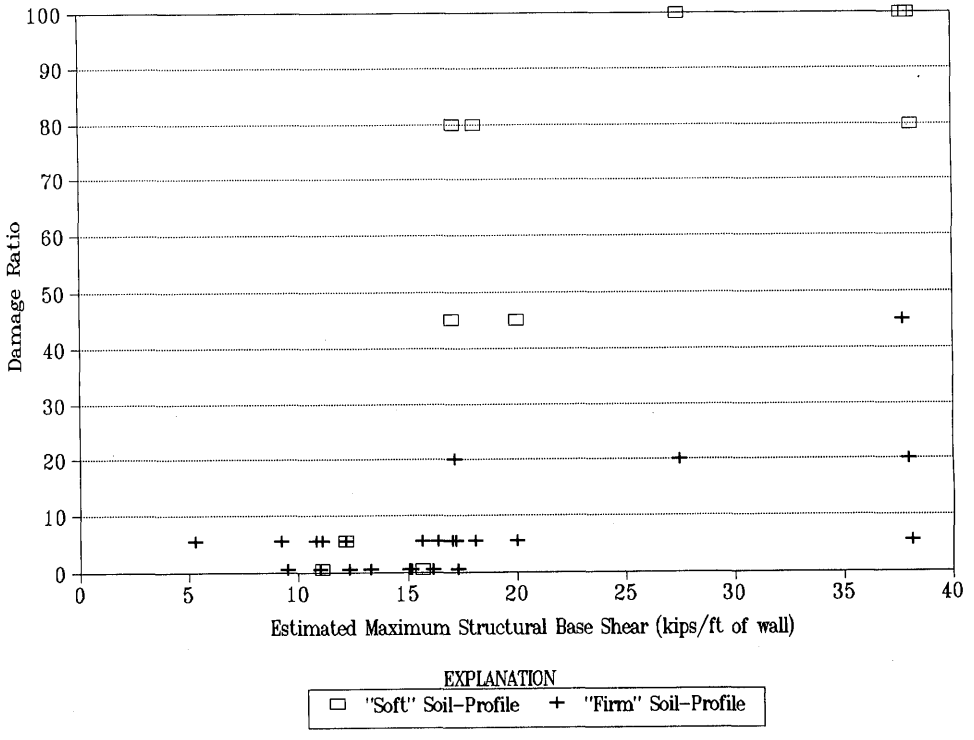


Figure 14.—Damage ratio versus estimated maximum structural base shear for all corner buildings studied except those within ground-failure zone. Base shear of about 15 to 20 kips/ft (225–300 kN/m) appears to be approximate lower bound of permanent lateral deformation observed in heavily damaged buildings.

not be so apparent. Longer durations, such as those expected from a repeat of the 1906 event, would be expected to cause severe damage or collapse to many corner buildings that were not severely damaged in the 1989 event. We note that San Francisco's recent postearthquake building-strengthening ordinance applied only to buildings with damage ratios of at least 10 percent; that is, lightly damaged buildings were not required to be strengthened.

Second, buildings similar to the corner buildings in the Marina District exist in several other San Francisco neighborhoods (including the Richmond and Mission Districts). Most of these buildings are not located on soft soils or fills and were not seriously affected by the 1989 earthquake. However, a repeat of the 1906 event could cause serious damage to these structures. Using the unreduced lateral-force formula (34–1) from the "Uniform Building Code" (International Conference of Building Officials, 1991, chap. 23),

$$V=ZICW/R_w,$$

where $V$ is the base shear, $Z$=0.4, $I$=1.0, $C$=2.75, $W$ is the building weight, and $R_w$=1.0. The spectral acceleration, $S_a$, defined as $V/W$, would be approximately 1.1 $g$ (425 in/s$^2$ [10.79 m/s$^2$]); this acceleration is intended to correspond to a 475-year event. Using this acceleration and a first-mode period of 0.9 s, the spectral displacement, $S_d$, may be computed from the standard formula

$$S_d = (2\pi/T)^2 S_a,$$

where $T$ is the (first) modal period. This computation results in a spectral displacement of 9 in. (0.22 m), approximately equal to the lower bound for severe damage shown in figure 13, from which we may conclude that the damage observed in the "soft"-soil-profile zone of the Marina District would be possible in similar buildings on firmer ground in a much larger earthquake.

Finally, building damage in the Marina District was highly sensitive to ground conditions, as well as to building construction. Accordingly, any conclusions drawn from performance data in the Marina District should be used with the knowledge that the observed building damage was a result of the coincidence of many factors, including seismologic, geologic, and structural parameters. Future earthquakes affecting the Marina District and other areas are likely to cause markedly different effects.

## REFERENCES CITED

ABK Joint Venture, 1981, Methodology for mitigation of seismic hazards in existing unreinforced masonry buildings; diaphragm testing: Report ABK–TR–03, 424 p.

Applied Technology Council, 1985, Earthquake damage evaluation data for California: Redwood City, Calif., 472 p.

Harris, S.K., Scawthorn, C.R., and Egan, J.A., 1990, Damage in the Marina District of San Francisco in the October 17, 1989 Loma Prieta earthquake: Japan Earthquake Engineering Symposium, 1990, Proceedings.

International Conference of Building Officials, 1991, Uniform building code: Whittier, Calif., 1050 p.

Kayen, R.E., Liu, H.-P., Fumal, T.E., Westerlund, R.E., Warrick, R.E., Gibbs, J.F., and Lee, H.J., 1990, Engineering and seismic properties of the soil column at Winfield Scott School, San Francisco, chap. G *of* Effects of the Loma Prieta earthquake on the Marina District, San Francisco, California: U.S. Geological Survey Open-File Report 90–253, p. G1–G18.

Real Estate Data, Inc., 1991, REALDEX real estate atlas of the county of San Francisco: San Francisco, 2,260 p.

Sadigh, K., Egan, J.A., and Youngs, R.R., 1986, Specification of ground motions for seismic design of long period structures: Earthquake Notes, v. 57, no. 1, p. 13.

Schlocker, Julius, 1974, Geology of the San Francisco North quadrangle, California: U.S. Geological Survey Professional Paper 782, 109 p.

Seed, H.B., Tokimatsu, K., Harder, L.F., and Chung, R.M., 1985, Influence of SPT procedures in soil liquefaction resistance evaluations: Journal of Geotechnical Engineering, v. 111, no. 12, p. 1425–1445.

Shakal, A., Huang, M., Reichle, M., Ventura, C., Cao, T., Sherburne, R., Savage, M., Darragh, R., and Petersen, C., 1989, CSMIP strong-motion records from the Santa Cruz Mountains (Loma Prieta), California earthquake of 17 October 1989: California Division of Mines and Geology, Office of Strong Motion Studies Report OSMS 89–06, 196 p.

U.S. Coast Survey, 1851, South shore Golden Gate from Point Lobos to San Francisco, California: scale 1:10,000.

MARINA DISTRICT

# PERFORMANCE OF EMERGENCY-RESPONSE SERVICES AFTER THE EARTHQUAKE

By Charles R. Scawthorn and Keith A. Porter, EQE Engineering and Design; and
Frank T. Blackburn, PWSS Co., Ltd.

## CONTENTS



ABSTRACT

Building collapses, gas leaks, and a large fire made the Marina District the primary focus of emergency response in the city of San Francisco. A total of 7 Marina District buildings collapsed, and 63 more were declared unsafe to enter or occupy. Police and emergency medical services were not generally overwhelmed, despite temporary loss of computer-aided dispatch. A fire that grew to near-conflagration proportions demonstrated both the strengths and weaknesses of emergency response. The fireboat *Phoenix*, the San Francisco Fire Department's Portable Water Supply System, and the tactics and training for using them were critical in controlling the fire. In contrast, the city's Auxiliary Water Supply System was poorly utilized because of overwhelmed procedures for emergency operations, communication, and command and control.

## INTRODUCTION

The earthquake severely tested the preparedness of emergency-response services throughout the San Francisco Bay area. San Francisco itself sustained moderate to strong ground shaking, with intensities ranging from VI to IX on the modified Mercalli intensity (MMI) scale (Benuska, 1990). The most severe damage occurred in the Marina District, an area of approximately ½ mi² with 14,000 residents at the end of the San Francisco peninsula. This area, assigned an MMI of IX by the U.S. Geological Survey, became the focus of the city's most intensive police and fire-service involvement. This report discusses the effectiveness of police, fire, and ambulance emergency services in the Marina District during the early hours after the earthquake. We first briefly review the setting of the Marina District and San Francisco's emergency-response capabilities before the earthquake, and we then describe police, ambulance, and, especially, fire-service response. We conclude with a summary of the lessons learned.

## THE MARINA DISTRICT BEFORE THE EARTHQUAKE

San Francisco's Marina District, located at the north end of the San Francisco peninsula (fig. 1), is primarily a residential neighborhood, bounded on the north by San Francisco Bay; on the south by Lombard Street, a major transit corridor; on the east by Fort Mason; and on the west by the Palace of Fine Arts and the Presidio of San Francisco

(figs. 1, 2). The land that composes the Marina District was reclaimed from San Francisco Bay, filled in stages during the years 1869 to 1917 (Bonilla, 1990). The 1915 Panama-Pacific International Exposition was held on the site of the Marina District; afterward, streets and lifeline services were installed, and the land was auctioned for housing. A typical Marina District apartment building is a 1920's-era wood-frame structure of one to three stories above a ground-level garage. Walls are typically constructed of stucco over straight wood sheathing, although some buildings have unreinforced-masonry or reinforced-concrete first stories.

## SAN FRANCISCO POLICE DEPARTMENT

On October 17, 1989, the San Francisco Police Department (SFPD) employed 1,768 officers, of whom approximately a third were on duty at 5:04 p.m. P.d.t. (Lt. Harper, oral commun., 1991). Officers operate out of nine police stations, or districts (fig. 3). Above the district level are three commanders, each in charge of three police districts; the Marina District is contained within the SFPD's Northern District.

The SFPD is responsible for emergency telephone (or 911) service. All calls to the 911 exchange are received at the Hall of Justice (fig. 1) at 6th and Bryant Streets. A dispatch officer determines whether the emergency is police related; if not, the call is routed to the appropriate municipal unit, such as the fire department or the paramedics, using a transfer line routed through Pacific Bell's central office on McCoppin Street. If the emergency is police related, the dispatch officer uses a computer-aided-dispatch (CAD) system to order the appropriate police district to respond.

## SAN FRANCISCO FIRE DEPARTMENT

On October 17, 1989, the San Francisco Fire Department (SFFD) employed approximately 1,300 firefighters and officers, not including staff at headquarters, training

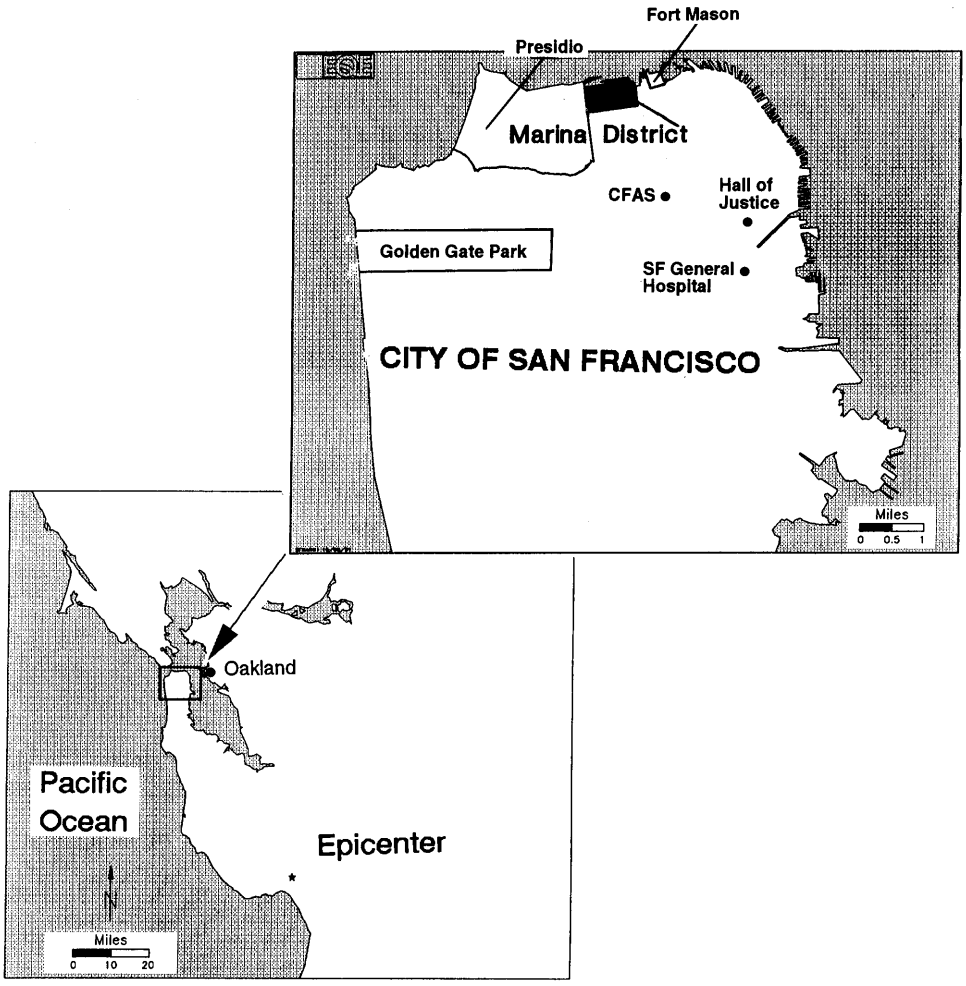


Figure 1.—Sketch maps of San Francisco Bay area and city of San Francisco, showing location of the Marina District (shaded area). CFAS, Central Fire Alarm Station.

center, and other support services. San Francisco's 41 fire stations are divided among 10 battalions of three to five stations each (fig. 4); each battalion is commanded by a battalion chief. The 10 battalions are organized into four divisions under the command of a division chief: three within the city of San Francisco and one at San Francisco International Airport. Department Chief Frederick Postel was out of town at the time of the earthquake. Three deputy chiefs, Michael Farrell, John Boscacci, and Frank Scales, report to Chief Postel; Deputy Chief Farrell was the acting chief in Chief Postel's absence. The units in service at 5:04 p.m. included 41 engine companies, 18 truck companies, 2 rescue companies, 1 air-service company, 1 fireboat company, and 1 equipment unit.

The SFFD typically responds to a 911 call as follows. When the call is received, the caller speaks first to a police dispatch officer. If the emergency is within the purview of the SFFD, the call is transferred to the SFFD's communications center at the Central Fire Alarm Station (CFAS, fig. 1) in Jefferson Square Park, on Turk Street between Gough and Laguna Streets. The caller then speaks to an SFFD dispatcher, who directly contacts the appropriate responding units. In an emergency such as an earthquake, the SFFD's communications center is designated the city's

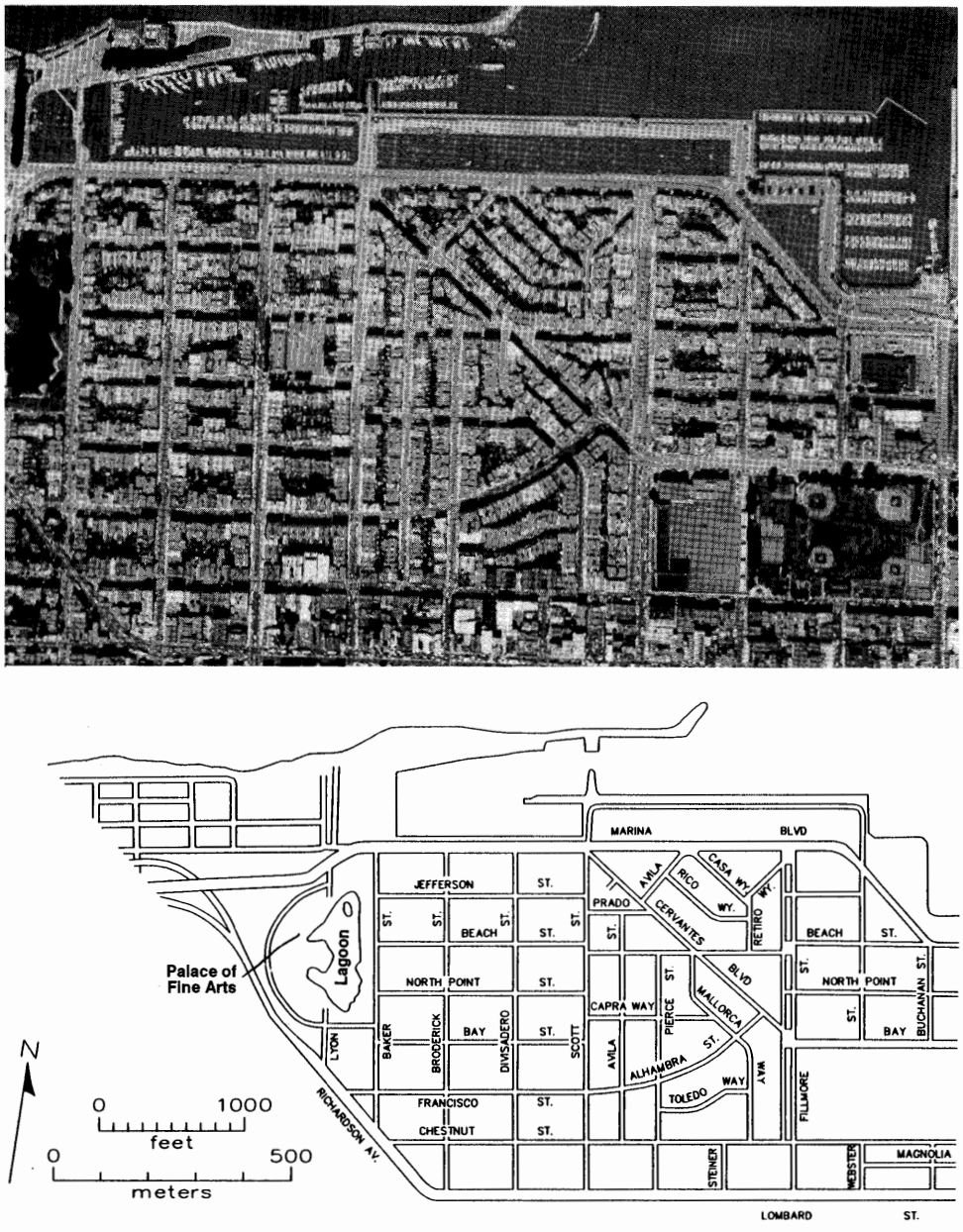


Figure 2.—Marina District, showing street grid.

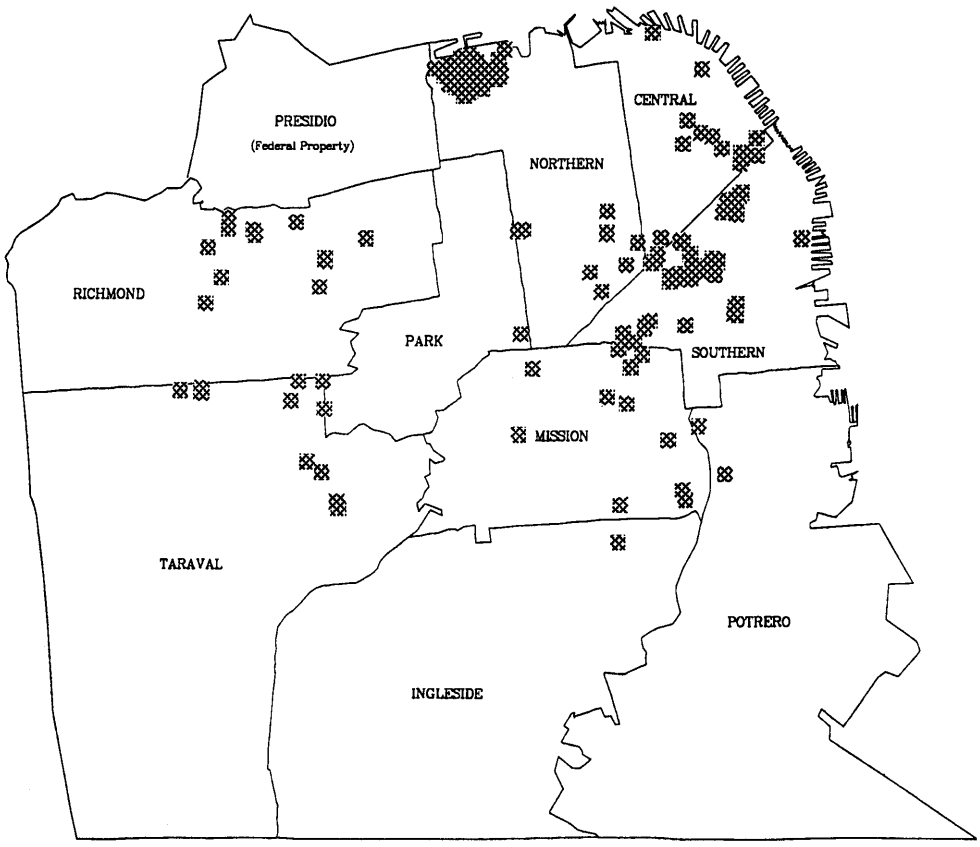


Figure 3.—Sketch map of San Francisco, showing locations of SFPD districts and areas of most extensive damage (shading). Map courtesy of SFPD.

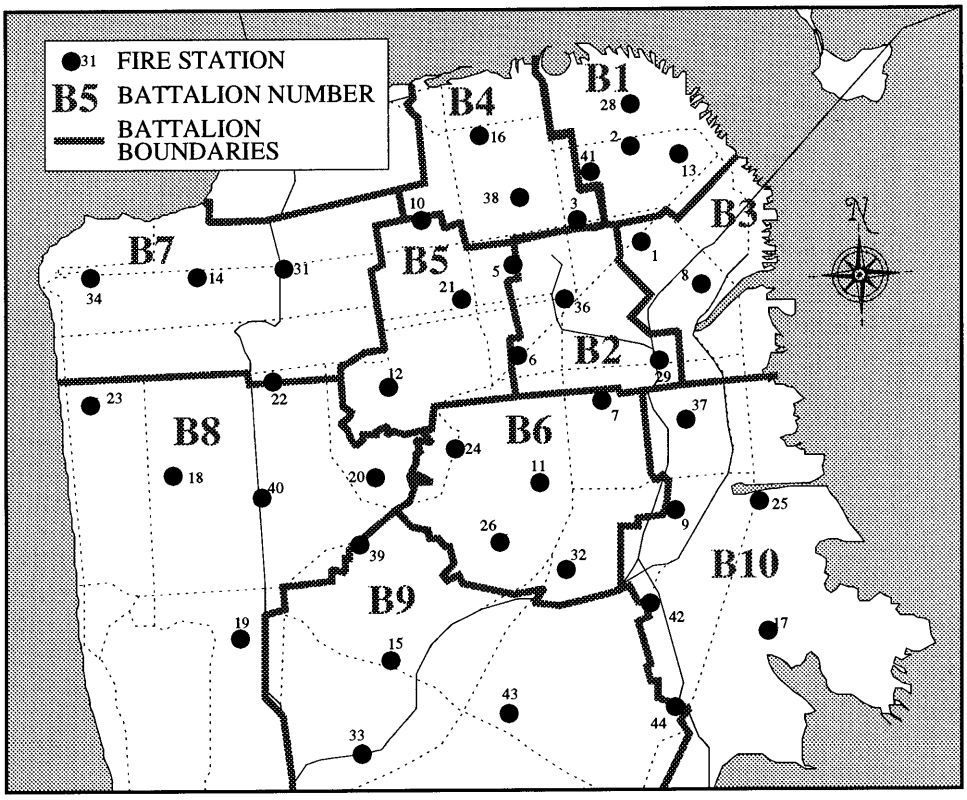


Figure 4.—Sketch map of San Francisco, showing locations of SFPD battalions and fire stations.

Emergency Operations Center (EOC), where the mayor, city-department heads, and all command and control are based.

Within minutes of the earthquake, 27 fires had broken out throughout the city, and the SFFD would turn out for more than 400 incidents in the next 4 hours (San Francisco Fire Fighters Local 798, 1990), the most significant of which were the fire and building collapses in the Marina District.

Normally, the SFFD has three available systems of water supply: the Municipal Water Supply System (MWSS), the Auxiliary Water Supply System (AWSS), and the Portable Water Supply System (PWSS). The MWSS serves the dual purpose of supplying potable water and providing water to fire hydrants. The AWSS is intended solely to ensure adequate water flow and pressure for firefighting purposes; it is separate and redundant to the MWSS, and is owned and controlled by the SFFD. Built in the decade after the 1906 earthquake and fire, the AWSS is concentrated primarily in the urbanized part of the city of 1906, still the central business district (fig. 5). It has been gradually extended to other parts of the city, although the original part still constitutes most of the AWSS. The AWSS network in the Marina District is mapped in figure 6.

The AWSS has been described in detail elsewhere (Scawthorn and others, 1990a, b). Briefly, it consists of several components:

- *Static supplies:* The 10-million-gal reservoir at Twin Peaks, the 750,000-gal Jones Street Tank, and the 500,000-gal Ashbury Tank (fig. 5).
- *Pump stations:* Two stations, each capable of pumping water from San Francisco Bay into the underground-pipe system at 10,000 gal/min and 300-lb/ft$^2$ pressure.
- *Pipe network:* 129 mi of cast-iron and ductile-iron pipe serving approximately 1,500 dedicated high-pressure hydrants. The pipe network is divided into three pressure zones: Twin Peaks, upper, and lower.
- *Fireboats:* At the time of the earthquake, San Francisco possessed only one fireboat, the *Phoenix*, whose pump capacity is 9,600 gal/min at 150-lb/ft$^2$ pressure. Fireboats may hook into the AWSS and pump seawater into the pipe network at any of five manifolds.
- *Cisterns:* In addition to the above components, San Francisco has 151 underground cisterns, again largely in the northeast quadrant of the city. These cisterns are generally of concrete construction, with a 75,000-gal capacity, about 1-hour supply for a typical SFFD pumper.

Control of the AWSS is centered at the Jones Street tankhouse, where gages provide pressure readings at a limited number of points in the network. A few gate valves can be operated remotely from this tankhouse by a signal transmitted over land lines. The water pressure in the lower pressure zone can be increased by opening valves at the tankhouse, and the Twin Peaks pressure zone can be "cut in" by remotely operating valves located at the Ashbury Tank. Remotely operable valves are presently powered by Pacific Gas & Electric Co. (PG&E), the local electric utility, but are being converted to a backup emergency battery system.

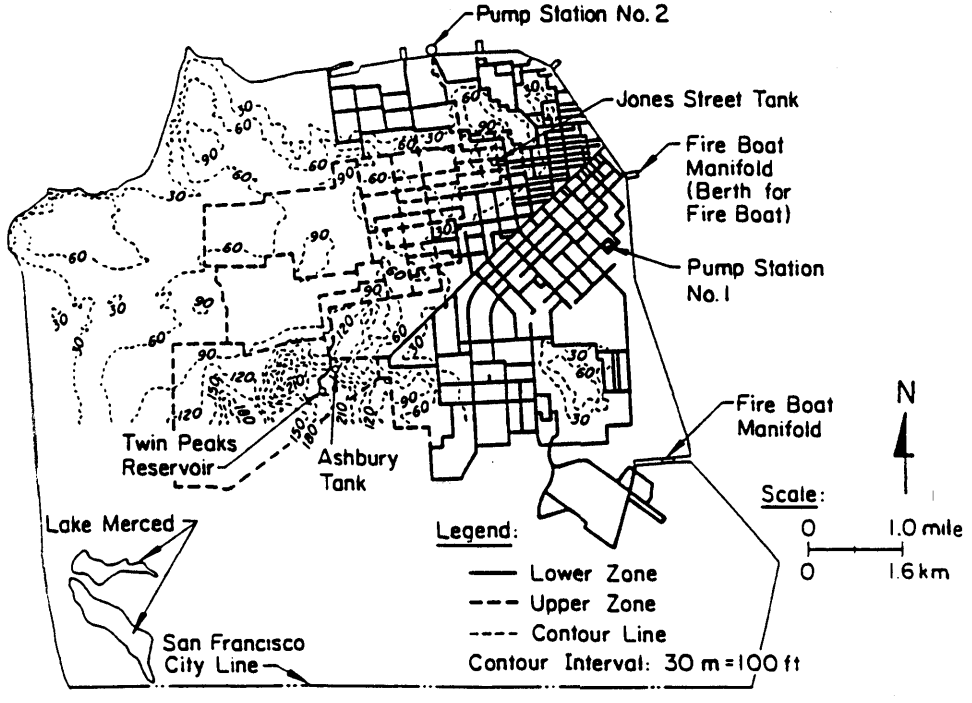


Figure 5.—Sketch map of San Francisco, showing location of AWSS pipe network. After Scawthorn and others (1990).

Although the AWSS provides high assurance of firefighting water supply in the northeast quadrant of the city, major fires can and do occur far from the AWSS pipe network. Experience in the 1906 earthquake, as well as in subsequent California earthquakes in 1971 (San Fernando) and 1983 (Coalinga), had also taught that earthquakes can damage piped water supply. In recognition of this fact, and to provide additional flexibility in deployment and to extend further the "reach" of the AWSS, since 1985 the SFFD has developed the PWSS. Its basic components are:

- Hosetenders, trucks capable of carrying 5,000 ft of large (5 in. diam) hose, with a high-pressure monitor for a master stream.
- Hose ramps, which allow vehicles to cross the hose when it is charged.
- Gated inlet Wye, allowing water supply into large-diameter from standard-diameter fire hose.
- Gleeson valve, a pressure-reducing valve connected to portable hydrants to draw water from the portable main at usable pressure.
- Portable hydrants, which allow water to be distributed from large-diameter hose.

Hosetenders, which carry all the hose, hydrants, valves, and other fittings, are capable of laying 5,000 ft of hose in about 20 minutes. Hose lengths are intermittently fitted with portable hydrants, permitting water supply at many locations along the hose. Hose can thus be gridded and, in effect, provide a system of above-ground water mains. At the time of the earthquake, the SFFD had four PWSS hosetenders.

## SAN FRANCISCO DEPARTMENT OF PUBLIC HEALTH, PARAMEDIC DIVISION

Emergency medical calls to the 911 exchange are routed to the Paramedic Division's Centralized Medical Dispatch Center (CMED) for response. Ambulances and crews are located at a staging area in Golden Gate Park (fig. 1) near Stanyan and Haight Streets. Normally, 15 ambulances are stationed there, and crews are available for 11 or 12 ambulances, with the others held in reserve. At the time of the earthquake, 11 ambulance crews were scheduled for duty.

## EARTHQUAKE DAMAGE IN THE MARINA DISTRICT

The earthquake caused severe damage and widespread liquefaction-induced, permanent ground displacements in the Marina District. Seven buildings in the Marina District collapsed; their locations are shown in figure 7. These were the only buildings in San Francisco or Oakland that collapsed in the earthquake, although several structures in

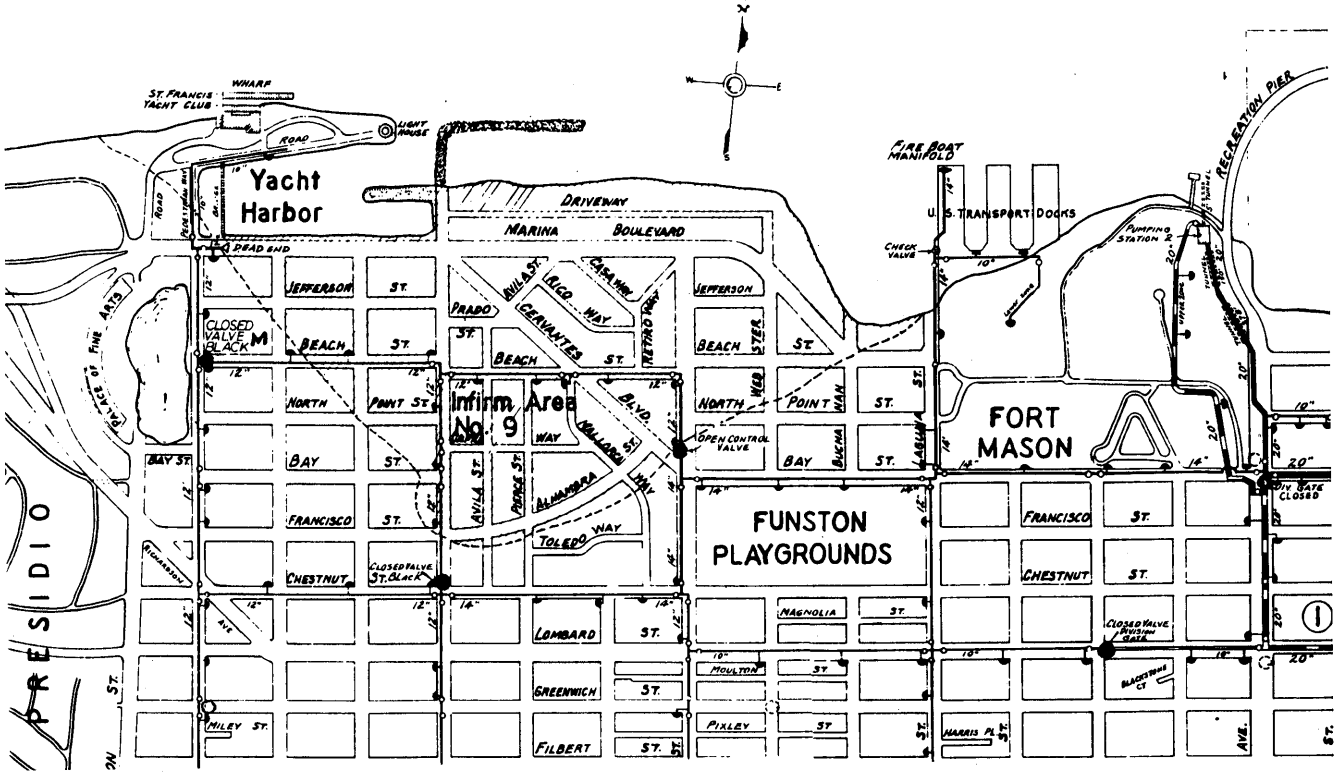


Figure 6.—Marina District, showing location of AWSS pipe network (heavy lines). Map courtesy of SFFD.

San Francisco and Oakland (fig. 1), outside the Marina District, sustained the loss of upper-story facades. At one brick building in downtown San Francisco, an upper-story facade collapsed, killing five people. Several other Marina District structures were on the verge of collapse. Eventually, 63 Marina District structures that had not collapsed were declared unsafe (red tagged), and many more were declared damaged and of questionable safety (yellow tagged); the locations of these structures are shown in figure 8.

The earthquake also caused widespread damage to underground facilities and other utilities. Electric power failed, and traffic signals went dark at a time when commuters were driving home, resulting in heavy, slow traffic in many places. The MWSS immediately sustained 123 main and service-line breaks within the Marina District, and 35 others outside the district (O'Rourke and others, 1990). The result in the Marina District was a total loss of flow to customers and to MWSS fire hydrants. The AWSS was undamaged in the Marina District. Elsewhere, however, the

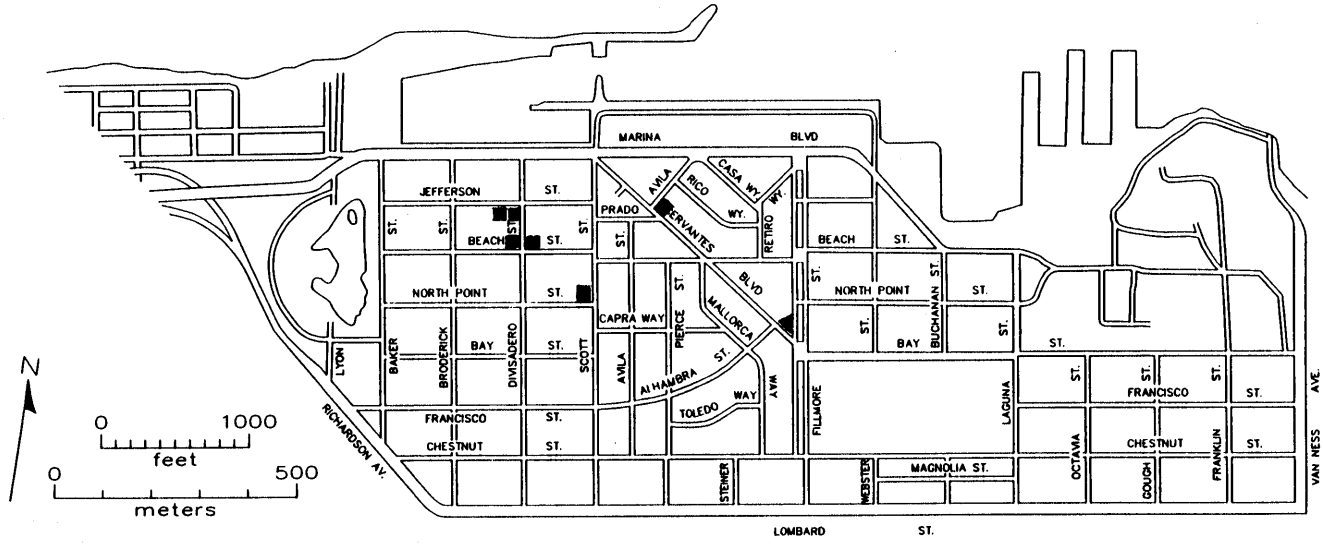


Figure 7.—Marina District, showing locations of collapsed buildings (dark areas). Base map from U.S. Geological Survey (1990).

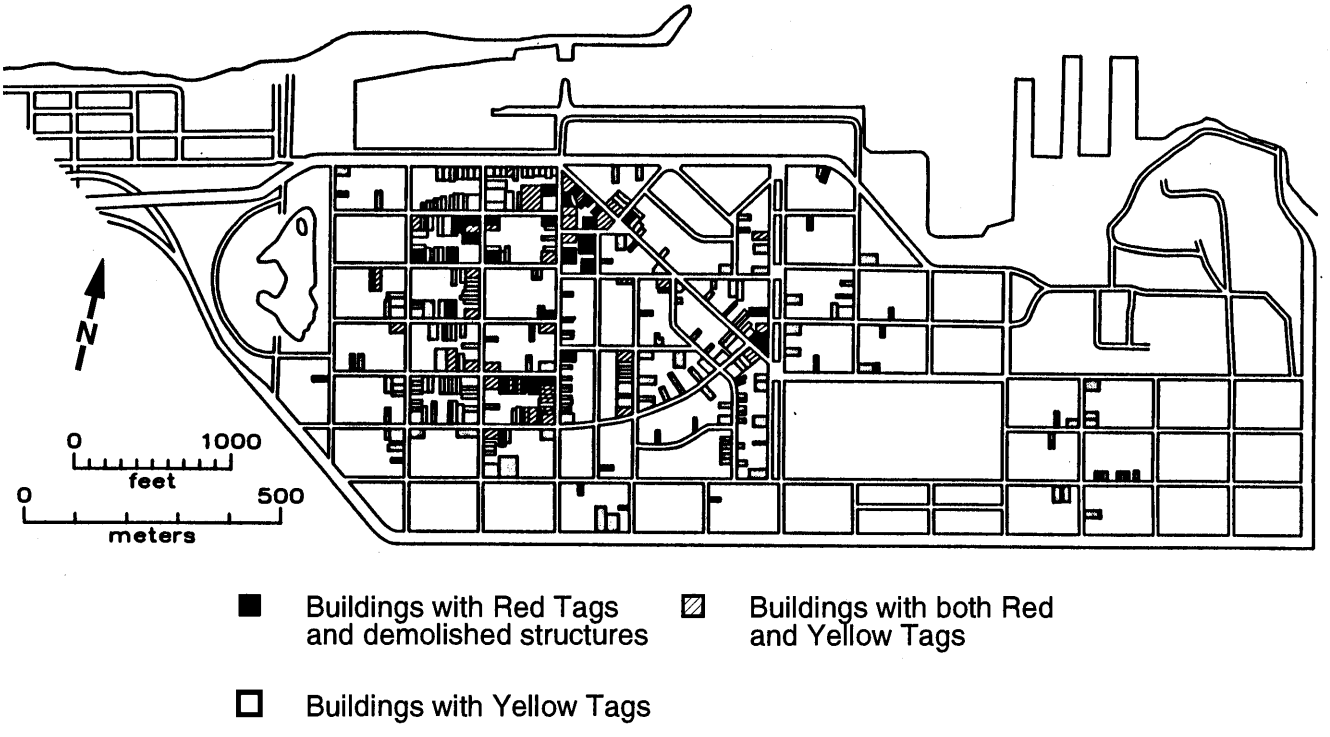


Figure 8.—Marina District, showing locations of damaged buildings. From Seekins and others (1990).

AWSS sustained one main break, one hydrant-branch break, and five hydrant-elbow breaks that soon made it ineffective (though not inoperative) in the Marina District. Long delays in getting a dial tone led many users to believe that the telephones were not working (Benuska, 1990). PG&E's low-pressure gas-distribution system sustained numerous breaks in the Marina District; soon after the earthquake, the smell of natural gas pervaded the district.

In summary, this was the situation confronting SFPD and SFFD personnel responding to the Marina District immediately after the earthquake: Traffic was stopped or severely congested at several key points in the city; people frightened by the earthquake were filling the streets; 7 structures had collapsed; 63 more structures were severely damaged, some of which threatened to collapse; building occupants were trapped, injured, or both; the odor of escaping gas filled the air, raising fears of fire; and, although the SFFD did not know it yet, MWSS fire hydrants in the Marina District lacked all pressure, and the high-pressure AWSS zone serving the Marina District was rapidly draining through breaks south of Market Street.

## SFPD RESPONSE

Damage to lifelines immediately reduced SFPD telecommunication and data-processing capabilities. The loss of commercial power and water, and limited interruption of telephone service, combined to force a temporary shutdown of the SFPD's computerized dispatch, and disrupted communications with the SFFD and the Paramedics Division. According to the SFPD's earthquake report:

> Mainframe equipment was physically shifted by the force of the earthquake, there was some minor failure of ancillary equipment, and the emergency power source failed because the generator's cooling system uses water (which was unavailable when the main was broken). . . . When emergency generator power failed, the mainframe went down, and so did the Computer Aided Dispatch (CAD) system. The 911 transfer line to other municipal units such as the fire department and paramedics was not operational, due to Pacific Bell's McCoppin Street switch failure.

Nonetheless, the emergency did not overwhelm the SFPD's ability to respond. The SFPD estimated that "police resources could have dealt successfully with twice the affected area and one additional major perimeter if other conditions (e.g., no major aftershocks, lack of looting, few reported offenses) remained the same."

Soon after the earthquake, the SFPD transmitted by local broadcast media an order recalling all offduty police officers and canceling all leaves. Many officers returned to duty on their own initiative, before the recall order was announced.

SFPD involvement was most extensive in their Northern District, which contains the Marina District, where activities focused on crowd and access control. A Marina Command Perimeter was established to control access into the more severely damaged part of the Marina District between Marina Boulevard, Chestnut Street, Baker Street, and Fillmore Street (fig. 9). The SFPD had some difficulty maintaining access control in the days after the earthquake. According to the SFPD's earthquake report:

> Reports of "tourists," tour buses, residents, interested third parties, and others attempting to enter affected areas and buildings are numerous. . . . changes in "policy" were made with enough frequency that maintaining access control became difficult; and many citizens were angered by the resulting delays and miscommunications. The authority of Parking Control Officers was often challenged when they were used to man the Marina perimeter. . . . This began to occur on October 18 and may have been largely due to confusion and the use of non-sworn personnel to man barricades.

## SFFD RESPONSE

### FIRST RESPONSE: BUILDING COLLAPSE AT 2 CERVANTES BOULEVARD

The SFFD's first recorded dispatch after the earthquake was at 5:06 p.m. P.d.t., according to official SFFD tape transcripts. The first response to the Marina District was at 5:11 p.m., when the communications center dispatched Engine 16 in reply to a report of people trapped at Fillmore Street and Cervantes Boulevard. Engine 16 arrived at the site by 5:14 p.m.; its crew reported finding the four-story structure at Fillmore Street and Cervantes Boulevard collapsed, with people trapped inside. The death toll from this collapse would turn out to be three, including Diane Laufer, 40, Paul Harris, 48, and 3½-month-old Scott Dickinson. Engine 16 also reported discovering a ruptured gas main nearby, and they asked the communications center to call PG&E, the owner of the main, to send crews to deal with the break. The communications center ordered Engine 16 to handle it themselves. Just 3 minutes later, at 5:17 p.m., they reported, "Get PG&E . . . gas all over the place."

The Battalion 4 chief on duty, Victor Shannon, heard Engine 16's initial report to the communications center regarding the collapsed building. Shannon signaled that he was going to respond to the scene, and he ordered that a rescue squad be dispatched as well. Rescue Squad 2 arrived 6 minutes later, at 5:20 p.m.

### A MAJOR GAS LEAK

At 5:23 p.m., Chief Shannon reported a major gas leak at Mallorca Way and Alhambra Street, that police were on the scene, and that PG&E was needed to deal with the gas leak right away. This leak turned out to be a cracked miter joint in a 12-in.-diameter steel feeder main, the only leak in the high-pressure steel feeder system in the Marina District; numerous other leaks in the district were in the low-

pressure cast-iron and steel system. Then, 3 minutes later at 5:26 p.m., Shannon requested more trucks at the scene; Truck 5 responded.

## COMMUNICATION PROBLEMS

At 5:28 p.m., Station 16 called the communications center, reporting "the collapse on Beach Street; there's a fire now in the collapse at Beach, between Divisadero and Broderick." This was the first indication of a fire in the Marina District on the SFFD's tape transcripts.

The communications center, however, did not acknowledge the message. Immense radio traffic was making contact extremely difficult. After analyzing the tape transcripts of radio communications between the communications center and field units, SFFD analysts later concluded:

> Throughout this time [from 5:04 until 7:30 p.m.], field units and the communications center interfered with one another on the radio. Units were cut off, and many messages were not acknowledged. Some field units failed to wait 1 second for the radio repeaters to open; thus, the first parts of their messages were not heard. Radio traffic was so heavy that units could not get through to the communications center. When they did, they were often not heard.

## FIRE, COLLAPSE, AND TRAPPED VICTIMS AT BEACH AND DIVISADERO STREETS

As Station 16 had reported, two four-story apartment buildings had collapsed at Beach and Divisadero Streets (fig. 10). The building on the northeast corner had collapsed onto Beach Street, covering an MWSS fire hydrant. Of its south facade, only one story remained; two stories remained at its rear on the north side (fig. 11). Sherra Cox, who was trapped in the rear of this building, would become the object of a difficult and dangerous rescue. Of the building on the northwest corner, two stories remained upright, leaning forward over an AWSS fire hydrant on the corner (fig. 12). This was the structure where the fire, which would eventually consume four buildings, began. As this building smoldered, a husband and wife, William and Janet Ray, lay trapped in a lower floor.

At about 5:30 p.m., Chief Shannon ordered Engine 38 to Cervantes Boulevard and Fillmore Street to assist with the rescue. He then requested an ambulance and another truck company, and he reported that a baby had been found in the collapsed building. The communications center dispatched both Truck 9 and Engine 41 to the scene.

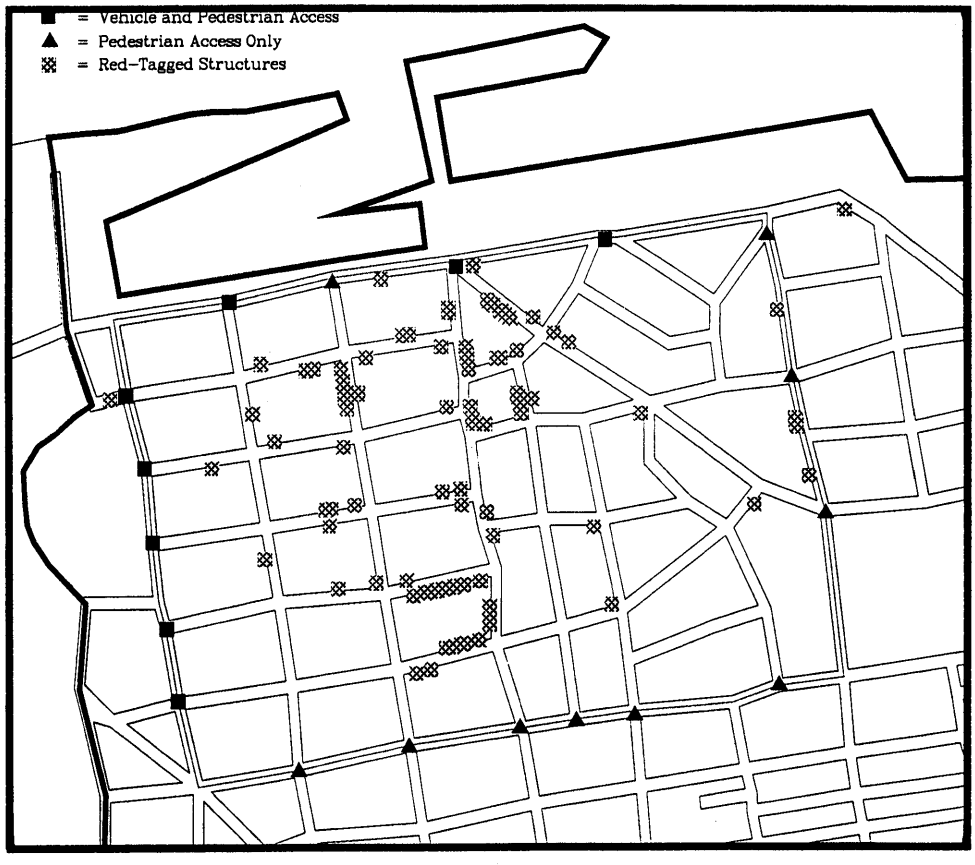


Figure 9.—Western part of the Marina District, showing location of SFPD North District's Marina Command Perimeter (outline). Map courtesy of SFPD.

At 5:35 p.m., Engine 10 reported a gas leak in front of 2359 Francisco Street, near Broderick Street. The crew of Engine 10 spent the next 20 minutes closing gas shutoff valves on Francisco Street while the fire three blocks to the north smoldered and grew.

At 5:37 p.m., the first unit to report from the fire scene was Truck 16, commanded by Capt. Robert Jabs. According to his report, Truck 16 had been on the way to the building collapse at Fillmore Street and Cervantes Boulevard when they were stopped by two offduty police offi-

Figure 10.—Two collapsed apartment buildings at Beach and Divisadero Streets. Building in foreground is 3701 Divisadero, where fire started; building in background is 2090 Beach Street, where Sherra Cox was trapped. Photograph taken at about 5:20 p.m. P.d.t. October 17, 1989, from Beach Street; view northeastward.

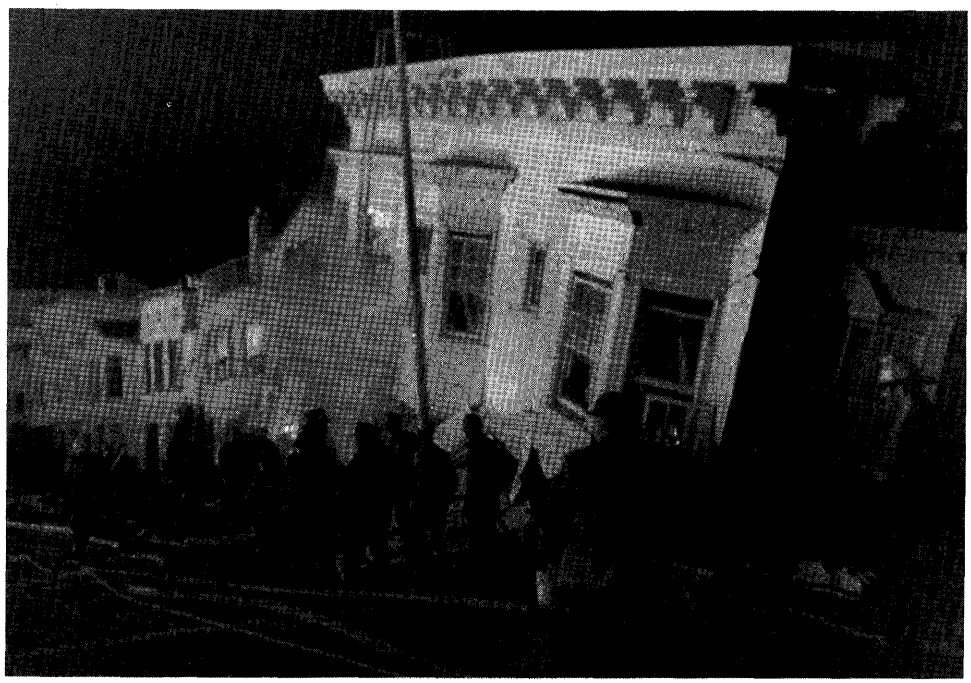

Figure 11.—Collapsed building at 2090 Beach Street, after fire was much advanced. Note firefighter directing water onto exposed side of building. Photograph by S.P. Harris, taken at about 7:00 p.m. P.d.t. October 17, 1989.

cers and told that buildings had collapsed, trapping people inside. Capt. Jabs ordered Truck 16 to Divisadero and Beach Streets, where they found the collapsed buildings. He radioed the communications center of Truck 16's location and of the situation: "We're at Divisadero and [garbled]. We've got 10 or 12 buildings collapsed. There's one starting on fire. We've got people trapped. We're going to need an engine company." The SFFD's tape transcripts indicate that the communications center mistook Truck 16 for Engine 16 and ordered Truck 10 to respond to the fire scene to assist Engine 16. As late as 5:47 p.m., the communications center believed that Engine 16 was at the fire.

## RESCUE AT 3701 DIVISADERO STREET

Capt. Jabs could see some of the trapped occupants of the northeast corner building at 2090 Beach Street. Civilians had been first on the scene and heard voices coming from inside this building. Because both corner buildings were in danger of further collapse, Capt. Jabs split his company of five and attempted both rescues. He sent firefighters Howard Cross and Wayne Martin into the northeast corner building, while he and the two remaining firefighters, John Reed and Thomas Bailon, began to search the burning building. Reed and Bailon went inside, while Capt. Jabs, aided by several civilians, tried to reach the trapped occupants from the side of the building, but they found the task impossible. Meanwhile, Reed and Bailon used axes to cut open the floor, and found the two trapped occupants, Janet Ray and her husband, William Ray. Capt. Jabs recorded, "They were trapped beneath debris from the collapsed building. I entered the building with four or five civilians to begin extraction." The building was on fire.

An explosion shook the building, and Capt. Jabs ordered the civilians out. He later wrote:

> Smoke was now starting to fill the floor ... and I could see flames coming from the front of the building. We could not free the trapped victims from the debris, so I had power saws and jacks brought into the building. We were racing against time, as the fire was spreading rapidly, and the only defense we had was a 1½-inch hose line working under reduced pressure. Voices from outside the building called, saying, "The building is going to collapse!" I looked out the window and saw that the top floor of the building was fully involved with fire. At this point, we chose to continue rescue attempts. Heat and smoke drove us from the building, but the male victim had crawled out through the hole we cut in the floor. Myself and a male civilian carried the victim across the partially collapsed roof to safety and awaited an ambulance.

Janet Ray, 28, perished.

## PG&E ARRIVES

By 5:52 p.m., two PG&E workers had arrived at Alhambra Street and Mallorca Way, determined that the gas leak was in the high-pressure system, and had Chief Shannon radio the communications center to ask for an additional PG&E crew.

Figure 12.—Collapsed building at 3701 Divisadero shortly after the earthquake. SFFD units had not yet arrived. Note dust or smoke from incipient fire at right. Photograph taken at about 5:20 p.m. October 17, 1989, from intersection of Beach and Divisadero Streets; view northwestward.

## ENGINE 41 ARRIVES AT THE FIRE

Firefighters Reed and Bailon were still attempting to cut through the floor of 3701 Divisadero Street when the first engine to report from the fire, Engine 41, arrived at 5:52 p.m. It had been ordered to report to Cervantes Boulevard and Fillmore Street to assist there, but when it arrived, a column of smoke was visible over the rooftops, and so Chief Shannon ordered Engine 41 to continue on to the fire. According to a report by Lt. Peter Cornyn of Engine 41, when Engine 41 reached Beach and Divisadero Streets, the fire was still small. Firefighters Baker and Fitzpatrick hooked up to the AWSS hydrant immediately in front of the burning building, leading a line from the hydrant to Engine 41. The engine was positioned on Beach Street to utilize its deck gun. Three large lines were led from the engine: one to the west end of the building, a second to the middle, and a third to Divisadero Street. Firefighters manned and charged the lines, but they found that the system pressure was inadequate to supply all three. According to Lt. Cornyn's report:

> Two large lines were left charged, but the hose stream didn't reach the fire. The fire was starting to escalate. Both ready lines were lead to the fire and charged, but there wasn't enough pressure to slow the fire down. At this point, Engine 41 was moved to Divisadero Street to escape the heat from the escalating fire.

Engine 41 withdrew to Divisadero Street, ripping the hose still connected to the hydrant in front of the burning building. While Engine 41 was still attacking the fire from Beach Street, Engine 2 from the Presidio Fire Department (PFD) arrived by way of Marina Boulevard. They attempted to draw water from an MWSS hydrant on the north side of the building, but they found the hydrant dry. They positioned their apparatus on Divisadero Street to the north of the burning building and, using water from their tank, provided protection for Capt. Jabs and the firefighters in 3701 Divisadero Street until the rescuers were forced from the building. When its water tank was empty, PFD Engine 2 was repositioned on Jefferson Street.

At 5:55 p.m., the communications center ordered Engine 14 to respond to Beach and Divisadero Streets, but then reversed the order, saying that a unit would be called from the PFD.

At 5:56 p.m., Engine 10 reported discovering another gas leak at 2240 Francisco Street. They asked whether they should ignore it and respond to the fire, which was only three blocks away. The communications center misunderstood this signal and believed that Engine 10 was going to the fire. Radio communication was confused; 3 minutes later, Engine 10 reported that they were available.

At about 5:55 p.m., Chief Shannon arrived at the fire and found the building in flames. At 5:58 p.m., he ordered Engine 16 to assist with the fire. The communications center reported to Shannon that a PFD unit was coming to the fire.

## AWSS WATER PRESSURE LOW

At 6:01 p.m., Chief Shannon reported that the fire crews were putting water on the fire but that system pressure was very low. This is the first recorded report that pressure in the AWSS system was low in the Marina District. The pressure had dropped because of breaks sustained by the AWSS in the lower pressure zone south of Market Street.

At 6:09 p.m., Truck 10 reported that two buildings were now on fire and were burning out of control. They requested at least one, preferably two, additional engines. The communications center dispatched Engine 14 to the fire. At the time, Engine 14 was 4 mi away at 25th Avenue and Geary Boulevard. Engine 10 again reported that they were at Scott and Alhambra Streets, four blocks from the fire, and asked whether they should report to the fire. They received no response and eventually informed the communications center that they were responding to the fire. From the previous communication with Engine 10, the communications center seemed to think that there was a fire at Scott and Alhambra Streets, and at 6:15 p.m. they ordered Engine 31 to a fire at that intersection.

## AWSS WATER SUPPLY NEVER EXHAUSTED

At 6:13 p.m., Engine 10 arrived at the fire and drove to Beach and Broderick Streets. The crew tested the low-pressure hydrant on the southeast corner and found it almost dry. They then hooked up Engine 10 to the AWSS hydrant on the northeast corner. The crew led two 3-in.-diameter hoses from the hydrant to the building immediately west of the fire, 2130 Beach Street. They found they had enough water to operate both leads, but only at reduced pressures. According to firefighter William Koenig of Engine 10, the pressure in the AWSS system ranged from 0 to 40 lb/in$^2$ at the engine. Somewhat later, Koenig reported:

> Both big lines were receiving 50 to 60 psi, certainly not the best. . . . It was necessary to prime No. 10 on about five to six occasions; however, most of the time water was there. . . . As the water supply fluctuated during this period, it was necessary to close down a line or two, depending on the fire situation.

Radiated heat began to ignite window casings on the building directly opposite the fire on Beach Street. In response, Koenig reported, "All lines were shut down to allow Lt. Donham [Truck 5] to have increased pressure to enable him to reach the third-floor window to extinguish this fire."

At 6:16 p.m., Engine 21 reported from the Marina District. Chief Shannon ordered Engine 21's crew to attack the fire from the west along Beach Street. They tried the AWSS hydrant at Beach and Broderick Streets, which was supplying lines, but they saw that the lines were limp, as

if the capacity of the hydrant were being exceeded. Its crew moved Engine 21 to the southeast corner of Beach and Baker Streets, tested the AWSS hydrant there, and found that it appeared to have enough water. They placed two Gleeson valves on the hydrant, led two lines to Beach and Broderick Streets, and charged the lines. According to the report by Capt. Guido Costella of Engine 21, "After charging both lines, the water supply went to zero."

## DRAFTING FROM THE LAGOON

Engine 21 abandoned the AWSS hydrant and fixed on another source of water: the lagoon at the Palace of Fine Arts, just two blocks to the west (fig. 13). According to Capt. Costella's report:

> We broke the lines at Beach and Broderick, connected both lines into E14 [Engine 14], and proceeded with E21 back to Baker and Beach. Our . . . plan was to draft from Palace of Fine Arts lagoon. All access to the lagoon was blocked. We found a car with the owner able to move it, and we were able to drive down the pathway.


Figure 13.—Western part of Marina District, showing location of fire relative to lagoon at the Palace of Fine Arts. Photograph taken October 18, 1989.

> We used one length of 6-inch suction [a rigid hose that does not collapse under vacuum from the engine's pump] to draft. We were supplying two 3-inch hose leads to E14 at Beach and Broderick and one supply lead to E3 that was working on Beach Street.

"Once the relay was established," recorded firefighter Koenig, "water was no problem, with both big lines now receiving 100 psi and the big multiversal in operation continuously." The fire by now had advanced westward to the three-story building at 2130 Beach Street. Before long, according to Koenig, "without warning, the second building, now 75 percent in flames from east to west, collapsed . . . into the first fire building and out into the street."

## FIREBOAT *PHOENIX* DISPATCHED

At 6:16 p.m., Chief Shannon reported that the AWSS in the Marina District was running out of water, and he requested the fireboat *Phoenix* to respond to the fire. About this time, offduty Battalion 4 chief, Greg Abell, arrived in the Marina District. Water pressure in the AWSS hydrants in the district had been low since the first fire crews had arrived, and there was no pressure in the MWSS hydrants. In response, Chief Abell called for a PWSS hosetender, carrying portable water-supply equipment, to lay an aboveground water main supplied with seawater pumped from the St. Francis Yacht Club Harbor by the *Phoenix*.

The communications center immediately dispatched Engine 22 and Hosetender 22 to the Marina, informing them they would lead from the fireboat. At 6:19 p.m., Chief Abell informed the communications center that the fire was five alarm. The communications center informed Chief Abell: "The fireboat's responding. They don't have a [firefighting] crew." This situation was normal. At the time of the earthquake, the fireboat *Phoenix* was assigned only its officer, Lt. Robert Banchero, Pilot Arvid Hanneras, and Engineer Nate Hardy. Lt. Banchero, when later questioned on what, in his opinion, could be done in the future to improve response, replied, "A: Have crew assigned to the fireboat. We couldn't wait for a cover co[mpany] the night of the quake."

Also at 6:19 p.m., Truck 2 reported that it was responding to the Marina District, and Truck 5 left the collapse at Fillmore and Cervantes Streets to respond to the fire.

## TWIN PEAKS RESERVOIR HELD IN RESERVE, PWSS ARRIVES

By 6:24 p.m., Engine 21 was asking the communications center about extra water supply to the AWSS. They were at the AWSS hydrant at Beach and Baker Streets, and were requesting water. The communications center did not know whether extra pressure had been cut in from the Twin Peaks Reservoir, and they informed Engine 21 that the Jones Street Tank had detected a leak. Within a few minutes, the communications center informed Chief Shan-

non that the Twin Peaks Reservoir had not been cut in and was being held in reserve.

About this time, Hosetender 25 arrived at Marina Boulevard and Divisadero Street, having been dispatched by telephone. This was the first PWSS equipment to arrive in the Marina District; its use would turn out to be critical. Normally, a hosetender and its engine travel together; one firefighter drives the hosetender, while two firefighters and the officer travel in the engine. Hosetender 25, however, had been dispatched alone to the Marina District, and carried only the driver.

By coincidence, Hosetender 25 arrived just as two offduty firefighters, Tom Kuhn and Steve Jones, returned to duty from their homes in Marin County. On their way into the city, the two firefighters had seen the fire and reported directly to the Marina District; they also saw PWSS Hosetender 25. Both firefighters Kuhn and Jones were normally assigned to Station 8, which houses another PWSS hosetender, No. 8. The two were assigned to assist Hosetender 25.

The now-complete crew of Hosetender 25 began immediately to make the initial 5-in.-diameter hose lead. It ran from Marina Boulevard up Divisadero Street to Beach Street and included two portable hydrants, with 900 ft of 5-in.-diameter hose. Hosetender 25 was then positioned on the east flank of the fire (fig. 14); from this position, they would be able to protect the buildings across, and farther north on, Divisadero Street.

By 6:27 p.m., the Division 2 chief, Assistant Chief Harry Brophy, had arrived in the Marina District, becoming the incident commander. He repeated the request for additional PG&E crews: "Send the PG&E out here to the area of Cervantes and Fillmore. You've got major gas in that area. Major gas leak . . . There's gas all over the place . . . You're gonna have a major one if we do not get it now."

By 6:41 p.m., Engine 21 was attempting to draft water from the lagoon at the Palace of Fine Arts, but its crew was having trouble getting the engine to the water because all access was blocked by parked cars. Engines 22 and 31 had attempted to draft water directly from the bay at the foot of Divisadero Street, but because of low tide, they were unable to find adequate access to the water over the harbor-bank riprap.

At 6:46 p.m., the second PWSS truck, Hosetender 22, arrived at the fire, along with Engine 22. It was ordered to lead hose up from Divisadero Street and Marina Boulevard one block south to Jefferson Street, along Jefferson Street one block west to Broderick Street, on Broderick Street one block south to Beach Street, and down Beach Street to the south flank of the fire. This hose lead was 3,000 ft long and had three portable hydrants. Chief Brophy had set it out to provide water all around the perimeter of the fire, preparing to make a stand on Jefferson Street to the north with aerial ladders and hand lines. Hosetender 22 was positioned on Beach Street to open up its own monitor on the fire's south flank.

## THE *PHOENIX* ARRIVES AT THE FIRE

About the same time as Hosetender 22 began to lay its hose, the Phoenix was arriving at the yacht harbor. It had trouble getting into position at the foot of Divisadero Street because of the outgoing tide. The water was so low that the *Phoenix* was dragging bottom, its screws churning mud. After the *Phoenix* was in position, the tide continued to drop, grounding the fireboat on the harbor bottom.

Engine 36, which had led hose from the high-pressure hydrant at Chestnut and Divisadero Streets, found that they had run out of hose half a block from the fire. Chief Brophy was still urgently calling for more hose.

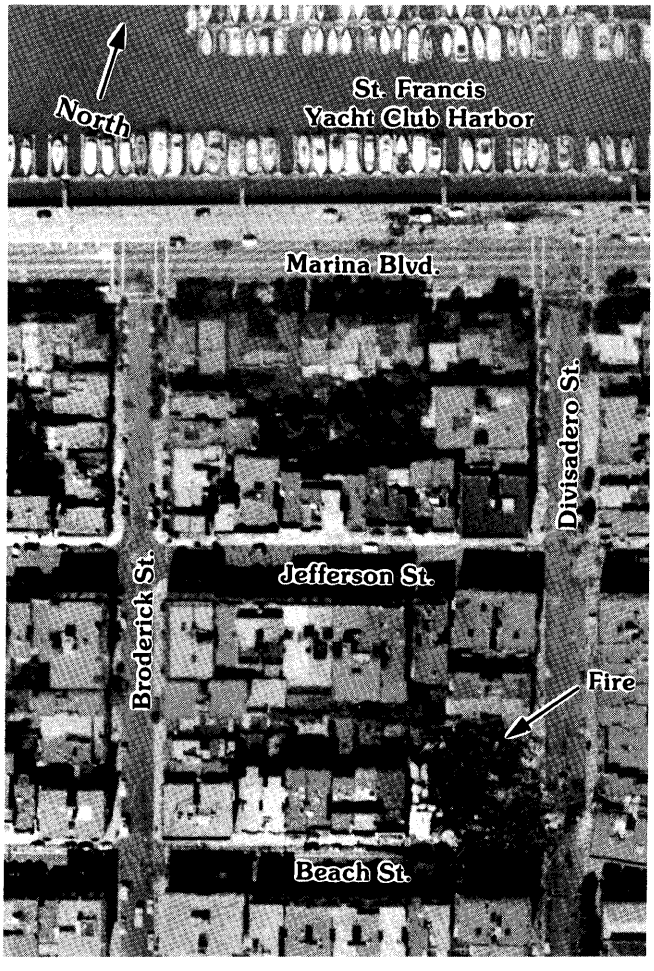


Figure 14.—Northwestern part of Marina District, showing location of the St. Francis Yacht Club Harbor. Hosetender 25 was located immediately to right of fire. PWSS hose leads from yacht harbor are visible on Divisadero and Broderick Streets. Photograph taken October 18, 1989.

At 6:57 p.m., Chief Abell reported that the fireboat had been hooked up and was ready to pump water. This was a turning point. Chief Brophy recorded, "Upon the arrival of the Fireboat . . . we changed from a defensive mode to offensive." Despite being aground, the *Phoenix* was able to pump because its intake sea chests were off the bottom and still under water. The fireboat's first lines had been put into the gated inlet Wye supplying Hosetender 25's 5-in.-diameter hose leads. Hosetender 25 had already been set up for some 10 minutes before receiving water from the *Phoenix*. The fire's radiant heat burnt the paint on the side of the truck but did not force it to withdraw as it waited for water. As soon as the *Phoenix* was hooked up, Chief Brophy ordered the line charged.

Hosetender 25 now had water and immediately opened up its high-pressure battery monitor on the fire's east flank. The effect was immediate and dramatic. Flowing 900 gal (3 tons) of water per minute, with 90 lb/in$^2$ of tip pressure and a 150-ft horizontal reach, Hosetender 25's monitor issued a powerful stream that knocked down the tremendous radiant heat threatening the exposure buildings on the east side of Divisadero Street. The fire in the buildings burning to the north began to darken.

### THREAT OF A CONFLAGRATION ENDED

At 7:00 p.m., Hosetender 8 was the last of the PWSS to arrive, 3 minutes after Hosetender 25 opened its monitor on the fire. Chief Brophy ordered it to make a lead from the fireboat, up Marina Boulevard to Broderick Street, south to Jefferson Street, and then east to Divisadero Street. This route provided an additional portable water main on the north flank, with three more portable hydrants and 2,400 ft of 5-in.-diameter hose supplying pumpers and aerial trucks on this side of the fire.

At 7:17 p.m., Chief Shannon reported that headway was being made against the fire. Then, 7 minutes later, a second aboveground main from the fireboat was ready to be charged. The fire was still out of control by 7:29 p.m., when the transcript ends. Half a block was still ablaze, but Chief Shannon was by then confident that the fire would go out, recording, "The threat of a big conflagration is over." About 9:30 p.m., the fire was brought under control.

### RESCUE OF SHERRA COX

Even while the *Phoenix* was still maneuvering into the yacht harbor, firefighter Gerald Shannon of Truck 9, Capt. Robert Boudoures of Truck 10, and firefighter Jerome Polizzi of Truck 2 had been working for some time on the difficult rescue of Sherra Cox. She was trapped in a lower floor of the collapsed four-story building at 2090 Beach Street, on the northeast corner of Divisadero and Beach Streets, directly across Divisadero Street from the fire. The heat of the fire was causing the buildings facing it to smoke, and igniting curtains inside their windows. The building containing Shannon, Boudoures, and Cox caught fire several times during the rescue; each time, the firefighters outside extinguished the flames. The heat was intense, but Shannon did not retreat; he had promised Cox that he would not leave until he brought her out. "After I saw her," he stated, "I just couldn't leave."

The rescue of Sherra Cox took 2 hours. Relief from the heat came when Hosetender 25's monitor opened up; all the crew of Truck 9 could feel the cooling effect of the water being put on the fire. Cox was pulled out on a backboard and taken to San Francisco General Hospital (see fig. 1). She later underwent surgery for a fractured pelvis (New York Times, 1989).

Relief began to come for the initial responders late into the night. Engine 41 was relieved around 11:30 p.m., and Engine 10 around midnight. Firefighters continued mopping-up operations for several days (fig. 15). The fire damaged seven structures, destroying four buildings containing 33 apartments and flats (Sanborn Map Co., 1988): 3701 Divisadero (21 apartments), 2130 Beach (12 apartments), 3717-19 Divisadero (2 flats), and 3723-25 Divisadero (2 flats). SFFD estimates place the losses from this fire at $7.4 million (fig. 16).

## SIGHTSEERS AND VOLUNTEERS

Civilians had been the first on the scene at 3701 Divisadero Street, and they remained long into the battle with the fire, some helping, some hindering. By 6:30 p.m., sightseers were becoming a problem, and Chief Abell instructed the communications center to notify the media to ask people to stay off the highways. Chief Brophy was becoming concerned about civilians as well; in a fragmented transmission recorded on the tape transcripts he said: ". . . people off to Marina Greens and Chestnut to the other. We have major, major damage. Buildings down everywhere. Gas leaks everywhere. Police Department seal off the area. Get civilians out."

At 6:33 a.m., the fire was still out of control (fig. 17), and the police were having trouble evacuating civilians. At 6:35 p.m., Chief Brophy radioed the communications center. Again, the transmission is fragmented, but its urgency is apparent: "The situation down here in the Marina is devastating. We've 20 or 30 buildings here off their foundations . . . this is a national . . . police cannot handle the sit. . . ."

### EMERGENT VOLUNTEERS

At 6:40 p.m., Chief Brophy requested all available hosetenders to the scene:

Get me all the hosetenders with the 5-inch hose that you can afford. Have them report in on Jefferson right where the yacht harbor is down there . . . Divisadero. We're going to have to take water from the bay. . . . We have three blocks that are going to be involved. We'll have to give away some houses to make a stop, but we need the hose. We have the manpower to pull it; we've got a lot of volunteers, but get it here.

Indeed, there were plenty of volunteers (fig. 18). An offduty police officer at home in his apartment on Divisadero Street near Beach Street felt the earthquake, took his daughter out of the building, went back inside to get his shield, and emerged again to take control of the area. Civil-

Figure 15.—Mopping-up operations on fire. Photograph taken October 18, 1989, from southeast corner of Beach and Divisadero Streets.

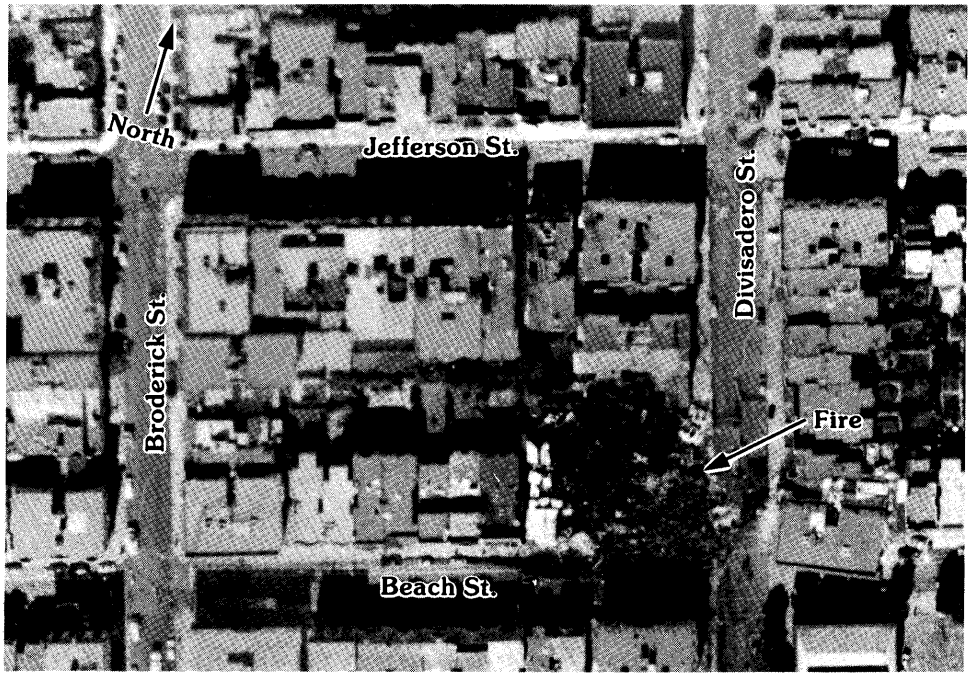


Figure 16.—Northwestern part of Marina District, showing area near Beach and Divisadero Streets. Fire destroyed corner building, another immediately to west, and two more immediately to north.

ians in the Marina District took it upon themselves to go from house to house, shutting off gas. Engine 41, while setting up at Divisadero and Beach Streets, was assisted by civilian men and women, offduty police officers, and retired firefighter Bill Koehler, formerly of Engine 41. These volunteers helped lead hose to the fire from the AWSS hydrant at Divisadero and Bay Streets, two blocks south; volunteers then manned the hoses (fig. 19). Lt. Peter Cornyn, in his report to Chief Postel, wrote of ". . . [T]hirty civilians, whose names I did not get, . . . manned lines attempting to

Figure 17.—Fire in the Marina District. Photograph by Martin Klimek, Marin *Independent Journal*, taken shortly after sunset October 17, 1989; view southeastward.

Figure 18.—Volunteers assisted SFFD at fire. Note firefighter at right. Photograph by C.R. Scawthorn.

stop the Marina fire. Both men and women manned the lines with total disregard to their own safety and well-being."

Engine 36 employed volunteers relaying messages about charging the hoses, and keeping people out of the way. The crew of Engine 10, while closing street gas valves on Francisco Street, was assisted by civilians who formed a human barricade to close the street to all traffic. Perhaps most striking were the civilians who assisted Capt. Robert Jabs and firefighters Bailon and Reed of Truck 16 as they tried to rescue the two trapped occupants of 3701 Divisa-dero Street while the building burned overhead. In his report to Chief Postel, Chief Shannon wrote: "The citizens did everything possible to assist. I will not forget the acts or faces of our heroic citizens, but I do not know the names."

## PARAMEDIC DIVISION RESPONSE

Paramedics responded to three Marina District locations. At 2 Cervantes Boulevard and 3701 Divisadero Street, paramedics treated the injured and examined the dead. In addition, they set up an incident command post half a block from the fire, with an ambulance and a multicasualty unit standing by throughout the night.

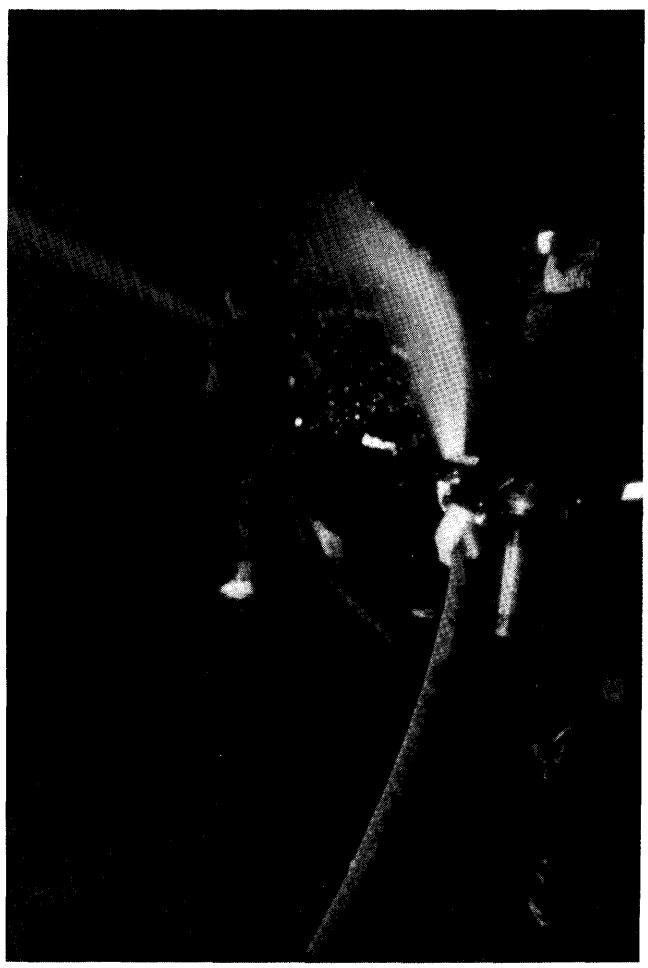

Figure 19.—Civilians helped to lead hoses and then man them at fire. Photograph by C.R. Scawthorn.

CMED dispatched an ambulance to the Marina District shortly after the earthquake. Charles Saunders, medical director of the San Francisco Department of Public Health's Paramedic Division, indicated that the initial response occurred within 5 or 6 minutes of the earthquake; a second ambulance was dispatched shortly afterward. Firefighters had discovered four occupants trapped within the building at 2 Cervantes Boulevard by the time paramedics arrived: Carol Dickinson, Scott Dickinson, Diane Laufer, and Paul Harris.

Moments before the earthquake, Carol Dickinson waved goodbye to her husband Walter as he left for a bicycle ride. She returned to apartment 104, 2 Cervantes Boulevard, just as the earthquake occurred. Carol tried to escape from the building, carrying her 3½-month-old infant Scott in her arms, but they were caught when the stairway collapsed. She was trapped, and the baby was underneath her. She recalled that the baby was breathing at first, but then it became difficult for her to breathe, and she realized that the baby had stopped breathing. Despite the danger of further collapse, firefighters and paramedics successfully extracted the mother and child, and an ambulance transported them to Pacific Medical Center, with paramedic Eberle in attendance. Paramedic Eberle attempted to revive the baby but was unsuccessful. Scott Dickinson was pronounced dead on arrival at Pacific Medical Center at 8:15 p.m. Carol Dickinson survived (Medical Examiner/ Coroner's Register 1303).

The other two victims, Diane Laufer and Paul Harris, were pronounced dead on arrival by a San Francisco Medical Examiner investigative team. The building had been pronounced structurally unsound, and the dead occupants were trapped beneath the debris; they were not extracted until the next day, after the building had been carefully disassembled. They were found lying amongst the rubble, partly pinned beneath a door jamb; Paul Harris appeared to be cradling Diane Laufer in his arms (Medical Examiner/Coroner's Registers 1306, 1307).

Paramedics were dispatched to treat William Ray when he was extracted from 3701 Divisadero Street, and, later, to treat Sherra Cox was she was removed from 2090 Beach Street. Both were taken to the hospital.

Throughout the night, paramedics manned the multicasualty unit and an ambulance standing by at the incident command post, half a block from the fire. The multicasualty unit was equipped with medical supplies, basic medical equipment, and communications equipment.

Injured Marina District residents generally were unable to communicate with the Paramedic Division because long delays getting a dial tone made it appear that telephone service within the district was inoperative. The Paramedic Division found that most earthquake victims near the dis-

trict self-reported to nearby Letterman Army Medical Center and St. Francis Hospital. Of 70 who arrived at these two hospitals, only about 12 were brought by Emergency Medical Services.

## CONCLUDING REMARKS

When examining the events related here, it is worthwhile contrasting San Francisco's experience in the 1989 earthquake with those in the 1906 earthquake. This section briefly summarizes observations and lessons learned, based on police, fire, and paramedic response in the Marina District, with reference to the record of the 1906 earthquake.

1. The city's fireboat *Phoenix* and the use of the PWSS proved crucial in stopping the blaze at 3701 Divisadero Street. The fire had burned out of control until PWSS equipment was deployed and supplied with water by the vast pumping capacity of the *Phoenix*. Without the fireboat *Phoenix* or the PWSS, the damage in the Marina District probably would have been substantially greater. Some firefighters also credit the limited damage to the unusual lack of wind. Estimates vary on the extent to which the fire might have burned, had winds been more typical of an October evening in the Marina District. One firefighter, in responding to a questionnaire by San Francisco Fire Fighters Local 798, noted, "Marina not in ashes because of (1) no wind, (2) fire boat, (3) portable hydrants and hose" (San Francisco Fire Fighter's Local 798, 1990).

In 1906, saltwater from the bay was the only source of water available to firefighters protecting buildings near the Embarcadero waterfront, the South Beach waterfront, and the channel. Pumping the saltwater were several military and private vessels, including the U.S. Navy destroyer U.S.S. *Preble*, the fireboat *Leslie*, the tugboats *Active* and *Fortune*, the U.S. Navy tugboat *Sotoyomo*, the two California fireboats *Governor Irwin* and *Governor Markham*, the Revenue cutter *Golden Gate*, and others (Hansen and Condon, 1989).

2. Planning and training in the use of the PWSS and the *Phoenix* worked. The strategies used with the PWSS had been carefully developed by SFFD staff, in anticipation of major events. When the time came to employ them, the plans proved well thought out and effective, and the time training PWSS crews proved well spent. We note that just 3 weeks before the earthquake, Chief Brophy had conducted a major training exercise at San Francisco's Pier 32, using the fireboat *Phoenix* to supply the PWSS. Firefighters interviewed after the earthquake remarked on how the use of the PWSS in the actual fire situation went just like the drill. This lesson demonstrates the effectiveness of thorough training and of tactics using high-pressure battery monitors to control large fires.

In 1906, SFFD leadership was centralized in Chief Dennis Sullivan. When he was incapacitated in the earthquake, the absence of institutionalized preparedness planning is generally thought to have contributed to the inability of SFFD to contain the fire.

3. Inadequate communications capacity and procedures aggravated the SFFD's difficulty in identifying the number and location of fires, advising incident commanders of in-service-unit location and status, and employing the AWSS. From the start of the emergency response, radio traffic between SFFD units and the communications center far exceeded the capacity of allotted channels. Additional radio channels would likely have made a substantial difference in the SFFD's response in the Marina District.

As congested as radio traffic was in 1989, it represented a vast improvement over conditions in 1906, when the Central Fire Alarm Station at 15 Brenham Place was badly damaged, making the city's fire-alarm system inoperative (Hansen and Condon, 1989).

4. Significant numbers of volunteers emerged to assist in the Marina District response. This pattern of emergent volunteers assisting emergency-service personnel during crises has been observed in past earthquakes as well. After the September 19, 1985, Mexico City earthquake, volunteer rescue teams worked around the clock searching for trapped victims of building collapse (EQE Engineering, 1986). In the May 2, 1983, Coalinga, Calif., earthquake, citizen volunteers manned firefighting hose lines and shut off their own and neighbors' gas (Scawthorn and Donelan, 1984). Lechat (1989) reported, "In Japan, it was observed that within half an hour after an earthquake (Niigata, 1964), 75 percent of the non-affected survivors were engaged in some kind of rescue activity." Emergency-response planning for fire and search and rescue should consider how best to employ emergent response. At a minimum, substantial supplies of clothing and equipment for volunteers should be cached or prearranged.

5. The value of preevent planning and standard operating procedures (SOP's) was demonstrated by the success of the PWSS and by the short-term ineffectiveness of the AWSS. Faced with the loss of water pressure, the SFFD had three options to increase AWSS water supply to the Marina District:

(a) Start the pumps at Pump Stations 1 and 2. Each station has a pumping capacity of 10,000 gal/min at 300-lb/in$^2$ pressure. Pump Station 2 alone could supply enough water flow and pressure for the fire (M. Khater, oral commun., 1991). The extent of damage to the AWSS pipe network, and potential flooding and washout, made this option problematic in the first hours after the earthquake.

(b) Order the fireboat *Phoenix* to the fireboat manifold at Fort Mason's Pier 1. Once attached to the fireboat manifold, the *Phoenix* could pump 9,600 gal/min at 150-lb/in$^2$ pressure directly into AWSS mains near the fire, thereby supplying similar flows to those from Pump Station 2. We note that the fireboat was dispatched directly to the Marina District, rather than to a manifold. In hindsight, this deci-

sion can be seen as proper because AWSS damage was unknown at the time and the fire's proximity to the shoreline permitted the fireboat to supply the PWSS directly.

(c) Cut the Twin Peaks Reservoir into the lower pressure zone. This option would have briefly prevented the Jones Street Tank from draining, but it would also have resulted in drawing down the Twin Peaks Reservoir within several hours, leaving the upper pressure zone unprotected by the AWSS.

In the end, no decision was made. Lacking SOP's, operators at the Jones Street Tank waited for instructions that they never received, leading to a temporary loss of water within the AWSS' lower pressure zone.

6. The SFFD and the local geotechnical- and earthquake-engineering communities had long been aware of the potential for liquefaction in the Marina District. The earthquake vulnerability of structures on made ground had been evident as early as 1868, after the Hayward earthquake of that year and the San Francisco earthquake of 1865. Nonetheless, the old City Hall, completed in 1896, was built on filled land and subsequently destroyed in the 1906 earthquake (Hansen and Condon, 1989).

Despite this past experience, the area's seismic vulnerability was not well known by residents in 1989, nor was it reflected in the city's emergency planning for earthquakes. Since the earthquake, the city of San Francisco has sponsored studies of several areas where a high potential for liquefaction is known to exist, including the Marina District (Harding Lawson Associates and others, 1991a, b). This type of study represents a bridge of knowledge between the engineering community and city officials. The conclusions of these studies should be integrated into future emergency plans.

7. Immediately after the earthquake, although the building collapse at 2 Cervantes Boulevard was known, surrounding areas in the Marina District were not reconnoitered for similar damage, allowing precious time for the fire to grow. Indeed, personnel at the SFFD's communications center (the City's EOC) long lacked a clear picture of the damage in the Marina District. They did not realize the magnitude of the emergency until they saw it on television, broadcast nationwide by the blimp that was on hand for the World Series.

After an earthquake, television and radio helicopters should be employed immediately for rapid reconnaissance. Their reports could be integrated within a disaster-information-management system, to transmit this data rapidly, effectively, and without unnecessary repetition to emergency-response authorities at the EOC. With a clear picture of the situation, these authorities can maximize scarce resources and respond effectively to the emergency.

The foregoing observations and lessons can provide the basis for improved disaster mitigation. However, some of these observations have been made before and not acted upon (for example, those regarding construction on made ground). Perhaps the most useful lesson is to observe a case in which recommendations based on "lessons learned" were implemented. Before 1906, SFFD officials and insurance underwriters had recognized that the city's water-supply system was inadequate to protect against conflagration. A design for the AWSS had been proposed but not implemented until after the 1906 disaster provided the final impetus. The AWSS has served San Francisco well, providing copious amounts of water for numerous large fires.

Earthquake losses were reduced only where responsible experts anticipated problems and communicated them effectively to appropriate authorities, who saw to it that solutions were promptly developed, implemented, and institutionalized with training and SOP's.

## ACKNOWLEDGMENTS

We gratefully appreciate the ongoing assistance and encouragement of Thomas D. O'Rourke of Cornell University, Ithaca, N.Y. Data were provided by Charles Saunders (San Francisco Department of Health, Paramedic Division), Ron Kramer (San Francisco Police Department), Tom Dickerman (San Francisco Water Department), and Andrew Nielsen and Steve Van Dyke (San Francisco Fire Department). This study was funded by research grants from the National Center for Earthquake Engineering Research, State University of New York, Buffalo.

## REFERENCES CITED

Benuska, Lee, ed., 1990, Loma Prieta earthquake reconnaissance report: Earthquake Spectra, supp. 90–01, 448 p.

Bonilla, G.G., 1990, Natural and artificial deposits in the Marina District, chap. A *of* Effects of the Loma Prieta earthquake on the Marina District, San Francisco, California: U.S. Geological Survey Open-File Report 90–253, p. A1–A24.

EQE Engineering, 1986, Summary of the September 19, 1985 Mexico earthquake: San Francisco, 30 p.

Hansen, Gladys, and Condon, Emmet, 1989, Denial of disaster: San Francisco, Cameron and Co., 160 p.

Harding Lawson Associates, Dames & Moore, Kennedy/Jenks/Chilton, and EQE Engineering, 1991a, Liquefaction study, Marina District and Sullivan Marsh area, San Francisco, California; final report prepared for San Francisco Department of Public Works: San Francisco, 144 p.

———1991b, Liquefaction study, North Beach, Embarcadero Waterfront, South Beach, and Upper Mission Creek area, San Francisco, California; report prepared for San Francisco Department of Public Works: San Francisco, 135 p.

Lechat, M., 1989, Corporal damage as related to building structure and design; the need for an international survey: International Workshop on Earthquake Epidemiology for Mitigation and Response, Baltimore, 1989, Proceedings, p. P–1 to P–16.

New York Times, 1989, In a collapsed building, heroism and the promise of coffee: October 19, 1989.

O'Rourke, T.D., Scawthorn, C.R., Blackburn, F.T., and Dickerman, T.S., 1990, Response of the San Francisco Water Supply System during the 1989 Loma Prieta earthquake, *in* Putting the pieces together: San Francisco.

Sanborn Map Co., 1988, San Francisco: v. 3.

San Francisco Fire Fighters Local 798, 1990, A report to the officers and members of the San Francisco Fire Department: San Francisco, Calif., 9 p.

Scawthorn, C.R., and Blackburn, F.T., 1990a, Performance of the San Francisco Auxiliary and Portable Water Supply Systems in the 17 October 1989 Loma Prieta Earthquake: U.S. National Conference on Earthquake Engineering, 4th, Palm Springs, 1990, Proceedings, v. 1, p. 171–180.

Scawthorn, C.R., and Donelan, J., 1984, Fire-related aspects of the Coalinga earthquake, *in* Coalinga, California, earthquake of May 2, 1983; reconnaissance report: Berkeley, University of California, Earthquake Engineering Research Institute Report 84–03, p. 675–685.

Scawthorn, C.R., O'Rourke, T.D., Khater, M.M., and Blackburn, F.T., 1990, Loma Prieta earthquake and the San Francisco AWSS; analysis and observed performance: Japan-U.S. Workshop on Earthquake Resistant Design of Lifeline Facilities and Countermeasures for Soil Liquefaction, 3d, San Francisco, 1990, Proceedings, p. 527–539.

Seekins, L.C., Lew, Frank, and Konfield, Lawrence, 1990, Areal distribution of damage to surface structures, chap. C *of* Effects of the Loma Prieta earthquake on the Marina District, San Francisco, California: U.S. Geological Survey Open-File Report 90–253, p. C1–C5.

U.S. Geological Survey, 1990, Effects of the Loma Prieta earthquake on the Marina District, San Francisco, California: Open-File Report 90–253.